PROTEOGLYCANS AND GLYCOSAMINOGLYCAN MODIFICATION IN IMMUNE REGULATION AND INFLAMMATION

EDITED BY: Rogier M. Reijmers, Aaron C. Petrey, Linda Troeberg and Megan S. Lord

PUBLISHED IN: Frontiers in Immunology

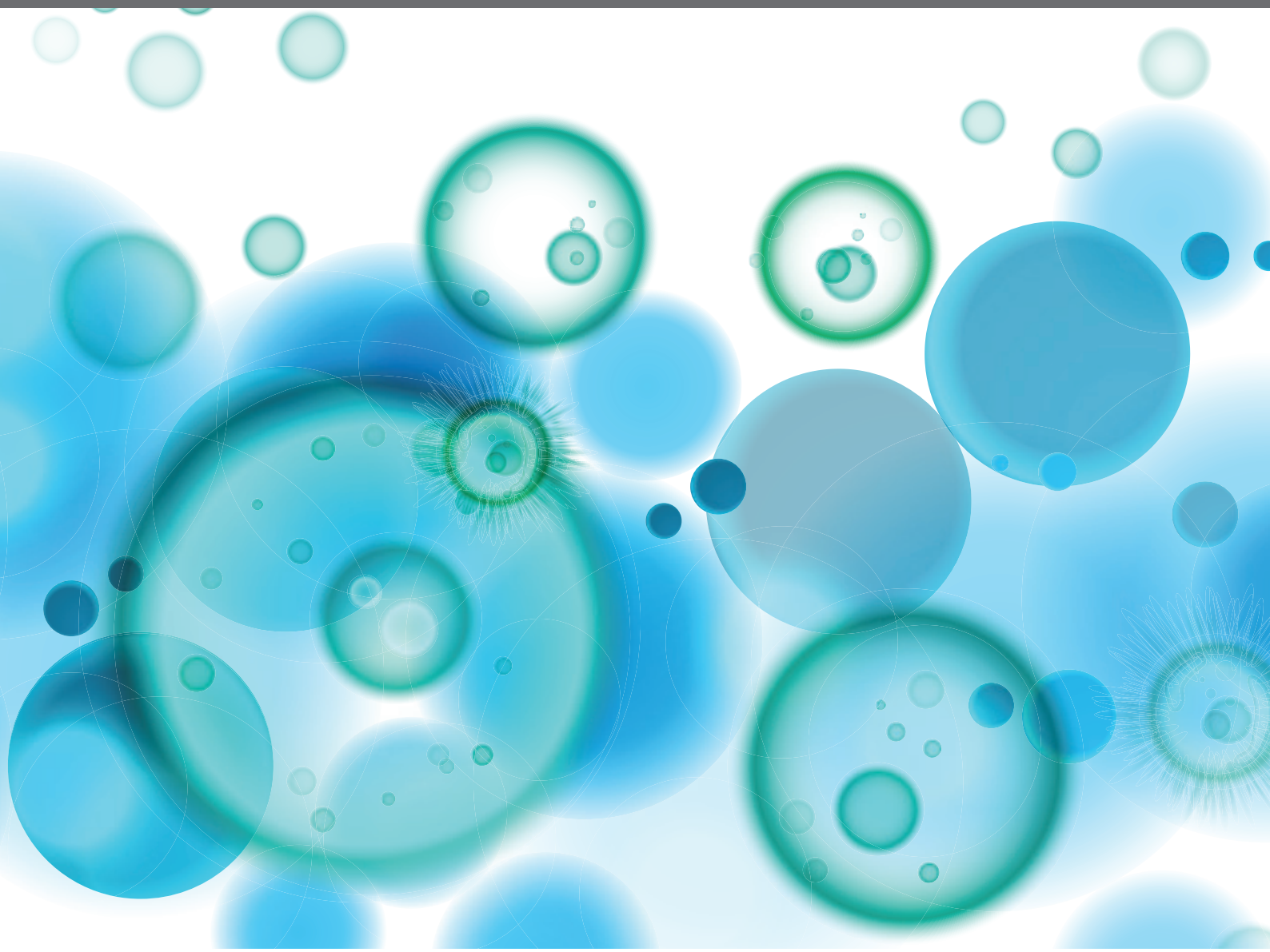

frontiers Research Topics

frontiers

ISSN 1664-8714
ISBN 978-2-88966-253-1
DOI 10.3389/978-2-88966-253-1

About Frontiers

Frontiers is more than just an open-access publisher of scholarly articles: it is a pioneering approach to the world of academia, radically improving the way scholarly research is managed. The grand vision of Frontiers is a world where all people have an equal opportunity to seek, share and generate knowledge. Frontiers provides immediate and permanent online open access to all its publications, but this alone is not enough to realize our grand goals.

Frontiers Journal Series

The Frontiers Journal Series is a multi-tier and interdisciplinary set of open-access, online journals, promising a paradigm shift from the current review, selection and dissemination processes in academic publishing. All Frontiers journals are driven by researchers for researchers; therefore, they constitute a service to the scholarly community. At the same time, the Frontiers Journal Series operates on a revolutionary invention, the tiered publishing system, initially addressing specific communities of scholars, and gradually climbing up to broader public understanding, thus serving the interests of the lay society, too.

Dedication to Quality

Each Frontiers article is a landmark of the highest quality, thanks to genuinely collaborative interactions between authors and review editors, who include some of the world's best academicians. Research must be certified by peers before entering a stream of knowledge that may eventually reach the public - and shape society; therefore, Frontiers only applies the most rigorous and unbiased reviews.
Frontiers revolutionizes research publishing by freely delivering the most outstanding research, evaluated with no bias from both the academic and social point of view. By applying the most advanced information technologies, Frontiers is catapulting scholarly publishing into a new generation.

What are Frontiers Research Topics?

Frontiers Research Topics are very popular trademarks of the Frontiers Journals Series: they are collections of at least ten articles, all centered on a particular subject. With their unique mix of varied contributions from Original Research to Review Articles, Frontiers Research Topics unify the most influential researchers, the latest key findings and historical advances in a hot research area! Find out more on how to host your own Frontiers Research Topic or contribute to one as an author by contacting the Frontiers Editorial Office: researchtopics@frontiersin.org

PROTEOGLYCANS AND GLYCOSAMINOGLYCAN MODIFICATION IN IMMUNE REGULATION AND INFLAMMATION

Topic Editors:
Rogier M. Reijmers, Leiden University Medical Center, Netherlands
Aaron C. Petrey, The University of Utah, United States
Linda Troeberg, University of East Anglia, United Kingdom
Megan S. Lord, University of New South Wales, Australia

Citation: Reijmers, R. M., Petrey, A. C., Troeberg, L., Lord, M. S., eds. (2020). Proteoglycans and Glycosaminoglycan Modification in Immune Regulation and Inflammation. Lausanne: Frontiers Media SA. doi: 10.3389/978-2-88966-253-1

Table of Contents

frontiers in Immunology

EDITORIAL
published: 15 October 2020
doi: 10.3389/fimmu.2020.595867

Editorial: Proteoglycans and Glycosaminoglycan Modification in Immune Regulation and Inflammation

Rogier M. Reijmers[1], Linda Troeberg[2]*, Megan S. Lord[3]* and Aaron C. Petrey[4,5]**

[1] LUMICKS B.V., Amsterdam, Netherlands, [2] Norwich Medical School, University of East Anglia, Norwich, United Kingdom, [3] Graduate School of Biomedical Engineering, University of New South Wales Sydney, Sydney, NSW, Australia, [4] University of Utah Molecular Medicine Program, Salt Lake City, UT, United States, [5] Division of Microbiology and Immunology, Department of Pathology, University of Utah, Salt Lake City, UT, United States

OPEN ACCESS

Edited and reviewed by:
Silvano Sozzani,
Sapienza University of Rome, Italy

***Correspondence:**
Rogier M. Reijmers
r.reijmers@lumicks.com
Linda Troeberg
l.troeberg@uea.ac.uk
Megan S. Lord
m.lord@unsw.edu.au
Aaron C. Petrey
aaron.petrey@u2m2.utah.edu

Specialty section:
This article was submitted to Cytokines and Soluble Mediators in Immunity, a section of the journal Frontiers in Immunology

Received: 17 August 2020
Accepted: 08 September 2020
Published: 15 October 2020

Citation:
Reijmers RM, Troeberg L, Lord MS and Petrey AC (2020) Editorial: Proteoglycans and Glycosaminoglycan Modification in Immune Regulation and Inflammation. Front. Immunol. 11:595867. doi: 10.3389/fimmu.2020.595867

Keywords: glycosaminoglycan (GAG), proteoglycans (PG), immune response, inflammation, heparan sulfate (HS), chondroitin sulfate (CS), dermatan sulfate (DS), hyaluronan

Editorial on the Research Topic

Proteoglycans and Glycosaminoglycan Modification in Immune Regulation and Inflammation

While many publications cover proteoglycan and glycosaminoglycan (GAG) research each year, to date there is still limited knowledge about the specific roles of these macromolecules in the regulation of immune responses and homeostasis. More specifically, the transcriptional control is understudied and largely unknown (1). For this reason, we initiated this Research Topic for Frontiers in Immunology, and challenged scientists to provide findings that uncover novel functions or summarize recent progress that connect these two fields of research. Our collection of 16 manuscripts consists of 7 Original Research papers, one Perspective, one Mini Review, and 7 Reviews covering different aspects of proteoglycan biology in immune processes, which are summarized below.

Proteoglycans are ubiquitously expressed intracellularly, on the cell surface and in the extracellular matrix. Attached to their core are one or a multitude of covalently linked linear anionic GAGs, which are subject to an array of synthetic and post-synthetic enzymatic modifications, leading to an almost infinite combination of configurations, each potentially harboring specific functions (2). As such, precise GAG modifications have been attributed to drive interactions with immune cells, pathogens, and specific protein ligands, while functions have also been attributed to the core proteins. Likewise, the immune system is extremely diverse with many different cell types and immunomodulators, such as chemokines and cytokines, each having specific and unique functions. All of these components need to be kept in strict balance and require tight spatiotemporal regulation to avoid development of autoimmunity or cancer, while combatting a limitless number of pathogens. Understanding this complexity is the greatest challenge in the field and requires detailed structural analysis of GAGs and proteoglycans (3).

Rajarathnam and Desai reviewed recent progress in understanding the molecular basis of chemokine interactions with GAGs and their CXCR1 and CXCR2 receptors. They argue that the range of GAG-binding affinities and geometries confers remarkable selectivity on the *in vivo* phenotype of individual chemokines, and that understanding these interactions is critical for clinical application. Crijns et al. more broadly address chemokine-GAG interactions, and suggest that limiting inflammation using different approaches like chemokine-derived GAG-binding peptides or dominant-negative chemokine mutants, might be beneficial, especially if required to reduce the inflammatory response, rather than completely eliminating it.

Specific effects of GAGs on inflammatory processes were addressed by several authors. For example, Talsma et al. extended our understanding of GAG effects on complement activation by demonstrating that heparin/heparan sulfate oligosaccharides inhibit the lectin pathway via inhibiting the activity of serine protease MASP-2 that cleaves C4. This work may enable the development of glycan-based inhibitors of the lectin pathway with therapeutic value. Arokiasamy, King et al. profiled the glycocalyx of lymphatic vessel endothelial cells, which is less well-understood than the glycocalyx associated with vascular endothelial cells. They showed that the lymphatic glycocalyx of murine cremaster muscles is remodeled in response to TNF-mediated inflammation. Blocking heparanase-mediated degradation of HS had no effect on neutrophil migration through the lymphatic vessels; but reduced lymphatic drainage of interstitial fluid. The responses and function of the lymphatic glycocalyx is thus distinct from that of blood vessels. El Masri et al. explored the role of SULFs in inflammation. Despite clear evidence for critical functions of these enzymes in various pathologies including cancer, the roles of SULFs in inflammatory processes are under-appreciated. To advance this field, further investigations are needed to fully understand their spatial and temporal expression and activity. How this could be strategically advanced in the near future is discussed in this Perspective article.

Use of disease models is progressing our understanding of the role of GAGs in complex *in vivo* scenarios. Pessentheiner et al. summarize the broad role of proteoglycans in obesity-related inflammation. Each class of proteoglycan is discussed, including their enzymatic modifications, and key clinical studies are highlighted implicating proteoglycans as therapeutic targets and biomarkers. Despite limited knowledge of syndecans in obesity-related inflammation, it is clear that syndecans are major players in inflammation. Gopal concisely reviewed the characteristics of syndecans, especially syndecan-1, -2 and -4, explaining their diverse role at the cell surface or as soluble proteins. Arokiasamy, Balderstone et al. focused on the role of syndecan-3 in inflammation and angiogenesis, discussing its impact in several distinct disease types and emphasizing that interactions with the GAG chains make syndecan-3 an inflammatory mediator.

In addition to research on HS, we are beginning to appreciate the roles of chondroitin sulfate (CS) in regulating inflammation. Hatano and Watanabe reviewed the roles of CS produced by antigen presenting cells, in contrast to the more widely studied roles of heparan sulfate (HS) and hyaluronan (HA). Importantly, this review suggests a structure-function relationship for CS based on sulfation with highly sulfated CS, such as CS-C, CS-D, and CS-E, possessing anti-inflammatory properties while the lesser sulfated CS-A possesses both pro- and anti-inflammatory properties. In addition, chain length is a determinant of function with oligosaccharides exhibiting pro-inflammatory properties. Wight et al. provide a comprehensive review on the regulatory roles of the HA-binding proteoglycan versican in the context of immunity and inflammation. The authors summarize how versican and its five different isoforms vary in function, and though not all contain CS chains, each mediates complex roles from development to inflammation by virtue of interacting with a host of diverse immune receptors. They provide insight into cell-type specific functions of versican and highlight how CS containing glycoforms allow versican to function as either a pro- or anti-inflammatory proteoglycan.

Although HA lacks the sulfation shared by the other GAGs, investigation into its regulatory role in inflammatory processes continues to reveal unexpected findings. Dong et al. report a previously unknown link between the HA receptor CD44 and clearance of lung surfactant by alveolar macrophages (AM), which constitutively bind to HA. Loss of CD44 in mice leads to reduced numbers of AMs, and dysregulation of genes involved in cholesterol metabolism. In addition, CD44 deficiency results in a buildup of lipid surfactant, foam-cell AMs, and oxidized lipids which exacerbate lung damage and inflammation. Reeves et al. demonstrate that RSV infection of pediatric human lung fibroblasts results in the formation of an HA-enriched ECM capable of recruiting mast cells and augmenting expression of mast cell proteases. Further, by disrupting HA synthesis or HA binding, the authors demonstrate that increased protease expression depends on mast cell interaction with the HA-matrix produced by infected cells.

Besides the impact on cells and immune modulators, effects of GAGs on bacterial pathogenesis were also explored. Martín et al. report that adhesion of *L. salivarius* Lv72 to HeLa cells induced expression of proteoglycan core proteins but reduced glycosaminoglycan chain biosynthesis by the HeLa cells. In addition, *L. salivarius* Lv72 increased expression of o*ppA* which aids in adhesion to mucosal cells. These results suggest communication between mucosa and microbiota. Galeev et al. demonstrated that proteoglycans not only play a role in bacterial adhesion and uptake by epithelial cells, but that they also play a critical role in the survival of bacteria once internalized via control of intracellular trafficking and endo-lysosomal fusion.

Clinical translation of GAG-based therapies is an exciting challenge. PG545, a synthetic heparanase inhibitor, has been demonstrated to affect tumor viability by preventing angiogenesis and non-neoplastic inflammatory disorders. PG545 acts through competing for GAG binding, and Koliesnik et al. show that it selectively induces Treg development and inhibits the formation of Th17 cells *in vitro* and during *in vivo* delayed type hypersensitivity (DTH). Unexpectedly, these effects were independent of heparanase, but the results support clinical application of PG545 in inflammatory responses associated with DTH. Furthermore, use of human milk glycans such as HA have captured attention for their potential as natural

products to enhance immune responses and their safety as therapeutic modalities. Kim and de la Motte summarize several pre-clinical studies highlighting the known roles of HA in intestinal host defense, detailing the receptors which mediate downstream mechanisms activated by exogenous HA including barrier function and anti-microbial effects.

Our Research Topic underscores the diverse role that proteoglycans have in inflammation and how they control different aspects of immunological processes. However, it also demonstrates that there is still much to discover about the specific mechanisms of their action, including transcriptional and translational regulation of proteoglycan and GAG biosynthesis (1).

AUTHOR CONTRIBUTIONS

All authors listed have made a substantial, direct and intellectual contribution to the work, and approved it for publication.

ACKNOWLEDGMENTS

We would like to thank all authors for their contribution to our Research Topic. This work was supported by Versus Arthritis (grant 21245, LT) and National Institutes of Health (HL135265, AP).

REFERENCES

1. Weiss RJ, Spahn PN, Toledo AG, Chiang AWT, Kellman BP, Li J, et al. ZNF263 is a transcriptional regulator of heparin and heparan sulfate biosynthesis. *Proc Natl Acad Sci USA*. (2020) 117:9311–7. doi: 10.1073/pnas.1920880117
2. Bishop JR, Schiksz M, Esko JD. Heparan sulphate proteoglycans fine-tune mammalian physiology. *Nature*. (2007) 446:1030–7. doi: 10.1038/nature05817
3. Kjellén L, Lindahl U. Specificity of glycosaminoglycan-protein interactions. *Curr Opin Struct Biol*. (2018) 50:101–8. doi: 10.1016/j.sbi.2017.12.011

Conflict of Interest: RR was employed by the company LUMICKS. ML is a Director of Glycos Pty Ltd, which is focused on the generation of bioengineered glycosaminoglycans as therapeutics.

The remaining authors declare that the research was conducted in the absence of any commercial or financial relationships that could be construed as a potential conflict of interest.

frontiers in Immunology

ORIGINAL RESEARCH
published: 04 October 2019
doi: 10.3389/fimmu.2019.02316

Heparanase-Dependent Remodeling of Initial Lymphatic Glycocalyx Regulates Tissue-Fluid Drainage During Acute Inflammation *in vivo*

Samantha Arokiasamy[1,2], *Ross King*[1], *Hidayah Boulaghrasse*[1], *Robin N. Poston*[1], *Sussan Nourshargh*[1], *Wen Wang*[2] *and Mathieu-Benoit Voisin*[1]*

[1] Barts and the London School of Medicine and Dentistry, William Harvey Research Institute, Queen Mary University of London, London, United Kingdom, [2] School of Engineering and Materials Science, Institute of Bioengineering, Queen Mary University of London, London, United Kingdom

OPEN ACCESS

Edited by:
Linda Troeberg, University of East Anglia, United Kingdom

Reviewed by:
Alvaro Teijeira, ETH Zürich, Switzerland
Christoph Reichel, Ludwig-Maximilians-Universität München, Germany

***Correspondence:**
Mathieu-Benoit Voisin
m.b.voisin@qmul.ac.uk

Specialty section:
This article was submitted to Inflammation, a section of the journal Frontiers in Immunology

Received: *09 May 2019*
Accepted: *12 September 2019*
Published: *04 October 2019*

Citation:
Arokiasamy S, King R, Boulaghrasse H, Poston RN, Nourshargh S, Wang W and Voisin M-B (2019) Heparanase-Dependent Remodeling of Initial Lymphatic Glycocalyx Regulates Tissue-Fluid Drainage During Acute Inflammation in vivo. Front. Immunol. 10:2316. doi: 10.3389/fimmu.2019.02316

The glycocalyx is a dense layer of carbohydrate chains involved in numerous and fundamental biological processes, such as cellular and tissue homeostasis, inflammation and disease development. Composed of membrane-bound glycoproteins, sulfated proteoglycans and glycosaminoglycan side-chains, this structure is particularly essential for blood vascular barrier functions and leukocyte diapedesis. Interestingly, whilst the glycocalyx of blood vascular endothelium has been extensively studied, little is known about the composition and function of this glycan layer present on tissue-associated lymphatic vessels (LVs). Here, we applied confocal microscopy to characterize the composition of endothelial glycocalyx of initial lymphatic capillaries in murine cremaster muscles during homeostatic and inflamed conditions using an anti-heparan sulfate (HS) antibody and a panel of lectins recognizing different glycan moieties of the glycocalyx. Our data show the presence of HS, α-D-galactosyl moieties, α2,3-linked sialic acids and, to a lesser extent, N-Acetylglucosamine moieties. A similar expression profile was also observed for LVs of mouse and human skins. Interestingly, inflammation of mouse cremaster tissues or ear skin as induced by TNF-stimulation induced a rapid (within 16 h) remodeling of the LV glycocalyx, as observed by reduced expression of HS and galactosyl moieties, whilst levels of α2,3-linked sialic acids remains unchanged. Furthermore, whilst this response was associated with neutrophil recruitment from the blood circulation and their migration into tissue-associated LVs, specific neutrophil depletion did not impact LV glycocalyx remodeling. Mechanistically, treatment with a non-anticoagulant heparanase inhibitor suppressed LV HS degradation without impacting neutrophil migration into LVs. Interestingly however, inhibition of glycocalyx degradation reduced the capacity of initial LVs to drain interstitial fluid during acute inflammation. Collectively, our data suggest that rapid remodeling of endothelial glycocalyx of tissue-associated LVs supports drainage of fluid and macromolecules but has no role in regulating neutrophil trafficking out of inflamed tissues via initial LVs.

Keywords: glycocalyx, lymphatic vessels, neutrophil trafficking, inflammation, lectins, heparan sulfate, heparanase, lymphatic drainage

INTRODUCTION

The glycocalyx is a carbohydrate-enriched layer surrounding all mammalian cells that is implicated in many biological and pathophysiological responses. *In vivo*, the glycocalyx of blood capillaries, the most studied cell surface glycan layer, spans between several 100 nm to a few micrometers on the luminal side, proportional to the size of vessels (1–3). Biochemically, this glycocalyx is composed of chains of carbohydrate residues attached to transmembrane glycoproteins, sulfated proteoglycans and to glycosaminoglycan (GAG) side chains. Among the glycoproteins forming the glycocalyx of blood vessels are cell adhesion molecules of short molecular length, such as intercellular adhesion molecules (e.g., ICAM-1/2 and VCAM-1) and selectins (4). Proteoglycans on the other hand are considered to be the "backbone" molecules of the glycocalyx (4) and are either anchored to the cell membrane (syndecans, glypicans) or secreted into the glycocalyx structure (mimecans, perlecans, and biglycans). GAG side chains are bound to these proteoglycans and are comprised of heparan sulfate (HS), chondroitin sulfate (CS), and hyaluronan (HA), with HS being the most abundant in the endothelial glycocalyx (5). GAGs are involved in numerous homeostatic and pathological functions of blood vessels through their interactions with a variety of proteins within the lumen of blood vessels. Indeed, the blood vascular endothelial cell (BEC) glycocalyx forms an integral part of the vascular barrier between flowing blood and the interstitium. As such, BEC glycocalyx plays a critical role in vascular permeability and the modulation of inflammatory processes (4, 6, 7). Specifically, the blood vascular glycocalyx acts as a mechano-transducer of sheer stress forces from the blood flow and induces the release of nitric oxide to regulate vascular tone (8). Furthermore, the sulfated GAG side-chains and the high density of glycans also provide strong negative electrostatic charges along the luminal surface of BECs that repulse red blood cells from the endothelium and restrict the diffusion of plasma proteins and solutes through the vessel wall into the interstitium. In contrast, thinning of BEC glycocalyx is strongly associated with increased vascular permeability and edema formation (9, 10).

The blood vascular glycocalyx is also intimately associated with the initial steps of leukocyte recruitment. Specifically, The BEC glycocalyx promotes the interaction between the leukocyte-expressed adhesion molecule L-selectin with its glycosylated receptor PSGL-1 on the luminal side of the endothelium. This interaction allows leukocyte integrins to access endothelial cell adhesion molecules, such as ICAM-1 and VCAM-1 during the rolling and adhesion stages of the recruitment cascade, respectively (11). Furthermore, the glycocalyx GAG side chains are known to bind, and to immobilize, leukocyte pro-inflammatory chemoattractants, in particular the neutrophil chemokines CXCL1 and CXCL2 (12). The latter promotes the transition from rolling to firm adhesion and supports directional crawling of neutrophils onto the luminal aspect of blood vessels. Similarly, HS chains present on high endothelial venules control CCL21 chemokine presentation during the recruitment of naïve lymphocytes and DCs to lymph nodes (13). Paradoxically, inflammation can modify the structure and function of blood vessel glycocalyx; and many cells including leukocytes and endothelial cells can release proteolytic enzymes and reactive oxygen/nitrogen species that degrade or modify the BEC glycocalyx. This phenomenon is particularly important for leukocyte recruitment as most of the adhesion molecules involved in neutrophil-EC interactions protrude $<$40 nm from the cell membrane whilst the thickness of the BEC glycocalyx is around 500 nm (14). Studies have demonstrated that inflammatory mediators, such as TNF or lipopolysaccharide (LPS) can reduce the thickness of BEC glycocalyx by at least a third (15–18), allowing leukocyte-expressed adhesion molecules to reach their binding partners on the BEC surface.

In sharp contrast, the characteristics and role of the glycocalyx on lymphatic vessels (LVs) have received little attention to date. The lymphatic vasculature is the second circulatory system of high vertebrates involved in tissue homeostasis, transport of interstitial fluid and macromolecules back into the blood circulation. The lymphatic system is characterized by a unidirectional network of vessels starting in most tissues with blind-end vessels also known as initial LVs or lymphatic capillaries. Initial LVs are composed of monolayer of oak leaf-shaped endothelial cells (LECs) with loose junctions and surrounded by a thin and discontinuous basement membrane (19). Those unique vessels drain into pre-collecting vessels, subsequently merging into large collectors and then afferent lymphatic venules that are connected to lymph nodes. Lymphatic vessels are thus crucial for immune surveillance as they contribute to the transport of antigens and trafficking of antigen-presenting cells from tissues to draining lymph nodes (dLNs). The latter provides a vital means through which adaptive immune responses are initiated during infections and vaccinations. Recently, the presence of a glycocalyx layer on the luminal side of large collecting lymphatic vessels in the rat mesentery was reported by electron microscopy on isolated vessels (20). It was proposed that the structure and composition of the glycocalyx of collecting LVs and BEC might be similar. Overall, LEC glycocalyx is believed to establish cytokine/chemokine gradients within the vessels, an effect that can aid lymphocyte rolling, maintain the homeostatic balance of the tissues, and contribute to pathogen clearance (4, 20, 21). Interestingly, lymphatic vessels express a unique receptor for the glycosaminoglycan hyaluronan, known as lymphatic vessel endothelial hyaluronan receptor 1 or LYVE-1 (22). Recently, LYVE-1 has been demonstrated to serve as a docking molecule for transmigrating dendritic cells and macrophages by binding to HA present on the surface of these leukocytes (23, 24). Despite these seminal but limited studies, there is to date insufficient insight into the exact composition of the

Abbreviations: BEC, blood endothelial cell; CS, chondroitin sulfate; CFA, complete Freund's adjuvant; dLN, draining lymph node; GAG, glycosaminoglycan; HS, heparan sulfate; IB4, isolectin-B4; ICAM-1, intercellular adhesion molecule 1; i. s., intrascrotal; LEC, lymphatic endothelial cell; LV, lymphatic vessel; PSGL-1, P-selectin glycoprotein ligand-1; MRP14, myeloid related protein 14; NAH, non-anticoagulant heparanase inhibitor N-desulfated/re-N-acetylated heparin; ROS, reactive oxygen species; TNF, tumor necrosis factor (alpha); MAL-1, *Maackia amurensis* Lectin-1; SNA, *Sambucus nigra* agglutinin; sWGA, succinylated wheat germ agglutinin; VCAM-1, vascular cell adhesion molecule 1.

glycocalyx of tissue-associated lymphatic capillaries *in vivo*. Moreover, little is known about the putative modifications and role of this LEC glycan layer during inflammation. To address this fundamental issue, we aimed to characterize the composition, remodeling and function of the glycocalyx of initial LVs of tissues in steady-state and inflamed conditions. This was achieved through analysis by confocal microscopy of the lymphatic vasculature in whole-mount murine cremaster muscles and ear dorsal skin as well as in human skin sections using several lectins (carbohydrate-binding proteins known to bind specific carbohydrate residues) and/or antibodies against HS and HA. We found that *in vivo*, the LV glycocalyx exhibited similarities with the glycocalyx of post-capillary venules with HS, α-D-galactosyl moieties, α2,3-linked sialic acids and N-acetylglucosamine chains being present. Interestingly, acute inflammation as induced by antigen-sensitization or TNF-stimulation resulted in the rapid remodeling of the LV glycocalyx as observed by reduced detection of HS and α-D-galactosyl moieties but not of sialic acids, a response associated with the migration of neutrophils into the lymphatic vasculature. Mechanistically, we observed that pharmacological blockade of endogenous heparanase inhibited TNF-induced HS cleavage. This inhibition of glycocalyx remodeling was associated with a reduced capacity of initial lymphatic capillaries to remove fluids out of the inflamed interstitium whilst neutrophil interactions with LVs were not affected. Collectively, our findings present a novel paradigm for the role and function of initial lymphatic glycocalyx, and demonstrate that its remodeling is important for the rapid drainage of inflamed tissues but not neutrophil recruitment to the lymphatic system *in vivo*.

MATERIALS AND METHODS

Reagents

Recombinant murine TNF was purchased from R&D Systems (Abingdon, UK), Complete Freund's Adjuvant (CFA) from AMSbio (Abingdon, UK), Ovalbumin and Evans blue from Sigma-Aldrich (Poole, UK). The following primary antibodies were used for immunofluorescence labeling for confocal imaging: rat anti–mouse LYVE-1 mAb (clone ALY7; Thermofisher, Hatfield, UK); rabbit anti-human LYVE-1 Ab (polyclonal PA1-16635, Thermofisher), non-blocking rat anti-mouse CD31 mAb (clone C390, Thermofisher); rat anti-mouse/human HEV mAb (clone MECA79, Thermofisher), rat anti-mouse GR1 mAb (clone RB6-8C5, Thermofisher), rat anti-mouse CD144 mAb (VE-Cadherin, clone BV14, Thermofisher), rat anti-mouse MRP14 mAb (clone 2B10; a gift from N. Hogg, Cancer Research UK, London, UK), rat anti-mouse F4/80 mAb (clone BM8, Biolegend, London, UK), rat anti-mouse CD115 mAb (clone AFS98, Biolegend), mouse anti-heparan sulfate (HS) mAb (10E4 epitope, clone F58-10E4, AMSbio), rabbit anti-hyaluronic acid Ab (polyclonal ab53842, Abcam, Cambridge, UK) and rabbit anti-mouse/human heparanase I Ab (polyclonal ab85543, Abcam). Isolectin-B4 (IB4), *Maackia amurensis* Lectin-1 (MAL-1), *Sambucus nigra* Agglutinin (SNA) and succinylated wheat germ agglutinin (sWGA) and their respective inhibitor carbohydrates (Galactose, lactose, N-acetylglucosamine) were purchased from Vector Labs (Peterborough, UK). All antibodies and lectins were fluorescently labeled using Alexa-fluor protein labeling kits as per manufacturer's recommendations (ThermoFisher Scientific, Paisley, UK). The non-anticoagulant heparanase inhibitor N-desulfated/re-N-acetylated heparin (NAH) was sourced from Iduron (Alderley Edge, UK).

Animals, Treatment and Induction of Tissue Inflammation

All experiments were approved by the local biological service unit Ethical Committee at Queen Mary University of London and carried out under the Home Office Project Licenses (70/7884 and P873F4263) according to the guidelines of the United Kingdom Animals Scientific Procedures Act (1986). Wild-type C57BL/6 male mice (8–12 weeks, Charles Rivers Margate, UK) were anesthetized with isofluorane and the cremaster muscles were stimulated for up to 16 h via intrascrotal (i.s.) injection of TNF (300 ng in 300 μl of PBS) or an emulsion (50:50, 300 μl per mouse) of CFA (200 μg) with ovalbumin (200 μg). Control mice were injected with 300 μl of PBS. To induce ear inflammation, anesthetized animals received a subcutaneous (s.c.) injection of 300 ng/30 μL of TNF (or PBS as control) in the dorsal ear skin for 16 h. To inhibit heparanase activity, the non-anticoagulant heparanase inhibitor N-desulfated/re-N-acetylated heparin (NAH) was injected locally (30 ug/mouse, i.s.) 3 h after the injection of TNF. For neutrophil depletion experiments, mice were injected intraperitoneally (i.p.) with 25 μg/mouse/day of anti-GR1 antibody for 3 days preceding the induction of the inflammatory response. This technique, developed in our lab (25) leads to a specific depletion of neutrophils (>99%) but not inflammatory monocytes from the blood circulation (**Supplementary Figure 3**). At the end of all *in vivo* experiments, animals were humanely killed by cervical dislocation in accordance with UK Home Office regulations and the tissues were removed for subsequent analysis.

Fluorescent Staining of Whole-Mount Murine Tissues

Cremaster Tissues

The labeling of blood and lymphatic vessels of the cremaster muscles *in vivo* was achieved as previously described (26). Briefly, the animals received an i.s. injection of the non-blocking dose of a fluorescently-labeled anti-LYVE-1 mAb (2 μg/mouse, Alexa555 conjugated) and/or a fluorescently-labeled non-blocking anti-CD31 mAb (2 μg/mouse, Alexa488, Alexa555, or Alexa647 conjugated depending on the antibody combination) 90 min to 2 h before the end of the inflammatory period to label the lymphatic and blood vasculatures, respectively. To label the glycocalyx sugar residues and HS, the animals also received an i.s. injection of 2 μg/animal of fluorescently labeled (Alexa647) lectins, anti-HS or anti-HA mAbs (both Alexa488 conjugated) 2 h prior to sacrificing the animals. To investigate neutrophil migration responses across post-capillary venules and migration into initial lymphatic vessels of the cremaster muscles, tissues were fixed in 4% PFA in PBS for 1 h at 4°C, then blocked and permeabilized in PBS (containing 12.5% goat serum, 12.5%

fetal bovine serum [FBS] and 0.5% Triton X-100) for 4 h at room temperature. To visualize neutrophils, macrophages or VE-Cadherin, tissues were incubated with Alexa647 conjugated anti-MRP14 (0.25 μg), Alexa647 conjugated anti-F4/80 (1 μg) or Alexa647 conjugated anti-CD144 (1 μg) mAbs, respectively, in 200 μl of PBS (with 10% FBS) per pair of cremaster tissues overnight or up to 48 h at 4°C. To visualize Heparanase I, tissues were incubated with 2 μg of anti-Heparanase I mAb in 200 μl of PBS (with 10% FBS) per pair of cremaster tissues for 48 h at 4°C post-fixation and permeabilization. After three washes in PBS (30 min each), tissues were incubated with an Alexa488 conjugated goat anti-rabbit secondary mAb (Thermofisher) for 4 h. For all immunostaining procedures, tissues where washed in PBS thrice for a minimum of 30 min per wash prior to the visualization of the samples by confocal microscopy.

Lymph Nodes

To quantify neutrophil infiltration of the cremaster draining lymph nodes, the tissues were harvested and fixed in 4% PFA in PBS for 24 h at 4°C, then halved, blocked and permeabilized in PBS (containing 12.5% goat serum, 12.5% fetal bovine serum [FBS] and 0.5% Triton X-100) for 4 h at room temperature. Tissues were then fluorescently immunostained for neutrophils (0.25 μg/100 μl anti-MRP14 mAb, Alexa647 conjugated), high endothelial venules (HEV, 0.25 μg/100 μl of anti-HEV mAb, Alexa488 conjugated) and capsula/trabeculae (0.25 μg/100 μl of anti-LYVE-1 mAb, Alexa555 conjugated), in PBS (with 10% FBS) overnight at 4°C prior to the visualization of the tissues by confocal microscopy.

Ear Skin

Ears were harvested and fixed in 4% PFA for 1 h at 4°C. The two ear flaps were then separated and the skin was blocked and permeabilized in PBS (containing 12.5% goat serum, 12.5% fetal bovine serum and 0.5% Triton X-100) for 4 h at room temperature. Tissues were then fluorescently incubated with 0.25 μg of Alexa488 conjugated anti-MRP14 mAb, 1 μg of Alexa647 conjugated lectin (IB4, MAL-1 or sWGA) and 1 μg of Alexa555 conjugated anti-LYVE-1 mAb in 200 μL per ear in PBS (with 10% FBS) overnight at 4°C prior to the visualization of the tissue by confocal microscopy.

Fluorescent Staining of Human Skin Sections

Paraffin sections of four human breast skin samples from breast carcinoma patients (6 μm thick sections) were obtained from the Breast Cancer Now Tissue Bank at the Barts Cancer Institute, QMUL, with ethical permission. The samples were from distal from breast carcinomas. Hematoxylin and eosin pre-staining from an independent pathologist confirmed the absence of tumor cells in our samples with low to moderate levels of perivascular lymphocytic infiltration. Sections were dewaxed in 2× xylene and 2× 100% ethanol baths for 5 min each, and antigen retrieval was performed at pH 9 in a citrate buffer (Vectorlabs) for 30 min at 95°C following the antibody supplier's guidelines. The sections were then blocked at room temperature with 10% FBS in PBS for 30 min followed by a 48 h incubation at 4°C with the rabbit anti-LYVE-1 antibody (1/200), anti-HS antibody (1/200) or one of our lectins (IB4, MAL-1, or sWGA) in PBS with 0.5% FBS. Samples were washed thrice with PBS for 15 min prior to visualization by confocal microscopy.

Confocal Microscopy and Image Analysis

All samples were imaged with either a Leica SP5 or Leica SP8 confocal microscope (Leica microsystem, Milton Keynes, UK) with the use of a 20× water-dipping objective (NA:1.0). Three-dimensional confocal images from mouse and human samples were analyzed using IMARIS software (Bitplane, Zurich, Switzerland) or FIJI/Image J (NIH, Bethesda, USA).

Mouse Cremaster Muscles and Ear Skin

Images of lymphatic initial capillary vessels (LVs) and blood post-capillary venules (BVs) (∼5 vessels per tissue) were acquired using sequential scanning of different channels at every 0.52 μm of tissue depth at a resolution of 1,024 × 470 and 1,024 × 800 pixels in the x × y plane, respectively. This resolution of pixels correspond to a voxel size of 0.45 × 0.45 × 0.52 μm in x × y × z. BV and LV were imaged at a zoom factor of ×1.9 and ×1.2, respectively. On average, a serial stack of ∼60 and ∼150 optical sections were acquired for BV and LV images, respectively. To assess the expression (i.e., mean fluorescence intensity measurements) of glycocalyx components, image settings (laser power, detector gain and offset) were first defined (and kept constant for each specific molecules and treatment groups) using samples stained with a control isotype-matched antibody (e.g., HS) or a lectin of interest pre-incubated with an inhibitory carbohydrate. To inhibit IB4, MAL-1 or sWGA binding activity, the lectins were pre-incubated with 50 mM of galactose, lactose or N-Acetylglucosamine, respectively, for 1 h prior to their use in murine tissues (**Supplementary Figure 1**). Quantification of neutrophil extravasation and migration into tissue-associated LVs were analyzed with IMARIS software as previously described (26). Specifically, extravasated neutrophils were defined as the number of neutrophils present in the interstitium across a 300 μm blood vessel segment and within 50 μm from each side of the venule of interest; and data are expressed as the number of neutrophils per volume of tissue. The neutrophil intravasation response was defined as the number of neutrophils present inside the lymphatic vessels as visualized in 3D and quantified by IMARIS Software and data were expressed as cell number per given volume of LV. LV volume were quantified by the IMARIS software following the creation of a 3D-isosurface on the LYVE-1 channel (thus excluding $MRP14^{+}$ and $CD31^{high}$ regions) and mean fluorescent intensity measurements of the glycocalyx components associated exclusively with LV where quantified within this isosurface. A similar strategy was done for the blood vessels (i.e., isosurface only on $CD31^{high}$ regions).

Lymph Nodes

Images (12 images per pair of LNs per mouse) were obtained with the use of sequential scanning of different channels at every 0.7 μm of tissue depth at a resolution of 1,024 × 1,024 pixels in

the x × y plane and with a zoom factor of 0.75, corresponding to a voxel size of 0.91 × 0.91 × 0.7 μm in x × y × z. On average, a serial stack of ∼30 optical sections were acquired. Quantification of neutrophil recruitment into the dLNs were analyzed with the 3D-reconstructing image processing software IMARIS. Recruited neutrophils were defined as the number of neutrophils per volume of tissue, excluding the blood circulating neutrophils present in HEVs.

Human Skin Sections

Images of lymphatic vessels (LVs) were acquired using sequential scanning of different channels at every 0.52 μm of tissue depth at a resolution of 1,024 × 300 pixels in the x × y plane with a zoom factor of 1, respectively with a resolution of 0.45 × 0.45 μm in x × y plans. On average, a serial stack of ∼30 optical sections were acquired, overlapping the 6 μm thick tissue section. Lymphatic vessels were confirmed by the presence of LYVE-1$^+$ vessels, morphology and the absence of erythrocytes in the lumen. The expression of lectin-binding moiety and HS on LVs was analyzed by FIJI/Image J by delimitating a surface area around LYVE-1$^+$ regions of LVs.

Lymphatic Drainage Analysis

To visualize the drainage capability of lymphatic vessels of the mouse cremaster muscle *in vivo*, animals received an i.s. injection of Evans Blue in PBS (1%, 300 μL) 20 min prior to the end of the inflammatory period. The cremaster muscles, draining (inguinal) and non-draining (brachial) LNs were then harvested, snap frozen in liquid nitrogen and the blood of the animal was recovered by cardiac puncture. The blood was then centrifuged and plasma collected. For the cremaster muscles and LNs, tissues were incubated in 100% formamide at 56°C overnight prior to spectrophotometry analysis. The quantity of Evans Blue in plasma and tissues samples was quantified with a spectrophotometer at an absorbance wavelength of 620 nm.

Blood Vascular Leakage Analysis

Blood vascular leakage (and lymphatic drainage) was assessed using the Mile's Assay (27). Briefly, 2 h before the end of the TNF stimulation (i.e., 16 h), Evans blue dye (0.5% in PBS, 5 μl/g) was injected i.v. At the end of the experiment, animals were sacrificed, and the cremaster muscles were harvested and incubated in 100% formamide (Sigma-Aldrich) at 56°C for 24 h. The amount of accumulated Evans blue in the tissue supernatant was then quantified by spectroscopy at 620 nm.

Statistical Analysis

Data are presented as mean ± S.E.M per mouse. Significant differences between multiple groups were identified by one-way or two-way analysis of variance (ANOVA), followed by Newman-Keuls/Sidak's Multiple Comparison Test. Whenever two groups were compared, Student's *t*-test was used. *P*-values < 0.05 were considered significant.

RESULTS

Characterization of the Glycocalyx of Initial Lymphatic Capillaries *in vivo*

To compensate for the lack of knowledge regarding the composition and role of initial lymphatic vessel (LV) glycocalyx, in this study we first aimed to investigate the expression profile of carbohydrate moieties present on initial LV of mouse cremaster tissues. This thin and transparent muscle contains an extensive lymphatic vasculature amenable for whole-mount fluorescent staining and 3-dimensional visualization of cellular and molecular structures *in vivo* by confocal microscopy (**Figure 1A**) (26). Interestingly, cremaster LVs are composed mainly of lymphatic endothelial cells (LECs) with discontinuous junctions organized in flaps and VE-Cadherin-enriched buttons (**Figure 1A**) (19). To visualize the glycocalyx of those initial lymphatic vessels we used several fluorescently-labeled lectins, namely Isolectin-B4 (IB4), Maackia Amurensis Lectin-1 (MAL-1), Sambucus Nigra Agglutinin (SNA) and succinylated Wheat Germ Agglutinin (sWGA). These lectins specifically recognize α-D-galactosyl moieties (IB4), sialic acid α2,3-linked (MAL-1) or α-2,6-linked (SNA) galactose/N-acetylgalactosamine residues and N-acetylglucosamine chains (sWGA). Additionally, an anti-heparan sulfate (HS) or anti-hyaluronic acid (HA) monoclonal antibody was employed to visualize heparan sulfate chains and hyaluronan, respectively. Lectins and anti-HS/anti-HA antibodies were injected i.s. in conjunction with non-blocking and fluorescently-labeled anti-LYVE-1 and anti-CD31 mAbs to differentiate the lymphatic and blood vasculatures, respectively, as described previously (26). Animals were sacrificed ∼2 h later, and the cremaster muscles were removed and fixed prior to visualization and image acquisition (whole mount) by confocal microscopy. Image series were then analyzed in 3-dimensions using IMARIS software to quantify the fluorescence intensity for each specific marker binding the glycocalyx moieties associated exclusively with LVs (i.e., LYVE-1$^+$ vessels). The specificity of lectin/antibody binding to their respective glycocalyx moieties in whole-mount tissues was confirmed using competitive sugar binding assays (with the use of specific inhibitory sugars for each lectins) or with isotype-matched control antibodies, respectively (**Supplementary Figure 1**). Our data show that *in vivo* the glycocalyx of initial lymphatic capillaries from cremaster tissues contains HS, α-D-galactosyl moieties, α-2,3-linked sialic acid residues and N-acetylglucosamine chains on as exemplified by the capacity of anti-HS mAb, IB4, MAL-1 and sWGA to bind the glycocalyx of these vessels whilst α-2,6-linked sialic acid residues (SNA ligand) could not be detected (**Figures 1B,C**). Interestingly, hyaluronan was minimally associated with lymphatic glycocalyx of naïve LVs (**Figures 1B,C**) but strongly expressed by interstitial cells morphologically resembling to macrophages or dendritic cells (**Supplementary Figure 2**). Of note, the deposition of those glycocalyx moieties was neither associated specific morphological structures of initial lymphatic ECs nor with the low expression regions of basement membrane of LVs (28). Further analysis of our images, however, demonstrated that the intensity of fluorescence of anti-HS Ab, IB4, and sWGA (but not MAL-1) was inversely proportional to the vessel size (**Figure 1D**);

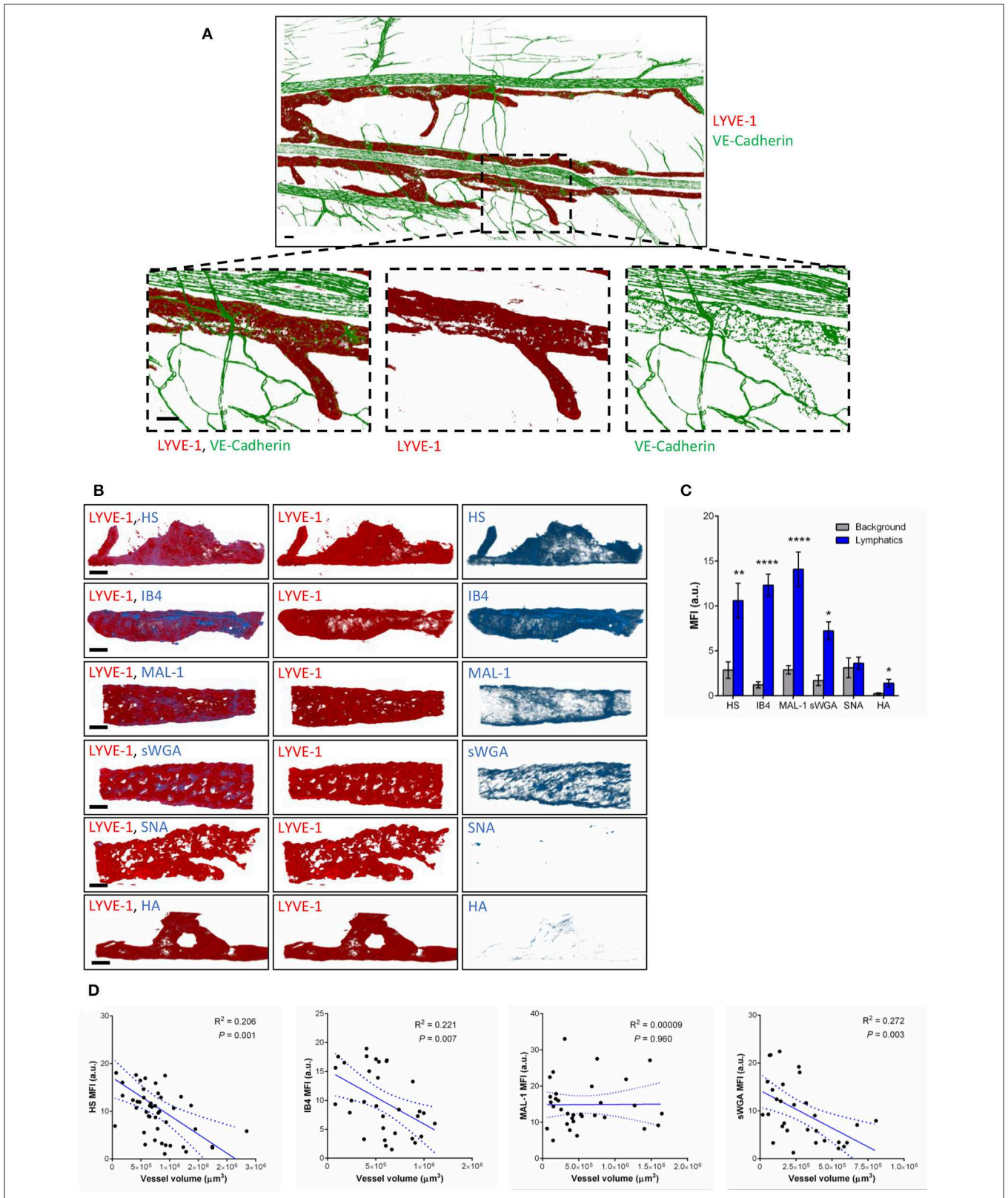

FIGURE 1 | Molecular composition of the glycocalyx on initial lymphatics of mouse cremaster muscles. **(A)** Representative 3D-reconstructed confocal tiled images showing the extent of the lymphatic vasculature (LYVE-1, red) in the cremaster muscles. Bottom panels are magnified images of a region within the tissue (dotted box)

(Continued)

FIGURE 1 | demonstrating the discontinuous expression of VE-Cadherin junctions (green) in LVs as compared to blood vessels. This lymphatic organization of junctions is characteristic of lymphatic endothelial cells from initial lymphatic capillaries. **(B)** Representative 3D-reconstructed confocal images of initial lymphatic vessel (LYVE-1, red) segments and their associated staining for several glycan chains. The images show that lymphatic glycocalyx contains HS (anti-HS Ab), α-D-Galactosyl moieties (IB4), sialic acid α2,3-linked (MAL-1) glycans, and N-Acetylglucosamine moieties (sWGA), whilst sialic acid α2,6-linked glycans (SNA), or hyaluronan (HA) minimally detected. **(C)** Quantification of the mean fluorescence intensity of HS, IB4, MAL-1, sWGA, SNA, HA as quantified on the lymphatic vessel using IMARIS software. **(D)** Linear relationship between the mean vessel size and the mean fluorescence intensity of multiple glycocalyx binding proteins (anti-HS Ab, IB4, MAL-1, and sWGA). Each point represents an individual vessel from cremaster muscles. Dotted curved lines in the correlation plots represent 95% confidence interval. Bar = 50 μm. Images are representative pictures from at least 8–10 vessels/animals, with at least 5 animals per group. Significant differences between lymphatic MFI and background MFI are indicated by asterisks: $^{*}P < 0.05$, $^{**}P < 0.01$, $^{****}P < 0.0001$.

suggesting that HS, α-D-galactosyl and N-acetylglucosamine moieties were more abundant on small initial capillaries than in larger vessels, whilst sialic acid levels were constant. Interestingly, similar pattern of expression of HS, α-D-galactosyl moieties, α-2,3-linked sialic acid residues and N-acetylglucosamine chains, were observed on the LVs of the mouse ear skin (**Figures 2A–C**) but also on the LVs in human breast skin tissue sections (**Figures 2D,E**). When comparing the intensity of fluorescence of the lectins binding to initial lymphatics and blood vessels (post-capillary venules) of the mouse cremaster muscles, we observed that both vasculatures were characterized by the presence of α-D-galactosyl moieties, α2,3-linked (but not α2,6-linked) sialic acids and N-acetylglucosamine chains. Of note, we noticed that IB4 had a greater affinity for the glycocalyx of blood post-capillary venules whilst MAL-1 showed a trend toward a higher binding to LVs (**Figures 3A,B**).

Collectively, our data demonstrate that *in vivo* the glycocalyx of initial lymphatic capillaries includes HS, α-D-galactosyl moieties, sialic acid α-2,3-linked glycans and, to a lesser extent N-acetylglucosamine residues in both mouse and human tissues.

The Glycocalyx of Initial Lymphatic Vessels Is Remodeled During Inflammation

Having observed the binding of the anti-HS mAb, IB4, and MAL-1, but not SNA to the lymphatic capillaries *in vivo*, we next investigated the potential regulation of LV glycocalyx during acute inflammation. For this purpose, the cremaster muscles of mice were first subjected to acute TNF-induced inflammation, a cytokine we have previously shown to induce the rapid migration of neutrophils into the tissue-associated lymphatic vessels (26). For this purpose, the cytokine was injected i.s. for 16 h prior to fluorescent staining of tissues with anti-HS Ab, anti-LYVE-1 and anti-MRP-14 mAb to visualize HS, lymphatic vasculature and neutrophils, respectively. Our data showed that TNF-stimulation induces the rapid migration of neutrophils into the tissue and the lymphatic vasculature (**Figures 4A–D)**. Of note, we did not observed preferred entry sites for neutrophils migration within LVs and with regards to glycocalyx components. However, we detected a significant decrease (∼64%) in HS expression on LVs of TNF-stimulated tissues as observed by a reduced binding of the anti-HS mAb (**Figures 4A,E)**. Similarly, we observed a reduction in staining for IB4 but not MAL-1, suggesting a decrease in galactosyl residues (∼3-fold decrease as compared to unstimulated lymphatic glycocalyx) but not sialic acid α-2,3-linked glycans following TNF-stimulation (**Figures 5A,B**). Similar results were obtained in another inflammatory model as induced by antigen sensitization (i.e., injection of an emulsion of ovalbumin in Complete Freund's Adjuvant, CFA + Ag) (**Figures 5A,B**). This remodeling of LV glycocalyx was associated with the recruitment of neutrophils into the interstitium and the tissue-associated lymphatic vessels in both inflammatory models (**Figures 5C,D**). Finally, to confirm that the LV glycocalyx remodeling was not restricted to inflamed cremaster muscles, similar analyses were performed in the mouse ear dorsal skin (**Figures 5E–H**). Our data clearly demonstrate that ear skin LVs also exhibit a cleavage of α-D-galactosyl moieties but not sialic acids following TNF-stimulation; a response associated with neutrophil infiltration into the tissue and migration into LVs (**Figures 5E–H**).

Collectively, these results provide evidence for moiety-specific remodeling of the LV glycocalyx in two distinct vascular beds, a response that is associated with neutrophil trafficking into inflamed tissues and LVs.

Neutrophils Do Not Contribute to the Remodeling of the LEC Glycocalyx of Initial Lymphatic Vessels

Having associated the remodeling of the glycocalyx of tissue-associated initial lymphatic capillaries with extensive neutrophil recruitment during acute inflammation, we then investigated the contribution of these leukocytes to this remodeling. Neutrophils from the blood circulation are known to secrete proteases (e.g., elastase) (29) and release reactive oxygen species (ROS) (30), that can cleave or modify glycoproteins at the surface of BECs during their recruitment (i.e., ICAM-1), thus contributing to the modification of the composition of the blood vascular glycocalyx. To directly assess a similar role of neutrophils during their entry into LVs, we performed antibody-based depletion of neutrophils prior to the induction of TNF-induced inflammation of the mouse cremaster muscles and analysis of the response (i.e., HS and IB4 expression profile, and neutrophil migration) by confocal microscopy. Antibody-based depletion efficiency was first confirmed by the absence of detection of neutrophils in the blood circulation (**Supplementary Figure 3**) and in the inflamed tissues and their associated LVs as compared to animals treated with an isotype-matched control Ab (**Figures 6A,B**). Interestingly, however, neutrophil-depleted animals showed a similar level of LV glycocalyx remodeling (reduced detection of both for α-D-galactosyl residues and HS) following TNF-stimulation that of non-depleted animals (**Figures 6C,D**). These observations suggest that neutrophils are not responsible for the shedding of HS and Galactosyl

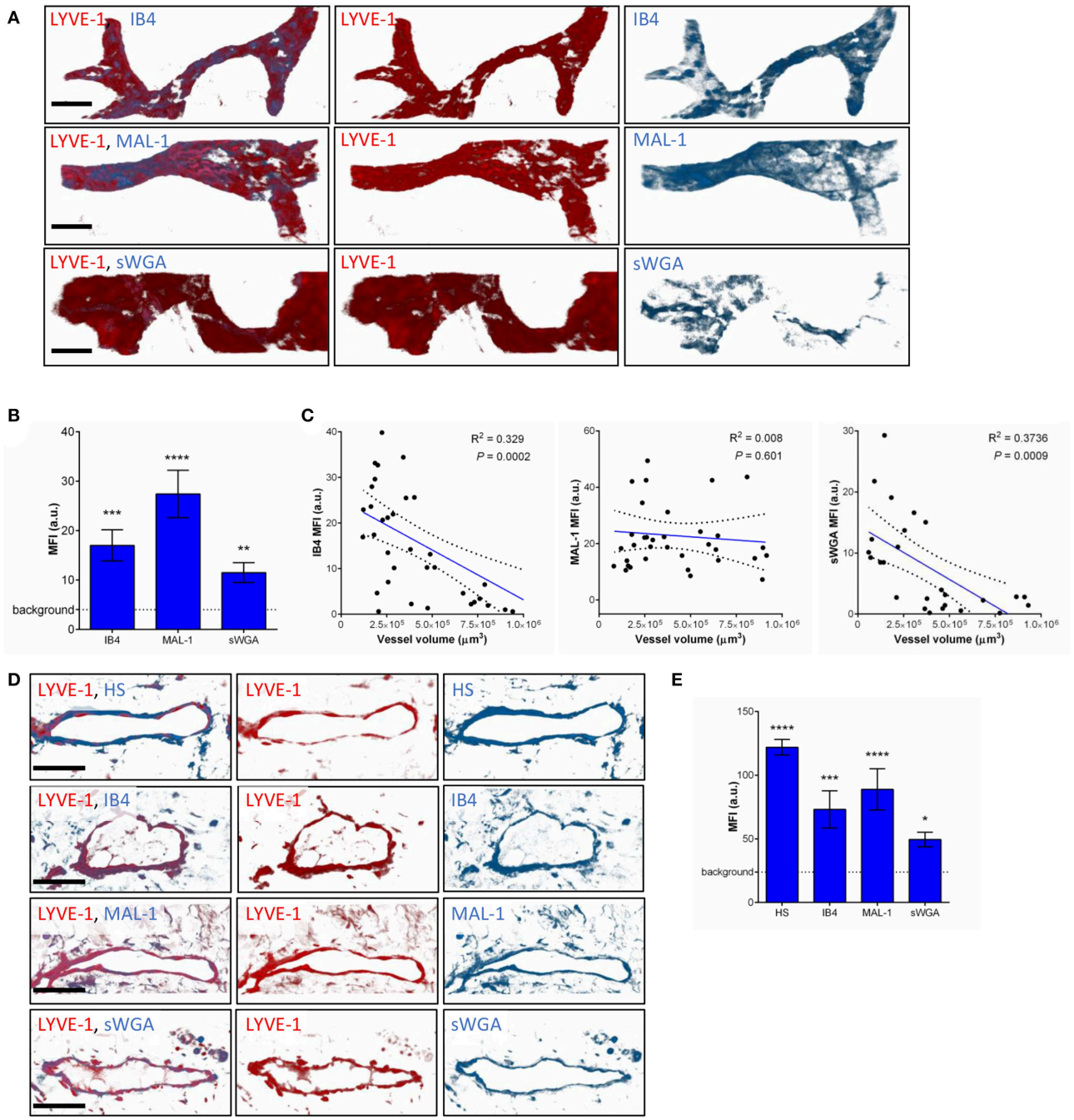

FIGURE 2 | Molecular composition of the glycocalyx on initial lymphatics of mouse and human skin. **(A)** The pictures are representative 3D-reconstructed confocal images of an initial lymphatic vessel (LYVE-1, red) segment from whole-mount fixed ears of naïve mice and fluorescently labeled with IB4, MAL-1 and sWGA lectins to visualize α-D-Galactosyl, sialic acid α2,3-linked and N-Acetylglucosamine glycan moieties, respectively. **(B)** Quantification of the mean fluorescence intensity of IB4, MAL-1 and sWGA as quantified on initial lymphatic vessels of mouse ear skins. **(C)** The graphs show the linear relationship between the mean vessel size and the mean fluorescence intensity (MFI) of individual lectins (IB4, MAL-1, and sWGA). Each point represents an individual vessel from cremaster muscles. Dotted curved lines in the correlation plots represent 95% confidence interval. **(D)** The pictures are representative 3D-reconstructed confocal images of a lymphatic vessel (LYVE-1, red) from human breast skin sections and fluorescently labeled with anti-HS Ab, IB4, MAL-1, and sWGA lectins to visualize HS, α-D-Galactosyl, sialic acid α2,3-linked and N-glucosamine glycan moieties, respectively. **(E)** Quantification of the mean fluorescence intensity (MFI) of anti-HS Ab, IB4, MAL-1, and sWGA as quantified on the lymphatic vessels of human skin samples. Bar = 50 µm. Images are representative pictures from at least 8–10 vessels/sample, with at least 5 animals/4 human samples per group. Significant differences between lymphatic vessel MFI and background MFI are indicated by asterisks: $^{*}P < 0.05$, $^{**}P < 0.01$, $^{***}P < 0.001$, $^{****}P < 0.0001$.

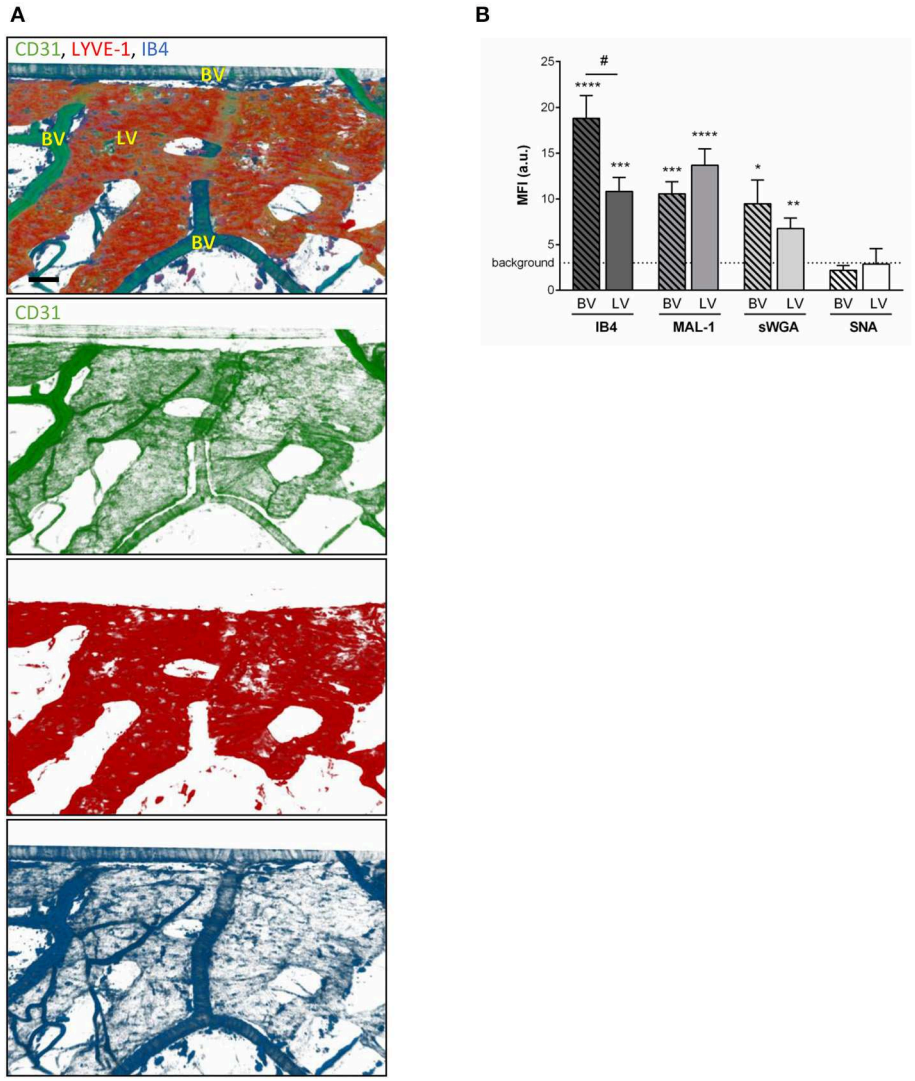

FIGURE 3 | Comparison of the glycocalyx composition between initial lymphatics and blood vessels. Cremaster muscles from WT mice were whole-mount immunostained for the visualization of endothelial cells (anti-CD31 Ab, green), lymphatic vessels (anti-LYVE-1 Ab, red) and glycosylic chains from glycocalyx (lectin, blue) via i.s. injection of the antibodies/lectin for 2 h prior to being observed by confocal microscopy. **(A)** Representative 3D-reconstructed confocal images of a region of the tissue showing that IB4 binds to the blood vessels (BV) and lymphatics (LVs). (Bar = 100 um). **(B)** Quantification of the mean fluorescence intensity (MFI) for IB4, MAL-1, sWGA, and SNA binding to the surface of initial lymphatics and blood vessels as detailed in the Material and Methods. Data are expressed as mean ± SEM from at least 8–10 vessels/animal, with at least 5 animals per group. Significant differences between BV/LV MFI and background MFI are indicated by asterisks: $^{*}P < 0.05$, $^{**}P < 0.01$, $^{***}P < 0.001$, $^{****}P < 0.001$; and between BV and LV groups by hash symbol: $^{\#}P < 0.05$.

moieties present lymphatic glycocalyx during TNF-induced inflammation *in vivo*.

Endogenous Heparanase Contributes to the Remodeling of Initial Lymphatic Glycocalyx

Since tissue-infiltrated neutrophils did not contribute to the remodeling of lymphatic glycocalyx *in vivo*, we next sought to investigate the role of endogenous glycosidases in glycocalyx degradation. Interestingly, a study by Schmidt et al. has demonstrated that the HS-specific endoglycosidase, Heparanase, is responsible for the cleavage of the glycan layer on the luminal side of blood capillaries in the lung during sepsis (16). To address the hypothesis that this enzyme may also be involved in the remodeling of the initial lymphatic glycocalyx during an acute inflammatory response, we first investigated its cellular source. For this purpose, TNF-stimulated cremaster muscles were immunostained with antibodies against Heparanase I (or with an isotype control antibody, **Supplementary Figure 4**), lymphatic (LYVE-1) and blood ($CD31^{high}$) vasculatures and neutrophils (MRP14) or macrophages (F4/80) prior to analysis by confocal microscopy. Heparanase I is an endo-β-glucuronidase implicated in the degradation of HS chains and known to be expressed by

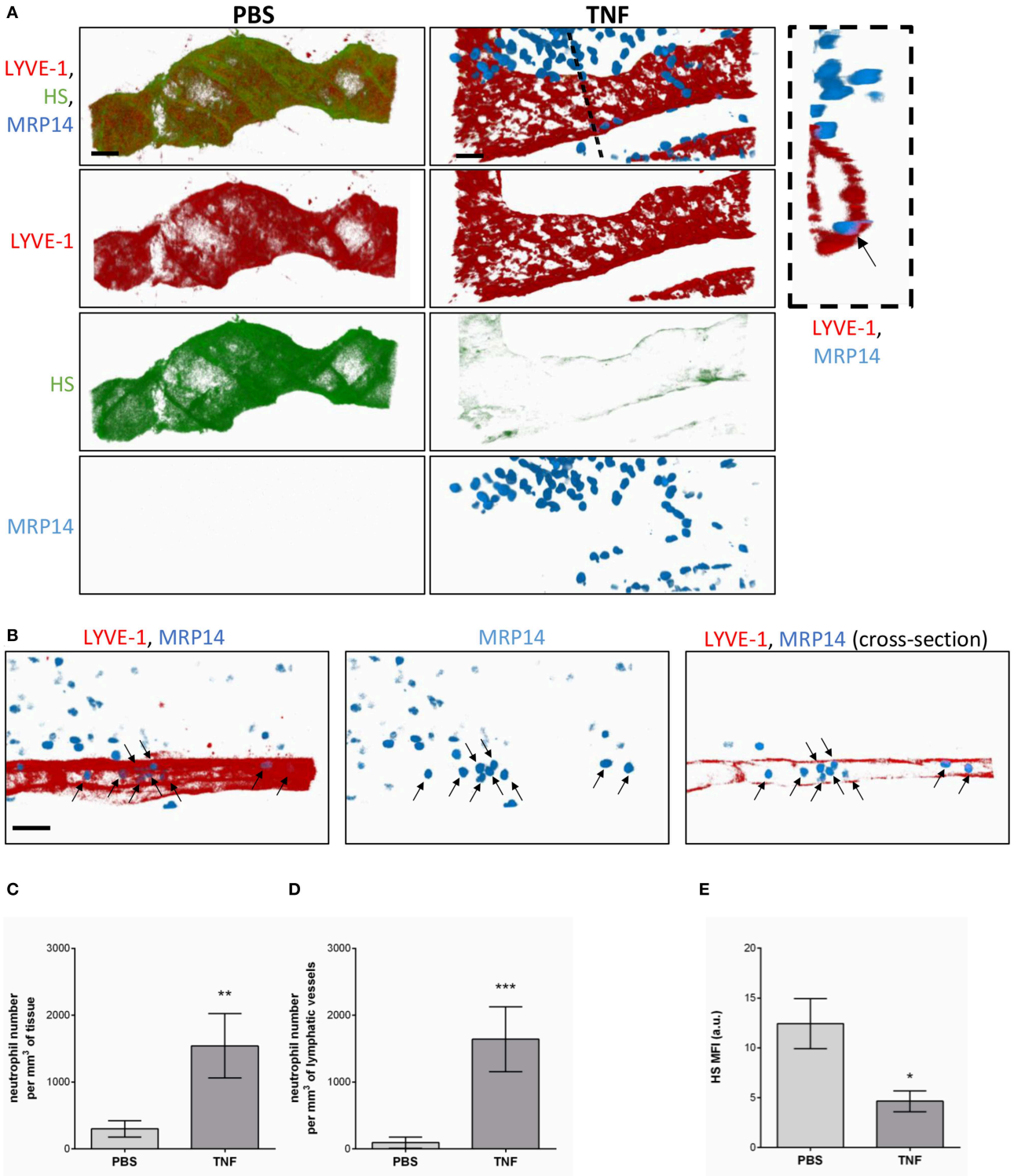

FIGURE 4 | Regulation of Heparan Sulfate expression in the glycocalyx of initial lymphatics and neutrophil migration responses upon inflammation. WT mice were intrascrotally (i.s.) injected with TNF (300 ng) and the inflammatory response was allowed to develop for 16 h. Two hours before the end of the inflammation period, mice were further injected i.s with anti-HS (green) and anti-LYVE-1 (red) Abs to visualize the heparan sulfate and lymphatic vasculature, respectively. The cremaster muscles were then harvested, fixed, permeabilized, and immunostained with an anti-MRP14 mAb to visualize the neutrophils (blue). Unstimulated controls received an i.s injection of PBS. **(A)** Representative 3D-reconstructed confocal images of an initial lymphatic vessel from PBS- (left panels) or TNF- (right panels) stimulated tissues.

(Continued)

FIGURE 4 | The image on the far right is a transversal cross-section view of the TNF-stimulated tissue image along the dotted line and showing the entry of a neutrophil (arrow) within the lymphatic vessel. **(B)** Representative 3D-reconstructed confocal images of an initial lymphatic vessel from a TNF-stimulated tissues. The right hand side panel is a longitudinal cross-section of the lymphatic capillary demonstrating the presence of numerous neutrophils (arrows) within the lymphatic vessel. **(C)** Quantification of the number of neutrophils that have infiltrated the interstitial tissues (per mm^3 of tissue). **(D)** Quantification of the number of neutrophils present within lymphatic vessels (per mm^3 of lymphatic vessel). **(E)** Quantification of the Mean Fluorescence Intensity (MFI) of HS expression on lymphatic vessels following PBS and TNF stimulation. Results are from $n = 8$–12 vessels per mouse with 3–6 animals per group. Statistically significant differences between isotype control PBS and TNF-treated groups are indicated by asterisks: $^{*}P < 0.05$, $^{**}P < 0.01$, $^{***}P < 0.001$. Bars = 50 μm.

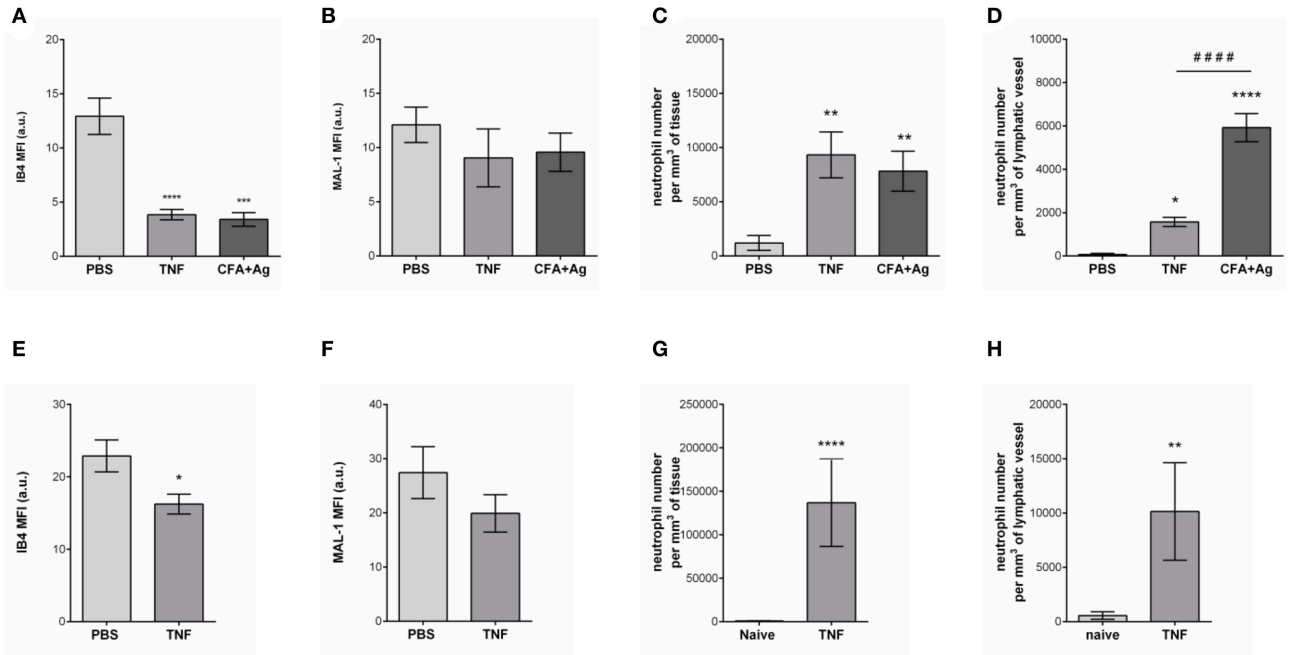

FIGURE 5 | Selective cleavage of initial lymphatic vessels glycocalyx during acute inflammation. The cremaster muscles of mice were stimulated following intrascrotal (i.s.) injection of TNF (300 ng) or CFA + Ag (200 μg). Control mice were injected with PBS. For 2 h before the end of the inflammation period, mice were further injected i.s. with IB4 or MAL-1 and anti-LYVE-1 Abs to reveal glycan chains and lymphatic vessels, respectively. At the end of the inflammation period, the cremaster muscles were harvested, fixed, and immunostained for neutrophils (anti-MRP14 mAb) prior to the visualization and quantification of the inflammatory response by confocal microscopy. For ear stimulation, the dorsal skin of mouse ears were injected with TNF (300 ng); and 16 h later, ears were harvested, fixed and stained whole-mount with fluorescently-labeled IB4 or MAL-1; anti-LYVE-1 and anti-MRP14 mAbs to reveal glycan chains, lymphatic vessels and neutrophils, respectively, prior to the visualization and quantification of the inflammatory response by confocal microscopy. Control mice were injected with PBS. The mean fluorescence intensity (MFI) for IB4 or MAL-1 binding to the lymphatic glycocalyx was quantified by creating an isosurface on lymphatic vessel channel (LYVE-1), excluding the signal from MRP14 channel using IMARIS software. **(A)** Mean fluorescence intensity (MFI) for IB4 staining on cremaster lymphatic vessels. **(B)** Mean fluorescence intensity (MFI) of MAL-1 staining on cremaster lymphatic vessels. **(C)** Number of neutrophils into the cremaster interstitium. **(D)** Number of neutrophils into the cremaster initial lymphatic vessels. **(E)** Mean fluorescence intensity (MFI) for IB4 staining on ear skin lymphatic vessels. **(F)** Mean fluorescence intensity (MFI) of MAL-1 staining on ear skin lymphatic vessels. **(G)** Number of neutrophils in the ear skin interstitium. **(H)** Number of neutrophils within the ear skin initial lymphatic vessels. Results are from $n = 4$–6 vessels per tissue with at least 5 animals per group. Statistically significant differences between stimulated and unstimulated treatment groups are indicated by: $^{*}P < 0.05$, $^{**}P < 0.01$, $^{***}P < 0.001$, $^{****}P < 0.0001$. Statistically significant differences between TNF-stimulated and CFA + Ag-stimulated tissues are indicated by: $^{\#\#\#\#}P < 0.0001$.

leukocytes, platelets and blood endothelial cells (31–33). In our *in vivo* inflammatory model, confocal image analyses showed that this enzyme was not associated with LVs post-TNF-stimulation but with interstitial cells (**Figure 7A**). In fact, Heparanase I was strongly detected in macrophages whilst the tissue-infiltrated neutrophils did not exhibit a positive immunostaining for this enzyme (**Figures 7B,C**). Similar pattern of Heparanase I expression was observed at an early (8 h) time-point of the inflammatory reaction (Data not shown).

To get further mechanistic insights into the role of Heparanase into the remodeling LV HS during inflammation, we tested the effect of local injection of a non-anticoagulant heparanase inhibitor N-desulfated/re-N-acetylated heparin (NAH). Briefly, TNF-stimulated cremaster muscles were treated locally (i.s. injection) with NAH, or its vehicle, 3 h post-administration of TNF. Two hours before the end of the inflammatory period (i.e., 16 h), the tissues were fluorescently immunostained with anti-LYVE-1 and anti-HS Abs to visualize the lymphatic vasculature and HS, respectively. In addition, at the end of the *in vivo* test period, tissues were harvested, fixed and immunostained with an anti-MRP14 Ab to enable quantification of neutrophil migration responses. In line with our previous results (**Figure 4**), vehicle-treated tissues exhibited a decrease in anti-HS Ab immunostaining on initial LVs upon

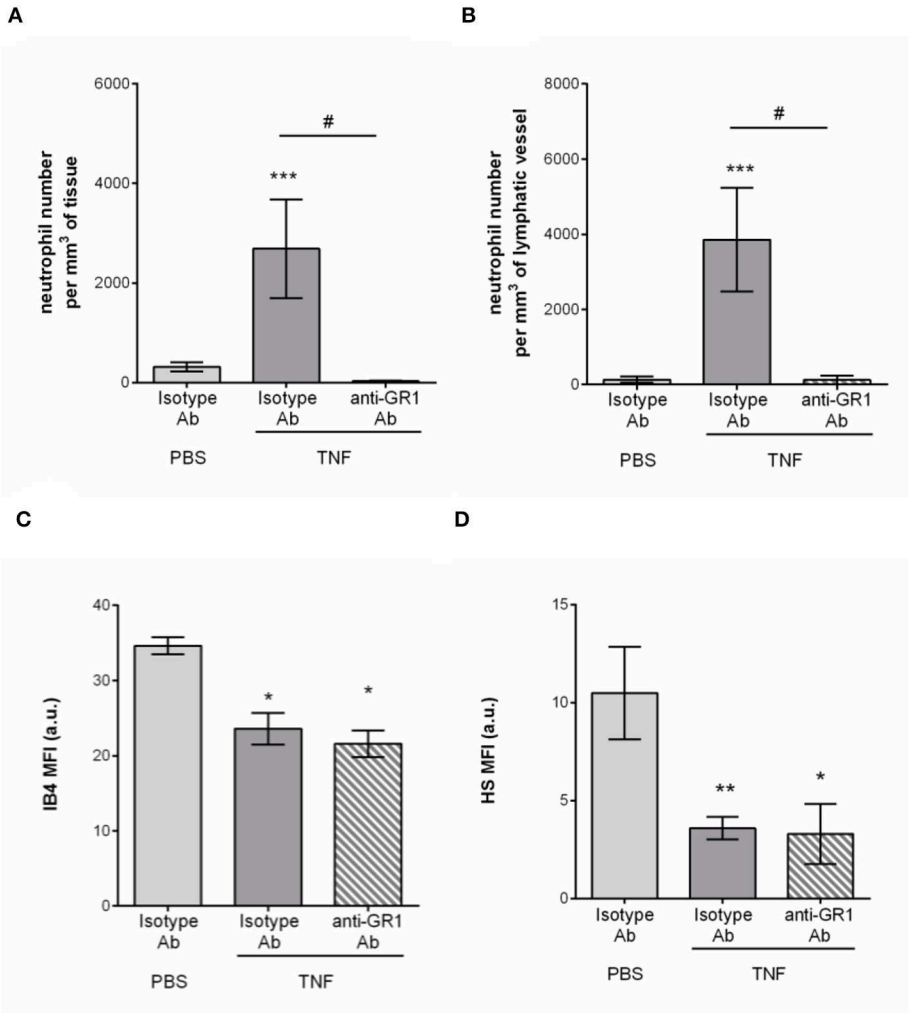

FIGURE 6 | Neutrophil-independent remodeling of initial lymphatic glycocalyx upon TNF-induced inflammation. Circulating neutrophils were depleted via a daily intraperitoneal (i.p.) injection of the anti-GR1 depleting antibody (25 μg) for 3 days prior to the induction of the inflammatory response. Inflammation of the cremaster muscles of WT mice was induced by the intrascrotal (i.s.) injection of TNF (300 ng) for 16 h. Non-depleted control mice received i.p. injections of an isotype control antibody; and unstimulated animals were injected i.s. with PBS. Two hours before the end of the inflammation period, mice were i.s injected with fluorescently labeled IB4/anti-HS Ab in conjunction with a non-blocking anti-LYVE-1 Ab to visualize the glycocalyx moieties and the lymphatic vessels, respectively. At the end of the inflammatory period, mice were sacrificed and their cremaster muscles harvested, fixed, and fluorescently-labeled with an anti-MRP14 Ab to detect the neutrophils. Neutrophil migration responses were analyzed in 3D by confocal microscopy. Lymphatic glycocalyx mean fluorescence intensity (MFI) was quantified with an isosurface generated on the lymphatic vessels (LYVE-1$^+$ vessels) using IMARIS software. **(A)** Number of neutrophils migrated into the tissue. **(B)** Number of neutrophils within the cremaster initial lymphatic vessels. **(C)** Mean fluorescence intensity (MFI) of IB4 staining on lymphatic vessels. **(D)** Mean fluorescence intensity (MFI) of anti-HS Ab staining on lymphatic vessels. Results are from at least 3 animals per group. Statistically significant differences between stimulated and unstimulated treatment groups are indicated by: $^*P < 0.05$, $^{**}P < 0.05$, $^{***}P < 0.001$. Statistically significant differences between neutrophil-depleted and non-depleted groups are indicated by: $^{\#}P < 0.01$.

TNF-stimulation (**Figures 8A,B**). Interestingly, inflamed tissues treated with NAH showed a similar deposition of HS as found in un-stimulated cremaster muscles (**Figures 8A,B**), confirming the role of endogenous heparanase for the remodeling of LEC glycocalyx during TNF-induced inflammation *in vivo*. In contrast, however, local administration of NAH had no significant impact on neutrophil migration into tissues and tissue-associated LVs as compared to vehicle-treated animals (**Figures 8C,D**). Furthermore, NAH-treatment did not inhibit neutrophil trafficking to the cremaster draining lymph nodes (**Figure 8E**). Collectively, these results suggest that local inhibition of heparanase-dependent shedding of HS on initial LVs does not affect the capacity of neutrophils to infiltrate the tissue-associated lymphatic vasculature.

Blockade of Initial LV Glycocalyx Shedding Prevents Local Fluid Drainage of TNF-Stimulated Cremaster Muscles

Whilst innate immune cell trafficking is an important aspect of lymphatic biology, a key function of tissue-associated initial

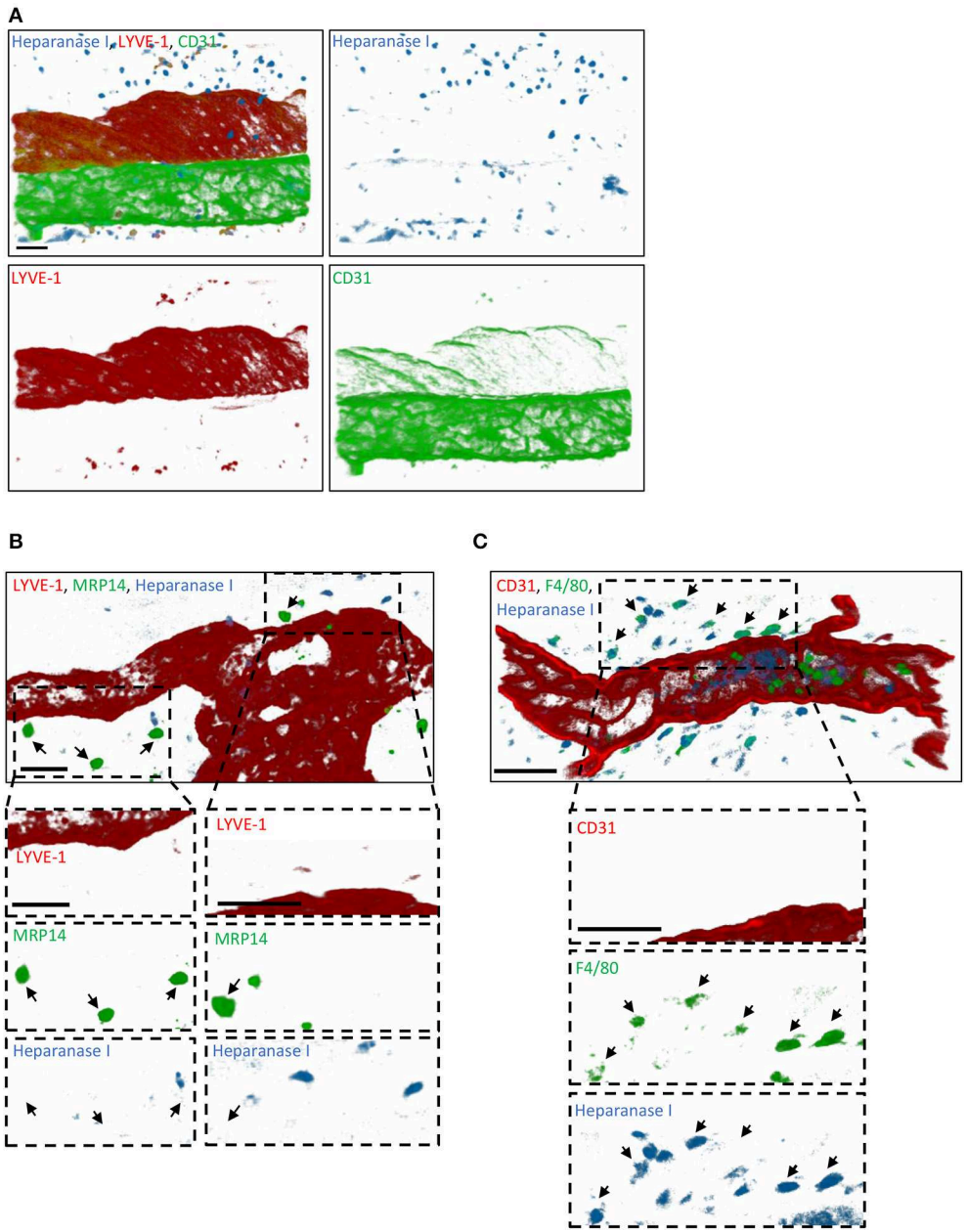

FIGURE 7 | Cellular source of Heparanase I in inflamed cremaster muscles. Mouse cremaster muscles were stimulated with TNF (i.s. 300 ng) followed by whole-mount immunostaining of the tissues with fluorescently labeled antibodies to reveal the HS-degrading enzyme Heparanase I, the lymphatic and/or blood vasculatures, and neutrophils/macrophages prior to the visualization of the samples by confocal microscopy. **(A)** Representative 3D-reconstructed confocal images of a region of the cremaster muscle showing that Heparanase I (blue) is not associated with cremaster lymphatic (LYVE-1, red) or blood (CD31, green) vasculatures but with cells present within the interstitial tissue. **(B)** Representative 3D-reconstructed confocal images of a region of the cremaster immunostained for lymphatic vessels (LYVE-1, red), neutrophils (MRP14, green) and Heparanase I (blue). Two magnified regions (dotted box) within the main image are provided in the bottom panels demonstrating that Heparanase I is neither associated with lymphatic endothelial cells nor neutrophils (arrows). **(C)** Representative 3D-reconstructed confocal images of a region of the cremaster immunostained for endothelial cells (CD31, red), macrophages (F4/80, green), and Heparanase I (blue). A magnified region (dotted box) within the main image are provided in the bottom panels demonstrating that Heparanase I is strongly associated with macrophages (arrows). Bar = 40 μm. Images are representative pictures from at least 5 vessels/animals, with at least 4 animals.

lymphatic capillaries is to transport fluids and macromolecules (including antigens) out of the interstitium into dLNs (for immune surveillance) and back into the blood circulation. Tissue drainage by LVs naturally occurs at steady state but also during inflammatory responses; but can be impaired during pathological conditions, such as aging (20). Nevertheless, the

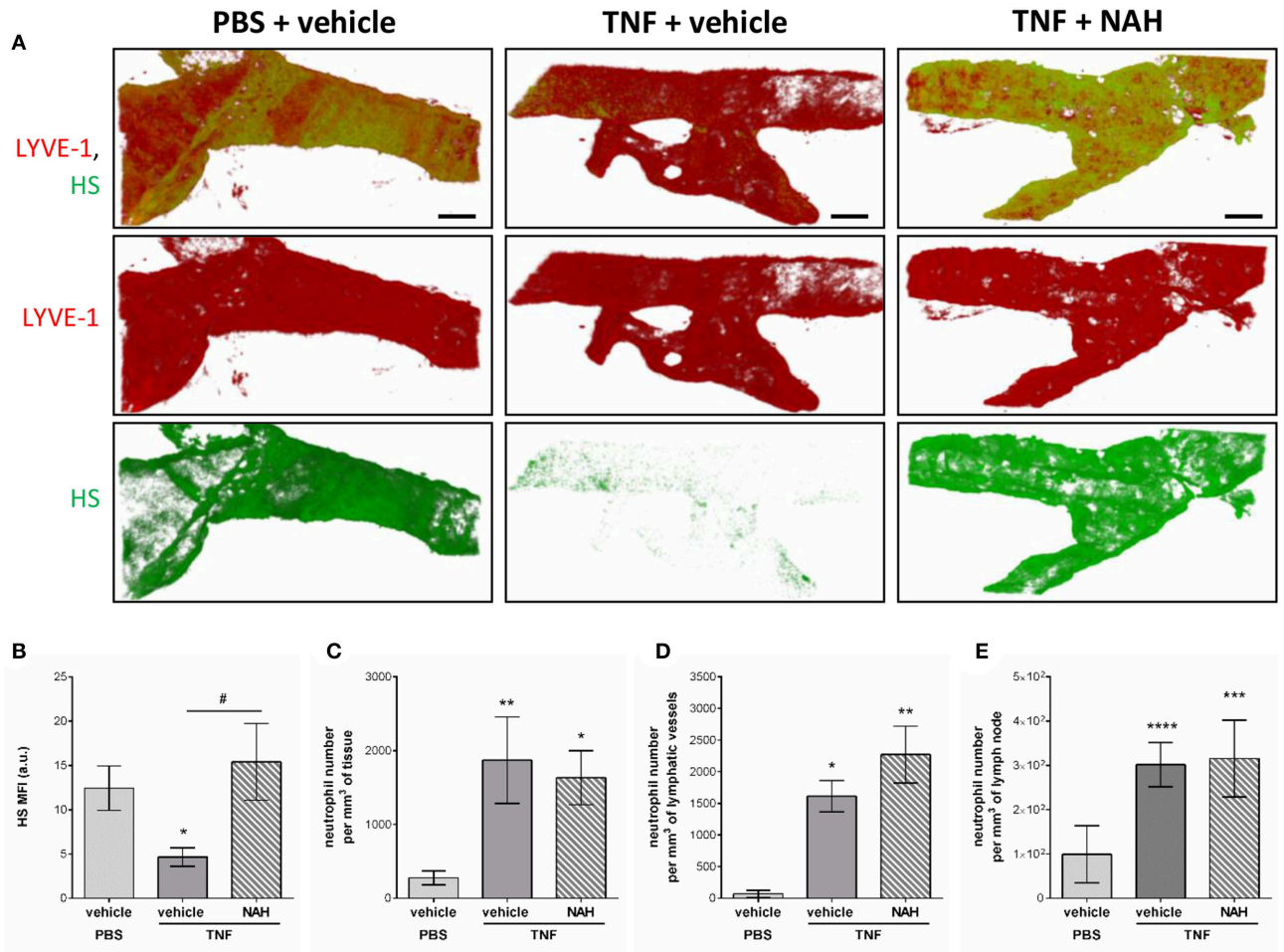

FIGURE 8 | Effect of a non-anticoagulant heparanase inhibitor (NAH) on TNF-induced HS remodeling of the lymphatic glycocalyx and neutrophil migration responses. TNF (300 ng) or PBS (as control) were administrated intrascrotally (i.s.). Three hours later, mice received an i.s. injection of 50 μg of non-anticoagulant heparanase inhibitor N-desulfated/re-N-acetylated heparin (NAH) or vehicle. At 14 h post-TNF-stimulation, mice were further i.s injected with anti-HS (green) and anti-LYVE-1 (red) mAbs to label *in vivo* and visualize the heparan sulfate layer and lymphatic vasculature, respectively. Sixteen hours post-TNF-stimulation, animals were sacrificed, their cremaster tissues and draining (i.e. inguinal) lymph nodes harvested and prepared for confocal microscopy to measure HS remodeling on tissue-associated initial lymphatic vessels and neutrophil migration responses. **(A)** The images show representative 3D-reconstructed confocal images of an initial lymphatic vessel from a PBS (left hand side panels) or TNF (middle and right-hand side panels)-stimulated tissues with or without NAH-pre-treatment ($N = 3$–6 mice per group; Bars = 50 μm). **(B)** Quantification of the Mean Fluorescence Intensity (MFI) of HS expression on initial lymphatic vessels of the cremaster muscles ($N = 3$–6 mice per group). **(C)** Quantification of the number of neutrophils present into the tissue's interstitium (per mm^3 of tissue) ($N = 6$–14 mice per group). **(D)** Quantification of the number of neutrophils present within initial lymphatic vessels (per mm^3 of lymphatic vessel) ($N = 5$–10 mice per group). **(E)** Quantification of the number of neutrophils present in the draining lymph nodes of the cremaster muscles (per mm^3 of lymph node) ($N = 3$ mice per group with two dLNs per animals). Statistical significance between PBS and TNF stimulated groups are indicated by asterisks: $^*P < 0.05$, $^{**}P < 0.01$, $^{***}P < 0.001$, $^{****}P < 0.0001$. Statistical significance between vehicle and NAH-treated groups are indicated by hash symbol: $^{\#}P < 0.05$.

current literature lacks convincing *in vivo* evidence for a role of lymphatic glycocalyx in this phenomenon in the context of acute inflammation. The aim of this last set of experiments was thus to determine how the remodeling of the lymphatic glycocalyx influences the draining capabilities of these vessels. For this purpose, we investigated the draining function of initial lymphatic capillaries of mouse cremaster muscles by injecting locally (i.s.) an isotonic solution of Evans Blue (EB) before measuring the quantity of the dye in cremaster muscles, draining and non-draining LNs as well as in the plasma of animals treated locally with the heparanase inhibitor NAH. Lymphatic drainage of EB was first confirmed by direct visualization of the dye in the lymph nodes and lymphatic venules (i.e., inguinal) draining the cremaster muscles (**Supplementary Figure 5A**). These observations were supported by the significant reduction of EB levels (∼30%) in TNF-stimulated cremaster muscles as compared to non-inflamed tissues (**Figure 9A**). Interestingly, whilst in non-inflamed conditions NAH did not modify EB drainage (**Supplementary Figure 5B**), treatment of TNF-stimulated tissues with this inhibitor restored EB levels to that seen in non-inflamed control tissues (**Figure 9A**). Furthermore, whilst TNF stimulation led to an increase in EB detection

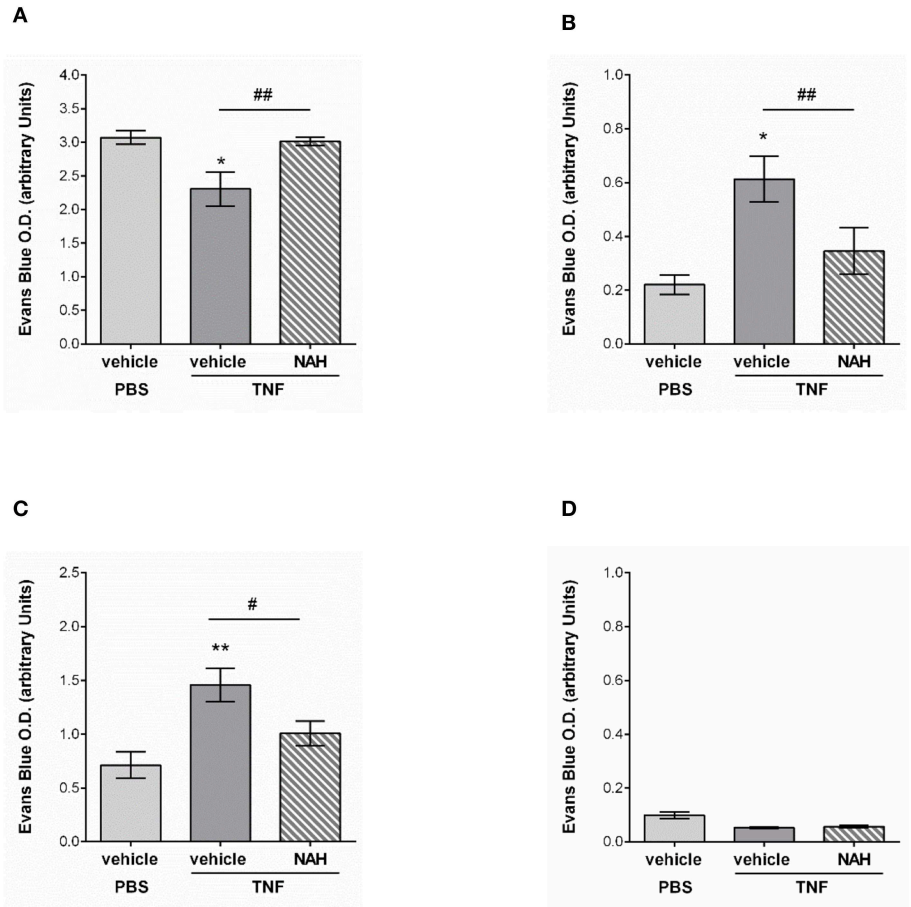

FIGURE 9 | Effect of a non-anticoagulant heparanase inhibitor (NAH) on lymphatic drainage in TNF-stimulated tissues. TNF (300 ng) or PBS (as control) were administrated intrascrotally. Three hours later, mice received an i.s. injection of 50 μg of non-anticoagulant heparanase inhibitor N-desulfated/re-N-acetylated heparin (NAH) or vehicle. Twenty min before the end of the inflammatory period (i.e., 16 h), mice received an i.s. injection of 1% Evans Blue. Animals were then sacrificed, their plasma, cremaster tissues, draining, and non-draining lymph nodes were collected and prepared for spectrophotometric analysis of Evans Blue content. **(A)** Quantification of the Evans Blue content in the mouse cremaster ($N = 6$–10 mice per group). **(B)** Quantification of the Evans Blue content in draining lymph (i.e., inguinal) nodes of the cremaster muscles ($N = 6$–7 mice per group). **(C)** Quantification of the Evans Blue content in mouse plasma samples ($N = 6$–10 mice per group). **(D)** Quantification of the Evans Blue content in non-draining (i.e., brachial) lymph nodes ($N = 4$ mice per group). Statistical significance between PBS and TNF stimulated groups are indicated by asterisks: $^{*}P < 0.05$, $^{**}P < 0.01$. Statistical significance between vehicle and NAH-treated groups are indicated by hash symbol: $^{\#}P < 0.05$, $^{\#\#}P<0.01$.

in dLNs (∼180% increase) and plasma (∼100% increase), as compared to unstimulated tissues, these responses were significantly suppressed in NAH-treated mice (**Figures 9B,C**). Of note, no EB could be detected in non-draining (i.e., brachial) LNs (**Figure 9D**), suggesting that our responses is mainly due to lymphatic drainage rather than potential diffusion of the locally-injected dye into blood capillaries. Furthermore, to exclude the possibility that blood vascular hyper-permeability may increase interstitial pressure (and thus, lymphatic drainage) within the tissues during inflammation, we sought to investigate the extent of blood vascular leakage at time of glycocalyx remodeling and lymphatic drainage using the Miles assay. Briefly, mice were injected with TNF (or PBS as control) prior to be treated locally with the heparanase inhibitor NAH (or vehicle control) 3 h later. Two hours before the end of the inflammatory period (i.e., 16 h), animals received an intravenous injection of 0.5% of Evans blue. The quantity of dye present in the cremaster muscles was then assessed by spectrophotometry. Our data show that of the accumulation of Evans blue in tissues was similar between unstimulated and TNF-stimulated groups (**Supplementary Figure 6**). Furthermore, NAH treatment did not affect vascular permeability response at this time point. These observations are supported by a previous study from our group demonstrating that *in vivo*, TNF promote a rapid but transient blood vascular leakage during the first 30 min post-stimulation (27). Together, these results suggest that the enhanced lymphatic drainage response that we observed during glycocalyx remodeling upon TNF-inflammation occurred independently of blood vascular leakage at the time-point analyzed.

Collectively, these results suggest that protecting the lymphatic glycocalyx HS from heparanase-induced shedding during TNF-induced inflammation reduces the capacity of initial lymphatic vessels to drain interstitial fluids toward draining lymph nodes and back into the blood circulation.

DISCUSSION

The lymphatic vasculature is the second circulatory system of high vertebrates and is formed by a unidirectional network of vessels and dLNs that starts in tissues with blunt-ended initial lymphatic capillaries. The main function of these specialized vessels is to remove interstitial fluids and macromolecules to counteract tissue edema and as such are essential for tissue homeostasis (19). Initial lymphatic capillaries also play a key role in immune surveillance by allowing not only the rapid drainage of antigens and migration of professional antigen-presenting cells, such as DCs and macrophages but also neutrophils toward the dLNs in order to initiate adaptive immune responses (26, 34). Initial lymphatic capillaries are composed of a monolayer of endothelial cells (LECs) that share some molecular similarities with blood endothelial cells (BECs) but also a few architectural and phenotypic differences (19). Furthermore, whilst both BECs and LECs contain a carbohydrate-rich glycocalyx layer on their cell surface, the characteristics of the glycocalyx of initial lymphatic vessels *in vivo* and its role in acute inflammation is unknown.

In an effort to gain insight into the characteristics of the composition of glycan residues forming the glycocalyx of initial lymphatic vessels, an antibody targeting the most abundant glycan moiety of endothelial glycocalyx, HS, alongside a panel of 4 lectins (IB4, MAL-1, SNA and sWGA) were used *in vivo* in the mouse cremaster muscle. Lectins are the most commonly employed glycan-binding glycoproteins used to label the blood vascular glycocalyx, especially IB4 that binds α-D-galactosyl moieties present at the luminal surface of microvascular endothelial cells (35). In contrast, lectins have not been systematically used to investigate the LEC glycocalyx *in vivo*. In our study, we demonstrate that IB4, MAL-1 and to a lesser extent sWGA, can successfully bind lymphatic vessels. Similar pattern of expression of those glycocalyx moieties was observed to be also present in lymphatic vessels from the mouse murine ear skin and in human breast skin samples. Interestingly, we noted a higher staining for IB4 on blood vessels than on initial lymphatic capillaries of mouse cremaster muscles. This difference in the binding level of IB4 on these two distinct vasculatures could be attributed to the fact that blood vessel walls are surrounded by smooth muscle cells and pericytes known to exhibit IB4-binding carbohydrate residues in their own glycocalyx (35) that would be also revealed by the local delivery of the lectin employed in our study. In contrast, initial lymphatic vessels are usually devoid of perivascular cells and are only composed of a monolayer of LECs surrounded by a thin and perforated basement membrane (28), hence the overall lower detection of α-D-galactosyl moieties on initial lymphatics as compared to blood vessels. In contrast, MAL-1 but not SNA, both of which have been used in a plethora of studies to detect different sialic acid-linked glycans (36–39) was found to bind the LEC glycocalyx to the same extent as BEC glycocalyx. MAL-1 expression on lymphatic glycocalyx could be related to the expression of lymphatic glycoproteins, such as of LYVE-1 and podoplanin by LECs, molecules exhibiting high levels of α2,3-linked sialic acid moieties (40, 41). In support of our findings, a study by Nightingale et al. showed that the level of MAL-1 binding to the surface of human dermal LECs *in vitro* was higher than of SNA (40), whilst being similar for other cell types (42). Altogether, these results suggest that the glycocalyx of LECs exhibit more α2,3-sialic acid linked moieties (i.e., MAL-1 ligands) than α2,6-sialic acid linked glycans (i.e., SNA ligand).

We further characterized the glycocalyx of tissue lymphatic capillaries by revealing the presence of HS on those vessels. HS proteoglycans represent the majority of all proteoglycans expressed by BECs, and as such HS is the major constituent of the blood vascular glycocalyx, representing more than 50% of the vascular GAGs present on those vessels (8). GAGs have the capacity to bind and immobilize chemokines for leukocyte recruitment to blood vessels. This is particularly the case for CXCL1 and CXCL2, two potent neutrophil chemoattractants (11, 43). HS was also shown to protect endothelial cells from oxidative stress damage by quenching reactive oxygen species (ROS) through the binding of superoxide dismutase enzyme to GAG HS and to maintain nitric oxide bioactivity (44). In the lymphatic system, HS has been implicated in the formation of a CCL21 gradient within the interstitium in the vicinity of the LVs in order to direct dermal DCs toward LVs, as indirectly demonstrated by the inhibitory effect of a bacterial heparinase on CCL21 gradient formation and DC recruitment to LVs (45). Similarly, transgenic mice exhibiting impairment in HS synthesis showed a defect in DC and naïve T-cell trafficking into the lymph nodes via high endothelial venules (13). In this context, we have recently demonstrated that during TNF-induced inflammation and antigen challenge, tissue-infiltrated neutrophils rapidly migrate into the lymphatic system through initial lymphatic capillaries (26), a process occurring in a strictly CCL21/CCR7 dependent manner. However, at present little is known about the regulation and role of tissue-associated lymphatic glycocalyx and HS during inflammation, and it is still unclear whether the LEC glycocalyx can regulate the migratory response of these leukocytes, a topic that needs further explorations.

Another important GAG associated with lymphatic vessels is Hyaluronan (HA). In fact, LECs from initial lymphatics are characterized by the expression of the specific marker LYVE-1, a transmembrane molecule that is known to be the lymphatic receptor for HA (23). Recently, an elegant study by Johnson et al. showed that LYVE-1 serves as a docking structure for migrating DCs. Specifically, the authors propose that HA, secreted by DCs, create a bridge between the receptor LYVE-1 and CD44 on LECs and the leukocytes, respectively (46). Whilst HA and CD44 are important for neutrophil adhesion to blood vessels (47, 48), to date, there is no evidence of a similar mechanism for neutrophil interaction with LECs. In fact, most studies have demonstrated that neutrophils preferentially use β2-integrins (binding to ICAM-1 on LECs) during their migration into lymphatic vessels (26, 49, 50).

There is an abundance of literature reporting the remodeling of the blood vascular glycocalyx during inflammation. Specifically, the BEC glycocalyx and in particular HS proteoglycans are rapidly shed in response to inflammation as induced by cytokines, such as TNF, but also in various experimental and pathological inflammatory conditions, such as ischemia reperfusion injury or sepsis (8, 51, 52). HS degradation during inflammation appears to allow the exposure of underlying adhesion molecules (e.g., ICAM-1, VCAM-1) and the release of pro-inflammatory chemokines, thus facilitating neutrophil adhesion and extravasation through the blood vessel wall (4, 16). Conversely, an intact layer of HS proteoglycans in physiological and homeostatic conditions has been associated with inhibition of neutrophil adhesion to BECs (16). Mechanistically, cleavage of BEC glycocalyx has been suggested to be partially as a consequence of the activation of leukocytes, such as neutrophils through their release of enzymes and ROS (15, 30, 53). However, there is no evidence to date of a similar phenomenon during acute inflammation at the level of tissue-associated lymphatic capillaries. Of relevance however, Zolla et al. have recently described the thinning of the glycocalyx of mesenteric afferent lymphatic collecting venules in aged rats (20). Here, we provide the first conclusive evidence for reduced HS and α-D-galacosyl moieties on initial lymphatic glycocalyx during acute inflammatory responses elicited in the mouse cremaster muscle. Furthermore, this response, elicited by TNF or antigen sensitization, was associated with the migration of neutrophils into the lymphatic vasculature. Interestingly, in neutrophil-depleted animals, the degradation of the lymphatic glycan layer still occurred, suggesting that in contrast to the cleavage of the BEC glycocalyx, this phenomenon in initial lymphatic capillaries is not mediated by neutrophils. In exploring other mechanistic pathways, we investigated the cellular source of Heparanase I, a β-D-endoglucuronidase known to be the enzyme capable to cleave HS in mammalian systems (31–33). Heparanase expression is mainly restricted to platelets and activated leukocytes, such as T-cells, macrophages, DCs and neutrophils (33), but can also be upregulated in other cell types during chronic inflammatory disorders, including BECs (54). Furthermore, neutrophil Heparanase expression, has been associated with degradation of sub-endothelial extracellular matrix of blood vessels (55, 56). However, in our acute inflammatory model, Heparanase I was neither associated with LECs nor with extravasated neutrophils but was found to be highly expressed by interstitial macrophages. Altogether, these set of data could suggest a distinct function of this enzyme during the interaction of this leukocyte with blood vessels vs. lymphatic vessels. This hypothesis is supported by our novel findings using neutrophil-depletion experiments and showing that these leukocytes are not responsible for HS remodeling of LVs during acute inflammation *in vivo*. In deciphering further the mechanisms of HS degradation, we demonstrated that a specific non-anticoagulant inhibitor of the endoglycosidase heparanase (NAH) blocked the shedding of HS GAGs on initial LVs. These results are supported by a study from Schmidt et al. who showed that endogenous TNF catalyzed the degradation of HS constituents of the BEC glycocalyx in a heparanase-dependent manner in an experimental model of sepsis-induced acute lung injury (16). Similarly, Lukasz et al. demonstrated both *in vitro* and *in vivo* that angiopoietin-2 can induce the secretion of heparanase by BECs, thus contributing to the cleavage of BEC glycocalyx and resulting in an increase in blood vascular leakage and leukocyte diapedesis (57). In our study however, inhibition of glycocalyx cleavage did not interfere with the capacity of neutrophils to migrate into tissue-associated LVs, offering a prominent difference in the functional roles of lymphatic vs. blood vessel glycocalyx for the trafficking of these leukocytes. Since HS plays an important role in the migration of DCs (45), it is also possible that our findings suggest potential differences in the function of HS with respect to controlling the recruitment of innate immune cells to LVs as compared to neutrophils.

To further understand the physiological relevance of glycocalyx shedding for lymphatic function during inflammation, we analyzed the capacity of initial LVs to drain interstitial fluids and macromolecules out of inflamed tissues. Here, we showed that glycocalyx remodeling on initial lymphatic capillaries was directly associated with a rapid decrease in Evans Blue (EB) dye (locally injected to mimic tissue edema) detection in inflamed cremaster muscles. More importantly the reduced level of EB in those tissues was inversely associated with an increase in EB detection in cremaster draining lymph nodes and within the blood circulation. Of note we did not observed differences in blood vascular permeability at this time point (i.e., 16 h post-TNF stimulation) between stimulated and unstimulated (or with NAH-treatment); suggesting that the enhanced lymphatic drainage was not the consequence of an increase in interstitial pressure due to vascular permeability but related to glycocalyx remodeling. This results is supported by our previous publication demonstrating that TNF-induced blood vascular leakage is a rapid but transient phenomenon occurring within the first 30 min post-cytokine stimulation (27). Interestingly, however, in TNF-stimulated tissues local blockade of HS shedding with the heparanase inhibitor, NAH, led to the detection of high levels of EB in the cremaster muscles, and conversely, a lower quantity in draining lymph nodes and plasma of the treated animals. Supported by the fact that EB is highly negatively charged, these results suggest that the glycocalyx of initial lymphatic capillaries may form an electrostatic barrier to interstitial solutes and macromolecules similarly to blood vessels due to the presence of negative electric charges of GAG molecules present on LEC glycocalyx (8, 58). The degradation of the lymphatic glycocalyx could therefore contribute to the rapid drainage of excessive interstitial fluids generated by the inflammatory response, and to promote the rapid transport of antigens toward the closest draining lymph node in order to mount an adaptive immune response as required. in sharp contrast, during aging, the thinning of the glycocalyx of large lymphatic collectors and the loss of extracellular matrix in the valve area of these vessels (20) were associated with a decrease in the capacity of lymphatic collectors to transport fluids correctly due to reduced investiture of smooth muscle cells and pericytes around the valves (59). However, our study clearly shows that the cleavage of initial lymphatic glycocalyx is important for more efficient drainage of the tissues. Initial lymphatic capillaries are in fact structurally distinct from lymphatic collectors (60, 61). Specifically, they exhibit an oak leaf-shaped monolayer of

overlapping endothelial cells facilitating the rapid absorption of fluids and macromolecules as well as contributing to the migration of immune cells (19). Initial lymphatics are also mostly devoid of perivascular cells in contrast to the large collector vessels that are covered with pericytes and smooth muscle cells. Initial lymphatics also express specific and highly glycosylated molecules, such as LYVE-1 (usually absent or reduced on collecting LVs) (22). Taken together, the unique molecular and architectural characteristics of initial lymphatics may suggest differences in the composition of the glycocalyx that may exhibit different functions as compared to the glycocalyx of large collecting venules. This is categorically supported by our findings that the cleavage of HS GAGs on initial lymphatic capillaries promotes a faster removal of interstitial fluids from inflamed tissues.

In conclusion, our study has revealed the presence of α-D-Galactosyl moieties, α2,3-sialic acid-linked glycans and HS as key components of the initial lymphatic capillary glycocalyx *in vivo*. We also demonstrate for the first time that HS and α-D-Galactosyl moieties are cleaved from the LEC glycocalyx upon inflammation, a response that appears to be mediated by endogenous heparanase activity. Interestingly, the shedding of glycocalyx components was not associated with enhanced neutrophil interaction and recruitment to lymphatic vessels, a response that is in sharp contrast with the importance of BEC glycocalyx cleavage for the migration of leukocytes through blood vessels (4). However, our data suggest that inflammation-induced shedding of initial lymphatic glycocalyx is important for the rapid drainage of interstitial fluids and macromolecules out of inflamed tissues into the draining lymph nodes and back into the blood circulation. This response is essential for immune surveillance and for the development of a specific adaptive immunity against foreign soluble antigens. Conversely, this phenomenon may also help with the dissemination of small pathogens and pro-inflammatory mediators into the body, thus potentially contributing to the induction of a rapid systemic inflammatory response.

DATA AVAILABILITY STATEMENT

The datasets generated for this study are available on request to the corresponding author.

ETHICS STATEMENT

All animal experiments were approved by the local biological service unit Ethical Committee at Queen Mary University of London and carried out under the Home Office Project Licenses (70/7884 165 & P873F4263) according to the guidelines of the United Kingdom Animals Scientific Procedures Act (1986).

This study was carried out in accordance with the recommendations of the NHS Health Research Authority and the NRES Committee East of England–Cambridge Central committee (15/EE/0192) with written informed consent from all subjects. All subjects gave written informed consent in accordance with the Declaration of Helsinki. The protocol was approved by the NRES Committee East of England–Cambridge Central.

AUTHOR CONTRIBUTIONS

M-BV provided the overall project supervision by designing and performing experiments, analyzing the data, and writing the manuscript. SA performed the experiments, analyzed the data, and contributed to the writing of the manuscript. RK, HB, and RP performed some experiments. WW secured the funding for SA and contributed to the supervision of the project. SN provided the valuable tools, secured funding for SA, and contributed to the supervision of the project and writing of the manuscript.

FUNDING

This work was supported by funds from Versus Arthritis UK (19913 to M-BV), William Harvey Research Foundation (to M-BV), British Heart Foundation (PG/14/62/31034 to M-BV and SN and supporting RK), and the Wellcome Trust (098291/Z/12/Z to SN). SA was supported by a QMUL Principal's Award Ph.D. Studentship.

ACKNOWLEDGMENTS

We thank Prof. N. Hogg for the gift of the anti-MRP14 mAb and Prof. A. Rot for critical assessment of the manuscript. The authors wish to acknowledge the role of the Breast Cancer Now Tissue Bank in collecting and making available the samples used in the generation of this publication.

SUPPLEMENTARY MATERIAL

The Supplementary Material for this article can be found online at: https://www.frontiersin.org/articles/10.3389/fimmu.2019.02316/full#supplementary-material

REFERENCES

1. Vink H, Duling BR. Identification of distinct luminal domains for macromolecules, erythrocytes, and leukocytes within mammalian capillaries. *Circ Res.* (1996) 79:581–9. doi: 10.1161/01.RES.79.3.581
2. Van Haaren PM, Vanbavel E, Vink H, Spaan JA. Localization of the permeability barrier to solutes in isolated arteries by confocal microscopy. *Am J Physiol Heart Circ Physiol.* (2003) 285:H2848–56. doi: 10.1152/ajpheart.00117.2003
3. Megens RT, Reitsma S, Schiffers PH, Hilgers RH, De Mey JG, Slaaf DW, et al. Two-photon microscopy of vital murine elastic and muscular arteries. Combined structural and functional imaging with subcellular resolution. *J Vasc Res.* (2007) 44:87–98. doi: 10.1159/000098259
4. Reitsma S, Slaaf DW, Vink H, Van Zandvoort MA, Oude Egbrink MG. The endothelial glycocalyx: composition, functions, and visualization. *Pflugers Arch.* (2007) 454:345–59. doi: 10.1007/s00424-007-0212-8
5. Oohira A, Wight TN, Bornstein P. Sulfated proteoglycans synthesized by vascular endothelial cells in culture. *J Biol Chem.* (1983) 258:2014–21.

6. Tarbell JM, Weinbaum S, Kamm RD. Cellular fluid mechanics and mechanotransduction. *Ann Biomed Eng.* (2005) 33:1719–23. doi: 10.1007/s10439-005-8775-z
7. Wang W. Change in properties of the glycocalyx affects the shear rate and stress distribution on endothelial cells. *J Biomech Eng.* (2007) 129:324–9. doi: 10.1115/1.2720909
8. Kolarova H, Ambruzova B, Svihalkova Sindlerova L, Klinke A, Kubala L. Modulation of endothelial glycocalyx structure under inflammatory conditions. *Mediators Inflamm.* (2014) 2014:694312. doi: 10.1155/2014/694312
9. Van Den Berg BM, Vink H, Spaan JA. The endothelial glycocalyx protects against myocardial edema. *Circ Res.* (2003) 92:592–4. doi: 10.1161/01.RES.0000065917.53950.75
10. Chelazzi C, Villa G, Mancinelli P, De Gaudio AR, Adembri C. Glycocalyx and sepsis-induced alterations in vascular permeability. *Crit Care.* (2015) 19:26. doi: 10.1186/s13054-015-0741-z
11. Wang L, Fuster M, Sriramarao P, Esko JD. Endothelial heparan sulfate deficiency impairs L-selectin- and chemokine-mediated neutrophil trafficking during inflammatory responses. *Nat Immunol.* (2005) 6:902–10. doi: 10.1038/ni1233
12. Proudfoot AE. The biological relevance of chemokine-proteoglycan interactions. *Biochem Soc Trans.* (2006) 34:422–6. doi: 10.1042/BST0340422
13. Bao X, Moseman EA, Saito H, Petryniak B, Thiriot A, Hatakeyama S, et al. Endothelial heparan sulfate controls chemokine presentation in recruitment of lymphocytes and dendritic cells to lymph nodes. *Immunity.* (2010) 33:817–29. doi: 10.1016/j.immuni.2010.10.018
14. Sundd P, Pospieszalska MK, Cheung LS, Konstantopoulos K, Ley K. Biomechanics of leukocyte rolling. *Biorheology.* (2011) 48:1–35. doi: 10.3233/BIR-2011-0579
15. Henry CB, Duling BR. TNF-α increases entry of macromolecules into luminal endothelial cell glycocalyx. *Am J Physiol Heart Circ Physiol.* (2000) 279:H2815–23. doi: 10.1152/ajpheart.2000.279.6.H2815
16. Schmidt EP, Yang Y, Janssen WJ, Gandjeva A, Perez MJ, Barthel L, et al. The pulmonary endothelial glycocalyx regulates neutrophil adhesion and lung injury during experimental sepsis. *Nat Med.* (2012) 18:1217–23. doi: 10.1038/nm.2843
17. Wiesinger A, Peters W, Chappell D, Kentrup D, Reuter S, Pavenstadt H, et al. Nanomechanics of the endothelial glycocalyx in experimental sepsis. *PLoS ONE.* (2013) 8:e80905. doi: 10.1371/journal.pone.0080905
18. Marki A, Esko JD, Pries AR, Ley K. Role of the endothelial surface layer in neutrophil recruitment. *J Leukoc Biol.* (2015) 98:503–15. doi: 10.1189/jlb.3MR0115-011R
19. Baluk P, Fuxe J, Hashizume H, Romano T, Lashnits E, Butz S, et al. Functionally specialized junctions between endothelial cells of lymphatic vessels. *J Exp Med.* (2007) 204:2349–62. doi: 10.1084/jem.20062596
20. Zolla V, Nizamutdinova IT, Scharf B, Clement CC, Maejima D, Akl T, et al. Aging-related anatomical and biochemical changes in lymphatic collectors impair lymph transport, fluid homeostasis, and pathogen clearance. *Aging Cell.* (2015) 14:582–94. doi: 10.1111/acel.12330
21. Levick JR, Michel CC. Microvascular fluid exchange and the revised Starling principle. *Cardiovasc Res.* (2010) 87:198–210. doi: 10.1093/cvr/cvq062
22. Banerji S, Ni J, Wang SX, Clasper S, Su J, Tammi R, et al. LYVE-1, a new homologue of the CD44 glycoprotein, is a lymph-specific receptor for hyaluronan. *J Cell Biol.* (1999) 144:789–801. doi: 10.1083/jcb.144.4.789
23. Jackson DG. Hyaluronan in the lymphatics: the key role of the hyaluronan receptor LYVE-1 in leucocyte trafficking. *Matrix Biol.* (2018) 78–79:219–35. doi: 10.1016/j.matbio.2018.02.001
24. Jackson DG. Leucocyte trafficking via the lymphatic vasculature-mechanisms and consequences. *Front Immunol.* (2019) 10:471. doi: 10.3389/fimmu.2019.00471
25. Voisin MB, Woodfin A, Nourshargh S. Monocytes and neutrophils exhibit both distinct and common mechanisms in penetrating the vascular basement membrane *in vivo*. *Arterioscler Thromb Vasc Biol.* (2009) 29:1193–9. doi: 10.1161/ATVBAHA.109.187450
26. Arokiasamy S, Zakian C, Dilliway J, Wang W, Nourshargh S, Voisin MB. Endogenous TNFalpha orchestrates the trafficking of neutrophils into and within lymphatic vessels during acute inflammation. *Sci Rep.* (2017) 7:44189. doi: 10.1038/srep44189
27. Finsterbusch M, Voisin MB, Beyrau M, Williams TJ, Nourshargh S. Neutrophils recruited by chemoattractants *in vivo* induce microvascular plasma protein leakage through secretion of TNF. *J Exp Med.* (2014) 211:1307–14. doi: 10.1084/jem.20132413
28. Pflicke H, Sixt M. Preformed portals facilitate dendritic cell entry into afferent lymphatic vessels. *J Exp Med.* (2009) 206:2925–35. doi: 10.1084/jem.20091739
29. Champagne B, Tremblay P, Cantin A, St Pierre Y. Proteolytic cleavage of ICAM-1 by human neutrophil elastase. *J Immunol.* (1998) 161:6398–405.
30. Van Golen RF, Van Gulik TM, Heger M. Mechanistic overview of reactive species-induced degradation of the endothelial glycocalyx during hepatic ischemia/reperfusion injury. *Free Radic Biol Med.* (2012) 52:1382–402. doi: 10.1016/j.freeradbiomed.2012.01.013
31. Miao HQ, Navarro E, Patel S, Sargent D, Koo H, Wan H, et al. Cloning, expression, and purification of mouse heparanase. *Protein Expr Purif.* (2002) 26:425–31. doi: 10.1016/S1046-5928(02)00558-2
32. Vlodavsky I, Iozzo RV, Sanderson RD. Heparanase: multiple functions in inflammation, diabetes and atherosclerosis. *Matrix Biol.* (2013) 32:220–2. doi: 10.1016/j.matbio.2013.03.001
33. Mayfosh AJ, Baschuk N, Hulett MD. Leukocyte heparanase: a double-edged sword in tumor progression. *Front Oncol.* (2019) 9:331. doi: 10.3389/fonc.2019.00331
34. Teijeira A, Rouzaut A, Melero I. Initial afferent lymphatic vessels controlling outbound leukocyte traffic from skin to lymph nodes. *Front Immunol.* (2013) 4:433. doi: 10.3389/fimmu.2013.00433
35. Scruggs AK, Cioffi EA, Cioffi DL, King JA, Bauer NN. Lectin-Based characterization of vascular cell microparticle glycocalyx. *PLoS ONE.* (2015) 10:e0135533. doi: 10.1371/journal.pone.0135533
36. Wang WC, Cummings RD. The immobilized leukoagglutinin from the seeds of *Maackia amurensis* binds with high affinity to complex-type Asn-linked oligosaccharides containing terminal sialic acid-linked alpha-2,3 to penultimate galactose residues. *J Biol Chem.* (1988) 263:4576–85.
37. Knibbs RN, Goldstein IJ, Ratcliffe RM, Shibuya N. Characterization of the carbohydrate binding specificity of the leukoagglutinating lectin from *Maackia amurensis*. Comparison with other sialic acid-specific lectins. *J Biol Chem.* (1991) 266:83–8.
38. Nicholls JM, Bourne AJ, Chen H, Guan Y, Peiris JS. Sialic acid receptor detection in the human respiratory tract: evidence for widespread distribution of potential binding sites for human and avian influenza viruses. *Respir Res.* (2007) 8:73. doi: 10.1186/1465-9921-8-73
39. Khatua B, Roy S, Mandal C. Sialic acids siglec interaction: a unique strategy to circumvent innate immune response by pathogens. *Indian J Med Res.* (2013) 138:648–62. Available online at: http://www.ijmr.org.in/text.asp?2013/138/5/648/124646
40. Nightingale TD, Frayne ME, Clasper S, Banerji S, Jackson DG. A mechanism of sialylation functionally silences the hyaluronan receptor LYVE-1 in lymphatic endothelium. *J Biol Chem.* (2009) 284:3935–45. doi: 10.1074/jbc.M805105200
41. Ochoa-Alvarez JA, Krishnan H, Shen Y, Acharya NK, Han M, Mcnulty DE, et al. Plant lectin can target receptors containing sialic acid, exemplified by podoplanin, to inhibit transformed cell growth and migration. *PLoS ONE.* (2012) 7:e41845. doi: 10.1371/journal.pone.0041845
42. Natunen S, Lampinen M, Suila H, Ritamo I, Pitkanen V, Nairn AV, et al. Metabolic glycoengineering of mesenchymal stromal cells with N-propanoylmannosamine. *Glycobiology.* (2013) 23:1004–12. doi: 10.1093/glycob/cwt039
43. Proudfoot AEI, Johnson Z, Bonvin P, Handel TM. Glycosaminoglycan interactions with chemokines add complexity to a complex system. *Pharmaceuticals.* (2017) 10:E70. doi: 10.3390/ph10030070
44. Gouverneur M, Spaan JA, Pannekoek H, Fontijn RD, Vink H. Fluid shear stress stimulates incorporation of hyaluronan into endothelial cell glycocalyx. *Am J Physiol Heart Circ Physiol.* (2006) 290:H458–2. doi: 10.1152/ajpheart.00592.2005
45. Weber M, Hauschild R, Schwarz J, Moussion C, De Vries I, Legler DF, et al. Interstitial dendritic cell guidance by haptotactic chemokine gradients. *Science.* (2013) 339:328–32. doi: 10.1126/science.1228456
46. Johnson LA, Banerji S, Lawrance W, Gileadi U, Prota G, Holder KA, et al. Dendritic cells enter lymph vessels by hyaluronan-mediated docking

to the endothelial receptor LYVE-1. *Nat Immunol.* (2017) 18:762–70. doi: 10.1038/ni.3750
47. Khan AI, Kerfoot SM, Heit B, Liu L, Andonegui G, Ruffell B, et al. Role of CD44 and hyaluronan in neutrophil recruitment. *J Immunol.* (2004) 173:7594–601. doi: 10.4049/jimmunol.173.12.7594
48. Mcdonald B, Kubes P. Interactions between CD44 and Hyaluronan in Leukocyte Trafficking. *Front Immunol.* (2015) 6:68. doi: 10.3389/fimmu.2015.00068
49. Gorlino CV, Ranocchia RP, Harman MF, Garcia IA, Crespo MI, Moron G, et al. Neutrophils exhibit differential requirements for homing molecules in their lymphatic and blood trafficking into draining lymph nodes. *J Immunol.* (2014) 193:1966–74. doi: 10.4049/jimmunol.1301791
50. Hampton HR, Bailey J, Tomura M, Brink R, Chtanova T. Microbe-dependent lymphatic migration of neutrophils modulates lymphocyte proliferation in lymph nodes. *Nat Commun.* (2015) 6:7139. doi: 10.1038/ncomms8139
51. Chappell D, Hofmann-Kiefer K, Jacob M, Rehm M, Briegel J, Welsch U, et al. TNF-α induced shedding of the endothelial glycocalyx is prevented by hydrocortisone and antithrombin. *Basic Res Cardiol.* (2009) 104:78–89. doi: 10.1007/s00395-008-0749-5
52. Becker BF, Chappell D, Jacob M. Endothelial glycocalyx and coronary vascular permeability: the fringe benefit. *Basic Res Cardiol.* (2010) 105:687–701. doi: 10.1007/s00395-010-0118-z
53. Vanteeffelen JW, Brands J, Jansen C, Spaan JA, Vink H. Heparin impairs glycocalyx barrier properties and attenuates shear dependent vasodilation in mice. *Hypertension.* (2007) 50:261–7. doi: 10.1161/HYPERTENSIONAHA.107.089250
54. Chen G, Wang D, Vikramadithyan R, Yagyu H, Saxena U, Pillarisetti S, et al. Inflammatory cytokines and fatty acids regulate endothelial cell heparanase expression. *Biochemistry.* (2004) 43:4971–7. doi: 10.1021/bi03 56552
55. Matzner Y, Bar-Ner M, Yahalom J, Ishai-Michaeli R, Fuks Z, Vlodavsky I. Degradation of heparan sulfate in the subendothelial extracellular matrix by a readily released heparanase from human neutrophils. Possible role in invasion through basement membranes. *J Clin Invest.* (1985) 76:1306–13. doi: 10.1172/JCI112104
56. Komatsu N, Waki M, Sue M, Tokuda C, Kasaoka T, Nakajima M, et al. Heparanase expression in B16 melanoma cells and peripheral blood neutrophils before and after extravasation detected by novel anti-mouse heparanase monoclonal antibodies. *J Immunol Methods.* (2008) 331:82–93. doi: 10.1016/j.jim.2007.11.014
57. Lukasz A, Hillgruber C, Oberleithner H, Kusche-Vihrog K, Pavenstadt H, Rovas A, et al. Endothelial glycocalyx breakdown is mediated by angiopoietin-2. *Cardiovasc Res.* (2017) 113:671–80. doi: 10.1093/cvr/cvx023
58. Curry FE, Adamson RH. Endothelial glycocalyx: permeability barrier and mechanosensor. *Ann Biomed Eng.* (2012) 40:828–39. doi: 10.1007/s10439-011-0429-8
59. Bridenbaugh EA, Nizamutdinova IT, Jupiter D, Nagai T, Thangaswamy S, Chatterjee V, et al. Lymphatic muscle cells in rat mesenteric lymphatic vessels of various ages. *Lymphat Res Biol.* (2013) 11:35–42. doi: 10.1089/lrb.2012. 0025
60. Hirakawa S, Detmar M, Karaman S. Lymphatics in nanophysiology. *Adv Drug Deliv Rev.* (2014) 74:12–8. doi: 10.1016/j.addr.2014.01.011
61. Kerjaschki D. The lymphatic vasculature revisited. *J Clin Invest.* (2014) 124:874–7. doi: 10.1172/JCI74854

Conflict of Interest: The authors declare that the research was conducted in the absence of any commercial or financial relationships that could be construed as a potential conflict of interest.

frontiers in Immunology

REVIEW
published: 09 January 2020
doi: 10.3389/fimmu.2019.03031

Syndecan-3 in Inflammation and Angiogenesis

Samantha Arokiasamy[1], *Michaela J. M. Balderstone*[1], *Giulia De Rossi*[2] *and James R. Whiteford*[1]*

[1] Barts and the London School of Medicine and Dentistry, William Harvey Research Institute, Queen Mary University of London, London, United Kingdom, [2] Department of Cell Biology, UCL Institute of Ophthalmology, London, United Kingdom

Syndecans are a four member multifunctional family of cell surface molecules with diverse biological roles. Syndecan-3 (SDC3) is the largest of these, but in comparison to the other family members relatively little is known about this molecule. SDC3 null mice grow and develop normally, all be it with subtle anatomical phenotypes in the brain. Roles for this molecule in both neuronal and brain tissue have been identified, and is associated with altered satiety responses. Recent studies suggest that SDC3 expression is not restricted to neuronal tissues and has important roles in inflammatory disorders such as rheumatoid arthritis, disease associated processes such as angiogenesis and in the facilitation of infection of dendritic cells by HIV. The purpose of this review article is to explore these new biological insights into SDC3 functions in inflammatory disease.

Keywords: heparan sulfate, syndecan, HIV, rheumatoid arthritis, angiogenesis

OPEN ACCESS

Edited by:
Rogier M. Reijmers, Leiden University Medical Center, Netherlands

Reviewed by:
Mark Morgan, University of Liverpool, United Kingdom
Jessica Bertrand, University Hospital Magdeburg, Germany

***Correspondence:**
James R. Whiteford
j.whiteford@qmul.ac.uk

Specialty section:
This article was submitted to Inflammation, a section of the journal Frontiers in Immunology

Received: *10 October 2019*
Accepted: *10 December 2019*
Published: *09 January 2020*

Citation:
Arokiasamy S, Balderstone MJM, De Rossi G and Whiteford JR (2020) Syndecan-3 in Inflammation and Angiogenesis. Front. Immunol. 10:3031. doi: 10.3389/fimmu.2019.03031

INTRODUCTION

The proteoglycans are a diverse family of molecules with multiple roles in development, health and disease (1). Heparan Sulfate Proteoglycans (HSPGs) form a subset of these, and these can be secreted extracellular matrix molecules or membrane associated (1). The principal families of membrane associated HSPGs are the glypicans and syndecans. Glypicans are distinguished from syndecans by the fact they are tethered to the cell membrane via glycosylphosphatidylinositol anchors. Syndecans (SDC) are a four member family of type 1 transmembrane proteins consisting of two related sub-families based on sequence homology. SDC2 and 4 form one family and SDC1 and 3 form the other. All syndecans have a short highly conserved cytoplasmic domain, a single transmembrane domain, and a larger extracellular core protein. Syndecan ectodomains are far less conserved between family members or species. However, they do possess Ser-Gly GAG attachment motifs usually surrounded by acidic amino acid residues. Every cell type expresses at least one syndecan, and roles in cell adhesion, migration, growth factor signaling, receptor trafficking and ion channel modulation have been identified [for reviews see (1–5)]. Of the four family members, perhaps the least well-understood is Syndecan-3 (SDC3). Predominantly, reported roles for this molecule have been exclusively related to the brain and nervous system, but recent studies are revealing roles for SDC3 in other important biological processes such as inflammation and angiogenesis. This review aims to explore this work and provide novel insight into the biology of SDC3.

SYNDECAN-3 MOLECULAR ARCHITECTURE

The syndecan-3 (N-syndecan) gene was first cloned from rat Schwann cells and was the third syndecan of the four member family to be identified (6, 7). It bears significant homology to syndecan-1, although unlike syndecan-1, it has a homolog in fish (8). Of the four family members, syndecan-3 (SDC3) is the largest, consisting of 442 amino acids in humans. In mammals, the SDC3 ectodomain contains seven potential glycosaminoglycan (GAG) attachment sites. Four are situated toward the N-terminus and the remaining three reside closer to the transmembrane domain (**Figure 1A**). The type and extent of GAG substitution on syndecan-3 is likely to be cell type and tissue dependent. Experiments using heparan sulfate (HS) and chondroitin sulfate (CS) degrading enzymes would suggest that SDC3 (at least when purified from brain tissue) possesses both HS and CS chains (9).

HS chains consist of repeated disaccharide units consisting of glucuronic acid and N-acetylglucosamine and chain lengths can range from 50 to 200 disaccharides. It is synthesized via a stepwise series of enzymatic reactions involving multiple transferases; briefly N-acetyglucosamine within a chain can undergo N-sulphation followed by the epimerisation of some glucuronic acids, this is followed by the sequential addition of first 2-O, 6-O, and 3-O sulfate groups. The complexity of this process means that HS chains are heterogenous in terms of sulphation and there is considerable evidence of HS chains having domains of high, intermediate and low sulphation [for review see (10), **Figure 1B**. CS is structurally distinct to HS on the basis that it is comprised of repeating disaccharide units consisting of glucuronic acid and n-acetylgalactosamine (**Figure 1B**). CS chains can also be sulphated although the extent and heterogeneity of this is not as great as HS. The majority of reported interactions between SDC3 and biologically active molecules are with its HS chains, and far less is understood as to the role or function of SDC3 CS chains. The extracellular core protein also possesses a domain rich in threonine and proline residues, which is characteristic of mucin-like proteins, and are potential sites for *O*-linked glycosylation (6).

Syndecan shedding is a regulated process whereby some or all of the extracellular domain of the molecule is cleaved from the cell surface by the action of matrix-metalloproteases (MMPs). Shed SDC3 has been observed in conditioned media in a variety of experimental systems, although the precise cleavage sites and proteases have yet to be confirmed (11). Predictive algorithms would suggest roles for MMP2, 9, and 14 at multiple cleavage sites but these have not been validated experimentally (3). SDC3, along with the other family members, form SDS insoluble dimers and this self-association is mediated both by residues in the transmembrane domain, and a membrane proximal ERKE motif (12).

The syndecan-3 cytoplasmic domain consists of 33 aa and in common with the rest of the family possesses two conserved domains (C1 and C2) flanking a variable sequence (V region), which is unique to each family member (**Figure 1C**). Syndecans all have the capability of interaction with PDZ proteins possessing a conserved EFYA motif at the C-terminus of the C2 region. Interactions between SDC3 and PDZ proteins such as syntenin, CASK, TIAM1, synectin, and synbindin have been reported. The SY sequence (Ser^{418}, Tyr^{419} in human SDC3, **Figure 1C**) in the C1 region of SDC3 is common to all syndecans. Studies with SDC4 have shown that phosphorylation of either residue is important for its functionality. Syndecans have proven remarkably recalcitrant to structural analysis, none more so than SDC3, for which there are no structural records in the databases (2). However, structural analysis of peptides corresponding to the syndecan-4 cytoplasmic domain in which this serine residue is phosphorylated show that this alters the conformation of this molecule considerably, and expression of phospho-mimetic mutants of this residue leads to enhanced cell migration (13). In other work, the Y (Tyr^{180} in human SDC4) was identified as a substrate for Src kinase and this has implications for the trafficking of integrins. It would not be surprising if phosphorylation of these conserved residues impacted on SDC3 functionality in a similar fashion (14). Additionally, *in vitro* studies have indicated that the other 2 tyrosines could potentially be phosphorylated, however no functional role for this has been demonstrated (15). The V region of SDC3 also bears similarities to other syndecans in that there are 2 lysine residues (Lys^{425} and Lys^{433}). Studies with syndecan-4 have shown the importance of these lysines for binding phospho-inositides (PIP3) and this not only stabilizes the structure of SDC4 cytoplasmic domain but this interaction is also associated with upregulating the activity of PKCα which promotes many of the downstream cell adhesion pathways associated with SDC4 (16, 17). It is therefore also conceivable that the interactions with the SDC3 V region and phospho-inositides could be important for SDC3 functionality.

SYNDECAN-3 IN THE BRAIN AND NERVOUS TISSUE

The association with SDC3 and cells of a neuronal lineage is well-established and a number of phenotypes associated with both the brain and nervous tissue have been identified (18, 19). Although no gross abnormalities are observed in the developing mouse brain, stereological analysis of sections revealed differences in the cellular density of key areas. Specifically, SDC3 null animals have a higher density of cells in deep cortical areas and a reduced number in the superficial cortical layers. This was found to be due to defects in neural cell migration during development and in particular, an interaction between SDC3 and heparin binding growth associated molecule (HBGAM) (20). Syndecans are known to be key players in cell adhesion and migration, so identifying a migration defect in neural cells associated with SDC3 is entirely consistent.

SDC3 is found in other tissues of the brain, immunostaining of wild-type mice revealed SDC3 to be expressed in the hypothalamus, particularly in the paraventricular nucleus and the lateral hypothalamic area (21). SDC3 expression (uniquely amongst the family members) is upregulated in the hypothalamus in response to food deprivation and the situation is reversible once starved animals are refed. Unsurprisingly, food

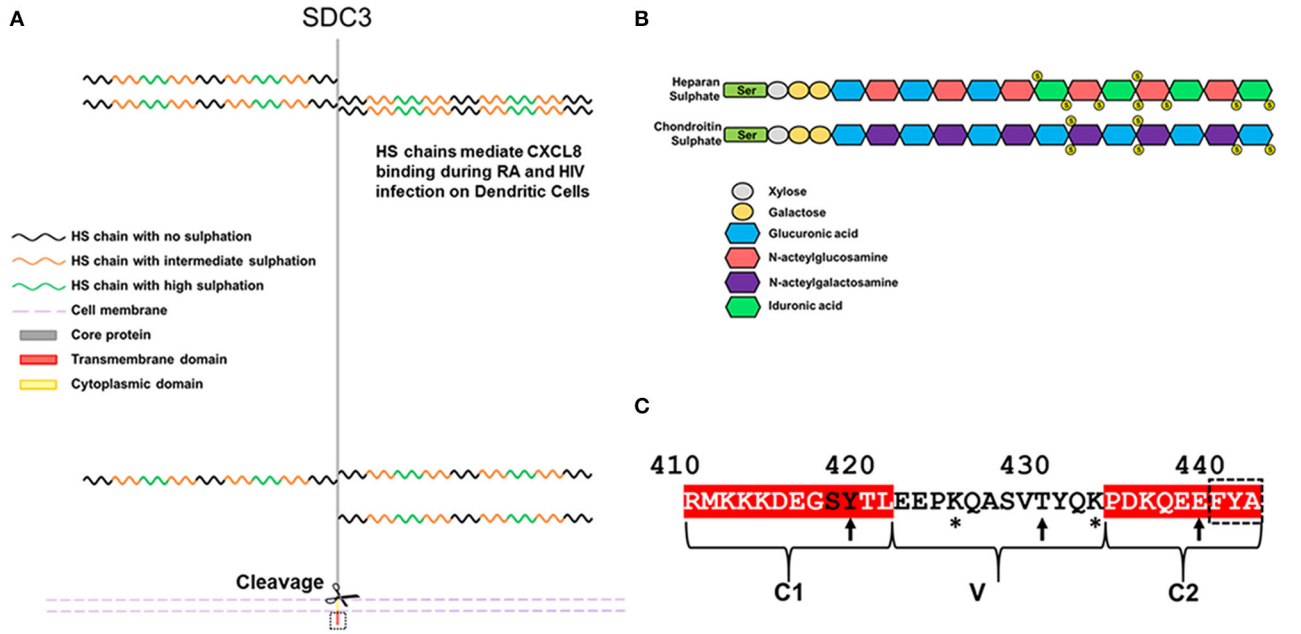

FIGURE 1 | Schematic diagram and features of SDC3. **(A)** Human SDC3 is 442aa in length and contains seven potential sites for GAG substitution. Most functions ascribed to SDC3 relate to interactions through its HS chains. HS chains are heterogenous in nature and contain regions of low, intermediate and high sulphation. **(B)** Structure of HS and CS. **(C)** The cytoplasmic domain of SDC3 is 33 amino acids in length and shares conserved C1 and C2 domains with other syndecan family members. The C-terminal PDZ binding domain is indicated by a dashed black box. Potential sites of tyrosine phosphorylation are indicated by arrows and lysine residues potentially involved in phosphoinositide binding are indicated by asterisks. The conserved SY in the C1 domain, which can be phosphorylated in other syndecan family members are denoted by black letters.

deprived animals exhibit an abnormal desire for food once the deprivation is ended. However, this response is lacking in animals null for SDC3, suggesting a role for SDC3 in feeding behaviors (21). This is further evidenced by the fact that SDC3 animals are partially resistant to obesity when given a high fat diet due to reduced food intake (22).

Several hypothalamic neuropeptides regulate feeding behaviors; for example, agouti-related protein (AgRP), melanin concentrating hormone (MCH) and neuropeptide Y stimulate increased feeding behaviors, whereas α-melanocyte stimulating hormone (αMSH) and corticotrophin releasing hormone (CRH) serve to inhibit pathways associated with increased feeding (23). It is known that many of the interactions between these peptides and their receptors at least in part have an HS involvement. There is a complex interplay between these neuropeptides and SDC3 is thought to have a role in promoting the antagonism between AgRP and αMSH for the melanocortin receptor MC-4R (24, 25). In essence, when animals are starved, SDC3 is upregulated and this promotes the binding of AgRP to MC-4R leading to a reduction in anti-satiety signals, and enhanced feeding. In animals null for SDC3, this interaction does not occur meaning αMSH is free to bind MC-4R leading to a reduction in the desire to feed in these animals. Interestingly, another consequence of starving is an upregulation of Tissue Inhibitor Metalloprotease-3 (TIMP3), this acts as an inhibitor to a variety of MMPs which also have key roles in syndecan shedding. This provides a means of regulating feeding behaviors since under conditions of starvation, SDC3 shedding is inhibited thus promoting occupation of MC-4R by AgRP and promoting feeding. On the other hand, under feeding conditions TIMP is down regulated, SDC3 shedding is up regulated and the satiety signal through the αMSH/MC-4R axis is promoted (26, 27). The hypothalamus also has key roles in modulating reward processing in addictive behaviors and SDC3 also has a role to play in these. Cocaine administration increases SDC3 expression in the lateral hypothalamic area and SDC3 knockout mice actually exhibit more addictive behaviors than wild-type counterparts. SDC3 null animals were more susceptible to cocaine addiction, a situation that could be reversed upon re-expression of SDC3. Glial cell line-derived growth factor (GDNF) acts to both increase and decrease cocaine self-administration behaviors in rodents through its interactions with a signaling complex consisting of the receptor GFR-α1 and the tyrosine kinase c-Ret (28). SDC3 is thought to disrupt this signaling complex since it can also bind GDNF and as such, is a potentially important target for treating addictions.

SYNDECAN-3 IN DISEASE

It is very evident from the studies described above that SDC3 plays a critical role in both brain development and behavior. However, other roles for SDC3 on endothelial cells (ECs) and leukocytes are emerging in inflammatory responses. The purpose of the remainder of this review is to examine the roles of SDC3

in the context of inflammatory disease (rheumatoid arthritis), angiogenesis and also HIV infection.

Syndecan-3 in Rheumatoid Arthritis

SDC3 is expressed on endothelia in both rheumatoid and non-rheumatoid synovia and is thought to have roles in binding chemokines, specifically CXCL8, during the progression of the disease (29, 30). Interestingly, mice null for SDC3 are protected in a model of antigen-induced arthritis (methylated BSA induced), in which clinical scores, leukocyte recruitment and cartilage damage were all significantly less than wild-type animals (31). This is a common feature of syndecan null animals, in that phenotypes only emerge when the animals are challenged and more often than not, deletion of syndecans leads to less severe disease progression, suggesting a role only in pathological scenarios. This study also highlighted a slight paradox; in models of both dermal and cremasteric inflammation, leukocyte rolling and adhesion was elevated in SDC3-null mice, suggesting an anti-inflammatory role for this molecule (31). This therefore suggests distinct roles for SDC3 depending on the vascular bed. SDC3 is thought to facilitate chemokine interactions via binding to its GAG chains, and it is likely that the extent and sulphation pattern of the HS chains in ECs from different tissues will vary. Administration of recombinant forms of SDC3 ectodomains, expressed in mammalian cells, have also been used in both collagen- and methylated BSA-induced murine inflammatory arthritis models with efficacious effects indicating both the therapeutic potential of targeting this molecule but also the importance of shed SDC3 in disease progression (32).

Syndecan-3 in Neovascular Diseases

Angiogenesis, the formation of new blood vessels from existing vasculature, and inflammation are intrinsically linked. SDC3-null mice exhibit no gross abnormalities suggesting that the formation of the vasculature in these animals is normal. However, in-depth studies on parameters such as vessel density, vessel diameter, vessel frequency and pericyte coverage have yet to be undertaken. SDC3 is expressed on ECs in early retinal development in rats (33), and has been found expressed on ECs from a variety of tissues. For example, along with SDC4, SDC3 is abundant on cultured human umbilical vein ECs (34), and human coronary artery endothelial cells as well as human coronary artery smooth muscle cells (35). Vascular endothelial growth factor A (VEGFA), alongside a number of other proangiogenic factors are known to bind HS (36, 37), so it would be tempting to propose a role for SDC3 in this context. Interestingly, sequences within the SDC3 extracellular core protein exert anti-angiogenic affects by blocking EC migration (38). A fusion protein consisting of GST fused to the N-terminus of the SDC3 ectodomain inhibits angiogenic sprout formation from aortic explants, and also inhibited EC micro-capillary formation and EC migration. Importantly, this protein was generated in a prokaryotic expression system so lacked any GAG substitutions, indicating that this is an intrinsic property of the core protein (38). This is also in common with other syndecan family members, whose core proteins also exhibit biological activity (39). SDC1, which is closely related to SDC3,

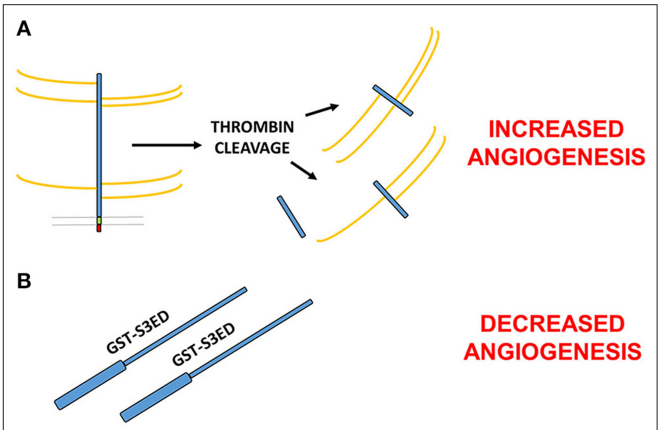

FIGURE 2 | Contrasting roles for the SDC3 ectodomain in angiogenesis. **(A)** Thrombin cleaved fragments of the SDC3 ectodomain promote pro-angiogenic processes such as EC junctional disassembly (43). **(B)** Full length bacterially expressed SDC3 extracellular core protein fused at the N-terminus to GST inhibits angiogenesis in a number of *in vitro* and *ex vivo* models (38). Since the thrombin cleavage sites of SDC3 are not known, it is possible that one or more of the cleavage products is pro-angiogenic whereas the full length sequence acts to inhibit new blood vessel formation.

has anti-angiogenic sequences within its core protein but they bear no homology to the SDC3 sequence suggesting that the anti-angiogenic properties of the latter may work via a distinct mechanism (40, 41). It remains unclear how these sequences affect the biology of the full length molecule—do they bind receptors *in cis*, as is the case for SDC1 (41) or *in trans* when shed as is the case for SDC2 (42)?

A key step in the formation of new blood vessels, and indeed inflammation, is the disassembly of EC junctions, enabling both the migration and proliferation of ECs and vascular leakage during disease. Thrombin-cleaved fragments of the SDC3 (and SDC4) ectodomain have been shown to promote this process in the human lung microvasculature, which has ramifications for conditions such as sepsis or thrombotic disease states, where thrombin is activated (43). This would suggest opposing roles for the SDC3 ectodomain in angiogenesis; on the one hand, studies would suggest that the core protein independent of GAG chains can inhibit the process (44), whereas fragments of SDC3 cleaved from mammalian cells with their GAGs intact appear to promote vascular permeability and EC migration. It is conceivable that since the thrombin cleavage sites in the SDC3 extracellular core proteins are not known, smaller fragments of the mature protein may in fact exhibit pro-angiogenic effects (**Figure 2**).

Syndecan-3 Interactions With Human Immunodeficiency Virus 1 (HIV-1)

Dendritic cells (DCs) are antigen presenting cells and play a critical role in identifying and capturing pathogens in peripheral tissues and subsequently priming T cells in the lymph nodes to initiate adaptive immune responses. Sexual transmission is the main route of HIV-1 dissemination and in the absence of surface lesions, the genital epithelia presents a barrier to viral crossing

(45, 46). HIV circumvents this by using DCs as molecular Trojan horses to cross this normally impenetrable epithelium (47). DCs induce virus-specific CD8+ T cell responses by presenting antigens bound by major histocompatibility complex molecules class-I (MHC-I) to these T cells, thus activating them. DCs infected with viruses can use viral proteins which are endogenously synthesized from viral replication as antigens for presentation on MHC-I in a process commonly called direct presentation (48). On the other hand, DCs not infected with viruses must engulf exogenous viral antigens for presentation to CD8+ T cells via a process known as cross-presentation (49). DCs have been shown to be susceptible to HIV-1 infection (50). Therefore, direct presentation usually takes place in the context of normal HIV transmission.

A number of cell surface receptors have been implicated in facilitating both the recognition, binding and transmission of the HIV-1 virus; different receptors have been shown to interact with HIV-1 on DCs, such as the C-type lectin DC-SIGN (51, 52), the mannose receptor (53), langerin (54), and CD4 (53). Most of these studies were carried out using HIV-1 glycoprotein gp120 but other experiments using HIV-1 particles suggest that other unknown receptors are also involved (55–57).

DC-SIGN, which binds with high affinity to ICAM-3 present on resting T cells, was discovered to play a key-role in the dissemination of HIV-1 by DCs (51, 58). It does not function as a receptor for HIV-1 virus entry into DCs but instead promotes efficient capture of HIV-1 viruses in the periphery and facilitate their transport to secondary lymphoid tissues to enhance infection *in trans* of cells that express CD4 and chemokine receptors (i.e., T cells) (51). More recently, de Witte et al. (59) found SDC3 to be highly expressed by DCs, namely immature monocyte-derived DCs, and was identified as a major specific HIV-1 attachment receptor. SDC3 captures HIV-1 through interaction with its HS chains and the viral envelope protein gp120; it also acts to stabilize the captured virus, enhance DC infection and like DC-SIGN, promotes HIV transmission to T cells. The authors also found that neutralization of both SDC3 and DC-SIGN leads to the complete impairment of HIV-1 binding to DCs and transmission to T cells. Neutralization of SDC3 alone led to partial inhibition of HIV-1 transmission. As current anti-viral treatments are only aimed at blocking viral replication in T-cells, this opens up a whole new avenue in terms of developing an HIV microbicide that targets DC-SIGN and SDC3 on DCs.

Interestingly, HIV-1 infected individuals known as HIV controllers (HICs) who are able to control viral replication without anti-retroviral therapy exist, but are rare. DCs from these individuals express higher levels of SDC3 and DC-SIGN and have been shown to be less susceptible to HIV-1 infection than cells from healthy donors. On the contrary, DCs from HICs show an enhanced capacity to capture HIV-1 when compared to cells from healthy donors or HIV-1 patients currently on anti-retroviral treatment with suppressed viral load (60). High levels of both SDC3 and DC-SIGN on DCs have previously been confirmed to play crucial roles in facilitating HIV-1 capture and this would, at first, seem contradictory (51, 58, 59). However, the combination of being less permissible to HIV-1 infection and having increased capacity to capture HIV-1 particles may allow DCs from HICs to preserve their function from the deleterious effect of infection—all of which might facilitate the induction of HIV-specific CD8+ T cells by cross-presentation in the context of low viremia.

CONCLUDING REMARKS

In this review, we have explored the diverse roles that the HSPG, SDC3, plays in a range of disease and developmental contexts. Although many phenotypes have been described, there is still a great deal to learn about how SDC3 is actually functioning in these scenarios. SDC1, 2 and 4 have been intrinsically linked with integrins and in particular modulating cell adhesion and migration responses. SDC1 has been shown to modulate the activity of a number of αV integrin heterodimers, as has SDC4 (14, 61). Similarly β1 integrin heterodimers have also been associated with SDC2 and 4 (14, 42, 62). The consequences of these interactions lead to cell migration and adhesion defects when they are compromised. Based on this, it seems likely that SDC3 would also interact and/or modulate integrin activity although further research is required to establish this for sure.

In many instances, it is interactions with SDC3 HS chains that appear to be driving the biological effects observed, whether it be acting to bind neuropeptides, inflammatory mediators or viral particles. However, this does raise the question as to what is driving this selectivity of the molecules toward SDC3 HS. In many cases, the other syndecans and indeed glypican family members are present in abundance but cannot perform the same functions as SDC3 despite possessing HS chains. One possibility is that sequences specific to SDC3 may influence the type and nature of GAG substitution, and it is this that differentiates SDC3 from other HSPGs. This would not be without precedent since studies have shown that sequences in the SDC2 ectodomain can influence the sulphation pattern of SDC2 HS (63). Alternatively, it could be that the expression and localization of SDC3 in cells could be more exquisitely regulated than first thought. Studies in the brain have shown that SDC3 expression can be induced both by starvation and narcotic substances and this is not the case for other family members. SDC3-null animals (like the other family members) develop normally for the most part and it is when challenged that phenotypes are observed. This is suggestive that SDC3 expression is governed by factors associated with these challenges. Molecules such as this make tempting therapeutic targets since it is to be expected that off-target effects would be negligible since the molecule is only having a role in the disease state. It is also entirely possible this selectivity of function of SDC3 HS is actually a combination of both of the above.

The studies described above point to important roles for SDC3 in inflammatory disease which require further investigation and hint that this molecule is important not just in the neuronal context but in other tissues. More detailed studies are required in both the SDC3 null mouse, and patient samples, to explore disease models where inflammation and angiogenesis are a feature. Greater mechanistic insight is required to understand how SDC3 exerts its functions. It remains a possibility that modulating SDC3 function could prove useful in the treatment

of the pathologies described above, however, the means by which this could be achieved requires elucidating.

AUTHOR CONTRIBUTIONS

JW and SA generated the text and performed the literature searches. MB prepared the figures and GD critically appraised and edited the manuscript.

FUNDING

SA, MB, GD, and JW gratefully acknowledge funding from Arthritis Research UK (Grant No. 21177), Fight for Sight (Grant No. 1558/59), Barts and The London Charity (Grant No. MGU0313), Queen Mary Innovations, William Harvey Research Foundation, The Macular Society and The Dunhill Medical Trust (Grant No. RPGF1906\173).

REFERENCES

1. Couchman JR. Transmembrane signaling proteoglycans. *Ann Rev Cell Dev Biol.* (2010) 26:89–114. doi: 10.1146/annurev-cellbio-100109-104126
2. Gondelaud F, Ricard-Blum S. Structures and interactions of syndecans. *FEBS J.* (2019) 286:2994–3007. doi: 10.1111/febs.14828
3. Bertrand J, Bollmann M. Soluble syndecans: biomarkers for diseases and therapeutic options. *Br J Pharmacol.* (2019) 176:67–81. doi: 10.1111/bph.14397
4. Mitsou I, Multhaupt HAB, Couchman JR. Proteoglycans, ion channels and cell-matrix adhesion. *Biochem J.* (2017) 474:1965–79. doi: 10.1042/BCJ20160747
5. Afratis NA. Nikitovic D, Multhaupt HA, Theocharis AD, Couchman JR, Karamanos NK. Syndecans—key regulators of cell signaling and biological functions. *FEBS J.* (2017) 284:27–41. doi: 10.1111/febs.13940
6. Carey DJ. Conner K, Asundi VK, O'Mahony DJ, Stahl RC, Showalter L, et al. cDNA cloning, genomic organization, and *in vivo* expression of rat N-syndecan. *J Biol Chem.* (1997) 272:2873–9. doi: 10.1074/jbc.272.5.2873
7. Carey DJ, Evans DM, Stahl RC, Asundi VK, Conner KJ, Garbes P, et al. Molecular cloning and characterization of N-syndecan, a novel transmembrane heparan sulfate proteoglycan. *J Cell Biol.* (1992) 117:191–201. doi: 10.1083/jcb.117.1.191
8. Chakravarti R, Adams JC. Comparative genomics of the syndecans defines an ancestral genomic context associated with matrilins in vertebrates. *BMC Genom.* (2006) 7:83. doi: 10.1186/1471-2164-7-83
9. Chernousov MA, Carey DJ. N-syndecan (syndecan 3) from neonatal rat brain binds basic fibroblast growth factor. *J Biol Chem.* (1993) 268:16810–4.
10. Li JP, Kusche-Gullberg M. Heparan Sulfate: biosynthesis, structure, and Function. *Int Rev Cell Mol Biol.* (2016) 325:215–73. doi: 10.1016/bs.ircmb.2016.02.009
11. Asundi VK, Erdman R, Stahl RC, Carey DJ. Matrix metalloproteinase-dependent shedding of syndecan-3, a transmembrane heparan sulfate proteoglycan, in Schwann cells. *J Neurosci Res.* (2003) 73:593–602. doi: 10.1002/jnr.10699
12. Asundi VK, Carey DJ. Self-association of N-syndecan (syndecan-3) core protein is mediated by a novel structural motif in the transmembrane domain and ectodomain flanking region. *J Biol Chem.* (1995) 270:26404–10. doi: 10.1074/jbc.270.44.26404
13. Koo BK, Jung YS, Shin J, Han I, Mortier E, Zimmermann P, et al. Structural basis of syndecan-4 phosphorylation as a molecular switch to regulate signaling. *J Mol Biol.* (2006) 355:651–63. doi: 10.1016/j.jmb.2005.09.087
14. Morgan MR, Hamidi H, Bass MD, Warwood S, Ballestrem C, Humphries MJ. Syndecan-4 phosphorylation is a control point for integrin recycling. *Dev Cell.* (2013) 24:472–85. doi: 10.1016/j.devcel.2013.01.027
15. Asundi VK, Carey DJ. Phosphorylation of recombinant N-syndecan (syndecan 3) core protein. *Biochem Biophys Res Commun.* (1997) 240:502–6. doi: 10.1006/bbrc.1997.7684
16. Oh ES, Woods A, Couchman JR. Syndecan-4 proteoglycan regulates the distribution and activity of protein kinase C. *J Biol Chem.* (1997) 272:8133–6. doi: 10.1074/jbc.272.13.8133
17. Oh ES, Woods A, Lim ST, Theibert AW, Couchman JR. Syndecan-4 proteoglycan cytoplasmic domain and phosphatidylinositol 4,5-bisphosphate coordinately regulate protein kinase C activity. *J Biol Chem.* (1998) 273:10624–9. doi: 10.1074/jbc.273.17.10624
18. Kim CW, Goldberger OA, Gallo RL, Bernfield M. Members of the syndecan family of heparan sulfate proteoglycans are expressed in distinct cell-, tissue-, and development-specific patterns. *Mol Biol Cell.* (1994) 5:797–805. doi: 10.1091/mbc.5.7.797
19. Kaksonen M, Pavlov I, Voikar V, Lauri SE, Hienola A, Riekki R, et al. Syndecan-3-deficient mice exhibit enhanced LTP and impaired hippocampus-dependent memory. *Mol Cell Neurosci.* (2002) 21:158–72. doi: 10.1006/mcne.2002.1167
20. Hienola A, Tumova S, Kulesskiy E, Rauvala H. N-syndecan deficiency impairs neural migration in brain. *J Cell Biol.* (2006) 174:569–80. doi: 10.1083/jcb.200602043
21. Reizes O, Lincecum J, Wang Z, Goldberger O, Huang L, Kaksonen M, et al. Transgenic expression of syndecan-1 uncovers a physiological control of feeding behavior by syndecan-3. *Cell.* (2001) 106:105–16. doi: 10.1016/S0092-8674(01)00415-9
22. Strader AD, Reizes O, Woods SC, Benoit SC, Seeley RJ. Mice lacking the syndecan-3 gene are resistant to diet-induced obesity. *J Clin Invest.* (2004) 114:1354–60. doi: 10.1172/JCI20631
23. Woods SC, Seeley RJ, Porte D Jr, Schwartz MW. Signals that regulate food intake and energy homeostasis. *Science.* (1998) 280:1378–83. doi: 10.1126/science.280.5368.1378
24. Reizes O, Clegg DJ, Strader AD, Benoit SC. A role for syndecan-3 in the melanocortin regulation of energy balance. *Peptides.* (2006) 27:274–80. doi: 10.1016/j.peptides.2005.02.030
25. Zheng Q, Zhu J, Shanabrough M, Borok E, Benoit SC, Horvath TL, et al. Enhanced anorexigenic signaling in lean obesity resistant syndecan-3 null mice. *Neuroscience.* (2010) 171:1032–40. doi: 10.1016/j.neuroscience.2010.09.060
26. Reizes O, Benoit SC, Strader AD, Clegg DJ, Akunuru S, Seeley RJ. Syndecan-3 modulates food intake by interacting with the melanocortin/AgRP pathway. *Ann N Y Acad Sci.* (2003) 994:66–73. doi: 10.1111/j.1749-6632.2003.tb03163.x
27. Reizes O, Benoit SC, Clegg DJ. The role of syndecans in the regulation of body weight and synaptic plasticity. *Int J Biochem Cell Biol.* (2008) 40:28–45. doi: 10.1016/j.biocel.2007.06.011
28. Chen J, Repunte-Canonigo V, Kawamura T, Lefebvre C, Shin W, Howell LL, et al. Hypothalamic proteoglycan syndecan-3 is a novel cocaine addiction resilience factor. *Nat Commun.* (2013) 4:1955. doi: 10.1038/ncomms2955
29. Patterson AM, Gardner L, Shaw J, David G, Loreau E, Aguilar L, et al. Induction of a CXCL8 binding site on endothelial syndecan-3 in rheumatoid synovium. *Arthritis Rheum.* (2005) 52:2331–42. doi: 10.1002/art.21222
30. Patterson AM, Cartwright A, David G, Fitzgerald O, Bresnihan B, Ashton BA, et al. Differential expression of syndecans and glypicans in chronically inflamed synovium. *Ann Rheum Dis.* (2008) 67:592–601. doi: 10.1136/ard.2006.063875
31. Kehoe O, Kalia N, King S, Eustace A, Boyes C, Reizes O, et al. Syndecan-3 is selectively pro-inflammatory in the joint and contributes to antigen-induced arthritis in mice. *Arthritis Res Ther.* (2014) 16:R148. doi: 10.1186/ar4610
32. Eustace AD, McNaughton EF, King S, Kehoe O, Kungl A, Mattey D, et al. Soluble syndecan-3 binds chemokines, reduces leukocyte migration *in vitro* and ameliorates disease severity in models of rheumatoid arthritis. *Arthritis Res Ther.* (2019) 21:172. doi: 10.1186/s13075-019-1939-2
33. Krempel PG, Matsuda M, Marquezini MV, Seixas TG, Ventura GM, Sholl-Franco A, et al. Bevacizumab reduces neurocan content and gene expression

in newborn rat retina *in vitro*. *Invest Ophthalmol Vis Sci.* (2014) 55:5109–15. doi: 10.1167/iovs.14-14466
34. Vuong TT, Reine TM, Sudworth A, Jenssen TG, Kolset SO. Syndecan-4 is a major syndecan in primary human endothelial cells *in vitro*, modulated by inflammatory stimuli and involved in wound healing. *J Histochem Cytochem.* (2015) 63:280–92. doi: 10.1369/0022155415568995
35. Tinholt M, Stavik B, Louch W, Carlson CR, Sletten M, Ruf W, et al. Syndecan-3 and TFPI colocalize on the surface of endothelial-, smooth muscle-, and cancer cells. *PLoS ONE.* (2015) 10:e0117404. doi: 10.1371/journal.pone.0117404
36. Ashikari-Hada S, Habuchi H, Kariya Y, Kimata K. Heparin regulates vascular endothelial growth factor165-dependent mitogenic activity, tube formation, and its receptor phosphorylation of human endothelial cells. Comparison of the effects of heparin and modified heparins. *J Biol Chem.* (2005) 280:31508–15. doi: 10.1074/jbc.M414581200
37. Robinson CJ, Mulloy B, Gallagher JT, Stringer SE. VEGF165-binding sites within heparan sulfate encompass two highly sulfated domains and can be liberated by K5 lyase. *J Biol Chem.* (2006) 281:1731–40. doi: 10.1074/jbc.M510760200
38. De Rossi G, Whiteford JR. A novel role for syndecan-3 in angiogenesis. *F1000Research.* (2013) 2:270. doi: 10.12688/f1000research.2-270.v1
39. De Rossi G, Whiteford JR. Novel insight into the biological functions of syndecan ectodomain core proteins. *BioFactors.* (2013) 39:374–82. doi: 10.1002/biof.1104
40. De Rossi G, Whiteford JR. Syndecans in angiogenesis and endothelial cell biology. *Biochem Soc Trans.* (2014) 42:1643–6. doi: 10.1042/BST20140232
41. Beauvais DM, Ell BJ, McWhorter AR, Rapraeger AC. Syndecan-1 regulates alphavbeta3 and alphavbeta5 integrin activation during angiogenesis and is blocked by synstatin, a novel peptide inhibitor. *J Exp Med.* (2009) 206:691–705. doi: 10.1084/jem.20081278
42. De Rossi G, Evans AR, Kay E, Woodfin A, McKay TR, Nourshargh S, et al. Shed syndecan-2 inhibits angiogenesis. *Development.* (2014) 141:e2207. doi: 10.1242/dev.118901
43. Jannaway M, Yang X, Meegan JE, Coleman DC, Yuan SY. Thrombin-cleaved syndecan-3/-4 ectodomain fragments mediate endothelial barrier dysfunction. *PLoS ONE.* (2019) 14:e0214737. doi: 10.1371/journal.pone.0214737
44. Braun KR, DeWispelaere AM, Bressler SL, Fukai N, Kenagy RD, Chen L, et al. Inhibition of PDGF-B induction and cell growth by syndecan-1 involves the ubiquitin and SUMO-1 ligase, Topors. *PLoS ONE.* (2012) 7:e43701. doi: 10.1371/journal.pone.0043701
45. Gill SK, Loveday C, Gilson RJ. Transmission of HIV-1 infection by oroanal intercourse. *Genitourin Med.* (1992) 68:254–7. doi: 10.1136/sti.68.4.254
46. Sullivan AK, Atkins MC, Boag F. Factors facilitating the sexual transmission of HIV-1. *AIDS Patient Care STDs.* (1997) 11:167–77. doi: 10.1089/apc.1997.11.167
47. Cameron PU, Freudenthal PS, Barker JM, Gezelter S, Inaba K, Steinman RM. Dendritic cells exposed to human immunodeficiency virus type-1 transmit a vigorous cytopathic infection to CD4+ T cells. *Science.* (1992) 257:383–7. doi: 10.1126/science.1352913
48. Xu RH, Remakus S, Ma X, Roscoe F, Sigal LJ. Direct presentation is sufficient for an efficient anti-viral CD8+ T cell response. *PLoS Pathogens.* (2010) 6:e1000768. doi: 10.1371/journal.ppat.1000768
49. van Montfoort N, van der Aa E, Woltman AM. Understanding MHC class I presentation of viral antigens by human dendritic cells as a basis for rational design of therapeutic vaccines. *Front Immunol.* (2014) 5:182. doi: 10.3389/fimmu.2014.00182
50. Smed-Sorensen A, Lore K, Vasudevan J, Louder MK, Andersson J, Mascola JR, et al. Differential susceptibility to human immunodeficiency virus type 1 infection of myeloid and plasmacytoid dendritic cells. *J Virol.* (2005) 79:8861–9. doi: 10.1128/JVI.79.14.8861-8869.2005
51. Geijtenbeek TB, Kwon DS, Torensma R, van Vliet SJ, van Duijnhoven GC, Middel J, et al. DC-SIGN, a dendritic cell-specific HIV-1-binding protein that enhances trans-infection of T cells. *Cell.* (2000) 100:587–97. doi: 10.1016/S0092-8674(00)80694-7
52. Arrighi JF, Pion M, Wiznerowicz M, Geijtenbeek TB, Garcia E, Abraham S, et al. Lentivirus-mediated RNA interference of DC-SIGN expression inhibits human immunodeficiency virus transmission from dendritic cells to T cells. *J Virol.* (2004) 78:10848–55. doi: 10.1128/JVI.78.20.10848-10855.2004
53. Turville SG, Cameron PU, Handley A, Lin G, Pohlmann S, Doms RW, et al. Diversity of receptors binding HIV on dendritic cell subsets. *Nat Immunol.* (2002) 3:975–83. doi: 10.1038/ni841
54. de Witte L, Nabatov A, Pion M, Fluitsma D, de Jong MA, de Gruijl T, et al. Langerin is a natural barrier to HIV-1 transmission by Langerhans cells. *Nat Med.* (2007) 13:367–71. doi: 10.1038/nm1541
55. Granelli-Piperno A, Pritsker A, Pack M, Shimeliovich I, Arrighi JF, Park CG, et al. Dendritic cell-specific intercellular adhesion molecule 3-grabbing nonintegrin/CD209 is abundant on macrophages in the normal human lymph node and is not required for dendritic cell stimulation of the mixed leukocyte reaction. *J Immunol.* (2005) 175:4265–73. doi: 10.4049/jimmunol.175.7.4265
56. Gummuluru S, Rogel M, Stamatatos L, Emerman M. Binding of human immunodeficiency virus type 1 to immature dendritic cells can occur independently of DC-SIGN and mannose binding C-type lectin receptors via a cholesterol-dependent pathway. *J Virol.* (2003) 77:12865–74. doi: 10.1128/JVI.77.23.12865-12874.2003
57. Gurney KB, Elliott J, Nassanian H, Song C, Soilleux E, McGowan I, et al. Binding and transfer of human immunodeficiency virus by DC-SIGN+ cells in human rectal mucosa. *J Virol.* (2005) 79:5762–73. doi: 10.1128/JVI.79.9.5762-5773.2005
58. Geijtenbeek TB, Torensma R, van Vliet SJ, van Duijnhoven GC, Adema GJ, van Kooyk Y, et al. Identification of DC-SIGN, a novel dendritic cell-specific ICAM-3 receptor that supports primary immune responses. *Cell.* (2000) 100:575–85. doi: 10.1016/S0092-8674(00)80693-5
59. de Witte L, Bobardt M, Chatterji U, Degeest G, David G, Geijtenbeek TB, et al. Syndecan-3 is a dendritic cell-specific attachment receptor for HIV-1. *Proc Natl Acad Sci USA.* (2007) 104:19464–9. doi: 10.1073/pnas.0703747104
60. Hamimi C, David A, Versmisse P, Weiss L, Bruel T, Zucman D, et al. Dendritic cells from HIV controllers have low susceptibility to HIV-1 infection *in vitro* but high capacity to capture HIV-1 particles. *PLoS ONE.* (2016) 11:e0160251. doi: 10.1371/journal.pone.0160251
61. Beauvais DM, Burbach BJ, Rapraeger AC. The syndecan-1 ectodomain regulates alphavbeta3 integrin activity in human mammary carcinoma cells. *J Cell Biol.* (2004) 167:171–81. doi: 10.1083/jcb.200404171
62. Woods A, Longley RL, Tumova S, Couchman JR. Syndecan-4 binding to the high affinity heparin-binding domain of fibronectin drives focal adhesion formation in fibroblasts. *Archiv Biochem Biophys.* (2000) 374:66–72. doi: 10.1006/abbi.1999.1607
63. Corti F, Wang Y, Rhodes JM, Atri D, Archer-Hartmann S, Zhang J, et al. N-terminal syndecan-2 domain selectively enhances 6-O heparan sulfate chains sulfation and promotes VEGFA165-dependent neovascularization. *Nat Commun.* (2019) 10:1562. doi: 10.1038/s41467-019-10205-0

Conflict of Interest: The authors declare that the research was conducted in the absence of any commercial or financial relationships that could be construed as a potential conflict of interest.

frontiers in Immunology

ORIGINAL RESEARCH
published: 09 January 2020
doi: 10.3389/fimmu.2019.03019

Adherence of *Lactobacillus salivarius* to HeLa Cells Promotes Changes in the Expression of the Genes Involved in Biosynthesis of Their Ligands

Carla Martín[1,2,3], *Iván Fernández-Vega*[2,3,4], *Juan E. Suárez*[1] *and Luis M. Quirós*[1,2,3]*

[1] *Área de Microbiología, Universidad de Oviedo, Oviedo, Spain,* [2] *Instituto Universitario Fernández-Vega, Universidad de Oviedo, Oviedo, Spain,* [3] *Instituto de Investigación Sanitaria del Principado de Asturias, Oviedo, Spain,* [4] *Hospital Universitario Central de Asturias, Oviedo, Spain*

The attachment of a variety of *Lactobacilli* to the mucosal surfaces is accomplished through the interaction of OppA, a superficial bacterial protein also involved in oligopeptide internalization, and the glycosaminoglycan moiety of the proteoglycans that form the epithelial cell glycocalyx. Upon the interaction of the vaginal isolate *Lactobacillus salivarius* Lv72 and HeLa cell cultures, the expression of *oppA* increased more than 50-fold over the following 30 min, with the overexpression enduring, albeit at a lower rate, for up to 24 h. Conversely, transcriptional analysis of 62 genes involved in proteoglycan biosynthesis revealed generalized repression of genes whose products catalyze different steps of the whole pathway. This led to decreases in the superficial concentration of heparan (60%) and chondroitin sulfate (40%), although the molecular masses of these glycosaminoglycans were higher than those of the control cultures. Despite this lowering in the concentration of the receptor, attachment of the *Lactobacilli* proceeded, and completely overlaid the underlying HeLa cell culture.

Keywords: bacterial adherence, glycosaminoglycan, OppA, *Lactobacillus*, proteoglycan, heparan sulfate, chondroitin sulfate

OPEN ACCESS

Edited by:
Megan S. Lord, University of New South Wales, Australia

Reviewed by:
Shuji Mizumoto, Meijo University, Japan
Hala Chaaban, University of Oklahoma Health Sciences Center, United States

***Correspondence:**
Luis M. Quirós
quirosluis@uniovi.es

Specialty section:
This article was submitted to Cytokines and Soluble Mediators in Immunity, a section of the journal Frontiers in Immunology

Received: *01 October 2019*
Accepted: *10 December 2019*
Published: *09 January 2020*

Citation:
Martín C, Fernández-Vega I, Suárez JE and Quirós LM (2020) Adherence of Lactobacillus salivarius to HeLa Cells Promotes Changes in the Expression of the Genes Involved in Biosynthesis of Their Ligands. Front. Immunol. 10:3019. doi: 10.3389/fimmu.2019.03019

INTRODUCTION

The organisms included in the genus *Lactobacillus* belong to the Filum Firmicutes. They are anaerobic, usually aerotolerant, bacteria that ferment sugars to lactic and other organic acids which are also auxotrophic for many essential nutrients. The genus comprises 241 species, according to the List of Prokaryotic Names with Standing in Nomenclature (July, 2019) and it is polyphyletic, to the extent that its division into 10 or 16 different genera, on the basis of their genome characteristics, has been proposed (1–3). *Lactobacilli* occupy many different habitats, ranging from the physical environment, where they behave as saprophytes, to the fact that they constitute a substantial part of the starter microbiota involved in food and feed fermentation, as well as being present within human body cavities, where they are an important part of the autochthonous microbiota. In the latter scenario, the lactic acid, H_2O_2 and bacteriocins produced by resident *Lactobacilli* protect the internal cavities from infection, while enhancing immune system maturation and tightening the boundaries between the epithelial cells that line the mucosa. This "microbial antagonism" is also based on *Lactobacilli*'s specific adherence to the mucosal surfaces, where they form biofilms that preclude pathogens coming into contact with epithelial cells (4–6).

There is some degree of specificity between the different body cavities and the species of *Lactobacilli* that thrive in each of them, and this preference depends not only on environmental conditions, but also on the ability of the bacterium to adhere to each mucosal surface (7). Attachment depends on the specific recognition between adhesins located on the exterior of the bacteria and the receptors that protrude from epithelial cells, and a variety of adhesins have been described for *Lactobacilli* (8–11). In addition, a variety of surface proteins have been found to act as adhesins, such as those that bind to mucus through the so called Mub-repeats (12), some of which depend on sortase-driven anchoring to the bacterial surface (13). Finally, some cytoplasmic proteins appear to reach the bacterial surface and behave as adhesins, in spite of them not presenting discernible membrane-translocating motives. Among them are the glycolytic enzymes glyceraldehyde 3-P-dehydrogenase (14, 15), enolase (16), and pyruvate dehydrogenase (17) and the protein synthesis factors EF-Tu (18) and GroEL (19).

The receptors to which *Lactobacilli* adhesins attach are part of the cells or the extracellular matrix present in the epithelium. The latter is made of polysaccharides (hyaluronic acid), fibrillar proteins of the collagen family and fibronectin (5, 20), and glycoproteins, with mucins and proteoglycans (PGs) being the most abundant. PGs are complex macromolecules whose core is made of specific proteins that, in turn, determine their location—either in the cell or at the extracellular matrix—and is covalently bound to glycosaminoglycans (GAGs). These are linear heteropolysaccharides consisting of repeating disaccharide units made of amino and uronic monosaccharides or galactose to which sulfate groups may be attached (21). Heparan sulfate proteoglycans (HSPGs) are usually the most prevalent GAG at the cell surface and in the pericellular matrix, and their structures may include not only heparan sulfate (HS), but also chondroitin sulfate (CS) moieties. Synthesis of HS and CS chains occurs mainly in the Golgi apparatus, and starts by the joining of a xylose to a specific serine residue on the core protein, followed by the successive addition of two galactoses and one glucuronic acid. The addition of the following residue determines the type of GAG that will be synthesized: *N*-acetylglucosamine will produce HS, while *N*-acetylgalactosamine leads to CS. The elongation of the chain is catalyzed by a series of enzymes that specifically recognize the sugars to be incorporated and act in a coordinated fashion. Finally, discrete regions of the polysaccharide may be modified through various reactions, including *N*-sulfation, epimerization and various *O*-sulfations (21). The specific combination of reactions that take place on each disaccharide gives rise to molecules with great structural diversity, resulting in them being able to interact with many biological ligands by means of the high affinity sequences they have for them. These interactions make PGs essential in the control of many biological processes, including organogenesis, cell junction, cell signaling or wound healing, among other functions (22).

Abbreviations: CS, chondroitin sulfate; GAG, glycosaminoglycan; HS, heparan sulfate; HSPG, Heparan sulfate proteoglycan.

In previous communications we reported that soluble GAGs antagonized the attachment of *L. salivarius* Lv72 and other *Lactobacilli* to epithelial cell cultures. Moreover, we found that heparin recognized a component of the external proteomes of *Lactobacilli* that turned out to be the oligopeptide-binding protein OppA (23), which is the surface component of an ATP-binding cassette (ABC) previously described as being involved in oligopeptide internalization (24). OppA modeling revealed the presence of a groove on its surface whose diameter matched the width of GAG-chains. The introduction of mutations on triplets encoding positively charged amino acids located on the vicinity of the groove blocked binding, thus confirming the role of OppA as a *Lactobacilli* adhesin, and that of GAGs, especially HS, as being its receptor on the mucosal surface (23–26).

These data suggest that the mutualistic relation established between mucosal surfaces and resident *Lactobacilli* is partially dependent on the specific interaction between OppA and the GAGs that cover the epithelial cells, mainly HS chains. Given this premise, we postulated that contact between the two cell types might induce changes in the expression of the genes encoding the bacterial adhesins, thus affecting their superficial concentrations. Moreover, considering that cells exercise exquisite control over both the composition and sequencing of HSPG in response to physiological and pathological changes, these changes might occur as part of the response of the epithelial cells to their interaction with the microbiota. This might result in tightening the bacterial and epithelial layers and in the efficient exclusion of undesirable microorganisms. The data obtained from the analysis of the molecular events resulting from the contact of both cell types are reported in this communication.

MATERIALS AND METHODS

Bacterial Strain, Eukaryotic Cell Line, and Growth Conditions

Lactobacillus salivarius Lv72 and HeLa cell cultures (ATCC CCL-2) were propagated in MRS medium (Becton, Franklin Lakes, USA) and Dulbecco's Modified Eagle's minimal essential medium (DMEM) (GibcoBRL, Eragny, France) supplemented with 10% (w/v) fetal bovine serum (GibcoBRL), respectively, as previously described (23).

Total RNA Isolation From Pure and Mixed *L. salivarius* Lv72/HeLa Cell Cultures and cDNA Synthesis

Confluent HeLa cell cultures in 25 cm^2 tissue culture flasks (Nunc, Roskilde, Denmark) were washed twice with DMEM and a suspension of freshly prepared exponentially growing *L. salivarius* Lv72 in the same medium was added (10^7 cells/ml, final concentration) and incubated for 1 h at 37°C under a 5% CO_2 atmosphere. Controls were treated in the same way except that only the sterile medium was added in the final step. The supernatants were discarded, and the cell cultures were washed twice with DMEM and overflowed with 12 ml of the same medium. Samples were taken at 10, 20, and 30 min and at 1, 2, 4, 6, and 24 h and subjected to RNA

extraction using the RNeasy kit (Qiagen; Hilden, Germany), following the manufacturer's specifications. To ensure removal of residual contaminating DNA, the samples were subjected to treatment with RNase-free DNase. The concentration of RNA was determined by measuring the absorbance at 260 nm. Aliquots of the samples were stored at −80°C until their future use. Synthesis of cDNA was carried out using the High Capacity cDNA Transcription Kit (Applied BioSystems; Foster City, CA) following the manufacturer's instructions. The reactions were performed in an iCycler IQ thermocycler (BioRad; Hercules, CA) using 2 μg RNA as substrate. The reaction products were cleaned using the PCR Clean-Up GenElute kit (Sigma-Aldrich, St. Louis, USA) as recommended by the provider. Finally, the aliquots containing the cDNA were diluted 1:20 with water and stored at −20°C until use. The data on eukaryotic gene expression throughout this paper were obtained from 24 h post-exposition samples since no significant differences compared to controls could be detected after shorter periods.

qRT-PCR Reactions

qRT-PCR reactions, and analysis of amplimer products were carried out according to the methods already detailed (27). Primers corresponding to the human and *Lactobacilli* versions of the glyceraldehyde 3-P-dehydrogenase genes were included on each plate as controls to monitor run variations and to normalize individual gene expression. The primer sequences used are detailed in **Supplemental Table 1**. The comparison of the individual sets of results corresponding to each experiment with respect to the results of its corresponding control was carried out using a Mann-Whitney *U*-test.

Immunohistochemistry

HeLa cells were propagated on culture microscope slides under the conditions described above. After incubation for 24 h, the cultures were washed three times with phosphate buffered saline (PBS), fixed with acetone for 20 min at −20°C, washed with the same buffer and incubated overnight at 4°C with appropriate dilutions of the primary antibodies (**Table 1**). The slides were then washed for 30 min with PBS, placed in the dark and incubated with the secondary antibodies (**Table 1**) for 90 min in a humid chamber. The samples were washed three times with PBS and incubated successively with 1 μg/ml phalloidin-TRITC conjugate (Sigma-Aldrich) for 90 min and 10 ng/ml DAPI (Southern Biotech; Birmingham, USA). The preparations were visually examined and photographed in a Leica DMR-XA fluorescence microscope coupled to Leica Qfluoro software in the Image Processing facility of the University of Oviedo. The quantification of fluorescence for the subsequent statistical analysis was carried out using ImageJ analysis software (28).

Adherence Assays

HeLa cell cultures grown on microscope slides were washed three times with DMEM on its own, after which a suspension of exponentially growing *L. salivarius* Lv72 suspended in the same medium was added to the slides (10^9 bacteria/ml, final concentration) and they were incubated for up to 24 h at 37°C under a 5% CO_2 atmosphere in a humid chamber. The supernatant was discarded, the slides were washed twice with PBS and the degree of adherence was established using immunochemical detection (see above) using OppA-specific primary antibodies.

TABLE 1 | Antibodies and dilution used.

Antigen	Species of origin	Dilution	Supplier
Syndecan 1 (CD138)	Mouse	1:100	Dakocytomation
Syndecan 2	Rabbit	1:250	Santa cruz biotechnology
Syndecan 3	Goat	1:50	Santa cruz biotechnology
Glypican 1	Rabbit	1:100	Thermoscientific
Perlecan	Rabbit	1:100	Santa cruz biotechnology
Agrin	Goat	1:100	Santa cruz biotechnology
TGFβ RIII	Mouse	1:100	Santa cruz biotechnology
HS (10E4 epitope)	Mouse	1:100	Amsbio
CS (Clone CS-56)	Mouse	1:100	Sigma-aldrich corp
OppA rabbit	Rabbit	1:100	Obtained from our own lab
Alexa Fluor 488	Goat anti-rabbit	1:200	Invitrogen
Alexa Fluor 488	Donkey anti-mouse	1:500	Invitrogen
Cy3	Donkey anti-mouse	1:50	Jackson immunoresearch laboratories
Cy3	Monkey anti-goat	1:100	Santa cruz biotechnology

Purification and Determination of GAGs

For the extraction of GAGs, HeLa cell cultures were kept pure or in contact with *L. salivarius* Lv72 for 24 h as explained above. After removing the medium by aspiration, the cell monolayers were washed with PBS. Next, 6 ml of 50 mM Tris-HCl buffer pH 8 containing 6 M guanidine chloride (Sigma-Aldrich) and 3 mM dithiothreitrol (DTT) (Sigma-Aldrich) were added and incubated with stirring at 60°C for 1 h. Subsequently, 15 ml of 50 mM Tris-HCl pH 8 containing 6.7 mM calcium chloride (Merck) and 50 μl of 1 mg/ml proteinase K (Sigma-Aldrich) were added, and the contents of the plates were extracted and incubated at 56°C for 16 h. GAGs were precipitated with 85% ethanol for a minimum of 2 h at −80°C, and collected by centrifugation at 4,000 rpm for 30 min at 4°C. The sediments were dried and resuspended in 2 ml of 10 mM phosphate buffer pH 6.8 containing 5 mM $CaCl_2$ and 20 μl of 1 mg/ml DNAse (Sigma-Aldrich), followed by incubation for 4 h at 37°C. Then, NaOH and $NaBH_4$ were added to the extracts to a final concentration of 0.2 M and 50 mM, respectively, and they were incubated at room temperature for 18 h. Next, the pH was equilibrated with 500 μl of 2 M HCl and 200 μl of 1 M sodium acetate for each ml of solution, and the samples were centrifuged at 4,000 rpm for 30 min at 4°C. The supernatant was collected, and the GAGs were precipitated again with 85% ethanol and resuspended in H_2O.

The purification of HS and CS chains was carried out by digestion with bacterial lyases. The CS was obtained by digesting the mixture of GAGs overnight at 37°C with a mixture of heparinase I, II, and III (Sigma-Aldrich) at a final concentration of 500 mU/ml each, in 0.1 M sodium acetate buffer pH 6.8 containing 10 mM NaCl. The HS was isolated by degradation with chondroitinase ABC (Sigma-Aldrich) at a

final concentration of 250 mU/ml in 50 mM Tris-HCl buffer pH 8 for 3 h at 37°C. In both cases, the resulting polysaccharide chains were obtained by precipitation with 85% ethanol at −80°C for 2 h.

The determination of GAG concentrations was carried out through spectrophotometry of their adducts with 1,9-dimethyl-methylene blue as previously reported (29).

GAG Analysis by Molecular Exclusion Chromatography

GAGs were labeled with 0.1 mg/ml FITC in 0.1 M sodium carbonate buffer pH 9, for 18 h at 4°C in the dark with shaking (30). Unreacted FITC was removed by precipitation with 85% ethanol for 2 h at −80°C, followed by centrifugation at 4,000 rpm for 20 min at 4°C. The sediment was resuspended in 0.1 M sodium carbonate buffer pH 9, and the precipitation was repeated until no FITC residues remained in the supernatant. Finally, the precipitate was resuspended in 300 µl of 50 mM phosphate buffer pH 7.2 containing 150 mM NaCl. Two-hundred microliter of each sample was subjected to molecular exclusion chromatography using a 10/300 Superose 12 column previously equilibrated in 50 mM phosphate buffer pH 7.2 and 150 mM NaCl, connected to a FPLC ÄKTA Design system (GE Healthcare, Chicago, USA). The column was eluted with a flow of 0.3 ml / min, and 0.5 ml fractions were collected. Aliquots of 350 µl of each of the fractions were added to a fluorescence plate (Nunc). Fluorescence was measured in a PerkinElmer LS55 fluorimeter (PerkinElmer, Waltham, Massachusetts, U.S.A), using wavelengths of 488 nm for excitation and 560 nm for emission.

RESULTS

Differential Expression of the Genes That Encode the Proteoglycan Core Proteins

Our previous studies have shown that HS chains present in HeLa cells play a prominent role in its interaction with *Lactobacilli* adhesins and the consequent adherence of the microorganism. Only a limited number of genes encode the core proteins of HSPGs, three of which, perlecan, agrin and collagen, encode molecules located in the extracellular matrix. The remaining HSPGs are all molecules located in the cell, mostly on the cell surface, although serglycin is found intracellularly.

Analysis of the core protein transcrips synthesized by HeLa cells in either pure culture or after their interaction with *L. salivarius* Lv72 (mixed cultures), revealed no expression of genes *GPC3*, *GPC4,* and *GPC6* among those that encode glypican isoforms. Conversely, the genes *GPC1*, *GPC2,* and *GPC5* were expressed under both conditions, although *GPC1* mRNA appeared underexpressed around 70% in mixed with respect to pure HeLa cell cultures. All four genes encoding syndecans were found to be expressed, although with significant reductions of 80, 70, and 70% for *SDC1*, *SDC2,* and *SDC3*, respectively in mixed cultures. Similar expression attenuations were found for the genes that encode the core proteins of perlecan (*PRCAN*), agrin (*AGRN*), and betaglycan (*TGFBR3*), while no changes were evidenced in the expression of *COL18A1* (collagen XVIII), *CD44v3* (CD44 isoform 3), and *SRGN* (serglycin) (**Figure 1A**).

When some of these changes were analyzed by immunohistochemistry, it was observed that the label intensity of syndecan 2, syndecan 3, glypican 1, perlecan and agrin decreased, the results being statistically significant ($p < 0.001$ in all cases). This therefore confirmed that differences in transcription correlated with net decreases in protein levels. In the case of betaglycan, no significant staining difference was observed in the presence of the microorganism ($p = 0.1$). However, in contrast to what was observed at the transcription level, the immunostaining of syndecan 1 significantly increased after the adhesion of lactobacillus ($p < 0.01$) (**Figure 1B**).

Comparison Between the Expression of the Determinants That Encode GAG Polymerization Enzymes

The proteins encoded by *XYLT1* and *XYLT2* catalyze the union of a xylose residue to the hydroxyl group of specific serine residues that form part of the core protein. This xylose unit can be phosphorylated by the product of *FAM20*, which appears to be involved in regulation of GAG synthesis. Next, biosynthesis continues through the successive addition of two galactose residues, both reactions being catalyzed by enzymes encoded by *B4GALT7* and *B4GALT6.* Finally, a tetrasaccharide, typical of HS and CS, is formed through the linking of glucuronic acid, which is mediated by the products of any of the three isoforms of *B3GAT1-3*, although in this study it was mainly transcripts of *B3GAT3* that were detected. Transcription of all these genes, with the exception of *B3GAT3*, were reduced by between 50 and 90% in HeLa cell cultures previously incubated with *L. salivarius* Lv72 (**Figure 2A**).

Further polymerization, in the case of HS, depends on the activity of an *N*-acetylglucosamine transferase (EXTL1-3) and of the copolymerases 1 and 2 (EXT1 and EXT2), which incorporate alternating glucuronic acid and *N*-acetylglucosamine residues to the growing chain. In the case of CS, elongation is initiated by the incorporation of an *N*-acetylgalactosamine (CSGALNACT1-2) followed by alternate additions of glucuronic acid and *N*-acetylgalactosamine, which are catalyzed by CS synthetase 1 and 3 (CHSY1 and CHSY3) and enhanced by the CS polymerization factor (CHPF). While expression of most of these genes was not significantly changed as a function of the contact of *L. salivarius* Lv72 with the HeLa cell cultures, the transcript concentrations of *EXTL3* and *EXTL2* and *CHPF* from the polymerization routes of HS and CS dropped by 50 and 70%, respectively (**Figure 2A**).

Differential Expression of the Genes That Mediate HS Modification

The fine structure of HS can change through *N*-deacetylation/*N*-sulfation in reactions catalyzed by bifunctional *N*-deacetylases/*N*-sulfotransferases encoded by genes *NDST1* to *NDST4.* In addition, glucuronic acid epimerization may generate iduronic acid (GLCE), which is sometimes followed by *O*-sulfation in position 2 of this residue (HS2ST1), and *O*-sulfations in positions 6

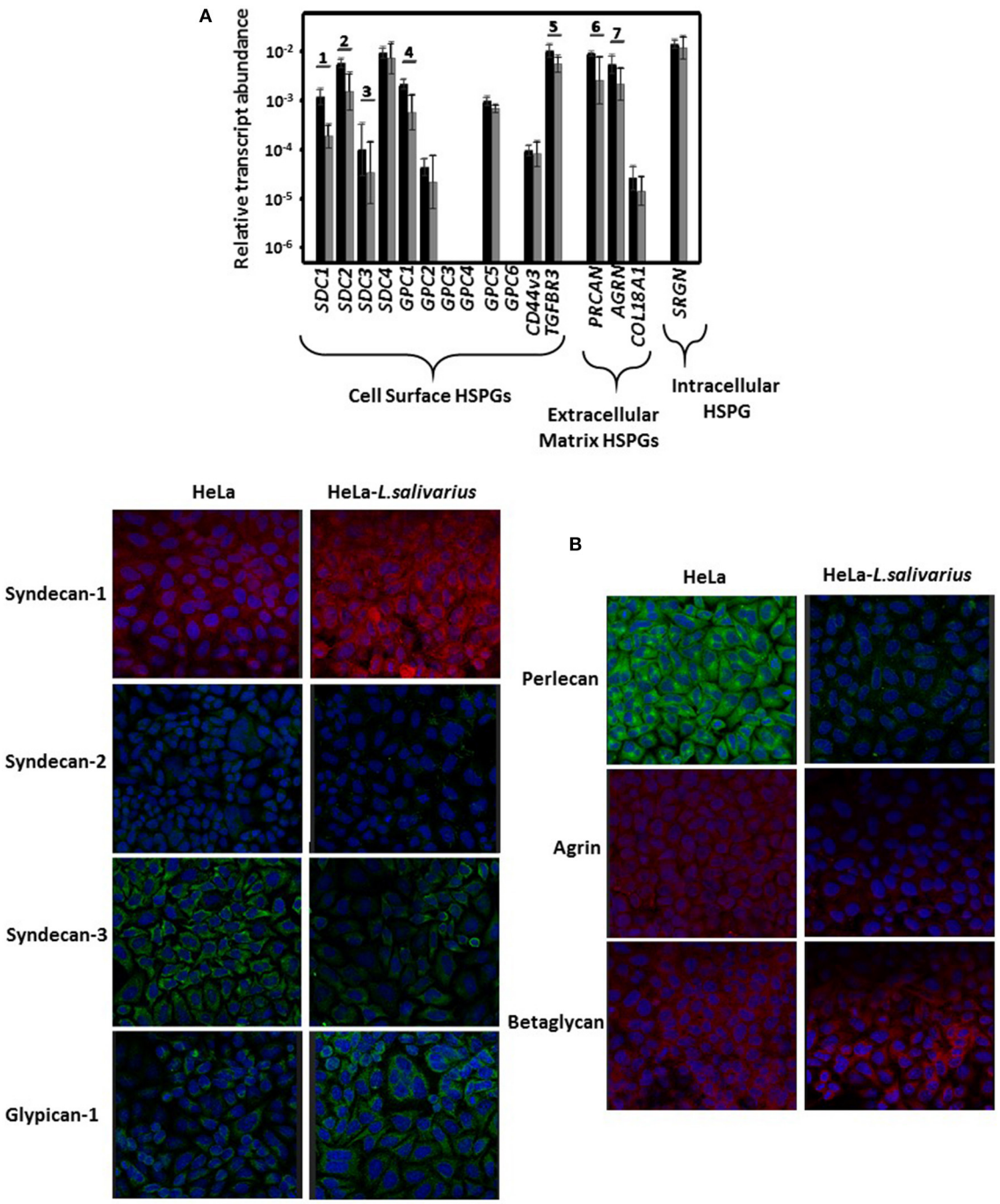

FIGURE 1 | Differential expression of the proteoglycan core proteins. **(A)** Differential expression of the genes that encode the PG core proteins of HeLa cells in pure culture (black bars) and after having been incubated for 1 h with *L. salivarius* Lv72 (gray bars). Note that the ordinates scale is logarithmic. Statistically significant differences ($p < 0.01$) are indicated by numbers. The data are the combined results of at least four independent determinations. **(B)** Immunolocalization of PGs in pure HeLa cell cultures (left) or those previously incubated with *L. salivarius* (right). The quantification of fluorescence using ImageJ analysis software and subsequent statistical analysis gave rise to significant results for syndecan 1 ($p < 0.01$), syndecan 2, syndecan 3, glypican 1, perlecan and agrin ($p < 0.001$ in all cases), but not for betaglycan ($p = 0.1$).

(HS6ST1 to HS6ST3) and 3 (HS3ST1 to HS3ST6) of the glucosamine residue. Following export from the cell, HS can be processed by heparanase (HPSE), an endo-β-D-glucuronidase that generates 10–20 residue oligosaccharides; a second isoform exists (HPSE2) which has no enzymatic activity but does have regulatory capacity. HS chains can also be desulfated through the action of two extracellular sulfatases (SULF1, SULF2).

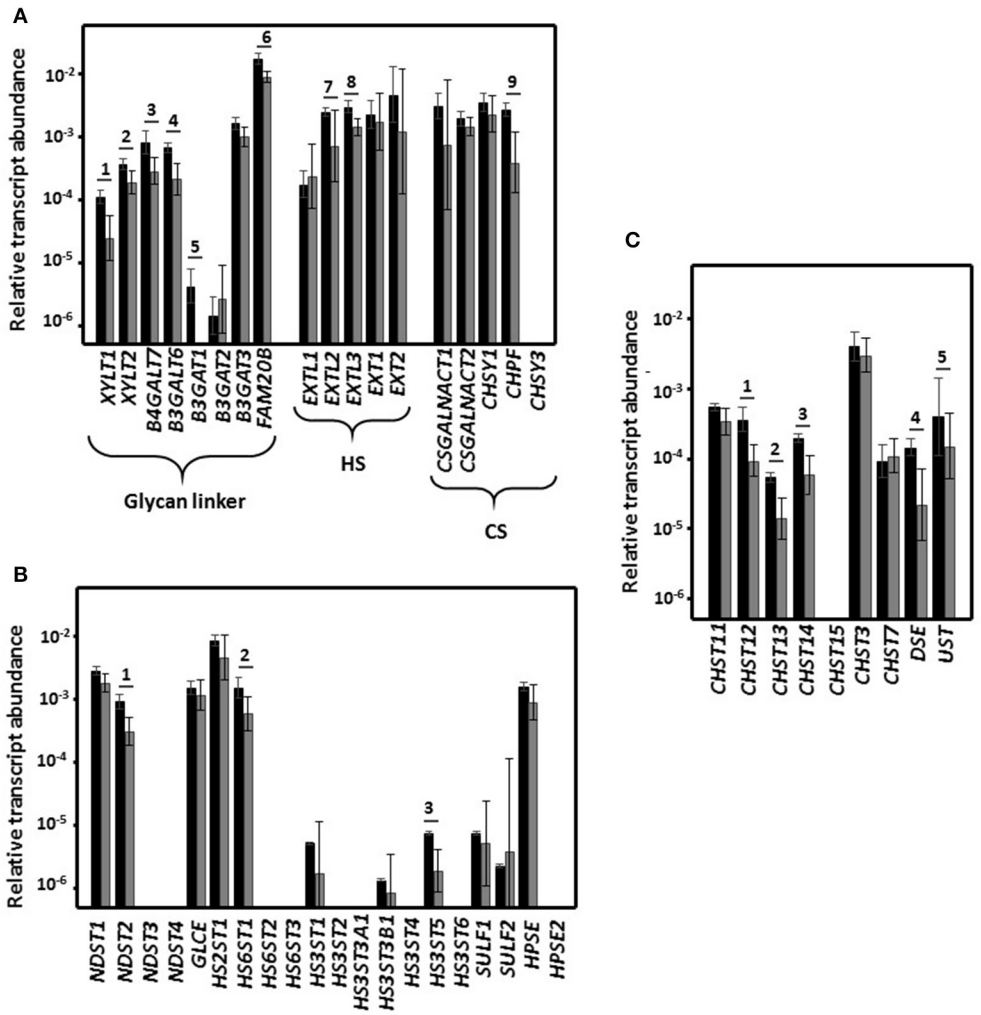

FIGURE 2 | Differential expression of the genes that encode the enzymes involved in the biosynthesis of GAGs. **(A)** Differential expression of genes encoding glycosyltransferases involved in common linkage region sequence and GAG chain synthesis. **(B)** Differential expression of genes involved in the modification of HS chains. **(C)** Differential expression of genes involved in the modification of CS chains. Relative transcript abundance of mRNAs for HeLa pure culture (black bars) and after HeLa cells were incubated for 1 h with *L. salivarius* Lv72 (gray bars) are plotted on a log scale for each gene assayed and the spreads represent standard deviations. Statistically significant differences ($p < 0.01$) are indicated by numbers. The data are the result of at least four independent determinations.

Of the 20 genes involved in HS structural fine-tuning, almost half were not expressed by the HeLa cell cultures under the experimental conditions in this work. Most of the remainder did not significantly change their expression level in response to contact with *L. salivarius* Lv72, although a reduction was observed for three genes, namely *NDST2*, *HS6ST1,* and *HS3ST5* (**Figure 2B**).

Differential Expression of the Genes That Mediate Chondroitin Sulfate Modification

The reactions that lead to CS diversification include 4-*O*-sulfation (CHST11 to CHST14) and 6-*O*-sulfation (CHST3, CHST7, and CHST15) of *N*-acetylgalactosamine, epimerization of the glucuronic acid in position 5 to iduronic acid (DSE) to give dermatan sulfate, and 2-*O*-sulfation of this residue (UST). The expression of five of these nine determinants was lower when HeLa cells had been in contact with the *Lactobacilli*, the drop ranging from 60 to 75% (**Figure 2C**).

Characterization of Glycosaminoglycans as a Function of the Interaction Between HeLa Cells and *L. salivarius* Lv72

The alterations observed in the expression of the genes responsible for the synthesis of GAGs in HeLa cells that had been in contact with *L. salivarius* Lv72 suggest that both the quantitative levels of these saccharide chains and their structural features (chain size and sulfation pattern) might be affected. To carry out quantifications, GAGs were extracted from cell cultures and their concentrations were determined through

the spectrophotometry of their adducts using 1,9-dimethylmethylene blue. The results showed significant reductions of more than 60% for HS and close to 40% for CS after the HeLa cell cultures were incubated with the bacterium (**Figure 3A**). Chain size characterization was performed by molecular exclusion chromatography. The data obtained showed a shift toward higher molecular weights, with the change for HS being greater than that for CS (**Figure 3B**).

The visualization of the chains of both GAGs in cell cultures was carried out by immunohistochemistry, using monoclonal antibodies against specific epitopes. 10E4 is a native HS epitope that includes *N*-sulfated glucosamine residues, and the monoclonal antibody CS-56, which was used to detect CS chains, reacts preferentially with CS-D (sulfated at C-2 and C-6) although it is also able to recognize other types of structures, including CS-A, -C, and -E (31). The results showed a decrease in the immunolabelling of HS after contact with the *Lactobacilli* ($p < 0.05$), while in the case of CS, no significant differences were observed ($p = 0.12$) (**Figure 3C**).

Differential Expression of *L. salivarius* Lv72 *oppA*

Interaction with HeLa cell cultures provoked the sustained enhancement of *oppA* expression by *L. salivarius* Lv72 with values reaching a more than 50-fold increment after between 30 min and 6 h of co-incubation. Even 24 h later the transcription of *oppA* from the *Lactobacilli* was several times higher than in pure bacterial cultures (**Figure 4A**).

L. salivarius does not proliferate in DMEM devoid of bovine fetal serum, as evidenced by the lack of increase over time in the viable counts of the cultures or the phenol red pH-dependent color change. The presence of OppA on its surface and the subsequent adherence of *L. salivarius* to HeLa cell cultures was followed by immunochemical detection for 24 h using OppA-specific as primary antibodies. As can be observed in **Figure 4B**, adherence of *L. salivarius* Lv72 gradually increased such that 24 h after incubation the HeLa cells were completely covered, as would be expected from the enhancement of *oppA* expression that occurred upon mixing the two cell types.

DISCUSSION

Lactobacilli are important members of the autochthonous microbiota, colonizing a variety of internal human cavities. In addition, *Lactobacilli* constitute the bulk of the human vaginal microbiota, this clearly being a very recent evolutionary accomplishment given that it does not colonize the vagina of any other mammal, not even the large primates (32). A variety of bacterial adhesins and eukaryotic receptors have been found to mediate the attachment of *Lactobacilli* to the mucosal surfaces. Among them, the mutual recognition between OppA and GAGs that are part of the epithelial glycocalix appears to play a significant role and several lines of evidence support this (23, 25, 26). The benefits linked to the mutualism derived from the interaction between *Lactobacilli* and the human mucosa suggest that both participants might have evolved mechanisms to strengthen their initial casual contact in order to stabilize their symbiotic relationship.

The existence of an inducible system to promote adherence was evident for the *Lactobacilli*, as observed in the enormous increase in *oppA* transcription upon contact of the bacterium with HeLa cell layers. In addition, this induction appeared to be long-lived in that it remained at the same level for 6 h post-contact, and even 24 h after co-incubation the generation of *oppA*-specific RNA was enhanced several-fold with respect to that of the pure *L. salivarius* Lv72 cultures used as controls. This finding suggests that induction of *oppA* might last for as long as the bacterium and the mucosal cells remain together. On the other hand, the initial promotion of the attachment appears to be delayed, despite the fast and intense transcriptional response of the bacterium, because it was seen to develop gradually over a period of several hours. This indicates that translation of the transcripts and export of the resulting polypeptides to the bacterial surface is a slow process. In this respect, it should be highlighted that *oppA* was initially described as the substrate recognition component of an oligopeptide ABC-transporter comprised of two additional and homologous integral membrane proteins (OppB and OppC), which form the translocation pore, and two cytoplasm proteins (OppD and OppF), which drive the transport process through binding and hydrolysis of ATP (24). It could be that export of OppA is dependent on the formation of the ABC-transport complex, which would probably account for the delay in its accumulation on the bacterial surface. This might have some advantages for *Lactobacilli*, since they are multiauxotrophic and could benefit from the putative increment of oligopeptide internalization, especially in a protein rich environment such as the epithelial glycocalyx. Alternatively, OppA might be secreted, which raises the question of how it would remain bound to the bacterial wall and exposed to the environment. Moreover, the Opp-ABC transporters have been implicated in the recognition of the oligopeptides involved in quorum sensing (bacterial pheromones) (33) that mediate diverse *Lactobacilli*-driven processes, some of which, such as the production of bacteriocins (34), the ability to form biofilms (35), and adherence to epithelial surfaces (36) might contribute to their beneficial role.

Most HSPGs appear associated with the cell surface, the two most important gene families being syndecans and glypicans, although other minor or "part time" species, such as betaglycan and CD44v3 isoform, may also appear. Apart from serglycin, which is located intracellularly, the other species are closely associated with the surface of many cell types, being located principally in the pericellular region or in basement membranes (37). *Lactobacilli* adhesion to HeLa cells induces a decrease in transcription in more than 50% of the HSPG species expressed. This reduction particularly affects the syndecans, which constitute the main group of molecules present on the cell surface of HeLa cells the isoforms of 3 of which appear underexpressed. This result is particularly interesting because in certain studies it has been described that syndecans, acting cooperatively, are primarily responsible for bacterial adhesion, as occurs in gastric epithelial cells and macrophages (38) and in corneal epithelial cells (39). Another implication of this result is

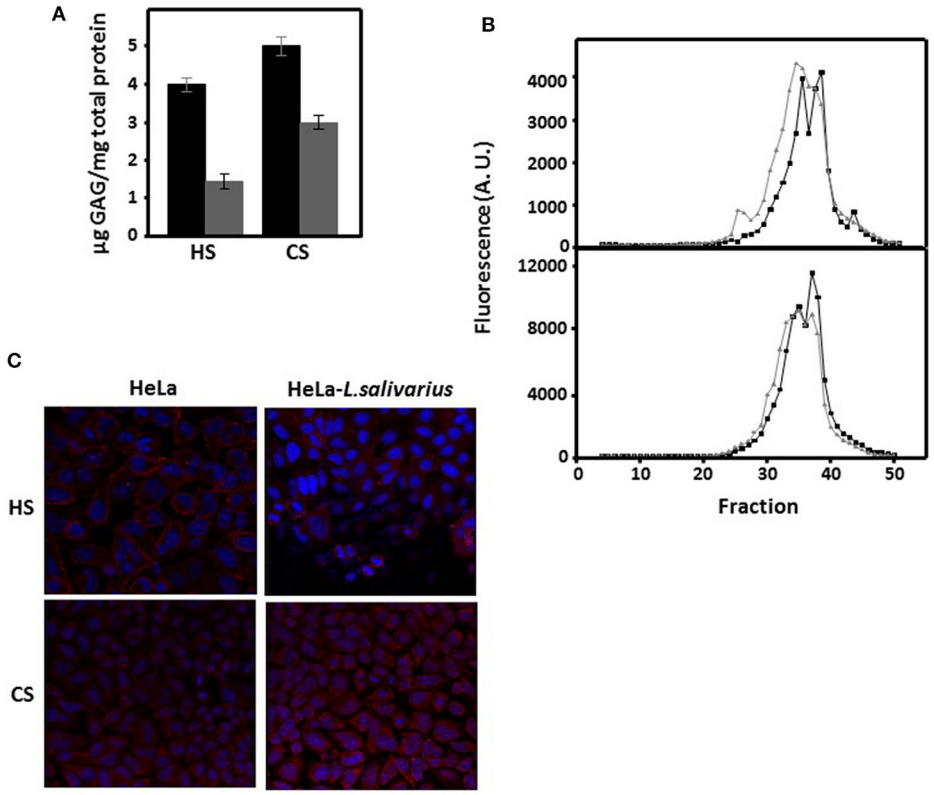

FIGURE 3 | Characterization of GAGs as a function of the interaction between HeLa cells and *L. salivarius* Lv72. **(A)** Quantification of HS and CS extracted from the surface of pure HeLa cell cultures (black bars) or those previously incubated with *L. salivarius* Lv72 (gray). The differences are statistically significant ($p < 0.001$ for HS) and ($p < 0.01$ for CS). The data are the result of at least four independent determinations. **(B)** Molecular exclusion chromatography of the HS (upper panel) and CS (bottom panel) chains extracted from the surface of pure HeLa cell cultures (black lines) or those previously incubated with *L. salivarius* Lv72 (gray). **(C)** Immunolocalization of HS and CS chains in pure HeLa cell cultures (left) or those previously incubated with *L. salivarius* Lv72 (right).

that, given that HS polysaccharides generally occur as HSPG, the decrease observed in core proteins should cause a decrease in the levels these saccharide chains on the cell surface and in the pericellular region.

Transcripts for 36 out of 47 genes involved in the biosynthesis of GAG chains could be detected, and 17 of them (47%) showed significant repression when the *Lactobacilli* were placed in contact with HeLa cell cultures. The genes affected are implicated in all production steps, i.e., synthesis of tetrasaccharide linker, initiation and polymerization of GAG chains, and fine-tuning the structure of the final macromolecule.

Although the organization and regulation of the synthesis of GAG chains is largely unknown, it is known that the expression levels of the enzymes involved play an essential role. It has also been proposed that these enzymes be grouped together in a hypothetical complex structure, referred to as a gagosome, which it is also hypothesized may contain regulatory proteins of an unknown nature (40). In addition, it is also known that regulation exists that is produced by some of the biosynthetic enzymes themselves, by the availability of precursors, or by enzymatic mechanisms such as phosphorylation of the xylose residue present in the binding tetrasaccharide (41). Our results show a particularly interesting reduction in the transcription of certain enzymes that are essential in the initiation and polymerization of GAG chains, such as those responsible for the initiation of HS chains (EXTL2 and EXTL3), the CS polymerization factor (CHPF) and, notably, those responsible for the synthesis of the tetrasaccharide linker and its phosphorylation (FAM20B). These data, together with the decrease in the transcription of the core proteins, strongly suggest the existence of a reduction in the synthesis of GAG chains is induced by the union of the microorganism. However, the GAGs had higher molecular masses, which might help the initial interaction of the glycocalyx components with the colonizing *Lactobacilli*. Nevertheless, the generalized gene-repression leading to the observed decrease in superficial GAGs seems puzzling, especially considering the extraordinary expression increase of *oppA* following the interaction of the two cell classes and the well-known mutualistic effect exerted by *Lactobacilli* colonization of the mucosae. However, this apparent paradox can be understood when the ecological conditions under which these two cell types live are taken into consideration. *Lactobacilli* colonize the external environment, where overexpression of *oppA* might not be as useful as in the internal cavities, where OppA is the anchor that enables fixation to the mucosae. On the other hand, from birth, the epithelial cells that form the walls of those cavities

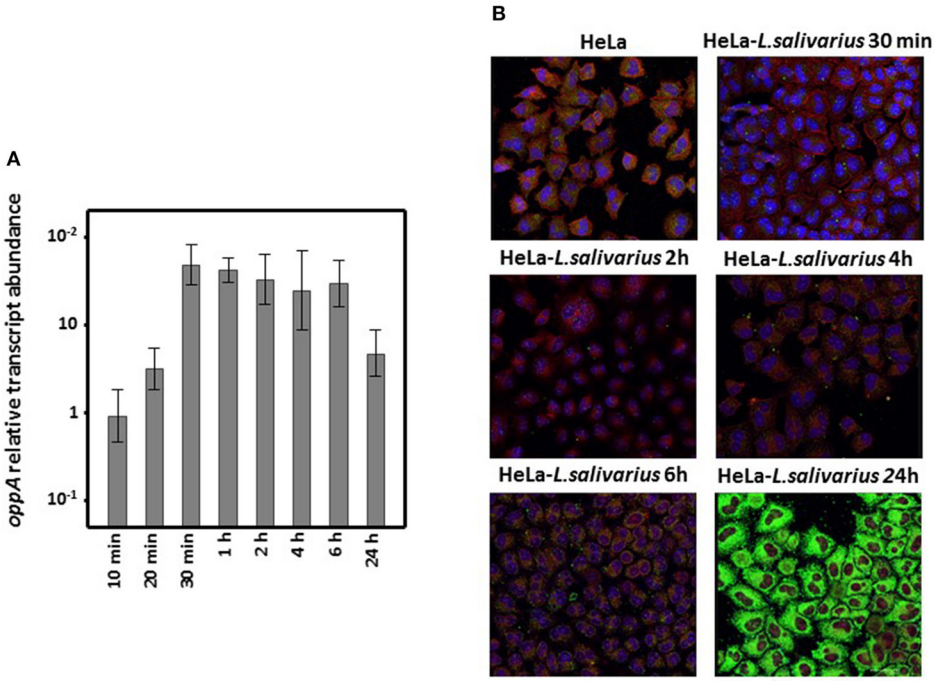

FIGURE 4 | Differential expression of *L. salivarius* Lv72 *oppA*. **(A)** Increase in *oppA*-specific RNA accumulation when extracted from mixed HeLa cell-*L. salivarius* Lv72 vs. pure bacterial cultures. The ordinates scale is logarithmic and standard deviations are indicated by spreads. The data are based on at least four independent determinations. **(B)** Immunolocalization of OppA in mixed HeLa cell *L. salivarius* Lv72 cultures. OppA antibody binding, nuclei and actin were revealed with Alexa 488 (green), DAPI (blue), and phalloidin (red), respectively.

are covered by evolving microbiotas (42, 43). Consequently, when these cells are grown in pure culture, they are confronted by an unexpected and potentially stressful situation. This may induce overexpression of the genes involved in PG biosynthesis in order to maximize the possibility of attachment by beneficial microbes that might be present in lumen fluid. Once the interaction is established, the epithelial cells may then relax their expression of the PG biosynthesis determinants to a level which simply maintains contact between its own glycocalyx and that of the microbe and, thus, the advantages conferred by their mutual association.

In conclusion, the results of the present work show that the adhesion of *Lactobacillus salivarius* Lv72 to HeLa cell cultures induces alterations in the expression levels of certain molecules involved in the process. These alterations involve overexpression of the *Lactobacilli* adhesin OppA, and also of genes encoding some PG core proteins, as well as genes encoding some of the enzymes involved in the synthesis of the GAG chains. The main modifications affect glycosyltransferases, which are responsible for the synthesis of GAGs, but other genes are also affected. These mechanisms are probably part of the communication system between epithelial cells and the microbiota.

DATA AVAILABILITY STATEMENT

All datasets generated for this study are included in the article/**Supplementary Material**.

AUTHOR CONTRIBUTIONS

CM and IF-V carried out most of the experiments. JS and LQ co-ordinated the study and drafted the manuscript. All authors have read and approved the final manuscript.

FUNDING

This work was supported by CICYT grant AGL2010-15097 from the Ministry of Science and Technology (Spain), and the Programa de Ciencia, Tecnología e Innovación of the Principado de Asturias for 2013–2017 (GRUPIN 14-139 to JS and GRUPIN 14-141 to LQ). CM held a scholarship within this project.

ACKNOWLEDGMENTS

The Instituto Universitario Fernández-Vega was supported in part by the Fundación de Investigación Oftalmológica through the Fundación Cristina Masaveu-Peterson and the Fundación Ramón Areces, Spain.

SUPPLEMENTARY MATERIAL

The Supplementary Material for this article can be found online at: https://www.frontiersin.org/articles/10.3389/fimmu.2019.03019/full#supplementary-material

REFERENCES

1. Salvetti E, Harris HMB, Felis GE, O'Toole PW. Comparative genomics of the genus *Lactobacillus* reveals robust phylogroups that provide the basis for reclassification. *Appl Environ Microbiol*. (2018) 84:e00993–18. doi: 10.1128/AEM.02052-18
2. Parks DH, Chuvochina M, Waite DW, Rinke C, Skarshewski A, Chaumeil PA, et al. A standardized bacterial taxonomy based on genome phylogeny substantially revises the tree of life. *Nat Biotechnol*. (2018) 36:996–1004. doi: 10.1038/nbt.4229
3. Wittouck S, Wuyts S, Lebeer S. Towards a genome-based reclassification of the genus *Lactobacillus*. *Appl Environ Microbiol*. (2019) 85:e02155–18. doi: 10.1128/AEM.02155-18
4. Bintsis T. Lactic acid bacteria as starter cultures: an update in their metabolism and genetics. *AIMS Microbiol*. (2018) 4:665–84. doi: 10.3934/microbiol.2018.4.665
5. Sengupta R, Altermann E, Anderson RC, McNabb WC, Moughan PJ, Roy NC. The role of cell surface architecture of *Lactobacilli* in host-microbe interactions in the gastrointestinal tract. *Mediators Inflamm*. (2013) 2013:237921. doi: 10.1155/2013/237921
6. Tannock GW. A special fondness for *Lactobacilli*. *Appl Environ Microbiol*. (2004) 70:3189–94. doi: 10.1128/AEM.70.6.3189-3194.2004
7. Petricevic L, Domig KJ, Nierscher FJ, Sandhofer MJ, Krondorfer I, Kneifel W, et al. Differences in the vaginal *Lactobacilli* of postmenopausal women and influence of rectal *Lactobacilli*. *Climacteric*. (2013) 16:356–61. doi: 10.3109/13697137.2012.725788
8. Granato D, Perotti F, Masserey I, Rouvet M, Golliard M, Servin A, et al. Cell surface-associated lipoteichoic acid acts as an adhesion factor for attachment of *Lactobacillus johnsonii* La1 to human enterocyte-like Caco-2 cells. *Appl Environ Microbiol*. (1999) 65:1071–7.
9. Avall-Jääskeläinen S, Lindholm A, Palva A. Surface display of the receptor-binding region of the *Lactobacillus brevis* S-layer protein in *Lactococcus lactis* provides non-adhesive lactococci with the ability to adhere to intestinal epithelial cells. *Appl Environ Microbiol*. (2003) 69:2230–6. doi: 10.1128/AEM.69.4.2230-2236.2003
10. Ruas-Madiedo P, Gueimonde M, Margolles A, de los Reyes-Gavilán CG, Salminen S. Exopolysaccharides produced by probiotic strains modify the adhesion of probiotics and enteropathogens to human intestinal mucus. *J Food Prot*. (2006) 69:2011–5. doi: 10.4315/0362-028X-69.8.2011
11. Kankainen M, Paulin L, Tynkkynen S, von Ossowski I, Reunanen J, Partanen P, et al. Comparative genomic analysis of *Lactobacillus rhamnosus* GG reveals pili containing a human- mucus binding protein. *Proc Natl Acad Sci USA*. (2009) 106:17193–8. doi: 10.1073/pnas.0908876106
12. Boekhorst J, Helmer Q, Kleerebezem M, Siezen RJ. Comparative analysis of proteins with a mucus-binding domain found exclusively in lactic acid bacteria. *Microbiology*. (2006) 152(Pt 1):273–80. doi: 10.1099/mic.0.28415-0
13. Muñoz-Provencio D, Rodríguez-Díaz J, Collado MC, Langella P, Bermúdez-Humarán LG, Monedero V. Functional analysis of the *Lactobacillus casei* BL23 sortases. *Appl Environ Microbiol*. (2012) 78:8684–93. doi: 10.1128/AEM.02287-12
14. Kinoshita H, Uchida H, Kawai Y, Kawasaki T, Wakahara N, Matsuo H, et al. Cell surface *Lactobacillus plantarum* LA 318 glyceraldehyde-3-phosphate dehydrogenase (GAPDH) adheres to human colonic mucin. *J Appl Microbiol*. (2008) 104:1667–74. doi: 10.1111/j.1365-2672.2007.03679.x
15. Martín R, Sánchez B, Urdaci MC, Langella P, Suárez JE, Bermúdez-Humarán LG. Effect of iron on the probiotic properties of the vaginal isolate *Lactobacillus jensenii* CECT 4306. *Microbiology*. (2015) 161:708–18. doi: 10.1099/mic.0.000044
16. Salzillo M, Vastano V, Capri U, Muscariello L. Identification and characterization of enolase as a collagen-binding protein in *Lactobacillus plantarum*. *J Basic Microbiol*. (2015) 55:890–7. doi: 10.1002/jobm.201400942
17. Salzillo M, Vastano V, Capri U, Muscariello L, Marasco R. Pyruvate dehydrogenase subunit β of *Lactobacillus plantarum* is a collagen adhesin involved in biofilm formation. *J Basic Microbiol*. (2017) 57:353–7. doi: 10.1002/jobm.201600575
18. Dhanani, AS, Bagchi, T. The expression of adhesin EF-Tu in response to mucin and its role in *Lactobacillus* adhesion and competitive inhibition of enteropathogens to mucin. *J Appl Microbiol*. (2013) 115:546–54. doi: 10.1111/jam.12249
19. Bergonzelli GE, Granato D, Pridmore RD, Marvin-Guy LF, Donnicola D, Corthésy-Theulaz IE. GroEL of *Lactobacillus johnsonii* La1 (NCC 533) is cell surface associated: potential role in interactions with the host and the gastric pathogen Helicobacter pylori. *Infect Immun*. (2006) 74:425–34. doi: 10.1128/IAI.74.1.425-434.2006
20. Lorca G, Torino MI, Font de Valdez G, Ljungh AA. *Lactobacilli* express cell surface proteins which mediate binding of immobilized collagen and fibronectin. *FEMS Microbiol Lett*. (2002) 206:31–7. doi: 10.1111/j.1574-6968.2002.tb10982.x
21. Esko JD, Kimata K, Lindahl U. Proteoglycans and sulfated glycosaminoglycans. In: Varki A, Cummings RD, Esko JD, Freeze HH, Stanley P, Bertozzi CR, editors. *Essentials of Glycobiology, 2nd Edn*. New York, NY: Cold Spring Harbor Laboratory Press (2009).
22. Whitelock JM, Iozzo RV. Heparan sulfate: a complex polymer charged with biological activity. *Chem Rev*. (2005) 105:2745–64. doi: 10.1021/cr010213m
23. Martín R, Martín C, Escobedo S, Suárez JE, Quirós LM. Surface glycosaminoglycans mediate adherence between HeLa cells and *Lactobacillus salivarius* Lv72. *BMC Microbiol*. (2013) 13:210. doi: 10.1186/1471-2180-13-210
24. Monnet V. Bacterial oligopeptide-binding proteins. *Cell Mol Life Sci*. (2003) 60:2100–14. doi: 10.1007/s00018-003-3054-3
25. Martín C, Escobedo S, Pérez-Martínez G, Coll-Marqués JM, Martín R, Suárez JE, et al. Two alkaline motifs in the *Lactobacillus salivarius* Lv72 OppA surface are important to its adhesin function. *Benef Microbes*. (2019) 10:101–9. doi: 10.3920/BM2018.0052
26. Martín C, Escobedo S, Suárez JE, Quirós LM. Widespread use of *Lactobacillus* OppA, a surface located protein, as an adhesin that recognises epithelial cell surface glycosaminoglycans. *Benef Microbes*. (2019) 10:463–72. doi: 10.3920/BM2018.0128
27. García B, García-Suárez O, Merayo-Lloves J, Alcalde I, Alfonso JF, Fernández-Vega Cueto L, et al. Differential expression of proteoglycans by corneal stromal cells in keratoconus. *Invest Ophthalmol Vis Sci*. (2016) 57:2618–28. doi: 10.1167/iovs.15-16692
28. Abramoff MD, Magalhaes PJ, Ram SJ. *Image Processing With ImageJ*. Biophotonics Int (2004).
29. Barbosa I, García S, Barbier-Chassefiere V, Caruelle JP, Martelly I, Papy-García D. Improved and simple micro assay for sulfated glycosaminoglycans quantification in biological extracts and its use in skin and muscle tissue studies. *Glycobiology*. (2003) 9:647–53. doi: 10.1093/glycob/cwg082
30. Toyoshima M, Nakajima M. Human heparanase. Human heparanase. Purification, characterization, cloning, and expression. *J Biol Chem*. (1999) 274:24153–60. doi: 10.1074/jbc.274.34.24153
31. Ito Y, Hikino M, Yajima Y, Mikami T, Sirko S, von Holst A, et al. Structural characterization of the epitopes of the monoclonal antibodies 473HD,CS-56, and MO-225 specific for chondroitin sulfate D-type using the oligosaccharide library. *Glycobiology*. (2005) 15:593–603. doi: 10.1093/glycob/cwi036
32. Miller EA, Beasley DE, Dunn RR, Archie EA. *Lactobacilli* dominance and vaginal pH: why is the human vaginal microbiome unique? *Front Microbiol*. (2016) 7:1936. doi: 10.3389/fmicb.2016.01936
33. Kareb O, Aïder M. Quorum sensing circuits in the communicating mechanisms of bacteria and its implication in the biosynthesis of bacteriocins by lactic acid bacteria: a review. *Probiotics Antimicrob Proteins*. (2019). P. 1–13. doi: 10.1007/s12602-019-09555-4
34. Skaugen M, Andersen EL, Christie VH, Nes IF. Identification, characterization, and expression of a second, bicistronic, operon involved in the production of lactocin S in *Lactobacillus sakei* L45. *Appl Environ Microbiol*. (2002) 68:720–7. doi: 10.1128/AEM.68.2.720-727.2002
35. Lebeer S, De Keersmaecker SC, Verhoeven TL, Fadda AA, Marchal K, Vanderleyden J. Functional analysis of luxS in the probiotic strain *Lactobacillus rhamnosus* GG reveals a central metabolic role important for growth and biofilm formation. *J Bacteriol*. (2007) 189:860–71. doi: 10.1128/JB.01394-06
36. Buck BL, Azcarate-Peril MA, Klaenhammer TR. Role of autoinducer-2 on the adhesion ability of *Lactobacillus acidophilus*. *J Appl Microbiol*. (2009) 107:269–79. doi: 10.1111/j.1365-2672.2009.04204.x

37. Iozzo RV, Schaefer L. Proteoglycan form and function: a comprehensive nomenclature of proteoglycans. *Matrix Biol*. (2015) 42:11–55. doi: 10.1016/j.matbio.2015.02.003
38. Smith MF Jr, Novotny J, Carl VS, Comeau LD. Helicobacter pylori and toll-like receptor agonists induce syndecan-4 expression in an NF-kappaB-dependent manner. *Glycobiology*. (2006) 16:221–9. doi: 10.1093/glycob/cwj061
39. García B, Merayo-Lloves J, Rodríguez D, Alcalde I, García-Suárez O, Alfonso JF, et al. Different use of cell surface glycosaminoglycans as adherence receptors to corneal cells by gram positive and gram negative pathogens. *Front Cell Infect Microbiol*. (2016) 6:173. doi: 10.3389/fcimb.2016.00173
40. Li JP, Kusche-Gullberg M. Heparan sulfate: biosynthesis, structure, and function. *Int Rev Cell Mol Biol*. (2016) 325:215–73. doi: 10.1016/bs.ircmb.2016.02.009
41. Nadanaka S, Zhou S, Kagiyama S, Shoji N, Sugahara K, Sugihara K, et al. EXTL2, a member of the EXT family of tumor suppressors, controls glycosaminoglycan biosynthesis in a xylose kinase-dependent manner. *J Biol Chem*. (2013) 288:9321–33. doi: 10.1074/jbc.M112.416909
42. Ferretti P, Pasolli E, Tett A, Asnicar F, Gorfer V, Fedi S, et al. Mother-to-infant microbial transmission from different body sites shapes the developing infant gut microbiome. *Cell Host Microbe*. (2018) 24:133–45.e5. doi: 10.1016/j.chom.2018.06.005
43. Sommer F, Bäckhed F. The gut microbiota–masters of host development and physiology. *Nat Rev Microbiol*. (2013) 11:227–38. doi: 10.1038/nrmicro2974

Conflict of Interest: The authors declare that the research was conducted in the absence of any commercial or financial relationships that could be construed as a potential conflict of interest.

frontiers in Immunology

ORIGINAL RESEARCH
published: 28 January 2020
doi: 10.3389/fimmu.2019.03159

Respiratory Syncytial Virus Infection of Human Lung Fibroblasts Induces a Hyaluronan-Enriched Extracellular Matrix That Binds Mast Cells and Enhances Expression of Mast Cell Proteases

Stephen R. Reeves[1,2,3]*, *Kaitlyn A. Barrow*[2], *Lucille M. Rich*[2], *Maria P. White*[2], *Nicholas J. Shubin*[2], *Christina K. Chan*[4], *Inkyung Kang*[4], *Steven F. Ziegler*[5], *Adrian M. Piliponsky*[2,3], *Thomas N. Wight*[4] and *Jason S. Debley*[1,2,3]

[1] Division of Pulmonary and Sleep Medicine, Seattle Children's Hospital, Seattle, WA, United States, [2] Center for Immunity and Immunotherapies, Seattle Children's Research Institute, Seattle, WA, United States, [3] Department of Pediatrics, University of Washington, Seattle, WA, United States, [4] Matrix Biology Program, Benaroya Research Institute, Seattle, WA, United States, [5] Immunology Program, Benaroya Research Institute, Seattle, WA, United States

OPEN ACCESS

Edited by:
Aaron C. Petrey,
The University of Utah, United States

Reviewed by:
Brooke Farrugia,
The University of Melbourne, Australia
Davide Vigetti,
University of Insubria, Italy

***Correspondence:**
Stephen R. Reeves
stephen.reeves@seattlechildrens.org

Specialty section:
This article was submitted to Molecular Innate Immunity, a section of the journal Frontiers in Immunology

Received: 20 November 2019
Accepted: 31 December 2019
Published: 28 January 2020

Citation:
Reeves SR, Barrow KA, Rich LM, White MP, Shubin NJ, Chan CK, Kang I, Ziegler SF, Piliponsky AM, Wight TN and Debley JS (2020) Respiratory Syncytial Virus Infection of Human Lung Fibroblasts Induces a Hyaluronan-Enriched Extracellular Matrix That Binds Mast Cells and Enhances Expression of Mast Cell Proteases. Front. Immunol. 10:3159. doi: 10.3389/fimmu.2019.03159

Human lung fibroblasts (HLFs) treated with the viral mimetic polyinosine-polycytidylic acid (poly I:C) form an extracellular matrix (ECM) enriched in hyaluronan (HA) that avidly binds monocytes and lymphocytes. Mast cells are important innate immune cells in both asthma and acute respiratory infections including respiratory syncytial virus (RSV); however, the effect of RSV on HA dependent mast cell adhesion and/or function is unknown. To determine if RSV infection of HLFs leads to the formation of a HA-enriched ECM that binds and enhances mast cell activity primary HLFs were infected with RSV for 48 h prior to leukocyte binding studies using a fluorescently labeled human mast cell line (LUVA). Parallel HLFs were harvested for characterization of HA production by ELISA and size exclusion chromatography. In separate experiments, HLFs were infected as above for 48 h prior to adding LUVA cells to HLF wells. Co-cultures were incubated for 48 h at which point media and cell pellets were collected for analysis. The role of the hyaladherin tumor necrosis factor-stimulated gene 6 (TSG-6) was also assessed using siRNA knockdown. RSV infection of primary HLFs for 48 h enhanced HA-dependent LUVA binding assessed by quantitative fluorescent microscopy. This coincided with increased HLF HA synthase (HAS) 2 and HAS3 expression and decreased hyaluronidase (HYAL) 2 expression leading to increased HA accumulation in the HLF cell layer and the presence of larger HA fragments. Separately, LUVAs co-cultured with RSV-infected HLFs for 48 h displayed enhanced production of the mast cell proteases, chymase, and tryptase. Pre-treatment with the HA inhibitor 4-methylumbelliferone (4-MU) and neutralizing antibodies to CD44 (HA receptor) decreased mast cell protease expression in co-cultured LUVAs implicating a direct role for HA. TSG-6 expression was increased over the 48-h infection. Inhibition of HLF TSG-6 expression by siRNA knockdown led

to decreased LUVA binding suggesting an important role for this hyaladherin for LUVA adhesion in the setting of RSV infection. In summary, RSV infection of HLFs contributes to inflammation via HA-dependent mechanisms that enhance mast cell binding as well as mast cell protease expression via direct interactions with the ECM.

Keywords: airway inflammation, airway remodeling, extracellular matrix, human lung fibroblasts, hyaluronan, mast cells, respiratory syncytial virus, tumor necrosis factor-stimulated gene 6

INTRODUCTION

Lower respiratory tract infections caused by respiratory syncytial virus (RSV) are the leading cause of hospital admissions for infants worldwide accounting for an estimated 3.4 million hospitalizations and leading to an estimated 239,000 deaths in children under the age of 5 years annually (1, 2). While these cases are generally related to the most severe episodes of RSV bronchiolitis, exposure to RSV is widespread with 50–65% of infants under the age of 1 year and nearly 100% of all children demonstrating evidence of prior RSV infection by the age of 2 years (3). In addition to the major public health concerns brought on by acute RSV infection in infancy, RSV infections have also been identified as a significant independent risk factor for the subsequent development of asthma, the most common chronic disease of childhood (4, 5).

Previous pathology specimen studies in humans have highlighted that ciliated bronchial epithelial cells (BECs) are the primary target for RSV lower respiratory tract infection; however, non-ciliated and non-epithelial cells also stain positively for RSV infection (6). Separate studies have identified a role for mesenchymal cells such as human lung fibroblasts (HLFs) in contributing to airway inflammatory changes in the setting of respiratory viruses, either by acting as an additional reservoir for replication or as an amplification site of proinflammatory signaling (7); however, the contributions of HLFs to the inflammatory response to RSV have yet to be elucidated *in vivo*. HLFs have been identified as an important regulator of the cellular microenvironment through the establishment of an extracellular matrix (ECM) that is permissive for inflammatory cell migration and enhances the retention of monocytes and lymphocytes at sites of inflammation (8–14). While several ECM constituents are likely to contribute to the establishment of a pro- or anti-inflammatory microenvironment, numerous studies have implicated the glycosaminoglycan hyaluronan (HA) as a significant contributor to the immunomodulatory functions of the ECM in both acute and chronic respiratory diseases (13, 15, 16).

Previous work has demonstrated that stimulation of HLFs with the viral mimetic, polyinosine-polycytidylic acid (poly I:C), a toll-like receptor 3 (TLR-3) agonist, led to the accumulation of an ECM that was enriched with HA and demonstrated an increased capacity to bind and retain monocytes in a HA-dependent manner (17). While these studies did not directly investigate the effects of HLF infection with RSV, the results of increased HA-dependent binding of monocytes and the establishment of a HA-enriched ECM within the cell layer were consistent with earlier studies that demonstrated intestinal smooth muscles stimulated with RSV or poly I:C produced a HA-enriched ECM that displayed enhanced binding of monocytes (18). Neither of these studies evaluated the subsequent effects on monocyte phenotype or cell signaling, thus the downstream effects of interacting with the HA-enriched ECM are unknown.

Mast cells are best characterized for their role in atopy and asthma; however, their contribution to the innate immune response to viral infection is of increasing interest (19). For example, recent studies have demonstrated that mast cell-derived serine protases are able to modulate innate immune signaling from epithelial cells leading to enhanced inflammatory responses (20). Mast cells are not typically present in the lungs of healthy children, but are recruited in the setting of respiratory viral infections, which may represent a link between early life respiratory infections and subsequent development of asthma (21). Furthermore, emerging evidence has demonstrated that mast cells express CD44, the major HA receptor, and that CD44 activity is critical for mast cell proliferation and differentiation (22, 23). To date, no studies investigating the interactions between HA and mast cells in the setting of RSV infection have been reported.

Based on the findings of these prior studies, we hypothesized that infection of primary healthy human HLFs with RSV would lead to the establishment of an HA-enriched ECM that would promote the retention of mast cells. Additionally, we hypothesized that HA-enriched ECM would promote protease expression by mast cells that were bound to the resultant ECM. To test these hypotheses, we employed a human mast cell line (LUVA) and examined the expression of mast cell proteases, which have been associated with proinflammatory mediators, following 48 h of co-culture on the RSV-induced ECM. Our findings demonstrate that RSV infection of healthy pediatric HLFs promotes the establishment of an ECM that is enriched with HA in the cell layer with enhanced capacity to adhere mast cells and enhance the production of mast cell proteases.

METHODS

Cell Culture Models

Primary healthy pediatric HLFs were obtained from Lonza. Cells were expanded until passage #5 and used for all studies described herein. HLFs were seeded at a density of ∼2,500 cells/cm^2 in 12-well plates (Corning® Life Sciences) and were maintained in 10% FBS DMEM supplemented with Pen/Strep and L-glutamine with media changes every 48 h.

LUVA cells were generously provided by Dr. John Steinke, University of Virginia (24) and were maintained in culture flasks using Stempro-34 media (Thermo Fisher Scientific) supplemented with Pen/Strep and L-glutamine with media changes every 48–72 h. RSV (line 19, A strain) was obtained and propagated as described (25). Knockdown of tumor necrosis factor-stimulated gene 6 (TSG-6) in HLFs was achieved using TSG-6 siRNA (4392420, Silencer® Select, Thermo Fisher) and Lipofectamine™ RNAiMAX Reagent (Thermo Fisher) according to the manufacturer's recommendations. Optimal transfection conditions were assessed based on manufacturer's suggested protocols leading to ∼95% reduction of TSG-6 expression detected by RT-PCR. For TSG-6 siRNA knockdown experiments, control conditions included transfection of non-coding scrambled siRNA.

LUVA-HLF Co-cultures

Confluent HLF monolayers were established and were infected with RSV 48 h as described above prior to the initiation of LUVA-HLF cocultures. LUVA cells were added to the HLF cultures in 12-well plates (5×10^5 cells per well) with a fresh media change. LUVA-HLF co-cultures with and without RSV infection were incubated for an additional 48 h after which LUVA cells were harvested for analysis as described below.

Time Course for Experiments

To establish the optimal timeline for experiments, preliminary studies were performed to investigate the time course for mast cell binding at 24, 48, and 96 h (data not shown). Maximal mast cell binding following RSV infection of HLFs was demonstrated at the 48-h timepoint and was unchanged by the 96-h timepoint, thus all additional experiments were conducted at 48 h post-RSV infection.

The timeline for experiments included two different paradigms depending on outcome measures. For all experiments, HLFs were seeded and grown for 3 days to achieve confluence following which HLFs were infected with RSV (MOI = 1) at experimental Day 0. The first set of studies included endpoint LUVA cell adhesion assays after 48 h of HLF RSV infection. In addition to LUVA cell binding assays, samples were isolated at this point for gene expression analysis of HLFs and characterization of HA accumulation and fragment size. The second paradigm included LUVA cells co-cultured with RSV-infected HLFs at the 48-h timepoint and maintained in co-culture for an additional 48 h at which point LUVA cells were collected following a brief hyaluronidase (from *Streptomyces hyalurolyticus;* Catalog # H1136, MilliporeSigma) treatment to remove adherent LUVA cells from the HA-enriched ECM, leading to ∼90% recovery of LUVA cells embedded in the HA-enriched ECM. HLFs and LUVA cell samples were collected and lysed for western blot. A subset of HLFs was treated with 2.5 mM 4-methylumbelliferone (4-MU; Catalog # M1381, MilliporeSigma), a HA synthase (HAS) inhibitor, at the time of RSV infection to inhibit formation of the HA-enriched ECM (26) and was re-dosed with each media change. In parallel, additional LUVA-HLF co-cultures were treated with monoclonal neutralizing antibodies against CD44 (30 μg/mL; Catalog # MA4400, Thermo Fisher) at the time of co-culture to block interactions between LUVAs and HA (27). A separate subset of HLFs was treated with siRNA to knockdown expression of TSG-6 24 h prior to RSV infection. LUVA cells were isolated following 48 h of co-culture for gene expression analysis, binding assays, and immunohistochemistry.

TABLE 1 | List of PCR primers.

PCR Target	Gene ID	Assay ID
Chymase	CMA1	Hs01095979_g1
Cluster of differentiation 44	CD44	Hs01075861_m1
Glyceraldehyde 3-phosphate dehydrogenase	GAPDH	Hs02758991_g1
Hyaluronan synthase 1	HAS1	Hs00987418_m1
Hyaluronan synthase 2	HAS2	Hs00193435_m1
Hyaluronan synthase 3	HAS3	Hs00193436_m1
Hyaluronidase 1	HYAL1	Hs00201046_m1
Hyaluronidase 2	HYAL2	Hs01117343_g1
Lymphatic vessel endothelial hyaluronan receptor 1	LYVE1	Hs00272659_m1
Receptor for hyaluronan mediated motility	RHAMM	Hs00234864_m1
Tryptase	TPSB2	Hs02576518_gH
Tumor necrosis factor-inducible gene 6	TNFAIP6	Hs01113602_m1
Versican	VCAN	Hs00171642_m1

RNA Extraction and Real-Time PCR

For gene expression analysis experiments, total RNA was isolated from either HLFs or LUVA cells according to manufacturer recommendations (RNAqueous kit, Ambion®-Applied Biosystems). RNA concentration and quality were determined using the NanoDrop™ One Microvolume UV-Vis Spectrophotometer (Thermo Fisher Scientific). RNA samples were reverse-transcribed using the SuperScript® VILO cDNA Synthesis Kit (Life Technologies). Real-time PCR was performed using validated TaqMan® probes (Life Technologies) for hyaluronan synthase (HAS) 1, HAS2, HAS3, hyaluronidase (HYAL) 1, HYAL2, CD44, receptor for HA mediated motility (RHAMM), lymphatic vessel endothelial HA receptor 1 (LYVE-1), versican (VCAN), TSG-6, chymase, tryptase, and glyceraldehyde 3-phosphate dehydrogenase (GAPDH, see **Table 1** for additional details). Assays were performed using the TaqMan® Fast Advanced Master Mix reagents and the Applied Biosystems StepOnePlus™ Real-Time PCR System (Life Technologies).

Western Blots

Samples were lysed with 1× lysis buffer (MPER + 1X Halt protease inhibitor cocktail + 5 μM EDTA; Thermo Scientific, San Jose, CA, USA), and total protein concentration determined using the Pierce BCA protein assay kit (Thermo Scientific), according to the manufacturer's protocol. Equal amounts of protein were electrophoresed on 4–20% polyacrylamide gels and transferred onto PVDF membranes. Tryptase and glyceraldehyde 3-phosphate dehydrogenase (GAPDH) were detected with human anti-mast cell tryptase (clone G3, Santa Cruz Biotechnology, Santa Cruz, CA, USA) and human anti-GAPDH (clone GA1R, Cell Sciences) antibodies, respectively.

HA Quantification and Characterization of Fragment Size

HA content and hydrodynamic size were assessed using a modification of reported methods (12, 28). Media and cell layer samples were isolated separately and digested with pronase (300 μg/ml, Roche) in 0.5 M Tris buffer (pH 6.5) for 18 h at 37°C. Following digestion, the pronase was heat inactivated by incubation at 100°C for 20 min. Media and cell layer concentrations of HA were measured using an Enzyme-Linked Immunosorbent Assay (ELISA) from R&D Systems® (kit DY3614-05). To determine the hydrodynamic size of HA fragments contained within the samples, equal amounts of HA were applied to an S-1000 column (GE Healthcare) in a 0.5 M sodium acetate buffer containing 0.025% Chaps, 0.02% sodium azide at pH 7.0. Samples were collected using a microtube fraction collector (Model 2110, BioRad) and were analyzed separately using the HA ELISA described above.

Mast Cell Binding Assays and Immunohistochemistry

Mast cell binding was assessed using a modification of reported methods (12, 18). Subsets of RSV-infected and control HLFs were used to assess the ability of the secreted ECM to bind LUVA cells. Parallel conditions pre-treated for 30 min at 37°C with hyaluronidase (4 U/mL; from *S. hyalurolyticus;* Catalog # H1136, MilliporeSigma) were included. LUVA cells were washed twice in phenol-free media and re-suspended (1×10^6 cells/mL) and were then incubated with calcein-AM (0.5 μg/ml; Life Technologies) for 45 min at 37°C. HLF wells were washed with RPMI. Afterward, 1.0 mL of the mast cell suspension was added to the wells and allowed to bind at 4°C for 90 min to inhibit enzymatic HA turnover. Cultures were washed 5 times in cold RPMI to remove non-adherent cells. Adherent cell area was quantified using live-cell fluorescent microscopy (ImageXpress Pico, Molecular Devices). Following live-cell imaging, subsets of cells were fixed using a 10% formalin/70% ethanol/5% acetic acid fixative for 10 min at room temperature, washed with PBS, and stained with biotinylated hyaluronan binding protein (HABP) primary (2.5 μg/ml; Catalog # H0161, MilliporeSigma) and a streptavidin conjugated Alexa Fluor 568 secondary (1:1,000, Thermo Fisher). Plates were then reimaged to using the ImageXpress Pico to highlight interactions between the HA matrix and LUVA cells.

Separate HLF specimens were grown on sterilized, collagen coated 12 mm glass coverslips under the experimental conditions described above. Staining for HA was achieved as described above, HLF specimens were also stained with a primary antibody to inter-alpha-trypsin inhibitor heavy chain 1 (ITIH1, 1:500, Thermo Fisher) and a rabbit secondary antibody conjugated to Alexa Fluor 488 (1:1,000, Thermo Fisher). Imaging was performed by either conventional epi-fluorescence microscopy (DM6000B, Leica, Wetzlar, Germany) or confocal microscopy (TCS SP5, Leica).

Statistical Analysis

Analyses of RT-PCR results were performed using GenEx version 6.0.5 (MultiD Analyses AB,) based on previously described methods (29). For all other data, the unpaired *t*-test was used for comparisons that were normally distributed within each group. For non-normally distributed data, the Mann-Whitney test was used. Statistical analyses were performed using Prism® 8.0 software (Graph-Pad Software Inc.). Statistical significance was set at $P < 0.05$.

RESULTS

RSV Infection Promotes Greater HA Synthesis by HLFs

Comparison of gene expression by HLFs with or without RSV infection demonstrated enhanced expression of mRNA for HA synthetic enzymes (i.e., HAS isoforms) and decreased expression of mRNA for the HA degradation enzyme (*HYAL2*). HLF expression of *HAS1* was essentially undetectable in both control and RSV-infected HLFs, thus precluding statistical comparisons between the groups (not shown). Expression of *HAS2*, the major HAS isoform expressed by HLFs, was significantly elevated following the 48-h RSV infection (13-fold, $P < 0.0006$, **Figure 1A**) as was the expression of *HAS3* (5.6-fold, $P < 0.0006$, **Figure 1B**). To investigate the contributions of HA degradation mechanisms to the accumulation of HA, expression of *HYAL1*, *HYAL2*, and *CD44* mRNA transcripts was also assessed with and without RSV infection. No significant differences in *HYAL1* and *CD44* expression were found between RSV-treated or control HLFs (**Figures 1C,E**); however, expression of *HYAL2* mRNA transcripts by RSV-infected HLFs was significantly decreased (∼80% decrease, $P < 0.0001$, **Figure 1D**).

In addition to characterization of gene expression of HA synthesis and degradation enzymes by HLFs, accumulation of HA in HLF cultures was assessed by immunofluorescence (**Figures 2A,B**). Staining for HA revealed an increase in HA accumulation in HLFs infected with RSV compared to control HLFs (**Figure 2C**; 3.5-fold increase, $P < 0.03$). Quantitative analysis of HA deposits assessed by ELISA demonstrated an increased total amount of HA contained within samples collected from RSV-infected HLFs compared to control HLFs (8,878 ± 114 ng/mL vs. 5,295 ± 389 ng/mL, $P < 0.0009$). This difference was driven by increased HA contained in the HLF cell layer following RSV infection (4,477 ± 56 ng/mL vs. 601 ± 128 ng/mL, $P < 0.0001$) without significant differences in the media compartment HA content (**Figure 2D**). In both the media and cell layer compartments, HA size was found to be skewed toward HMW-HA in RSV-infected samples compared to control HLFs with a more polydisperse pattern seen in the control samples (**Figures 2E,F**).

HA-Enriched ECM Produced by RSV-Infected HLFs Promotes the Increased Adhesion of LUVA Cells as Well as the Expression of Mast Cell Proteases

To determine if the HA-enriched ECM produced by HLFs following RSV infection would promote greater adhesion of mast cells compared to that of control HLFs, adhesion of LUVA cells using quantitative fluorescent live-cell imaging was assessed. Compared to control HLFs (**Figure 3A**) adhesion of LUVA cells to the ECM generated by RSV-infected HLFs (**Figure 3B**) was

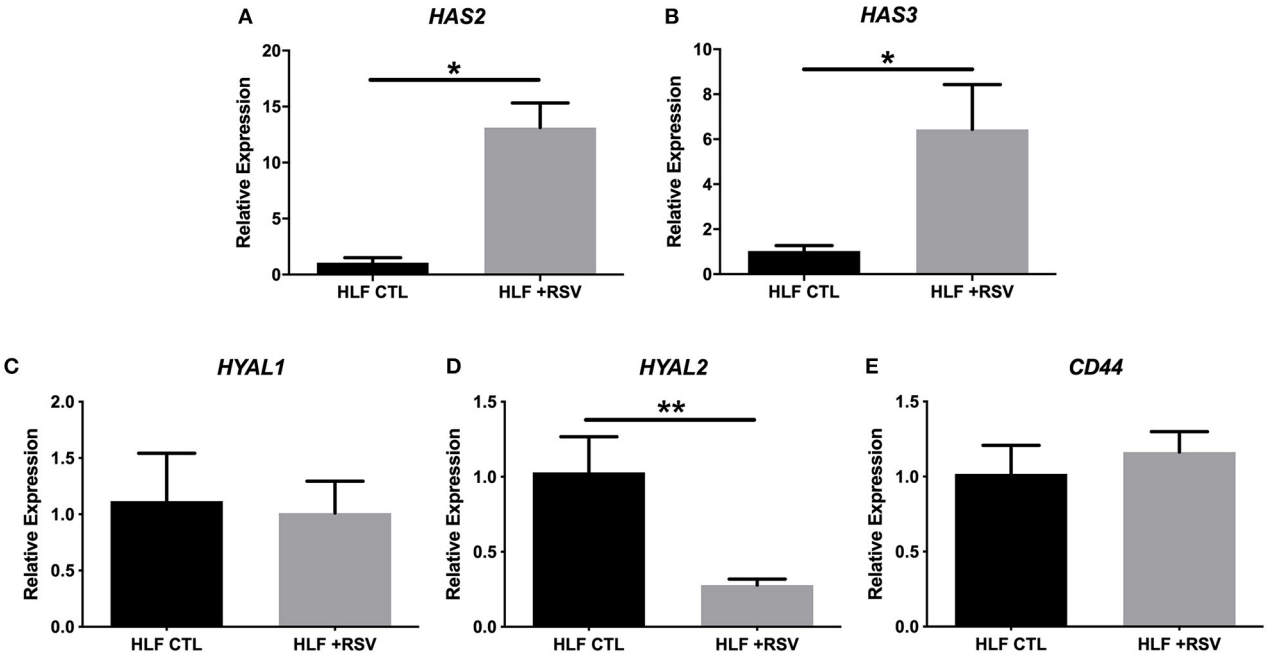

FIGURE 1 | Expression of hyaluronan synthase (HAS) and hyaluronidase (HYAL) isoforms by human lung fibroblasts (HLFs) infected with respiratory syncytial virus (RSV). Expression of **(A)** *HAS2* and **(B)** *HAS3* were both significantly increased following RSV infection (13-fold, $^{*}P < 0.0006$ and 5.6-fold, $^{*}P < 0.0006$, respectively). HLF expression of **(C)** *HYAL1* was not significantly altered by RSV infection. Expression of **(D)** *HYAL2* was significantly decreased (~80% reduction, $^{**}P < 0.0001$) following RSV infection. Expression of CD44 was not significantly altered **(E)**. Gene expression was normalized to GAPDH and is shown as normalized mean ± SD relative to control HLFs for $N = 7$ replicates/group.

significantly greater. The increased binding in RSV-infected conditions compared to controls was reversible by pretreating the wells with *Streptomyces* hyaluronidase (**Figures 3C,D**). Quantitative analysis of the staining area in each of these conditions revealed a 2-fold increase in LUVA binding in adhesion studies conducted with RSV-infected HLFs compared to control HLFs (401.6 ± 18.9 units vs. 213.2 ± 9.8 units, $P < 0.0001$). The enhanced binding was eliminated in samples pre-treated with hyaluronidase ($P < 0.0001$, **Figure 3E**).

To assess whether the interactions with the ECM generated by RSV-infected HLFs would lead to alterations in mast cell phenotype beyond increased adhesion, co-cultures of LUVA cells with HLFs following the establishment of the HA-enriched ECM for an additional 48 h were performed. LUVA cells were then isolated and assayed for expression of mast cell proteases as well as expression of HA receptors. Expression of the three major HA receptors (*CD44*, *RHAMM*, and *LYVE1*) was evaluated by PCR. Co-culture with RSV infected HLFs led to a 3-fold increase in CD44 expression by LUVA cells ($P = 0.002$, **Figure 4A**) without significant changes in RHAMM or LYVE1 expression (**Figures 4B,C**). To determine the role of HA in the induction of protease expression, a condition with the HAS inhibitor 4-MU as well as a condition using a monoclonal neutralizing antibody to the HA receptor, CD44, were included (**Figure 5**). LUVA cells co-cultured with RSV-infected HLFs exhibited an increased expression of chymase mRNA compared to LUVA cells alone ($P = 0.01$, **Figure 5A**) or to LUVA cells co-cultured with uninfected controls ($P = 0.002$). RSV infection of LUVA cells alone lead to a small increase in chymase expression at baseline (1.7-fold, $P = 0.03$); however, the magnitude of this increase is small in comparison to the HLF/RSV-infected co-culture condition. Pre-treatment with the HAS inhibitor 4-MU decreased the expression of chymase by LUVA cells co-cultured with RSV-infected HLFs to levels similar to LUVA cells alone ($P = 0.02$). Addition of monoclonal anti-CD44 antibodies also significantly attenuated the expression of chymase by LUVA cells co-cultured with HLFs following RSV infection ($P = 0.01$). LUVA cells co-cultured with RSV-infected HLFs also demonstrated an increased expression of tryptase mRNA compared to LUVA cells alone ($P = 0.01$) or to LUVA cells co-cultured with uninfected controls ($P = 0.002$, **Figure 5B**). Similar to chymase mRNA expression, RSV infection of LUVA cells alone led to a slight increase in tryptase expression at baseline ($P = 0.03$). Additionally, pre-treatment with 4-MU also decreased the expression of tryptase by LUVA cells co-cultured with RSV-infected HLFs ($P = 0.02$). Similarly, the addition of monoclonal CD44 blocking antibodies significantly attenuated the expression of tryptase by LUVA cells co-cultured with HLFs following RSV infection ($P = 0.01$). Tryptase expression assayed by western blot confirmed a pattern of protein expression that was similar to the gene expression analysis (**Figure 5C**).

Impact of RSV on the Expression of Hyaladherins

Previous work with HLFs demonstrated an important role for versican (VCAN), a large chondroitin sulfate proteoglycan

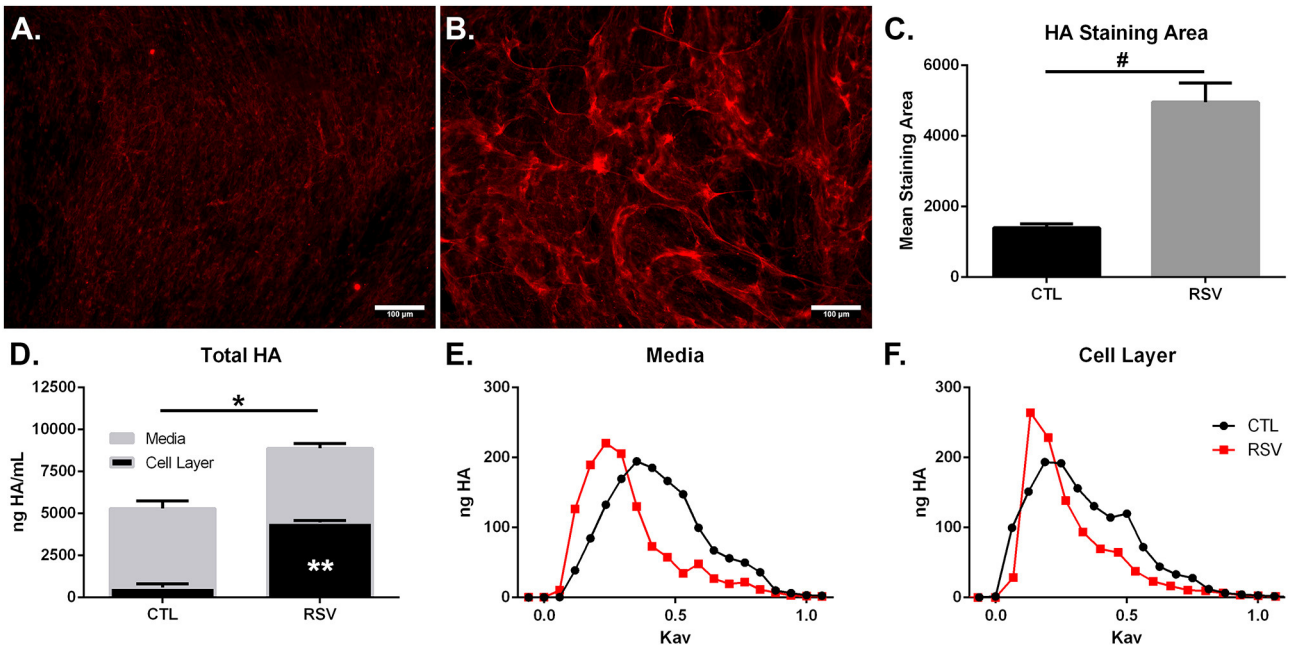

FIGURE 2 | Imaging studies were performed to label HA deposition (red) by HLFs in **(A)** control HLFs and **(B)** RSV-infected HLFs. **(C)** Quantitative analysis of staining area demonstrated a 3.5-fold increase in the staining of HA ($^{\#}P < 0.03$). **(D)** Quantitative analysis of HA accumulation revealed that HLFs infected with RSV displayed increased total HA accumulation (8,878 ± 114.4 ng/mL vs. 5,295 ± 389.6 ng/mL, $^{*}P < 0.0009$). Differences were driven by increased HA contained in the HLF cell layer following RSV infection (4,477 ± 56.13 ng/mL vs. 600.8 ± 128.3 ng/mL, $^{**}P < 0.0001$) without significant differences in the media compartment HA content. Data shown as mean ± SD for $N = 3$ replicates/group. HLFs infected with RSV demonstrated a greater abundance of HMW-HA species compared to HLF controls in both **(E)** media and **(F)** cell layer compartments. A representative plot of HA profiles measured by S-1000 size exclusion chromatography is shown. Data is plotted as ng HA vs. the partition coefficient (K_{av}) for $N = 3$ replicates/group.

that interacts with HA, in the enhanced binding of leukocytes following the application of the viral mimetic poly I:C (17). Thus, we examined the role of VCAN in our model system as well. We found that *VCAN* mRNA expression by HLFs was significantly suppressed following a 48-h infection with RSV (10-fold decrease, $P < 0.0001$, **Figure 6A**). HLF gene expression of versicanases (ADAMSTS1, ADAMSTS4, and ADAMSTS5) was elevated following the 48-h RSV infection (**Figures 6B–D**). Given the decreased VCAN synthesis and enhanced expression of VCAN degradation enzymes it seems unlikely that VCAN is driving the HA related effects in this model system. In contrast, we observed a 6-fold increase in the expression of mRNA for the hyaladherin TSG-6 in RSV-infected HLFs by 48 h ($P < 0.0001$, **Figure 7A**). Given that TSG-6 has been shown to be an important mediator of HA cable formation and HA-dependent inflammatory changes (30), and that it plays a critical role in the establishment of airway inflammation in murine models (31), we hypothesized that TSG-6 may also be contributing to the enhanced HA-dependent mast cell binding that we have demonstrated.

To determine the role of TSG-6 in our model, we repeated the mast cell adhesion assays following siRNA knockdown of TSG-6 expression in control and RSV-infected HLFs. This led to a significant reduction in the HA-dependent binding of LUVA cells observed in the RSV-infected HLF condition (54% reduction, $P < 0.002$, **Figure 7B**). Following live-cell adhesion assays, samples were fixed, stained, and re-examined for HA staining (representative images shown in **Figures 7C,D**). Wells from the RSV-infected HLFs demonstrated increased HA accumulation with LUVA cells embedded in the HA-enriched ECM (**Figure 7D**). Closer inspection revealed that LUVA cells were associated with dense cable-like structures of HA (**Figure 7E**) and that siRNA knockdown of TSG-6 expression prevented this association, contributing to the decreased binding of LUVA cells in that condition (**Figure 7F**).

Immunofluorescent staining for HA and ITIH1, a heavy chain (HC) covalently bound to HA via TSG-6 activity, in the ECM by HLFs during control conditions demonstrated a modest amount of HA production and relatively little incorporation of ITIH1 into the ECM (**Figure 8A**). Conversely, RSV infected HLFs demonstrated increased HA staining and organization of the ECM in higher order structures that stained positively for ITIH1, i.e., HC-HA (**Figure 8B**). Inhibition of TSG-6 expression did not alter the pattern observed in control HLFs (**Figure 8C**); however, inhibition of TSG-6 expression decreased staining for ITIH1 and decreased the presence of higher order HA structures observed in the RSV infected HLFs (**Figure 8D**).

Finally, we examined the role of TSG-6 knockdown on mast cell protease expression by the LUVA cells after a 48-h co-culture period. In these studies, we observed a modest 1.3-fold reduction

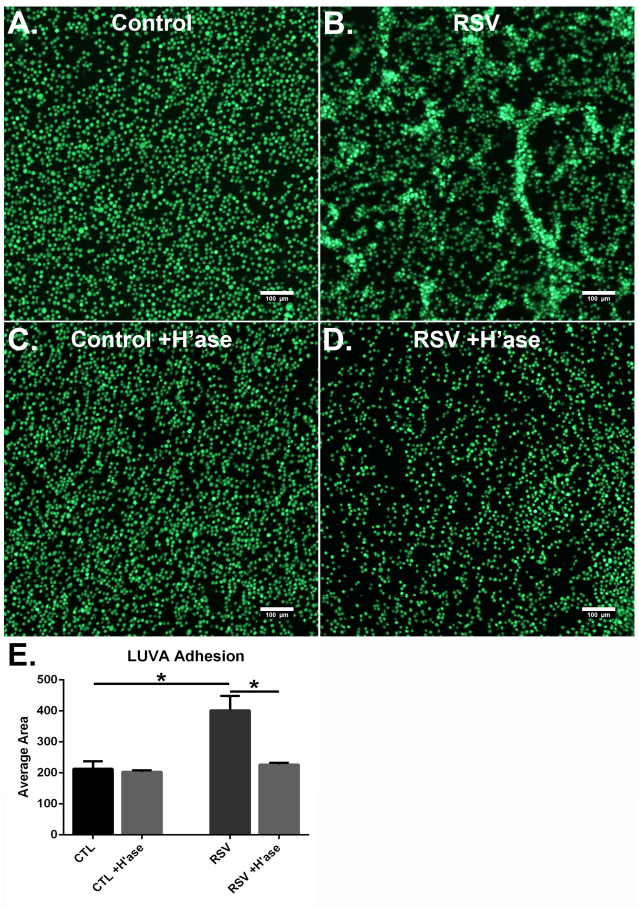

FIGURE 3 | Adhesion of LUVA cells (green) to the ECM generated by **(A)** control HLFs compared to **(B)** RSV-infected HLFs. Note that LUVA cells aggregated in clusters in a pattern similar to that shown in **Figure 2**. Panels **(C,D)** depict LUVA binding following pre-treatment of the wells with *Streptomyces* hyaluronidase for control HLFs and RSV-infected HLFs, respectively. **(E)** Quantitative analysis of the staining area revealed a 2-fold increase in LUVA binding in adhesion studies conducted with RSV-infected HLFs compared to control HLFs (401.6 ± 18.94 units vs. 213.2 ± 9.818 units, $^*P < 0.0001$). The enhanced binding was eliminated in samples pre-treated with hyaluronidase ($^*P < 0.0001$). Data shown as mean ± SD for $N = 6$ replicates/group.

in chymase expression ($P = 0.03$) and no significant changes in tryptase expression (**Figure 9**).

DISCUSSION

The findings of the present study demonstrate for the first time that RSV infection of primary pediatric donor-derived HLFs produces an ECM that is enriched with HA that is more adhesive for mast cells. The accumulation of HA in the cell layer was accompanied by the enhanced expression of HAS2 and HAS3 while HYAL2 expression was decreased in RSV infected HLFs. Furthermore, we have demonstrated that this binding is accompanied by augmented expression of the mast cell proteases, chymase and tryptase. The increased mast cell binding was dependent on the presence of HA following specific digestion of the ECM by hyaluronidase. Furthermore, inhibition of HA-enriched ECM formation through the use of 4-MU, an inhibitor of HA synthesis, or blockade of the HA receptor CD44 with monoclonal antibodies, demonstrated that enhanced mast cell protease expression was dependent on the interaction with this HA-enriched ECM. Additional studies to evaluate the contributions of the hyaladherin, TSG-6, demonstrated that knockdown of TSG-6 expression partially decreased enhanced binding of the LUVA cells to the ECM and partially decreased the expression of chymase, but did not alter expression of tryptase. These data implicate the formation of an HA-enriched ECM in promoting a proinflammatory milieu during acute respiratory viral infections (Summary **Figure 10**).

Mast cells have been long recognized to play a critical role in allergic airway inflammation and asthma (32, 33); however, their contributions to innate immunity and host defense during acute respiratory infections have also been increasingly recognized (34, 35). Unlike circulating white blood cells, mast cells mature in tissues and the local microenvironment plays a critical role in the differentiation of mast cells and the establishment of their phenotype. Serine proteases are unique to mast cells and have been recognized for their contributions in several inflammatory diseases including asthma (36). Furthermore, the expression of proteases by mature mast cells is shaped by local environmental factors (35). Previous studies have demonstrated an important role for interactions with HA via the CD44 receptor during proliferation and differentiation of mast cells (23, 37, 38), thus for these studies we chose to investigate the effect of interacting with the RSV-induced ECM in LUVA cells, a human mast cell line (24). Other studies have examined the direct effects of RSV infection of mast cells and shown that inflammatory cytokines such as type-I interferon production is significantly increased; however, mast cell protease production was not assessed (39). In our experiments, LUVA cells alone did display slight increases in chymase and tryptase following RSV exposure, but the magnitude of this increase was relatively small compared to that displayed by LUVA cells cultured on the HA-enriched ECM generated by RSV-infected HLFs. While we cannot rule out that signaling mediators produced by HLFs may contribute to the enhanced protease production by the LUVA cells, the reduction in protease expression following the inhibition of the HA-enriched matrix produced by HLFs with 4-MU would suggest a direct effect of this ECM in driving this process. Furthermore, inhibition of modifications to HA by TSG-6, i.e., HC-HA, via siRNA knockdown suggests an important role for HA in either directly signaling to the LUVA cells or holding them in close apposition to the HLFs so that other direct or indirect signaling may occur. These findings are interesting in that we are demonstrating for the first time that ECM induced by RSV infection of HLFs can alter the expression of inflammatory mediators by mast cells. It is possible that other proinflammatory mediators expressed by mast cells, as well as IgE-dependent and IgE-independent stimuli of mast cells are altered by the interaction with this "pathological"

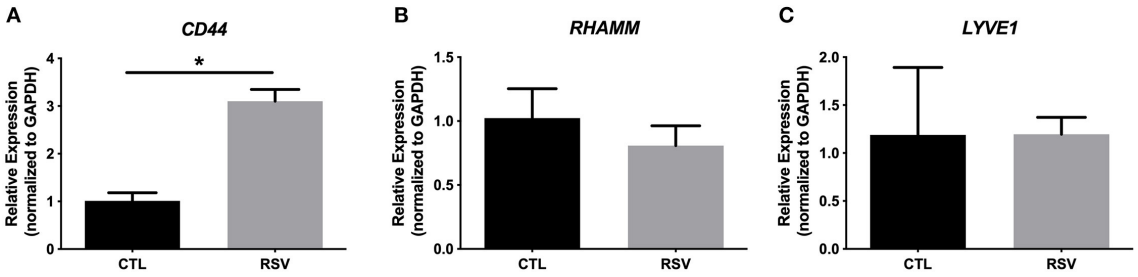

FIGURE 4 | Gene expression of HA receptors by LUVA cells co-cultured with HLFs with or without RSV infection for 48 h. **(A)** LUVA cells co-cultured with RSV-infected HLFs demonstrated an increased expression of *CD44* mRNA compared to LUVA cells alone (*$P = 0.002$). No differences in LUVA cell expression of *RHAMM* or *LYVE1* were observed **(B,C)**. Gene expression was normalized to GAPDH and is shown as normalized mean ± SD relative to control LUVA cells for $N = 6$ replicates/group.

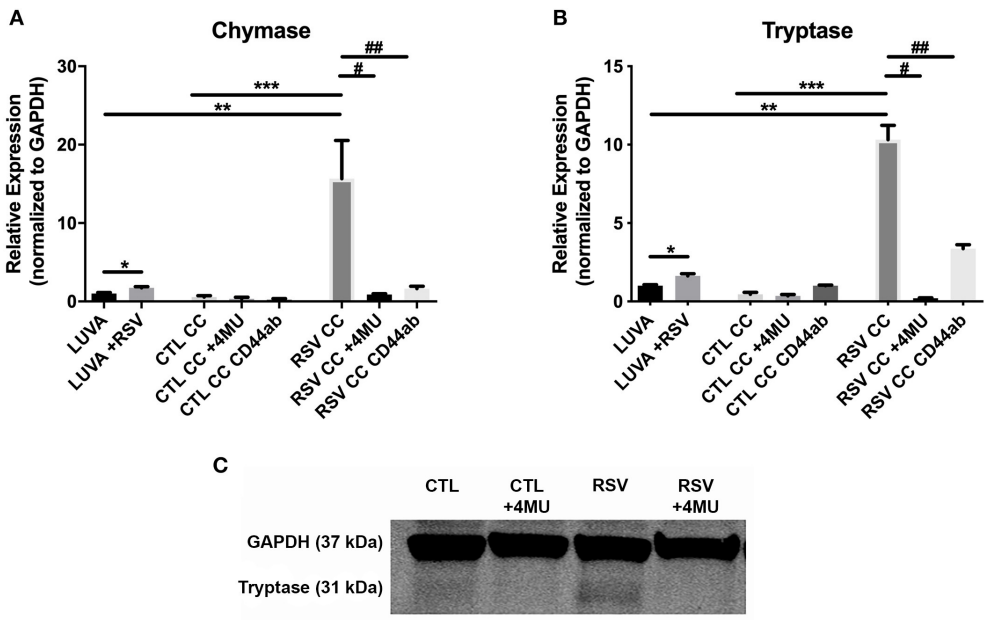

FIGURE 5 | Gene expression of mast cell proteases by LUVA cells co-cultured (CC) with HLFs with or without RSV infection for 48 h (RSV CC and CTL CC, respectively). **(A)** LUVA cells co-cultured with RSV-infected HLFs demonstrated an increased expression of chymase mRNA compared to LUVA cells alone (**$P =$ 0.01) and LUVA cells co-cultured with uninfected HLFs (***$P = 0.002$). RSV infection of LUVA cells alone did lead to a small increase in chymase expression at baseline (*1.7-fold, $P = 0.03$). Treatment with either 4-MU or neutralizing antibody to CD44 significantly decreased chymase expression by LUVA cells co-cultured with RSV-infected HLFs ($^{\#}P = 0.02$; $^{\#\#}P = 0.01$, respectively). **(B)** Expression of tryptase by LUVA cells co-cultured with RSV-infected HLFs was increased compared to LUVA cells alone (**$P = 0.01$) and LUVA cells co-cultured with uninfected HLFs (***$P = 0.002$). RSV infection of LUVA cells alone led to a slight increase in tryptase expression at baseline (*1.7-fold, $P = 0.03$). Treatment with either 4-MU or neutralizing antibody to CD44 decreased the expression of tryptase by LUVA cells co-cultured with RSV-infected HLFs ($^{\#}P = 0.02$; $^{\#\#}P = 0.01$, respectively). **(C)** Tryptase protein assayed by western blot confirmed a similar pattern as the gene expression analysis. Gene expression was normalized to GAPDH and is shown as normalized mean ± SD relative to control LUVA cells for $N = 3$–6 replicates/group.

HA matrix; however, examination of these factors is beyond the scope of this report and will be an interesting area for future investigation.

The role of HLFs in establishing a HA-enriched, proinflammatory ECM has been previously explored (17). In those studies, sub-confluent primary HLFs treated with poly I:C produced an ECM that was enriched with HA and VCAN that led to increased binding of a human monocyte cell line (U937 cells). Furthermore, treatment with poly I:C led to a shift in the HA content from the culture media to the cell layer and an increase in the hydrodynamic size of the HA (i.e., HMW-HA), but only a modest increase in the total amount of HA accumulation in the HLF cultures. Interestingly, Potter-Perigo et al. found that the increased accumulation of HA and VCAN was secondary to relative decreases in degradation pathways (17). While there are several similarities between the findings of that study and the findings that we report herein, there are also several important differences. In the present study, HLFs were

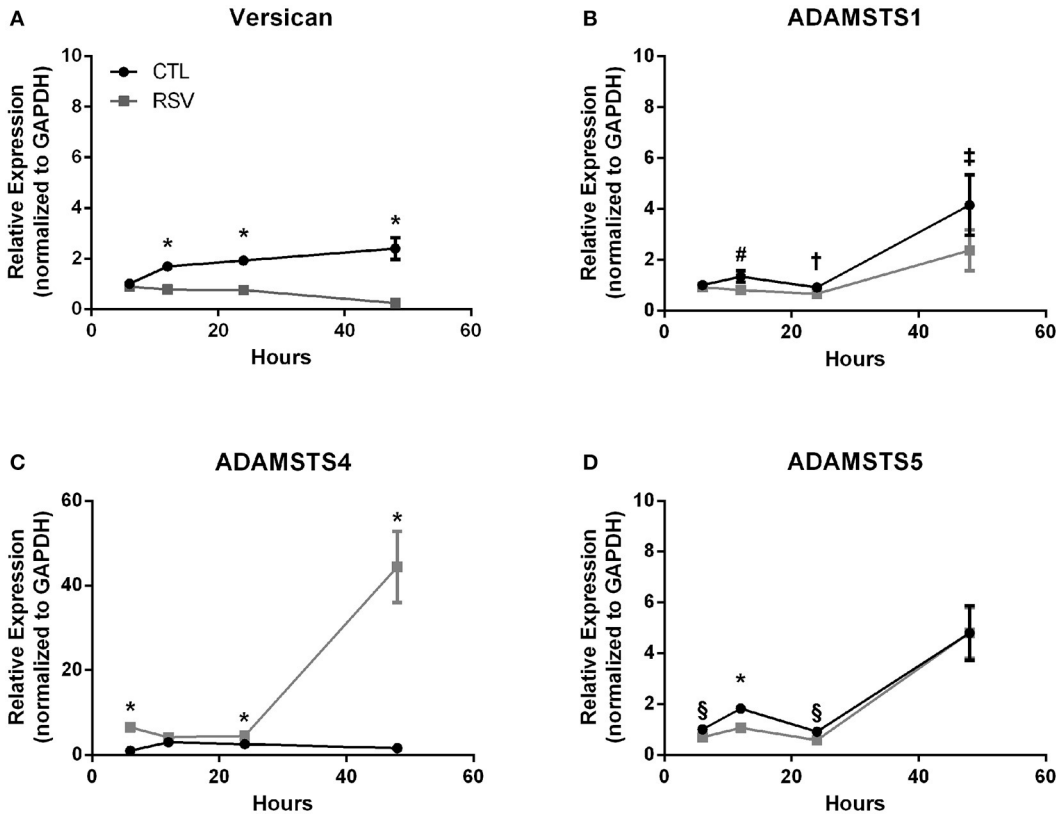

FIGURE 6 | Time course of versican and versicanase expression by HLFs following infection with RSV. **(A)** Beginning at the 12-h timepoint, versican gene expression was decreased in RSV-infected HLFs compared to control HLFs ($P > 0.0001$, each comparison). **(B)** No significant differences were observed for ADAMSTS1 gene expression between the groups at 6 h. Expression of ADAMSTS1 was decreased at 12 h ($^{\#}P < 0.005$), 24 h ($^{\dagger}P < 0.05$), and 48 h ($^{\ddagger}P < 0.002$) following RSV infection. **(C)** Gene expression of ADAMSTS4 was significantly increased at 6 h, 24 h, and 48 h in RSV-infected HLFs compared to control HLFs ($^{*}P < 0.0001$, each comparison). **(D)** Gene expression of ADAMSTS5 was significantly decreased in RSV-infected HLFs at 6 h ($^{\S}P < 0.01$), 12 h ($^{*}P < 0.0001$), and 24 h ($^{\S}P < 0.01$), but not at the 48-h timepoint.

infected with RSV capable of replication resulting in a sustained infection of the HLFs which may lead to a very different exposure profile compared to single-dose poly I:C exposure. We also sought to examine VCAN expression in our model system and found that it was significantly reduced in HLFs following a 48-h RSV infection. Thus, VCAN expression was unlikely to explain the enhanced mast cell binding that was observed in the present study.

In a more recent study, Gaucherand et al. demonstrated that co-culture of HLFs with activated T lymphocytes produced an HA-enriched, leukocyte adhesive ECM (11). Similar to our findings, the authors reported a decreased expression of versican along with an increase in versican degrading enzyme expression. Additionally, that study reported increased expression of TSG-6 by HLFs following co-culture with activated T lymphocytes leading to the hypothesis that increased TSG-6 expression was contributing to the enhanced retention of monocytes in leukocyte binding assays. Similar to our data, HLFs co-cultured with the activated T lymphocytes produced a greater amount of total HA, which was largely retained in the cell layer (11).

A similarity between our studies is that TSG-6 seems to be an important player in the establishment of the leukocyte-adhesive ECM. Previous work has demonstrated an important role for TSG-6 in promoting the crosslinking of HA into larger cable-like structures (30, 40). Separate studies have also identified an important role for TSG-6 in other models of lung inflammation, including asthma and allergen challenge (41, 42). Additionally, the presence of TSG-6 has been shown to enhance the production of HA-enriched matrices and increase the ability of these matrices to adhere leukocytes (43). Knockdown of TSG-6 expression in our system led to a significant reduction in the retention of LUVA cells; however, this did not decrease LUVA cell binding to the degree that digestion of the matrix HA content with hyaluronidase did, suggesting that while TSG-6 is important for LUVA cell binding in our system, other factors may also contribute.

In another recent study from our group, we have reported that co-culture of primary airway epithelial cells (AECs) obtained from asthmatic pediatric donors with healthy donor-derived primary HLFs led to increased synthesis of an ECM that was enriched with HA and led to increased retention of

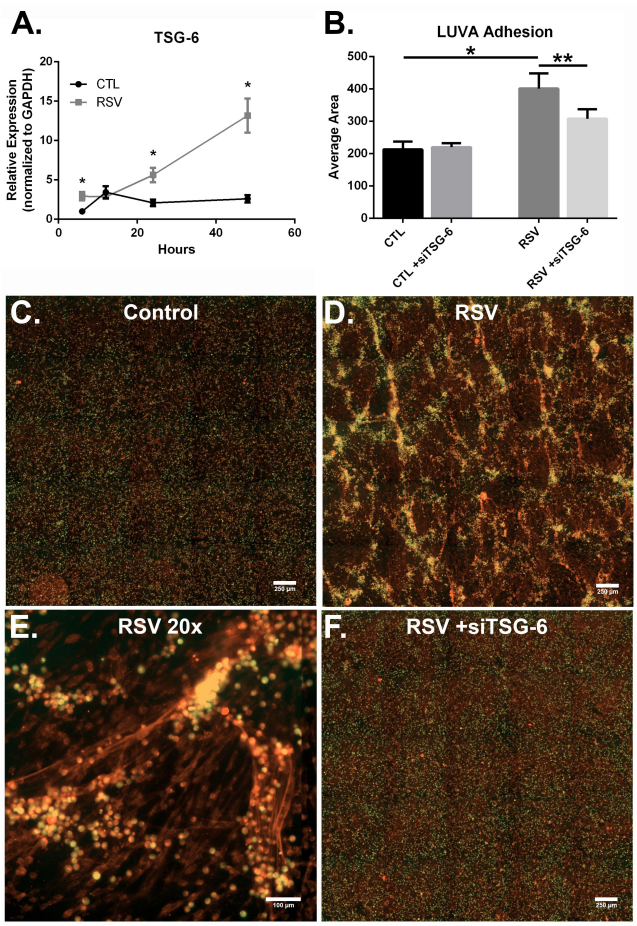

FIGURE 7 | The effect of TSG-6 expression by HLFs following RSV infection on mast cell binding. **(A)** TSG-6 expression by HLFs was significantly increased following 6, 24, and 48 h of RSV infection (*$P < 0.0001$, each comparison). Gene expression was normalized to GAPDH and is shown as normalized mean ± SD relative to control HLFs at 6 h. **(B)** Quantitative analysis of LUVA cells following knockdown of TSG-6 in a live-cell binding assay revealed a significant reduction in the binding of LUVA cells observed in HLF following RSV infection (54% reduction, **$P < 0.002$). Immunohistochemistry of adherent LUVA cells (green) to the HA ECM (red) generated by **(C)** control HLFs compared to **(D)** RSV-infected HLFs. Binding of LUVA cell aggregates is demonstrated in the RSV-infected HLF cultures along HA cable structures **(E)**. Aggregates of bound LUVA cells decreased following pre-treatment with siRNA to inhibit TSG-6 expression **(F)**. Data shown as mean ± SD for $N = 6$ replicates/group.

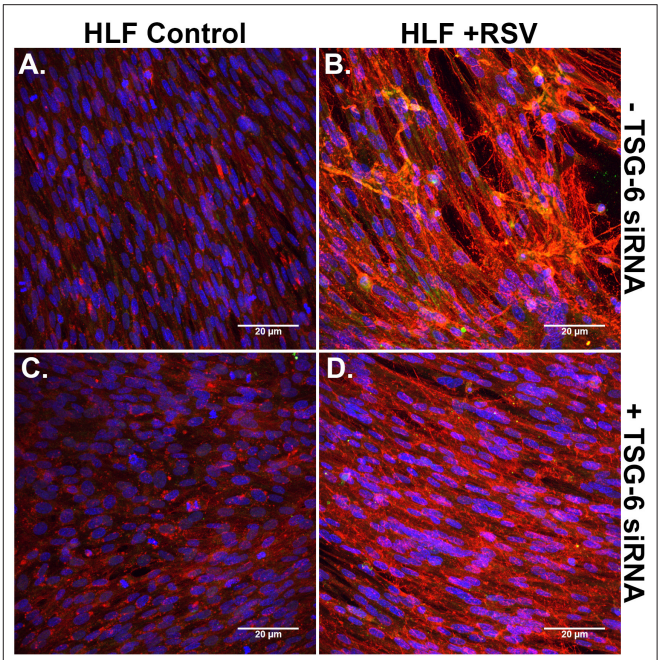

FIGURE 8 | Immunohistochemistry for HA (red) and ITIH1, i.e., HC1 (green), accumulated in the ECM generated by HLFs following a 48-h RSV infection. **(A)** Uninfected control HLFs displayed a modest amount of HA production and relatively little incorporation of ITIH1 into the ECM. **(B)** RSV-infected HLFs demonstrated increased HA staining and organization of the ECM in higher order structures that also stained positively for ITIH1. Inhibition of TSG-6 expression did not alter the pattern observed in control conditions **(C)**; however, inhibition of TSG-6 expression decreased the amount of staining for ITIH1 and decreased the number of higher order HA structures observed in the RSV-infected HLFs **(D)**.

leukocytes compared to co-culture of HLFs with AECs derived from healthy donors (12). That study taken together with the findings of the present study and the studies discussed above (11, 17) reveal some important similarities about the behavior of HLFs despite exposure to somewhat different pro-inflammatory conditions. In each of these studies, expansion of the amount of HA contained within the cell layer as well as a shift toward increased HMW-HA species were present. Although what causes the retention of the HMW-HA in the cell layer in these experiments is unknown, one possible explanation is that the HA is somehow being protected from degradation and/or turnover by the presence of hyaladherins such as TSG-6 or HA modifications such as HC-HA. While this hypothesis remains to be directly tested in HLFs, it is possible that this could be an important mechanism for the establishment of pro-inflammatory or "pathological" HA matrices that promote lung inflammation given the elegant series of studies that have implicated TSG-6 as an important mediator of inflammation and airway hyperresponsiveness in asthma (15, 31, 42–44).

While the present study has several strengths, there are also some important limitations to consider. We have demonstrated that increased HA accumulation following RSV infection of HLFs is accompanied by increased transcription of *HAS2* and *HAS3* mRNA with concurrent downregulation of *HYAL2* transcription. While the altered balance of HA syntheses and degradation may be sufficient to explain the greater accumulation of HA during RSV infection it is important to note that HASes are also subject to post-translational modifications that can affect their enzymatic activity, stability, and localization (45–47). Investigation of these mechanisms is beyond the scope of the present study but would be important considerations in future studies as these mechanisms may also be important targets for regulating the formation of a proinflammatory RSV-induced ECM. Similarly, signaling pathways proximal to the upregulation of HASes such as NF-κB signaling or transcription co-factors such as HAS2-AS1 have been explored in other models and may also be important mechanisms for the regulation of HAS expression and

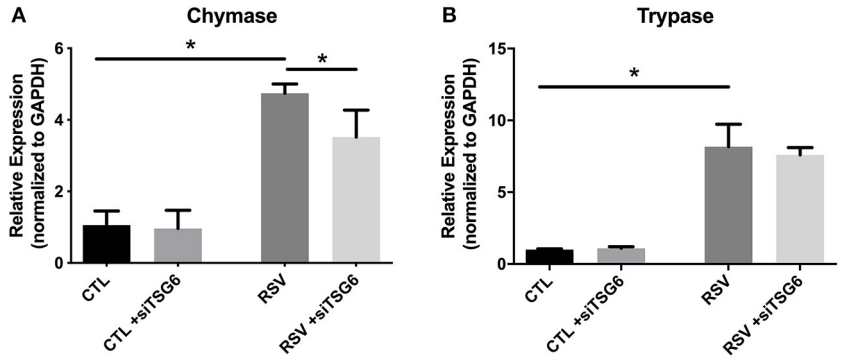

FIGURE 9 | Gene expression by LUVA cells co-cultured with RSV-infected HLFs with or without knockdown of TSG-6 expression by siRNA. **(A)** LUVA chymase expression was increased following co-culture with RSV-infected HLFs (*$P = 0.03$) but was found to be significantly reduced by treatment of HLFs with TSG-6 siRNA (*$P = 0.03$), HLFs (*$P = 0.03$). **(B)** Expression of tryptase was also increased following co-culture with RSV-infected HLFs (*$P = 0.03$); however, it was not significantly different following treatment of HLFs with TSG-6 siRNA. Gene expression was normalized to GAPDH and is shown as normalized mean ± SD relative to control HLFs for $N = 4$ replicates/group.

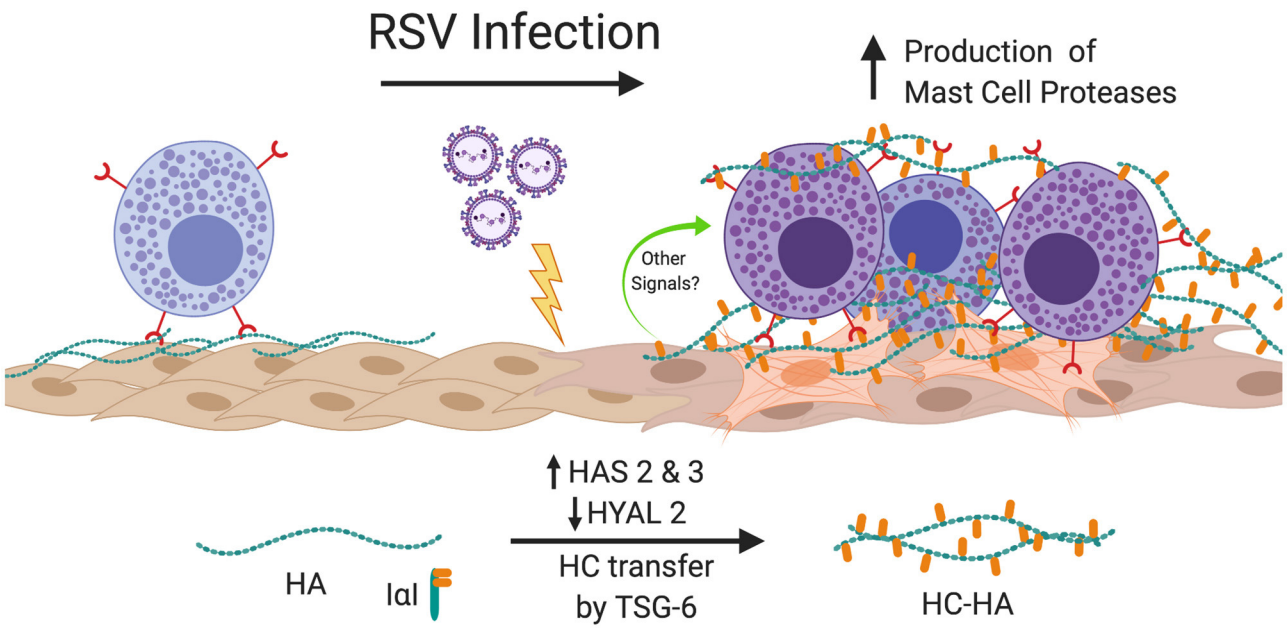

FIGURE 10 | Summary of findings. In this study, we have shown that infection of HLFs with RSV induces upregulation of HAS2 and HAS3 with concomitant downregulation of HYAL2 leading to greater accumulation of HA in the HLF cell layer that displays greater adherence of mast cells via direct interactions with the HA-enriched ECM via a CD44 dependent mechanism. Furthermore, RSV infected HLFs display increased expression of TSG-6, which in turn catalyzes the transfer of ITIH1 to form HC-HA and enhances the binding of mast cells to the ECM. Mast cells bound to the RSV-induced ECM upregulate expression mast cell proteases contributing to the proinflammatory milieu. Blocking the formation of the HA-enriched ECM or blocking the CD44 receptor with neutralizing antibodies attenuates this process. Figure created with BioRender.com.

accumulation of HA in the microenvironment in our model (48). Future studies aimed at addressing these considerations are needed.

In conclusion, we have demonstrated that infection of healthy pediatric HLFs with RSV leads to the establishment of a HA-enriched ECM that not only displays enhanced binding of mast cells, but also directly alters the phenotype of the cells that are interacting with this matrix. Additional molecules such as TSG-6 may be important in the establishment of this matrix through the formation of HC-HA, thus implicating its activity during inflammatory processes during acute viral infections. These studies raise the question as to whether HA or TSG-6 may be targets for therapeutic intervention during acute viral respiratory illnesses; however, further work will need to be done to characterize their contributions in *in vivo* model systems.

DATA AVAILABILITY STATEMENT

The raw data supporting the conclusions of this article will be made available by the authors, without undue reservation, to any qualified researcher.

AUTHOR CONTRIBUTIONS

SR, AP, TW, and JD drafted/edited the manuscript. SR, IK, SZ, AP, TW, and JD designed experiments. KB, LR, MW, NS, and CC made significant contributions to experiments, maintenance of the model system, and data analysis.

FUNDING

This work was supported by NIH U19AI125378 (PI: SZ), NIH R01HL128361 (PI: JD), and NIH K08HL135266 (PI: SR).

ACKNOWLEDGMENTS

The authors would like to thank Dr. Virginia M. Green for her careful reading and editing of the manuscript. LUVA cells were generously provided by Dr. John Steinke, University of Virginia.

REFERENCES

1. Nair H, Nokes DJ, Gessner BD, Dherani M, Madhi SA, Singleton RJ, et al. Global burden of acute lower respiratory infections due to respiratory syncytial virus in young children: a systematic review and meta-analysis. *Lancet*. (2010) 375:1545–55. doi: 10.1016/S0140-6736(10)60206-1
2. Lozano R, Naghavi M, Foreman K, Lim S, Shibuya K, Aboyans V, et al. Global and regional mortality from 235 causes of death for 20 age groups in 1990 and 2010: a systematic analysis for the Global Burden of Disease Study 2010. *Lancet*. (2012) 380:2095–128. doi: 10.1016/S0140-6736(12)61728-0
3. Openshaw PJ. Immunopathological mechanisms in respiratory syncytial virus disease. *Springer Semin Immunopathol*. (1995) 17:187–201. doi: 10.1007/BF00196165
4. Stein RT, Sherrill D, Morgan WJ, Holberg CJ, Halonen M, Taussig LM, et al. Respiratory syncytial virus in early life and risk of wheeze and allergy by age 13 years. *Lancet*. (1999) 354:541–5. doi: 10.1016/S0140-6736(98)10321-5
5. Sigurs N, Bjarnason R, Sigurbergsson F, Kjellman B. Respiratory syncytial virus bronchiolitis in infancy is an important risk factor for asthma and allergy at age 7. *Am J Respir Crit Care Med*. (2000) 161:1501–7. doi: 10.1164/ajrccm.161.5.9906076
6. Johnson JE, Gonzales RA, Olson SJ, Wright PF, Graham BS. The histopathology of fatal untreated human respiratory syncytial virus infection. *Mod Pathol*. (2007) 20:108–19. doi: 10.1038/modpathol.3800725
7. Bedke N, Haitchi HM, Xatzipsalti M, Holgate ST, Davies DE. Contribution of bronchial fibroblasts to the antiviral response in asthma. *J Immunol*. (2009) 182:3660–7. doi: 10.4049/jimmunol.0802471
8. Katoh S, Matsumoto N, Kawakita K, Tominaga A, Kincade PW, Matsukura S. A role for CD44 in an antigen-induced murine model of pulmonary eosinophilia. *J Clin Invest*. (2003) 111:1563–70. doi: 10.1172/JCI16583
9. Kai Y, Yoneyama H, Koyama J, Hamada K, Kimura H, Matsushima K. Treatment with chondroitinase ABC alleviates bleomycin-induced pulmonary fibrosis. *Med Mol Morphol*. (2007) 40:128–40. doi: 10.1007/s00795-007-0370-y
10. Evanko SP, Potter-Perigo S, Bollyky PL, Nepom GT, Wight TN. Hyaluronan and versican in the control of human T-lymphocyte adhesion and migration. *Matrix Biol*. (2012) 31:90–100. doi: 10.1016/j.matbio.2011.10.004
11. Gaucherand L, Falk BA, Evanko SP, Workman G, Chan CK, Wight TN. Crosstalk between T lymphocytes and lung fibroblasts: generation of a hyaluronan-enriched extracellular matrix adhesive for monocytes. *J Cell Biochem*. (2017) 118:2118–30. doi: 10.1002/jcb.25842
12. Reeves SR, Kang I, Chan CK, Barrow KA, Kolstad TK, White MP, et al. Asthmatic bronchial epithelial cells promote the establishment of a Hyaluronan-enriched, leukocyte-adhesive extracellular matrix by lung fibroblasts. *Respir Res*. (2018) 19:146. doi: 10.1186/s12931-018-0849-1
13. Garantziotis S, Savani RC. Hyaluronan biology: a complex balancing act of structure, function, location and context. *Matrix Biol*. (2019) 78–9:1–10. doi: 10.1016/j.matbio.2019.02.002
14. Petrey AC, de la Motte CA. Hyaluronan, a crucial regulator of inflammation. *Front Immunol*. (2014) 5:101. doi: 10.3389/fimmu.2014.00101
15. Lauer ME, Dweik RA, Garantziotis S, Aronica MA. The rise and fall of hyaluronan in respiratory diseases. *Int J Cell Biol*. (2015) 2015:712507. doi: 10.1155/2015/712507
16. Wight TN, Frevert CW, Debley JS, Reeves SR, Parks WC, Ziegler SF. Interplay of extracellular matrix and leukocytes in lung inflammation. *Cell Immunol*. (2017) 312:1–14. doi: 10.1016/j.cellimm.2016.12.003
17. Potter-Perigo S, Johnson PY, Evanko SP, Chan CK, Braun KR, Wilkinson TS, et al. Polyinosine-polycytidylic acid stimulates versican accumulation in the extracellular matrix promoting monocyte adhesion. *Am J Respir Cell Mol Biol*. (2010) 43:109–20. doi: 10.1165/rcmb.2009-0081OC
18. de La Motte CA, Hascall VC, Calabro A, Yen-Lieberman B, Strong SA. Mononuclear leukocytes preferentially bind via CD44 to hyaluronan on human intestinal mucosal smooth muscle cells after virus infection or treatment with poly(I.C). *J Biol Chem*. (1999) 274:30747–55. doi: 10.1074/jbc.274.43.30747
19. Pejler G, Ronnberg E, Waern I, Wernersson S. Mast cell proteases: multifaceted regulators of inflammatory disease. *Blood*. (2010) 115:4981–90. doi: 10.1182/blood-2010-01-257287
20. Lefrancais E, Duval A, Mirey E, Roga S, Espinosa E, Cayrol C, et al. Central domain of IL-33 is cleaved by mast cell proteases for potent activation of group-2 innate lymphoid cells. *Proc Natl Acad Sci USA*. (2014) 111:15502–7. doi: 10.1073/pnas.1410700111
21. Andersson CK, Shikhagaie M, Mori M, Al-Garawi A, Reed JL, Humbles AA, et al. Distal respiratory tract viral infections in young children trigger a marked increase in alveolar mast cells. *ERJ Open Res*. (2018) 4:00038-2018. doi: 10.1183/23120541.00038-2018
22. Fukui M, Whittlesey K, Metcalfe DD, Dastych J. Human mast cells express the hyaluronic-acid-binding isoform of CD44 and adhere to hyaluronic acid. *Clin Immunol*. (2000) 94:173–8. doi: 10.1006/clim.1999.4830
23. Takano H, Nakazawa S, Shirata N, Tamba S, Furuta K, Tsuchiya S, et al. Involvement of CD44 in mast cell proliferation during terminal differentiation. *Lab Invest*. (2009) 89:446–55. doi: 10.1038/labinvest.2008.159
24. Laidlaw TM, Steinke JW, Tinana AM, Feng C, Xing W, Lam BK, et al. Characterization of a novel human mast cell line that responds to stem cell factor and expresses functional FcepsilonRI. *J Allergy Clin Immunol*. (2011) 127:815–22.e1–5. doi: 10.1016/j.jaci.2010.12.1101
25. Lee HC, Headley MB, Loo YM, Berlin A, Gale M Jr, Debley JS, et al. Thymic stromal lymphopoietin is induced by respiratory syncytial virus-infected airway epithelial cells and promotes a type 2 response to infection. *J Allergy Clin Immunol*. (2012) 130:1187–96.e5. doi: 10.1016/j.jaci.2012.07.031
26. Kultti A, Pasonen-Seppanen S, Jauhiainen M, Rilla KJ, Karna R, Pyoria E, et al. 4-Methylumbelliferone inhibits hyaluronan synthesis by depletion of cellular UDP-glucuronic acid and downregulation of hyaluronan synthase 2 and 3. *Exp Cell Res*. (2009) 315:1914–23. doi: 10.1016/j.yexcr.2009.03.002
27. Zheng Z, Katoh S, He Q, Oritani K, Miyake K, Lesley J, et al. Monoclonal antibodies to CD44 and their influence on hyaluronan recognition. *J Cell Biol*. (1995) 130:485–95. doi: 10.1083/jcb.130.2.485
28. Evanko SP, Johnson PY, Braun KR, Underhill CB, Dudhia J, Wight TN. Platelet-derived growth factor stimulates the formation of versican-hyaluronan aggregates and pericellular matrix expansion

in arterial smooth muscle cells. *Arch Biochem Biophys*. (2001) 394:29–38. doi: 10.1006/abbi.2001.2507
29. Pfaffl MW. A new mathematical model for relative quantification in real-time RT-PCR. *Nucleic Acids Res*. (2001) 29:e45. doi: 10.1093/nar/29.9.e45
30. Day AJ, de la Motte CA. Hyaluronan cross-linking: a protective mechanism in inflammation? *Trends Immunol*. (2005) 26:637–43. doi: 10.1016/j.it.2005.09.009
31. Swaidani S, Cheng G, Lauer ME, Sharma M, Mikecz K, Hascall VC, et al. TSG-6 protein is crucial for the development of pulmonary hyaluronan deposition, eosinophilia, and airway hyperresponsiveness in a murine model of asthma. *J Biol Chem*. (2013) 288:412–22. doi: 10.1074/jbc.M112.389874
32. Velez TE, Bryce PJ, Hulse KE. Mast Cell interactions and crosstalk in regulating allergic inflammation. *Curr Allergy Asthma Rep*. (2018) 18:30. doi: 10.1007/s11882-018-0786-6
33. Gonzalez-de-Olano D, Alvarez-Twose I. Mast cells as key players in allergy and inflammation. *J Investig Allergol Clin Immunol*. (2018) 28:365–78. doi: 10.18176/jiaci.0327
34. Piliponsky AM, Romani L. The contribution of mast cells to bacterial and fungal infection immunity. *Immunol Rev*. (2018) 282:188–97. doi: 10.1111/imr.12623
35. Krystel-Whittemore M, Dileepan KN, Wood JG. Mast cell: a multi-functional master cell. *Front Immunol*. (2015) 6:620. doi: 10.3389/fimmu.2015.00620
36. Dai H, Korthuis RJ. Mast cell proteases and inflammation. *Drug Discov Today Dis Models*. (2011) 8:47–55. doi: 10.1016/j.ddmod.2011.06.004
37. Tanaka S. Targeting CD44 in mast cell regulation. *Expert Opin Ther Targets*. (2010) 14:31–43. doi: 10.1517/14728220903473186
38. Girodet PO, Ozier A, Trian T, Begueret H, Ousova O, Vernejoux JM, et al. Mast cell adhesion to bronchial smooth muscle in asthma specifically depends on CD51 and CD44 variant 6. *Allergy*. (2010) 65:1004–12. doi: 10.1111/j.1398-9995.2009.02308.x
39. Al-Afif A, Alyazidi R, Oldford SA, Huang YY, King CA, Marr N, et al. Respiratory syncytial virus infection of primary human mast cells induces the selective production of type I interferons, CXCL10, and CCL4. *J Allergy Clin Immunol*. (2015) 136:1346–54.e1. doi: 10.1016/j.jaci.2015.01.042
40. Jessen TE, Odum L. Role of tumour necrosis factor stimulated gene 6 (TSG-6) in the coupling of inter-alpha-trypsin inhibitor to hyaluronan in human follicular fluid. *Reproduction*. (2003) 125:27–31. doi: 10.1530/rep.0.1250027
41. Forteza R, Casalino-Matsuda SM, Monzon ME, Fries E, Rugg MS, Milner CM, et al. TSG-6 potentiates the antitissue kallikrein activity of inter-alpha-inhibitor through bikunin release. *Am J Respir Cell Mol Biol*. (2007) 36:20–31. doi: 10.1165/rcmb.2006-0018OC
42. Lauer ME, Majors AK, Comhair S, Ruple LM, Matuska B, Subramanian A, et al. Hyaluronan and its heavy chain modification in asthma severity and experimental asthma exacerbation. *J Biol Chem*. (2015) 290:23124–34. doi: 10.1074/jbc.M115.663823
43. Lauer ME, Cheng G, Swaidani S, Aronica MA, Weigel PH, Hascall VC. Tumor necrosis factor-stimulated gene-6 (TSG-6) amplifies hyaluronan synthesis by airway smooth muscle cells. *J Biol Chem*. (2013) 288:423–31. doi: 10.1074/jbc.M112.389882
44. Stober VP, Johnson CG, Majors A, Lauer ME, Cali V, Midura RJ, et al. TNF-stimulated gene 6 promotes formation of hyaluronan-inter-alpha-inhibitor heavy chain complexes necessary for ozone-induced airway hyperresponsiveness. *J Biol Chem*. (2017) 292:20845–58. doi: 10.1074/jbc.M116.756627
45. Passi A, Vigetti D, Buraschi S, Iozzo RV. Dissecting the role of hyaluronan synthases in the tumor microenvironment. *FEBS J*. (2019) 286:2937–49. doi: 10.1111/febs.14847
46. Vigetti D, Passi A. Hyaluronan synthases posttranslational regulation in cancer. *Adv Cancer Res*. (2014) 123:95–119. doi: 10.1016/B978-0-12-800092-2.00004-6
47. Melero-Fernandez de Mera RM, Arasu UT, Karna R, Oikari S, Rilla K, Vigetti D, et al. Effects of mutations in the post-translational modification sites on the trafficking of hyaluronan synthase 2 (HAS2). *Matrix Biol*. (2019) 80:85–103. doi: 10.1016/j.matbio.2018.10.004
48. Moretto P, Karousou E, Viola M, Caon I, D'Angelo ML, De Luca G, et al. Regulation of hyaluronan synthesis in vascular diseases and diabetes. *J Diabetes Res*. (2015) 2015:167283. doi: 10.1155/2015/167283

Conflict of Interest: The authors declare that the research was conducted in the absence of any commercial or financial relationships that could be construed as a potential conflict of interest.

frontiers in Immunology

ORIGINAL RESEARCH
published: 30 January 2020
doi: 10.3389/fimmu.2020.00029

CD44 Loss Disrupts Lung Lipid Surfactant Homeostasis and Exacerbates Oxidized Lipid-Induced Lung Inflammation

Yifei Dong[1], *Arif A. Arif*[1,2], *Jian Guo*[3], *Zongyi Ha*[1], *Sally S. M. Lee-Sayer*[1], *Grace F. T. Poon*[1], *Manisha Dosanjh*[1], *Calvin D. Roskelley*[2], *Tao Huan*[3] *and Pauline Johnson*[1]*

[1] *Department of Microbiology and Immunology, University of British Columbia, Vancouver, BC, Canada,* [2] *Department of Cellular and Physiological Sciences, University of British Columbia, Vancouver, BC, Canada,* [3] *Department of Chemistry, University of British Columbia, Vancouver, BC, Canada*

Alveolar macrophages (AMs) are CD44 expressing cells that reside in the alveolar space where they maintain lung homeostasis by serving critical roles in immunosurveillance and lipid surfactant catabolism. AMs lacking CD44 are unable to bind the glycosaminoglycan, hyaluronan, which compromises their survival and leads to reduced numbers of AMs in the lung. Using RNA sequencing, lipidomics and multiparameter flow cytometry, we demonstrate that CD44$^{-/-}$ mice have impaired AM lipid homeostasis and increased surfactant lipids in the lung. CD44$^{-/-}$ AMs had increased expression of CD36, a lipid scavenger receptor, as well as increased intracellular lipid droplets, giving them a foamy appearance. RNA sequencing revealed the differential expression of genes associated with lipid efflux and metabolism in CD44$^{-/-}$ AMs. Lipidomic analysis showed increased lipids in both the supernatant and cell pellet extracted from the bronchoalveolar lavage of CD44$^{-/-}$ mice. Phosphatidylcholine species, cholesterol, oxidized phospholipids and levels of reactive oxygen species (ROS) were increased in CD44$^{-/-}$ AMs. Oxidized phospholipids were more cytotoxic to CD44$^{-/-}$ AMs and induced greater lung inflammation in CD44$^{-/-}$ mice. Reconstitution of CD44$^{+/+}$ mice with CD44$^{-/-}$ bone marrow as well as adoptive transfer of CD44$^{-/-}$ AMs into CD44$^{+/+}$ mice showed that lipid accumulation in CD44$^{-/-}$ AMs occurred irrespective of the lung environment, suggesting a cell intrinsic defect. Administration of colony stimulating factor 2 (CSF-2), a critical factor in AM development and maintenance, increased AM numbers in CD44$^{-/-}$ mice and decreased phosphatidylcholine levels in the bronchoalveolar lavage, but was unable to decrease intracellular lipid accumulation in CD44$^{-/-}$ AMs. Peroxisome proliferator-activated receptor gamma (PPARγ), downstream of CSF-2 signaling and a regulator of lipid metabolism, was reduced in the nucleus of CD44$^{-/-}$ AMs, and PPARγ inhibition in normal AMs increased their lipid droplets. Thus, CD44 deficiency causes defects in AMs that lead to abnormal lipid accumulation and oxidation, which exacerbates oxidized lipid-induced lung inflammation. Collectively, these findings implicate CD44 as a regulator of lung homeostasis and inflammation.

Keywords: CD44, alveolar macrophage, lung surfactant lipids, oxidized lipids, lipidomics, flow cytometry, RNA sequencing, lung inflammation

OPEN ACCESS

Edited by:
Aaron C. Petrey,
The University of Utah, United States

Reviewed by:
Toshiyuki Murai,
Osaka University, Japan
Eva Turley,
University of Western Ontario, Canada

***Correspondence:**
Pauline Johnson
pauline@mail.ubc.ca

Specialty section:
This article was submitted to Inflammation, a section of the journal Frontiers in Immunology

Received: *01 October 2019*
Accepted: *08 January 2020*
Published: *30 January 2020*

Citation:
Dong Y, Arif AA, Guo J, Ha Z, Lee-Sayer SSM, Poon GFT, Dosanjh M, Roskelley CD, Huan T and Johnson P (2020) CD44 Loss Disrupts Lung Lipid Surfactant Homeostasis and Exacerbates Oxidized Lipid-Induced Lung Inflammation. Front. Immunol. 11:29. doi: 10.3389/fimmu.2020.00029

INTRODUCTION

Alveolar macrophages (AMs) are important for lung homeostasis, playing key roles in immunosurveillance and lipid surfactant catabolism (1). They are fetal monocyte-derived tissue resident macrophages (2) in the alveolar space that require colony stimulating factor 2 (CSF-2 also known as GM-CSF) (2, 3), peroxisome proliferator-activated receptor gamma (PPARγ) (4), and transforming growth factor beta (TGFβ) (5) for their development, maturation and survival. The deficiency of any of these factors leads to the accumulation of immature macrophages which are unable to catabolize surfactant lipids, and this leads to the buildup of lipids in the immature AMs which take on a foamy appearance. Consequently, lung surfactant lipids build up in the alveolar space and this can lead to pulmonary alveolar proteinosis (PAP) (6, 7). While primary PAP is attributed to defective CSF-2 signaling, the causes of secondary PAP are largely unknown (7). CSF-2 induces the expression of PPARγ in fetal lung monocytes, which is critical for the generation of the AM gene signature (4). PPARγ is also important for lipid catabolism (8–10) in mature AMs (4). TGFβ upregulates PPARγ expression and conditional deletion of the TGFβ receptor in macrophages leads to the accumulation of immature, lipid-laden foamy macrophages, showing a key role for TGFβ signaling in AM development (5). Autocrine TGFβ, produced by mature AMs, also contributes to their self-maintenance and survival (5).

AMs have an important role in the clearance of pulmonary surfactant produced by alveolar epithelial cells which is typically made up of 80% polar lipids [primarily phosphatidylcholine (PC)], 10% neutral lipids including cholesterol, and 10% proteins (1, 7, 11). AM numbers are reduced during lung damage and inflammation (12–14) and this leads to the accumulation of surfactant lipids in the alveolar space where they become susceptible to oxidation in the oxygen-rich environment of the lung, especially during inflammation when reactive oxygen species (ROS) are generated by inflammatory cells (15). Oxidized lipids are cytotoxic, and if they build up in AMs, lung function is compromised (16). For example, bleomycin-induced lung injury leads to inflammation, ROS production, phospholipid oxidation and the generation of foamy macrophages, which all contribute to lung dysfunction (16). In contrast, mice lacking a NADPH-oxidase subunit that cannot generate ROS were protected from bleomycin-induced pulmonary damage and fibrosis (17). In humans, oxidized lipid cytotoxicity can lead to the life-threatening acute respiratory distress syndrome (18) and lung phospholipid peroxidation is associated with asthma and chronic obstructive pulmonary disease progression (19). Furthermore, oxidized phosphatidylcholine (OxPC) is found in AMs from patients diagnosed with idiopathic interstitial pneumonia (20). Thus, oxidized lipids are an important component of the pathophysiology of lung disease, and the removal of excess surfactant lipids and oxidized lipids from the alveolar space by AMs is essential to maintain vital lung function and homeostasis.

Unlike most other macrophages at steady state, mature murine AMs express high levels of CD11c, Siglec F, and constitutively bind hyaluronan (HA) via its receptor, CD44 (21, 22). HA, a component of the extracellular matrix, is implicated in both lung homeostasis and inflammation (23). At homeostasis, CD44-dependent HA binding by AMs results in the formation of a pericellular HA coat that promotes their survival (12). AMs from $CD44^{-/-}$ mice lack the HA coat, leading to a decrease in their viability and $CD44^{-/-}$ mice have approximately half the normal number of AMs (12). In humans, CD44 expression is lower on AMs isolated from patients with diffuse panbronchiolitis (24) and chronic obstructive pulmonary disease (COPD) (25), and in mice, the depletion of AMs exaggerates pulmonary inflammatory responses (26, 27). Furthermore, $CD44^{-/-}$ mice treated with bleomycin are unable to resolve lung inflammation, resulting in a buildup of HA and apoptotic neutrophils (28, 29). Here, we investigated the impact of CD44 in lung homeostasis and inflammation by studying AMs from $CD44^{-/-}$ mice.

MATERIALS AND METHODS

Mice

C57BL/6J ($CD45.2^{+}$), B6.SJL-$Ptprc^{a}Pepc^{b}$/BoyJ ($CD45.1^{+}$), C57BL/6J x BoyJ heterozygotes ($CD45.1^{+}$, $CD45.2^{+}$), and $CD44^{-/-}$ mice were housed and bred in specific pathogen free facilities, as previously described (12). Experiments used 6–14 week-old, age and sex matched mice and were conducted with protocols approved by the University Animal Care Committee in accordance with the Canadian Council of Animal Care guidelines for ethical animal research.

Reagents

Fluorescein-conjugated HA (FL-HA), used to measure the ability of cells to bind HA, was prepared from rooster comb HA sodium salt of expected molecular mass 1–4 million and <2% protein contamination, catalog no 5388 (Sigma-Aldrich), as previously described (12). *Streptomyces hyaluronlyticus* hyaluronidase (HA'se) and biotinylated HA-binding protein (HABP) were from Millipore, and streptavidin was from Thermo Fisher Scientific or eBioscience. Recombinant mouse CSF-2 (carrier free) was from BioLegend. L-α-phosphatidylcholine (PC) was from Sigma-Aldrich. 1-palmitoyl-2-(5′-oxo-valeroyl)-sn-glycero-3-phosphocholine (POVPC) was from Avanti Polar Lipids. Fatty acid free (FAF) BSA was from Roche Diagnostics. BODIPY 493/503, N-(7-Nitrobenz-2-Oxa-1,3-Diazol-4-yl)-1,2-Dihexadecanoyl-sn-Glycero-3-Phosphoethanolamine (NBD-PE), and 2′,7′-dichlorodihydrofluorescein diacetate (H_2DCFDA) were from Thermo Fisher Scientific. The PPARγ antagonist, T0070907, was from Tocris Bioscience. Fluorescent or biotinylated labeled CD11c (N418), CD11b (M1/70), Ly6C (HK1.4), CD14 (SA2-8), CD45.1 (A20), CD45.2 (104), CD200R (OX110), MHC II (M5/114.15.2), Siglec F (1RNM44N), and SIRPα (P84) were from Thermo Fisher Scientific; CD36 (HM36) and CD206 (C068C2) were from Biolegend; CD44 (IM7) was from Ablab; Ly6G (1A8), Siglec F (E50-2440), and mouse IgG1κ isotype were from BD Biosciences; CD116 (698423) and MerTK (polyclonal BAF591) were from R&D; PPARγ (81B8) was from Cell Signaling Technologies, and anti-OxPC (E06) was from Avanti Polar Lipids.

In vivo Experiments

Bone marrow (BM) reconstitution into irradiated recipients was essentially as described in Dong et al. (12). POVPC (200 μg) in 50 μl PBS, or CSF-2 (2 μg daily) was given to mice by intratracheal instillation (i.t.) by laryngoscopic manipulation, and the bronchoalveolar lavage (BAL) analyzed 3 or 7 days later, respectively. For adoptive transfer experiments, 2–3 × 10^5 $CD44^{+/+}$ or $CD44^{-/-}$ AMs were transferred by i.t. into $CD45.1^+$ $CD44^{+/+}$ or $CD45.2^+$ $CD44^{-/-}$ mice, and BAL was analyzed on day 7.

Isolation of Bronchoalveolar Lavage (BAL) Cells for RNAseq, Flow Cytometry or *in vitro* Analysis

BAL was isolated from $CD44^{+/+}$ and $CD44^{-/-}$ mice using 4 × 700 μl PBS, 2 mM EDTA and the BAL cells (>95% AMs from naïve mice) were treated by RBC lysis buffer (0.84% NH_4Cl in 10 mM Tris pH 7.2) for 5 min, centrifuged and either subjected to RNA extraction using RNeasy Mini Kit (Qiagen) or counted manually using the hemocytometer and trypan blue, and prepared for flow cytometry as previously described (12). Alternatively, AMs were washed once with PBS and incubated with 2.5 μM BODIPY 493/503 in PBS, 5 μM H_2DCFDA in PBS, or 10 μM NBD-PE in RPMI for 30 min at 37°C prior to flow cytometry. Or, AMs were incubated with 1% EtOH (vehicle solvent), 50 μM PC, or 50 μM POVPC in PBS for 1 h at 37°C, then analyzed with Annexin V-PE and DAPI by flow cytometry (12). HABP was used to detect cell surface HA by flow cytometry (12). For blocking FL-HA binding on AMs, *ex vivo* $CD44^{+/+}$ and $CD44^{-/-}$ AMs were incubated with the CD44 blocking antibody KM81 (1:100 from tissue culture supernatant) for 30 min at 4°C. All flow cytometry was performed using the BD LSR II.

In vitro AM Culture

AMs were cultured with 20 ng/ml of recombinant CSF-2 in RPMI containing 1% BSA, in the presence or absence of 500 μM PC or 1 μM T0070907 in a 96-well non-tissue culture treated plate for 48 h, harvested using versene, and the cells analyzed by flow cytometry. For culture with PC, 1% FAF BSA was used.

Intracellular Labeling of AMs

AMs were isolated by BAL with PBS 2 mM EDTA and fixed with 2% paraformaldehyde immediately for 10 min at room temperature, washed twice with PBS, labeled with the E06 or PPARγ antibody intracellularly using the Intracellular Fixation & Permeabilization Buffer Set (Thermo Fisher Scientific).

Analysis of BAL Fluid

BAL isolated using PBS 2 mM EDTA was centrifuged and the supernatant and cell pellet collected. Hyaluronan Quantikine ELISA Kit (R&D Systems) was used to determine the HA concentration in the BAL supernatant. Total protein was determined using the Pierce BCA Protein Assay Kit (Thermo Fisher Scientific). Total PC concentration was determined using the Phospholipase C assay kit (Wako Diagnostics).

Gas Chromatography Analysis for Cholesterol

Lipids were extracted twice from 1 ml BAL supernatant by adding 6 ml of 2:1 v/v chloroform: methanol, with 1% acetic acid. Organic solvents were evaporated under a stream of nitrogen gas. Lipid extracts were resuspended in pyridine and then an equal part of N,O-bis(trimethylsilyl)trifluoro-acetamide with trimethylchlorosilane. Samples were spiked with 10 μM cholestane as an internal standard and analyzed by gas-chromatography mass spectrometry (GC-MS).

Flow Cytometric Analysis

Flow cytometry was analyzed using FlowJo VX (Treestar). Flow cytometry plots shown were first gated by size, singlets, and live/dead stain. AMs were then gated as $CD11c^+$ and Siglec F^+ (**Supplementary Figures 1A,B**). Fold difference was calculated by dividing each $CD44^{+/+}$ and $CD44^{-/-}$ biological replicate by the mean of $CD44^{+/+}$ samples in each experiment.

Confocal Microscopy

AMs labeled with BODIPY or E06 and DAPI were mounted onto Superfrost$^+$ microscope slides (Thermo Fisher Scientific). Whole cell image stacks were acquired using a Leica Sp8 microscope. Maximum stack projections were analyzed using ImageJ 1.51 (NIH). BODIPY stained lipid droplets were identified using a trainable segmentation function in ImageJ, followed by particle analysis, and droplet masks were applied onto the raw images to measure number, pixel intensity, and droplet size. E06 labeled droplets were also counted. PPARγ and DAPI labeled AMs were acquired using a Leica Sp5. Total nuclear PPARγ was measured within the $DAPI^+$ nuclear area and quantified as mean pixel intensity (MPI). Immunofluorescence of 12 μm lung tissue cryosections was measured as previously described (12) and analyzed using ImageJ for HABP mean pixel intensity (MPI), where HA-rich bronchioles were excluded from the analysis.

RNAseq Analysis

RNA from three independent $CD44^{+/+}$ and three $CD44^{-/-}$ samples were pooled from the BAL of 4, 2, or 2 female mice, respectively.

Illumina RNA Sequencing

RNA was sequenced by the UBC Biomedical Research Center. RNA quality, *18S* and *28S* ribosomal RNA with RIN = 9.6, was determined by Agilent 2100 Bioanalyzer following the standard protocol for NEBNext Ultra II Stranded mRNA (New England Biolabs). Sequencing was performed on the Illumina NextSeq 500 with paired end 42bp × 42bp reads. De-multiplexed read sequences were then aligned to the *Mus musculus* (mm10) reference sequence using Spliced Transcripts Alignment to a Reference, STAR (https://www.ncbi.nlm.nih.gov/pubmed/23104886), aligners. The sequence data is available at GEO database, accession number: GSE138445.

Cufflinks and Cuffdiff

Assembly and differential expression were estimated using Cufflinks (http://cole-trapnell-lab.github.io/cufflinks/) through

Cufflinks Assembly & DE version 2.1.0 which included Cuffdiff analysis (30). Gene differences with a q value (p-value adjusted for false discovery rate) <0.05 were considered significant.

Metascape Analysis

Metascape analysis was performed on the genes annotated as significantly different from the Cuffdiff analysis (31). Gene IDs were entered and analyzed as *M. musculus*. Significantly different GO pathways were obtained as an output from Metascape.

R Scripts and Heatmaps

R language was used for bioinformatic analysis of RNA sequencing results using RStudio Version 1.1.442. Gene ID was converted to Entrez ID using Annotables: Ensembl 90 conversion chart (32). Heatmaps were created using R library, "pheatmap()." The input for heatmaps were a list of differentially expressed genes in specific GO pathways and their corresponding fragments per kilobase of transcript per million mapped reads (FPKMs). FPKM values were obtained from Illumina RNA-Sequencing.

String Analysis

All 200 significant genes ($q < 0.05$) were input into the String Consortium (33). String Consortium maps the interactions between genes based on text mining, experiments, databases, co-expression, neighborhood, gene fusion, and co-occurrence.

Mass Spectrometry, Lipidomics, and Analysis

BAL Cell Pellet and Supernatant Sample Preparation

The BAL from 8 $CD44^{+/+}$ and 8 $CD44^{-/-}$ female mice were spun down to generate a supernatant and cell pellet for each sample. Lipids were extracted from the BAL pellets, $CD44^{+/+}$ (WT1-8) and $CD44^{-/-}$ (KO1-8) with 400 µl ice cold extraction solvent [methanol:acetonitrile (ACN):water = 2:1:1, v:v:v] followed by three freeze-thaw cycles. Proteins were precipitated at −20°C for 2 h, then 900 µl methyl tert-butyl ether (MTBE) was added and vortexed for 90 min on an open-air microplate shaker. One hundred and seventy microliter H_2O was then added into the solution followed by centrifugation (17,530 g, 4°C, 1 min) to accelerate the phase separation. $CD44^{+/+}$ (WT1-8) and $CD44^{-/-}$ (KO1-8) BAL supernatant samples (3 ml each) were thawed on ice and 3 ml MTBE added and vortexed for 90 min on an open-air microplate shaker. In both cases, the upper organic phase was carefully transported to a 1.5 ml Eppendorf vial and concentrated by Speed-vac at 4°C. The concentrated pellets were subsequently reconstituted with ACN:isopropyl alcohol(IPA) = 1:1, v:v for LC-MS analysis. One method control (MC) was prepared using the same procedure but with no sample in the vial. One quality control (QC) was prepared by pooling 10 µl from each of the 16 reconstituted solutions (8 WT+8 KO). QC was injected between every four sample injections to ensure the instrument was stable and the sample injection volume was optimized.

Liquid Chromatography Mass Spectrometry (LC-MS) Analysis

The LC-MS analysis was performed on Bruker Impact II™ UHR-QqTOF (Ultra-High Resolution Qq-Time-Of-Flight) mass spectrometer coupled with a Agilent 1290 Infinity™ II LC system. LC separation was performed on a Waters ACQUITY UPLC BEH C18 Column (130 Å, 1.7 µm, 1.0 mm × 100 mm). Two microliter sample solutions of each replicate, MC and QC were injected in a random order. Two microliter Sodium formate was injected within each run for internal calibration. The mobile phase A was 60% ACN 40% H_2O [2 mM ammonium acetate (NH_4Ac) in positive mode, 5 mM NH_4Ac in negative mode]; mobile phase B was 90% IPA 10% ACN (2 mM NH_4Ac in positive mode, 5 mM NH_4Ac in negative mode). The chromatographic gradient was run at a flow rate of 0.100 ml/min as follows: 0–8 min: linear gradient from 95 to 60% A; 8–14 min: linear gradient from 60 to 30% A; 14–20 min: linear gradient from 30 to 5% A; 20–23 min: hold at 5% A; 23–24 min: linear gradient from 5 to 95% A; 24–33 min: hold at 95% A. The mass spectrometer was operated in Auto MS/MS mode. The ionization source capillary voltage was set to 4.5 kV in positive scanning mode and −3.5 kV in negative scanning mode. The nebulizer gas pressure was set to 1.0 bar. The dry gas temperature was set to 220°C. The collision energy for MS/MS was set to 7 eV. The data acquisition was performed in a range of 50–1,200 m/z at a frequency of 8 Hz.

Data Interpretation

Bruker Data Analysis software was used to calibrate the spectra using sodium formate as the internal reference. Then the raw data files with format of ".d" were converted to format of ".abf" using AbfConverter. The converted files were then uploaded onto MS-DIAL for lipid feature extraction and alignment. Lipids identification was carried out using LipidBlast available in MS-DIAL (34, 35). The parameters were set as follows: MS1 tolerance was 0.01 Da; MS2 tolerance was 0.05 Da; retention time tolerance was 0.5 min. The alignment result was exported in a "csv." file. Fold change (FC, calculated as $CD44^{-/-}/CD44^{+/+}$) and p-values between $CD44^{+/+}$ and $CD44^{-/-}$ groups were calculated using a two tails distribution, homoscedastic t test in Microsoft Excel. The lipids with FC > 1.5 or FC < 0.67, and $p < 0.05$ were selected as being significantly different between the $CD44^{+/+}$ and $CD44^{-/-}$ groups.

Statistics

Statistical analysis used is described in the figure legends. The majority of graphs were generated using GraphPad Prism 6 and the data shown are the average ± standard deviation. Significance was defined as $^{*}p < 0.05$, $^{**}p < 0.01$, $^{***}p < 0.001$. Non-paired Student's t-tests were used to compare biological replicates from individual $CD44^{+/+}$ and $CD44^{-/-}$ mice. Paired Student's t-tests were used in adoptive transfer experiments, where $CD44^{+/+}$ and $CD44^{-/-}$ cells are within the same mouse, in each biological replicate. Welch's t-test, which does not assume equal variance, was used to compare HA deposition in the lung, to account for the variability that can arise in inflammation between each animal, and between $CD44^{+/+}$ and $CD44^{-/-}$

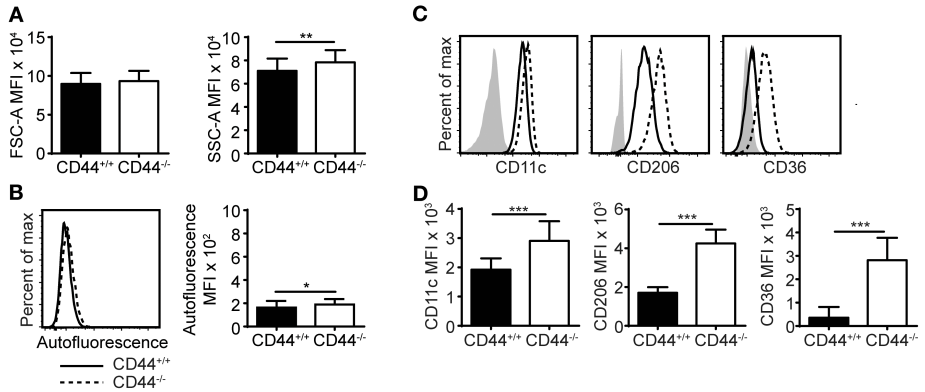

FIGURE 1 | CD44$^{-/-}$ mice have abnormal AMs. **(A,B)** Bar graphs and representative flow cytometry histograms comparing the FSC-A (cell size), SSC-A (cell granularity), and autofluorescence of CD44$^{+/+}$ and CD44$^{-/-}$ AMs from BAL of naïve mice. **(C,D)** Representative flow cytometry histograms and graphs comparing the MFI of cell surface phenotype of CD44$^{+/+}$ and CD44$^{-/-}$ AMs, where the background MFI of autofluorescence from unlabeled CD44$^{+/+}$ or CD44$^{-/-}$ cells was subtracted from the values shown. Data show an average of two experiments ± SD, each with three to five CD44$^{+/+}$ and CD44$^{-/-}$ mice, except for in **(A)** which was the average of BAL AMs from 44 CD44$^{+/+}$ and CD44$^{-/-}$ mice over 12 experiments. Significance indicated as $^{*}p < 0.05$, $^{**}p < 0.01$, $^{***}p < 0.001$, non-paired Student's *t*-test.

groups. The homoscedastic *t*-test, which assumes equal variance, was performed on the lipidomics data.

RESULTS

CD44$^{-/-}$ AMs Have Increased Cellular Granularity and Cell Surface Receptor Expression

CD44$^{-/-}$ mice have approximately 50% less AMs compared to normal C57Bl/6J mice, as previously reported (12). These CD44$^{-/-}$ AMs express the characteristic AM markers: CD11c and Siglec F, but are unable to bind hyaluronan, an extracellular matrix glycosaminoglycan that promotes their survival (12). Here, flow cytometric analysis showed that CD44$^{-/-}$ AMs, gated as in **Supplementary Figure 1A**, were unable to bind fluorescein labeled HA (FL-HA), had a greater granularity (SSC) and a slightly higher autofluorescence than CD44$^{+/+}$ AMs (**Figures 1A,B** and **Supplementary Figures 1B,E**). In addition, there was a slight increase in the mean fluorescence intensity (MFI) of several cell surface molecules normally expressed on resident AMs (CD11c, CD206, CD200R, Sirpα, MerTK) but Siglec F levels remained unchanged (**Figures 1C,D** and **Supplementary Figures 1C,D**). Adjusting for increased autofluorescence did not account for these changes. There was also increased expression of molecules not normally expressed on mature AMs (CD36, MHCII, CD11b, and PD-1) (**Figures 1C,D** and **Supplementary Figures 1C,D**). CD36 is a scavenger receptor for fatty acids and oxidized lipids (36, 37), raising the possibility that the increased SSC and autofluorescence may represent increased lipid content. To determine if cell surface HA bound on normal AMs physically affected the binding of antibodies and thus contributed to the phenotypic differences observed by flow cytometry, CD44$^{+/+}$ and CD44$^{-/-}$ AMs were treated with hyaluronidase (HA'se). This decreased the binding of HABP on CD44$^{+/+}$ AMs, indicating the removal of HA. HABP binding was reduced to the levels observed on CD44$^{-/-}$ AMs, but not quite to the level of unstained cells, suggesting either some non-specific binding of HABP or incomplete removal of HA by HA'se. The HA'se treatment on CD44$^{+/+}$ AMs did not change the MFI of cell surface receptors (**Supplementary Figures 1F,G**). These differences suggest CD44 deficiency causes changes in AMs.

CD44$^{+/+}$ and CD44$^{-/-}$ AMs Have Different Transcriptional Profiles at Steady-State

To understand how the loss of CD44 could be impacting AMs, we performed RNAseq analysis on CD44$^{+/+}$ and CD44$^{-/-}$ AMs. Approximately 200 genes with a q value of 0.05 or less were differentially expressed (**Figure 2A** and **Supplementary Table 1**). The RNAseq data showed several transcriptional changes in CD44$^{-/-}$ AMs that could affect lipid homeostasis in the CD44$^{-/-}$ AMs, notably *ApoE, ApoC1, ABCA1, DGAT2, LipN, and PLA2γ7* transcripts. Gene ontology analysis was performed to determine the pathways most affected by the loss of CD44 and this identified the greatest changes in the "sterol metabolic process," followed by differences in "the response to external stimulus," "protein phosphorylation pathways," "regulation of homeostatic process," and "regulation of sterol metabolic process" (**Figures 2B,C**). String analysis of the differentially expressed genes led to the identification of a gene cluster associated with sterol/cholesterol synthesis, and a broader cluster of genes involved in cell signaling, adhesion and migration (**Supplementary Figure 2**). Dissection of the sterol pathways led to a significant number of up and down-regulated genes associated with sterol/cholesterol synthesis and trafficking. Upregulated genes included those involved in lipid/cholesterol transport (*ApoE, ApoC1, ABCA1*), triacylglycerol synthesis (*DGAT2),* lipid catabolism (*LipN*), signaling (*Src, Igf1, Igf2r*), and immune function/antigen presentation (*CD74, MHCII*). Down regulated genes included phospholipase (*PL)A2γ7*, *PLCβ1*, *Plin1, Srebf2, LDLR*, all involved in lipid homeostasis or its regulation. The transcription factor, Srebf2, is one of the

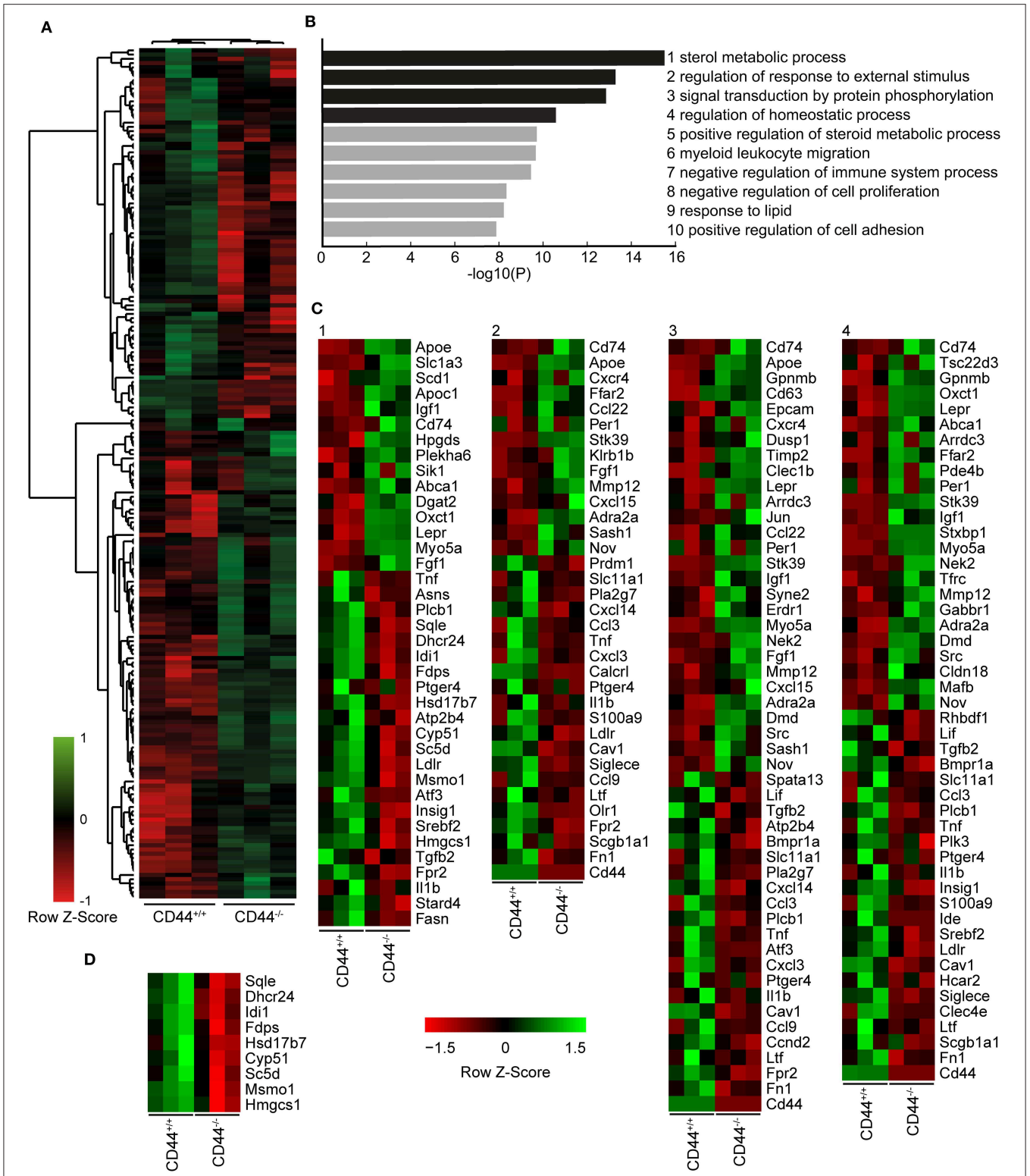

FIGURE 2 | RNA sequencing analysis comparing $CD44^{+/+}$ and $CD44^{-/-}$ AMs. **(A)** Cuffdiff RNA sequencing analysis showing 200 significant differentially expressed genes ($q < 0.05$) between $CD44^{+/+}$ and $CD44^{-/-}$ AMs. Eighty-seven genes were decreased, and 113 genes were increased in $CD44^{-/-}$ AMs. **(B)** Top 10 most significant Gene Ontology pathways associated with the significant differentially expressed genes analyzed by Metascape. **(C)** Heatmap of normalized FPKM of differentially expressed genes in the top four pathways of Metascape. **(D)** Heatmap of normalized FPKM of differentially expressed genes associated with the Cholesterol Biosynthesis Process, R-MMU-191273. Data are from three independent samples from a total of eight mice for both $CD44^{+/+}$ and $CD44^{-/-}$ AMs.

master regulators of cholesterol homeostasis (38). In keeping with this, several genes in sterol/cholesterol synthesis were also downregulated (**Figure 2D**). The down regulation of genes involved in cholesterol synthesis and LDL uptake, and the upregulation of genes involved in sequestering lipids/cholesterol (*ApoE*) (39) and trafficking them out of the cell (*ABCA1*) (40), raised the possibility that the $CD44^{-/-}$ AMs were responding to increased lipids/cholesterol.

Lipidomic Analysis Reveals Altered Lipid Levels in the BAL Supernatant and Cell Pellet of $CD44^{-/-}$ Mice

To investigate if the transcriptional changes in $CD44^{-/-}$ AMs affected lung lipid surfactant homeostasis in $CD44^{-/-}$ mice, we employed a lipidomic approach. Lipids were extracted from the BAL supernatant and cell pellet of $CD44^{+/+}$ and $CD44^{-/-}$ mice and subjected to LC-MS analysis. From principal component analysis, the lipids from the cell pellet showed a clear difference between the $CD44^{+/+}$ and $CD44^{-/-}$ samples, whereas the difference between the lipids from the BAL supernatant was less clear (**Figures 3A,B**). The volcano plots showed a general trend of more lipids present in the $CD44^{-/-}$ samples, with greater differences observed in the cell pellet (**Figures 3C,D**). There were 429 lipid moieties identified from the BAL supernatant, and out of these, 52 were significantly changed ($p < 0.05$) by 1.5-fold or more in the $CD44^{-/-}$ samples. The majority of these, 49/52, were increased in the $CD44^{-/-}$ AMs, typically by 1.5–2-fold (**Supplementary Table 2**). The five most significantly changed lipids were three moieties of PC and lysophosphatidylglycerol (LPG) which were upregulated, while phosphatidyl serine (PS) was downregulated 4-fold. In the BAL cell pellet, 658 lipids moieties were detected, and out of these, 241 were significantly different: 186 lipids were more abundant and 55 were less abundant in the $CD44^{-/-}$ samples (**Supplementary Table 3**). In these samples the fold differences varied from 10-fold less to 18 times more. Six out of the top ten most significant changes were increases in PC moieties in the $CD44^{-/-}$ cell pellet. Over 5-fold increases were observed with specific TAG, DAG, PA, PC, PG, and PE moieties. Notably, specific oxidized phospholipids (OxPLs) were increased up to 11-fold in the $CD44^{-/-}$ cell pellet, and cholesterol was 2.6-fold higher. Overall, there were many lipid moieties that were present at higher levels in the $CD44^{-/-}$ BAL supernatant and cell pellet. When the lipids were grouped into their main classes and compared, the overall differences in the BAL supernatant were small, with a 1.1–1.5-fold increase in the $CD44^{-/-}$ samples, yet significant changes occurred for PC and lysophospholipids. Larger increases (1.7–2.6-fold) were observed in the $CD44^{-/-}$ cell pellet for cholesterol and the most prevalent lipids: PC, PE, PG and fatty acids, with 3.6-fold greater levels observed for OxPLs (**Figure 3E**).

$CD44^{-/-}$ AMs Have More Lipid Droplets, Increased ROS and Higher OxPC Levels

To corroborate the findings from the lipidomic experiments, PC and cholesterol levels were measured by ELISA and gas chromatography, respectively, and both were significantly increased in the BAL supernatant from $CD44^{-/-}$ mice (**Figures 4A,B**). In addition, BODIPY 493/503, a dye that labels neutral lipids/lipid droplets was used to measure lipid levels in AMs. By confocal microscopy, we observed an increase in the number and size of lipid droplets in $CD44^{-/-}$ AMs, and by flow cytometry we observed a significant increase in MFI of BODIPY, indicating a higher neutral lipid content (**Figures 4C,D**). These data further support a buildup of lipids in the BAL supernatant and AMs from $CD44^{-/-}$ mice.

To further investigate the increased presence of oxidized phospholipids in $CD44^{-/-}$ AMs, we used the E06 antibody that recognizes oxidized phosphatidylcholine (OxPC) (41). By confocal microscopy there was an increased number of OxPC droplets per cell and flow cytometry revealed a greater MFI in the $CD44^{-/-}$ AMs (**Figures 4E,F**). Labeling the AMs with a cell permeant fluorogenic dye that measures cellular ROS activity (H_2DCFDA), showed a small but significant increase in ROS activity in the $CD44^{-/-}$ AMs compared to the $CD44^{+/+}$ AMs (**Figure 4G**). An increased accumulation of lipids and oxidized lipids in the cell are signs of a foamy macrophage and phospholipidosis (42), and this was further supported by the increased labeling of NBD-PE by $CD44^{-/-}$ AMs (**Figure 4H**). To determine if the increased lipid and OxPC accumulation in $CD44^{-/-}$ AMs resulted in increased oxidized lipid-induced toxicity, $CD44^{+/+}$ and $CD44^{-/-}$ AMs were incubated with the oxidized phospholipid, POVPC, *in vitro* and compared with PC or the vehicle control (1% ethanol). The loss in AM viability caused by POVPC relative to ethanol or PC treatment was significantly greater in $CD44^{-/-}$ AMs compared to $CD44^{+/+}$ AMs (**Figure 4I**), indicating increased sensitivity to OxPC-induced cellular toxicity.

The Inflammatory Response to OxPC Is Exacerbated in $CD44^{-/-}$ Mice

During an inflammatory response, there is increased oxidation of lung surfactant lipids, which can be cytotoxic to AMs if they accumulate. This oxidized lipid-induced cytotoxicity causes lung damage and further drives the inflammatory response (15, 16). To determine if the increased sensitivity of $CD44^{-/-}$ AMs to OxPC observed *in vitro* translated into a more severe inflammatory response in $CD44^{-/-}$ mice, we used a mouse model of OxPC-driven lung inflammation. POVPC was delivered i.t. to $CD44^{+/+}$ and $CD44^{-/-}$ mice and their weight loss was monitored over time (**Figure 5A**). Analysis of the cells in the BAL 3 days after POVPC instillation, showed leukocyte infiltration including monocytes, neutrophils, eosinophils, and $CD11b^{-}$ cells, indicative of an inflammatory response in both $CD44^{+/+}$ and $CD44^{-/-}$ mice (**Figure 5B**). Apart from the tissue resident AMs, there were significantly greater numbers of other leukocytes (neutrophils, monocytes, eosinophils) in the BAL from $CD44^{-/-}$ mice (**Figure 5C**). Protein and HA levels, both indicators of lung inflammation and damage (23, 28, 29), were also increased after POVPC treatment and were higher in the BAL from $CD44^{-/-}$ mice

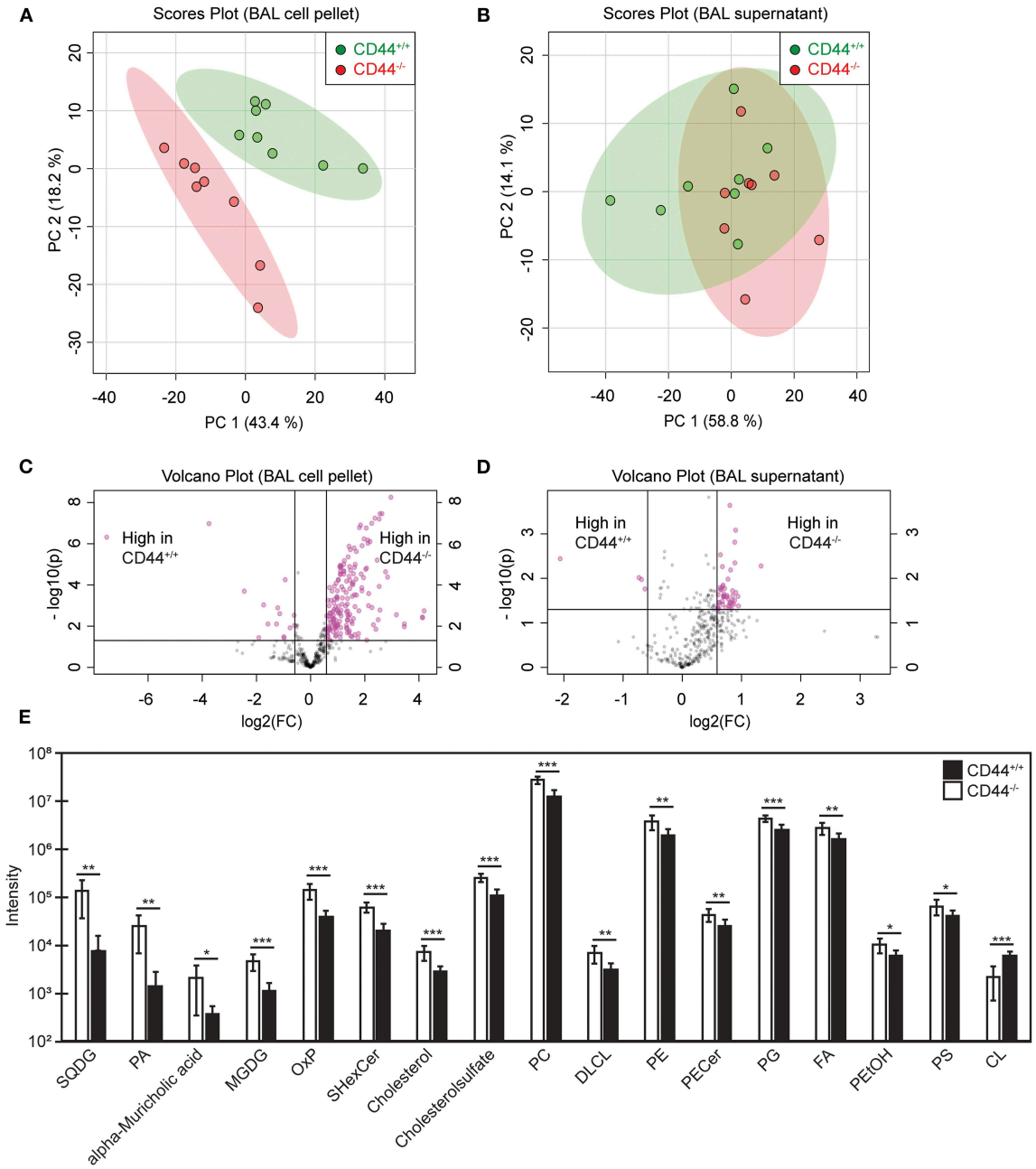

FIGURE 3 | Univariant and multivariant analysis of the differences in lipid composition between CD44$^{+/+}$ and CD44$^{-/-}$ BAL samples. **(A,B)** Principal component analysis showing lipid differences from the BAL cell pellets and supernatants from CD44$^{+/+}$ and CD44$^{-/-}$ mice. **(C,D)** Volcano plots comparing the differences in lipid levels measured from the BAL cell pellets and supernatants from CD44$^{+/+}$ and CD44$^{-/-}$ mice. Pink dots represent lipid species with >1.5-fold difference between CD44$^{+/+}$ and CD44$^{-/-}$ samples, with $p < 0.05$. **(E)** Graph showing lipids and lipid classes that are significantly different between CD44$^{+/+}$ and CD44$^{-/-}$ BAL cell pellets. Data show the average from 8 CD44$^{+/+}$ and 8 CD44$^{-/-}$ female mice. Significance indicated as *$p < 0.05$, **$p < 0.01$, ***$p < 0.001$, using a two tails distribution, homoscedastic *t* test in Microsoft Excel.

(**Figures 5D,E**). There was also increased HA detected by HABP labeling in the lung tissue of CD44$^{-/-}$ mice 3 days after POVPC treatment, a sign of increased lung inflammation (**Figures 5F,G**). Thus, the increased sensitivity to OxPC toxicity in CD44$^{-/-}$ AMs leads to increased lung damage and greater lung inflammation.

The Effect of the Alveolar Environment on CD44$^{-/-}$ AMs

To further understand the cause of this lipid accumulation in the AMs and the BAL of CD44$^{-/-}$ mice, we sought to distinguish between intrinsic and extrinsic AM factors. To address the contributions of the alveolar environment on the

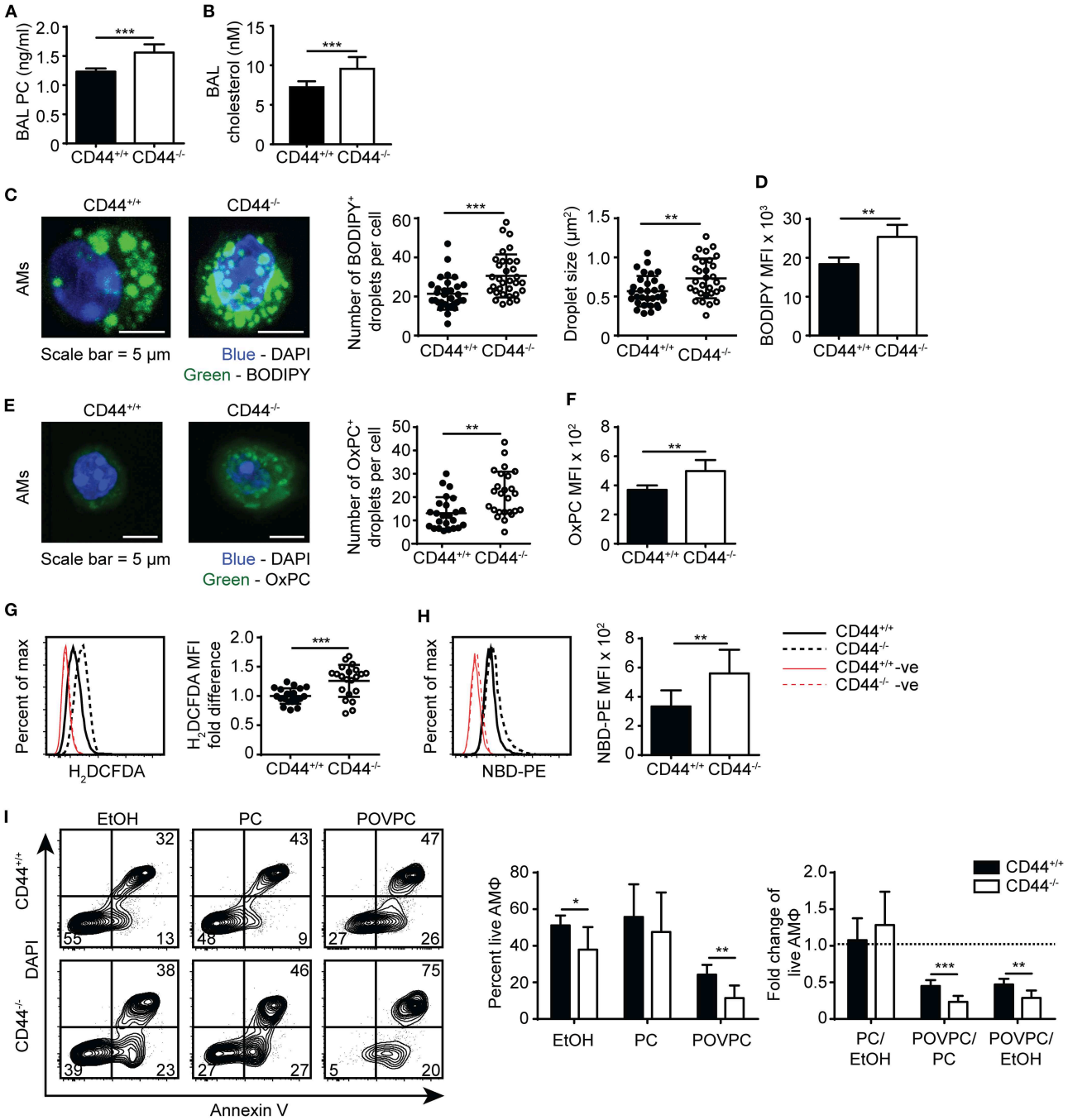

FIGURE 4 | Lipid droplet and oxidized PC levels are elevated in CD44$^{-/-}$ AMs. **(A)** Surfactant PC levels in the BAL supernatant of CD44$^{+/+}$ and CD44$^{-/-}$ mice measured by ELISA. **(B)** Concentration of cholesterol in BAL from CD44$^{+/+}$ and CD44$^{-/-}$ mice measured by thin layer chromatography. **(C)** Representative confocal microscopy (z-stack) of *ex vivo* CD44$^{+/+}$ and CD44$^{-/-}$ AMs labeled with BODIPY and DAPI, and the number and size of BODIPY^{+} droplets per CD44$^{+/+}$ or CD44$^{-/-}$ AM. **(D)** MFI of BODIPY labeled CD44$^{+/+}$ and CD44$^{-/-}$ AMs by flow cytometry, after subtraction of autofluorescence MFI. **(E)** Representative confocal microscopy (z-stack) of *ex vivo* CD44$^{+/+}$ and CD44$^{-/-}$ AMs labeled with the anti-OxPC antibody, E06, and DAPI, and the number of E06^{+} droplets per CD44$^{+/+}$ or CD44$^{-/-}$ AM. **(F)** MFI of OxPC levels in CD44$^{+/+}$ and CD44$^{-/-}$ AMs (after subtraction of autofluorescence MFI) using the anti-OxPC antibody E06 and flow cytometry. **(G)** Representative histograms and graphs comparing H_2DCFDA labeling of ROS and **(H)** NBD-PE in CD44$^{+/+}$ and CD44$^{-/-}$ AMs. **(I)** Representative flow cytometry plots of CD44$^{+/+}$ and CD44$^{-/-}$ AMs treated with EtOH, PC, or POVPC labeled with Annexin V and DAPI. Bar graphs show the percent live CD44$^{+/+}$ or CD44$^{-/-}$ AMs (Annexin V^{-} DAPI^{-}) after EtOH, PC, or POVPC treatment for 1 h, and compares the fold change in percent live CD44$^{+/+}$ or CD44$^{-/-}$ AMs with different treatments. Data show an average of three to five CD44$^{+/+}$ and CD44$^{-/-}$ mice from each experiment ± SD, repeated twice, or five times **(G)**; three to four cells were analyzed per mouse in confocal imaging, from three to five mice per experiment, over two experiments. Significance indicated as $^{*}p < 0.05$, $^{**}p < 0.01$, $^{***}p < 0.001$, non-paired Student's *t*-test.

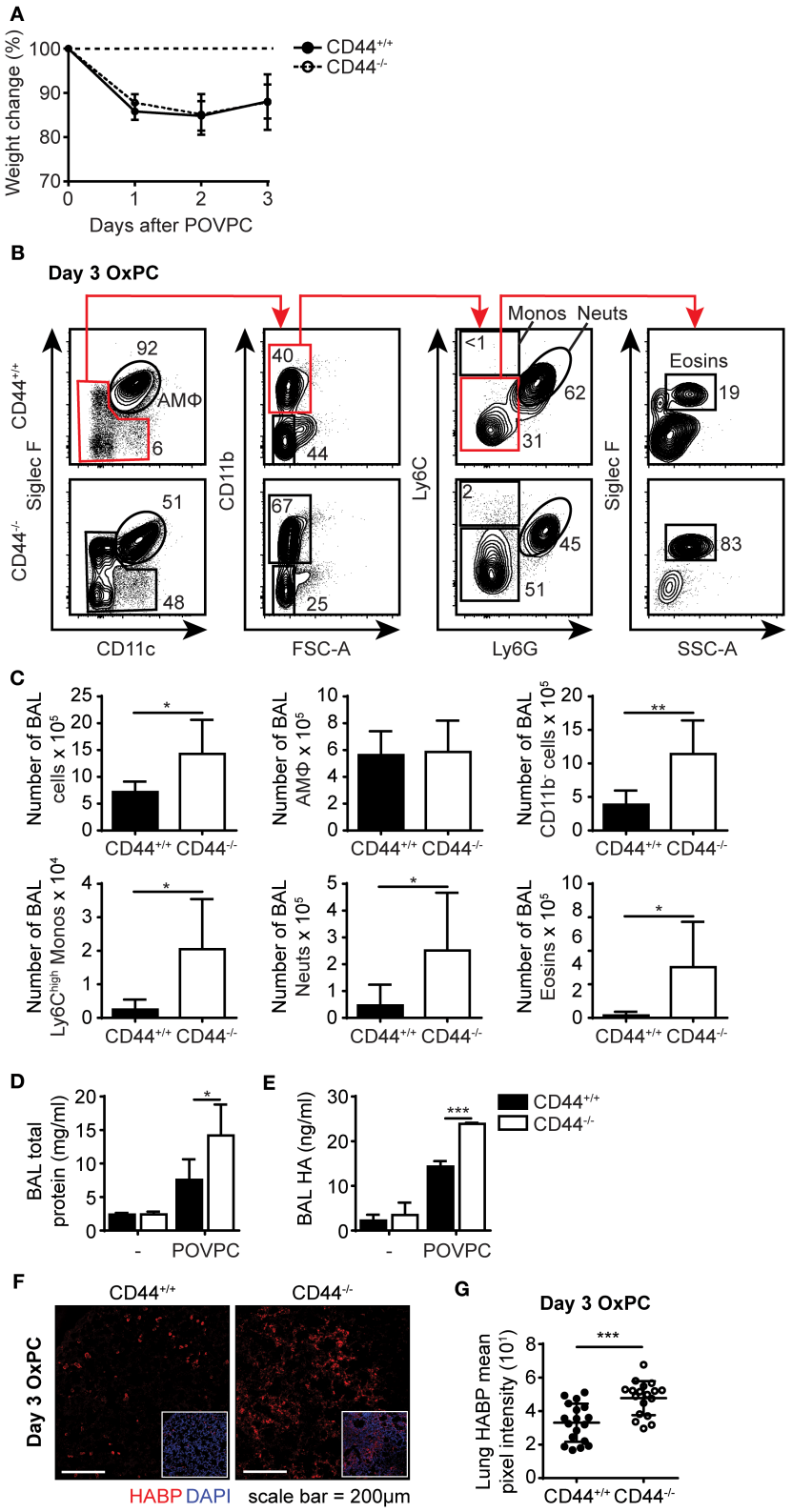

FIGURE 5 | POVPC induced pulmonary inflammation is exacerbated in CD44$^{-/-}$ mice. **(A)** Percent weight change over 3 days from CD44$^{+/+}$ and CD44$^{-/-}$ mice treated with i.t. POVPC. **(B)** Representative flow cytometry plots showing the gating (after live/dead and sizing gating) and proportion of AMs, Ly6C^{high} monocytes, neutrophils, eosinophils, and CD11b^{-} cells in the BAL of CD44$^{+/+}$ and CD44$^{-/-}$ mice 3 days after POVPC instillation. **(C)** Graphs comparing the number of total BAL

(Continued)

FIGURE 5 | cells, AMs, CD11b^{-} cells, Ly6c^{high} monocytes, neutrophils, and eosinophils in the BAL of CD44$^{+/+}$ and CD44$^{-/-}$ mice 3 days after POVPC instillation **(D)** Level of total protein in the BAL supernatant of CD44$^{+/+}$ and CD44$^{-/-}$ mice treated with or without POVPC measured by BCA. **(E)** Level of HA in the BAL of CD44$^{+/+}$ and CD44$^{-/-}$ mice treated with or without POVPC measured by ELISA. **(F)** Confocal microscopy and **(G)** graphs comparing HABP mean pixel intensity from CD44$^{+/+}$ and CD44$^{-/-}$ lung sections at 3 days after POVPC treatment. Data show an average of two experiments ± SD, each with three to five CD44$^{+/+}$ and CD44$^{-/-}$ mice. Data from confocal microscopy are pooled from 18 CD44$^{+/+}$ and CD44$^{-/-}$ POVPC lung sections, from two experiments each with three to five mice. Significance indicated as $^{*}p < 0.05$, $^{**}p < 0.01$, $^{***}p < 0.001$, non-paired Student's *t*-test and (**G** only) Welch's *t*-test with Welch's correction.

AMs, we performed short-term adoptive transfer of CD44$^{-/-}$ AMs into the alveolar space of CD44$^{+/+}$ mice and vice versa. CD44$^{-/-}$AMs expressing the CD45.2 allele, were instilled into the trachea of CD44$^{+/+}$ BoyJ mice expressing the CD45.1 allele and the BAL analyzed 7 days later (**Figure 6A**). After being transferred to a normal alveolar environment, the CD45.2^{+} CD44$^{-/-}$ AMs decreased expression of CD36 (**Figures 6B,C**), consistent with CD36 expression responding to the reduced lipid surfactant environment of the CD44$^{+/+}$ mice and indicative of an extrinsic effect. However, BODIPY, SSC-A and CD11c levels did not drop significantly, suggesting an intrinsic defect. In contrast, when CD45.1^{+} CD44$^{+/+}$ AMs were transferred into the trachea of the CD45.2^{+} CD44$^{-/-}$ mice and analyzed 7 days later (**Figure 6D**), these AMs dramatically increased CD36 expression, to levels higher than the CD44$^{-/-}$ AMs (**Figures 6E,F**). In addition, SSC-A and BODIPY levels increased to similar levels observed in CD44$^{-/-}$ AMs, consistent with the wild-type cells responding to extrinsic changes in lipid surfactant levels in the lungs of CD44$^{-/-}$ mice. To evaluate if the CD44$^{+/+}$ AMs were directly responding to increased lipid levels in the lung surfactant of CD44$^{-/-}$ mice, *ex vivo* CD44$^{+/+}$ AMs were incubated with PC for 48 h *in vitro* then analyzed for neutral lipids using BODIPY, and CD36 expression. Both showed a significant increase in CD44$^{+/+}$ AMs (**Figures 6G–I**), demonstrating a direct response to extrinsic changes in extracellular PC. Together, these data suggest both intrinsic and extrinsic defects affect CD44$^{-/-}$ AMs, which impact intracellular lipid levels and CD36 expression, respectively.

To further evaluate the defects in CD44$^{-/-}$ AMs, we performed bone marrow reconstitution experiments on irradiated mice. We reconstituted irradiated CD45.1^{+} CD44$^{+/+}$ mice with CD45.2^{+} CD44$^{-/-}$ bone marrow (**Figure 7A**). After allowing several weeks for reconstitution of the AM compartment, CD44$^{-/-}$ AMs were isolated from the BAL and had a similar phenotype to CD44$^{-/-}$ AMs isolated from CD44$^{-/-}$ mice, namely similar levels of BODIPY, CD36 and CD11c (**Figures 7B,C**). We also reconstituted irradiated CD44$^{+/+}$ mice with 50% CD44$^{+/+}$ and 50% CD44$^{-/-}$ bone marrow and analyzed both CD44$^{+/+}$ and CD44$^{-/-}$ AMs from the same lung environment after allowing at least 7 weeks for reconstitution of the lung macrophage compartment (**Figure 7D**). This competitive transfer leads to the dominance of CD44$^{+/+}$ AMs over CD44$^{-/-}$ AMs in an 80:20 ratio, as CD44$^{-/-}$ AMs are less able to survive (12). Analysis of both the CD44$^{+/+}$ and CD44$^{-/-}$ AMs from the same mice showed that the CD44$^{-/-}$ AMs were significantly higher in SSC and CD11c levels (**Figure 7E**), indicative of an intrinsic defect. Together, these results show the ability of CD44$^{-/-}$ AMs to regulate CD36 expression in response to changes in the lung environment, but an inability to decrease their lipid content or reduce CD11c levels, indicating both cell extrinsic and intrinsic changes in CD44$^{-/-}$ AMs.

CSF-2 Partially Restored Lipid Surfactant Homeostasis in CD44$^{-/-}$ BAL but Did Not Reduce Lipid Droplets in CD44$^{-/-}$ AMs

While the reduced numbers of CD44$^{-/-}$ AMs (12) could contribute to increased PC and cholesterol levels in the BAL, the adoptive transfer and competitive reconstitution experiments suggested an intrinsic defect in the ability to catabolize lipids in the CD44$^{-/-}$ AMs, which was also supported by the lipidomic data. Lipid droplet accumulation and the foamy AM phenotype is a feature of immature AMs that arise after the deletion of CSF-2, PPARγ or TGFβ, which are important for maturation and survival (2–5). While the RNAseq data showed reduced TGFβ2 transcript levels in CD44$^{-/-}$ AMs, these transcripts were very low compared to the levels of TGFβ1 transcripts, which did not differ between normal and CD44$^{-/-}$ AMs (geo accession no: GSE138445). CSF-2 induces PPARγ expression (4) and upregulates CD11c expression in bone marrow derived macrophages (12), and both CSF-2 and PPARγ agonists promote CD44-mediated HA binding (12). It is possible that some of the downstream effects of CSF-2 or PPARγ could be mediated via CD44 and its interaction with HA, which then promotes AM survival (12). Since CSF-2 also attenuates bleomycin-induced lipid accumulation in the alveolar space (16), we determined if CSF-2 could rescue the defects in surfactant lipid homeostasis caused by CD44 deficiency. CSF-2 was given daily to the CD44$^{-/-}$ mice by i.t. for 7 days, then the BAL from the mice was analyzed. While CSF-2 instillation did not significantly alter the composition of cells in the BAL (**Figure 8A**), it did increase CD44$^{-/-}$ AM numbers (**Figure 8B**) and decrease the concentration of PC in the BAL (**Figure 8C**). There was a concomitant reduction in CD36 expression in the CD44$^{-/-}$ AMs, but no significant changes were observed in their granularity (SSC-A), neutral lipid content (measured by BODIPY), or the expression of CD11c (**Figures 8D,E**). This suggests that the reduced number of AMs contributes to increased lipid surfactant levels and concomitantly, increased levels of CD36. However, CSF-2 does not rescue the cell intrinsic defect of accumulated lipids in CD44$^{-/-}$ AMs.

CD44$^{-/-}$ AMs Have Reduced PPARγ Expression

PPARγ is an important transcriptional regulator of lipid metabolism (10) and this, coupled with its key role in AM maturation and survival (4), make it a potential candidate

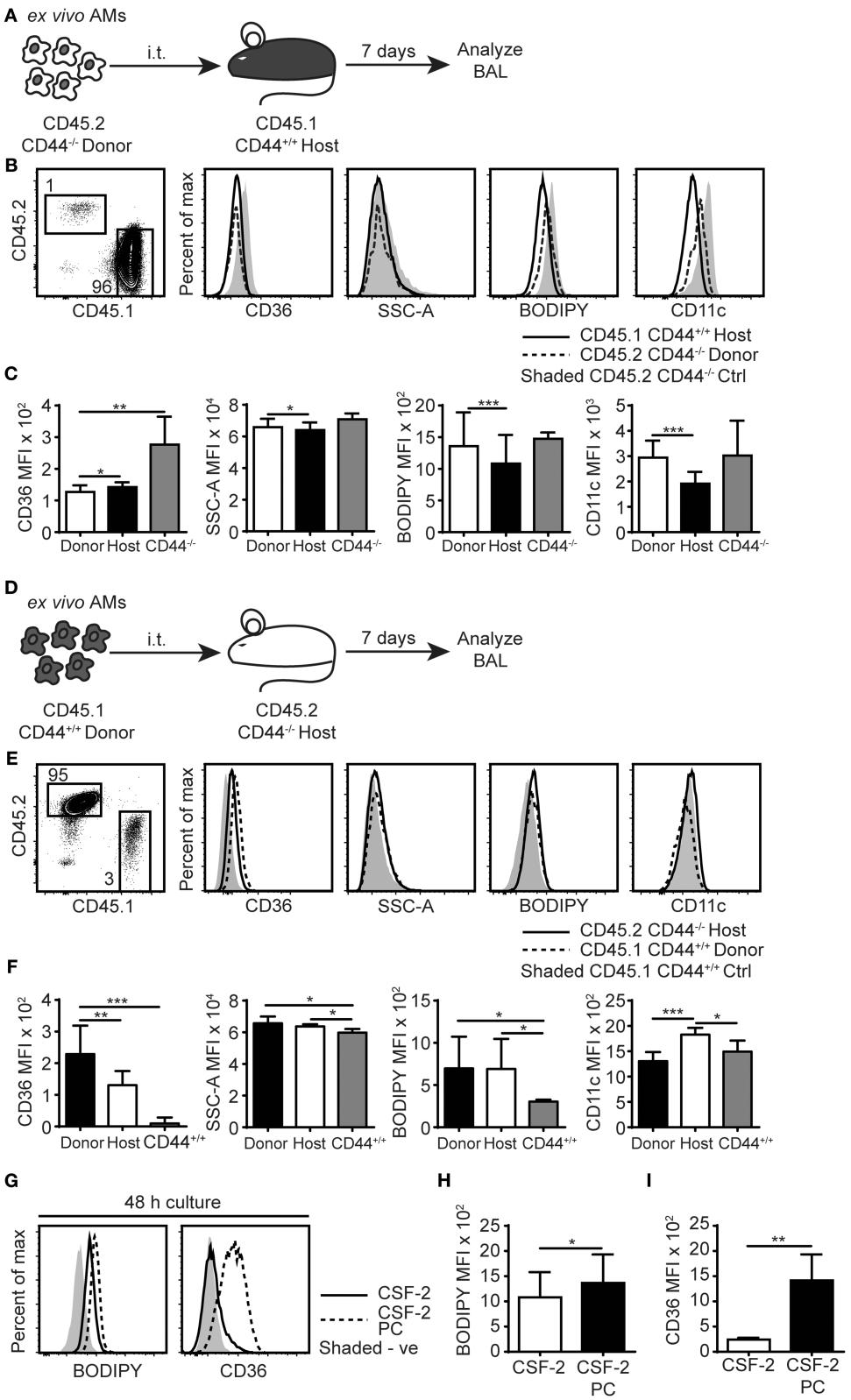

FIGURE 6 | AMs lipid homeostasis is controlled by the extracellular milieu and the expression of CD44. **(A)** Schematic diagram showing donor AMs isolated from CD45.2^{+} CD44$^{-/-}$ mice are transferred by i.t. into CD45.1^{+} CD44$^{+/+}$ host mice and analyzed 7 days later. **(B)** Representative flow cytometry plots comparing the SSC-A, BODIPY, CD36, and CD11c levels by CD45.2^{+} CD44$^{-/-}$ donor AMs and CD45.1^{+} CD44$^{+/+}$ host AMs with control CD45.2^{+} CD44$^{-/-}$ mice, 7 days after

(Continued)

FIGURE 6 | adoptive transfer. **(C)** Graphs comparing SSC-A, BODIPY, CD36, and CD11c MFI of CD45.2$^+$ CD44$^{-/-}$ donor AMs, CD45.1$^+$ CD44$^{+/+}$ host AMs, and *ex vivo* CD44$^{-/-}$ AMs. **(D)** Schematic diagram showing donor AMs isolated from CD45.1$^+$ CD44$^{+/+}$ mice are transferred by i.t. into CD45.2$^+$ CD44$^{-/-}$ host mice and analyzed 7 days later. **(E)** Representative flow cytometry plots comparing the SSC-A, BODIPY, CD36, and CD11c levels in CD45.1$^+$ CD44$^{+/+}$ donor AMs and CD45.2$^+$ CD44$^{-/-}$ host AMs compared with CD45.1$^+$ CD44$^{+/+}$ control mice, 7 days after adoptive transfer. **(F)** Graphs comparing SSC-A, BODIPY, CD36, and CD11c MFI of CD45.1$^+$ CD44$^{+/+}$ donor AMs, CD45.2$^+$ CD44$^{-/-}$ host AMs, and *ex vivo* CD44$^{+/+}$ AMs. **(G)** Representative flow cytometry histograms comparing the BODIPY and CD36 MFI of AMs after 48 h culture in CSF- 2, or CSF-2 and PC. **(H,I)** Graphs comparing BODIPY labeling and CD36 expression by AMs cultured in CSF- 2, or CSF-2 and PC for 48 h. For adoptive transfer experiments, data show an average of two experiments ± SD, each with three to five mice. Significance indicated as $^*p < 0.05$, $^{**}p < 0.01$, $^{***}p < 0.001$, paired (donor AMs vs. host AMs) and non-paired Student's *t*-test (CD44$^{-/-}$ donor AMs vs. *ex vivo* CD44$^{-/-}$ AMs or CD44$^{-/-}$ host AMs vs. *ex vivo* CD44$^{+/+}$ AMs). For *in vitro* cell culture experiments, data show an average of two experiments ± SD, each with three to five mice. Significance indicated as $^*p < 0.05$, $^{**}p < 0.01$, $^{***}p < 0.001$, paired Student's *t*-test.

for contributing to the cell intrinsic defects present in the CD44$^{-/-}$ AMs. Although no differences in PPARγ transcript levels were apparent from the RNAseq data, other forms of regulation such as PPARγ activation, cellular localization, or protein levels may be defective in CD44$^{-/-}$ AMs. Confocal microscopy showed that the majority of PPARγ in *ex vivo* CD44$^{+/+}$ and CD44$^{-/-}$ AMs was localized to the nucleus (**Figure 9A**). Both confocal microscopy and flow cytometry showed PPARγ protein was expressed at a slightly lower level in CD44$^{-/-}$ AMs (**Figures 9B,C**). To determine if this was of functional significance, *ex vivo* CD44$^{+/+}$ AMs were incubated for 48 h in the presence of CSF-2 and treated with a selective PPARγ antagonist, T-0070907 (43), to mimic conditions in the CD44$^{-/-}$ AMs. The antagonist increased the levels of BODIPY, as well as CD36 and CD11c (**Figures 9D,E**). This suggests that the reduced expression/activation of PPARγ could contribute to the accumulation of lipids in CD44$^{-/-}$ AMs.

DISCUSSION

AMs play an important role in maintaining lung homeostasis and are responsible for the uptake of surfactant and oxidized surfactant lipids, their storage and catabolism (1). Here we report that CD44 deficiency disrupted lipid surfactant homeostasis in the alveolar space and led to intracellular lipid accumulation in AMs. CD44$^{-/-}$ AMs accumulated PC and cholesterol and had increased intracellular lipid droplets, giving the AMs a foamy appearance, with increased side scatter (SSC) and autofluorescence. CD44 deficiency in AMs led to the differential expression of 200 genes, several of which were involved in lipid metabolism and trafficking. The inability of CD44$^{-/-}$ AMs to reduce intracellular lipid levels coupled with the reduced numbers of AMs in CD44$^{-/-}$ mice resulted in the increase in lung surfactant lipids in the BAL supernatant. The inability to reduce intracellular lipid accumulation in CD44$^{-/-}$ AMs may be attributed, at least in part, to the dysregulation of PPARγ.

Transcriptional analysis of CD44$^{+/+}$ and CD44$^{-/-}$ AMs identified the upregulation of genes involved in cholesterol efflux and trafficking in CD44$^{-/-}$ AMs. These included *ApoE* (39), which was validated by qPCR (data not shown) and *ABCA1* (40), key genes downstream of PPARγ signaling. Although *CD36* gene levels were not significantly different by transcriptomic analysis, cell surface expression of CD36 was increased in CD44$^{-/-}$ AMs, and this correlated with extracellular lipid levels. CD36 is a multi-functional scavenger receptor that binds oxidized lipids and fatty acids (37) and CD36 signaling promotes cholesterol efflux and inhibits cholesterol synthesis by activating PPARγ (44). The transcriptional analysis also predicted the down regulation of several genes in CD44$^{-/-}$ AMs, including *srebf2*, a master transcriptional regulator of cholesterol and fatty acid synthesis (38, 45) and a cluster of genes associated with sterol/cholesterol synthesis. Together, these data suggest that CD44$^{-/-}$ AMs are responding to increased exposure to lipids by activating gene pathways responsible for reducing lipid content, yet are still unable to reduce intracellular lipid content. Although PPARγ is a master transcriptional regulator of lipid metabolism (8–10), its effects can be cell-type specific and complicated by the activation of its heterodimeric partner, RXR and other lipid regulated transcription factors such as LXR. While one may have predicted that PPARγ would have been more active in CD44$^{-/-}$ AMs, transcript levels were not different and slightly less, not more, PPARγ protein levels were found in the nucleus of CD44$^{-/-}$ AMs.

In AMs, PPARγ expression is induced by CSF-2 and TGFβ and is critical for their development (4). PPARγ upregulates genes important for the transcriptional identity of AMs, including molecules involved in the intracellular binding, storage and metabolism of lipids, which help prevent foam-cell formation and protect against lipotoxicity (4, 9, 10, 46). PPARγ deficiency in AMs causes significant accumulation of cholesterol and phospholipids in the BAL supernatant (47, 48) and leads to immature AMs that have increased lipid droplets (4). This is consistent with the results here, where we found slightly reduced levels of PPARγ in the nucleus of CD44$^{-/-}$ AMs. The upregulation of BODIPY$^+$ lipid droplets and CD36 on CD44$^{+/+}$ AMs after *in vitro* culture with a PPARγ antagonist also supports the idea that reduced PPARγ activity mimics the CD44$^{-/-}$ AM phenotype. However, in addition to lipid induced activation of PPARγ, its activity can also be regulated at the translational and protein level. PPARγ protein is degraded via ubiquitination after ligand mediated activation (49), and so it is possible that CD44$^{-/-}$ AMs have lower nuclear PPARγ levels because they have been exposed to greater levels of activating PPARγ ligands, leading to greater degradation.

Whether CD44 directly or indirectly modulates PPARγ activity remains to be addressed. In IL-1β stimulated chondrosarcoma cells, the addition of high molecular weight HA increases PPARγ expression at both the mRNA and protein level (50). It will be of interest to determine if there

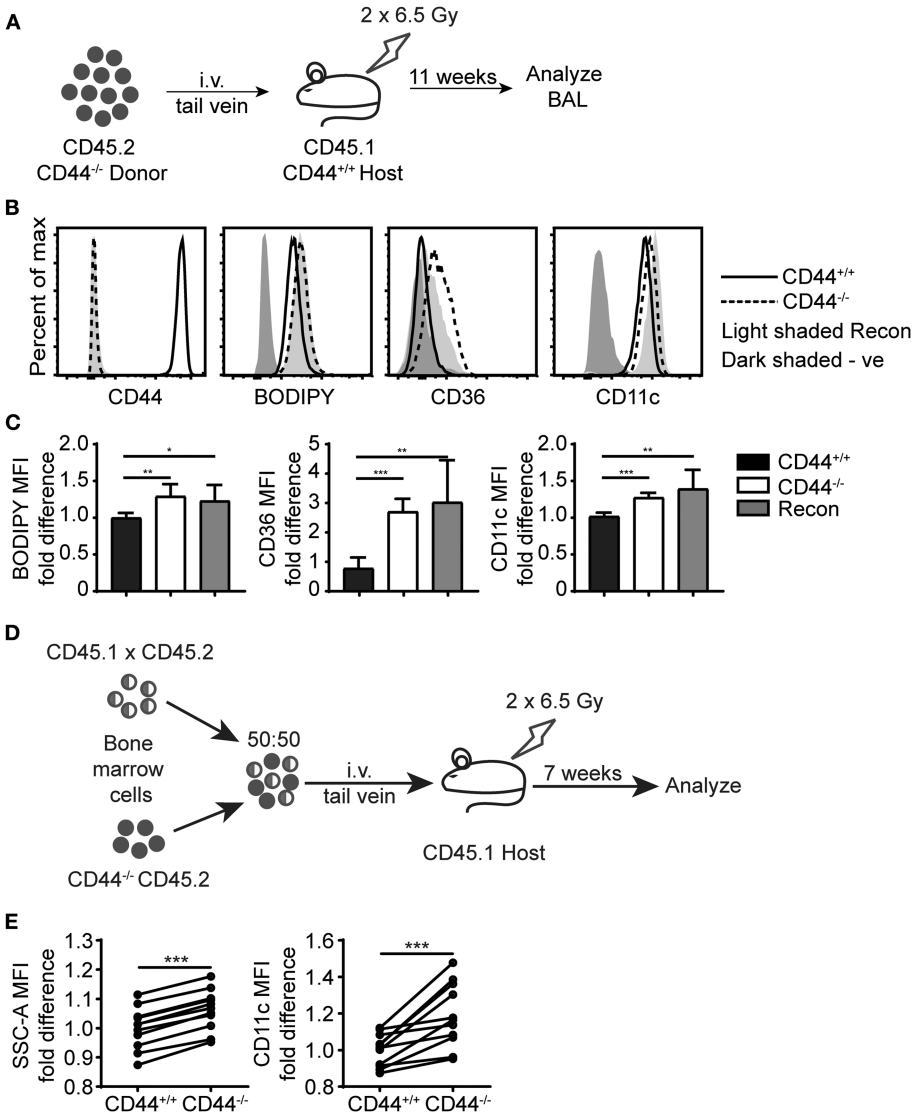

FIGURE 7 | Cell intrinsic defects in CD44$^{-/-}$ AMs are preserved after long term BM reconstitution. **(A)** Schematic showing the BM reconstitution experiment where BM cells from CD44$^{-/-}$ mice were injected into lethally irradiated CD44$^{+/+}$ host mice and analyzed 11 weeks later. **(B)** Representative flow cytometry plots comparing the CD44, BODIPY, CD36, and CD11c levels of AMs from CD44$^{+/+}$ mice and CD44$^{-/-}$ mice, as well CD44$^{-/-}$ AMs reconstituted in CD44$^{+/+}$ mice. **(C)** Graphs comparing the fold difference of BODIPY, CD36, and CD11c of AMs from CD44$^{+/+}$ mice and CD44$^{-/-}$ mice, as well CD44$^{-/-}$ AMs reconstituted in CD44$^{+/+}$ mice. **(D)** Schematic showing the BM reconstitution experiment where BM cells from CD44$^{+/+}$ and CD44$^{-/-}$ mice were injected at equal proportions into lethally irradiated host mice to study the role of CD44 in AM repopulation. **(E)** Graphs comparing the fold difference in the granularity (SSC-A) and CD11c between CD44$^{+/+}$ and CD44$^{-/-}$ AMs in the BAL after 7 weeks in competition, as measured by flow cytometry. Data show an average of two experiments ± SD, each with three to five mice. Significance indicated as $*p < 0.05$, $**p < 0.01$, $***p < 0.001$ unpaired Student's *t*-test.

is a link between HA engagement by CD44 and PPARγ levels or activation. Alternatively, TGFβ can upregulate PPARγ expression (4) and RNAseq data did predict a reduction in TGFβ2 expression in CD44$^{-/-}$ AMs, although not for the more highly expressed TGFβ1. In other cell types, CD44 and HA-binding modulate TGFβ responses by facilitating TGFβ cleavage and activation (51), or by promoting TGFβ receptor signaling (52).

Mice deficient in CSF-2, or harboring an AM-specific deletion of PPARγ, or the conditional deletion of TGFβR2, all produce CD11b^{+} immature foamy macrophages, which are unable to regulate lipid turnover leading to surfactant accumulation in the BAL and ultimately PAP (3–5). Their immature CD11b^{+} CD11c^{low} Siglec F^{low} phenotype is distinct from the phenotype of CD44$^{-/-}$ AMs, which have high levels of mature AM markers: Siglec F, CD11c, CD206, CD200R, and Sirpα. However, CD44$^{-/-}$ AMs also express low levels of CD11b and MHCII, and RNAseq analysis predicted an upregulation of *mafB*, a transcription factor that is normally down-regulated in mature cells, to allow self-renewal and

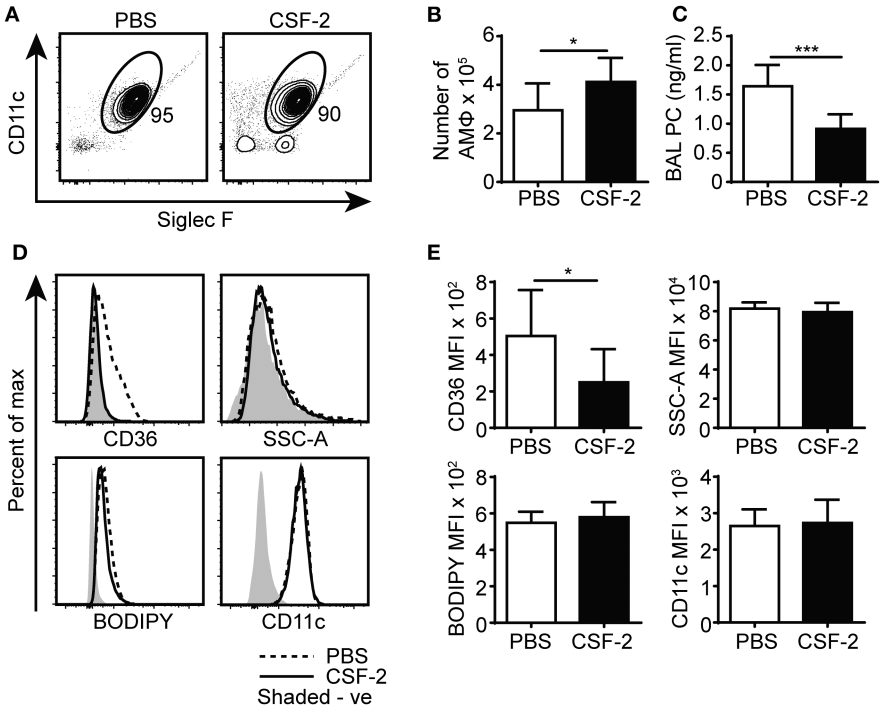

FIGURE 8 | CSF-2 induces AM proliferation and rescues aberrant pulmonary surfactant PC accumulation in CD44$^{-/-}$ mice. **(A)** Representative flow cytometry plots showing the proportion of BAL AMs from CD44$^{-/-}$ mice after 7 days of PBS or CSF-2 treatment. **(B)** Number of AMs in the BAL from CD44$^{-/-}$ mice after PBS or CSF-2 treatment. **(C)** BAL PC concentration from CD44$^{-/-}$ mice after PBS or CSF-2 treatment. **(D)** Representative flow cytometry histograms comparing the phenotype of AMs from CD44$^{-/-}$ mice after 7 days of PBS or CSF-2 treatment. **(E)** Graphs comparing the MFI of SSC-A, BODIPY, CD36, and CD11c between AMs from CD44$^{-/-}$ mice after 7 days of PBS or CSF-2 treatment. Data show an average of two experiments ± SD, each with three to five mice. Background MFI of autofluorescence from unlabeled CD44$^{+/+}$ and CD44$^{-/-}$ cells were, respectively, subtracted in the flow cytometry analysis. Significance indicated as $^{*}p < 0.05$, $^{***}p < 0.001$, non-paired Student's *t*-test.

terminal differentiation (53). It is possible some of the effects of CSF-2 on AMs maybe mediated by CD44 as CSF-2 induces HA binding by CD44 and this is known to promote the survival of AMs (12). Although exogenous CSF-2 restored AM numbers and reduced PC levels in the BAL of CD44$^{-/-}$ mice, it did not impact the intracellular lipid accumulation in CD44$^{-/-}$ AMs.

RNAseq predicted the altered expression of genes involved in cholesterol/sterol synthesis and trafficking, triglyceride synthesis and phospholipid catabolism in CD44$^{-/-}$ AMs. This suggested dysregulation of lung lipid surfactant metabolism in CD44$^{-/-}$ AMs, which was validated by measuring the lipids present in the BAL supernatant and cell pellet of the CD44$^{+/+}$ and CD44$^{-/-}$ mice. Although the molecular composition of lung surfactant has been analyzed in young and old mice (54), to our knowledge, this study is the first to provide a full lipidomic analysis of the lung surfactant and AMs. The major lipids present in lung surfactant include PC moieties (1, 7, 11), which were elevated in the CD44$^{-/-}$ BAL supernatant and cell pellet. Lipidomic MS analysis of the cell pellets from CD44$^{+/+}$ and CD44$^{-/-}$ AMs showed greater accumulation of intracellular lipids including PC, PE, PG, fatty acids, cholesterol, and OxPLs in CD44$^{-/-}$ AMs. These results were consistent with the observations from flow cytometry and confocal microscopy experiments which showed CD44$^{-/-}$ AMs had higher BODIPY labeled neutral lipids and OxPC levels than CD44$^{+/+}$ AMs. The increased cytotoxicity of OxPC in CD44$^{-/-}$ AMs coupled with the observed increase in ROS and OxPC levels in these cells, resulted in an increased inflammatory response in the lungs of CD44$^{-/-}$ mice exposed to oxidized lipids. This is of significance as oxidized lipids propagate an inflammatory response. Interestingly, mice exposed to bleomycin generate oxidized lipids (16) and CD44$^{-/-}$ mice have significantly worse bleomycin-induced inflammation and lung damage compared to wild-type mice (28).

Overall, this work demonstrates a new role for CD44 in AMs in maintaining lipid surfactant homeostasis, a key function of AMs in the alveolar space. Dysregulation of lipid surfactant homeostasis in CD44$^{-/-}$ AMs leads to a buildup of lipid surfactant and foamy AMs, and an increase in oxidized lipids exacerbates lung damage and inflammation. This work also raises the possibility that reduced numbers of AMs and compromised lipid surfactant metabolism, leading to increased lung damage and inflammation, are contributing factors to the development of secondary pulmonary alveolar proteinosis.

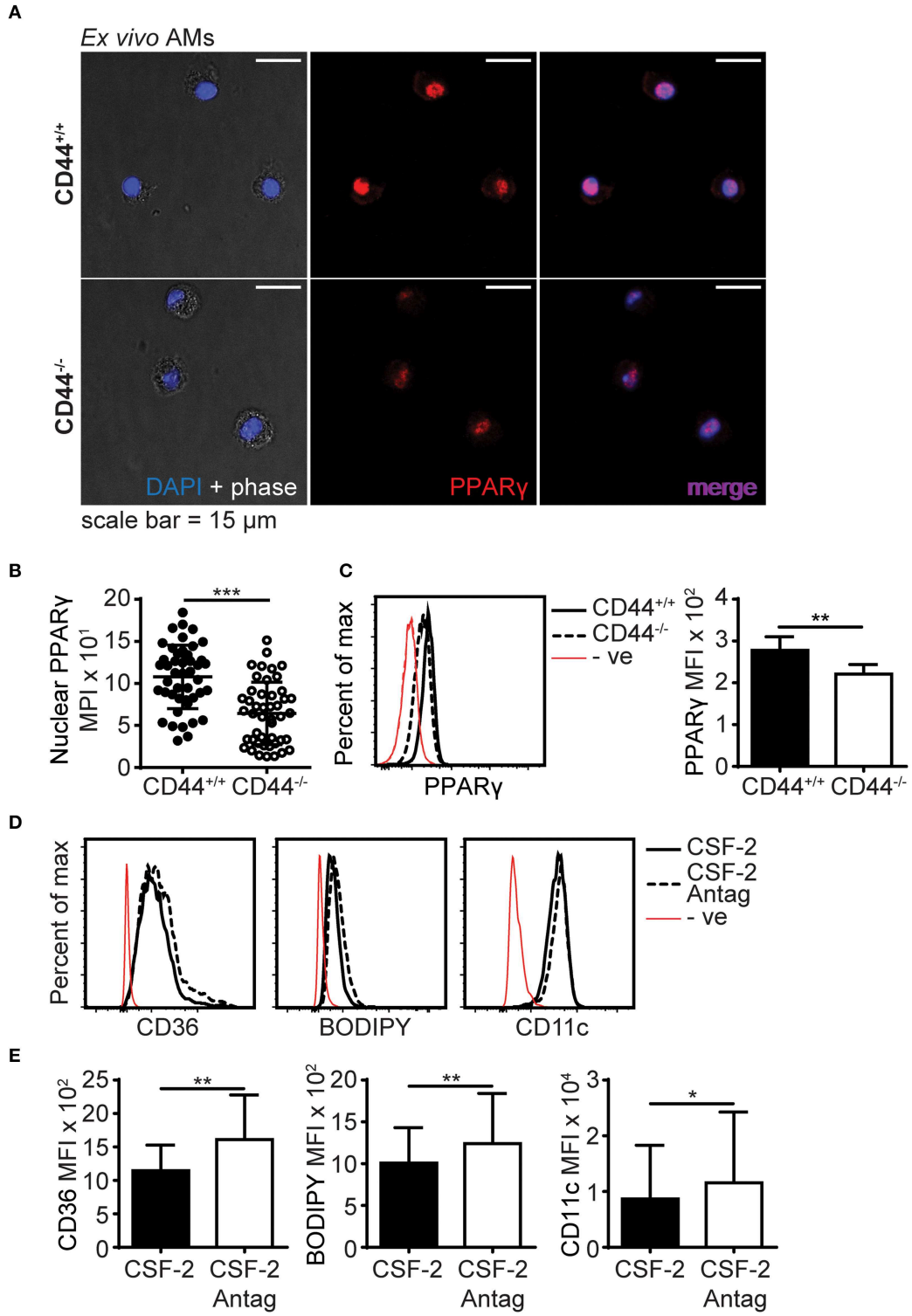

FIGURE 9 | PPARγ expression is defective in CD44$^{-/-}$ AMs. **(A)** Representative confocal microscopy showing CD44$^{+/+}$ and CD44$^{-/-}$ AMs labeled with intracellular PPARγ antibody and DAPI. **(B)** Comparison of nuclear PPARγ mean pixel intensity (MPI) between CD44$^{+/+}$ and CD44$^{-/-}$ AMs, determined by confocal microscopy. **(C)** Representative flow cytometry histograms and graphs comparing intracellular PPARγ expression between CD44$^{+/+}$ and CD44$^{-/-}$ AMs. **(D,E)** Representative flow cytometry histograms and graphs comparing the levels of CD36, BODIPY and CD11c levels by MFI (after subtraction of background autofluorescence) in CD44$^{+/+}$ AMs cultured with CSF-2 or CSF-2 and the PPARγ antagonist T0070907 (Antag) for 48 h in culture. Data show an average of three to five mice from each experiment ± SD, repeated twice or three times; for confocal imaging three to four fields containing cells were analyzed per mice. Significance indicated as $^{*}p < 0.05$, $^{**}p < 0.01$, $^{***}p < 0.001$, non-paired Student's *t*-test.

DATA AVAILABILITY STATEMENT

The datasets generated for this study can be found in the Geo database & SRA. GEO accession number: GSE138445.

ETHICS STATEMENT

The animal study was reviewed and approved by the University of British Columbia Animal Care Committee.

AUTHOR CONTRIBUTIONS

YD initiated and developed the project and performed most of the experiments. AA, ZH, JG, GP, and SL-S provided input and performed experiments. MD provided technical support. CR provided supervision. TH oversaw the lipidomic experiments, provided financial support, and supervision. PJ developed and oversaw the project, provided supervision, and acquired funds. YD and PJ wrote the manuscript, with contributions from JG, which was reviewed by all authors.

FUNDING

This work was supported by grants from the Natural Sciences and Engineering Research Council of Canada (NSERC) and the Canadian Institutes of Health Research (MOP 119503, PJT-153455) to PJ and UBC startup grant (F18-03001) and Canadian Foundation for Innovation (38159) to TH. AA and YD acknowledge fellowships from NSERC and UBC, respectively.

ACKNOWLEDGMENTS

We acknowledge invaluable assistance from the UBC Animal and Flow cytometry Facilities, as well as excellent service from the BRC-Seq Next-Gen sequencing core.

SUPPLEMENTARY MATERIAL

The Supplementary Material for this article can be found online at: https://www.frontiersin.org/articles/10.3389/fimmu.2020.00029/full#supplementary-material

REFERENCES

1. Hussell T, Bell TJ. Alveolar macrophages: plasticity in a tissue-specific context. *Nat Rev Immunol.* (2014) 14:8-93. doi: 10.1038/nri3600
2. Guilliams M, De Kleer I, Henri S, Post S, Vanhoutte L, De Prijck S, et al. Alveolar macrophages develop from fetal monocytes that differentiate into long-lived cells in the first week of life via GM-CSF. *J Exp Med.* (2013) 210:1977-92. doi: 10.1084/jem.20131199
3. Shibata Y, Berclaz PY, Chroneos ZC, Yoshida M, Whitsett JA, Trapnell BC. GM-CSF regulates alveolar macrophage differentiation and innate immunity in the lung through PU.1. *Immunity.* (2001) 15:557-67. doi: 10.1016/S1074-7613(01)00218-7
4. Schneider C, Nobs SP, Kurrer M, Rehrauer H, Thiele C, Kopf M. Induction of the nuclear receptor PPAR-gamma by the cytokine GM-CSF is critical for the differentiation of fetal monocytes into alveolar macrophages. *Nat Immunol.* (2014) 15:1026-37. doi: 10.1038/ni.3005
5. Yu X, Buttgereit A, Lelios I, Utz SG, Cansever D, Becher B, et al. The cytokine TGF-beta promotes the development and homeostasis of alveolar macrophages. *Immunity.* (2017) 47:903-12.e4. doi: 10.1016/j.immuni.2017.10.007
6. Trapnell BC, Carey BC, Uchida K, Suzuki T. Pulmonary alveolar proteinosis, a primary immunodeficiency of impaired GM-CSF stimulation of macrophages. *Curr Opin Immunol.* (2009) 21:514-21. doi: 10.1016/j.coi.2009.09.004
7. Trapnell BC, Nakata K, Bonella F, Campo I, Griese M, Hamilton J, et al. Pulmonary alveolar proteinosis. *Nat Rev Dis Primers.* (2019) 5:16. doi: 10.1038/s41572-019-0066-3
8. Schoonjans K, Staels B, Auwerx J. Role of the peroxisome proliferator-activated receptor (PPAR) in mediating the effects of fibrates and fatty acids on gene expression. *J Lipid Res.* (1996) 37:907-25.
9. Tontonoz P, Spiegelman BM. Fat and beyond: the diverse biology of PPARgamma. *Annu Rev Biochem.* (2008) 77:289-312. doi: 10.1146/annurev.biochem.77.061307.091829
10. Ahmadian M, Suh JM, Hah N, Liddle C, Atkins AR, Downes M, et al. PPARgamma signaling and metabolism: the good, the bad and the future. *Nat Med.* (2013) 19:557-66. doi: 10.1038/nm.3159
11. Vangolde LMG, Batenburg JJ, Robertson B. The pulmonary surfactant system - biochemical aspects and functional-significance. *Physiol Rev.* (1988) 68:374-455. doi: 10.1152/physrev.1988.68.2.374
12. Dong Y, Poon GFT, Arif AA, Lee-Sayer SSM, Dosanjh M, Johnson P. The survival of fetal and bone marrow monocyte-derived alveolar macrophages is promoted by CD44 and its interaction with hyaluronan. *Mucosal Immunol.* (2017) 11:60114. doi: 10.1038/mi.2017.83
13. Ghoneim HE, Thomas PG, McCullers JA. Depletion of alveolar macrophages during influenza infection facilitates bacterial superinfections. *J Immunol.* (2013) 191:1250-9. doi: 10.4049/jimmunol.1300014
14. Dagvadorj J, Shimada K, Chen S, Jones HD, Tumurkhuu G, Zhang W, et al. Lipopolysaccharide induces alveolar macrophage necrosis via CD14 and the P2X7 receptor leading to interleukin-1alpha release. *Immunity.* (2015) 42:640-53. doi: 10.1016/j.immuni.2015.03.007
15. Imai Y, Kuba K, Neely GG, Yaghubian-Malhami R, Perkmann T, van Loo G, et al. Identification of oxidative stress and toll-like receptor 4 signaling as a key pathway of acute lung injury. *Cell.* (2008) 133:235-49. doi: 10.1016/j.cell.2008.02.043
16. Romero F, Shah D, Duong M, Penn RB, Fessler MB, Madenspacher J, et al. A pneumocyte-macrophage paracrine lipid axis drives the lung toward fibrosis. *Am J Respir Cell Mol Biol.* (2015) 53:74-86. doi: 10.1165/rcmb.2014-0343OC
17. Manoury B, Nenan S, Leclerc O, Guenon I, Boichot E, Planquois JM, et al. The absence of reactive oxygen species production protects mice against bleomycin-induced pulmonary fibrosis. *Respir Res.* (2005) 6:11. doi: 10.1186/1465-9921-6-11
18. Lamb NJ, Gutteridge JM, Baker C, Evans TW, Quinlan GJ. Oxidative damage to proteins of bronchoalveolar lavage fluid in patients with acute respiratory distress syndrome: evidence for neutrophil-mediated hydroxylation, nitration, and chlorination. *Crit Care Med.* (1999) 27:1738-44. doi: 10.1097/00003246-199909000-00007
19. Kirkham P, Rahman I. Oxidative stress in asthma and COPD: antioxidants as a therapeutic strategy. *Pharmacol Ther.* (2006) 111:476-94. doi: 10.1016/j.pharmthera.2005.10.015
20. Yoshimi N, Ikura Y, Sugama Y, Kayo S, Ohsawa M, Yamamoto S, et al. Oxidized phosphatidylcholine in alveolar macrophages in idiopathic interstitial pneumonias. *Lung.* (2005) 183:109-21. doi: 10.1007/s00408-004-2525-0
21. Poon GF, Dong Y, Marshall KC, Arif A, Deeg CM, Dosanjh M, et al. Hyaluronan binding identifies a functionally distinct alveolar macrophage-like population in bone marrow-derived dendritic cell cultures. *J Immunol.* (2015) 195:632-42. doi: 10.4049/jimmunol.1402506
22. Culty M, O'Mara TE, Underhill CB, Yeager H Jr, Swartz RP. Hyaluronan receptor (CD44) expression and function in human peripheral blood monocytes and alveolar macrophages. *J Leukoc Biol.* (1994) 56:605-11. doi: 10.1002/jlb.56.5.605

23. Johnson P, Arif AA, Lee-Sayer SSM, Dong Y. Hyaluronan and its interactions with immune cells in the healthy and inflamed lung. *Front Immunol.* (2018) 9:2787. doi: 10.3389/fimmu.2018.02787
24. Katoh S, Matsubara Y, Taniguchi H, Fukushima K, Mukae H, Kadota J, et al. Characterization of CD44 expressed on alveolar macrophages in patients with diffuse panbronchiolitis. *Clin Exp Immunol.* (2001) 126:545-50. doi: 10.1046/j.1365-2249.2001.01699.x
25. Pons AR, Noguera A, Blanquer D, Sauleda J, Pons J, Agusti AGN. Phenotypic characterisation of alveolar macrophages and peripheral blood monocytes in COPD. *Eur Respir J.* (2005) 25:647-52. doi: 10.1183/09031936.05.00062304
26. Thepen T, Van Rooijen N, Kraal G. Alveolar macrophage elimination *in vivo* is associated with an increase in pulmonary immune response in mice. *J Exp Med.* (1989) 170:499-509. doi: 10.1084/jem.170.2.499
27. Knapp S, Leemans JC, Florquin S, Branger J, Maris NA, Pater J, et al. Alveolar macrophages have a protective antiinflammatory role during murine pneumococcal pneumonia. *Am J Resp Crit Care.* (2003) 167:171-9. doi: 10.1164/rccm.200207-698OC
28. Teder P, Vandivier RW, Jiang D, Liang J, Cohn L, Pure E, et al. Resolution of lung inflammation by CD44. *Science.* (2002) 296:155-8. doi: 10.1126/science.1069659
29. Liang JR, Jiang DH, Griffith J, Yu S, Fan J, Zhao XJ, et al. CD44 is a negative regulator of acute pulmonary inflammation and lipopolysaccharide-TLR signaling in mouse macrophages. *J Immunol.* (2007) 178:2469-75. doi: 10.4049/jimmunol.178.4.2469
30. Trapnell C, Hendrickson DG, Sauvageau M, Goff L, Rinn JL, Pachter L. Differential analysis of gene regulation at transcript resolution with RNA-seq. *Nat Biotechnol.* (2013) 31:46-53. doi: 10.1038/nbt.2450
31. Tripathi S, Pohl MO, Zhou Y, Rodriguez-Frandsen A, Wang G, Stein DA, et al. Meta- and orthogonal integration of influenza "OMICs" data defines a role for UBR4 in virus budding. *Cell Host Microbe.* (2015) 18:723-35. doi: 10.1016/j.chom.2015.11.002
32. Steinbaugh M, Turner S, Wolen A. *stephenturner/annotables: Ensembl 90 (Version v0.1.90)*. Charlottesville, VA:Zenodo (2017).
33. Szklarczyk D, Gable AL, Lyon D, Junge A, Wyder S, Huerta-Cepas J, et al. STRING v11: protein-protein association networks with increased coverage, supporting functional discovery in genome-wide experimental datasets. *Nucleic Acids Res.* (2019) 47:D607-13. doi: 10.1093/nar/gky1131
34. Tsugawa H, Cajka T, Kind T, Ma Y, Higgins B, Ikeda K, et al. MS-DIAL: data-independent MS/MS deconvolution for comprehensive metabolome analysis. *Nat Methods.* (2015) 12:523-6. doi: 10.1038/nmeth.3393
35. Kind T, Liu KH, Lee DY, DeFelice B, Meissen JK, Fiehn O. LipidBlast *in silico* tandem mass spectrometry database for lipid identification. *Nat Methods.* (2013) 10:755-8. doi: 10.1038/nmeth.2551
36. Su X, Abumrad NA. Cellular fatty acid uptake: a pathway under construction. *Trends Endocrinol Metab.* (2009) 20:72-7. doi: 10.1016/j.tem.2008.11.001
37. Silverstein RL, Febbraio M. CD36, a scavenger receptor involved in immunity, metabolism, angiogenesis, and behavior. *Sci Signal.* (2009) 2:re3. doi: 10.1126/scisignal.272re3
38. Eberle D, Hegarty B, Bossard P, Ferre P, Foufelle F. SREBP transcription factors: master regulators of lipid homeostasis. *Biochimie.* (2004) 86:839-48. doi: 10.1016/j.biochi.2004.09.018
39. Yue L, Mazzone T. Peroxisome proliferator-activated receptor {gamma} stimulation of adipocyte ApoE gene transcription mediated by the liver receptor X pathway. *J Biol Chem.* (2009) 284:10453-61. doi: 10.1074/jbc.M808482200
40. Chawla A, Boisvert WA, Lee CH, Laffitte BA, Barak Y, Joseph SB, et al. A PPAR gamma-LXR-ABCA1 pathway in macrophages is involved in cholesterol efflux and atherogenesis. *Mol Cell.* (2001) 7:161-71. doi: 10.1016/S1097-2765(01)00164-2
41. Horkko S, Bird DA, Miller E, Itabe H, Leitinger N, Subbanagounder G, et al. Monoclonal autoantibodies specific for oxidized phospholipids or oxidized phospholipid-protein adducts inhibit macrophage uptake of oxidized low-density lipoproteins. *J Clin Invest.* (1999) 103:117-28. doi: 10.1172/JCI4533
42. Schmitz G, Grandl M. Endolysosomal phospholipidosis and cytosolic lipid droplet storage and release in macrophages. *Biochim Biophys Acta.* (2009) 1791:524-39. doi: 10.1016/j.bbalip.2008.12.007
43. Lee G, Elwood F, McNally J, Weiszmann J, Lindstrom M, Amaral K, et al. T0070907, a selective ligand for peroxisome proliferator-activated receptor gamma, functions as an antagonist of biochemical and cellular activities. *J Biol Chem.* (2002) 277:19649-57. doi: 10.1074/jbc.M200743200
44. Rodrigue-Way A, Caron V, Bilodeau S, Keil S, Hassan M, Levy E, et al. Scavenger receptor CD36 mediates inhibition of cholesterol synthesis via activation of the PPARgamma/PGC-1alpha pathway and Insig1/2 expression in hepatocytes. *FASEB J.* (2014) 28:1910-23. doi: 10.1096/fj.13-240168
45. Shimano H, Sato R. SREBP-regulated lipid metabolism: convergent physiology - divergent pathophysiology. *Nat Rev Endocrinol.* (2017) 13:710-30. doi: 10.1038/nrendo.2017.91
46. Ginhoux F. Fate PPAR-titioning: PPAR-gamma 'instructs' alveolar macrophage development. *Nat Immunol.* (2014) 15:1005-7. doi: 10.1038/ni.3011
47. Baker AD, Malur A, Barna BP, Ghosh S, Kavuru MS, Malur AG, et al. Targeted PPAR{gamma} deficiency in alveolar macrophages disrupts surfactant catabolism. *J Lipid Res.* (2010) 51:1325-31. doi: 10.1194/jlr.M001651
48. Baker AD, Malur A, Barna BP, Kavuru MS, Malur AG, Thomassen MJ. PPARgamma regulates the expression of cholesterol metabolism genes in alveolar macrophages. *Biochem Biophys Res Commun.* (2010) 393:682-7. doi: 10.1016/j.bbrc.2010.02.056
49. Hauser S, Adelmant G, Sarraf P, Wright HM, Mueller E, Spiegelman BM. Degradation of the peroxisome proliferator-activated receptor gamma is linked to ligand-dependent activation. *J Biol Chem.* (2000) 275:18527-33. doi: 10.1074/jbc.M001297200
50. Chang CC, Hsieh MS, Liao ST, Chen YH, Cheng CW, Huang PT, et al. Hyaluronan regulates PPARgamma and inflammatory responses in IL-1beta-stimulated human chondrosarcoma cells, a model for osteoarthritis. *Carbohydr Polym.* (2012) 90:1168-75. doi: 10.1016/j.carbpol.2012.06.071
51. Acharya PS, Majumdar S, Jacob M, Hayden J, Mrass P, Weninger W, et al. Fibroblast migration is mediated by CD44-dependent TGF beta activation. *J Cell Sci.* (2008) 121:1393-402. doi: 10.1242/jcs.021683
52. Bourguignon LYW, Singleton PA, Zhu HB, Zhou B. Hyaluronan promotes signaling interaction between CD44 and the transforming growth factor beta receptor I in metastatic breast tumor cells. *J Biol Chem.* (2002) 277:39703-12. doi: 10.1074/jbc.M204320200
53. Aziz A, Soucie E, Sarrazin S, Sieweke MH. MafB/c-Maf deficiency enables self-renewal of differentiated functional macrophages. *Science.* (2009) 326:867-71. doi: 10.1126/science.1176056
54. Moliva JI, Rajaram MV, Sidiki S, Sasindran SJ, Guirado E, Pan XJ, et al. Molecular composition of the alveolar lining fluid in the aging lung. *Age.* (2014) 36:9633. doi: 10.1007/s11357-014-9633-4

Conflict of Interest: The authors declare that the research was conducted in the absence of any commercial or financial relationships that could be construed as a potential conflict of interest.

frontiers in Immunology

ORIGINAL RESEARCH
published: 06 February 2020
doi: 10.3389/fimmu.2020.00132

The Heparan Sulfate Mimetic PG545 Modulates T Cell Responses and Prevents Delayed-Type Hypersensitivity

Ievgen O. Koliesnik[1†], Hedwich F. Kuipers[1,2†], Carlos O. Medina[1], Svenja Zihsler[1], Dan Liu[1], Jonas D. Van Belleghem[1] and Paul L. Bollyky[1]*

[1] Division of Infectious Diseases and Geographic Medicine, Department of Medicine, Beckman Center, Stanford University School of Medicine, Stanford, CA, United States, [2] Department of Clinical Neurosciences, University of Calgary, Calgary, AB, Canada

The heparan sulfate mimetic PG545 (pixatimod) is under evaluation as an inhibitor of angiogenesis and metastasis including in human clinical trials. We have examined the effects of PG545 on lymphocyte phenotypes and function. We report that PG545 treatment suppresses effector T cell activation and polarizes T cells away from Th17 and Th1 and toward Foxp3+ regulatory T cell subsets *in vitro* and *in vivo*. Mechanistically, PG545 inhibits Erk1/2 signaling, a pathway known to affect both T cell activation and subset polarization. Interestingly, these effects are also observed in heparanase-deficient T cells, indicating that PG545 has effects that are independent of its role in heparanase inhibition. Consistent with these findings, administration of PG545 in a Th1/Th17-dependent mouse model of a delayed-type hypersensitivity led to reduced footpad inflammation, reduced Th17 memory cells, and an increase in FoxP3+ Treg proliferation. PG545 also promoted Foxp3+ Treg induction by human T cells. Finally, we examined the effects of other heparan sulfate mimetics PI-88 and PG562 on lymphocyte polarization and found that these likewise induced Foxp3+ Treg *in vitro* but did not reduce Th17 numbers or improve delayed-type hypersensitivity in this model. Together, these data indicate that PG545 is a potent inhibitor of Th1/Th17 effector functions and inducer of FoxP3+ Treg. These findings may inform the adaptation of PG545 for clinical applications including in inflammatory pathologies associated with type IV hypersensitivity responses.

Keywords: heparan sulfate mimetic, PG545, Th17 cells, regulatory T cells, inflammation

OPEN ACCESS

Edited by:
Rogier M. Reijmers, Leiden University Medical Center, Netherlands

Reviewed by:
Wendy W. J. Unger, Sophia Children's Hospital, Netherlands
Behdad Afzali, National Institute of Diabetes and Digestive and Kidney Diseases (NIDDK), United States

****Correspondence:***
Ievgen O. Koliesnik
kolesnik@stanford.edu

† These authors share first authorship

Specialty section:
This article was submitted to Inflammation, a section of the journal Frontiers in Immunology

Received: *11 October 2019*
Accepted: *17 January 2020*
Published: *06 February 2020*

Citation:
Koliesnik IO, Kuipers HF, Medina CO, Zihsler S, Liu D, Van Belleghem JD and Bollyky PL (2020) The Heparan Sulfate Mimetic PG545 Modulates T Cell Responses and Prevents Delayed-Type Hypersensitivity. Front. Immunol. 11:132. doi: 10.3389/fimmu.2020.00132

INTRODUCTION

Heparan sulfate mimetics have emerged as potential therapies against various types of cancer (1–4). These agents are thought to work via inhibition of heparanase (5–7), an enzyme associated with tumor cell invasion and angiogenesis (6, 8, 9). Heparanase is also known to be involved in normal immune cell functions (10–13). In particular, heparanase overexpression facilitates T cell effector functions and migration, as well as macrophage and NK cell activation (12, 14).

The first such inhibitor, PI-88, demonstrated promising results in mouse cancer models (15). However, a phase III clinical trial using PI-88 as an adjuvant in hepatocellular carcinoma therapy did not reach its primary end point (16).

PG545 is a member of a novel class of synthetic heparanase inhibitors, the PG500 family (17, 18). A fully sulfated oligosaccharide attached to a lipophilic moiety, PG545 has improved pharmacokinetics and much weaker anticoagulant activity relative to other heparanase inhibitors, including PI-88 (19). PG545 is reported to function by blocking the catalytic center of heparinase and competing for the HS-binding domain (11, 19). PG545 is currently under evaluation in human clinical trials for use in treating solid tumors after having demonstrated efficacy against tumor angiogenesis and metastasis in multiple animal studies (1, 3, 20, 21). PG545 has also demonstrated efficacy against lymphoma and may also have utility in other, non-neoplastic inflammatory disorders, such as acute kidney injury, atherosclerosis, and viral infection (2, 9, 22, 23). However, it remains unclear how PG545 impacts immune cells, particularly T-lymphocytes. This knowledge is likely to be important, given the key role of T-lymphocytes in cancer immunology and inflammation.

We sought to evaluate the impact of PG545 on T cells and T cell subsets, including pro-inflammatory Th1 and Th17 cells and anti-inflammatory FoxP3+ regulatory T cells (24, 25). To this end, we studied this agent in the context of *in vitro* T cell activation and proliferation, antigenic responses *in vivo*, and in a skin hypersensitivity model.

We report that *in vitro*, PG545 promotes expansion of Treg while suppressing effector T cells, particular Th17 T cells. *In vivo*, PG545 suppresses antigen-specific T cell generation and cytokine production, leading to improvement in a Th17-dependent delayed hypersensitivity model. Together, these data indicate that PG545 has profound effects on T cell polarization and function.

MATERIALS AND METHODS

Mice

C75BL/6J mice for the experiments were obtained from the Jackson laboratories at the age of 8–10 weeks and kept in specific pathogen free facility on a standard chow. $HPSE^{-/-}$ mice were a kind gift of I. Vlodavsky (26). OT-II B6 transgenic mice were from the Jackson Laboratory. $Foxp3^{gfp}$ reporter mice (27) were a kind gift of Dr. Alexander Rudensky. All mice were maintained in a specific pathogen-free AAALAC-accredited animal facility at Stanford University. All experiments were approved by the Stanford IACUC.

Human Lymphocyte Isolation

Human peripheral blood mononuclear cells (PBMCs) were obtained and isolated as previously described (28). Human naïve CD4 cells were isolated from frozen PBMC using EasySep™ human CD4 isolation kit (Stemcell technologies, Vancouver, Canada). The cells were then resuspended in RPMI 1640 (Invitrogen) supplemented with 10% FBS (Hyclone, Logan, UT), 100 μg/ml Penicillin, 100 U/ml Streptomycin, 50 μM βme, 2 mM glutamine, and 1 mM sodium pyruvate (Invitrogen).

Mouse Lymphocyte Isolation and Culture

Primary T cells were isolated from spleen and lymph node cell suspensions as previously described (29) using a CD4 isolation kit (Stemcell technologies). For T cell activation studies, 1×10^5 cells were cultured and activated as previously described (30) using plate bound anti-CD3 (145-2C11, Biolegend) and soluble anti-CD28 (37.51, Biolegend) at concentrations of 2 and 1 μg/ml, respectively. Bone marrow derived dendritic cells were differentiated as previously described (28) Briefly, 10×10^6 bone marrow cells were cultured in complete T cell medium (RMPI 1640, 10% FBS, 100 U/ml Streptomycin, 50 μM βme, 2 mM glutamine, and 1 mM sodium pyruvate) for 7 days in the presence of 10 ng/ml mouse GM-CSF and 2 ng/ml IL-4 (Peprotech). On day 3 and 5 fresh medium with cytokines was added. For co-culture experiments 2×10^4 BMDCs were incubated with 1 μg/ml anti-CD3 antibody (145-2C11, Biolegend) and 1×10^5 naïve CD4 T cells.

Flow Cytometry

Flow cytometry was performed as previously described (31). Antibodies used included anti-CD4-BV785 (RM4-5), anti-CD8-BV711 (53-6.7), anti-CD62L-BV421 (MEl-14), anti-CD44-APC-Cy7 (IM7), anti-CD25-PE-Cy7-(PC61), anti-CD3-PE-Cy7 (17A2), anti-CD69-APC (H1. 2F3), anti-CD154-PE (MR1), all from BioLegend. For Foxp3, RORγt, and T-bet staining, cells were fixed, permeabilized and stained using Foxp3 Transcription factor staining kit (Thermo Fisher Scientific). The antibodies used for nuclear staining were anti-Foxp3-EF660 (FJK-16s; Thermo Fisher Scientific), anti-Ki-67- PECy7 (SolA 15; Thermo Fisher Scientific), anti-T-bet-Alexa Fluor 647 (4B10, BioLegend), anti-RORγt (Q31-378, BD Biosciences). For cytokine staining 5×10^6 cells were stimulated with 50 ng/ml PMA and 500 ng ionomycin (Sigma-Aldrich) in the presence of Brefeldin A (Bioelegend) for 5 h. Cells were fixed using IC buffer (Thermo Fisher Scientific), permeabilized with 0.5% saponin (Sigma-Aldrich) and stained with anti-IFNg-APC (XMG1.12, anti-IL-17-PE (TC11-18H10.1), anti-TNFa-PE (MP6-XT22). For phosphoflow experiments mouse total CD4 T cells were activated for 3 days with or without PG545, rested for 6 h and restimulated with Dynabeads mouse T cell activator (Thermo Fisher Scientific) for 12 h with or with or without PG545. Cells were fixed in Phosphoflow fixation buffer (BD Biosciences), permeabilized with 90% methanol for 30 min on ice and stained with anti-phospho-Erk44/42-APC (Cell Signaling Technology). Flow cytometry was performed using LSRII (BD Biosciences) or Cytek Aurora (Cytek Biosciences) and the sorting was done at the FACS Aria III (BD Biosciences). Data was analyzed using Flowjo 10 software (Treestar Inc.).

In vitro T-Cell Differentiation

Th1 and Th17 cells were induced as previously described (31). In brief, 1×10^5 naïve CD4 cells were activated with anti-CD3 (145-2C11, Biolegend) and anti-CD28 (37.51, Biolegend) antibodies in presence of 50 ng/ml mouse recombinant IL-12 or 5 ng/ml of human recombinant TGFβ (Biolegend) and 25 ng/ml mouse recombinant IL-6 (Peprotech) for 3 days. For iTreg induction cells were cultured with 50 ng/ml of human

recombinant TGFβ with 100 IU/ml recombinant IL-2 (Chiron), as previously described (32). For T cell proliferation cells were stained with 5 uM Cell Trace Violet (Thermo Fisher Scientific) in PBS for 15 min at RT, washed with cell culture media, counted and plated as mentioned earlier. Cells were cultured in RPMI 1640 media containing 2.05 mM L-Glutamine, 10% FBS and 1× penicillin/streptomycin (GE Healthcare). For some experiments MAPK Kinase Inhibitor PD98059 (Sigma Aldrich) was used.

In vitro Suppression Assays

Suppression assays were performed as previously described (33). In brief, iTregs induced either in the absence or presence of PG545 were co-cultured with Cell Trace labeled responder CD4 cells and T cell-depleted splenocytes as antigen presenting cells. Activation was provided by 1 μg/ml of soluble anti-CD3 (145-2C11, Biolegend).

Ovalbumin Immunization

Naïve CD4 T cells from OT-II mice were stained with eFlour 450 cell proliferation dye (Thermo Fisher Scientific) and 1×10^6 of the cells adoptively transferred via intravenous tail injections into B6 recipients. The next day mice were immunized with 50 μg of OVA protein emulsified in 100 μL alum (Thermo Fisher Scientific).

Western Blotting

Protein lysate from CTLL2 cells (ATCC) cells was prepared using RIPA buffer (Thermo Fisher Scientific) and 20 μg of protein per sample were separated on a NuPAGE 4–12% Bis-Tris Protein gel (Thermo Fisher Scientific) and blotted onto a 0.22 μm Odyssey nitrocellulose membrane (LI-COR). Phospho Erk1/2 was detected using a pErk antibody Thr202/204 #9101 (Cell Signaling Technology).

In vivo Delayed Type Hypersensitivity Experiments

These experiments were performed as previously described (34). In brief, 8–10 week old mice were sensitized subcutaneously with 200 μg of mBSA (Sigma-Aldrich) emulsified in Complete Freund's Adjuvant (Santa Cruz Biotechnology) and challenged with 200 μg of mBSA solution in the foot pad of a hind limb. Control foot pad was injected with an equal volume of PBS. Footpad swelling was measured starting at day 0 using a digital caliper (Traceable). The reading of the "PBS" foot were subtracted from the "mBSA" foot for each individual mouse. PG545 dissolved in PBS was administered to mice intraperitoneally at a concentration of 400 μg/mouse at the indicated time point.

Generation of Murine Bone Marrow–Derived Dendritic Cells

BMDC were generated as described (28). Bone marrow from femurs of 6–10 week old mice was flushed out using a 27 G Precision Glide needle (BD Biosciences, Cat. No. 305109). Cells were plated at 1×10^6 cells in 10 ml of media per Petri Dish (Fisherbrand, Cat. No. FB0875711), supplemented with 10 ng/ml of recombinant mouse granulocyte-macrophage colony-stimulating factor (GM-CSF) (STEMCELL Technologies, Cat. No. 78206.1) and 2 ng/ml of recombinant mouse IL-4 (Invitrogen, Cat. No. 14-8041-62). An equivalent amount of fresh media containing cytokines was added 3 days after plating, and 50% of media was changed on day 5 after plating. BMDCs were harvested for use on day 6.

Induction of EAE

EAE was induced as described previously (35). In brief, C57BL/6J mice were immunized with 200 μg of myelin oligodendrocyte glycoprotein (35–55) (MOG_{35-55}) in complete Freund's adjuvant containing 400 ng of mycobacterium tuberculosis H37RA (Difco Laboratories, Detroit, MI). All mice were administered 400 ng of pertussis toxin (List Biological, Campbell, CA) intraperitoneally (i.p.) at 0 and 48 h post-immunization. Mice were monitored daily for clinical symptoms and scored as follows: 0, no clinical disease; 1, tail weakness; 2, hindlimb weakness; 3, complete hindlimb paralysis; 4, hindlimb paralysis and some forelimb weakness; 5, moribund or dead.

Statistical Analysis

Statistical analysis was performed using Prism software, version 7.0 (GraphPad). Data are presented as mean SD. In samples with Gaussian distribution, an unpaired *t*-test was used to determine significant differences between groups or a 2-way ANOVA was used to identify effects of multiple parameters. A $p < 0.05$ was considered statistically significant.

RESULTS

PG545 Inhibits Effector T Cell Activation *in vitro* and *in vivo*

We first asked whether PG545 affects T cell activation *in vitro*. To test this, we stimulated CD4+ T cells in a polyclonal manner. We observed that PG545 did not inhibit the activation of CD4+ T cells, as measured by the expression of CD69 and CD25 (**Figures 1A,B**).

We next examined cytokine production by these cells via intracellular staining. We observed that PG545 treatment resulted in altered cytokine production, including reduced IFNg and IL-17 in Th1 and Th17 polarizing conditions, respectively. This is seen for a representative staining example as well as across multiple samples (**Figures 1C,D**). This was also accompanied by decreased expression of T-bet and RORgt in the setting of PG545 treatment (**Figure 1G**; **Supplemental Figure 1A**). PG545 also inhibited IL-17 production by activated total CD4 T cells, while sparing IFNg-competent T cells (**Figures 1E,F**), suggesting that PG545 acts early on during Th1 differentiation but not on mature Th1 memory cells.

Together, these data indicate that PG545 potently polarizes T helper differentiation away from Th1 and Th17 cells.

We next examined the impact of PG545 on adaptive immunity *in vivo*. To this end, we transferred Cell Trace-labeled, ovalbumin (OVA)-specific OT-II naïve CD4 cells from CD45.1 mice into naïve CD45.2 autologous recipient mice on day−2. These recipient animals then received either a single dose of PG545 or the same volume of phosphate buffered saline (PBS) as a control via intraperitoneal (i.p.) injection on day−1

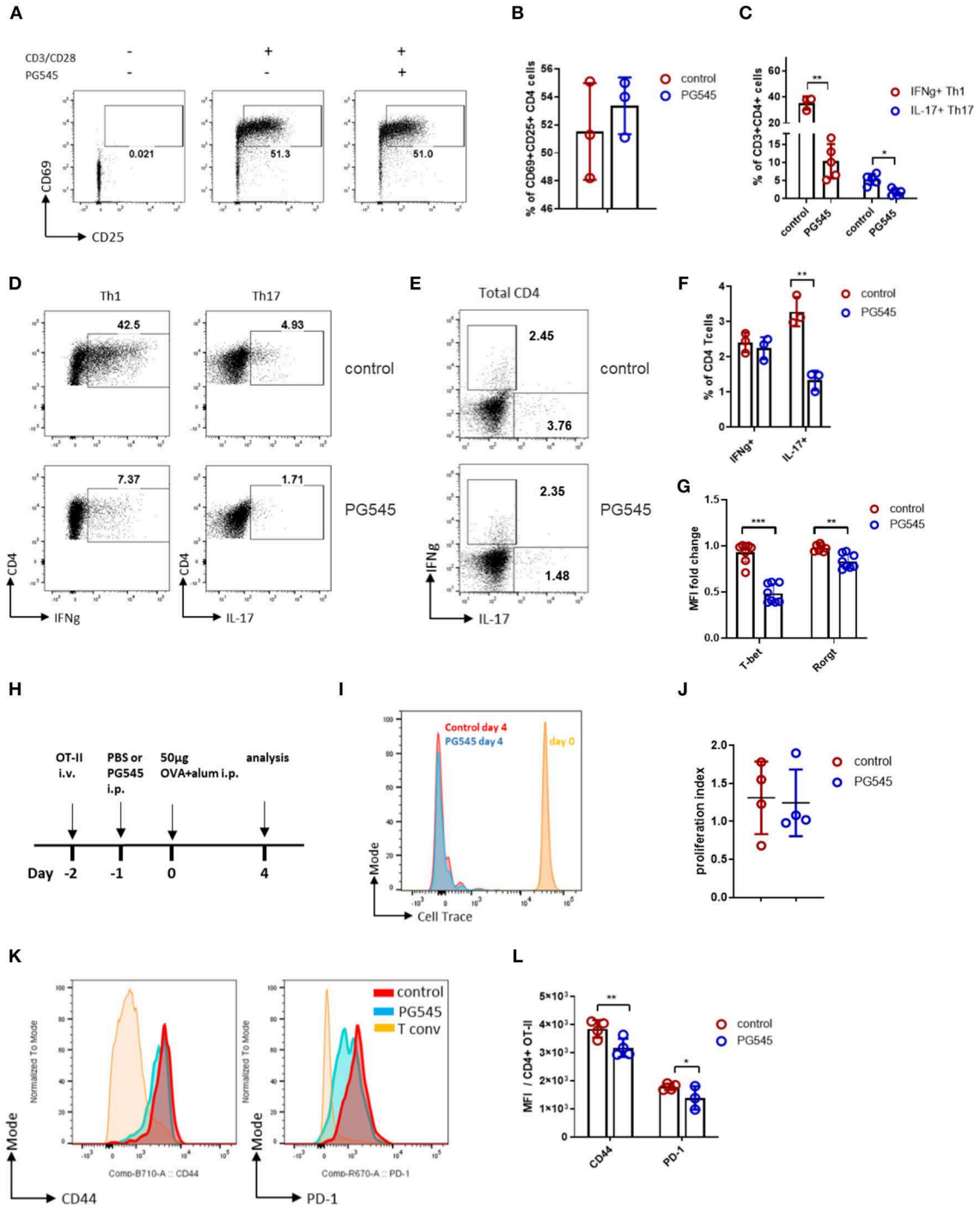

FIGURE 1 | PG545 inhibits effector T cell differentiation. **(A)** FACS plot showing the expression of CD25 and CD69 by mouse CD4 cells in response to CD3/CD28 stimulation in the absence or presence of PG545. **(B)** Cumulative bar diagram of CD25 and CD69 expression. Data are representative of three experiments. **(C)** Aggregate data on T helper cell differentiation in the presence of PG545. Data are representative of three experiments. **(D)** FACS plot of Th1 and Th17 differentiation of naïve T cells in the absence or presence of PG545. **(E,F)** IFNg and IL-17 profile of memory CD4 T cells cultured with PG545 for 48 h. Data are representative of two experiments. **(G)** T-bet and RORgt expression in T cells from Th1 and Th17 polarization, respectively. **(H)** Schematic of the experimental protocol used to generate the data in this figure. **(I)** Overlaid histograms showing the proliferation of transferred OT-II cells in B6 recipients following OVA-alum immunization and injection with either PBS (control) or PG545 (20 µg/g of weight). **(J)** Proliferation index of transferred OT-II cells. **(K)** Representative histograms showing CD44 and PD-1 expression on transferred OT-II cells. **(L)** Aggregated mean fluorescence index (MFI) data from **(K)**. Each data point represents an individual mouse. Data represent mean ± SD; $*p < 0.05$, $**p < 0.01$, $***p < 0.001$ vs. respective control by unpaired *t*-test or one way ANOVA with multiple comparisons where appropriate.

followed by i.p. immunization with OVA on day 0. Then, on day 4 we euthanized the mice, isolated lymphatic tissue, and examined the proliferation and phenotype of these transferred cells via flow cytometry. A schematic of this protocol is shown in **Figure 1H**.

Following OVA immunization, transferred OT-II cells underwent rapid proliferation as measured by Cell Trace dilution. Mice that received either PG545 or control injections had equivalent proliferation of OT-II cells (**Figures 1I,J**). However, these cells from mice that received PG545 had lower expression of CD44 and PD-1 than control OT-II cells. This was seen for a representative staining example (**Figure 1K**) as well as across samples from multiple mice (**Figure 1L**). Neither CD25 nor CD69 levels were altered (not shown). This is consistent with the effects of PG545 *in vitro* where we likewise did not observe effects on early T cell activation (**Figure 1A**). Together, these data suggest that PG545 modestly impacts T cell activation but not proliferation.

We also examined PG545 effects on other aspects of murine health in this system. Mice treated with PG545 developed splenomegaly (**Supplemental Figure 1B**) a mild albeit not significant weight loss (**Supplemental Figure 1C**) without an increase in the lymphocyte count (**Supplemental Figure 1D**).

Together these data demonstrate that PG545 inhibits effector T cell phenotype without affecting their proliferation.

PG545 Enhances Induction of FoxP3+ Treg *in vitro*

Because CD44 expression is reported to influence the number of Foxp3+ Treg by promoting Treg homeostasis but inhibiting expansion (36, 37) we considered whether PG545 might impact Treg. We did indeed observe that PG545 induced more Foxp3+ cells among OT-II T cells recovered from the spleen and draining lymph nodes of recipient mice. This was seen for a representative staining example (**Figure 2A**) as well as across samples from multiple mice (**Figure 2B**). We believe that these cells represent *de novo* induced Foxp3+ cells rather than the expanded pre-existing Tregs, since the transferred naïve OT-II cells have undergone multiple rounds of division before expressing Foxp3 (**Supplemental Figure 1F**). In comparison to these effects with PG545, we did not observe an increase in Treg upon treatment with either another heparan sulfate mimetic PI88 (**Figure 2C**) or with heparan sulfate itself using the same OT-II transfer model (data not shown). These data suggest that PG545 promotes the induction of Tregs *in vivo*. Given recent reports of the anti-inflammatory properties of PG545 in several systems (9, 22), we asked whether this agent promotes expansion of FoxP3+ Treg *in vitro*. To interrogate the effect of PG545 on T cells, we performed a Treg induction assay using a previously established protocol (33, 38). Addition of PG545 increased the percentage of Foxp3+ Treg in the presence of IL-2 and TGFβ (**Figures 2D,E**). In addition, the total frequencies of Foxp3+ cell per sample were also increased in the presence of PG545 (**Figure 2F**). PG545 promoted Treg induction at a range of concentrations (**Figures 2G,H**). PG545 was more effective at promoting Foxp3+ Treg induction at lower TGFβ concentrations (**Figures 2I,J**) indicating a high sensitivity of T cells to PG545 during suboptimal Treg differentiation conditions.

To test whether PG545-induced Foxp3+ cells were functional, we used a previously described *in vitro* suppression assay that uses induced Foxp3+ Treg in conjunction with autologous, CFSE-labeled CD4+ T cells and autologous irradiated CD4- cells as antigen presenting cells (APC) (39). Using this system, we determined that Tregs induced in the presence of PG545 were equally potent in suppressing effector T cell activation *in vitro* (**Supplemental Figure 1E**).

We also tested the effects of PG545 on human cells. PG545 favored Treg induction of naïve human CD4 cells, most potently at low concentrations of TGFβ (**Figures 2K,L**).

Together, these data demonstrate that PG545 promotes the expansion of both human and mouse Treg numbers *in vitro* and *in vivo*. Moreover, these data suggest that iTregs derived in the context of PG545 are functionally competent.

PG545-Mediated Effects on Treg Induction Do Not Depend on HPSE Expression

We next asked whether the effect of PG545 on Treg induction was dependent on HPSE expression. To this end, we repeated our *in vitro* Treg induction assay using CD4+ T cells isolated from heparanase knock-out mice ($HPSE^{-/-}$) mice. To interrogate this, we bred $HPSE^{-/-}$ mice on a C57Bl6 background to strain-matched mice expressing a GFP/Foxp3 reporter (26, 27).

We found that PG545 doubled Foxp3 frequencies of wild type as well as HPSE-deficient CD4 cells (**Figures 3A,B**). Interestingly, $HPSE^{-/-}$ CD4 T cells on their own produced higher frequencies of Foxp3+ cells, indicating that HPSE protein could inhibit iTreg induction. Nonetheless, the Treg-promoting effect of PG545 seems to be heparanase-dependent.

PG545 Inhibits Erk Signaling in Lymphoid Cells

We then asked how PG545 might promote Treg induction but inhibit Th1 and Th17 polarization. Erk1/2 signaling is known to inhibit Foxp3+ Treg induction and to promote Th1 polarization via suppression of Foxp3 and RORγt expression (40–42). We therefore asked whether PG545 might impact Erk1/2 signaling. To address this question, we examined Erk1/2 phosphorylation in CTLL2 T cells.

We observed a potent inhibition of basal Erk1/2 phosphorylation after treatment with PG545 (**Figures 4A,B**). Similarly, PG545 strongly diminished pErk signaling in primary activated mouse CD4 T cells (**Figures 4C,D**). These data suggest that PG545 inhibits basal Erk1/2 signaling. In agreement with previous findings (40, 41), we observed a significant increase of Foxp3+ frequencies in the presence of Erk inhibitor (**Figure 4E**; **Supplemental Figure 1G**). This effect was dose-dependent, as higher concentrations of inhibitor suppresses Foxp3 induction and caused higher cell death (not shown). These findings are highly consistent with our observations that PG545 promotes Treg expansion and prevents polarization toward Th1.

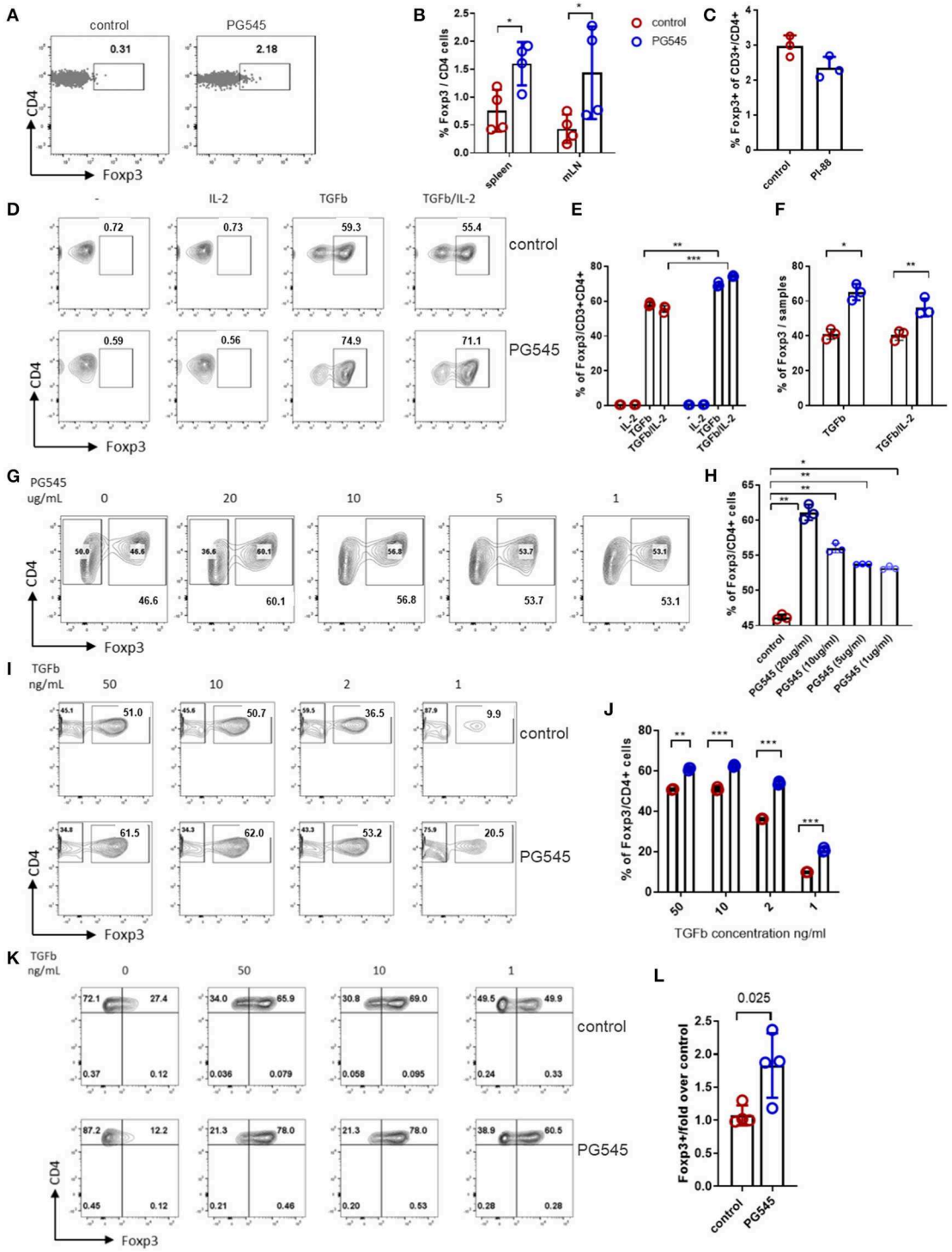

FIGURE 2 | PG545 promotes Treg induction. Treg induction protocols were performed using established protocols and naïve mouse CD4+ cells isolated from spleen and LN of 3–4 month old Foxp3^{GFP} mouse. **(A)** Representative FACS plots of Foxp3 expression in OT-II cells. **(B)** Bar diagram with frequencies of Foxp3+ CD4 cells from **(A)**. **(C)** Foxp3+ frequencies among the adoptively transferred CD4+ OT-II cells after PI-88 administration. **(D,E)** FACS plots and bar diagrams for the frequencies of Foxp3+ CD4+ cells across different culture conditions. **(F)** Percentage of Foxp3+ cells from the Treg induction experiment in **(D)**. **(G,H)** Treg percentages following Treg induction across indicated PG545 concentrations of **(I,J)**. Treg differentiation assay with decreasing concentrations of TGFβ. Experiments A–I are representative experiments that were each performed at least three times. **(K,L)** Treg differentiation assay of naïve human CD4+ cells in the presence of PG545 for 96 h. Representative of three independent experiments with four donors in total. Data represent mean fold change ± SD for the condition with 50 ng/ml of TGFbeta; $^{*}p < 0.05$, $^{**}p < 0.01$, $^{***}p < 0.001$ vs. respective control by unpaired *t*-test or one-way ANOVA with multiple comparisons where appropriate.

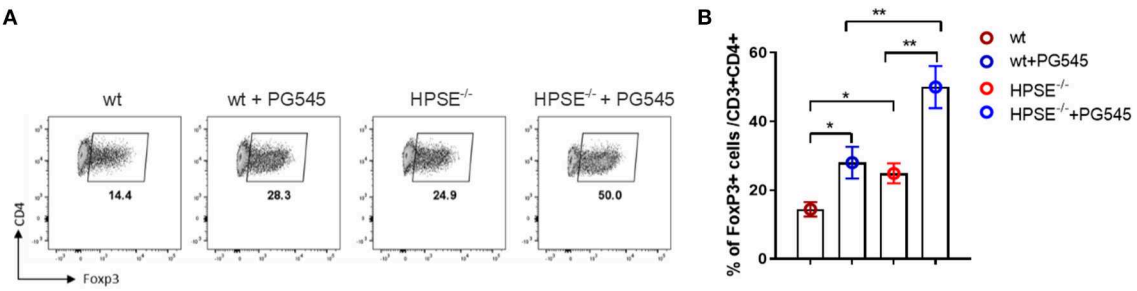

FIGURE 3 | PG545 acts on Treg in heparanase-independent manner. **(A)** Treg differentiation of wild type and HPSE$^{-/-}$ CD4 T cells in the presence of PG545. **(B)** Bar diagrams showing the frequencies of Foxp3+ CD4+ cells. Data are representative of three independent experiments. Mean ± SD, two-tailed unpaired *t*-test. $^{*}p < 0.05$, $^{**}p < 0.01$.

PG545 Inhibits Th17 and Promotes Treg Cells *in vivo*

We next sought to evaluate the functional impact of PG545 in a model of Th1/Th17-dependent inflammation. One such model is the methylated bovine serum albumin (mBSA) induced delayed type hypersensitivity (DTH) model (34). Here, the sensitization phase is initiated by immunization with mBSA, which is delivered subcutaneously as an emulsion with complete Freund's adjuvant (CFA). The elicitation phase of the reaction is then triggered by a second injection of mBSA into the hind paws. Footpad inflammation is then measured 24 h later. To test the impact of PG545 in this system, mice were treated with PG545 via a series of i.p. injections. A schematic of this protocol is shown in **Figure 5A**.

We observed that mice treated with PG545 showed a dramatically blunted hypersensitivity response (**Figures 5B,C**). Of note, there was no difference in footpad swelling between mice that received a single injection of PG545 1 day post-sensitization vs. those that received an additional injection on the day of challenge (elicitation phase) (**Figure 5C**).

To assess the effect of PG545 on priming vs. recall response, we treated DTH-immunized mice with PG545 at different time points. For this analysis, we also included HPSE$^{-/-}$ mice, previously used in the iTreg induction experiment (**Figure 3A**). Remarkably, irrespective of the treatment protocol, PG545 potently suppressed footpad swelling in all the experimental groups (**Supplemental Figure 2A**). While HPSE$^{-/-}$ mice mounted a normal DTH response, a single PG545 administration at day−6 fully prevented the swelling. Together these data demonstrate that PG545 has potent therapeutic effects in this model, irrespective of the administration.

We also assessed the impact of PG545 on the immune profile of these animals in this model. PG545 treated mice had a decrease in the draining LN cellularity (**Figure 5D**). This was accompanied with the decreased numbers of CD154+ CD4+ antigen-specific memory cells in the PG545-treated mice (**Figures 5E,F**). PG545 did not affect the systemic frequencies of Foxp3+ Tregs in this model (**Figure 5G**), but increased the proliferation of Tregs (**Figure 5H**).

Finally, we assessed the impact of PG545 on T cell polarization in this model. The fraction of IL-17 producing CD154+ T cells was dramatically diminished (**Figures 5F,I**). This also correlated with the cytokine staining obtained with the memory cell from the draining lymph node (**Figure 1E**). Likewise, memory cells from the mice treated at different times points all had impaired IL-17 production (**Supplemental Figure 2B**).

Since PG545 exhibits a strong inhibition of Th17 lineage, we wondered if this was the case for another Th17-mediated autoimmune model experimental autoimmune encephalomyelitis (EAE). Surprisingly, PG545 administration was not able to make mice resistant to EAE, although it did significantly delay its onset (**Figure 5J**). Interestingly, analysis of the spinal cord infiltrate revealed decreased frequencies of Th17 cells in mice treated with PG545, whereas Tregs remained unchanged (**Figure 5K**; **Supplemental Figure 2C**). This supports our observation in DTH model with respect to Th17 inhibition, but not the overall immune suppression.

Together these data indicate that PG545 is a potent inhibitor of DTH responses in mice and that PG545 may act in part by suppressing memory Th17 differentiation and priming.

PG545 Inhibits LPS Mediated Dendritic Cell Maturation

Considering the very potent anti-inflammatory effect of PG545 irrespective of the administration regimen, we wondered if PG545 could have an effect on the antigen presenting cells. For this, we administered PG545 into naïve mice and assessed their dendritic cell compartment 7 days later. After *in vivo* PG545 administration to naïve mice we observed lower relative DC frequencies in the spleen, probably due to splenomegaly (**Figures 6A,B**), but slightly higher frequencies in the lymph node relative to B220^{lo} CD3- cells. In contrast, DC frequencies relative to total live cells in both the spleen and lymphatic tissue were unchanged (**Figures 6A–C**). Next, we sought to analyze the DC response to LPS in the presence of PG545. For this, we generated bone marrow-derived dendritic cells and assessed their phenotype and functionality *in vitro* in the context of PG545. Strikingly, while the treatment with PG545 alone did not have a major effect of BMDC phenotype, PG545 greatly

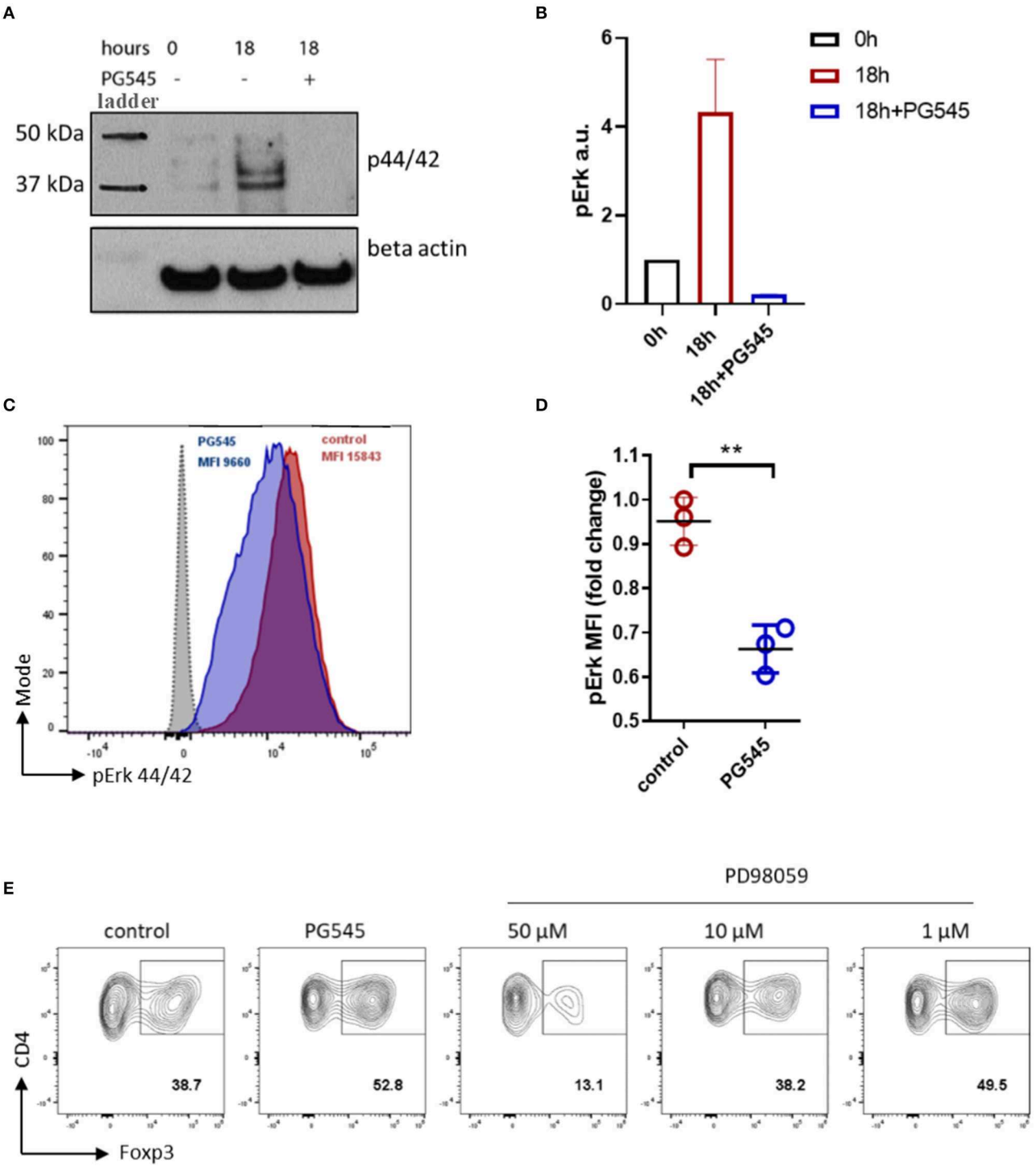

FIGURE 4 | PG545 inhibits Erk signaling in lymphoid cell line and primary CD4 cells. **(A)** Immunoblot of pErk1/2 in 6 h serum starved CTLL2 cells. Time = 0 h indicate pErk in serum starved cells before adding the medium. 18 h = 18 h of incubation in CTLL2 medium ±PG545. **(B)** Densitometry of pErk signal against beta actin. **(C)** Phospho-flow analysis for pErk44/42 of primary CD3/CD28 activated mouse CD4 cells in the presence of PG545 for 72 h. **(D)** MFI quantification of pErk1/2 expression. Data are representative of experiments that were each performed at least three times. The fold change was normalized to 1. **(E)** iTreg differentiation in the presence of the selective inhibitor of MAPKK PD98059. Shown is the representative FACS plots, gate is on live CD3+ CD4+ lymphocytes. Data represent mean ± SD; $*p < 0.05$, $**p < 0.01$ vs. respective control by unpaired *t*-test.

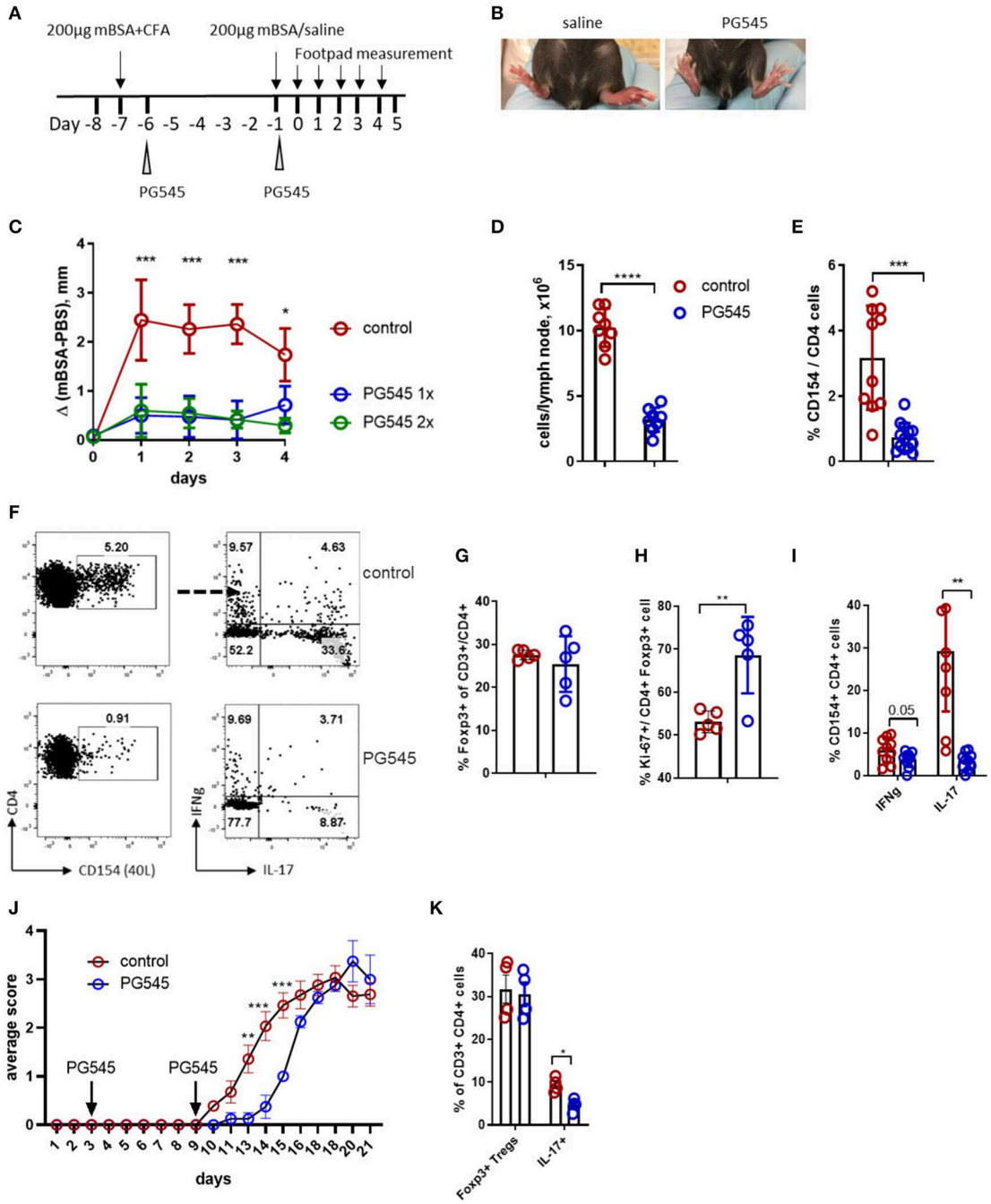

FIGURE 5 | PG545 inhibits DTH response through decreasing Th17 potential. **(A)** Schematics of the DTH experiment. **(B)** Image of the footpad swelling in control and PG545-treated mice. **(C)** Footpad swelling shown as the difference between the control (saline) and mBSA footpad of each individual mouse. **(D)** Draining lymph node cellularity from mice in the DTH experiment. **(E)** Frequencies of the CD154+ cells after re-stimulation with mBSA in the presence of Brefeldin A for 6 h. **(F)** Representative flow cytometry for the T cell analysis from the popliteal (draining) LN of DTH mice. **(G)** Frequencies of Tregs in the draining LN. **(H)** *Ex vivo* proliferation of Tregs in the draining lymph node of mice. **(I)** Cytokine profile of CD154+ (antigen-specific) CD4 T cells from DTH experiments. **(J)** Clinical score of EAE in mice treated with PG545 and control mice. $n = 11$ for control, $n = 5$ for PG545. Statistical significance was assessed using mixed-effect analysis with multiple comparisons. **(K)** Frequencies of Tregs and Th17 cells in the spinal cord infiltrates of EAE animals. Bar diagram represent two independent experiments. Experiments A–I are representative experiments that were each performed at least three times. Data shown are for mean ± SD using a two-tailed unpaired *t*-test. $^{*}p < 0.05$, $^{**}p < 0.01$, $^{***}p < 0.001$, $^{****}p < 0.0001$.

diminished their LPS response as demonstrated by the decrease of maturation markers (**Figure 6D**). This is in contrast to the activation effect of PG545 on CpG treated BMDCs which was previously reported by Brennan et al. (23). Interestingly, we also observed a synergistic effect of PG545 and CpG toward DC maturation (data not shown).

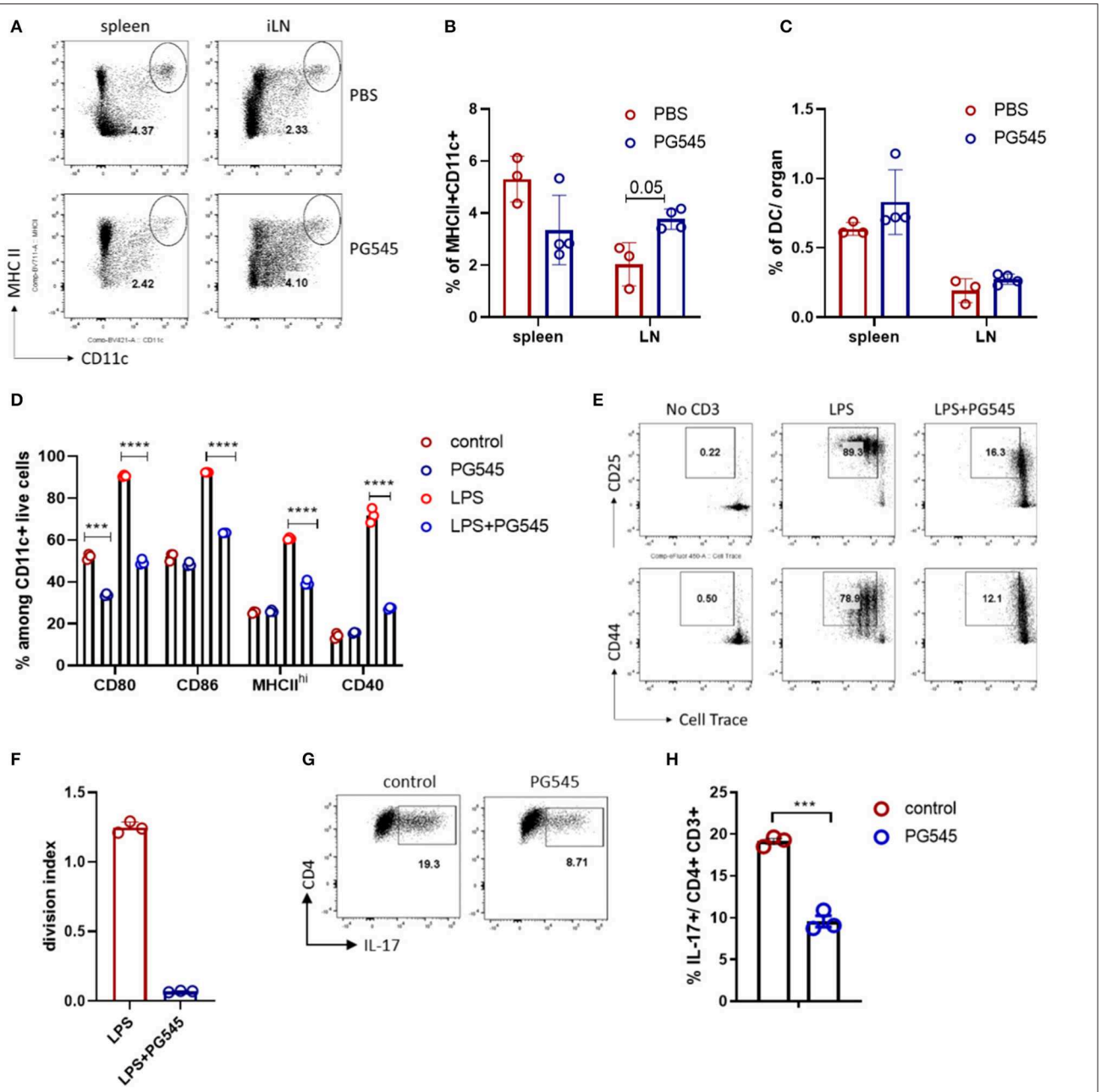

FIGURE 6 | PG545 inhibits LPS response of dendritic cells (DC). **(A)** FACS plot depicting dendritic cell staining in PBS and PG545 treated mice. The gate is Zombie Aqua- CD3-B220^{lo} lymphocytes. **(B,C)** Bar diagrams with relative and total DC frequencies. **(D)** Bar diagram depicting maturation/activation markers on BMDC after LPS/PG545 stimulation for 24 h. Representative of three independent experiments. **(E,F)** Activation markers expression and proliferation of CD4 T cells after co-culture with BMDC from **(D)** for 3 days. Shown is one out of two experiments. **(G,H)** Th17 differentiation in the presence of BMDC. Data are expressed as mean ± SD. **(B–D)** were analyzed using two-way ANOVA with Turkeys's multiple comparisons; **(F,H)**- two-tailed unpaired *t*-test. $^{*}p < 0.05$, $^{**}p < 0.01$, $^{***}p < 0.001$, $^{****}p < 0.0001$.

In addition, while control BMDC potently activated T cells and promoted their proliferation in a polyclonal manner, PG545-treated BMDC failed to do so (**Figures 6E,F**). Since the inhibition of BMDC could contribute to the reduced polarization toward Th17 phenotypes observed in our *in vivo* models, we also assessed the Th17 polarization in the presence of BMDC. We find that the fraction of Th17 cells after *in vitro* activation was reduced in the setting of PG545 (**Figures 6G,H**).

PI-88 and PG562 Favor Treg Induction *in vitro* but Do Not Suppress DTH

We also tested the effect of PI-88 and PG562 on Treg induction and T-cell mediated response. Both PI-88 and PG562 promoted Treg induction *in vitro* (**Figures 7A–D**) although less potently than PG545. This was true whether the Tregs were induced in the presence of anti-CD3/CD28 with TGFb (**Figures 7A,B**) or BMDCs with soluble anti-CD3 and TGFb (**Figures 7C,D**).

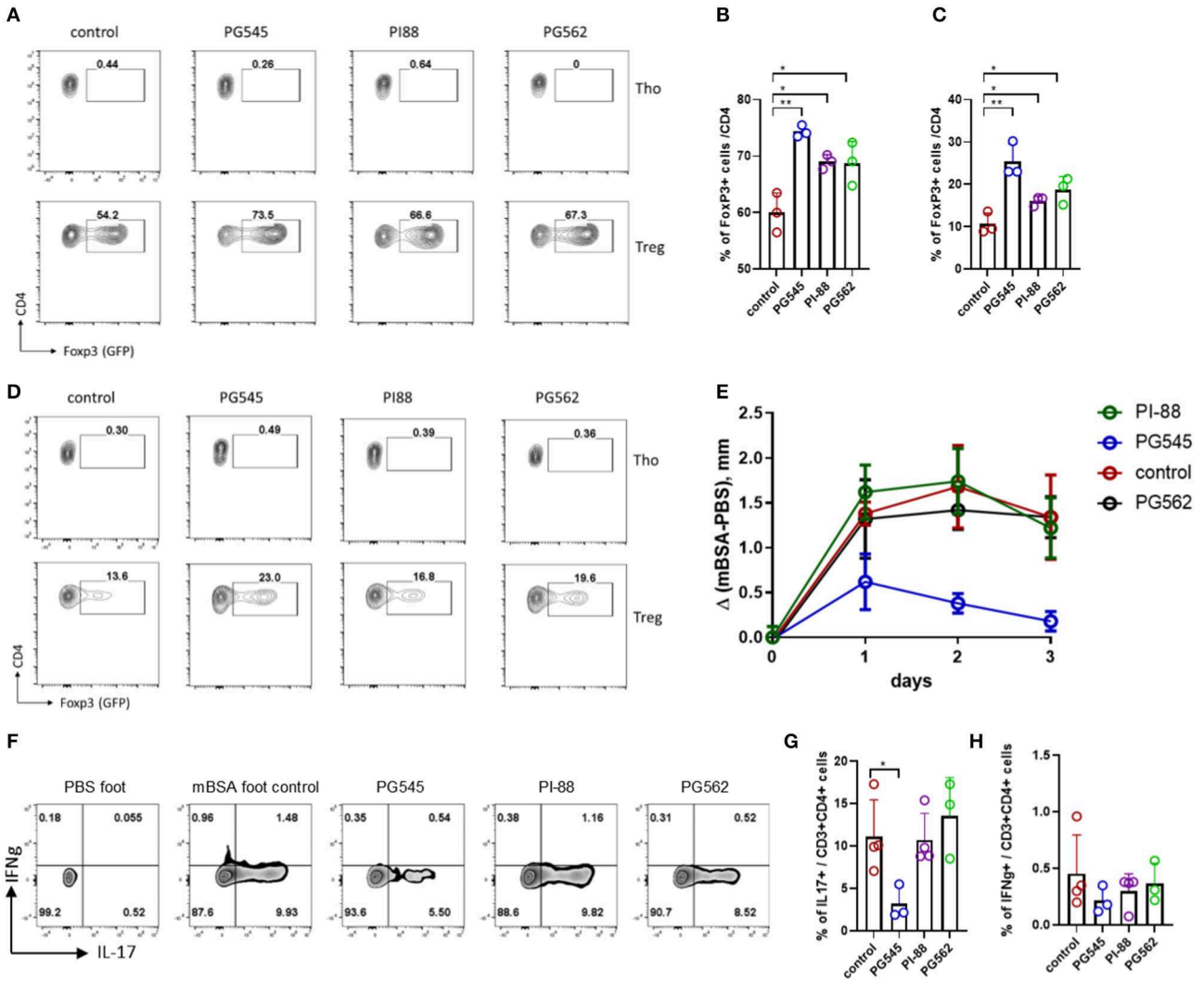

FIGURE 7 | PI-88 and PG562 promote Treg induction but do not affect DTH response. **(A)** Treg induction assay in the presence of HS mimetics (all at 20 μg/ml) from mouse naïve CD4+ cells upon CD3/28 activation and TGFβ. **(B)** Aggregate bar diagram depicting Foxp3+ cell frequencies. **(C,D)** Aggregate bar diagram and FACS plot of Treg induction as in **(A)** from naïve CD4 cells co-cultured with mouse bone marrow derived dendritic cells (BMDC) in the presence of soluble aCD3 and TGFβ. **(E)** Footpad swelling depicted as the difference between the control (saline) and mBSA footpad of each mouse treated with HS mimetics (two injections, 400 μg/mouse). Mean ± SD, one-way ANOVA with Turkey *post-hoc* test. **(F)** Cytokine staining of the PMA/Ionomycin stimulated lymphocytes from the draining LN of DTH mice. Shown is the CD3+ CD4+ live dye+. Day 4 after mBSA challenge. **(G,H)** Summarized IL-17 and IFNg staining of the DTH mice. $^{*}p < 0.05$, $^{**}p < 0.01$, $^{***}p < 0.001$.

However, only PG545 was able to prevent footpad inflammation in a DTH model when all three components were tested side by side (**Figure 7E**). In agreement with the previous experiments, PG545 administration effectively suppressed the recall Th17 response in the draining LN of the animals, but neither PI-88 nor PG562 affected Th17 cells (**Figures 7F,G**). Of note, IFNg+ cells were not changed (**Figure 7H**).

Together these data indicate that while all three heparinase inhibitors tested promote Treg induction *in vitro*, PG545 is unique in its ability to inhibit Th17-mediate DTH responses in mice.

DISCUSSION

Here we report that the HS mimetic PG545 affects T cell differentiation and function. In particular, PG545 selectively promotes the induction of anti-inflammatory Tregs while inhibiting the development of Th17 both *in vitro* and *in vivo*. Consistent with these effects, PG545 inhibits Erk1/2 signaling, a pathway known to inhibit Foxp3+ Treg induction and promote Th1 and Th17 polarization (40–42).

These data expand on our understanding of PG545 beyond its impact on tumor models, where it decreased angiogenesis and metastasis and improved survival (43–46). More recently,

several groups have shown a beneficial effect of PG545 treatment in atherosclerosis (47) and acute kidney injury (22). These effects were attributed to the reduction of pro-inflammatory markers, though neither increased Foxp3+ Treg nor reduced Th17 numbers were implicated.

Moreover, it appears that PG545 has both heparinase dependent and independent effects. Previously, the anti-angiogeneic effects of PG545, for example, were attributed to inhibition of heparinase and heparan sulfate-binding angiogenic growth factors (17). However, our data indicate that PG545 promotes the expansion of Foxp3+ Treg independently of heparanase. Consistent with this, PG545 was recently reported to have apoptotic effects on lymphoma cell lines that lack heparanase expression (2).

One question that this study raises is how an anti-inflammatory effect of PG545 observed here reconciles with its anti-tumor activity shown in other studies. Since cytotoxic T cells are the main effector T cells involved in cancer immunotherapy, it may be that these are less sensitive to the effect of PG545 treatment than tumor cells (48). It may also be that the effects of PG545 are context dependent. A recent study has shown that MEK inhibition can reactivate tumor-infiltrating CD8 lymphocytes by preventing their exhaustion (48). Finally, it may also be that the impact of PG545 on Erk signaling or other pathways in those models may trump effects on lymphocytes.

It is tempting to consider that both the anti-tumor and anti-inflammatory properties of PG545 may be attributable in part to inhibition of Erk1/2 signaling. However, PG545 has effects that are difficult to entirely attribute to Erk1/2 inhibition. For example, PG545 is reported to decrease glucose uptake, downregulate glycolytic machinery, inhibit Wnt signaling, and induces autophagy in cancer cell lines (2, 43, 44). Moreover, while Erk1/2 signaling inhibits Th17 polarization in some settings, it promotes Th17 in others, suggesting that both the regulation of these signaling cascades and their inhibition is likely to be complex (40, 49–51). Finally, we demonstrate effects similar to Erk signaling on Foxp3+ Treg but do not conclusively demonstrate that these are Erk-mediated. In the aggregate, our interpretation of the data is that it suggests that PG545 may acts via multiple mechanisms of which Erk1/2 inhibition is a part.

A report from Brennan et al. (23) suggested an activation effect of PG545 on dendritic cells. However, while Brennan et al. activated BMDC with the CpG mimic we used LPS stimulation, indicating the context-dependent properties of the HS mimetic.

Overall, we show that PG545 promotes regulatory T cells *in vitro*. This effect is accompanied with the inhibition of Th17 cells and to some extent Th1 cells. PG545 acts on T cells in heparanase-independent manner and impairs Erk signaling in proliferating cells without affecting an early activation program. PG545 administration effectively suppressed DTH in mice. These findings may inform the adaptation of PG545 for clinical applications including in inflammatory pathologies associated with DTH.

DATA AVAILABILITY STATEMENT

All datasets generated for this study are included in the article/**Supplementary Material**.

ETHICS STATEMENT

All experiments were approved by the Stanford IACUC.

AUTHOR CONTRIBUTIONS

IK and HK designed and performed the experiments. CM edited the manuscript and performed some experiments with SZ and JV. DL helped with BMDC experiments. IK and PB conceptualized the study and wrote the manuscript.

FUNDING

This work was supported by grants R21AI133240, R01AI12492093 to PB. CM was supported by the Stanford Molecular and Cellular Immunobiology Training Grant (5 T32 AI07920, PI Olivia Martinez), the National Academies of Sciences, Engineering and Medicine Ford Foundation Pre-Doctoral Fellowship and the Stanford Diversifying Academia, Recruiting Excellence Fellowship.

ACKNOWLEDGMENTS

We would like to thank K. Dredge (Paragen Bio) and E. Hammond (Zucero Therapeutics) for providing HS mimetics and discussing the data, Peggy Ho (Steinman lab, Stanford University) for help with the CFA emulsification. We thank Stanford Shared FACS facility for their assistance.

SUPPLEMENTARY MATERIAL

The Supplementary Material for this article can be found online at: https://www.frontiersin.org/articles/10.3389/fimmu.2020.00132/full#supplementary-material

Supplemental Figure 1 | (A) Histograms of T-bet and RORgt expression in CD4 T cells at Th1 and Th17 condition, respectively. **(B)** Spleen enlargement in mice after PG545 treatment. **(C)** Mouse body weight after PG545 treatment. **(D)** Spleen cellularity in mice on PG545. **(E)** Treg suppression assay with mouse iTregs induced in the presence of PG545. Representative CFSE dilution of effector CD4 T cells after co-culture with control iTregs, PG545 iTregs or alone. **(F)** Foxp3+ Tregs frequencies among the transferred OT-II cells followed by immunization with OVA/alum. **(G)** iTreg induction in the presence of MAPK kinase inhibitor. Data shown are for mean ± SD using a two-tailed unpaired *t*-test. $^{**}p < 0.01$, $^{***}p < 0.001$.

Supplemental Figure 2 | (A) Footpad swelling of DTH mice treated with different regimen of PG545. Data are from one experiment with 4–5 mice per group. **(B)** FACS profile of the CD4 T cell cytokine staining from DTH mice with various PG545 treatment. **(C)** Representative bar diagram with Foxp3+ and IL-17+ cell frequencies among spinal cord CD3+CD4+ T cells in EAE mice. Data shown are for mean ± SD using a two-tailed unpaired *t*-test or two-way ANOVA test. $^{*}p < 0.05$, $^{**}p < 0.01$.

REFERENCES

1. Hammond E, Haynes NM, Cullinane C, Brennan TV, Bampton D, Handley P, et al. Immunomodulatory activities of pixatimod: emerging nonclinical and clinical data, and its potential utility in combination with PD-1 inhibitors. *J Immunother Cancer*. (2018) 6:54. doi: 10.1186/s40425-018-0363-5
2. Weissmann M, Bhattacharya U, Feld S, Hammond E, Ilan N, Vlodavsky I. The heparanase inhibitor PG545 is a potent anti-lymphoma drug: Mode of action. *Matrix Biol.* (2018) 77:58-72. doi: 10.1016/j.matbio.2018.08.005
3. Dredge K, Brennan TV, Hammond E, Lickliter JD, Lin L, Bampton D, et al. A Phase I study of the novel immunomodulatory agent PG545 (pixatimod) in subjects with advanced solid tumours. *Br J Cancer*. (2018) 118:1035–41. doi: 10.1038/s41416-018-0006-0
4. Heyman B, Yang, Y. Mechanisms of heparanase inhibitors in cancer therapy. *Exp Hematol.* (2016) 44:1002–12. doi: 10.1016/j.exphem.2016.08.006
5. Vlodavsky I, Ilan N, Naggi A, Casu B. Heparanase: structure, biological functions, and inhibition by heparin-derived mimetics of heparan sulfate. *Curr. Pharm. Des.* (2007) 13:2057–73. doi: 10.2174/138161207781039742
6. Parish CR, Freeman C, Hulett MD. Heparanase: a key enzyme involved in cell invasion. *Biochim Biophys Acta Rev Cancer*. (2001) 1471:M99–108. doi: 10.1016/S0304-419X(01)00017-8
7. Dempsey LA, Brunn GJ, Platt JL. Heparanase, a potential regulator of cell–matrix interactions. *Trends Biochem Sci.* (2000) 25:349–51. doi: 10.1016/S0968-0004(00)01619-4
8. Roy M, Marchetti D. Cell surface heparan sulfate released by heparanase promotes melanoma cell migration and angiogenesis. *J Cell Biochem.* (2009) 106:200–9. doi: 10.1002/jcb.22005
9. Vlodavsky I, Blich M, Li JP, Sanderson RD, Ilan N. Involvement of heparanase in atherosclerosis and other vessel wall pathologies. *Matrix Biol.* (2013) 32:241–51. doi: 10.1016/j.matbio.2013.03.002
10. Parish CR, Freeman C, Ziolkowski AF, He YQ, Sutcliffe EL, Zafar A, et al. Unexpected new roles for heparanase in Type 1 diabetes and immune gene regulation. *Matrix Biol.* (2013) 32:228–33. doi: 10.1016/j.matbio.2013.02.007
11. Putz EM, Mayfosh AJ, Kos K, Barkauskas DS, Nakamura K, Town L, et al. NK cell heparanase controls tumor invasion and immune surveillance. *J Clin Invest.* (2017) 127:2777–88. doi: 10.1172/JCI92958
12. Digre A, Singh K, Åbrink M, Reijmers RM, Sandler S, Vlodavsky I, et al. Overexpression of heparanase enhances T lymphocyte activities and intensifies the inflammatory response in a model of murine rheumatoid arthritis. *Sci. Rep.* (2017) 7:46229. doi: 10.1038/srep46229
13. Hermano E, Meirovitz A, Meir K, Nussbaum G, Appelbaum L, Peretz T, et al. Macrophage polarization in pancreatic carcinoma: role of heparanase enzyme. *JNCI J Natl Cancer Inst.* (2014) 106:dju332. doi: 10.1093/jnci/dju332
14. Caruana I, Savoldo B, Hoyos V, Weber G, Liu H, Kim ES, et al. Heparanase promotes tumor infiltration and antitumor activity of CAR-redirected T-lymphocytes. *Nat Med.* (2015) 21:524. doi: 10.1038/nm.3833
15. Mohamed S, Coombe DR. Heparin mimetics: their therapeutic potential. *Pharmaceuticals*. (2017) 10:78. doi: 10.3390/ph10040078
16. Imported from https://oncologypro.esmo.org/Meeting-Resources/ESMO-2017-Congress/Low-grade-glioma-patients-with-IDH-mutation-and-1p19q-codeletion-what-to-do-after-surgery
17. Ferro V, Liu L, Johnstone KD, Wimmer N, Karoli T, Handley P, et al. Discovery of PG545: a highly potent and simultaneous inhibitor of angiogenesis, tumor growth, and metastasis. *J Med Chem.* (2012) 55:3804–13. doi: 10.1021/jm201708h
18. Hammond E, Brandt R, Dredge, K. PG545, a heparan sulfate mimetic, reduces heparanase expression *in vivo*, blocks spontaneous metastases and enhances overall survival in the 4T1 breast carcinoma model. *PLoS ONE*. (2012) 7:e52175. doi: 10.1371/journal.pone.0052175
19. Hammond E, Handley P, Dredge K, Bytheway I. Mechanisms of heparanase inhibition by the heparan sulfate mimetic PG545 and three structural analogues. *FEBS Open Bio.* (2013) 3:346–51. doi: 10.1016/j.fob.2013.07.007
20. Barash U, Lapidot M, Zohar Y, Loomis C, Moreira A, Feld S, et al. Involvement of heparanase in the pathogenesis of mesothelioma: basic aspects and clinical applications. *JNCI J Natl Cancer Inst.* (2018) 110:1102–14. doi: 10.1093/jnci/djy032
21. Lapidot M, Barash U, Vlodavsky I, Pass H. Heparanase inhibitors restrain mesothelioma. *Oncotarget*. (2018) 9:36830–2. doi: 10.18632/oncotarget.26243
22. Abassi Z, Hamoud S, Hassan A, Khamaysi I, Nativ O, Heyman SN, et al. Involvement of heparanase in the pathogenesis of acute kidney injury: nephroprotective effect of PG545. *Oncotarget*. (2017) 8:34191–204. doi: 10.18632/oncotarget.16573
23. Brennan TV, Lin L, Brandstadter JD, Rendell VR, Dredge K, Huang X, et al. Heparan sulfate mimetic PG545-mediated antilymphoma effects require TLR9-dependent NK cell activation. *J Clin Invest.* (2016) 126:207–19. doi: 10.1172/JCI76566
24. Zhu J, Paul WE. CD4 T cells: fates, functions, and faults. *Blood*. (2008) 112:1557–69. doi: 10.1182/blood-2008-05-078154
25. Hori S, Nomura T, Sakaguchi S. Control of regulatory T cell development by the transcription factor Foxp3. *J Immunol.* (2017) 198:981–5. doi: 10.1126/science.1079490
26. Zcharia E, Jia J, Zhang X, Baraz L, Lindahl U, Peretz T, et al. Newly generated heparanase knock-out mice unravel co-regulation of heparanase and matrix metalloproteinases. *PLoS ONE*. (2009) 4:e5181. doi: 10.1371/journal.pone.0005181
27. Fontenot JD, Rasmussen JP, Williams LM, Dooley JL, Farr AG, Rudensky AY. Regulatory T cell lineage specification by the forkhead transcription factor Foxp3. *Immunity*. (2005) 22:329–41. doi: 10.1016/j.immuni.2005.01.016
28. Sweere JM, Van Belleghem JD, Ishak H, Bach MS, Popescu M, Sunkari V, et al. Bacteriophage trigger antiviral immunity and prevent clearance of bacterial infection. *Science*. (2019) 363:eaat9691. doi: 10.1126/science.aat9691
29. Ruppert SM, Falk BA, Long SA, Bollyky PL. Regulatory T cells resist cyclosporine-induced cell death via CD44-mediated signaling pathways. *Int J Cell Biol.* (2015) 2015:1–10. doi: 10.1155/2015/614297
30. Bollyky PL, Falk BA, Long SA, Preisinger A, Braun KR, Wu RP, et al. CD44 costimulation promotes FoxP3+ regulatory T cell persistence and function via production of IL-2, IL-10, and TGF-. *J Immunol.* (2009) 183:2232–41. doi: 10.4049/jimmunol.0900191
31. Koliesnik IO, Andreas N, Romanov VS, Sreekantapuram S, Krljanac B, Haenold R, et al. RelB regulates Th17 differentiation in a cell-intrinsic manner. *Immunobiology*. (2017) 223:191–9. doi: 10.1016/j.imbio.2017.10.026
32. Bollyky PL, Falk BA, Wu RP, Buckner JH, Wight TN, Nepom GT. Intact extracellular matrix and the maintenance of immune tolerance: high molecular weight hyaluronan promotes persistence of induced CD4+CD25+ regulatory T cells. *J Leukoc Biol.* (2009) 86:567–72. doi: 10.1189/jlb.0109001
33. Bollyky PL, Lord JD, Masewicz SA, Evanko SP, Buckner JH, Wight TN, et al. Cutting edge: high molecular weight hyaluronan promotes the suppressive effects of CD4+CD25+ regulatory T cells. *J Immunol.* (2007) 179:744–7. doi: 10.4049/jimmunol.179.2.744
34. Sido JM. Methylated bovine serum albumin (mBSA)-induced delayed-type hypersensitivity in mice. *Methods Mol Biol.* (2018) 1803:95–9. doi: 10.1007/978-1-4939-8549-4_7
35. Kuipers HF, Rieck M, Gurevich I, Nagy N, Butte MJ, Negrin RS, et al. Hyaluronan synthesis is necessary for autoreactive T-cell trafficking, activation, and Th1 polarization. *Proc Natl Acad Sci USA*. (2016) 113:1339–44. doi: 10.1073/pnas.1525086113
36. Firan M, Dhillon S, Estess P, Siegelman MH. Suppressor activity and potency among regulatory T cells is discriminated by functionally active CD44. *Blood*. (2006) 107:619–27. doi: 10.1182/blood-2005-06-2277
37. Liu T, Soong L, Liu G, König R, Chopra AK. CD44 expression positively correlates with Foxp3 expression and suppressive function of CD4+ Treg cells. *Biol Direct*. (2009) 4:40. doi: 10.1186/1745-6150-4-40
38. Walker MR, Carson BD, Nepom GT, Ziegler SF, Buckner JH. *De novo* generation of antigen-specific CD4+CD25+ regulatory T cells from human CD4+CD25- cells. *Proc Natl Acad Sci USA*. (2005) 102:4103–8. doi: 10.1073/pnas.0407691102
39. Walker MR, Kasprowicz DJ, Gersuk VH, Benard A, Van Landeghen M, Buckner JH, et al. Induction of FoxP3 and acquisition of T regulatory activity by stimulated human CD4+CD25- T cells. *J Clin Invest.* (2003) 112:1437–43. doi: 10.1172/JCI19441
40. Liu H, Yao S, Dann SM, Qin H, Elson CO, Cong Y. ERK differentially regulates Th17- and Treg-cell development and contributes to the pathogenesis of colitis. *Eur J Immunol.* (2013) 43:1716–26. doi: 10.1002/eji.201242889

41. Luo X, Zhang Q, Liu V, Xia Z, Pothoven KL, Lee C. Cutting edge: TGF-beta-induced expression of Foxp3 in T cells is mediated through inactivation of ERK. *J Immunol.* (2008) 180:2757–61. doi: 10.4049/jimmunol.180.5.2757
42. Nagy N, Kaber G, Johnson PY, Gebe JA, Preisinger A, Falk BA, et al. Inhibition of hyaluronan synthesis restores immune tolerance during autoimmune insulitis. *J Clin Invest.* (2015) 125:3928–40. doi: 10.1172/JCI79271
43. Jung DB, Yun M, Kim EO, Kim J, Kim B, Jung JH, et al. The heparan sulfate mimetic PG545 interferes with Wnt/β-catenin signaling and significantly suppresses pancreatic tumorigenesis alone and in combination with gemcitabine. *Oncotarget.* (2015) 6:4992–5004. doi: 10.18632/oncotarget.3214
44. Mondal S, Roy D, Camacho-Pereira J, Khurana A, Chini E, Yang L, et al. HSulf-1 deficiency dictates a metabolic reprograming of glycolysis and TCA cycle in ovarian cancer. *Oncotarget.* (2015) 6:33705–19. doi: 10.18632/oncotarget.5605
45. Winterhoff B, Freyer L, Hammond E, Giri S, Mondal S, Roy D, et al. PG545 enhances anti-cancer activity of chemotherapy in ovarian models and increases surrogate biomarkers such as VEGF in preclinical and clinical plasma samples. *Eur J Cancer.* (2015) 51:879–92. doi: 10.1016/j.ejca.2015.02.007
46. Singh P, Blatt A, Feld S, Zohar Y, Saadi E, Barki-Harrington L, et al. The heparanase inhibitor PG545 attenuates colon cancer initiation and growth, associating with increased p21 expression. *Neoplasia.* (2017) 19:175–84. doi: 10.1016/j.neo.2016.12.001
47. Muhammad RS, Abu-Saleh N, Kinaneh S, Agbaria M, Sabo E, Grajeda-Iglesias C, et al. Heparanase inhibition attenuates atherosclerosis progression and liver steatosis in E0 mice. *Atherosclerosis.* (2018) 276:155–62. doi: 10.1016/j.atherosclerosis.2018.07.026
48. Klebanoff CA, Gattinoni L, Restifo NP. CD8+ T-cell memory in tumor immunology and immunotherapy. *Immunol Rev.* (2006) 211:214–24. doi: 10.1111/j.0105-2896.2006.00391.x
49. Huang X, Yu P, Liu M, Deng Y, Dong Y, Liu Q, et al. ERK inhibitor JSI287 alleviates imiquimod-induced mice skin lesions by ERK/IL-17 signaling pathway. *Int Immunopharmacol.* (2019) 66:236–41. doi: 10.1016/j.intimp.2018.11.031
50. Tan AH, Lam KP. Pharmacologic inhibition of MEK-ERK signaling enhances Th17 differentiation. *J Immunol.* (2010) 184:1849–57. doi: 10.4049/jimmunol.0901509
51. Chang CF, D'Souza WN, Ch'en IL, Pages G, Pouyssegur J, Hedrick SM. Polar opposites: Erk direction of CD4 T cell subsets. *J Immunol.* (2012) 189:721–31. doi: 10.4049/jimmunol.1103015

Conflict of Interest: The authors declare that the research was conducted in the absence of any commercial or financial relationships that could be construed as a potential conflict of interest.

frontiers in Immunology

MINI REVIEW
published: 18 February 2020
doi: 10.3389/fimmu.2020.00227

Syndecans in Inflammation at a Glance

*Sandeep Gopal**

Development and Stem Cells Program, Department of Anatomy and Developmental Biology, Monash Biomedicine Discovery Institute, Monash University, Melbourne, VIC, Australia

Syndecans are transmembrane proteoglycans with heparan and chondroitin sulfate chains attached to their extracellular domain. Like many proteoglycans, they interact with a large number of ligands, such as growth factors, adhesion receptors, soluble small molecules, proteinases, and other extracellular matrix proteins to initiate downstream signaling pathways. Syndecans play a major role in inflammation, mainly by regulating leukocyte extravasation and cytokine function. At the same time, syndecans can undergo cytokine mediated changes in their expression levels during inflammation. The function of syndecans during inflammation appears to depend on the stage of inflammation, sulfation of heparan/chondroitin sulfate chains, the rate of ectodomain shedding and the solubility of the ectodomains. From the current literature, it is clear that syndecans are not only involved in the initial recruitment of pro-inflammatory molecules but also in establishing a balanced progression of inflammation. This review will summarize how cell surface and soluble syndecans regulate multiple aspects of inflammation.

Keywords: syndecan, proteoglycan, extravasation, inflammation, shedding, cytokines, chemokine gradient

OPEN ACCESS

Edited by:
Rogier M. Reijmers, Leiden University Medical Center, Netherlands

Reviewed by:
Ida Gjervold Lunde, Oslo University Hospital, Norway
Martin Götte, University of Münster, Germany

***Correspondence:**
Sandeep Gopal
sandeep.gopal@monash.edu

Specialty section:
This article was submitted to Inflammation, a section of the journal Frontiers in Immunology

Received: *29 November 2019*
Accepted: *28 January 2020*
Published: *18 February 2020*

Citation:
Gopal S (2020) Syndecans in Inflammation at a Glance. Front. Immunol. 11:227. doi: 10.3389/fimmu.2020.00227

INTRODUCTION

Inflammation is the immediate response of the body to combat an infection or injury. It is a cascade of complex immunological events resulting from the disruption of tissue homeostasis, which acts to remove the source of infection or restore damaged tissue. When left unchecked, inflammation will result in further tissue damage and injury (1). Inflammation can either be acute or chronic. Acute inflammation (e.g., wounding) is a controlled short-term process that results in the healing of the damaged tissue or the removal of infection, whereas chronic inflammation (e.g., cancers) is a persistent response that leads to further tissue damage. Chronic inflammation often does not present visible cardinal signs of inflammation, such as redness (rubor), increased heat (calor), swelling (tumor), pain (dolor), or loss of function (functio laesa) (2). However, it can lead to more serious conditions, such as fibrosis and cancers (3, 4). Inflammation is associated with modifications to the local vasculature and elevated blood flow that permits the recruitment of leukocytes, plasma proteins, and soluble molecules to the site of inflammation (5). Key steps in inflammation involve recognition of the inducers, signal transduction, release of pro-inflammatory molecules, activation of the effectors of inflammation, and resolution of the inflammation (6). The inducers are recognized by a range of receptors, such as toll-like receptors and nucleotide-binding domain and leucine-rich-repeat-containing receptors, leading to the activation and nuclear translocation of the transcription factor NF-κB (7–9). This induces the expression of a number of pro-inflammatory cytokines, such as interleukin-1β (IL-1β), IL-6, IL-8, IL-12, and Tumor Necrosis Factor-α (TNF-α). While several molecules are involved in inflammation, cytokines play a central role as both pro-inflammatory and anti-inflammatory molecules (6). However, the classification

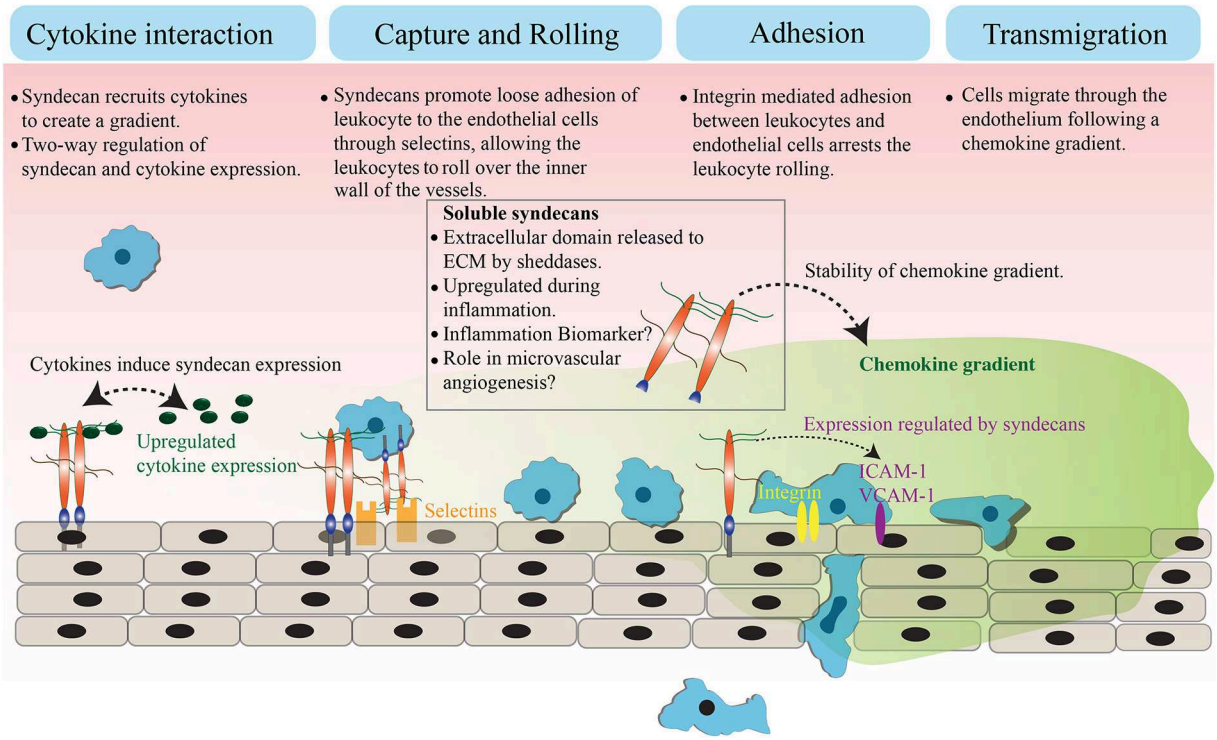

FIGURE 1 | Role of syndecans in extravasation. Syndecans bind to inflammatory cytokines and chemokines through GAG chains. This interaction appears to trigger a feedback signaling, which results in an elevated expression of both syndecan and cytokines. The GAG chain mediated binding of syndecan with chemokine and the subsequent shedding of syndecan-chemokine complex results in a stable chemokine gradient. Syndecans mediate a loose interaction between leukocytes and endothelial cells through selectins, which reduces the pace of leukocyte movement and they bigin to roll over the vessel surface. The adhesion between leukocytes and endothelial cells is strengthened by an integrin controlled signaling and other cell adhesion molecules, leading to the arrest of leukocyte rolling. Attached leukocytes begin transmigration directed by a stable chemokine gradient to the site of inflammation.

of pro-inflammatory and anti-inflammatory is not absolute, as some of the cytokines are known to play both roles (10). In the next stage, effector cells, such as neutrophils and monocytes are recruited to the site of inflammation leading to a process called degranulation (11). Neutrophils expedite the release of reactive oxygen species, reactive nitrogen species, and protein degrading enzymes. This creates a highly toxic environment for pathogens as well as the host tissue, leading to the destruction of both. In the final phase of inflammation, macrophages ensure minimal damage to the host tissue by restricting neutrophil migration while enhancing monocyte recruitment to the site of inflammation (11, 12).

SYNDECANS IN INFLAMMATION

Syndecans are transmembrane proteoglycans that can interact with a large number of ligands including growth factors, adhesion receptors, cytokines, chemokines, proteinases, and other extracellular matrix proteins (13). As a result of these ligand interactions, syndecans initiate a number of biological signaling events relevant to cell adhesion, angiogenesis, inflammation, and tissue repair (14–18). The mammalian genome encodes four syndecans; syndecan−1, −2, −3, and −4. Syndecans not only maintain cell homeostasis under normal conditions but also regulate inflammatory responses during infection and trauma (**Figure 1**). Syndecans are one of the major sources of glycosaminoglycan (GAG) chains on the cell surface. They control a large number of cytokines though GAG chain mediated binding to stimulate inflammatory response (19–21). While syndecan-1 is the most studied syndecan in the context of inflammation, other syndecans are also shown to have roles in inflammatory response in various models. Syndecan-1 and -4 knockout mouse models have provided a great deal of information about the role of syndecans in inflammation, where they appear to be involved in multiple aspects of inflammation from leukocyte recruitment through to the resolution of inflammation (22, 23). One common observation during inflammation is that the total expression of syndecans at protein level can be significantly upregulated (21, 24). For instance, the levels of syndecan-1 and syndecan-4 are elevated during myocardial injury. Similarly, syndecan-2 expression is upregulated in endothelial cells, fibroblasts and intestinal epithelial cells by inflammatory stimuli, such as TNFα or hypoxia (25, 26). It has been previously reported that the level of syndecans in the serum of animals is directly related to the severity of the inflammation (27, 28). Other reports suggest that the loss of syndecans from cells, possibly by shedding, regulates inflammatory responses (28). This review will discuss the role

of cell surface and soluble syndecans in cytokine regulation and leukocyte extravasation with a focus on syndecan−1,−2, and−4, while syndecan-3 is discussed in detail in another review of this issue.

During leukocyte extravasation, the leukocytes move out of circulation and adhere in proximity to the sites of inflammation (6). Syndecans, along with glypicans are the major heparan sulfate proteoglycans (HSPG) that control this process (22, 29, 30). HSPGs loosely bind to L- and/or P-selectins on the inner wall of vessels to slow down the flow of leukocytes (31), leading to leukocyte rolling on the surface of the endothelium. This suggests the involvement of HSPGs as pro-inflammatory molecules, specifically to support leukocyte rolling. However, knockout studies showed an elevated inflammatory response in the absence of syndecan-1 or syndecan-4 in mice, indicating that syndecans are inflammation antagonists instead (22, 28, 32). These observations were explained when an increase in leukocyte adhesion and transendothelial migration with prolonged edema formation was identified in syndecan-1 knockout mice subjected to a myocardial infarction (33). Another report suggests that syndecan-1 is essential to limit inflammation and apoptosis during lung injury after an influenza infection (34). Similarly, syndecan-1 is required to maintain the motility of macrophages during chronic inflammation in atherosclerosis, where the absence of syndecan-1 resulted in persistent inflammation (35). In addition to that, syndecan-1 knockout mice exhibit increased expression of pro-inflammatory cytokines (TNFα, IL-6, CCL-5, and CCL-3) and adhesion molecules (ICAM-1 or VCAM-1) during oxazolone-induced delayed-type hypersensitivity and dextran sodium sulfate-induced colitis (36, 37). These data support the idea that syndecan-1 is anti-inflammatory. The negative regulation of strong leukocyte adhesion to endothelium by syndecan-1 is proposed to be the reason behind its anti-inflammatory role. In general, strengthening of leukocyte adhesion to the endothelium is the penultimate step of leukocyte extravasation, which is mediated by integrins and adhesion molecules (e.g., ICAM-1, VCAM-1). It has been suggested that syndecan-1 may oppose integrins, likely by competition for ligands to control strong leukocyte adhesion. Therefore, the absence of syndecan-1 may have promoted integrin mediated leukocyte adhesion to the endothelium (38). Taken together, syndecan-1 appears to support the initial regulation of leukocyte movement whereas it negatively regulates the later leukocyte adhesion and migration. Similar observations were made with syndecan-4, where chemotaxis experiments revealed that syndecan-4 mediates anti-thrombin induced inhibition of leukocyte migration in a heparan sulfate chain-dependent manner (39). These observations indicate that syndecans function to create a balanced inflammatory response by controlling distinct aspects of leukocyte extravasation. In some chronic inflammatory diseases, such as asthma, syndecan-4 also control T-helper 2 (Th2) derived immune response. Asthma is characterized by airway inflammation, which is caused by an inappropriate Th2 cell response. The blocking of syndecan-4 in ovalbumin sensitized mice resulted in a reduced inflammation due to the defective migration of antigen presenting dendritic cells. This affects the Th2 derived immune response where dendritic cells failed to deliver signals to Th2 cells (40).

It is well-known that the balancing of pro-inflammatory and anti-inflammatory molecules dictates the final outcome of an inflammatory response. The increase in leukocyte recruitment to the inflammation site is usually supported by an increase in the expression of cytokines and adhesion molecules. It has been reported that HSPGs can promote or inhibit both pro-inflammatory and anti-inflammatory cytokines by direct binding through their GAG chains (41–43). Depending on the model under investigation, different syndecans have shown to bind either pro-inflammatory or anti-inflammatory cytokines. Syndecans facilitate a gradient of a group of small cytokines, known as chemokines, during leukocyte rolling. For example, the binding of chemokines (e.g., IL-8) to syndecan-1 through GAG chains allows the stabilization of the chemokines on the endothelial surface and creates a tethering effect for the chemokine. The later shedding of the chemokine-Syndecan-1 complex leads to a stable chemokine gradient (44, 45). This chemokine gradient appears to be crucial for maintaining the directionality of leukocyte migration (46). Another report showed that syndecan-1 regulates pro-inflammatory cytokine IL-17 during Psoriasiform Dermatitis, where the absence of syndecan-1 resulted in increased skin inflammation (47). Both syndecan-1 and IL-17 are shown to be increased in nasal polyps, a chronic inflammation in the nasal cavity (48). Syndecan-2 expression is elevated in endothelial cells during inflammation, where they can directly bind with cytokines (e.g., CXCL-8) and induce the expression of other cytokines (e.g., IL-1α, IL-17A^{+}) (25, 49). The silencing of syndecan-4 in HUVEC cells resulted in an elevation of pro-inflammatory factors (e.g., CXCL-8), which suggests that a loss of syndecan-4 may result in an aggravated inflammatory response. This appears to agree with syndecan-4 knockout mice studies, where lipopolysaccharide (LPS) induced pulmonary inflammation resulted in increased early neutrophil migration and higher titers of chemokines in bronchoalveolar lavage fluid. In this case, the expression of chemokines was reduced when the bronchial epithelial cells were pre-treated with heparin or syndecan-4 before LPS treatment (50). While syndecans appears to control inflammatory cytokines, the inverse is also possible, with the expression of syndecans being regulated by cytokines. In some cases, the same cytokines even have opposite effects on the expression of different syndecans. For instance, IL-1β and IL-6 treatment downregulated syndecan-1 expression in isolated rat hepatocytes while syndecan-2 expression is upregulated by the same (51). The same study also reported an increase in syndecan-1 expression in response to a TNF-α treatment. Similar observations were made in human periodontal fibroblasts and osteoblasts (52). Growing HUVEC endothelial cells in the presence of inflammatory mediators, such as IL-1β and LPS resulted in a rapid elevation of syndecan-4 expression (53). On the other hand, TNF-α treatment of HT29 cells resulted in the downregulation of syndecan-1 expression (54). These findings clearly indicate a feedback mechanism to control the expression of syndecans during inflammation.

Further investigations are required to provide clarity to the effect of this feedback regulation on inflammation.

As syndecans show both pro- and anti-inflammatory roles in knockout models, one might wonder the reason behind this. For instance, an arthritis model generated by injecting CXCL1 into mice knee showed a decreased disease severity in syndecan-3 null mice compared to wildtype, possibly through a reduced neutrophil accumulation and cartilage degradation in null mice (55). However, the administration of CXCL1 into the skin resulted in increased neutrophil recruitment compared to wildtype animals (55). One explanation for this opposite effect could be, that syndecan-3 is promoting pro-inflammatory cytokines in skin and anti-inflammatory cytokines in the cartilage. Another explanation is that the deletion of syndecan-3 resulted in distinct response from other syndecans in each system under evaluation. This study did not examine the expression changes of other syndecans after syndecan-3 deletion. This becomes relevant when the deletion of one syndecan leads to opposite inflammatory responses to same stimulus in different tissues. It is possible that the removal of syndecan-3 may have influenced the expression of different members syndecan family in each system, eventually leading to a compensatory or opposite response. Earlier studies regarding the role of syndecans in inflammation did not take potential compensation between syndecans into account. There is no obvious developmental phenotype for mice lacking syndecan-1 or syndecan-4, which may indicate compensation between syndecans. However, when these mice are injured, they exhibit profound phenotypes. This leads to the question on whether the phenotype observed is a result of the loss of one syndecan or due to the compensatory effect by an alternate syndecan. In addition, each syndecan may be interacting with distinct cytokines and the second syndecan may be signaling through different ligands instead of simply compensating for the deleted syndecan.

Another aspect of syndecan function in inflammation yet to be addressed is their role in matrix turnover and mechanotransduction. ECM remodeling is observed during chronic inflammation, which is usually mediated by matrix degrading enzymes (e.g., Matrix metalloproteinases) (56). Cytokines promote the expression of catabolic enzymes leading to matrix degradation and turnover (57, 58). Since syndecans are one of the key regulators of cytokine function during inflammation, it is safe to assume that syndecans contribute to matrix turnover. ECM remodeling and increased deposition of ECM components are common during the development of fibrosis, a prominent outcome of chronic inflammation (59). Cardiac disease models showed that syndecan-1 mediates fibrosis resulting from an enhanced deposition of collagen (60, 61). Similar observations were made in the lung where syndecan-4 plays an important role in limiting lung fibrosis during inflammation (62, 63). ECM remodeling contributes significantly to the mechanical properties of the matrix. The role of mechanosignaling in leukocyte extravasation has been reported previously (64). While the role of syndecans as mechanosensors is not fully elucidated, they can play a significant role in mechanotransduction. Syndecan mediation of cell-matrix and cell-cell adhesion, and cytoskeleton organization has been extensively studied (13, 14, 65–67). Therefore, it is safe to assume that syndecans may control mechanical forces generated by the adhesion associated molecules during inflammation. A previous report supports this notion, where the syndecan-1 knockout endothelial cells failed to form a phospho-paxillin gradient in response to the shear stress generated by atheroprotective flow. Paxillin is a structural protein in the focal adhesions and the defective phosphorylation of paxillin resulted in a pro-inflammatory phenotype (28). In addition, syndecan-1 and−4 have shown to control the function of stretch-activated calcium channels in epithelial cells and fibroblasts, respectively. This could well be relevant for inflammation, where calcium is not only a known influencer, but also important in conditions, such as wound contraction and shear (68).

SOLUBLE SYNDECANS IN INFLAMMATION

Syndecans exist either as transmembrane form or as soluble extracellular domains (69). Proteolytic cleavage of syndecan core proteins at the juxtamembrane site is associated with inflammation, mainly as a result of the actions by enzymes called sheddases (e.g., MMPs, ADAMTS) (70). The cleavage of the core protein results in the delivery of extracellular domain to the matrix and then to the circulation. Several cytokines (e.g., IL-8, IL-17, TNFα) can induce core protein cleavage by sheddases, likely by directly interacting with GAG chains (45). The cleaved core proteins, carrying glycosaminoglycan chains, are released to the extracellular matrix where they can bind to more extracellular matrix ligands. The shedding can have multiple effects on cell signaling. One, they rapidly downregulate signal transduction at the cell surface. Two, they can quench ligands and make them unavailable to the remaining syndecans on the cell surface. Three, they can initiate more signaling pathways as circulating soluble effectors, independent of cell surface signaling. The increase in the levels of soluble syndecans-1 and syndecan-4 in the dermal wound fluid and high levels of syndecan-3 in the serum during rheumatoid arthritis have been observed (41, 71). Early studies showed that MMP-7 mediated syndecan-1 shedding to alveolar epithelium resulted in a stable CXCL1 chemokine gradient to promote neutrophil migration (44, 72, 73). While this may depict syndecan-1 shedding as pro-inflammatory, it however allows a tight control of inflammation. The gradient formation restricts neutrophil migration at the site of epithelial injury, thus preventing further tissue damage (73). The CXCL1 secretion levels are reduced in syndecan-1 or MMP-7 knockout animals, resulting in reduced neutrophil migration (72). In addition to CXCL1, shed syndecan is known to bind with chemokines, such as CCL7, CCL11, and CCL17, minimizing the Th2 cell recruitment to the lungs (74). More recent studies showed that syndecan-1 shedding is essential for the resolution of inflammation, likely by removing the sequestered CXC chemokines (75). It is also known that soluble syndecan-1 can reduce the expression of pro-inflammatory cytokines. For example, the administration of exosomes containing syndecan-1 can be used to mitigate the expression of pro-inflammatory

cytokines (e.g., IL-1β, IL-6, TNFα) and alleviate LPS induced acute lung edema and inflammation (76). While these results show that syndecan-1 shedding is required to alleviate or control inflammatory response, the opposite observations were also made. For instance, intestinal epithelial cells expressing shedding resistant syndecan-1 appears to be less prone to inflammatory damage. These experiments showed reduced neutrophil migration and TNFα expression (72). A possibility worth considering is that the transient expression of shedding resistant syndecan may have resulted in very high levels of cell bound syndecan-1, leading to the activation of other signaling pathways. Similarly, hemorrhagic shock increases systemic shedding and a decrease in the pulmonary presence of syndecan-1, leading to increased inflammation (77). In light of the observations that soluble syndecan-1 is elevated under inflammatory conditions, it has been proposed that syndecan-1 serum levels can be used as a biomarker for inflammation (78, 79). The increase in soluble syndecan-1 may occur in the later stages of inflammation. Therefore, the effectiveness of using soluble syndecan-1 as a marker in early inflammation will need further study and more effective detection tools. On the other hand, the presence of soluble syndecan-1 may be used as a marker for the severity of diseases, such as neuromyelitis optica or inflammatory breast cancers (27, 80). A final aspect of inflammation that may have been associated with syndecan shedding is angiogenesis. Inflammation promotes angiogenesis, which further enhances chronic inflammation. In other words, inflammation and angiogenesis are mutually dependent (81, 82). Previous reports showed that syndecan-1 knockout mice have increased angiogenesis due to an increase in leukocyte adhesion (83). Similarly, soluble syndecan-1 ectodomain alters angiogenesis in syndecan-1 overexpressing mice. However, this may be due to the excess proteolytic activity resulted from the modulation of proteolytic enzymes by heparan sulfate chains on the shed syndecan-1 ectodomain (84). Previous reports shows that syndecan-2 signaling is essential for angiogenesis during development, while the shed syndecan-2 is known to inhibit angiogenesis (17, 85). Syndecan-4 ectodomain shedding is associated with both acute and chronic inflammation as well as angiogenesis. One report showed that pro-inflammatory molecule LPS induces the shedding of syndecan-4 from the heart, possibly as a result of ADAMTS1, ADAMTS4, or MMP9 (61). The syndecan-4 shedding during chronic inflammation caused by diabetes mellitus resulted in an impaired macrovascular angiogenesis (86). The same report showed that treating HUVEC cells with advanced glycation end products (AGEs) leads to syndecan-4 shedding. AGEs are the harmful compounds formed by sugar and protein or fat in the blood that are typically high during diabetes mellitus. These compounds are known to enhance the expression and function of pro-inflammatory cytokine TNFα, which can also promote syndecan shedding. The TNFα mediated shedding of syndecan-4 could well be the reason for the defective angiogenesis during inflammation caused by diabetes mellitus (86).

PERSPECTIVES AND CONCLUSIONS

The current findings conclude that, irrespective of the type, syndecans are elevated during inflammation. Independent studies have indicated that syndecans can act as both pro-inflammatory and anti-inflammatory molecules, with cell surface and soluble syndecans having distinct roles. The elevation in syndecan expression is required for initial leukocyte rolling and recruitment of chemokines. However, this needs to be limited as the signaling progresses. At this point, the expression of syndecans on the cell surface may have to be controlled, which could be achieved by shedding of syndecans. The shedding of syndecans can not only reduce the signaling from cell surface, but also create a stable chemokine gradient that directs the migration of leukocytes only to the vicinity of inflammation. These limiting steps may be crucial later on, in helping the clearance of inflammation. Even though the role of syndecans in inflammation is well-studied, there are several aspects that need further investigation. Previous reports have shown that pathogens exploit GAG chains on syndecans to infect the host (87, 88). However, there is no data supporting the idea that syndecans can recognize the inflammation inducers. This is an area worth exploring in the future. In addition, the impacts of syndecan-mediated calcium regulation and matrix turnover in inflammation is still not clear and requires further studies. Finally, syndecans may influence the expression of each other, which warrants further investigation to determine how the balancing of syndecans may help to regain tissue homeostasis during inflammation. Moreover, the temporal expression levels and the rate of shedding of syndecans during different stages of inflammation is unknown. Therefore, more studies need to be done in order to establish the potential use of syndecans as biomarkers of inflammation.

AUTHOR CONTRIBUTIONS

SG collected the data and compiled the review.

FUNDING

SG was supported by grants from the National Health and Medical Research Council, Australia (APP1161439) and Australian Research Council (DE190100174).

ACKNOWLEDGMENTS

The author thanks Prof. John Couchman, University of Copenhagen and Dr. Roger Pocock, Monash University for the comments on the manuscript.

REFERENCES

1. Medzhitov R. Origin and physiological roles of inflammation. *Nature.* (2008) 454:428–35. doi: 10.1038/nature07201
2. Punchard NA, Whelan CJ, Adcock I. The journal of inflammation. *J Inflamm.* (2004) 1:1. doi: 10.1186/1476-9255-1-1
3. Ueha S, Shand FH, Matsushima K. Cellular and molecular mechanisms of chronic inflammation-associated organ fibrosis.

Front Immunol. (2012) 3:71. doi: 10.3389/fimmu.2012.00071
4. Costa C, Incio J, Soares R. Angiogenesis and chronic inflammation: cause or consequence? *Angiogenesis.* (2007) 10:149–66. doi: 10.1007/s10456-007-9074-0
5. Pober JS, Sessa WC. Inflammation and the blood microvascular system. *Cold Spring Harb Perspect Biol.* (2014) 7:a016345. doi: 10.1101/cshperspect.a016345
6. Ashley NT, Weil ZM, Nelson RJ. Inflammation: mechanisms, costs, and natural variation. *Ann Rev Ecol Evol Syst.* (2012) 43:385–406. doi: 10.1146/annurev-ecolsys-040212-092530
7. Roach JC, Glusman G, Rowen L, Kaur A, Purcell MK, Smith KD, et al. The evolution of vertebrate Toll-like receptors. *Proc Natl Acad Sci USA.* (2005) 102:9577–82. doi: 10.1073/pnas.0502272102
8. Ye Z, Ting JP. NLR, the nucleotide-binding domain leucine-rich repeat containing gene family. *Curr Opin Immunol.* (2008) 20:3–9. doi: 10.1016/j.coi.2008.01.003
9. Liu T, Zhang L, Joo D, Sun SC. NF-κB signaling in inflammation. *Signal Transduct Target Ther.* (2017) 2:17023. doi: 10.1038/sigtrans.2017.23
10. Zhang JM, An J. Cytokines, inflammation, and pain. *Int Anesthesiol Clin.* (2007) 45:27–37. doi: 10.1097/AIA.0b013e318034194e
11. Lacy P. Mechanisms of degranulation in neutrophils. *Allergy Asthma Clin Immunol.* (2006) 2:98–108. doi: 10.1186/1710-1492-2-3-98
12. Nathan C. Points of control in inflammation. *Nature.* (2002) 420:846–52. doi: 10.1038/nature01320
13. Xian X, Gopal S, Couchman JR. Syndecans as receptors and organizers of the extracellular matrix. *Cell Tissue Res.* (2010) 339:31–46. doi: 10.1007/s00441-009-0829-3
14. Gopal S, Bober A, Whiteford JR, Multhaupt HA, Yoneda A, Couchman JR. Heparan sulfate chain valency controls syndecan-4 function in cell adhesion. *J Biol Chem.* (2010) 285:14247–58. doi: 10.1074/jbc.M109.056945
15. Oh ES, Woods A, Couchman JR. Syndecan-4 proteoglycan regulates the distribution and activity of protein kinase C. *J Biol Chem.* (1997) 272:8133–6. doi: 10.1074/jbc.272.13.8133
16. Oh ES, Woods A, Lim ST, Theibert AW, Couchman JR. Syndecan-4 proteoglycan cytoplasmic domain and phosphatidylinositol 4,5-bisphosphate coordinately regulate protein kinase C activity. *J Biol Chem.* (1998) 273:10624–9. doi: 10.1074/jbc.273.17.10624
17. De Rossi G, Evans AR, Kay E, Woodfin A, McKay TR, Nourshargh S, et al. Shed syndecan-2 inhibits angiogenesis. *J Cell Sci.* (2014) 127:4788–99. doi: 10.1242/jcs.153015
18. De Rossi G, Whiteford JR. Syndecans in angiogenesis and endothelial cell biology. *Biochem Soc Trans.* (2014) 42:1643–6. doi: 10.1042/BST20140232
19. Segaliny AI, Brion R, Mortier E, Maillasson M, Cherel M, Jacques Y, et al. Syndecan-1 regulates the biological activities of interleukin-34. *Biochim Biophys Acta.* (2015) 1853:1010–21. doi: 10.1016/j.bbamcr.2015.01.023
20. Hassan H, Greve B, Pavao MS, Kiesel L, Ibrahim SA, Götte M. Syndecan-1 modulates beta-integrin-dependent and interleukin-6-dependent functions in breast cancer cell adhesion, migration, and resistance to irradiation. *FEBS J.* (2013) 280:2216–27. doi: 10.1111/febs.12111
21. Götte M. Syndecans in inflammation. *FASEB J.* (2003) 17:575–91. doi: 10.1096/fj.02-0739rev
22. Götte M, Joussen AM, Klein C, Andre P, Wagner DD, Hinkes MT, et al. Role of syndecan-1 in leukocyte-endothelial interactions in the ocular vasculature. *Invest Ophthalmol Vis Sci.* (2002) 43:1135–41.
23. Ishiguro K, Kadomatsu K, Kojima T, Muramatsu H, Iwase M, Yoshikai Y, et al. Syndecan-4 deficiency leads to high mortality of lipopolysaccharide-injected mice. *J Biol Chem.* (2001) 276:47483–8. doi: 10.1074/jbc.M106268200
24. Alexopoulou AN, Multhaupt HA, Couchman JR. Syndecans in wound healing, inflammation and vascular biology. *Int J Biochem Cell Biol.* (2007) 39:505–28. doi: 10.1016/j.biocel.2006.10.014
25. Halden Y, Rek A, Atzenhofer W, Szilak L, Wabnig A, Kungl AJ. Interleukin-8 binds to syndecan-2 on human endothelial cells. *Biochem J.* (2004) 377:533–8. doi: 10.1042/bj20030729
26. Choi S, Chung H, Hong H, Kim SY, Kim SE, Seoh JY, et al. Inflammatory hypoxia induces syndecan-2 expression through IL-1beta-mediated FOXO3a activation in colonic epithelia. *FASEB J.* (2017) 31:1516–30. doi: 10.1096/fj.201601098R
27. Pei S, Zheng D, Wang Z, Hu X, Pan S, Wang H. Elevated soluble syndecan-1 levels in neuromyelitis optica are associated with disease severity. *Cytokine.* (2018) 111:140–5. doi: 10.1016/j.cyto.2018.08.017
28. Voyvodic PL, Min D, Liu R, Williams E, Chitalia V, Dunn AK, et al. Loss of syndecan-1 induces a pro-inflammatory phenotype in endothelial cells with a dysregulated response to atheroprotective flow. *J Biol Chem.* (2014) 289:9547–59. doi: 10.1074/jbc.M113.541573
29. Couchman JR. Transmembrane signaling proteoglycans. *Annu Rev Cell Dev Biol.* (2010) 26:89–114. doi: 10.1146/annurev-cellbio-100109-104126
30. Couchman JR, Pataki CA. An introduction to proteoglycans and their localization. *J Histochem Cytochem.* (2012) 60:885–97. doi: 10.1369/0022155412464638
31. Giuffrè L, Cordey AS, Monai N, Tardy Y, Schapira M, Spertini O. Monocyte adhesion to activated aortic endothelium: role of L-selectin and heparan sulfate proteoglycans. *J Cell Biol.* (1997) 136:945–56. doi: 10.1083/jcb.136.4.945
32. Echtermeyer F, Streit M, Wilcox-Adelman S, Saoncella S, Denhez F, Detmar M, et al. Delayed wound repair and impaired angiogenesis in mice lacking syndecan-4. *J Clin Invest.* (2001) 107:R9-r14. doi: 10.1172/JCI10559
33. Vanhoutte D, Schellings MW, Götte M, Swinnen M, Herias V, Wild MK, et al. Increased expression of syndecan-1 protects against cardiac dilatation and dysfunction after myocardial infarction. *Circulation.* (2007) 115:475–82. doi: 10.1161/CIRCULATIONAHA.106.644609
34. Brauer R, Ge L, Schlesinger SY, Birkland TP, Huang Y, Parimon T, et al. Syndecan-1 attenuates lung injury during influenza infection by potentiating c-Met signaling to suppress epithelial apoptosis. *Am J Respir Crit Care Med.* (2016) 194:333–44. doi: 10.1164/rccm.201509-1878OC
35. Angsana J, Chen J, Smith S, Xiao J, Wen J, Liu L, et al. Syndecan-1 modulates the motility and resolution responses of macrophages. *Arterioscler Thromb Vasc Biol.* (2015) 35:332–40. doi: 10.1161/ATVBAHA.114.304720
36. Kharabi Masouleh B, Ten Dam GB, Wild MK, Seelige R, van der Vlag J, Rops AL, et al. Role of the heparan sulfate proteoglycan syndecan-1 (CD138) in delayed-type hypersensitivity. *J Immunol.* (2009) 182:4985–93. doi: 10.4049/jimmunol.0800574
37. Floer M, Götte M, Wild MK, Heidemann J, Gassar ES, Domschke W, et al. Enoxaparin improves the course of dextran sodium sulfate-induced colitis in syndecan-1-deficient mice. *Am J Pathol.* (2010) 176:146–57. doi: 10.2353/ajpath.2010.080639
38. Hyun YM, Lefort CT, Kim M. Leukocyte integrins and their ligand interactions. *Immunol Res.* (2009) 45:195–208. doi: 10.1007/s12026-009-8101-1
39. Kaneider NC, Reinisch CM, Dunzendorfer S, Römisch J, Wiedermann CJ. Syndecan-4 mediates antithrombin-induced chemotaxis of human peripheral blood lymphocytes and monocytes. *J Cell Sci.* (2002) 115:227–36. doi: 10.1186/cc1575
40. Polte T, Petzold S, Bertrand J, Schütze N, Hinz D, Simon JC, et al. Critical role for syndecan-4 in dendritic cell migration during development of allergic airway inflammation. *Nat Commun.* (2015) 6:7554. doi: 10.1038/ncomms8554
41. Eustace AD, McNaughton EF, King S, Kehoe O, Kungl A, Mattey D, et al. Soluble syndecan-3 binds chemokines, reduces leukocyte migration *in vitro* and ameliorates disease severity in models of rheumatoid arthritis. *Arthritis Res Ther.* (2019) 21:172. doi: 10.1186/s13075-019-1939-2
42. Kuschert GS, Coulin F, Power CA, Proudfoot AE, Hubbard RE, Hoogewerf AJ, et al. Glycosaminoglycans interact selectively with chemokines and modulate receptor binding and cellular responses. *Biochemistry.* (1999) 38:12959–68. doi: 10.1021/bi990711d
43. Webb LM, Ehrengruber MU, Clark-Lewis I, Baggiolini M, Rot A. Binding to heparan sulfate or heparin enhances neutrophil responses to interleukin 8. *Proc Natl Acad Sci USA.* (1993) 90:7158–62. doi: 10.1073/pnas.90.15.7158
44. Li Q, Park PW, Wilson CL, Parks WC. Matrilysin shedding of syndecan-1 regulates chemokine mobilization and transepithelial efflux of neutrophils in acute lung injury. *Cell.* (2002) 111:635–46. doi: 10.1016/S0092-8674(02)01079-6
45. Marshall LJ, Ramdin LS, Brooks T, DPhil PC, Shute JK. Plasminogen activator inhibitor-1 supports IL-8-mediated neutrophil transendothelial migration by inhibition of the constitutive shedding of endothelial IL-8/heparan sulfate/syndecan-1 complexes. *J Immunol.* (2003) 171:2057–65. doi: 10.4049/jimmunol.171.4.2057

46. Sarris M, Masson JB, Maurin D, Van der Aa LM, Boudinot P, Lortat-Jacob H, et al. Inflammatory chemokines direct and restrict leukocyte migration within live tissues as glycan-bound gradients. *Curr Biol.* (2012) 22:2375–82. doi: 10.1016/j.cub.2012.11.018
47. Jaiswal AK, Sadasivam M, Archer NK, Miller RJ, Dillen CA, Ravipati A, et al. Syndecan-1 regulates psoriasiform dermatitis by controlling homeostasis of IL-17-Producing γδ T Cells. *J Immunol.* (2018) 201:1651–61. doi: 10.4049/jimmunol.1800104
48. Gong GQ, Ren FF, Wang YJ, Wan L, Chen S, Yuan J, et al. Expression of IL-17 and syndecan-1 in nasal polyps and their correlation with nasal polyps. *J Huazhong Univ Sci Technolog Med Sci.* (2017) 37:412–8. doi: 10.1007/s11596-017-1749-1
49. Hong H, Song HK, Hwang ES, Lee AR, Han DS, Kim SE, et al. Up-regulation of syndecan-2 in proximal colon correlates with acute inflammation. *FASEB J.* (2019) 33:11381–95. doi: 10.1096/fj.201900561R
50. Tanino Y, Chang MY, Wang X, Gill SE, Skerrett S, McGuire JK, et al. Syndecan-4 regulates early neutrophil migration and pulmonary inflammation in response to lipopolysaccharide. *Am J Respir Cell Mol Biol.* (2012) 47:196–202. doi: 10.1165/rcmb.2011-0294OC
51. Sebestyén A, Gallai M, Knittel T, Ambrust T, Ramadori G, Kovalszky I. Cytokine regulation of syndecan expression in cells of liver origin. *Cytokine.* (2000) 12:1557–60. doi: 10.1006/cyto.2000.0754
52. Worapamorn W, Tam SP, Li H, Haase HR, Bartold PM. Cytokine regulation of syndecan-1 and−2 gene expression in human periodontal fibroblasts and osteoblasts. *J Periodontal Res.* (2002) 37:273–8. doi: 10.1034/j.1600-0765.2002.01610.x
53. Vuong TT, Reine TM, Sudworth A, Jenssen TG, Kolset SO. Syndecan-4 is a major syndecan in primary human endothelial cells *in vitro*, modulated by inflammatory stimuli and involved in wound healing. *J Histochem Cytochem.* (2015) 63:280–92. doi: 10.1369/0022155415568995
54. Day RM, Mitchell TJ, Knight SC, Forbes A. Regulation of epithelial syndecan-1 expression by inflammatory cytokines. *Cytokine.* (2003) 21:224–33. doi: 10.1016/S1043-4666(03)00091-7
55. Kehoe O, Kalia N, King S, Eustace A, Boyes C, Reizes O, et al. Syndecan-3 is selectively pro-inflammatory in the joint and contributes to antigen-induced arthritis in mice. *Arthritis Res Ther.* (2014) 16:R148. doi: 10.1186/ar4610
56. Bonnans C, Chou J, Werb Z. Remodelling the extracellular matrix in development and disease. *Nat Rev Mol Cell Biol.* (2014) 15:786–801. doi: 10.1038/nrm3904
57. Siwik DA, Colucci WS. Regulation of matrix metalloproteinases by cytokines and reactive oxygen/nitrogen species in the myocardium. *Heart Fail Rev.* (2004) 9:43–51. doi: 10.1023/B:HREV.0000011393.40674.13
58. Manicone AM, McGuire JK. Matrix metalloproteinases as modulators of inflammation. *Semin Cell Dev Biol.* (2008) 19:34–41. doi: 10.1016/j.semcdb.2007.07.003
59. Cox TR, Erler JT. Remodeling and homeostasis of the extracellular matrix: implications for fibrotic diseases and cancer. *Dis Model Mech.* (2011) 4:165–78. doi: 10.1242/dmm.004077
60. Lunde IG, Herum KM, Carlson CC, Christensen G. Syndecans in heart fibrosis. *Cell Tissue Res.* (2016) 365:539–52. doi: 10.1007/s00441-016-2454-2
61. Strand ME, Aronsen JM, Braathen B, Sjaastad I, Kvaløy H, Tønnessen T, et al. Shedding of syndecan-4 promotes immune cell recruitment and mitigates cardiac dysfunction after lipopolysaccharide challenge in mice. *J Mol Cell Cardiol.* (2015) 88:133–44. doi: 10.1016/j.yjmcc.2015.10.003
62. Tanino Y, Wang X, Nikaido T, Misa K, Sato Y, Togawa R, et al. Syndecan-4 inhibits the development of pulmonary fibrosis by attenuating TGF-β signaling. *Int J Mol Sci.* (2019) 20:4989. doi: 10.3390/ijms20204989
63. Jiang D, Liang J, Campanella GS, Guo R, Yu S, Xie T, et al. Inhibition of pulmonary fibrosis in mice by CXCL10 requires glycosaminoglycan binding and syndecan-4. *J Clin Invest.* (2010) 120:2049–57. doi: 10.1172/JCI38644
64. Schaefer A, Hordijk PL. Cell-stiffness-induced mechanosignaling - a key driver of leukocyte transendothelial migration. *J Cell Sci.* (2015) 128:2221–30. doi: 10.1242/jcs.163055
65. Okina E, Grossi A, Gopal S, Multhaupt HA, Couchman JR. Alpha-actinin interactions with syndecan-4 are integral to fibroblast-matrix adhesion and regulate cytoskeletal architecture. *Int J Biochem Cell Biol.* (2012) 44:2161–74. doi: 10.1016/j.biocel.2012.08.017
66. Gopal S, Multhaupt HAB, Pocock R, Couchman JR. Cell-extracellular matrix and cell-cell adhesion are linked by syndecan-4. *Matrix Biol.* (2017) 60–61:57–69. doi: 10.1016/j.matbio.2016.10.006
67. Couchman JR, Gopal S, Lim HC, Nørgaard S, Multhaupt HA. Syndecans: from peripheral coreceptors to mainstream regulators of cell behaviour. *Int J Exp Pathol.* (2015) 96:1–10. doi: 10.1111/iep.12112
68. Gopal S, Søgaard P, Multhaupt HA, Pataki C, Okina E, Xian X, et al. Transmembrane proteoglycans control stretch-activated channels to set cytosolic calcium levels. *J Cell Biol.* (2015) 210:1199–211. doi: 10.1083/jcb.201501060
69. Subramanian SV, Fitzgerald ML, Bernfield M. Regulated shedding of syndecan-1 and−4 ectodomains by thrombin and growth factor receptor activation. *J Biol Chem.* (1997) 272:14713–20. doi: 10.1074/jbc.272.23.14713
70. Manon-Jensen T, Multhaupt HA, Couchman JR. Mapping of matrix metalloproteinase cleavage sites on syndecan-1 and syndecan-4 ectodomains. *FEBS J.* (2013) 280:2320–31. doi: 10.1111/febs.12174
71. Kainulainen V, Wang H, Schick C, Bernfield M. Syndecans, heparan sulfate proteoglycans, maintain the proteolytic balance of acute wound fluids. *J Biol Chem.* (1998) 273:11563–9. doi: 10.1074/jbc.273.19.11563
72. Zhang Y, Wang Z, Liu J, Zhang Z, Chen Y. Suppressing syndecan-1 shedding ameliorates intestinal epithelial inflammation through inhibiting NF-κB Pathway and TNF-α. *Gastroenterol Res Pract.* (2016) 2016:6421351. doi: 10.1155/2016/6421351
73. Gill SE, Nadler ST, Li Q, Frevert CW, Park PW, Chen P, et al. Shedding of syndecan-1/CXCL1 complexes by matrix metalloproteinase 7 functions as an epithelial checkpoint of neutrophil activation. *Am J Respir Cell Mol Biol.* (2016) 55:243–51. doi: 10.1165/rcmb.2015-0193OC
74. Xu J, Park PW, Kheradmand F, Corry DB. Endogenous attenuation of allergic lung inflammation by syndecan-1. *J Immunol.* (2005) 174:5758–65. doi: 10.4049/jimmunol.174.9.5758
75. Hayashida K, Parks WC, Park PW. Syndecan-1 shedding facilitates the resolution of neutrophilic inflammation by removing sequestered CXC chemokines. *Blood.* (2009) 114:3033–43. doi: 10.1182/blood-2009-02-204966
76. Zhang C, Guo F, Chang M, Zhou Z, Yi L, Gao C, et al. Exosome-delivered syndecan-1 rescues acute lung injury via a FAK/p190RhoGAP/RhoA/ROCK/NF-κB signaling axis and glycocalyx enhancement. *Exp Cell Res.* (2019) 384:111596. doi: 10.1016/j.yexcr.2019.111596
77. Gonzalez Rodriguez E, Cardenas JC, Cox CS, Kitagawa RS, Stensballe J, Holcomb JB, et al. Traumatic brain injury is associated with increased syndecan-1 shedding in severely injured patients. *Scand J Trauma Resusc Emerg Med.* (2018) 26:102. doi: 10.1186/s13049-018-0565-3
78. Yablecovitch D, Oren A, Ben-Horin S, Fudim E, Eliakim R, Saker T, et al. Soluble syndecan-1: a novel biomarker of small bowel mucosal damage in children with celiac disease. *Dig Dis Sci.* (2017) 62:755–60. doi: 10.1007/s10620-016-4415-8
79. Patterson AM. Soluble syndecan-1: does this biomarker address a seemingly insoluble problem in inflammatory bowel disease? *Dig Dis Sci.* (2015) 60:2222–4. doi: 10.1007/s10620-015-3669-x
80. Ibrahim SA, Gadalla R, El-Ghonaimy EA, Samir O, Mohamed HT, Hassan H, et al. Syndecan-1 is a novel molecular marker for triple negative inflammatory breast cancer and modulates the cancer stem cell phenotype via the IL-6/STAT3, Notch and EGFR signaling pathways. *Mol Cancer.* (2017) 16:57. doi: 10.1186/s12943-017-0621-z
81. Walsh DA, Pearson CI. Angiogenesis in the pathogenesis of inflammatory joint and lung diseases. *Arthritis Res.* (2001) 3:147–53. doi: 10.1186/ar292
82. Szade A, Grochot-Przeczek A, Florczyk U, Jozkowicz A, Dulak J. Cellular and molecular mechanisms of inflammation-induced angiogenesis. *IUBMB Life.* (2015) 67:145–59. doi: 10.1002/iub.1358
83. Götte M, Bernfield M, Joussen AM. Increased leukocyte-endothelial interactions in syndecan-1-deficient mice involve heparan sulfate-dependent and -independent steps. *Curr Eye Res.* (2005) 30:417–22. doi: 10.1080/02713680590956289
84. Elenius V, Götte M, Reizes O, Elenius K, Bernfield M. Inhibition by the soluble syndecan-1 ectodomains delays wound repair in mice overexpressing syndecan-1. *J Biol Chem.* (2004) 279:41928–35. doi: 10.1074/jbc.M404506200

85. Chen E, Hermanson S, Ekker SC. Syndecan-2 is essential for angiogenic sprouting during zebrafish development. *Blood.* (2004) 103:1710–9. doi: 10.1182/blood-2003-06-1783
86. Li R, Xie J, Wu H, Li G, Chen J, Chen Q, et al. Syndecan-4 shedding impairs macrovascular angiogenesis in diabetes mellitus. *Biochem Biophys Res Commun.* (2016) 474:15–21. doi: 10.1016/j.bbrc.2016.03.112
87. Aquino RS, Park PW. Glycosaminoglycans and infection. *Front Biosci.* (2016) 21:1260–77. doi: 10.2741/4455
88. Rajas O, Quirós LM, Ortega M, Vazquez-Espinosa E, Merayo-Lloves J, Vazquez F, et al. Glycosaminoglycans are involved in bacterial adherence to lung cells. *BMC Infect Dis.* (2017) 17:319. doi: 10.1186/s12879-017-2418-5

Conflict of Interest: The author declares that the research was conducted in the absence of any commercial or financial relationships that could be construed as a potential conflict of interest.

frontiers in Immunology

MINI REVIEW
published: 03 March 2020
doi: 10.3389/fimmu.2020.00232

Regulation of Macrophage and Dendritic Cell Function by Chondroitin Sulfate in Innate to Antigen-Specific Adaptive Immunity

Sonoko Hatano and Hideto Watanabe*

Institute for Molecular Science of Medicine, Aichi Medical University, Nagakute, Japan

Chondroitin sulfate (CS), a type of glycosaminoglycan (GAG), is a linear acidic polysaccharide comprised of repeating disaccharides, modified with sulfate groups at various positions. Except for hyaluronan (HA), GAGs are covalently bound to core proteins, forming proteoglycans (PGs). With highly negative charges, GAGs interact with a variety of physiologically active molecules, including cytokines, chemokines, and growth factors, and control cell behavior during development and in the progression of diseases, including cancer, infections, and inflammation. Heparan sulfate (HS), another type of GAG, and HA are well reported as regulators for leukocyte migration at sites of inflammation. There have been many reports on the regulation of immune cell function by HS and HA; however, regulation of immune cells by CS has not yet been fully understood. This article focuses on the regulatory function of CS in antigen-presenting cells, including macrophages and dendritic cells, and refers to CSPGs, such as versican and biglycan, and the cell surface proteoglycan, syndecan.

Keywords: chondroitin sulfate, glycosaminoglycan, proteoglycan, antigen-presenting cell, receptor type of protein tyrosine phosphatase sigma

OPEN ACCESS

Edited by:
Megan S. Lord,
University of New South Wales, Australia

Reviewed by:
Charles W. Frevert,
University of Washington Tacoma, United States
Paul Proost,
KU Leuven, Belgium
Brooke Farrugia,
The University of Melbourne, Australia

****Correspondence:***
Sonoko Hatano
shatano@aichi-med-u.ac.jp

Specialty section:
This article was submitted to Cytokines and Soluble Mediators in Immunity, a section of the journal Frontiers in Immunology

Received: *11 October 2019*
Accepted: *28 January 2020*
Published: *03 March 2020*

Citation:
Hatano S and Watanabe H (2020) Regulation of Macrophage and Dendritic Cell Function by Chondroitin Sulfate in Innate to Antigen-Specific Adaptive Immunity. Front. Immunol. 11:232. doi: 10.3389/fimmu.2020.00232

INTRODUCTION

Glycosaminoglycans (GAGs) are linear polysaccharides consisting of repeating disaccharide units and modified with sulfate groups at various positions on the sugar residues. The GAG chains retain negatively charged domains due to characteristics of the sulfate groups, allowing for the absorption of water and other positively charged soluble ligands, such as chemokines (1, 2), cytokines (3), growth factors (4, 5), and cell surface receptors (6, 7). They are classified into chondroitin sulfate/dermatan sulfate (CS/DS), heparin/heparan sulfate (HP/HS), hyaluronan (HA), and keratan sulfate (KS).

At the site of injury or infection, macrophages release cytokines to activate endothelial cells, and HS on endothelial cells binds to L-selectins on leukocyte, leading to leukocyte rolling (8). Macrophages also release substantial amounts of chemokines that bind to GAGs at the endothelial surface (9). Leukocytes adhere to endothelial cells firmly and then migrate through the endothelial barrier. Therefore, the roles of GAGs in inflammation and immunity are linked to chemokines due to their highly polar nature. HA is best studied in clinical applications for its influence on inflammation, and its role is varying depending on its molecular weight. High-molecular-weight HA has anti-angiogenic, anti-inflammatory, and immunosuppressive effects (10). Conversely, low-molecular-weight HA promotes angiogenesis, inflammation, and cell migration (10, 11). HA

forms provisional matrices with a CS proteoglycan (PG) versican. In the versican-null lung, there are no such matrices, and numbers of infiltrated leukocytes do not increase (12). The HA–versican interaction is important for the recruitment of inflammatory cells including neutrophils, macrophages, and T cells (13, 14). An early work showed a significant increase in CS synthesis in the normal lung after intravenous administration of a single dose of endotoxin (15).

Therefore, PGs accumulate in inflammatory areas and induce inflammatory cell infiltration. Increasing evidence suggests an anti-inflammatory activity of CS through suppression of pro-inflammatory cytokine activities (16–18). While the structure–function relationship of CS is controversial, we aim to introduce the latest information on the role of CS in inflammation.

STRUCTURE OF CHONDROITIN SULFATE

Chondroitin sulfate (CS) is a natural biomacromolecule abundantly distributed in virtually all invertebrates and vertebrates and involved in many biological processes (19, 20). Based on its structure, chain length, and sulfation patterns, CS provides specific biological functions at molecular, cellular, and organ levels, such as cell adhesion, cell division and differentiation, morphogenesis, organogenesis, and neural network formation (6, 21). CS is composed of a repeating glucuronic acid (GlcA) and *N*-acetylgalactosamine (GalNAc) and modified with sulfate groups at varying positions on sugar residues. The major disaccharide structures of CS are as follows: a non-sulfated unit (CH, GlcA-GalNAc), a monosulfated unit at the C-4 position of the GalNAc residue (chondroitin 4-sulfate: CSA, GlcA-GalNAc4S), a monosulfated unit at the C-6 position of GalNAc (chondroitin 6-sulfate: CSC, GlcA-GalNAc6S), a disulfated unit at the C-4 and C-6 positions of GalNAc (chondroitin 4, 6-sulfate: CSE, GlcA-GalNAc4S6S), a disulfated unit at the C-2 position of GlcA and the C-4 position of GalNAc (chondroitin 2,4-sulfate, GlcA2S-GalNAc4S), a disulfated unit at the C-2 position of GlcA and the C-6 position of GalNAc (chondroitin 2, 6-sulfate: CSD, GlcA2S-GalNAc6S), and a trisulfated unit at the C-2 position of GlcA and the C-4 and C-6 positions of GalNAc (GlcA2S-GalNAc4S6S). Certain GlcA residues are epimerized to iduronic acid (IdoA); the chain containing IdoA residues is designated as CSB or DS (**Figure 1**).

Thus, CS possesses a heterogeneous structure and physical–chemical profile in different species and tissues and is responsible for the various and more specialized functions in the extracellular matrix (ECM). To understand the structure–function relationship of CS, our group developed a sequence determination method of synthesized CS dodecasaccharides (22) and generated a CS library *via* chemo-enzymatic synthesis (23). This CS library showed that CSA interacts with a malarial variant surface antigen 2-CSA (VAR2CSA) protein and may potentially serve as a target in therapeutic strategies against placental malaria (24).

Abbreviations: CS, chondroitin sulfate; GAG, glycosaminoglycan; HA, hyaluronan; PG, proteoglycan; CSPG, chondroitin sulfate proteoglycan; HS, heparan sulfate; DS, dermatan sulfate; HP, heparin; KS, keratan sulfate; GlcA, glucuronic acid; GalNAc, *N*-acetylgalactosamine; CSA, chondroitin 4-sulfate; CSC, chondroitin 6-sulfate; CSD, chondroitin 2,6-sulfate; CSE, chondroitin 4,6-sulfate; IdoA, iduronic acid; ECM, extracellular matrix; VAR2CSA, variant surface antigen 2-CSA; APC, antigen-presenting cell; DC, dendritic cell; PAMP, pathogen-associated molecular pattern; DAMP, damage-associated molecular pattern; PRR, pattern recognition receptor; TLR, Toll-like receptor; MHC, major histocompatibility complex; TNF-α, tumor necrosis factor-alpha; IL, interleukin; LPS, lipopolysaccharide; IFN, interferon; EAE, experimental autoimmune encephalomyelitis; CNS, central nervous system; RPTPσ, receptor type of protein tyrosine phosphatase sigma; LAR, leukocyte common antigen-related; SLRP, small leucine-rich proteoglycan; LRR, leucine-rich repeat; LDL, low-density lipoprotein; SDC, syndecan.

THE EFFECT OF CHONDROITIN SULFATE ON ANTIGEN-PRESENTING CELLS (IDEM FOR MACROPHAGES AND DENDRITIC CELLS)

Antigen-presenting cells (APCs), including macrophages, dendritic cells (DCs), and B cells, trigger innate immunity by different mechanisms (**Figure 2**). In the innate immune system, the recognition of extracellular pathogen is mainly mediated by macrophages and DCs in the mononuclear phagocyte system. They recognize pathogen-associated molecular patterns (PAMPs) brought by microbes and damage-associated molecular patterns (DAMPs) produced by damaged host cells through antigen-specific surface receptors, including pattern recognition receptors (PRRs) (25). Toll-like receptors (TLRs) represent a major PRR family. Once their extracellular domains bind PAMPs or DAMPs, the TLRs trigger an intracellular signaling pathway to activate various transcription factors such as nuclear factor-κB (NF-κB). After recognizing their specific molecular patterns, APCs internalize antigens by phagocytosis, process them, and display the fragment of antigen on their surface with major histocompatibility complex (MHC) (26, 27). In general, macrophages remain at the inflammatory sites to eliminate pathogens and apoptotic cells by phagocytosis and clearance and produce pro-inflammatory cytokines. In contrast, DCs can travel to the draining lymph nodes and stimulate T cells (28, 29).

The Role of Chondroitin Sulfate in Macrophages

Macrophages are typically activated in a pro-inflammatory phenotype (M1) or an anti-inflammatory phenotype (M2). Furthermore, M2 macrophage is classified into four subdivisions, M2a, M2b, M2c, and M2d, depending on the applied stimuli and their protein expression profile (30). M1 secretes various pro-inflammatory cytokines and chemokines, such as tumor necrosis factor-alpha (TNF-α), interleukin (IL)-1β, IL-6, IL-8, etc., to scavenge pathogens (31), and M2 produces inflammation inhibitory factors, such as IL-10 and Arginase 1, to avoid excessive inflammation and promote tissue repair (32). Most tissue-resident macrophages are not originated from circulating hematopoietic stem cell-derived monocytes but developed from embryonic precursors including the yolk-sac macrophage or fetal liver monocytes (33, 34).

The anti-inflammatory activity of CS has been studied concerning macrophages. CS influences inflammatory processes by limiting NF-κB signaling (16, 35) and also inhibits IL-1β-induced liberation of pro-inflammatory genes, such as IL-6,

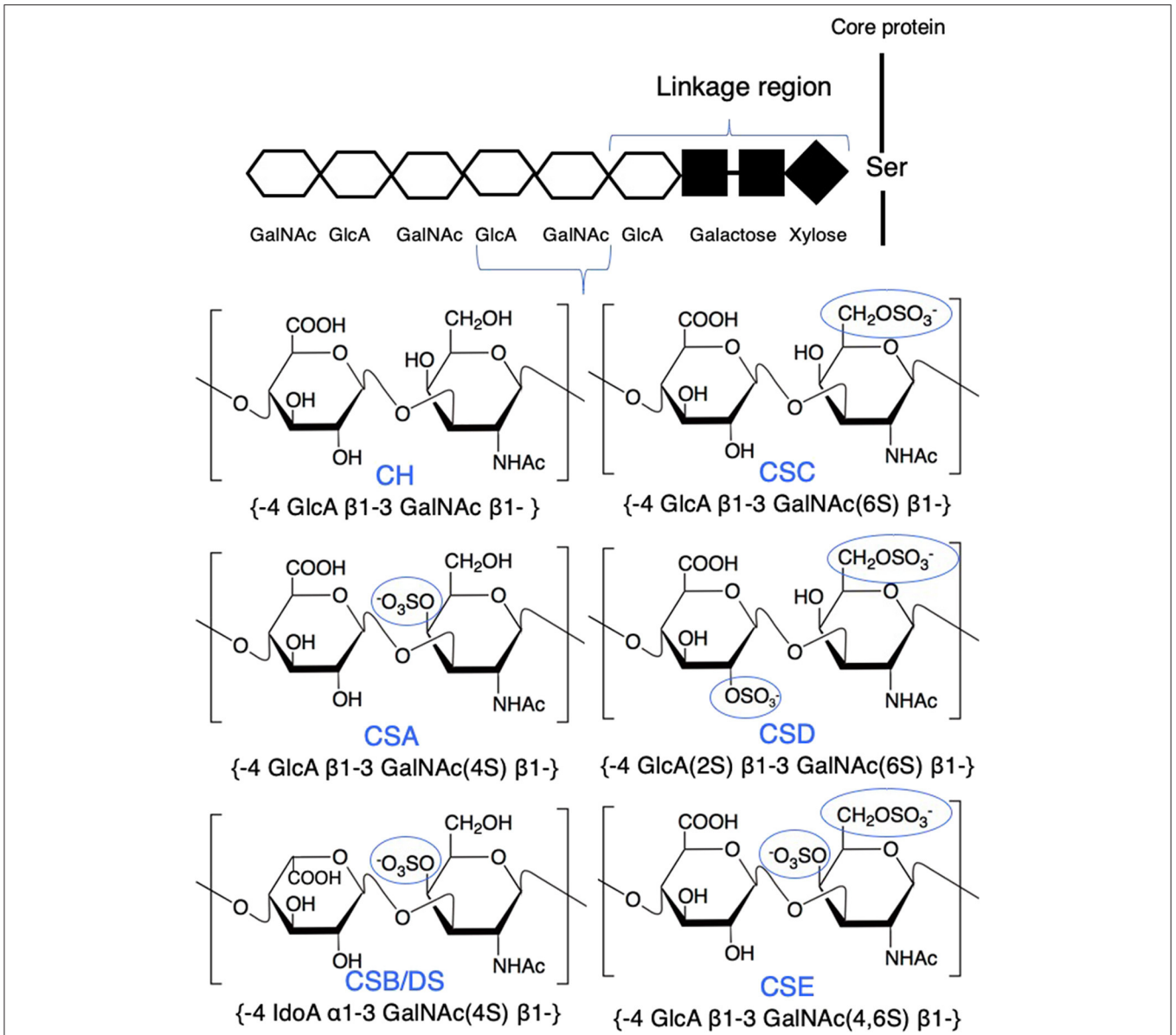

FIGURE 1 | Structure of major chondroitin sulfate (CS) disaccharides. CS is linked to a serine residue of a core protein *via* a linkage region. Repeating disaccharides form a linear polysaccharide chain, which is modified with sulfate groups at varying positions on sugar residues. The major disaccharide structures of CS are as follows: a non-sulfated unit (CH, GlcA-GalNAc); a monosulfated unit at the C-4 position of the GalNAc residue (CSA, GlcA-GalNAc4S); a monosulfated unit at the C-6 position of the GalNAc residue (CSC, GlcA-GalNAc6S); a disulfated unit at the C-2 position of GlcA and the C-6 position of the GalNAc residue (CSD, GlcA2S-GalNAc6S); and a disulfated unit at the C-4 and the C-6 positions of the GalNAc residue (CSE, GlcA-GalNAc4S6S). Certain GlcA residues are epimerized to IdoA (CSB or DS, IdoA-GalNAc4S).

nitric oxide synthase 2, and prostaglandin E2 synthase (36, 37). Further, CS blocks lipopolysaccharide (LPS) binding to CD44 on rat bone marrow-derived macrophages to inhibit the LPS/CD44/NF-κB pathway (38). In CS structure, CSA and its *N*-deacetylated derivative can activate NF-κB in macrophages and induce TNF-α production (39). In contrast, CSC attenuates the inflammatory response in macrophages *via* suppression of NF-κB nuclear translocation (40). Moreover, CSA or CSC inhibited the LPS-induced expression of TNF-α, IL-1β, IL-6, and nitric oxide (NO) on bone marrow-derived macrophages (36). The functions of the CS sulfated structures on macrophages are still in argument.

The Role of Chondroitin Sulfate in Dendritic Cells

Dendritic cells (DCs) are more potent APCs than macrophages and the major instructors of T cells (41). In local tissues, including

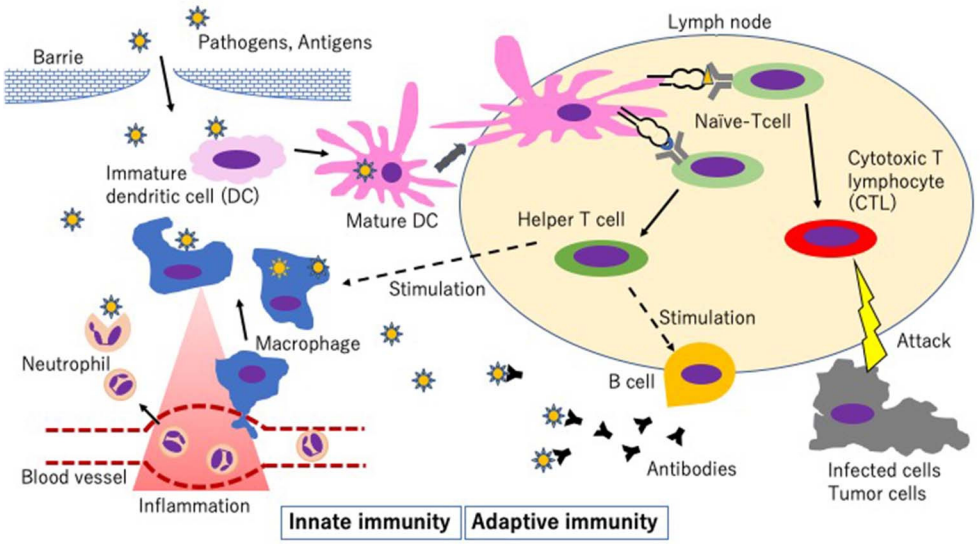

FIGURE 2 | Schematic diagram of innate immunity and adaptive immunity. Step 1: Activation of pattern recognition receptors (PRRs) on tissue-resident macrophages and/or dendritic cells (DCs) by pathogen-associated molecular patterns (PAMPs) resulting in activation of the innate immune response and the following events.
1. Migration of monocytes that mature into recruited macrophages and neutrophils in the systemic circulation.
2. Maturation of DCs, which then migrate to the lymph node.
Step 2: Processing of the antigens and presentation of an antigen on major histocompatibility complex I (MHC-I) or MHC-II to the T cell receptor on T cells.
Step 3: Development of adaptive immunity.

skin and intestine, DCs recognize PAMPs or DAMPs through a large variety of PRRs and phagocytose the antigens and become activated during this process. A variety of factors, such as IL-1 (42) and TNF-α (43), whole bacteria and microbial cell wall component LPS (44), CpG motifs in bacterial DNA (45), haptens (44), and apoptotic cells (44), stimulate DC maturation and promote the expression of MHC-antigen-presenting and costimulatory molecules. The mature DCs migrate to nearby lymphoid organs to present the peptide to naive T cells in a complex with MHC proteins (28). Naive T cells can differentiate into several types of effector T cells *via* MHC class II complex and $CD8^+$ T cells *via* MHC class I complex (41, 46–48). Effector cells include four types of helper T cells, namely, Th1, Th2, T_{FH}, Th17, and regulatory T cells, depending on the cytokines they encounter (49, 50). The mature DCs are divided into three major subsets of conventional DCs (cDC1s and cDC2s) and plasmacytoid DCs (pDCs). cDC1 has a high intrinsic capacity to cross-present antigens *via* MHC class I to activate $CD8^+$ T cells and to promote Th1. cDC2 influences a wide range of naive T cell differentiation to Th1, Th2, Th17, and $CD8^+$ T cells (51). Although pDCs are specialized to respond to viral infection with a massive production of type I interferons (IFNs), they also act as APCs and control T cell responses (28).

Both sulfate group content and position in CS are important for Th1 cell-promoted activity of murine splenocytes in terms of cytokine production (52). CSA exhibits the highest cytokine production activity in murine splenocytes. In contrast, CSE decreases Th1-promoted and Th2-inhibitory activity (53). A CSPG fraction mainly of aggrecan extracted from salmon nasal cartilage attenuates the severity of experimental autoimmune encephalomyelitis (EAE), by suppressing the differentiation of the Th17 lineage, and enhances regulatory T cell expansion (54). In EAE mice, treatment with CSD disaccharides inhibits the expression of IFN-γ in the brain (55). CSD treatment also obviously alleviates the clinical symptoms of EAE by limiting T cell infiltration and microglial activation. However, CSA treatment exacerbates EAE symptoms by stimulating T cell infiltration in the central nervous system (CNS) and inducing their differentiation into Th1 and Th17 lineages (56). Moreover, CSC displayed a neuroprotective effect in EAE and may inhibit the spread of pathogenic T cells in the CNS (57). DCs play a pivotal role in promoting unbalanced active immune responses, resulting in the progression of autoimmune diseases. These results suggest that CS could regulate DC function, which leads to designated T cell differentiation.

RECEPTORS OF CHONDROITIN SULFATE ON ANTIGEN-PRESENTING CELLS

Toll-Like Receptors

The components of ECM are recognized by TLRs as DAMPs. To date, 13 mammalian TLRs have been identified. Each TLR recognizes specific PAMPs and DAMPs including lipopeptides for TLR1, TLR2, and TLR6, LPS for TLR4, bacterial flagellin for TLR5, dsRNA for TLR3, ssRNA for TLR7 and TLR8, and DNA for TLR9 (58). TLR2 and TLR4 can also be activated by endogenous ligands or DAMPs (59, 60). A small proteoglycan biglycan stimulates macrophage activation *via* TLR2 or TLR4. The effect is significantly reduced in

TLR4-mutant and TLR2$^{-/-}$ macrophages and abolished in TLR2$^{-/-}$/TLR4-mutant macrophages (61). In cancer-associated inflammation, tumor-derived versican causes a dysfunction of DCs *via* activation of their TLR2 (62). Versican also facilitates Lewis lung carcinoma metastasis through TLR2 and its co-receptor TLR6 (63). Although versican and biglycan are CSPGs, these reports did not mention whether CS or core protein is responsible for these effects. In macrophage-like cell line, smaller sized CSA or its disaccharides suppress IL-6 secretion, whereas no such size-dependent suppression was apparent for CSC (21). CSA and CSC significantly inhibit NF-κB activity and inflammatory cytokines *via* TLR4 (64). To elucidate the structure–function relationship between CSs and TLRs, further studies are expected.

Receptor-Type Protein Tyrosine Phosphatase Sigma

The receptor-type protein tyrosine phosphatase sigma (RPTPσ) is found as an inhibitor of axonal growth and nerve regeneration with CS (65), and is a cell-surface protein that has intracellular tyrosine phosphatase activity and extracellular domains. RPTPσ is one of the type IIa RPTPs, and others are leukocyte common antigen-related (LAR) and RPTPδ. Out of the three, RPTPσ is expressed in several immune cells, including DCs, and is essential for regulating immune cell activation, cytokine production, and inflammation (66, 67). RPTPσ interacts with both CS and HP/HS in the nervous system, with a resembling binding affinity (65, 68, 69). CS and HP/HS compete for the same binding site of RPTPσ in the first Ig-like domain and result in opposing effects on axon elongation. Crystallographic analysis suggests that CS can prevent RPTPσ dimerization, while HS induces RPTPσ clustering (70). Using a biotin-conjugated CS GAG library composed of chemoenzymatically synthesized CS species, RPTPσ binds to CSE with 10-kDa molecular mass, but not to CSA or CSC (71).

RPTPσ acts as a receptor to inhibit autoimmune-related inflammation by preventing DC hyperactivation (66). Since RPTPσ is crucial for suppressing immune responses mediated by DCs, the CS function through RPTPσ might contribute to various immune-related diseases.

CD44

CD44 is a transmembrane glycoprotein that exhibits extensive molecular heterogeneity. The CD44 ectodomain is responsible for binding HA; low-molecular-weight HA triggers TLR-mediated inflammation (72–74). In macrophages, biglycan and HA induce autophagy through interaction with CD44 (75, 76). Besides biglycan and HA, versican (77), osteopontin (78, 79), and macrophage migration inhibitory factor (80) are also ligands of CD44. The cytoplasmic domain modulates inflammatory signaling in a ligand-dependent manner *via* TLR2 and TLR4 activity (76, 79, 80).

CD44 is dramatically overexpressed on the surface of activated macrophages found at sites of inflammation, as such, it has been widely used as a receptor for targeted drug delivery (81–83). Given the relationship between CS and CD44, CS can be used to modify nanoparticles to enhance the cellular uptake of nanoparticles *via* CD44-mediated endocytosis (84, 85). Remarkably, CS exhibits a high affinity for CD44 and facilitates cell internalization *via* CD44-mediated endocytosis (86, 87).

THE ROLE OF CORE PROTEIN IN CHONDROITIN SULFATE PROTEOGLYCAN

Versican

Versican is a large CSPG in the ECM and comprises a core protein of approximately 400 kDa, with approximately 20 attachment sites for CS side chains (88, 89). The core protein contains an N-terminal G1 domain and a C terminal G3 domain, with CS-attached domains between the two globular domains, and comprises four alternative splicing forms (V0, V1, V2, and V3). Versican interacts with HA at the G1 domain and other ECM molecules at the G3 domain. Versican acts on inflammatory responses as a DAMP *via* cell surface proteins such as CD44 (77, 90), CD162 (91), TLR2, TLR6, and CD14 (63, 92).

The versican gene is upregulated in monocytes/macrophages in some pro-inflammatory states, such as myocardial infarction (93), coronary stenosis (94), and autoimmunity (95–97). Experiments performed *in vitro* using classically activated murine bone marrow-derived macrophages treated with LPS showed that M1 type of macrophages exhibited a high expression level of versican mRNA, as well as versican accumulation (98). In human monocyte-to-macrophage differentiation and polarization, the versican gene expression level of M1 macrophages is higher than that of M2 macrophages (99). CSA and V1 core protein were upregulated in the perivascular cuff of multiple sclerosis and EAE and migration of leukocytes including macrophages across the glia limitans into the CNS parenchyma (100).

Versican secreted by Lewis lung carcinoma cells interacts with TLR2 on DCs and sensitizes DCs to respond with IL-6 and IL-10 by increasing the expression of cell surface receptors for IL-6 and IL-10 (62). This result indicates the protumor properties of intact versican. On the other hand, versikine, a degradation product of versican, also interacts with TLR2 on macrophages and acts with antitumor properties (101–103). Versikine is a 70-kDa N-terminal fragment (104), including the G1 domain and lacking CS-attached and the G3 domains. As the intact versican possesses a lot of functional domains including CS, there might be different manners to interact with TLR2.

We previously showed that embryonic fibroblasts, which express the mutant versican lacking the A-subdomain of the G1 domain, attain cell senescence (105). As there is a higher content of CSC and CSE in their conditioned media, the CS composition of the mutant versican could be altered (106). Changes in CS composition are probably caused by the changed core proteins.

Biglycan

The small leucine-rich proteoglycans (SLRPs) in the ECM regulate cell function in the inflammatory sites. Their core proteins have leucine-rich repeat (LRR) motifs and are attached with the CS and/or DS side chains. Biglycan is one of the SLRPs (107, 108) and consists of a 42-kDa core protein containing 10 LRRs and up to two covalently bound CS and/or DS side chains. Biglycan interacts with types I, II, III, and VI collagen

and regulates collagen fibrillogenesis (109–112). This regulation is mediated by the core protein, whereas the CS/DS side chains maintain interfibrillar space by extending outward from the protein core (113). The soluble form of biglycan initiates and perpetuates the inflammatory response by activating TLR2 and TLR4, and biglycan-deficient mice are less susceptible to death caused by TLR2- or TLR4-dependent sepsis (61). It is important that the biglycan core protein directly binds to CD44, and the GAG side chains enhance this interaction (75). Both the biglycan core protein and GAG side chain are also necessary for IL-1β maturation of macrophages (114). Sulfated CS/DS side chains are also implicated in lipid retention by direct interaction with low-density lipoprotein (LDL). In atherosclerotic plaque, LDL colocalizes with biglycan. The interaction between LDL and PGs promotes modification and aggregation of LDL, and uptake of LDL by macrophages leads to foam cell formation (115). Therefore, biglycan core protein plays a pivotal role in the suppression of inflammation and the transition from innate to adaptive immunity (116). Recently, an excellent review reported that biglycan, HA, and versican as the matrix-derived DAMPs regulate TLR-, CD14-, and CD44-signaling cross talk between inflammation and autophagy (85).

Syndecan

The syndecan (SDC) family of cell surface heparan sulfate proteoglycan mediates cell–cell and cell–matrix interactions *via* the GAG chains and is also important in the regulation of inflammation. SDCs are type I transmembrane proteoglycans and consist of four distinct members whose ectodomain varies among the members. SDC1 is widely expressed in epithelia and leukocytes. SDC2 is mainly expressed in endothelial cells and fibroblasts. SDC3 is expressed in neural tissues (117). SDC4 is abundant in many cell types and a soluble protein isoform lacking the transmembrane and cytoplasmic domains (118). Though HS is usually covalently attached to SDCs, SDC1 and SDC3 also bear two CS chains (119). Deletion of SDC1 leads to an exacerbation of allergic asthma (120). SDC4-deficient mice exhibit increased susceptibility to endotoxin shock (121). Although ubiquitous SDC4 expression is low in a steady state, SDC4 expression elevates in mice post-LPS stimulation of macrophages (122). Immature DCs express increased glypican-1 and SDC1 compared to mature DCs, whereas mature DCs express glypican-3, which was not present in immature DCs (123). Research has illustrated that SDC1 on DC negatively regulates DC migration; therefore, lower SDC1 expression levels are often associated with mature DCs (124). Furthermore, the functional switch from SDC1 to SDC4 expression during DC maturation controls DC motility and subsequent migration from peripheral sites to lymphoid tissues (125).

CONCLUSION

This mini-review described regulation of CS on APCs with their different structures through their specific receptors at inflammatory sites. CS exhibits both pro- and anti-inflammatory activities with their heterogeneous structures. Even with the same structure, CS affects differently depending on the target cells and their microenvironments. Regarding their sulfation patterns, CSC and CSD have anti-inflammatory activity, whereas CSA has both pro- and anti-inflammatory activities. In many cases, CSE has a potential anti-inflammatory activity, although a recent report suggests its stimulatory effect on tumor progression with the pro-inflammatory activity (6). Regarding the CS chain length, short chains such as oligosaccharides or disaccharides mostly activate inflammation, whereas the long chains serve as anti-inflammatory factors. CS structure and length may vary by the different core proteins and their expressing cells. To understand detailed CS functions in immunity, further investigations into the structure–function relationship of CS are needed.

AUTHOR CONTRIBUTIONS

SH and HW contributed to the conception and design of the study. SH wrote the first draft of the manuscript and wrote sections of the manuscript. All authors contributed to manuscript revision, read and approved the submitted version.

SH took primary responsibility for communication with the journal and editorial office during the submission process, throughout peer review and during publication, ensuring that the submission adheres to all journal requirements including, but not exclusive to, details of authorship, study ethics and ethics approval, clinical trial registration documents and conflict of interest declaration, and available post-publication to respond to any queries or critiques.

FUNDING

This work was supported by JSPS KAKENHI (Grant No. 18H02646 to HW).

ACKNOWLEDGMENTS

We would like to thank Dr. Nobuo Sugiura and Dr. Tatsumasa Shioiri for their advice on CS structures.

REFERENCES

1. Hirose J, Kawashima H, Yoshie O, Tashiro K, Miyasaka M. Versican interacts with chemokines and modulates cellular responses. *J Biol Chem*. (2001) 276:5228–34. doi: 10.1074/jbc.M007542200
2. Luster AD, Greenberg SM, Leder P. The IP-10 chemokine binds to a specific cell surface heparan sulfate site shared with platelet factor 4 and inhibits endothelial cell proliferation. *J Exp Med*. (1995) 182:219–31. doi: 10.1084/jem.182.1.219
3. Kuschert GS, Hoogewerf AJ, Proudfoot AE, Chung CW, Cooke RM, Hubbard RE, et al. Identification of a glycosaminoglycan binding surface on human interleukin-8. *Biochemistry*. (1998) 37:11193–201. doi: 10.1021/bi972867o
4. Mizuguchi S, Uyama T, Kitagawa H, Nomura KH, Dejima K, Gengyo-Ando K, et al. Chondroitin proteoglycans are involved in cell division of *Caenorhabditis elegans*. *Nature*. (2003) 423:443–8. doi: 10.1038/nature01635
5. Kawakami Y, Kurihara Y, Saito Y, Fujita Y, Yamashita T, Takei K. The soluble form of LOTUS inhibits nogo receptor-mediated signaling

by interfering with the interaction between nogo receptor type 1 and p75 neurotrophin receptor. *J Neurosci*. (2018) 38:2589–604. doi: 10.1523/JNEUROSCI.0953-17.2018
6. Kastana P, Choleva E, Poimenidi E, Karamanos N, Sugahara K, Papadimitriou E. Insight into the role of chondroitin sulfate E in angiogenesis. *FEBS J*. (2019) 286:2921–36. doi: 10.1111/febs.14830
7. Zhang F, Zheng L, Cheng S, Peng Y, Fu L, Zhang X, et al. Comparison of the interactions of different growth factors and glycosaminoglycans. *Molecules*. (2019) 24:E3360. doi: 10.3390/molecules24183360
8. Parish CR. The role of heparan sulphate in inflammation. *Nat Rev Immunol*. (2006) 6:633–43. doi: 10.1038/nri1918
9. Webb LM, Ehrengruber MU, Clark-Lewis I, Baggiolini M, Rot A. Binding to heparan sulfate or heparin enhances neutrophil responses to interleukin 8. *Proc Natl Acad Sci USA*. (1993) 90:7158–62. doi: 10.1073/pnas.90.15.7158
10. Petrey AC, de la Motte CA. Hyaluronan, a crucial regulator of inflammation. *Front Immunol*. (2014) 5:101. doi: 10.3389/fimmu.2014.00101
11. Stern R, Asari AA, Sugahara KN. Hyaluronan fragments: an information-rich system. *Eur J Cell Biol*. (2006) 85:699–715. doi: 10.1016/j.ejcb.2006.05.009
12. Kang I, Harten IA, Chang MY, Braun KR, Sheih A, Nivison MP, et al. Versican deficiency significantly reduces lung inflammatory response induced by polyinosine-polycytidylic acid stimulation. *J Biol Chem*. (2017) 292:51–63. doi: 10.1074/jbc.M116.753186
13. Andersson-Sjoland A, Hallgren O, Rolandsson S, Weitoft M, Tykesson E, Larsson-Callerfelt AK, et al. Versican in inflammation and tissue remodeling: the impact on lung disorders. *Glycobiology*. (2015) 25:243–51. doi: 10.1093/glycob/cwu120
14. Wight TN. Provisional matrix: a role for versican and hyaluronan. *Matrix Biol*. (2017) 60–61:38–56. doi: 10.1016/j.matbio.2016.12.001
15. Blackwood RA, Cantor JO, Moret J, Mandl I, Turino GM. Glycosaminoglycan synthesis in endotoxin-induced lung injury. *Proc Soc Exp Biol Med*. (1983) 174:343–9. doi: 10.3181/00379727-174-41746
16. Xu CX, Jin H, Chung YS, Shin JY, Woo MA, Lee KH, et al. Chondroitin sulfate extracted from the styela clava tunic suppresses TNF-alpha-induced expression of inflammatory factors, VCAM-1 and iNOS by blocking Akt/NF-kappaB signal in JB6 cells. *Cancer Lett*. (2008) 264:93–100. doi: 10.1016/j.canlet.2008.01.022
17. Du Y, Carlson EC, Funderburgh ML, Birk DE, Pearlman E, Guo N, et al. Stem cell therapy restores transparency to defective murine corneas. *Stem Cells*. (2009) 27:1635–42. doi: 10.1002/stem.91
18. Stabler TV, Huang Z, Montell E, Verges J, Kraus VB. Chondroitin sulphate inhibits NF-kappaB activity induced by interaction of pathogenic and damage associated molecules. *Osteoarthritis Cartilage*. (2017) 25:166–74. doi: 10.1016/j.joca.2016.08.012
19. Volpi N. Anti-inflammatory activity of chondroitin sulphate: new functions from an old natural macromolecule. *Inflammopharmacology*. (2011) 19:299–306. doi: 10.1007/s10787-011-0098-0
20. du Souich P, Garcia AG, Verges J, Montell E. Immunomodulatory and anti-inflammatory effects of chondroitin sulphate. *J Cell Mol Med*. (2009) 13:1451–63. doi: 10.1111/j.1582-4934.2009.00826.x
21. Jin M, Iwamoto T, Yamada K, Satsu H, Totsuka M, Shimizu M. Effects of chondroitin sulfate and its oligosaccharides on toll-like receptor-mediated IL-6 secretion by macrophage-like J774.1 cells. *Biosci Biotechnol Biochem*. (2011) 75:1283–9. doi: 10.1271/bbb.110055
22. Shioiri T, Tsuchimoto J, Watanabe H, Sugiura N. Sequence determination of synthesized chondroitin sulfate dodecasaccharides. *Glycobiology*. (2016) 26:592–606. doi: 10.1093/glycob/cww008
23. Sugiura N, Shioiri T, Chiba M, Sato T, Narimatsu H, Kimata K, et al. Construction of a chondroitin sulfate library with defined structures and analysis of molecular interactions. *J Biol Chem*. (2012) 287:43390–400. doi: 10.1074/jbc.M112.412676
24. Sugiura N, Clausen TM, Shioiri T, Gustavsson T, Watanabe H, Salanti A. Molecular dissection of placental malaria protein VAR2CSA interaction with a chemo-enzymatically synthesized chondroitin sulfate library. *Glycoconj J*. (2016) 33:985–94. doi: 10.1007/s10719-016-9685-z
25. ten Broeke T, Wubbolts R, Stoorvogel W. MHC class II antigen presentation by dendritic cells regulated through endosomal sorting. *Cold Spring Harb Perspect Biol*. (2013) 5:a016873. doi: 10.1101/cshperspect.a016873
26. Steinman RM. The dendritic cell system and its role in immunogenicity. *Annu Rev Immunol*. (1991) 9:271–96. doi: 10.1146/annurev.iy.09.040191.001415
27. Gaudino SJ, Kumar P. Cross-talk between antigen presenting cells and T cells impacts intestinal homeostasis, bacterial infections, and tumorigenesis. *Front Immunol*. (2019) 10:360. doi: 10.3389/fimmu.2019.00360
28. Geissmann F, Manz MG, Jung S, Sieweke MH, Merad M, Ley K. Development of monocytes, macrophages, and dendritic cells. *Science*. (2010) 327:656–61. doi: 10.1126/science.1178331
29. Grabowska J, Lopez-Venegas MA, Affandi AJ, den Haan JMM. CD169^{+} macrophages capture and dendritic cells instruct: the interplay of the gatekeeper and the general of the immune system. *Front Immunol*. (2018) 9:2472. doi: 10.3389/fimmu.2018.02472
30. Roszer T. Understanding the mysterious M2 macrophage through activation markers and effector mechanisms. *Mediators Inflamm*. (2015) 2015:816460. doi: 10.1155/2015/816460
31. Liao WT, You HL, Li C, Chang JG, Chang SJ, Chen CJ. Cyclic GMP-dependent protein kinase II is necessary for macrophage M1 polarization and phagocytosis via toll-like receptor 2. *J Mol Med*. (2015) 93:523–33. doi: 10.1007/s00109-014-1236-0
32. Zhang X, Xu F, Liu L, Feng L, Wu X, Shen Y, et al. (+)-Borneol improves the efficacy of edaravone against DSS-induced colitis by promoting M2 macrophages polarization via JAK2-STAT3 signaling pathway. *Int Immunopharmacol*. (2017) 53:1–10. doi: 10.1016/j.intimp.2017.10.002
33. Guilliams M, van de Laar L. A hitchhiker's guide to myeloid cell subsets: practical implementation of a novel mononuclear phagocyte classification system. *Front Immunol*. (2015) 6:406. doi: 10.3389/fimmu.2015.00406
34. Gordon S, Plüddemann A. The mononuclear phagocytic system. Generation of diversity. *Front Immunol*. (2019) 10:1893. doi: 10.3389/fimmu.2019.01893
35. Jomphe C, Gabriac M, Hale TM, Heroux L, Trudeau LE, Deblois D, et al. Chondroitin sulfate inhibits the nuclear translocation of nuclear factor-kappaB in interleukin-1beta-stimulated chondrocytes. *Basic Clin Pharmacol Toxicol*. (2008) 102:59–65. doi: 10.1111/j.1742-7843.2007.00158.x
36. da Cunha AL, Aguiar JAK, Correa da Silva FS, Michelacci YM. Do chondroitin sulfates with different structures have different activities on chondrocytes and macrophages?. *Int J Biol Macromol*. (2017) 103:1019–31. doi: 10.1016/j.ijbiomac.2017.05.123
37. Gouze JN, Gouze E, Popp MP, Bush ML, Dacanay EA, Kay JD, et al. Exogenous glucosamine globally protects chondrocytes from the arthritogenic effects of IL-1beta. *Arthritis Res Ther*. (2006) 8:R173. doi: 10.1186/ar2082
38. Taraballi F, Corradetti B, Minardi S, Powel S, Cabrera F, Van Eps JL, et al. Biomimetic collagenous scaffold to tune inflammation by targeting macrophages. *J Tissue Eng*. (2016) 7:2041731415624667. doi: 10.1177/2041731415624667
39. Zhang W, Sun F, Niu H, Wang Q, Duan J. Mechanistic insights into cellular immunity of chondroitin sulfate A and its zwitterionic N-deacetylated derivatives. *Carbohydr Polym*. (2015) 123:331–8. doi: 10.1016/j.carbpol.2015.01.059
40. Tan GK, Tabata Y. Chondroitin-6-sulfate attenuates inflammatory responses in murine macrophages via suppression of NF-kappaB nuclear translocation. *Acta Biomater*. (2014) 10:2684–92. doi: 10.1016/j.actbio.2014.02.025
41. Kaufmann SHE. Immunology's coming of age. *Front Immunol*. (2019) 10:684. doi: 10.3389/fimmu.2019.01214
42. Yamada N, Katz SI. Generation of mature dendritic cells from a CD14+ cell line (XS52) by IL-4, TNF-alpha, IL-1 beta, and agonistic anti-CD40 monoclonal antibody. *J Immunol*. (1999) 163:5331–7.
43. Banchereau J, Steinman RM. Dendritic cells and the control of immunity. *Nature*. (1998) 392:245–52. doi: 10.1038/32588

44. Rescigno M, Granucci F, Citterio S, Foti M, Ricciardi-Castagnoli P. Coordinated events during bacteria-induced DC maturation. *Immunol Today*. (1999) 20:200–3. doi: 10.1016/S0167-5699(98)01427-3
45. Jakob T, Walker PS, Krieg AM, Udey MC, Vogel JC. Activation of cutaneous dendritic cells by CpG-containing oligodeoxynucleotides: a role for dendritic cells in the augmentation of Th1 responses by immunostimulatory DNA. *J Immunol*. (1998) 161:3042–9.
46. Nierkens S, Tel J, Janssen E, Adema GJ. Antigen cross-presentation by dendritic cell subsets: one general or all sergeants? *Trends Immunol*. (2013) 34:361–70. doi: 10.1016/j.it.2013.02.007
47. Iwasaki A, Medzhitov R. Regulation of adaptive immunity by the innate immune system. *Science*. (2010) 327:291–5. doi: 10.1126/science.1183021
48. Iwasaki A, Medzhitov R. Control of adaptive immunity by the innate immune system. *Nat Immunol*. (2015) 16:343–53. doi: 10.1038/ni.3123
49. Huang C, Yang X, Huang J, Liu X, Yang X, Jin H, et al. Porcine beta-defensin 2 provides protection against bacterial infection by a direct bactericidal activity and alleviates inflammation via interference with the TLR4/NF-kappaB pathway. *Front Immunol*. (2019) 10:1673. doi: 10.3389/fimmu.2019.01673
50. Zhu J, Paul WE. CD4 T cells: fates, functions, and faults. *Blood*. (2008) 112:1557–69. doi: 10.1182/blood-2008-05-078154
51. Collin M, Bigley V. Human dendritic cell subsets: an update. *Immunology*. (2018) 154:3–20. doi: 10.1111/imm.12888
52. Akiyama H, Sakai S, Linhardt RJ, Goda Y, Toida T, Maitani T. Chondroitin sulphate structure affects its immunological activities on murine splenocytes sensitized with ovalbumin. *Biochem J*. (2004) 382:269–78. doi: 10.1042/BJ20031851
53. Toida T, Sakai S, Akiyama H, Linhardt RJ. Immunological activity of chondroitin sulfate. *Adv Pharmacol*. (2006) 53:403–15. doi: 10.1016/S1054-3589(05)53019-9
54. Sashinami H, Asano K, Yoshimura S, Mori F, Wakabayashi K, Nakane A. Salmon proteoglycan suppresses progression of mouse experimental autoimmune encephalomyelitis via regulation of Th17 and Foxp3(+) regulatory T cells. *Life Sci*. (2012) 91:1263–9. doi: 10.1016/j.lfs.2012.09.022
55. Rolls A, Cahalon L, Bakalash S, Avidan H, Lider O, Schwartz M. A sulfated disaccharide derived from chondroitin sulfate proteoglycan protects against inflammation-associated neurodegeneration. *FASEB J*. (2006) 20:547–9. doi: 10.1096/fj.05-4540fje
56. Zhou J, Nagarkatti P, Zhong Y, Nagarkatti M. Immune modulation by chondroitin sulfate and its degraded disaccharide product in the development of an experimental model of multiple sclerosis. *J Neuroimmunol*. (2010) 223:55–64. doi: 10.1016/j.jneuroim.2010.04.002
57. Miyamoto T, Inoue H, Sakamoto Y, Kudo E, Naito T, Mikawa T, et al. Identification of a novel splice site mutation of the CSPG2 gene in a Japanese family with wagner syndrome. *Invest Ophthalmol Vis Sci*. (2005) 46:2726–35. doi: 10.1167/iovs.05-0057
58. Sun L, Liu W, Zhang LJ. The role of toll-like receptors in skin host defense, psoriasis, and atopic dermatitis. *J Immunol Res*. (2019) 2019:1824624. doi: 10.1155/2019/1824624
59. Gallo RL, Bernard JJ. Innate immune sensors stimulate inflammatory and immunosuppressive responses to UVB radiation. *J Invest Dermatol*. (2014) 134:1508–11. doi: 10.1038/jid.2014.32
60. Yu L, Wang L, Chen S. Endogenous toll-like receptor ligands and their biological significance. *J Cell Mol Med*. (2010) 14:2592–603. doi: 10.1111/j.1582-4934.2010.01127.x
61. Schaefer L, Babelova A, Kiss E, Hausser HJ, Baliova M, Krzyzankova M, et al. The matrix component biglycan is proinflammatory and signals through toll-like receptors 4 and 2 in macrophages. *J Clin Invest*. (2005) 115:2223–33. doi: 10.1172/JCI23755
62. Tang M, Diao J, Gu H, Khatri I, Zhao J, Cattral MS. Toll-like receptor 2 activation promotes tumor dendritic cell dysfunction by regulating IL-6 and IL-10 receptor signaling. *Cell Rep*. (2015) 13:2851–64. doi: 10.1016/j.celrep.2015.11.053
63. Kim S, Takahashi H, Lin WW, Descargues P, Grivennikov S, Kim Y, et al. Carcinoma-produced factors activate myeloid cells through TLR2 to stimulate metastasis. *Nature*. (2009) 457:102–6. doi: 10.1038/nature07623
64. Campo GM, Avenoso A, Campo S, Traina P, D'Ascola A, Calatroni A. Glycosaminoglycans reduced inflammatory response by modulating toll-like receptor-4 in LPS-stimulated chondrocytes. *Arch Biochem Biophys*. (2009) 491:7–15. doi: 10.1016/j.abb.2009.09.017
65. Shen Y, Tenney AP, Busch SA, Horn KP, Cuascut FX, Liu K, et al. PTPsigma is a receptor for chondroitin sulfate proteoglycan, an inhibitor of neural regeneration. *Science*. (2009) 326:592–6. doi: 10.1126/science.1178310
66. Ohtake Y, Wong D, Abdul-Muneer PM, Selzer ME, Li S. Two PTP receptors mediate CSPG inhibition by convergent and divergent signaling pathways in neurons. *Sci Rep*. (2016) 6:37152. doi: 10.1038/srep37152
67. Ohtake Y, Saito A, Li S. Diverse functions of protein tyrosine phosphatase sigma in the nervous and immune systems. *Exp Neurol*. (2018) 302:196–204. doi: 10.1016/j.expneurol.2018.01.014
68. Fisher D, Xing B, Dill J, Li H, Hoang HH, Zhao Z, et al. Leukocyte common antigen-related phosphatase is a functional receptor for chondroitin sulfate proteoglycan axon growth inhibitors. *J Neurosci*. (2011) 31:14051–66. doi: 10.1523/JNEUROSCI.1737-11.2011
69. Dickendesher TL, Baldwin KT, Mironova YA, Koriyama Y, Raiker SJ, Askew KL, et al. NgR1 and NgR3 are receptors for chondroitin sulfate proteoglycans. *Nat Neurosci*. (2012) 15:703–12. doi: 10.1038/nn.3070
70. Coles CH, Shen Y, Tenney AP, Siebold C, Sutton GC, Lu W, et al. Proteoglycan-specific molecular switch for RPTPsigma clustering and neuronal extension. *Science*. (2011) 332:484–8. doi: 10.1126/science.1200840
71. Tadai K, Shioiri T, Tsuchimoto J, Nagai N, Watanabe H, Sugiura N. Interaction of receptor type of protein tyrosine phosphatase sigma (RPTPsigma) with a glycosaminoglycan library. *J Biochem*. (2018) 164:41–51. doi: 10.1093/jb/mvy027
72. Ruppert SM, Hawn TR, Arrigoni A, Wight TN, Bollyky PL. Tissue integrity signals communicated by high-molecular weight hyaluronan and the resolution of inflammation. *Immunol Res*. (2014) 58:186–92. doi: 10.1007/s12026-014-8495-2
73. Powell JD, Horton MR. Threat matrix: low-molecular-weight hyaluronan (HA) as a danger signal. *Immunol Res*. (2005) 31:207–18. doi: 10.1385/IR:31:3:207
74. Hauser-Kawaguchi A, Luyt LG, Turley E. Design of peptide mimetics to block pro-inflammatory functions of HA fragments. *Matrix Biol*. (2019) 78–79:346–56. doi: 10.1016/j.matbio.2018.01.021
75. Poluzzi C, Nastase MV, Zeng-Brouwers J, Roedig H, Hsieh LT, Michaelis JB, et al. Biglycan evokes autophagy in macrophages via a novel CD44/Toll-like receptor 4 signaling axis in ischemia/reperfusion injury. *Kidney Int*. (2019) 95:540–62. doi: 10.1016/j.kint.2018.10.037
76. Taylor KR, Yamasaki K, Radek KA, Di Nardo A, Goodarzi H, Golenbock D, et al. Recognition of hyaluronan released in sterile injury involves a unique receptor complex dependent on toll-like receptor 4, CD44, and MD-2. *J Biol Chem*. (2007) 282:18265–75. doi: 10.1074/jbc.M606352200
77. Wu YJ, La Pierre DP, Wu J, Yee AJ, Yang BB. The interaction of versican with its binding partners. *Cell Res*. (2005) 15:483–94. doi: 10.1038/sj.cr.7290318
78. Kahles F, Findeisen HM, Bruemmer D. Osteopontin: a novel regulator at the cross roads of inflammation, obesity and diabetes. *Mol Metab*. (2014) 3:384–93. doi: 10.1016/j.molmet.2014.03.004
79. Castello LM, Raineri D, Salmi L, Clemente N, Vaschetto R, Quaglia M, et al. Osteopontin at the crossroads of inflammation and tumor progression. *Mediators Inflamm*. (2017) 2017:4049098. doi: 10.1155/2017/4049098
80. Shi X, Leng L, Wang T, Wang W, Du X, Li J, et al. CD44 is the signaling component of the macrophage migration inhibitory factor-CD74 receptor complex. *Immunity*. (2006) 25:595–606. doi: 10.1016/j.immuni.2006.08.020
81. Alam MM, Han HS, Sung S, Kang JH, Sa KH, Al Faruque H, et al. Endogenous inspired biomineral-installed hyaluronan nanoparticles as pH-responsive carrier of methotrexate for rheumatoid arthritis. *J Control Release*. (2017) 252:62–72. doi: 10.1016/j.jconrel.2017.03.012
82. Xiao B, Zhang Z, Viennois E, Kang Y, Zhang M, Han MK, et al. Combination therapy for ulcerative colitis: orally targeted nanoparticles prevent mucosal damage and relieve inflammation. *Theranostics*. (2016) 6:2250–66. doi: 10.7150/thno.15710
83. Rios de la Rosa JM, Tirella A, Gennari A, Stratford IJ, Tirelli N. The CD44-Mediated uptake of hyaluronic acid-based carriers in macrophages. *Adv Healthc Mater*. (2017) 6:201601012. doi: 10.1002/adhm.201601012

84. Lee JY, Chung SJ, Cho HJ, Kim DD. Bile acid-conjugated chondroitin sulfate a-based nanoparticles for tumor-targeted anticancer drug delivery. *Eur J Pharm Biopharm*. (2015) 94:532–41. doi: 10.1016/j.ejpb.2015.06.011
85. Roedig H, Damiescu R, Zeng-Brouwers J, Kutija I, Trebicka J, Wygrecka M, et al. Danger matrix molecules orchestrate CD14/CD44 signaling in cancer development. *Semin Cancer Biol*. (2019). doi: 10.1016/j.semcancer.2019.07.026. [Epub ahead of print].
86. Zhou B, Weigel JA, Fauss L, Weigel PH. Identification of the hyaluronan receptor for endocytosis (HARE). *J Biol Chem*. (2000) 275:37733–41. doi: 10.1074/jbc.M003030200
87. Tsai HY, Chiu CC, Lin PC, Chen SH, Huang SJ, Wang LF. Antitumor efficacy of doxorubicin released from crosslinked nanoparticulate chondroitin sulfate/chitosan polyelectrolyte complexes. *Macromol Biosci*. (2011) 11:680–8. doi: 10.1002/mabi.201000456
88. Zimmermann DR, Ruoslahti E. Multiple domains of the large fibroblast proteoglycan, versican. *Embo J*. (1989) 8:2975–81. doi: 10.1002/j.1460-2075.1989.tb08447.x
89. Shinomura T, Nishida Y, Ito K, Kimata K, Kern, Kern CB. CDNA cloning of PG-M, a large chondroitin sulfate proteoglycan expressed during chondrogenesis in chick limb buds. Alternative spliced multiforms of PG-M and their relationships to versican. *J Biol Chem*. (1993) 268:14461–9.
90. Kawashima H, Hirose M, Hirose J, Nagakubo D, Plaas AH, Miyasaka M. Binding of a large chondroitin sulfate/dermatan sulfate proteoglycan, versican, to L-selectin, P-selectin, and CD44. *J Biol Chem*. (2000) 275:35448–56. doi: 10.1074/jbc.M003387200
91. Zheng PS, Wen J, Ang LC, Sheng W, Viloria-Petit A, Wang Y, et al. Versican/PG-M G3 domain promotes tumor growth and angiogenesis. *Faseb J*. (2004) 18:754–6. doi: 10.1096/fj.03-0545fje
92. Wang W, Xu GL, Jia WD, Ma JL, Li JS, Ge YS, et al. Ligation of TLR2 by versican: a link between inflammation and metastasis. *Arch Med Res*. (2009) 40:321–3. doi: 10.1016/j.arcmed.2009.04.005
93. Toeda K, Nakamura K, Hirohata S, Hatipoglu OF, Demircan K, Yamawaki H, et al. Versican is induced in infiltrating monocytes in myocardial infarction. *Mol Cell Biochem*. (2005) 280:47–56. doi: 10.1007/s11010-005-8051-4
94. Wingrove JA, Daniels SE, Sehnert AJ, Tingley W, Elashoff MR, Rosenberg S, et al. Correlation of peripheral-blood gene expression with the extent of coronary artery stenosis. *Circ Cardiovasc Genet*. (2008) 1:31–8. doi: 10.1161/CIRCGENETICS.108.782730
95. Olsen NJ, Moore JH, Aune TM. Gene expression signatures for autoimmune disease in peripheral blood mononuclear cells. *Arthritis Res Ther*. (2004) 6:120–8. doi: 10.1186/ar1190
96. Shou J, Bull CM, Li L, Qian HR, Wei T, Luo S, et al. Identification of blood biomarkers of rheumatoid arthritis by transcript profiling of peripheral blood mononuclear cells from the rat collagen-induced arthritis model. *Arthritis Res Ther*. (2006) 8:R28. doi: 10.1186/ar1883
97. Masuda A, Yasuoka H, Satoh T, Okazaki Y, Yamaguchi Y, Kuwana M. Versican is upregulated in circulating monocytes in patients with systemic sclerosis and amplifies a CCL2-mediated pathogenic loop. *Arthritis Res Ther*. (2013) 15:R74. doi: 10.1186/ar4251
98. Chang MY, Tanino Y, Vidova V, Kinsella MG, Chan CK, Johnson PY, et al. A rapid increase in macrophage-derived versican and hyaluronan in infectious lung disease. *Matrix Biol*. (2014) 34:1–12. doi: 10.1016/j.matbio.2014.01.011
99. Martinez FO, Gordon S, Locati M, Mantovani A. Transcriptional profiling of the human monocyte-to-macrophage differentiation and polarization: new molecules and patterns of gene expression. *J Immunol*. (2006) 177:7303–11. doi: 10.4049/jimmunol.177.10.7303
100. Stephenson EL, Mishra MK, Moussienko D, Laflamme N, Rivest S, Ling CC, et al. Chondroitin sulfate proteoglycans as novel drivers of leucocyte infiltration in multiple sclerosis. *Brain*. (2018) 141:1094–110. doi: 10.1093/brain/awy033
101. Hope C, Foulcer S, Jagodinsky J, Chen SX, Jensen JL, Patel S, et al. Immunoregulatory roles of versican proteolysis in the myeloma microenvironment. *Blood*. (2016) 128:680–5. doi: 10.1182/blood-2016-03-705780
102. Hope C, Emmerich PB, Papadas A, Pagenkopf A, Matkowskyj KA, Van De Hey DR, et al. Versican-derived matrikines regulate batf3-dendritic cell differentiation and promote T cell infiltration in colorectal cancer. *J Immunol*. (2017) 199:1933–41. doi: 10.4049/jimmunol.1700529
103. Binder MJ, McCoombe S, Williams ED, McCulloch DR, Ward AC. The extracellular matrix in cancer progression: role of hyalectan proteoglycans and ADAMTS enzymes. *Cancer Lett*. (2017) 385:55–64. doi: 10.1016/j.canlet.2016.11.001
104. Sandy JD, Westling J, Kenagy RD, Iruela-Arispe ML, Verscharen C, Rodriguez-Mazaneque JC, et al. Versican V1 proteolysis in human aorta in vivo occurs at the Glu441-Ala442 bond, a site that is cleaved by recombinant ADAMTS-1 and ADAMTS-4. *J Biol Chem*. (2001) 276:13372–8. doi: 10.1074/jbc.M009737200
105. Suwan K, Choocheep K, Hatano S, Kongtawelert P, Kimata K, Watanabe H. Versican/PG-M assembles hyaluronan into extracellular matrix and inhibits CD44-mediated signaling toward premature senescence in embryonic fibroblasts. *J Biol Chem*. (2009) 284:8596–604. doi: 10.1074/jbc.M806927200
106. Suwan K, Hatano S, Kongtawelert P, Pothacharoen P, Watanabe H. Alteration of chondroitin sulfate composition on proteoglycan produced by knock-in mouse embryonic fibroblasts whose versican lacks the A subdomain. *Ups J Med Sci*. (2009) 114:73–81. doi: 10.1080/03009730902761722
107. Nastase MV, Young MF, Schaefer L. Biglycan: a multivalent proteoglycan providing structure and signals. *J Histochem Cytochem*. (2012) 60:963–75. doi: 10.1369/0022155412456380
108. Schaefer L, Schaefer RM. Proteoglycans: from structural compounds to signaling molecules. *Cell Tissue Res*. (2010) 339:237–46. doi: 10.1007/s00441-009-0821-y
109. Wiberg C, Hedbom E, Khairullina A, Lamande SR, Oldberg A, Timpl R, et al. Biglycan and decorin bind close to the n-terminal region of the collagen VI triple helix. *J Biol Chem*. (2001) 276:18947–52. doi: 10.1074/jbc.M100625200
110. Wiberg C, Heinegard D, Wenglen C, Timpl R, Morgelin M. Biglycan organizes collagen VI into hexagonal-like networks resembling tissue structures. *J Biol Chem*. (2002) 277:49120–6. doi: 10.1074/jbc.M206891200
111. Wiberg C, Klatt AR, Wagener R, Paulsson M, Bateman JF, Heinegard D, et al. Complexes of matrilin-1 and biglycan or decorin connect collagen VI microfibrils to both collagen II and aggrecan. *J Biol Chem*. (2003) 278:37698–704. doi: 10.1074/jbc.M304638200
112. Douglas T, Heinemann S, Bierbaum S, Scharnweber D, Worch H. Fibrillogenesis of collagen types I, II, and III with small leucine-rich proteoglycans decorin and biglycan. *Biomacromolecules*. (2006) 7:2388–93. doi: 10.1021/bm0603746
113. Iozzo RV. The biology of the small leucine-rich proteoglycans. Functional network of interactive proteins. *J Biol Chem*. (1999) 274:18843–6. doi: 10.1074/jbc.274.27.18843
114. Babelova A, Moreth K, Tsalastra-Greul W, Zeng-Brouwers J, Eickelberg O, Young MF, et al. Biglycan, a danger signal that activates the NLRP3 inflammasome via toll-like and P2X receptors. *J Biol Chem*. (2009) 284:24035–48. doi: 10.1074/jbc.M109.014266
115. Hultgardh-Nilsson A, Boren J, Chakravarti S. The small leucine-rich repeat proteoglycans in tissue repair and atherosclerosis. *J Intern Med*. (2015) 278:447–61. doi: 10.1111/joim.12400
116. Zeng-Brouwers J, Beckmann J, Nastase MV, Iozzo RV, Schaefer L. *De novo* expression of circulating biglycan evokes an innate inflammatory tissue response via MyD88/TRIF pathways. *Matrix Biol*. (2014) 35:132–42. doi: 10.1016/j.matbio.2013.12.003
117. Gondelaud F, Ricard-Blum S. Structures and interactions of syndecans. *FEBS J*. (2019) 286:2994–3007. doi: 10.1111/febs.14828
118. Xing Y, Xu Q, Lee C. Widespread production of novel soluble protein isoforms by alternative splicing removal of transmembrane anchoring domains. *FEBS Lett*. (2003) 555:572–8. doi: 10.1016/S0014-5793(03)01354-1
119. Couchman JR. Transmembrane signaling proteoglycans. *Annu Rev Cell Dev Biol*. (2010) 26:89–114. doi: 10.1146/annurev-cellbio-100109-104126
120. Xu J, Park PW, Kheradmand F, Corry DB. Endogenous attenuation of allergic lung inflammation by syndecan-1. *J Immunol*. (2005) 174:5758–65. doi: 10.4049/jimmunol.174.9.5758

121. Ishiguro K, Kojima T, Muramatsu T. Syndecan-4 as a molecule involved in defense mechanisms. *Glycoconj J*. (2002) 19:315–8. doi: 10.1023/A:1025308702966
122. Ishiguro K, Kadomatsu K, Kojima T, Muramatsu H, Iwase M, Yoshikai Y, et al. Syndecan-4 deficiency leads to high mortality of lipopolysaccharide-injected mice. *J Biol Chem*. (2001) 276:47483–8. doi: 10.1074/jbc.M106268200
123. Wegrowski Y, Milard AL, Kotlarz G, Toulmonde E, Maquart FX, Bernard J. Cell surface proteoglycan expression during maturation of human monocytes-derived dendritic cells and macrophages. *Clin Exp Immunol*. (2006) 144:485–93. doi: 10.1111/j.1365-2249.2006.03059.x
124. Averbeck M, Kuhn S, Buhligen J, Gotte M, Simon JC, Polte T. Syndecan-1 regulates dendritic cell migration in cutaneous hypersensitivity to haptens. *Exp Dermatol*. (2017) 26:1060–7. doi: 10.1111/exd.13374
125. Averbeck M, Gebhardt C, Anderegg U, Termeer C, Sleeman JP, Simon JC. Switch in syndecan-1 and syndecan-4 expression controls maturation associated dendritic cell motility. *Exp Dermatol*. (2007) 16:580–9. doi: 10.1111/j.1600-0625.2007.00568.x

Conflict of Interest: The authors declare that the research was conducted in the absence of any commercial or financial relationships that could be construed as a potential conflict of interest.

frontiers in Immunology

REVIEW
published: 24 March 2020
doi: 10.3389/fimmu.2020.00512

Versican—A Critical Extracellular Matrix Regulator of Immunity and Inflammation

Thomas N. Wight[1]*, *Inkyung Kang*[1], *Stephen P. Evanko*[1], *Ingrid A. Harten*[1], *Mary Y. Chang*[2], *Oliver M. T. Pearce*[3], *Carys E. Allen*[3] and *Charles W. Frevert*[2]

[1] Matrix Biology Program, Benaroya Research Institute at Virginia Mason, Seattle, WA, United States, [2] Division of Pulmonary/Critical Care Medicine, Center for Lung Biology, University of Washington School of Medicine, Seattle, WA, United States, [3] Centre for the Tumour Microenvironment, Barts Cancer Institute, Queen Mary University of London, London, United Kingdom

The extracellular matrix (ECM) proteoglycan, versican increases along with other ECM versican binding molecules such as hyaluronan, tumor necrosis factor stimulated gene-6 (TSG-6), and inter alpha trypsin inhibitor (IαI) during inflammation in a number of different diseases such as cardiovascular and lung disease, autoimmune diseases, and several different cancers. These interactions form stable scaffolds which can act as "landing strips" for inflammatory cells as they invade tissue from the circulation. The increase in versican is often coincident with the invasion of leukocytes early in the inflammatory process. Versican interacts with inflammatory cells either indirectly via hyaluronan or directly via receptors such as CD44, P-selectin glycoprotein ligand-1 (PSGL-1), and toll-like receptors (TLRs) present on the surface of immune and non-immune cells. These interactions activate signaling pathways that promote the synthesis and secretion of inflammatory cytokines such as TNFα, IL-6, and NFκB. Versican also influences inflammation by interacting with a variety of growth factors and cytokines involved in regulating inflammation thereby influencing their bioavailability and bioactivity. Versican is produced by multiple cell types involved in the inflammatory process. Conditional total knockout of versican in a mouse model of lung inflammation demonstrated significant reduction in leukocyte invasion into the lung and reduced inflammatory cytokine expression. While versican produced by stromal cells tends to be pro-inflammatory, versican expressed by myeloid cells can create anti-inflammatory and immunosuppressive microenvironments. Inflammation in the tumor microenvironment often contains elevated levels of versican. Perturbing the accumulation of versican in tumors can inhibit inflammation and tumor progression in some cancers. Thus versican, as a component of the ECM impacts immunity and inflammation through regulating immune cell trafficking and activation. Versican is emerging as a potential target in the control of inflammation in a number of different diseases.

Keywords: versican, hyaluronan, immunity, inflammation, macrophages, T lymphocytes

OPEN ACCESS

Edited by:
Aaron C. Petrey,
The University of Utah, United States

Reviewed by:
Anna Maria Piccinini,
University of Nottingham,
United Kingdom
Katherina Psarra,
Evaggelismos General Hospital, Greece

***Correspondence:**
Thomas N. Wight
twight@benaroyaresearch.org

Specialty section:
This article was submitted to Inflammation, a section of the journal Frontiers in Immunology

Received: *08 January 2020*
Accepted: *06 March 2020*
Published: *24 March 2020*

Citation:
Wight TN, Kang I, Evanko SP, Harten IA, Chang MY, Pearce OMT, Allen CE and Frevert CW (2020) Versican—A Critical Extracellular Matrix Regulator of Immunity and Inflammation. Front. Immunol. 11:512. doi: 10.3389/fimmu.2020.00512

INTRODUCTION

Inflammation occurs during tissue infection or injury and involves the migration of leukocytes out of the blood vessels and into damaged areas of tissue (1, 2). Inflammation is driven by receptors on the surface of immune and non-immune cells (pattern recognition receptors, PRR) (1). PRRs recognize three classes of molecular patterns resulting from either pathogens generated by infectious agents such as virus and bacteria (pathogen-associated molecular patterns or PAMPs), molecules released from damaged tissues (damage-associated molecular patterns or DAMPs), or from molecular patterns on "self" tissues, often upregulated during malignancy (self-associated molecular patterns, SAMPs) (3). Activation of these receptors initiates an inflammatory response involving inflammatory cytokine production and recruitment of leukocytes. While inflammation is important in repairing tissue after insult, it often results in an exacerbation of tissue injury and promotion of disease.

Recent studies have indicated an important role for the ECM in the inflammatory response (4–10). Leukocytes cross the endothelial barrier and interact with the ECM which influences their adhesion, retention, migration, and activation. Leukocyte trafficking and localization are critical to events associated with the immune response. Specific components of the ECM can act as DAMPs or matrikines (11) promoting inflammatory cytokine synthesis and release by immune and non-immune cells (4, 12, 13). Proteoglycans, as components of the ECM, play a key part in providing intrinsic signals needed to coordinate critical events in the inflammatory cascade (4–6, 10, 14–23).

We have been interested in versican, which is a chondroitin sulfate proteoglycan (CSPG) and a member of the hyalectin family of ECM components (24), as one of the principal drivers of immunity and inflammation in a variety of different diseases, such as cardiovascular and lung disease, autoimmune diseases, and several different cancers. Interestingly, like many other ECM components, versican has "two faces"—functioning both in a pro- and an anti-inflammatory manner. The goal of this review will be to highlight the involvement of versican as a component in inflammation, discuss its role in recruiting and activating leukocytes, and provide examples and possible mechanisms by which this "versatile" ECM molecule can exhibit both pro- and anti-inflammatory properties.

VERSICAN

The expression and accumulation of versican, a large ECM proteoglycan, increases dramatically during inflammation in most diseases [reviewed in (4–6, 10, 23, 25, 26)]. Versican, named for its versatility in being a highly interactive molecule (27), is encoded from a single gene locus on chromosome 5q14.3 in humans (28) and its full-length isoform shares 76% nucleotide and 62% amino acid sequence identity between mouse and human.

There are at least five different isoforms of versican, V0, V1, V2, V3, V4, due to the alternative splicing of the major exons that code for the attachment regions for the chondroitin sulfate (CS) glycosaminoglycans (GAG) in the core protein (27, 29–33). Four of these isoforms contain CS GAGs that are attached by covalent linkage to the core protein, while one of the isoforms, V3, contains no GAGs due to the splicing together of the N- and C- terminal regions. V0, V1, V2, and V3 differ in the size of the core proteins and the size and number of the GAG chains. Additional variation within these isoforms has also been observed with an alternatively spliced C-terminus "Vint tail" (33).

The calculated molecular masses from cDNA sequencing studies for human versican core proteins are 370 kDa for V0, 262 kDa for V1, and 72 kDa for V3. These theoretical values are significantly lower than deduced from SDS PAGE gels where V0 migrates at around 550 kDa, and V1 around 500 kDa after chondroitin ABC lyase digestion (34). These differences are due to the high content of O- and N-linked oligosaccharides associated with the versican core protein (34–36). Interestingly, the different isoforms exhibit functional differences regarding their impact on cell phenotype, such as the ability of V1 to promote proliferation and inhibit apoptosis, while V2 exhibits antiproliferative activity (37, 38). In contrast, V3 regulates ECM assembly and inhibits cell proliferation and migration (39–45). A new V5 isoform has been recently described and shown to be expressed by injured rat neurons (46). While the biological importance of the "Vint tail" has yet to be elucidated, it likely provides fine tuning of interactions with the G3 region of the molecule. Thus, the different molecular domains of versican make the biology of this molecule quite complex given that both the alternative splicing of the mRNA as well as the controlled degradation of the intact versican molecule generate many different molecular forms which themselves can have their own effects on key events associated with immunity and inflammation. Much work remains to be done to sort out these complex interactions and their effects on the biology of this highly interactive molecule.

There is variation in the number, size, and composition of the CS chains attached to the different isoforms of versican. For example, consensus sequence for the number of CS attachment sites on the core protein of human versican reveals 17–23 sites for V0, 12–15 for V1, 5–8 for V2, and 0 for V3 (36, 47). Growth factors that increase during inflammation such as platelet-derived growth factor (PDGF) and transforming growth factor-beta (TGFβ) increase CS chains length and alter CS composition, impacting the ability of versican to interact with other molecules (35, 48–50). The CS isolated from versican interacts with inflammatory cytokines and impacts cytokine activity (51) [also see reviews (52, 53)]. Interestingly, the machinery and signaling pathways that control the composition and elongation of the CS chain differ from those controlling the transcription of versican core protein synthesis (48). For example, we found that stimulation of versican core protein synthesis by PDGF in non-human primate arterial smooth muscle cells encoded both the PKC and ERK pathways, whereas the elongation of the CS chains attached to the versican core protein was PKC dependent, but ERK independent. Since GAG chain length is a critical factor in determining the interactive nature of versican as well as other proteoglycans (54), targeting the pathways that regulate GAG chain elongation (55) may be a useful therapeutic

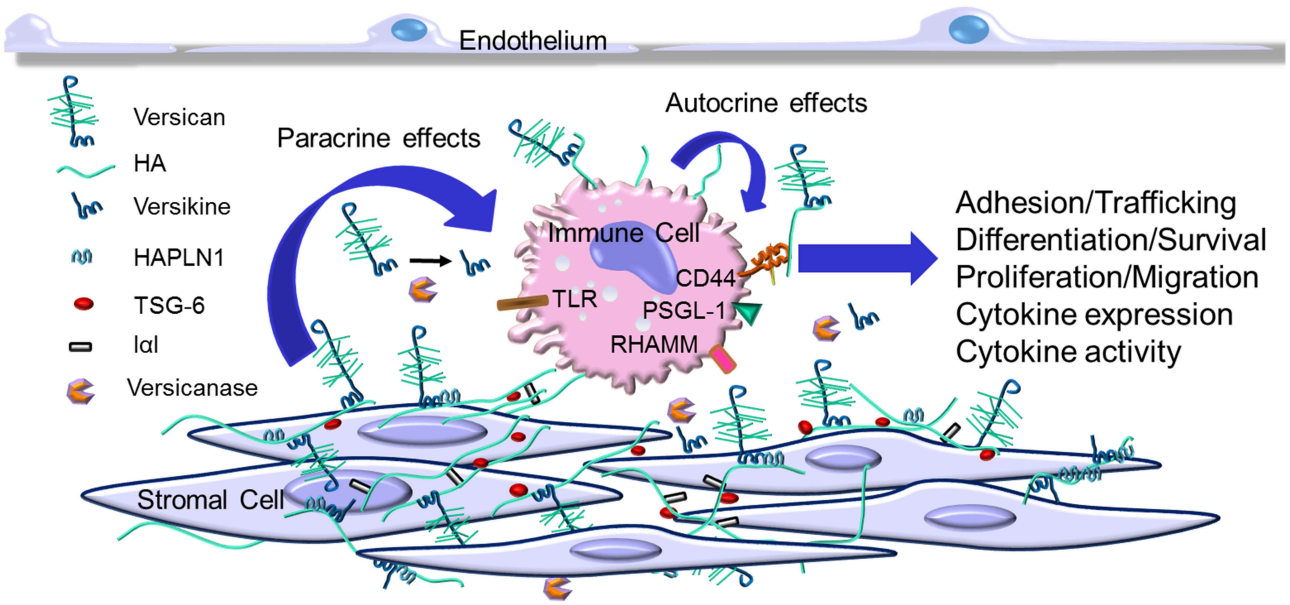

FIGURE 1 | Versican increases in the extracellular matrix (ECM) as part of the early inflammatory response. Immune cells invade the tissue from the blood stream and interact with specific ECM components including versican, versican fragments such as versikine (generated by versicanases), and other ECM components that associate with versican. This interaction may involve receptors on the immune cells such as CD44, P-selectin glycoprotein 1 (PSGL-1), receptor for hyaluronan-mediated motility (RHAMM), and toll-like receptors (TLRs). This interaction impacts several aspects of immune cell activation as part of the immune and inflammatory response.

approach to alter the immune and inflammatory properties of this ECM component.

Versican is synthesized by many different types of cells, including epithelial, endothelial, and stromal cells as well as leukocytes. This synthesis is regulated by a host of proinflammatory cytokines and growth factors [reviewed in (26, 56)]. Versican expression is regulated through two signaling pathways. Rhamani et al. first described the role of the canonical Wnt/β-catenin/T-cell factor (TCF) pathway in regulating versican expression in airway smooth muscle cells (57–59). Using polyinosinic-polycytidylic acid (poly I:C) and lipopolysaccharide (LPS) to activate TLR3 and TLR4, respectively, we showed that the signaling cascade that includes TLR3 or TLR4, the TLR adaptor molecule, Trif, type I interferons (IFNs), and the type I IFN receptor (IFNAR1), increases versican expression by mouse macrophages, which implicates versican as an IFN-stimulated gene (60). Versican synthesis is also controlled by several different miRNAs which are modulated during inflammation (61–63).

The degradation of versican is affected by several different families of proteases that increase during inflammation. Such proteases include matrix metalloproteinases (MMPs), i.e., MMP-1,−2,−3,−7, and−9 (64–66), serine protease plasmin (67), and at least five ADAMTS (a disintegrin and metalloproteinase with thrombospondin motifs) MMPs, specifically ADAMTS-1,−4,−5,−9, and−20 [see reviews (12, 13, 68–70)]. Cleavage of versican by ADAMTS-1,−4,−5, and−9 leads to production of an amino-terminal fragment, termed versikine, that can be detected using an antibody recognizing the neoepitope sequence DPEAAE (DPE) (12, 71, 72). Fragments such as versikine can act as DAMPs, interacting with immune and non-immune cells stimulating pro- and anti-inflammatory cytokine release and a modified immune response in both human and murine models (13, 73–75). Thus, many mechanisms are in place to regulate the expression and degradation of versican during the inflammatory process which ultimately influence key cellular events including cell adhesion, proliferation, migration, and ECM remodeling.

VERSICAN: A COMPONENT OF THE INFLAMMATORY RESPONSE

Versican is essential during development (76, 77) and it is now becoming apparent that it is an important component of the tissue inflammation caused by infection and tissue injury (10). Versican accumulates as part of the early inflammatory response in a number of human diseases often associated with the invasion of leukocytes including those in the vascular system (10, 40, 78–84), lung (5, 6, 60, 77, 85–89), brain and spinal cord (53, 90–92), intestine (93–96), heart (97), liver (63), skin (98, 99), eye (100, 101), pancreatic islets (102), and many different forms of cancer [reviewed in (103–105)]. The accumulation of versican in these tissues is usually associated with other ECM components that bind versican, such as hyaluronan (106, 107), link protein, TSG-6, IαI, and CD44 (95, 96, 108–111) (**Figure 1**). Complexes form as a result of this interaction which shape the microenvironment which impacts immunity and inflammation (95, 96, 109–113). Versican is usually found co-localized with hyaluronan, however,

inflammatory situations exist where each can be found separately (114, 115). Like versican, hyaluronan is also well-known for having both pro- and anti-inflammatory properties [reviewed in (95, 96, 111, 113, 116, 117)]. It remains to be determined whether the respective pro- or anti-inflammatory activities of versican and hyaluronan are interdependent. Usually, when interventions are used to reduce either versican or hyaluronan in cells and tissues, both components are similarly affected, adding to the challenge of determining the independent contributions of each molecule in the inflammatory process.

Versican interacts with receptors, such as CD44, PSGL-1, TLR2 (118), found on the surface of immune cells, and P- or L-selectins (20, 51, 52, 119–123). This interaction initiates a signaling cascade that influences the phenotypes of immune and inflammatory cells. For the TLRs, versican, like hyaluronan, does not possess the biochemical homology common to ligands for TLR2 and TLR4, such as LPS, so the precise interaction of versican with the TLRs is a bit unclear. No doubt interaction with the TLRs for versican, and maybe hyaluronan as well, involves a complex with molecules that have an affinity for the TLRs (113). In addition, it is interesting to compare the consequences of postulated versican–TLR interactions to other proteoglycans that have peptide motifs that bind TLRs, such as biglycan (18, 124). Whereas biglycan impacts inflammation by activating TLR4 and inflammasomes through activation of Trif-dependent signaling pathways (4, 6, 14, 19, 125), versican appears to mediate TLR2 interaction and activate MyD88-dependent signaling (118, 119). The functional significance of these two separate pathways in governing the inflammatory response is not clear. It will be important to determine if versican has unique immunogenic properties when compared to other ECM molecules.

The negatively charged CS chains in large part control the ability of versican to interact with a multitude of other molecules including chemokines, growth factors and proteases (51, 52, 122, 126–128) impacting their bioavailability and bioactivity (129–131). A number of studies demonstrate that CS chains can also promote the release of proinflammatory cytokines from macrophages and splenocytes, regulate MHCII intracellular trafficking, antigen presentation and T-cell activation [reviewed in (53)].

While a majority of studies show versican as having proinflammatory properties (see below), some studies have indicated that versican can operate in an immunosuppressive manner under certain conditions. For example, Xu et al. (132) found that treatment of mice exposed to LPS with siRNA to versican V1 resulted in increases in TNFα, NFκB, and TLR2 which were accompanied by increases in leukocytes in the lung. Interestingly, we found that LPS stimulated the expression of versican by macrophages in a type I IFN-dependent manner and that deletion of versican from macrophages promoted increased leukocyte invasion in mice exposed to poly I:C (60, 87). These studies are important since they suggest that macrophage-derived versican may possess immunosuppressive characteristics. Additionally, Coulson-Thomas and colleagues showed that the surface of human umbilical cord mesenchymal stem cells contains a glycocalyx enriched in hyaluronan, versican, TSG-6, and IαI, protecting the stem cells from immunodestruction (133) and affecting T-cell and macrophage phenotype. Interestingly, in tumors, human cancer stem cells synthesize and secrete prominent pericellular coat matrices enriched in hyaluronan and versican (134). Such a "cell coat" may account, in part, for the resistance to chemotherapy that these cells exhibit, as well as protection from immune surveillance as has been described for hyaluronan (135, 136) (see below).

VERSICAN: INTERPLAY WITH LEUKOCYTES

Leucocytes interact with the ECM as they invade tissue as part of the inflammatory response (5, 7–9, 17, 21) (see **Figure 1**). To explore this interaction, Carol de la Motte's laboratory at the Cleveland Clinic pioneered the use of co-cultures of leukocytes with stromal cells to explore the mechanisms and consequences responsible for the interaction of leukocytes with the ECM. Using agonists that promote ER stress, these models demonstrated that stromal cells produce an ECM organized into cable like structures that bound leukocytes [see reviews (96, 116, 137)]. These cable-like structures contain hyaluronan, versican, TSG-6, and IαI that bind different subsets of leukocytes (93, 94, 112, 114–116, 137–147). Such structures have not only been found *in vitro*, but also in diseased tissues, such as in atherosclerosis (10, 84), inflammatory bowel disease (IBD) (94), and in brain and spinal cord injury (53, 91). Further studies are needed to determine the contribution of each of the components in the complex on leukocyte phenotype. For example, we found that blocking versican accumulation in the ECM generated by cultured human lung fibroblasts using a neutralizing antibody significantly reduced monocyte adhesion *in vitro* (115). In addition, we showed that manipulating the expression of versican by overexpressing the V3 isoform in experimentally-induced atherosclerotic lesions in rabbits significantly reduced macrophage infiltration, inhibiting the development of lipid-filled atherosclerotic lesions (84). Furthermore, our *in vitro* studies using rat arterial smooth muscle cells demonstrated that the V3 expression effect is anti-inflammatory and decreased the expression of the CS-containing versican isoforms, V0 and V1, and the formation of elastic fibers which are a poor substrate for macrophages (42, 43). Such results further support a critical role for versican in myeloid cell accumulation in atherosclerosis and perhaps in other diseases as well (39).

Lymphoid cells also interact with the ECM. An effective immune response requires that T cells are able to adhere to and migrate through the ECM (7, 145). For example, activated human CD4+ T cells bind to the ECM generated by human synoviocytes and human lung fibroblasts treated with poly I:C, but not to the ECM generated by the stromal cells in the absence of poly I:C treatment (145). This binding blocked the ability of T cells to spread and migrate and was reversed by pretreatment of the ECM with chondroitin ABC lyase. Additionally, versican blocked hyaluronan binding to T cells and inhibited IL-10 synthesis reducing the immunosuppressive capacity of these cells (145). Versican also inhibited human T-cell invasion of collagen gels consistent with influencing T-cell migration and

immunosuppression. These activities, of course, could be critical to influencing the ability of T cells to invade and destroy tumor cells (see below). In addition, versican was identified as one of the most upregulated genes in lymphocytes isolated from patients with Sezary syndrome which is a leukemic variant of cutaneous T cell lymphoma. In this setting, versican promoted the invasive and homing capacity of the lymphocytes from these patients (148). Interestingly, the cleavage of versican by ADAMTS enzymes is critical for T-cell trafficking in mouse models of influenza virus infection (149).

Whether versican is intact or degraded may affect its impact on disease cell phenotype. For example, we showed that the G1 fragment of versican promoted extensive ECM cable formation that interconnected adjacent cells and inhibited proliferation, while the intact form had no activity (150). Using the CRISPR/Cas9 system, Hideto Watanabe's group recently developed mice that synthesized versican lacking the ADAMTS versicanase cleavage site (99). They found that accumulation of intact versican in these mice facilitated TGFβ activity coupled to fibroblast proliferation and myofibroblast differentiation and accelerated wound healing. Interestingly, wounds from the versican cleavage-resistant mice contained elevated levels of M1 macrophages and T cells, suggesting in this context that intact versican enhances inflammatory cell infiltration. These studies highlight the importance of ECM molecules such as versican in regulating the ability of both myeloid cells and T cells to invade tissue which is critical to the immune destruction of tumors in many forms of cancer (see below).

VERSICAN: EXPRESSION BY MYELOID CELLS AND THE IMPACT ON INFLAMMATION

Versican is also expressed by myeloid cells and upregulated as part of the inflammatory response (see **Figure 1**). For example, versican expression is elevated by myeloid cells in autoimmunity (127, 151, 152), coronary stenosis (153), myocardial infarction (154), and in response to proinflammatory stimulants such as hypoxia (155, 156) and LPS (60, 87, 157). Versican is differentially expressed in M1 macrophages, as opposed to M2 macrophages, as they differentiate from monocytes (87, 156, 158). On the other hand, a recent study shows that versican enhances mesothelioma growth by promoting M2 polarization and inhibiting phagocytosis (159). More work is needed to sort out whether specific isoforms of versican play a role in determining and/or regulating macrophage phenotype. In patients with systemic sclerosis, CD14-positive monocytes (127) show elevated expression of versican that is accompanied by elevated expression of CCL2 [also known as Monocyte Chemoattractant Protein 1 (MCP-1)]. Interestingly, versican protects CCL2 from degradation which in turn promotes monocyte migration (127). Earlier studies showed that in a model of neuronal inflammation hyperalgesia, CCL2 binds to versican and impacts inflammation (160). A similar relationship has been seen among versican, macrophages, and CCL2 and the promotion of inflammation in mouse models of cancer (161, 162) (see below). Versican also interacts with CCL5 which is important in recruiting CD8 T cells in the inflammatory response (51). Versican has also been identified as a gene common for classical monocytes ($CD14^{++}$ $CD16^{-}$) and classical CD11c dendritic cells (163).

LPS and poly I:C, two TLR agonists, stimulate versican expression in both murine bone marrow-derived macrophages and alveolar macrophages *in vitro* (87) and in murine alveolar macrophages as well as in stromal cells *in vivo* (60, 88). To determine the role of versican derived from macrophages in the innate immune response *in vivo*, we developed two models of conditional versican deficiency by floxing exon 4 of the versican gene. LysM/$Vcan^{-/-}$ mice have constitutive myeloid cell-specific versican deficiency (60), and $R26R^{ert2}Cre^{+}/Vcan^{-/-}$ mice, when treated with tamoxifen, are globally deficient in versican (88). *In vitro* studies with macrophages from LysM/$Vcan^{-/-}$ mice indicate that versican is important for production of type I IFNs and IL-10 by macrophages in response to poly I:C. This is supported by *in vivo* studies with LysM/$Vcan^{-/-}$ mice which indicate that myeloid-derived versican restrains recruitment of inflammatory cells into lungs and promotes production of the key anti-inflammatory cytokines, IFN-β and IL-10, in the pulmonary response to poly I:C. In contrast, *in vivo* studies with $R26R^{ert2}Cre^{+}/Vcan^{-/-}$ mice suggest that stromal-derived versican promotes pulmonary inflammatory cell recruitment in response to poly I:C. When considered in tandem, these results identify versican derived from macrophages as an immunomodulatory molecule with anti-inflammatory properties whereas versican derived from stromal cells has proinflammatory properties. Some of the factors that determine the pro- or anti-inflammatory properties of versican include cellular source, surface receptors, signaling pathways affected, nature of the binding partners that associate with versican and/or whether versican is intact or degraded. It should also be noted that reducing versican by genetic manipulation or other means frequently reduces the accumulation of hyaluronan (88) raising some question as to whether the opposing inflammatory properties of versican may be governed by hyaluronan?

VERSICAN AND INFLAMMATION IN CANCER: PRO- AND/OR ANTI-INFLAMMATORY?

Versican is a central player in cancer development in that it impacts tumor-promoting inflammation, immune surveillance evasion, and immunomodulation (164). Versican expression increases as part of the inflammatory response in a number of cancers [reviewed in (22, 103, 105, 165)]. In both breast cancer and Lewis lung carcinoma, the presence of versican produced by the tumor cells leads to an accumulation and activation of tumor-associated macrophages (TAMs) via TLR2 and its co-receptors TLR6 and CD14 (118, 119, 159, 165–167). Tumor cell-derived versican in turn promotes accumulation and secretion of proinflammatory TNFα and IL-6. In addition, we found significantly elevated expression and accumulation of versican in leiomyosarcoma (LMS), a metastatic uterine cancer,

when compared to the more benign leiomyomas and control healthy tissue (103, 168). Importantly, cultured human LMS cells synthesized large quantities of versican, forming extensive pericellular coats around the tumor cells. Blocking versican synthesis with siRNA to versican reduced the thickness of the cell coats and inhibited their proliferation and migration *in vitro* and tumor formation in vivo (103, 168).

Stromal cells are a major source of versican as well. In breast and ovarian cancer, TGFβ is overexpressed and contributes to strong stromal versican upregulation (169, 170). Cervical and endometrial cancers are characterized by increases in versican originating from both tumor and stromal cells (171, 172). On the other hand, lack of versican expression in a mouse fibrosarcoma model resulted in a decrease in the number and density of cancer-associated fibroblasts (CAFs) in stroma (173). Such changes led to larger tumors and poorer prognosis in pancreatic cancer (174). In Lewis lung carcinoma, stromal cell-derived versican and its fragment, versikine are associated with increased angiogenesis as part of the inflammatory response contributing to this tumor (175). Accumulation of versican in tumors is positively correlated with the number of microvessels within tumor stroma (176, 177). We found, for example, that human stromal stem cells that produce elevated levels of versican formed an extensive vascular network enriched in hyaluronan and versican when cultured with vascular endothelial cells (178). Furthermore, when patches containing these proangiogenic cells were transplanted onto athymic rat hearts they developed 50-fold more vessels than patches containing stromal cells with low versican expression (178). In other studies, we demonstrated that versican was actively processed in the early stages of VEGF-induced pathological angiogenesis generating extensive DPEAAE (versikine) fragments that associated with the endothelial cells (179). These results suggest that versican, in some form, may be critical for the early stages of angiogenesis as part of the events associated with inflammation.

Myeloid cells are also a major source of versican in tumor inflammation. Versican from myeloid cells promotes tumor metastasis in breast cancer (180). Versican expressed by CD11b+ Ly6C^{high} myeloid cells promotes lung metastasis in a TGFβ-dependent manner in mouse models (181). Intriguingly, versican expression is upregulated by macrophages when co-cultured with carcinoma cells (161, 162), suggesting that the source of versican includes both myeloid cells associated with cancer cells (182, 183). These studies raise the possibility of "crosstalk" among different cell types within the tumor that may influence the nature of versican accumulation and bioactivity which would provide key links to the inflammation associated with cancer initiation, promotion, and metastatic progression (see **Figure 1**).

Infiltrating myeloid cells secrete versican which can also exhibit immunosuppressive activities in some cancers (74, 75, 103, 118, 184, 185). For example, ADAMTS-generated versikine regulates mouse BATF3-dendritic cell (BATF3-DC) differentiation (74). BATF3-DCs control CD8+ abundance in the tumor microenvironment (186). These observations support a role for versican as being tolerogenic. In addition, a recent study (187) using bone marrow biopsies from 35 myeloma patients revealed a significant correlation of versikine accumulation with infiltration of CD8+ T cells supporting a model in which macrophages and regulatory DCs secrete tolerogenic versican which is subsequently degraded, generating versikine and further altering the immunosuppressive nature of the tumor microenvironment. Thus, taken together, these studies establish that both intact versican and a proteolytic degradation product of versican have immunomodulatory properties and suggest that the anti-tumor properties of versikine might antagonize the pro-tumor properties of intact versican (13, 23, 73, 75, 188). The juxtaposition of these findings indicates that the consequences of ECM-derived–DAMP interactions with PRRs can have sharply differing outcomes depending on the contextual specifics of versican structure.

The tumor stromal ECM microenvironment is characteristic of a wound that does not heal (189, 190) and is functionally analogous to an immune privileged site in normal tissue such as in the eye [reviewed in (191)]. Versican and hyaluronan are enriched in immune privileged sites. The expression and accumulation of versican in the microenvironment of some tumors is associated with reduced numbers of CD8-positive T cells indicating that versican may interfere with T-cell invasion as part of an immunosuppressive activity (192). In addition, versican may be a player in regulating the expression of PD-L1 as part of the autoimmune checkpoint involved in tumor escape from the T-cell immune response. Hartley and colleagues showed that versican produced by mouse tumor cells stimulated monocytes to produce TNFα in a TLR2-dependent manner which in turn upregulated the expression of PD-L1 by mouse monocyte/macrophages (193). The involvement of versican in regulating PD-L1 expression in T cells awaits further investigation. However, such results overall suggest that versican may be part of the exclusionary zone in the microenvironment impacting and preventing T cells access to the tumor (191, 194–196). Such an involvement should be considered as a potential target in immunotherapy treatment of cancer. For example, versican accumulation in the stroma could interfere with T cell-mediated tumor destruction by displacing the T cells from the appropriate tumor target (191).

While the CS containing isoforms of versican appear to be pro-inflammatory, V3 which contains no CS chains when overexpressed in arterial smooth muscle cells inhibits the expression of pro inflammatory cytokines such as CXCL1, CCL20, and CCL2 resulting in blockade of epidermal growth factor receptor and NFκB signaling activity (42, 43). V3 expression also reduced the rate of tumor growth of melanoma by inhibiting tumor cell proliferation as well as increasing the rate of apoptosis. Such experiments highlight a potential role for V3 in counteracting the inflammatory response associated with cancer (197–199).

CONCLUSIONS

Studies indicating a causal role of versican regulating events that drive immunity and inflammation are increasing. There is no doubt that versican, either intact or degraded, as an ECM participant, has a role, but whether it acts alone or

in combination with other components during inflammatory events is still not fully understood. Published studies indicate that versican has both pro- and anti-inflammatory activities depending upon the context in which versican is presented to cells. Versican's role in inflammation also depends on temporal and spatial considerations and it may play different roles whether it is involved early or late in disease and whether it is intact or degraded. Furthermore, versican's versatility in binding to multiple receptors and other components involved in the inflammatory response identifies it as a "keystone molecule" regulating inflammation. Developing targeted reagents and therapeutic strategies to interfere with versican accumulation should further identify key mechanisms regulating versican's biological activity. Versican is increasingly being seen as a potential therapeutic target in multiple diseases.

Thus, future directions will be to take advantage of the mouse models we have developed in which versican has been deleted conditionally in the whole animal or specifically in myeloid cells and determine the impact of selectively removing versican in mouse models of cardiovascular and lung disease, autoimmune diseases such as type 1 diabetes and multiple sclerosis, and in some cancers, particularly breast cancer. Such studies have not been possible in the past due to the unavailability of the versican KO mouse. We are interested in focusing on the impact of the different versican variants, such as V3 to better define their role in inflammation and immunity since our preliminary data indicates that V3 acts differently than V0 or V1 in influencing events that drive the immune and inflammatory response. Our cell biology studies will focus on how versican influences immune cells and the immune response focusing on its role in antigen presentation, immune synapse formation, and immune activation important, for example, in the destruction of tumors. Indeed versican, as part of the ECM, is "versatile" and a "keystone" molecule in the regulation of immunity and inflammation.

AUTHOR CONTRIBUTIONS

TW wrote the manuscript. IK, SE, IH, MC, OP, CA, and CF edited and revised the manuscript. All authors have reviewed and approved the final version of this article.

FUNDING

This study was supported by National Institutes of Health grants R01 DK 096087 and U19 AI 125378 (TW) and R01 AI 130280 (CF and TW) and by Cancer Research UK career establishment award A27947 (OMTP).

ACKNOWLEDGMENTS

We thank Dr. Virginia M. Green for her careful editing and preparation of the manuscript. We also thank all past and present collaborators and lab members for their dedication to furthering our understanding of the role of this important ECM macromolecule in disease pathogenesis. We apologize to those authors whose original contributions were not cited in lieu of reviews due to space requirements.

REFERENCES

1. Liu J, Cao X. Cellular and molecular regulation of innate inflammatory responses. *Cell Mol Immunol.* (2016) 13:711–21. doi: 10.1007/1038/cmi.2016.58
2. Fullerton JN, Gilroy DW. Resolution of inflammation: a new therapeutic frontier. *Nat Rev Drug Discov.* (2016) 15:551–67. doi: 10.1007/1038/nrd.2016.39
3. Laubli H, Varki A. Sialic acid-binding immunoglobulin-like lectins (Siglecs) detect self-associated molecular patterns to regulate immune responses. *Cell Mol Life Sci.* (2019). doi: 10.1007/s00018-019-03288-x
4. Frevert CW, Felgenhauer J, Wygrecka M, Nastase MV, Schaefer L. Danger-associated molecular patterns derived from the extracellular matrix provide temporal control of innate immunity. *J Histochem Cytochem.* (2018) 66:213–27. doi: 10.1007/1369/0022155417740880
5. Gill S, Wight TN, Frevert CW. Proteoglycans: key regulators of pulmonary inflammation and the innate immune response to lung infection. *Anat Rec.* (2010) 293:968–81. doi: 10.1002/ar.21094
6. Kang I, Chang MY, Wight TN, Frevert CW. Proteoglycans as immunomodulators of the innate immune response to lung infection. *J Histochem Cytochem.* (2018) 66:241–59. doi: 10.1369/0022155417751880
7. Sorokin L. The impact of the extracellular matrix on inflammation. *Nat Rev Immunol.* (2010) 10:712–23. doi: 10.1038/nri2852
8. Vaday GG, Franitza S, Schor H, Hecht I, Brill A, Cahalon L, et al. Combinatorial signals by inflammatory cytokines and chemokines mediate leukocyte interactions with extracellular matrix. *J Leukoc Biol.* (2001) 69:885–92. doi: 10.1189/jlb.69.6.885
9. Vaday GG, Lider O. Extracellular matrix moieties, cytokines, and enzymes: dynamic effects on immune cell behavior and inflammation. *J Leukoc Biol.* (2000) 67:149–59. doi: 10.1002/jlb.67.2.149
10. Wight TN, Kang I, Merrilees MJ. Versican and the control of inflammation. *Matrix Biol.* (2014) 35:152–61. doi: 10.1016/j.matbio.2014.01.015
11. Maquart FX, Pasco S, Ramont L, Hornebeck W, Monboisse JC. An introduction to matrikines: extracellular matrix-derived peptides which regulate cell activity. Implication in tumor invasion. *Crit Rev Oncol Hematol.* (2004) 49:199–202. doi: 10.1016/j.critrevonc.2003.06.007
12. Nandadasa S, Foulcer S, Apte SS. The multiple, complex roles of versican and its proteolytic turnover by ADAMTS proteases during embryogenesis. *Matrix Biol.* (2014) 35:34–41. doi: 10.1016/j.matbio.2014.01.005
13. Timms K, Maurice SB. Context-dependent bioactivity of versican fragments. *Glycobiology.* (2019). doi: 10.1093/glycob/cwz090. [Epub ahead of print].
14. Frey H, Schroeder N, Manon-Jensen T, Iozzo RV, Schaefer L. Biological interplay between proteoglycans and their innate immune receptors in inflammation. *FEBS J.* (2013) 280:2165–79. doi: 10.1111/febs.12145
15. Karamanos NK, Piperigkou Z, Theocharis AD, Watanabe H, Franchi M, Baud S, et al. Proteoglycan chemical diversity drives multifunctional cell regulation and therapeutics. *Chem Rev.* (2018) 118:9152–232. doi: 10.1021/acs.chemrev.8b00354
16. Karamanos NK, Theocharis AD, Neill T, Iozzo RV. Matrix modeling and remodeling: a biological interplay regulating tissue homeostasis and diseases. *Matrix Biol.* (2019) 75–76:1–11. doi: 10.1016/j.matbio.2018.08.007
17. Parish CR. The role of heparan sulphate in inflammation. *Nat Rev Immunol.* (2006) 6:633–43. doi: 10.1038/nri1918
18. Roedig H, Damiescu R, Zeng-Brouwers J, Kutija I, Trebicka J, Wygrecka M, et al. Danger matrix molecules orchestrate CD14/CD44 signaling in cancer development. *Semin Cancer Biol.* (2019). doi: 10.1016/j.semcancer.2019.07.026
19. Schaefer L, Babelova A, Kiss E, Hausser HJ, Baliova M, Krzyzankova M, et al. The matrix component biglycan is proinflammatory and signals through

Toll-like receptors 4 and 2 in macrophages. *J Clin Invest.* (2005) 115:2223–33. doi: 10.1172/JCI23755
20. Taylor KR, Gallo RL. Glycosaminoglycans and their proteoglycans: host-associated molecular patterns for initiation and modulation of inflammation. *FASEB J.* (2006) 20:9–22. doi: 10.1096/fj.05-4682rev
21. Wight TN, Frevert CW, Debley JS, Reeves SR, Parks WC, Ziegler SF. Interplay of extracellular matrix and leukocytes in lung inflammation. *Cell Immunol.* (2017) 312:1–14. doi: 10.1016/j.cellimm.2016.12.003
22. Theocharis AD, Skandalis SS, Tzanakakis GN, Karamanos NK. Proteoglycans in health and disease: novel roles for proteoglycans in malignancy and their pharmacological targeting. *FEBS J.* (2010) 277:3904–23. doi: 10.1111/j.1742-4658.2010.07800.x
23. Zhang Z, Miao L, Wang L. Inflammation amplification by versican: the first mediator. *Int J Mol Sci.* (2012) 13:6873–82. doi: 10.3390/ijms13066873
24. Wight TN, Heinegård DK, Hascall VC. Proteoglycans: structure and function. In: Hay ED, editor. *Cell Biology of Extracellular Matrix.* New York, NY: Plenum Press (1991). p. 45–78.
25. Wight TN. The pathobiology of versican. In: Karamanos N, editor. *Extracellular Matrix: Pathobiology and Signaling.* Berlin: Walter De Gruyter GMBH & Co., KG (2012). p. 154–70.
26. Wight TN, Kinsella MG, Evanko SP, Potter-Perigo S, Merrilees MJ. Versican and the regulation of cell phenotype in disease. *Biochim Biophys Acta.* (2014) 1840:2441–51. doi: 10.1016/j.bbagen.2013.12.028
27. Zimmermann DR, Ruoslahti E. Multiple domains of the large fibroblast proteoglycan, versican. *EMBO J.* (1989) 8:2975–81. doi: 10.1002/j.1460-2075.1989.tb08447.x
28. Iozzo RV, Naso MF, Cannizzaro LA, Wasmuth JJ, McPherson JD. Mapping of the versican proteoglycan gene (CSPG2) to the long arm of human chromosome 5 (5q12-5q14). *Genomics.* (1992) 14:845–51. doi: 10.1016/s0888-7543(05)80103-x
29. Zako M, Shinomura T, Ujita M, Ito K, Kimata K. Expression of PG-M (V3), an alternatively spliced form of PG-M without a chondroitin sulfate attachment region in mouse and human tissues. *J Biol Chem.* (1995) 270:3914–8. doi: 10.1074/jbc.270.8.3914
30. Dours-Zimmermann MT, Zimmerman DR. A novel glycosaminoglycan attachment domain identified in two alternative splice variants of human versican. *J Biol Chem.* (1994) 269:32992–8.
31. Ito K, Shinomura T, Zako M, Ujita M, Kimata K. Multiple forms of mouse PG-M, a large chondroitin sulfate proteoglycan generated by alternative splicing. *J Biol Chem.* (1995) 270:958–65. doi: 10.1074/jbc.270.2.958
32. Kischel P, Waltregny D, Dumont B, Turtoi A, Greffe Y, Kirsch S, et al. Versican overexpression in human breast cancer lesions: known and new isoforms for stromal tumor targeting. *Int J Cancer.* (2010) 126:640–50. doi: 10.1002/ijc.24812
33. Lemire JM, Braun KR, Maurel P, Kaplan ED, Schwartz SM, Wight TN. Versican/PG-M isoforms in vascular smooth muscle cells. *Arterioscler Thromb Vasc Biol.* (1999) 19:1630–9. doi: 10.1161/01.atv.19.7.1630
34. Evanko SP, Chan CK, Johnson PY, Frevert CW, Wight TN. The biochemistry and immunohistochemistry of versican. In: Mecham RP, editor. *Methods in Extracellular Matrix Biology*. Cambridge, MA: Academic Press (Elsevier Inc.) (2018). p. 261–79.
35. Chang Y, Yanagishita M, Hascall VC, Wight TN. Proteoglycans synthesized by smooth muscle cells derived from monkey (Macaca nemestrina) aorta. *J Biol Chem.* (1983) 258:5679–88.
36. Zimmermann D. Versican. In: Iozzo R, editor. *Proteoglycans: Structure, Biology and Molecular Interactions*. New York, NY: Marcel Dekker, Inc. (2000). p. 327–41.
37. Sheng W, Wang G, Wang Y, Liang J, Wen J, Zheng PS, et al. The roles of versican V1 and V2 isoforms in cell proliferation and apoptosis. *Mol Biol Cell.* (2005) 16:1330–40. doi: 10.1091/mbc.e04-04-0295
38. Wu Y, Zhang Y, Cao L, Chen L, Lee V, Zheng PS, et al. Identification of the motif in versican G3 domain that plays a dominant-negative effect on astrocytoma cell proliferation through inhibiting versican secretion and binding. *J Biol Chem.* (2001) 276:14178–86. doi: 10.1074/jbc.M100618200
39. Merrilees MJ, Wight TN. *Targeting the Matrix: Potential Benefits for Versican Therapeutics. Current Comments*. Elsevier (2012). Available online at: http://www.elsevierblogs.com/currentcomments/?p=519 (accessed June 04, 2019).
40. Wight TN. A role for proteoglycans in vascular disease. *Matrix Biol.* (2018) 71–72:396–420. doi: 10.1016/j.matbio.2018.02.019
41. Wight TN, Merrilees MJ. Proteoglycans in atherosclerosis and restenosis: key roles for versican. *Circ Res.* (2004) 94:1158–67. doi: 10.1161/01.RES.0000126921.29919.51
42. Kang I, Barth JL, Sproul EP, Yoon DW, Braun KR, Argraves WS, et al. Expression of V3 versican by rat arterial smooth muscle cells promotes differentiated and anti-inflammatory phenotypes. *J Biol Chem.* (2015) 290:21629–41. doi: 10.1074/jbc.M115.657486
43. Kang I, Yoon DW, Braun KR, Wight TN. Expression of versican V3 by arterial smooth muscle cells alters TGFβ-, EGF-, and NFκB-dependent signaling pathways, creating a microenvironment that resists monocyte adhesion. *J Biol Chem.* (2014) 289:15393–404. doi: 10.1074/jbc.M113.544338
44. Lemire JM, Merrilees MJ, Braun KR, Wight TN. Overexpression of the V3 variant of versican alters arterial smooth muscle cell adhesion, migration, and proliferation *in vitro*. *J Cell Physiol.* (2002) 190:38–45. doi: 10.1002/jcp.10043
45. Merrilees MJ, Lemire JM, Fischer JW, Kinsella MG, Braun KR, Clowes AW, et al. Retrovirally mediated overexpression of versican v3 by arterial smooth muscle cells induces tropoelastin synthesis and elastic fiber formation *in vitro* and in neointima after vascular injury. *Circ Res.* (2002) 90:481–7. doi: 10.1161/hh0402.105791
46. Bogen O, Bender O, Alvarez P, Kern M, Tomiuk S, Hucho F, et al. Expression of a novel versican variant in dorsal root ganglia from spared nerve injury rats. *Mol Pain.* (2019) 15:1744806919874557. doi: 10.1177/1744806919874557
47. Naso MF, Zimmermann DR, Iozzo RV. Characterization of the complete genomic structure of the human versican gene and functional analysis of its promoter. *J Biol Chem.* (1994) 269:32999–3008.
48. Cardoso LE, Little PJ, Ballinger ML, Chan CK, Braun KR, Potter-Perigo S, et al. Platelet-derived growth factor differentially regulates the expression and post-translational modification of versican by arterial smooth muscle cells through distinct protein kinase C and extracellular signal-regulated kinase pathways. *J Biol Chem.* (2010) 285:6987–95. doi: 10.1074/jbc.M109.088674
49. Little PJ, Tannock L, Olin KL, Chait A, Wight TN. Proteoglycans synthesized by arterial smooth muscle cells in the presence of transforming growth factor-beta1 exhibit increased binding to LDLs. *Arterioscler Thromb Vasc Biol.* (2002) 22:55–60. doi: 10.1161/hq0102.101100
50. Schönherr E, Järveläinen HT, Sandell LJ, Wight TN. Effects of platelet-derived growth factor and transforming growth factor-β 1 on the synthesis of a large versican-like chondroitin sulfate proteoglycan by arterial smooth muscle cells. *J Biol Chem.* (1991) 266:17640–7.
51. Hirose J, Kawashima H, Yoshie O, Tashiro K, Miyasaka M. Versican interacts with chemokines and modulates cellular responses. *J Biol Chem.* (2001) 276:5228–34. doi: 10.1074/jbc.M007542200
52. Wu YJ, La Pierre DP, Wu J, Yee AJ, Yang BB. The interaction of versican with its binding partners. *Cell Res.* (2005) 15:483–94. doi: 10.1038/sj.cr.7290318
53. Stephenson EL, Yong VW. Pro-inflammatory roles of chondroitin sulfate proteoglycans in disorders of the central nervous system. *Matrix Biol.* (2018) 71–72:432–42. doi: 10.1016/j.matbio.2018.04.010
54. Chait A, Wight TN. Interaction of native and modified low-density lipoproteins with extracellular matrix. *Curr Opin Lipidol.* (2000) 11:457–63. doi: 10.1097/00041433-200010000-00003
55. Little PJ, Osman N, O'Brien KD. Hyperelongated biglycan: the surreptitious initiator of atherosclerosis. *Curr Opin Lipidol.* (2008) 19:448–54. doi: 10.1097/MOL.0b013e32830dd7c4
56. Kinsella MG, Bressler SL, Wight TN. The regulated synthesis of versican, decorin, and biglycan: extracellular matrix proteoglycans that influence cellular phenotype. *Crit Rev Eukaryot Gene Expr.* (2004) 14:203–34. doi: 10.1615/critreveukaryotgeneexpr.v14.i3.40
57. Rahmani M, Carthy JM, McManus BM. Mapping of the Wnt/beta-catenin/TCF response elements in the human versican promoter. *Methods Mol Biol.* (2012) 836:35–52. doi: 10.1007/978-1-61779-498-8_3
58. Rahmani M, Read JT, Carthy JM, McDonald PC, Wong BW, Esfandiarei M, et al. Regulation of the versican promoter by the beta-catenin-T-cell factor complex in vascular smooth muscle cells. *J Biol Chem.* (2005) 280:13019–28. doi: 10.1074/jbc.M411766200

59. Rahmani M, Wong BW, Ang L, Cheung CC, Carthy JM, Walinski H, et al. Versican: signaling to transcriptional control pathways. *Can J Physiol Pharmacol.* (2006) 84:77–92. doi: 10.1139/y05-154
60. Chang MY, Kang I, Gale M Jr, Manicone AM, Kinsella MG, Braun KR, et al. Versican is produced by Trif- and type I interferon-dependent signaling in macrophages and contributes to fine control of innate immunity in lungs. *Am J Physiol Lung Cell Mol Physiol.* (2017) 313:L1069–86. doi: 10.1152/ajplung.00353.2017
61. Rutnam ZJ, Wight TN, Yang BB. miRNAs regulate expression and function of extracellular matrix molecules. *Matrix Biol.* (2013) 32:74–85. doi: 10.1016/j.matbio.2012.11.003
62. Wang X, Hu G, Zhou J. Repression of versican expression by microRNA-143. *J Biol Chem.* (2010) 285:23241–50. doi: 10.1074/jbc.M109.084673
63. Yan Y, Qin D, Hu B, Zhang C, Liu S, Wu D, et al. Deletion of miR-126a promotes hepatic aging and inflammation in a mouse model of cholestasis. *Mol Ther Nucleic Acids.* (2019) 16:494–504. doi: 10.1016/j.omtn.2019.04.002
64. Halpert I, Sires U, Potter-Perigo S, Wight TN, Shapiro DS, Welgus HG, et al. Matrilysin is expressed by lipid-laden macrophages at sites of potential rupture in atherosclerotic lesions and localized to areas of versican deposits. *Proc Natl Acad Sci USA.* (1996) 93:9748–53.
65. Passi A, Negrini D, Albertini R, Miserocchi G, De Luca G. The sensitivity of versican from rabbit lung to gelatinase A (MMP-2) and B (MMP-9) and its involvement in the development of hydraulic lung edema. *FEBS Lett.* (1999) 456:93–6. doi: 10.1016/s0014-5793(99)00929-1
66. Perides G, Asher RA, Lark MW, Lane WS, Robinson RA, Bignami A. Glial hyaluronate-binding protein: a product of metalloproteinase digestion of versican? *Biochem J.* (1995) 312:377–84. doi: 10.1042/bj3120377
67. Kenagy RD, Fischer JW, Davies MG, Berceli SA, Hawkins SM, Wight TN, et al. Increased plasmin and serine proteinase activity during flow-induced intimal atrophy in baboon PTFE grafts. *Arterioscler Thromb Vasc Biol.* (2002) 22:400–4. doi: 10.1161/hq0302.105376
68. Apte SS. A disintegrin-like and metalloprotease (reprolysin type) with thrombospondin type 1 motifs: the ADAMTS family. *Int J Biochem Cell Biol.* (2004) 36:981–5. doi: 10.1016/j.biocel.2004.01.014
69. Apte SS. A disintegrin-like and metalloprotease (reprolysin-type) with thrombospondin type 1 motif (ADAMTS) superfamily: functions and mechanisms. *J Biol Chem.* (2009) 284:31493–7. doi: 10.1074/jbc.R109.052340
70. Kenagy RD, Plaas AH, Wight TN. Versican degradation and vascular disease. *Trends Cardiovasc Med.* (2006) 16:209–15. doi: 10.1016/j.tcm.2006.03.011
71. Sandy JD, Westling J, Kenagy RD, Iruela-Arispe ML, Verscharen C, Rodriguez-Mazaneque JC, et al. Versican V1 proteolysis in human aorta *in vivo* occurs at the Glu^{441}-Ala^{442} bond, a site that is cleaved by recombinant ADAMTS-1 and ADAMTS-4. *J Biol Chem.* (2001) 276:13372–8. doi: 10.1074/jbc.M009737200
72. Somerville RP, Longpre JM, Jungers KA, Engle JM, Ross M, Evanko S, et al. Characterization of ADAMTS-9 and ADAMTS-20 as a distinct ADAMTS subfamily related to Caenorhabditis elegans GON-1. *J Biol Chem.* (2003) 278:9503–13. doi: 10.1074/jbc.M211009200
73. Schmitt M. Versican vs versikine: tolerance vs attack. *Blood.* (2016) 128:612–3. doi: 10.1182/blood-2016-06-721092
74. Hope C, Emmerich PB, Papadas A, Pagenkopf A, Matkowskyj KA, Van De Hey DR, et al. Versican-derived matrikines regulate Batf3-dendritic cell dfferentiation and pomote T cell infiltration in colorectal cancer. *J Immunol.* (2017) 199:1933–41. doi: 10.4049/jimmunol.1700529
75. Hope C, Foulcer S, Jagodinsky J, Chen SX, Jensen JL, Patel S, et al. Immunoregulatory roles of versican proteolysis in the myeloma microenvironment. *Blood.* (2016) 128:680–5. doi: 10.1182/blood-2016-03-705780
76. Mjaatvedt CH, Yamamura H, Capehart AA, Turner D, Markwald RR. The Cspg2 gene, disrupted in the hdf mutant, is required for right cardiac chamber and endocardial cushion formation. *Dev Biol.* (1998) 202:56–66. doi: 10.1006/dbio.1998.9001
77. Snyder JM, Washington IM, Birkland T, Chang MY, Frevert CW. Correlation of versican expression, accumulation, and degradation during embryonic development by quantitative immunohistochemistry. *J Histochem Cytochem.* (2015) 63:952–67. doi: 10.1369/0022155415610383
78. Otsuka F, Kramer MC, Woudstra P, Yahagi K, Ladich E, Finn AV, et al. Natural progression of atherosclerosis from pathologic intimal thickening to late fibroatheroma in human coronary arteries: a pathology study. *Atherosclerosis.* (2015) 241:772–82. doi: 10.1016/j.atherosclerosis.2015.05.011
79. Burke AP, Jarvelainen H, Kolodgie FD, Goel A, Wight TN, Virmani R. Superficial pseudoaneurysms: clinicopathologic aspects and involvement of extracellular matrix proteoglycans. *Mod Pathol.* (2004) 17:482–8. doi: 10.1038/modpathol.3800060
80. Evanko S, Raines EW, Ross R, Gold LI, Wight TN. Proteoglycan distribution in lesions of atherosclerosis depends on lesion severity, structural characteristics and the proximity of platelet-derived growth factor and transforming growth factor-b. *Am J Pathol.* (1998) 152:533–46.
81. Farb A, Kolodgie FD, Hwang JY, Burke AP, Tefera K, Weber DK, et al. Extracellular matrix changes in stented human coronary arteries. *Circulation.* (2004) 110:940–7. doi: 10.1161/01.CIR.0000139337.56084.30
82. Olive M, Harten I, Mitchell R, Beers J, Djabali K, Cao K, et al. Cardiovascular pathology in Hutchinson-Gilford Progeria: Correlation with the vascular pathology of aging. *Arterioscler Thromb Vasc Biol.* (2010) 30:2301–9. doi: 10.1161/ATVBAHA.110.209460
83. Wight T, Evanko S, Kinsella MG, Chang MY, Yeop Han C, Sakr S, et al. The pro-inflammatory nature of the extracellular matrix. In: Matsuzawa Y, Kita T, Nagai R, Teramoto T, editors. *Atherosclerosis XIII*. Amsterdam: Elsevier B.V. (2004). p. 404–6.
84. Merrilees MJ, Beaumont BW, Braun KR, Thomas AC, Kang I, Hinek A, et al. Neointima formed by arterial smooth muscle cells expressing versican variant v3 is resistant to lipid and macrophage accumulation. *Arterioscler Thromb Vasc Biol.* (2011) 31:1309–16. doi: 10.1161/ATVBAHA.111.225573
85. Andersson-Sjoland A, Hallgren O, Rolandsson S, Weitoft M, Tykesson E, Larsson-Callerfelt AK, et al. Versican in inflammation and tissue remodeling: the impact on lung disorders. *Glycobiology.* (2015) 25:243–51. doi: 10.1093/glycob/cwu120
86. Bensadoun ES, Burke AK, Hogg JC, Roberts CR. Proteoglycan deposition in pulmonary fibrosis. *Am J Respir Crit Care Med.* (1996) 154:1819–28.
87. Chang MY, Tanino Y, Vidova V, Kinsella MG, Chan CK, Johnson PY, et al. A rapid increase in macrophage-derived versican and hyaluronan in infectious lung disease. *Matrix Biol.* (2014) 34:1–12. doi: 10.1016/j.matbio.2014.01.011
88. Kang I, Harten IA, Chang MY, Braun KR, Sheih A, Nivison MP, et al. Versican deficiency significantly reduces lung inflammatory response induced by polyinosine-polycytidylic acid stimulation. *J Biol Chem.* (2017) 292:51–63. doi: 10.1074/jbc.M116.753186
89. Reeves SR, Kaber G, Sheih A, Cheng G, Aronica MA, Merrilees MJ, et al. Subepithelial accumulation of versican in a cockroach antigen-induced murine model of allerigic asthma. *J Histochem Cytochem.* (2016) 64:364–80. doi: 10.1369/0022155416642989
90. Sobel RA, Ahmed AS. White matter extracellular matrix chondroitin sulfate/dermatan sulfate proteoglycans in multiple sclerosis. *J Neuropathol Exp Neurol.* (2001) 60:1198–207. doi: 10.1093/jnen/60.12.1198
91. Stephenson EL, Mishra MK, Moussienko D, Laflamme N, Rivest S, Ling CC, et al. Chondroitin sulfate proteoglycans as novel drivers of leucocyte infiltration in multiple sclerosis. *Brain.* (2018) 141:1094–110. doi: 10.1093/brain/awy033
92. Haylock-Jacobs S, Keough MB, Lau L, Yong VW. Chondroitin sulphate proteoglycans: extracellular matrix proteins that regulate immunity of the central nervous system. *Autoimmun Rev.* (2011) 10:766–72. doi: 10.1016/j.autrev.2011.05.019
93. de la Motte C, Hascall VC, Drazba JA, Strong SA. Poly I:C induces mononuclear leukocyte-adhesive hyaluronan structures on colon smooth muscle cells: IαI and versican facilitate adhesion. In: Kennedy JF, Phillips GO, Williams PA, Hascall VC, editors. *Hyaluronan: Chemical, Biochemical and Biological Aspects*. Cambridge, UK: Woodhead Publishing Limited. (2002). p. 381–8.
94. de la Motte CA, Hascall VC, Drazba J, Bandyopadhyay SK, Strong SA. Mononuclear leukocytes bind to specific hyaluronan structures on colon mucosal smooth muscle cells treated with polyinosinic acid:polycytidylic acid: inter-α-trypsin inhibitor is crucial to structure and function. *Am J Pathol.* (2003) 163:121–33. doi: 10.1016/s0002-9440(10)63636-x
95. Petrey AC, de la Motte CA. Hyaluronan, a crucial regulator of inflammation. *Front Immunol.* (2014) 5:101. doi: 10.3389/fimmu.2014.00101

96. Petrey AC, de la Motte CA. Hyaluronan in inflammatory bowel disease: cross-linking inflammation and coagulation. *Matrix Biol.* (2019) 78–79:314–23. doi: 10.1016/j.matbio.2018.03.011
97. Rienks M, Papageorgiou AP, Frangogiannis NG, Heymans S. Myocardial extracellular matrix: an ever-changing and diverse entity. *Circ Res.* (2014) 114:872–88. doi: 10.1161/CIRCRESAHA.114.302533
98. Kunisada M, Yogianti F, Sakumi K, Ono R, Nakabeppu Y, Nishigori C. Increased expression of versican in the inflammatory response to UVB- and reactive oxygen species-induced skin tumorigenesis. *Am J Pathol.* (2011) 179:3056–65. doi: 10.1016/j.ajpath.2011.08.042
99. Islam S, Chuensirikulchai K, Khummuang S, Keratibumrungpong T, Kongtawelert P, Kasinrerk W, et al. Accumulation of versican facilitates wound healing: implication of its initial ADAMTS-cleavage site. *Matrix Biol.* (2020) 87:77–93. doi: 10.1016/j.matbio.2019.10.006
100. Mukhopadhyay A, Nikopoulos K, Maugeri A, de Brouwer AP, van Nouhuys CE, Boon CJ, et al. Erosive vitreoretinopathy and wagner disease are caused by intronic mutations in CSPG2/Versican that result in an imbalance of splice variants. *Invest Ophthalmol Vis Sci.* (2006) 47:3565–72. doi: 10.1167/iovs.06-0141
101. Tang PH, Velez G, Tsang SH, Bassuk AG, Mahajan VB. VCAN canonical splice site mutation is associated with vitreoretinal degeneration and disrupts an MMP proteolytic site. *Invest Ophthalmol Vis Sci.* (2019) 60:282–93. doi: 10.1167/iovs.18-25624
102. Bogdani M, Johnson PY, Potter-Perigo S, Nagy N, Day AJ, Bollyky PL, et al. Hyaluronan and hyaluronan binding proteins accumulate in both human type 1 diabetic islets and lymphoid tissues and associate with inflammatory cells in insulitis. *Diabetes.* (2014) 63:2 727–43. doi: 10.2337/db13-1658
103. Keire PA, Kang I, Wight TN. Versican: Role in cancer tumorigenesis. In: Brekken RA, Stupack DG, editors. *Extracellular Matrix in Tumor Biology*. Cham: Springer International Publishing (2017). p. 51–74.
104. Theocharis AD, Karamanos NK. Proteoglycans remodeling in cancer: underlying molecular mechanisms. *Matrix Biol.* (2019) 75-76:220–59. doi: 10.1016/j.matbio.2017.10.008
105. Ricciardelli C, Sakko AJ, Ween MP, Russell DL, Horsfall DJ. The biological role and regulation of versican levels in cancer. *Cancer Metastasis Rev.* (2009) 28:233–45. doi: 10.1007/s10555-009-9182-y
106. LeBaron RG, Zimmermann DR, Ruoslahti E. Hyaluronate binding properties of versican. *J Biol Chem.* (1992) 267:10003–10.
107. Matsumoto K, Shionyu M, Go M, Shimizu K, Shinomura T, Kimata K, et al. Distinct interaction of versican/PG-M with hyaluronan and link protein. *J Biol Chem.* (2003) 278:41205–12. doi: 10.1074/jbc.M305060200
108. Kohda D, Morton CJ, Parkar AA, Hatanaka H, Inagaki FM, Campbell ID, et al. Solution structure of the link module: a hyaluronan-binding domain involved in extracellular matrix stability and cell migration. *Cell.* (1996) 86:767–75.
109. Day AJ, Prestwich GD. Hyaluronan-binding proteins: tying up the giant. *J Biol Chem.* (2002) 277:4585–8. doi: 10.1074/jbc.R100036200
110. Day AJ, Milner CM. TSG-6: A multifunctional protein with anti-inflammatory and tissue-protective properties. *Matrix Biol.* (2019) 78–79:60–83. doi: 10.1016/j.matbio.2018.01.011
111. Garantziotis S, Savani RC. Hyaluronan biology: A complex balancing act of structure, function, location and context. *Matrix Biol.* (2019) 78–79:1–10. doi: 10.1016/j.matbio.2019.02.002
112. Day AJ, de la Motte CA. Hyaluronan cross-linking: a protective mechanism in inflammation? *Trends Immunol.* (2005) 26:637–43. doi: 10.1016/j.it.2005.09.009
113. Tighe RM, Garantziotis S. Hyaluronan interactions with innate immunity in lung biology. *Matrix Biol.* (2019) 78–79:84–99. doi: 10.1016/j.matbio.2018.01.027
114. Gaucherand L, Falk BA, Evanko SP, Workman G, Chan CK, Wight TN. Crosstalk between T lymphocytes and lung fibroblasts: generation of a hyaluronan-enriched extracellular matrix adhesive for monocytes. *J Cell Biochem.* (2017) 118:2118–30. doi: 10.1002/jcb.25842
115. Potter-Perigo S, Johnson PY, Evanko SP, Chan CK, Braun KR, Wilkinson TS, et al. Polyinosine-polycytidylic acid stimulates versican accumulation in the extracellular matrix promoting monocyte adhesion. *Am J Respir Cell Mol Biol.* (2010) 43:109–20. doi: 10.1165/rcmb.2009-0081OC
116. Hascall VC, Majors AK, De La Motte CA, Evanko SP, Wang A, Drazba JA, et al. Intracellular hyaluronan: a new frontier for inflammation? *Biochim Biophys Acta.* (2004) 1673:3–12. doi: 10.0.1016/j.bbagen.2004.02.013
117. Jiang D, Liang J, Noble PW. Hyaluronan as an immune regulator in human diseases. *Physiol Rev.* (2011) 91:221–64. doi: 10.1152/physrev.00052.2009
118. Tang M, Diao J, Gu H, Khatri I, Zhao J, Cattral MS. Toll-like receptor 2 activation promotes tumor dendritic cell dysfunction by regulating IL-6 and IL-10 receptor signaling. *Cell Rep.* (2015) 13:2851–64. doi: 10.1016/j.celrep.2015.11.053
119. Kim S, Takahashi H, Lin WW, Descargues P, Grivennikov S, Kim Y, et al. Carcinoma-produced factors activate myeloid cells through TLR2 to stimulate metastasis. *Nature.* (2009) 457:102–6. doi: 10.1038/nature07623
120. Zheng PS, Vais D, Lapierre D, Liang YY, Lee V, Yang BL, et al. PG-M/versican binds to P-selectin glycoprotein ligand-1 and mediates leukocyte aggregation. *J Cell Sci.* (2004) 117:5887–95. doi: 10.1242/jcs.01516
121. Kawashima H, Atarashi K, Hirose M, Hirose J, Yamada S, Sugahara K, et al. Oversulfated chondroitin/dermatan sulfates containing GlcAbeta1/IdoAalpha1-3GalNAc(4,6-O-disulfate) interact with L- and P-selectin and chemokines. *J Biol Chem.* (2002) 277:12921–30. doi: 10.1074/jbc.M200396200
122. Kawashima H, Hirose M, Hirose J, Nagakubo D, Plaas AH, Miyasaka M. Binding of a large chondroitin sulfate/dermatan sulfate proteoglycan, versican, to L-selectin, P-selectin, and CD44. *J Biol Chem.* (2000) 275:35448–56. doi: 10.1074/jbc.M003387200
123. Wang W, Xu GL, Jia WD, Ma JL, Li JS, Ge YS, et al. Ligation of TLR2 by versican: a link between inflammation and metastasis. *Arch Med Res.* (2009) 40:321–3. doi: 10.1016/j.arcmed.2009.04.005
124. Poluzzi C, Nastase MV, Zeng-Brouwers J, Roedig H, Hsieh LT, Michaelis JB, et al. Biglycan evokes autophagy in macrophages via a novel CD44/Toll-like receptor 4 signaling axis in ischemia/reperfusion injury. *Kidney Int.* (2019) 95:540–62. doi: 10.1016/j.kint.2018.10.037
125. Zeng-Brouwers J, Beckmann J, Nastase MV, Iozzo RV, Schaefer L. De novo expression of circulating biglycan evokes an innate inflammatory tissue response via MyD88/TRIF pathways. *Matrix Biol.* (2014) 35:132–42. doi: 10.1016/j.matbio.2013.12.003
126. Kawashima H, Li YF, Watanabe N, Hirose J, Hirose M, Miyasaka M. Identification and characterization of ligands for L-selectin in the kidney. I. Versican, a large chondroitin sulfate proteoglycan, is a ligand for L-selectin. *Int Immunol.* (1999) 11:393–405. doi: 10.1093/intimm/11.3.393
127. Masuda A, Yasuoka H, Satoh T, Okazaki Y, Yamaguchi Y, Kuwana M. Versican is upregulated in circulating monocytes in patients with systemic sclerosis and amplifies a CCL2-mediated pathogenic loop. *Arthritis Res Ther.* (2013) 15:R74. doi: 10.1186/ar4251
128. Malla N, Berg E, Theocharis AD, Svineng G, Uhlin-Hansen L, Winberg JO. *In vitro* reconstitution of complexes between pro-matrix metalloproteinase-9 and the proteoglycans serglycin and versican. *FEBS J.* (2013) 280:2870–87. doi: 10.1111/febs.12291
129. Ra HJ, Harju-Baker S, Zhang F, Linhardt RJ, Wilson CL, Parks WC. Control of promatrilysin (MMP7) activation and substrate-specific activity by sulfated glycosaminoglycans. *J Biol Chem.* (2009) 284:27924–32. doi: 10.1074/jbc.M109.035147
130. Ra HJ, Parks WC. Control of matrix metalloproteinase catalytic activity. *Matrix Biol.* (2007) 26:587–96. doi: 10.1016/j.matbio.2007.07.001
131. Tocchi A, Parks WC. Functional interactions between matrix metalloproteinases and glycosaminoglycans. *FEBS J.* (2013) 280:2332–41. doi: 10.1111/febs.12198
132. Xu L, Xue T, Zhang J, Qu J. Knockdown of versican V1 induces a severe inflammatory response in LPS-induced acute lung injury via the TLR2-NF-kappaB signaling pathway in C57BL/6J mice. *Mol Med Rep.* (2016) 13:5005–12. doi: 10.3892/mmr.2016.5168
133. Coulson-Thomas VJ, Gesteira TF, Hascall V, Kao W. Umbilical cord mesenchymal stem cells suppress host rejection: The role of the glycocalyx. *J Biol Chem.* (2014) 289:23465–81. doi: 10.1074/jbc.M114.557447
134. Avnet S, Cortini M. Role of pericellular matrix in the regulation of cancer stemness. *Stem Cell Rev.* (2016) 12:464–75. doi: 10.1007/s12015-016-9660-x
135. Schwertfeger KL, Cowman MK, Telmer PG, Turley EA, McCarthy JB. Hyaluronan, inflammation, and breast cancer progression. *Front Immunol.* (2015) 6:236. doi: 10.3389/fimmu.2015.00236

136. Turley EA, Wood DK, McCarthy JB. Carcinoma cell hyaluronan as a "portable" cancerized prometastatic microenvironment. *Cancer Res.* (2016) 76:2507–12. doi: 10.1158/0008-5472.CAN-15-3114
137. de la Motte CA. Hyaluronan in intestinal homeostasis and inflammation: implications for fibrosis. *Am J Physiol Gastrointest Liver Physiol.* (2011) 301:G945–9. doi: 10.1152/ajpgi.00063.2011
138. de la Motte CA, Hascall VC, Calabro A, Yen-Lieberman B, Strong SA. Mononuclear leukocytes preferentially bind via CD44 to hyaluronan on human intestinal mucosal smooth muscle cells after virus infection or treatment with poly(I.C). *J Biol Chem.* (1999) 274:30747–55. doi: 10.1074/jbc.274.43.30747
139. Evanko SP, Potter-Perigo S, Johnson PY, Wight TN. Organization of hyaluronan and versican in the extracellular matrix of human fibroblasts treated with the viral mimetic poly I:C. *J Histochem Cytochem.* (2009) 57:1041–60. doi: 10.1369/jhc.2009.953802
140. Lauer ME, Fulop C, Mukhopadhyay D, Comhair S, Erzurum SC, Hascall VC. Airway smooth muscle cells synthesize hyaluronan cable structures independent of inter-alpha-inhibitor heavy chain attachment. *J Biol Chem.* (2009) 284:5313–23. doi: 10.1074/jbc.M807979200
141. Lauer ME, Mukhopadhyay D, Fulop C, de la Motte CA, Majors AK, Hascall VC. Primary murine airway smooth muscle cells exposed to poly(I,C) or tunicamycin synthesize a leukocyte-adhesive hyaluronan matrix. *J Biol Chem.* (2009) 284:5299–312. doi: 10.1074/jbc.M807965200.
142. Majors AK, Austin RC, de la Motte CA, Pyeritz RE, Hascall VC, Kessler SP, et al. Endoplasmic reticulum stress induces hyaluronan deposition and leukocyte adhesion. *J Biol Chem.* (2003) 278:47223–31. doi: 10.1074/jbc.M304871200
143. Wang A, Hascall VC. Hyaluronan structures synthesized by rat mesangial cells in response to hyperglycemia induce monocyte adhesion. *J Biol Chem.* (2004) 279:10279–85. doi: 10.1074/jbc.M312045200
144. Lauer ME, Erzurum SC, Mukhopadhyay D, Vasanji A, Drazba J, Wang A, et al. Differentiated murine airway epithelial cells synthesize a leukocyte-adhesive hyaluronan matrix in response to endoplasmic reticulum stress. *J Biol Chem.* (2008) 283:26283–96. doi: 10.1074/jbc.M803350200
145. Evanko SP, Potter-Perigo S, Bollyky PL, Nepom GT, Wight TN. Hyaluronan and versican in the control of human T-lymphocyte adhesion and migration. *Matrix Biol.* (2012) 31:90–100. doi: 10.1016/j.matbio.2011.10.004
146. Selbi W, de la Motte CA, Hascall VC, Day AJ, Bowen T, Phillips AO. Characterization of hyaluronan cable structure and function in renal proximal tubular epithelial cells. *Kidney Int.* (2006) 70:1287–95. doi: 10.1038/sj.ki.5001760
147. Wang A, de la Motte C, Lauer M, Hascall V. Hyaluronan matrices in pathobiological processes. *FEBS J.* (2011) 278:1412–8. doi: 10.1111/j.1742-4658.2011.08069.x
148. Fujii K, Karpova MB, Asagoe K, Georgiev O, Dummer R, Urosevic-Maiwald M. Versican upregulation in Sezary cells alters growth, motility and resistance to chemotherapy. *Leukemia.* (2015) 29:2024–32. doi: 10.1038/leu.2015.103
149. McMahon M, Ye S, Izzard L, Dlugolenski D, Tripp RA, Bean AG, et al. ADAMTS5 Is a critical regulator of virus-specific T cell immunity. *PLoS Biol.* (2016) 14:e1002580. doi: 10.1371/journal.pbio.1002580
150. Merrilees MJ, Zuo N, Evanko SP, Day AJ, Wight TN. G1 domain of versican regulates hyaluronan organization and the phenotype of cultured human dermal fibroblasts. *J Histochem Cytochem.* (2016) 64:353–63. doi: 10.1369/0022155416643913
151. Olsen NJ, Moore JH, Aune TM. Gene expression signatures for autoimmune disease in peripheral blood mononuclear cells. *Arthritis Res Ther.* (2004) 6:120–8. doi: 10.1136/ard.2003.017194
152. Shou J, Bull CM, Li L, Qian HR, Wei T, Luo S, et al. Identification of blood biomarkers of rheumatoid arthritis by transcript profiling of peripheral blood mononuclear cells from the rat collagen-induced arthritis model. *Arthritis Res Ther.* (2006) 8:R28. doi: 10.1186/ar1883
153. Wingrove JA, Daniels SE, Sehnert AJ, Tingley W, Elashoff MR, Rosenberg S, et al. Correlation of peripheral-blood gene expression with the extent of coronary artery stenosis. *Circ Cardiovasc Genet.* (2008) 1:31–8. doi: 10.1161/CIRCGENETICS.108.782730
154. Toeda K, Nakamura K, Hirohata S, Hatipoglu OF, Demircan K, Yamawaki H, et al. Versican is induced in infiltrating monocytes in myocardial infarction. *Mol Cell Biochem.* (2005) 280:47–56. doi: 10.1007/s11010-005-8051-4
155. Asplund A, Ostergren-Lunden G, Camejo G, Stillemark-Billton P, Bondjers G. Hypoxia increases macrophage motility, possibly by decreasing the heparan sulfate proteoglycan biosynthesis. *J Leukoc Biol.* (2009) 86:381–8. doi: 10.1189/jlb.0908536
156. Asplund A, Friden V, Stillemark-Billton P, Camejo G, Bondjers G. Macrophages exposed to hypoxia secrete proteoglycans for which LDL has higher affinity. *Atherosclerosis.* (2011) 215:77–81. doi: 10.1016/j.atherosclerosis.2010.12.017
157. Lang R, Patel D, Morris JJ, Rutschman RL, Murray PJ. Shaping gene expression in activated and resting primary macrophages by IL-10. *J Immunol.* (2002) 169:2253–63. doi: 10.4049/jimmunol.169.5.2253
158. Martinez FO, Gordon S, Locati M, Mantovani A. Transcriptional profiling of the human monocyte-to-macrophage differentiation and polarization: new molecules and patterns of gene expression. *J Immunol.* (2006) 177:7303–11. doi: 10.4049/jimmunol.177.10.7303
159. Pappas AG, Magkouta S, Pateras IS, Skianis I, Moschos C, Vazakidou ME, et al. Versican modulates tumor-associated macrophage properties to stimulate mesothelioma growth. *Oncoimmunology.* (2019) 8:e1537427. doi: 10.1080/2162402X.2018.1537427
160. Bogen O, Dina OA, Gear RW, Levine JD. Dependence of monocyte chemoattractant protein 1 induced hyperalgesia on the isolectin B4-binding protein versican. *Neuroscience.* (2009) 159:780–6. doi: 10.1016/j.neuroscience.2008.12.049
161. Said N, Sanchez-Carbayo M, Smith SC, Theodorescu D. RhoGDI2 suppresses lung metastasis in mice by reducing tumor versican expression and macrophage infiltration. *J Clin Invest.* (2012) 122:1503–18. doi: 10.1172/JCI61392
162. Said N, Theodorescu D. RhoGDI2 suppresses bladder cancer metastasis via reduction of inflammation in the tumor microenvironment. *Oncoimmunology.* (2012) 1:1175–7. doi: 10.4161/onci.20594
163. Villani AC, Satija R, Reynolds G, Sarkizova S, Shekhar K, Fletcher J, et al. Single-cell RNA-seq reveals new types of human blood dendritic cells, monocytes, and progenitors. *Science.* (2017) 356:eaah4573. doi: 10.1126/science.aah4573
164. Hanahan D, Weinberg RA. Hallmarks of cancer: the next generation. *Cell.* (2011) 144:646–74. doi: 10.1016/j.cell.2011.02.013
165. Du WW, Yang W, Yee AJ. Roles of versican in cancer biology–tumorigenesis, progression and metastasis. *Histol Histopathol.* (2013) 28:701–13. doi: 10.14670/HH-28.701
166. Grivennikov SI, Greten FR, Karin M. Immunity, inflammation, and cancer. *Cell.* (2010) 140:883–99. doi: 10.1016/j.cell.2010.01.025
167. Dos Reis DC, Damasceno KA, de Campos CB, Veloso ES, Pegas GRA, Kraemer LR, et al. Versican and tumor-associated macrophages promotes tumor progression and metastasis in canine and murine models of breast carcinoma. *Front Oncol.* (2019) 9:577. doi: 10.3389/fonc.2019.00577
168. Keire PA, Bressler SL, Lemire JM, Edris B, Rubin BP, Rahmani M, et al. A role for versican in the development of leiomyosarcoma. *J Biol Chem.* (2014) 289:34089–103. doi: 10.1074/jbc.M114.607168
169. Derynck R, Goeddel DV, Ullrich A, Gutterman JU, Williams RD, Bringman TS, et al. Synthesis of messenger RNAs for transforming growth factors alpha and beta and the epidermal growth factor receptor by human tumors. *Cancer Res.* (1987) 47:707–12.
170. Van Bockstal M, Lambein K, Van Gele M, De Vlieghere E, Limame R, Braems G, et al. Differential regulation of extracellular matrix protein expression in carcinoma-associated fibroblasts by TGF-beta1 regulates cancer cell spreading but not adhesion. *Oncoscience.* (2014) 1:634–48. doi: 10.18632/oncoscience.87
171. Kodama J, Hasengaowa, Kusumoto T, Seki N, Matsuo T, Nakamura K, et al. Versican expression in human cervical cancer. *Eur J Cancer.* (2007) 43:1460–6. doi: 10.1016/j.ejca.2007.02.007
172. Kodama J, Hasengaowa, Kusumoto T, Seki N, Matsuo T, Ojima Y, et al. Prognostic significance of stromal versican expression in human endometrial cancer. *Ann Oncol.* (2007) 18:269–74. doi: 10.1093/annonc/mdl370

173. Fanhchaksai K, Okada F, Nagai N, Pothacharoen P, Kongtawelert P, Hatano S, et al. Host stromal versican is essential for cancer-associated fibroblast function to inhibit cancer growth. *Int J Cancer.* (2016) 138:630–41. doi: 10.1002/ijc.29804
174. Ozdemir BC, Pentcheva-Hoang T, Carstens JL, Zheng X, Wu CC, Simpson TR, et al. Depletion of carcinoma-associated fibroblasts and fibrosis induces immunosuppression and accelerates pancreas cancer with reduced survival. *Cancer Cell.* (2014) 25:719–34. doi: 10.1016/j.ccr.2014.04.005
175. Asano K, Nelson CM, Nandadasa S, Aramaki-Hattori N, Lindner DJ, Alban T, et al. Stromal versican regulates tumor growth by promoting angiogenesis. *Sci Rep.* (2017) 7:17225. doi: 10.1038/s41598-017-17613-6
176. Ghosh S, Albitar L, LeBaron R, Welch WR, Samimi G, Birrer MJ, et al. Up-regulation of stromal versican expression in advanced stage serous ovarian cancer. *Gynecol Oncol.* (2010) 119:114–20. doi: 10.1016/j.ygyno.2010.05.029
177. Labropoulou VT, Theocharis AD, Ravazoula P, Perimenis P, Hjerpe A, Karamanos NK, et al. Versican but not decorin accumulation is related to metastatic potential and neovascularization in testicular germ cell tumours. *Histopathology.* (2006) 49:582–93. doi: 10.1111/j.1365-2559.2006.02558.x
178. Kreutziger KL, Muskheli V, Johnson P, Braun K, Wight TN, Murry CE. Developing vasculature and stroma in engineered human myocardium. *Tissue Eng Part A.* (2011) 17:1219–28. doi: 10.1089/ten.TEA.2010.0557
179. Fu Y, Nagy JA, Brown LF, Shih SC, Johnson PY, Chan CK, et al. Proteolytic cleavage of versican and involvement of ADAMTS-1 in VEGF-A/VPF-induced pathological angiogenesis. *J Histochem Cytochem.* (2011) 59:463–73. doi: 10.1369/0022155411401748
180. Gao D, Vahdat LT, Wong S, Chang JC, Mittal V. Microenvironmental regulation of epithelial-mesenchymal transitions in cancer. *Cancer Res.* (2012) 72:4883–9. doi: 10.1158/0008-5472.CAN-12-1223
181. Gao D, Joshi N, Choi H, Ryu S, Hahn M, Catena R, et al. Myeloid progenitor cells in the premetastatic lung promote metastases by inducing mesenchymal to epithelial transition. *Cancer Res.* (2012) 72:1384–94. doi: 10.1158/0008-5472.CAN-11-2905
182. Gutmann DH. Microglia in the tumor microenvironment: taking their TOLL on glioma biology. *Neuro Oncol.* (2015) 17:171–3. doi: 10.1093/neuonc/nou346
183. Senda M, Fukuyama R, Nagasaka T. Kinetics of versican-expressing macrophages in bone marrow after cord blood stem cell transplantation for treatment of acute myelogenous leukaemia. *J Clin Pathol.* (2016) 69:906–11. doi: 10.1136/jclinpath-2015-203496
184. Hope C, Ollar SJ, Heninger E, Hebron E, Jensen JL, Kim J, et al. TPL2 kinase regulates the inflammatory milieu of the myeloma niche. *Blood.* (2014) 123:3305–15. doi: 10.1182/blood-2014-02-554071
185. Arana P, Zabaleta A, Lasa M, Maiso P, Alignani D, Jelinek T, et al. High-throughput characterization and new insight into the role of tumor associated macrophages (TAMs) in multiple myeloma (MM). *Blood.* (2016) 128:482. doi: 10.1182/blood.V128.22.482.482
186. Spranger S, Dai D, Horton B, Gajewski TF. Tumor-residing Batf3 dendritic cells are required for effector T cell trafficking and adoptive T cell therapy. *Cancer Cell.* (2017) 31:711–23 e4. doi: 10.1016/j.ccell.2017.04.003
187. Dhakal B, Pagenkopf A, Umair Mushtaq M, Cunningham AM, Flietner E, Morrow Z, et al. Versican proteolysis predicts immune effector infiltration and post-transplant survival in myeloma. *Leuk Lymphoma.* (2019) 60:2558–62. doi: 10.1080/10428194.2019.1585836
188. Binder MJ, McCoombe S, Williams ED, McCulloch DR, Ward AC. The extracellular matrix in cancer progression: Role of hyalectan proteoglycans and ADAMTS enzymes. *Cancer Lett.* (2017) 385:55–64. doi: 10.1016/j.canlet.2016.11.001
189. Dvorak HF. Tumors: wounds that do not heal. Similarities between tumor stroma generation and wound healing. *N Engl J Med.* (1986) 315:1650–9.
190. Dvorak HF. Tumors: wounds that do not heal-redux. *Cancer Immunol Res.* (2015) 3:1–11. doi: 10.1158/2326-6066.CIR-14-0209
191. Joyce JA, Fearon DT. T cell exclusion, immune privilege, and the tumor microenvironment. *Science.* (2015) 348:74–80. doi: 10.1126/science.aaa6204
192. Gorter A, Zijlmans HJ, van Gent H, Trimbos JB, Fleuren GJ, Jordanova ES. Versican expression is associated with tumor-infiltrating CD8-positive T cells and infiltration depth in cervical cancer. *Mod Pathol.* (2010) 23:1605–15. doi: 10.1038/modpathol.2010.154
193. Hartley G, Regan D, Guth A, Dow S. Regulation of PD-L1 expression on murine tumor-associated monocytes and macrophages by locally produced TNF-alpha. *Cancer Immunol Immunother.* (2017) 66:523–35. doi: 10.1007/s00262-017-1955-5
194. Jiang H, Hegde S, DeNardo DG. Tumor-associated fibrosis as a regulator of tumor immunity and response to immunotherapy. *Cancer Immunol Immunother.* (2017) 66:1037–48. doi: 10.1007/s00262-017-2003-1
195. Nicholas NS, Apollonio B, Ramsay AG. Tumor microenvironment (TME)-driven immune suppression in B cell malignancy. *Biochim Biophys Acta.* (2016) 1863:471–82. doi: 10.1016/j.bbamcr.2015.11.003
196. Tang H, Wang Y, Chlewicki LK, Zhang Y, Guo J, Liang W, et al. Facilitating T cell infiltration in tumor microenvironment overcomes resistance to PD-L1 blockade. *Cancer Cell.* (2016) 29:285–96. doi: 10.1016/j.ccell.2016.02.004
197. Hernandez D, Miquel-Serra L, Docampo MJ, Marco-Ramell A, Cabrera J, Fabra A, et al. V3 versican isoform alters the behavior of human melanoma cells by interfering with CD44/ErbB-dependent signaling. *J Biol Chem.* (2011) 286:1475–85. doi: 10.1074/jbc.M110.127522
198. Miquel-Serra L, Serra M, Hernández D, Domenzain C, Docampo MJ, Rabanal R, et al. V3 versican isoform expression has a dual role in human melanoma tumor growth and metastasis. *Lab Invest.* (2006) 86:889–901. doi: 10.1038/labinvest.3700449
199. Serra M, Miquel L, Domenzain C, Docampo MJ, Fabra A, Wight TN, et al. V3 versican isoform expression alters the phenotype of melanoma cells and their tumorigenic potential. *Int J Cancer.* (2005) 114:879–86. doi: 10.1002/ijc.20813

Conflict of Interest: The authors declare that the research was conducted in the absence of any commercial or financial relationships that could be construed as a potential conflict of interest.

frontiers in Immunology

REVIEW
published: 31 March 2020
doi: 10.3389/fimmu.2020.00483

Targeting Chemokine—Glycosaminoglycan Interactions to Inhibit Inflammation

*Helena Crijns, Vincent Vanheule and Paul Proost**

Laboratory of Molecular Immunology, Department of Microbiology, Immunology and Transplantation, Rega Institute for Medical Research, KU Leuven, Leuven, Belgium

Leukocyte migration into tissues depends on the activity of chemokines that form concentration gradients to guide leukocytes to a specific site. Interaction of chemokines with their specific G protein-coupled receptors (GPCRs) on leukocytes induces leukocyte adhesion to the endothelial cells, followed by extravasation of the leukocytes and subsequent directed migration along the chemotactic gradient. Interaction of chemokines with glycosaminoglycans (GAGs) is crucial for extravasation *in vivo*. Chemokines need to interact with GAGs on endothelial cells and in the extracellular matrix in tissues in order to be presented on the endothelium of blood vessels and to create a concentration gradient. Local chemokine retention establishes a chemokine gradient and prevents diffusion and degradation. During the last two decades, research aiming at reducing chemokine activity mainly focused on the identification of inhibitors of the interaction between chemokines and their cognate GPCRs. This approach only resulted in limited success. However, an alternative strategy, targeting chemokine-GAG interactions, may be a promising approach to inhibit chemokine activity and inflammation. On this line, proteins derived from viruses and parasites that bind chemokines or GAGs may have the potential to interfere with chemokine-GAG interactions. Alternatively, chemokine mimetics, including truncated chemokines and mutant chemokines, can compete with chemokines for binding to GAGs. Such truncated or mutated chemokines are characterized by a strong binding affinity for GAGs and abrogated binding to their chemokine receptors. Finally, Spiegelmers that mask the GAG-binding site on chemokines, thereby preventing chemokine-GAG interactions, were developed. In this review, the importance of GAGs for chemokine activity *in vivo* and strategies that could be employed to target chemokine-GAG interactions will be discussed in the context of inflammation.

Keywords: chemokine, chemotaxis, heparin, heparan sulfate, leukocyte migration

OPEN ACCESS

Edited by:
Rogier M. Reijmers, Leiden University Medical Center, Netherlands

Reviewed by:
Sergey Samsonov, University of Gdansk, Poland
Douglas Philip Dyer, University of Manchester, United Kingdom

****Correspondence:***
Paul Proost
paul.proost@kuleuven.be

Specialty section:
This article was submitted to Cytokines and Soluble Mediators in Immunity, a section of the journal Frontiers in Immunology

Received: *30 November 2019*
Accepted: *02 March 2020*
Published: *31 March 2020*

Citation:
Crijns H, Vanheule V and Proost P (2020) Targeting Chemokine—Glycosaminoglycan Interactions to Inhibit Inflammation. Front. Immunol. 11:483. doi: 10.3389/fimmu.2020.00483

INTRODUCTION

Chemotactic cytokines or chemokines, complement fragments C3a and C5a, bioactive lipids such as leukotrienes, and formylated peptides interact with specific G protein-coupled receptors (GPCRs) on leukocytes and are predominant mediators of leukocyte migration to an inflammatory site (1). Chemokines constitute a family of about 50 small, mostly secreted proteins comprising between 60 and 90 amino acids (2, 3). Chemokines are the only group of cytokines that interact

with GPCRs (4, 5). In contrast to other chemoattractants, chemokines are characterized by their specificity for leukocyte subsets (5). Accordingly, chemokine receptors are expressed on different groups of leukocytes in a cell-specific manner (3, 6). Pathogen-associated molecular patterns (PAMPs), derived from an infectious microorganism, can directly induce the production of chemokines through pattern recognition receptors (PRRs) by tissue-resident immune cells, including macrophages, and numerous parenchymal and stromal cells. In addition, chemokine production can be caused by endogenous molecules associated with injury or infection, including defensins and elastase, and by signaling of danger molecules through PRRs (7). Binding of locally produced chemokines to their chemokine receptors induces leukocyte adhesion to the endothelial cells, followed by extravasation of the leukocytes and subsequent directed migration to the site of inflammation (2, 3). To be exposed on the endothelial layer of blood vessels and to create a concentration gradient, chemokines need to bind to glycosaminoglycans (GAGs) such as heparan sulfate (HS) on endothelial cells and in tissues (8–10). In addition to regulating leukocyte trafficking, chemokines play a role in cell survival, effector responses such as degranulation and the coordination of recirculation and homing of lymphocytes. However, the function of chemokines is not restricted to leukocyte physiology alone, since they contribute to several processes such as tumor growth and metastasis, haematopoiesis, angiogenesis, and organogenesis (3, 5, 11).

Chemokines can be classified into functional groups. Inflammatory chemokines are involved in the recruitment of effector leukocytes to the site of inflammation. They are induced upon infection, inflammation, tissue injury, tumors or other stress factors. Examples of inflammatory chemokines include CXCL1-3, CXCL5-6, and CXCL8, which regulate neutrophil recruitment. Homeostatic chemokines, by contrast are constitutively expressed and regulate basal leukocyte migration. An example of a homeostatic chemokine is CCL27, which plays a role in skin homing of T cells. Some chemokines demonstrate both inflammatory and homeostatic activities, hence they are referred to as dual-function chemokines (3, 11–13). These include CXCL12, which is important for the retention of neutrophils in the bone marrow (BM), and also synergizes with other chemoattractants to attract inflammatory cells (14).

Alternatively, chemokines can be classified based on their structure according to a conserved tetra-cysteine motif that forms two disulphide bridges and that determines the specific tertiary chemokine structure. Four subfamilies can be defined based on the position of the two NH_2-terminal cysteine residues. In the CC chemokine subgroup, the two first cysteine residues are adjacent, whereas these residues are separated by one or three amino acids in the CXC and CX3C chemokine subfamilies, respectively. C chemokines are an exception, since they lack two conserved cysteine residues (3, 7, 12). The CXC chemokines can be subdivided in either ELR^+ or ELR^- CXC chemokines. ELR^+ CXC chemokines include a Glu-Leu-Arg amino acid sequence preceding the CXC sequence and are neutrophil attractants with angiogenic activity (3, 15). CXC chemokines lacking the ELR motif that bind to CXC chemokine receptor 3 (CXCR3) act on natural killer (NK) cells and activated T lymphocytes and display angiostatic activity. Members of this group include CXCL4, CXCL4L1, CXCL9, CXCL10, and CXCL11 (16). Although chemokines demonstrate low amino acid sequence homology, their tertiary structure is characterized by remarkable similarities (3).

TWO MAIN INTERACTION PARTNERS OF CHEMOKINES: CHEMOKINE RECEPTORS AND GLYCOSAMINOGLYCANS

Chemokines Receptors

GPCRs with seven transmembrane domains mediate the recognition of chemokine-encoded messages (7). These GPCRs comprise a polypeptide chain with three intracellular and three extracellular loops, a serine/threonine-rich intracellular COOH-terminal and an acidic NH_2-terminal extracellular domain. Receptor signaling and internalization is mediated by the transmembrane domains, cytoplasmic loops and COOH-terminal domain. The NH_2-terminal domain and a pocket created by the transmembrane domains and extracellular loops are involved in ligand recognition (1). A unique structural feature of the chemokine receptors is the DRYLAIV amino acid sequence present in the second intracellular loop domain, which is required for efficient coupling with G proteins of the $G_{\alpha i}$ class (5, 12). The chemokine receptors are classified into four subfamilies in accordance with the cysteine motifs of their main ligands: CXCR, CCR, CX3CR, and XCR (1, 12). Upon binding of chemokines, chemokine receptors undergo conformational changes giving rise to the activation of intracellular effectors via G proteins and/or β-arrestins, initiating signal transduction pathways and cellular responses (17–23).

In addition, several atypical chemokine receptors (ACKRs) have been identified (6, 24). These atypical receptors are characterized by a modified or lacking DRYLAIV motif, resulting in the inability of eliciting conventional G protein-coupled signaling processes. The ACKRs influence the internalization and function of chemokines through interaction with β-arrestin signaling pathways. They regulate inflammatory and immune responses by functioning as scavenger or decoy receptors or chemokine transporters (1, 3, 12).

Most inflammatory chemokines bind to several receptors and most chemokine receptors recognize multiple ligands. This binding promiscuity is characteristic for the chemokine network (3, 5). Thus, the chemokine/chemokine receptor network seems highly redundant (25). However, this functional redundancy is not absolute (26, 27). It has been suggested that chemokines are under temporal and spatial control *in vivo*, and that the localization and timing determine a different biological outcome in different tissues. To ensure appropriate inflammatory responses and to avoid undesirable inflammation, this complex system must be tightly controlled, thereby enabling fine-tuning of leukocyte responses to different inflammatory stimuli. The mechanisms which regulate the interactions between chemokines and chemokine receptors, including down-regulation of chemokine activity by atypical

receptors, alternative signaling responses and posttranslational modifications (PTMs), have recently been reviewed (28–30). In contrast to the originally expected redundancy of the chemokine network, recent work demonstrates extreme specificity of the chemokine/chemokine receptor system. Girbl et al., identified distinct and non-redundant roles for two murine CXCR2 ligands CXCL1 and CXCL2 in neutrophil transendothelial migration (31). In addition, Coombs et al. revealed that differential trafficking of the chemokine receptors CXCR1 and CXCR2 regulates neutrophil clustering and dispersal at sites of tissue damage in zebrafish (32). Furthermore, Dyer et al. provide evidence for both redundancy and specificity of the chemokine receptors CCR1, CCR2, CCR3 and CCR5 dependent on the context (33).

The interactions of chemokines and chemokine receptors were traditionally described by a two-step/two-site mechanism (34–36). In the spatial formulation (i.e., two-site), the NH_2-terminus of the receptor recognizes the chemokine globular core (site 1 interaction), followed by the insertion of the unstructured chemokine NH_2-terminus into the receptor transmembrane bundle (site 2 interaction). In the functional formulation (i.e., two-step), site 1 provides affinity and specificity, whereas site 2 elicits receptor activation. With this knowledge, it is not surprising that minor modifications at the NH_2-terminus of chemokines may have profound effects on their activity. However, more and more evidence supports a more complex model (multiple steps/multiple binding sites in the interaction of chemokines and their receptors) to mediate increasingly diverse outcomes (37). The new paradigms in chemokine receptor signal transduction have recently been reviewed by Kleist et al. (38). These authors indicate that we should move beyond the two-site model, since chemokine receptor signaling is influenced by PTMs of chemokine receptors, chemokine, and chemokine receptor dimerization and endogenous non-chemokine ligands.

Glycosaminoglycans (GAGs)

GAGs are negatively charged, linear polysaccharides comprising repeated disaccharide units, varying in basic composition of the saccharide, linkage, and patterns of acetylation and N- and O-sulphation. The structures of GAGs are highly variable in composition and length, ranging from 1 to 25,000 disaccharide units. Therefore, these polysaccharides exhibit the largest diversity among biological macromolecules (8, 39). GAGs interact with a wide variety of proteins, including proteases, growth factors, cytokines, chemokines and adhesion molecules, enabling them to participate in physiological processes, such as protein function, cellular adhesion and signaling (9, 40). GAGs can be classified into six groups: heparan sulfate (HS), heparin, chondroitin sulfate (CS), dermatan sulfate (DS), keratan sulfate (KS), and hyaluronic acid (HA) (39). The structures and disaccharide composition of GAGs are shown in **Figure 1**. The disaccharide subunits are composed of an amino sugar residue [N-acetyl-D-galactosamine (GalNAc) or N-acetyl-D-glucosamine (GlcNAc)] and an uronic

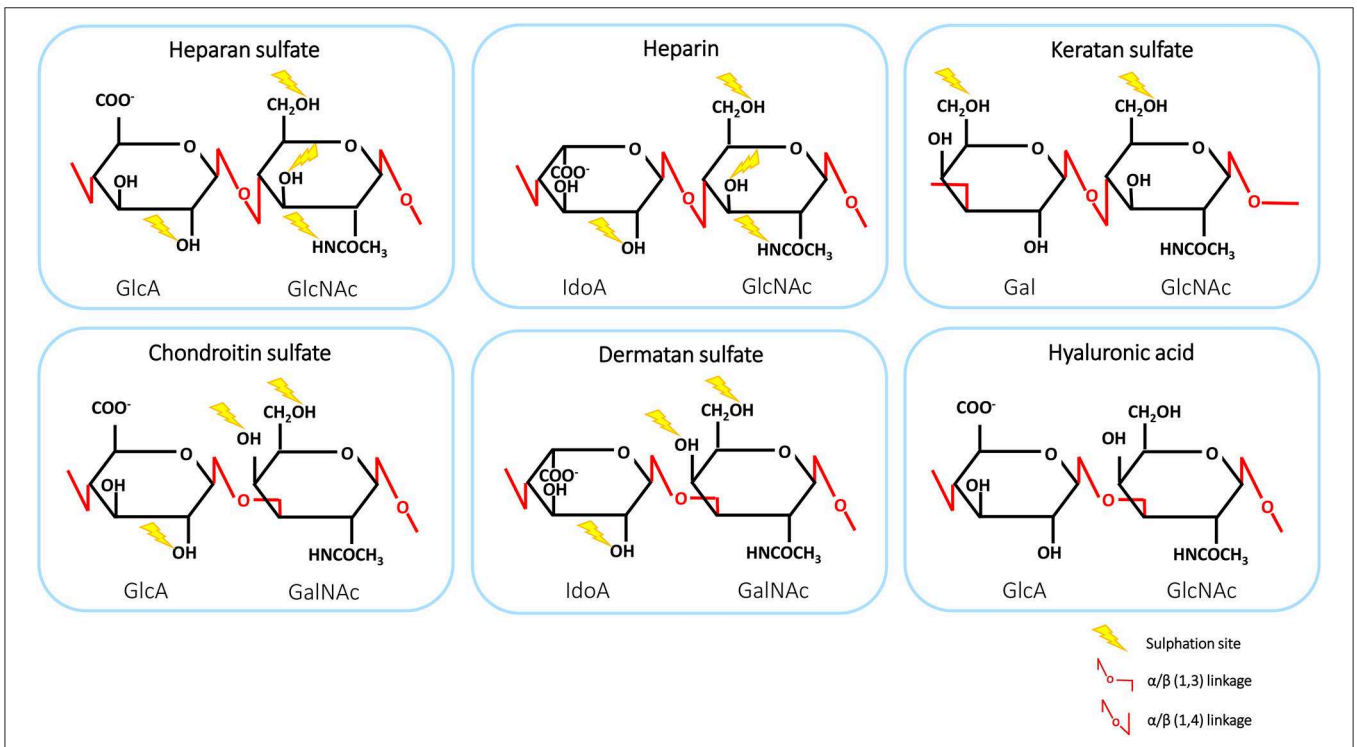

FIGURE 1 | The structure and disaccharide composition of glycosaminoglycans (GAGs). The backbone of GAGs consists of repeating disaccharide subunits, composed of uronic acid or galactose and an amino sugar. Linkages are shown in red and sites of sulphation are indicated by yellow lightning bolts. GlcA, D-glucuronic acid; GlcNAc, N-acetyl-D-glucosamine; GalNAc, N-acetyl-D-galactosamine; Gal, D-galactose; IdoA, L-iduronic acid.

acid residue [D-glucuronic acid (GlcA) or L-iduronic acid (IdoA)] or D-galactose (Gal) (41, 42). Interestingly, HS has a multidomain structure with sulphated IdoA-containing domains or NS-domains (usually 5-10 disaccharides) separated by flexible spacers of low sulphation that have an acetylated GlcA-GlcNAc sequence (43). HS proteoglycans (HSPGs) account for 50 to 90% of total endothelial proteoglycans (PGs) (44). GAGs, including heparin and HA, can be present in plasma as soluble molecules. Alternatively, GAGs are encountered in surface-bound forms as PGs (8, 39). GAGs, other than heparin and HA, are frequently found covalently attached to protein cores, thereby forming PGs (9). These structures are ubiquitously present on cell surfaces as well as in the extracellular matrix (ECM). There, the PGs serve as a macromolecular coating, also known as glycocalyx, which can interact with proteins such as chemokines (8).

Chemokine binding to GAGs is required for chemokine-induced leukocyte migration *in vivo*. Mutants demonstrating impaired GAG-binding capacity retained the ability to induce chemotaxis *in vitro*, but failed to elicit cell migration *in vivo* (45–49). Chemokines interact with GAGs of the ECM and endothelial cell surfaces (39, 45, 50, 51). Immobilization of chemokines enables the formation of a chemokine gradient, which is indispensable for leukocyte recruitment. This tethering mechanism prevents the diffusion of the chemokines in the blood stream and facilitates localized high concentrations of chemokines that are produced (39, 45). Furthermore, GAGs may play a role in the abluminal-to-luminal transcytosis of chemokines (52, 53). In addition, GAGs may protect chemokines against proteolysis and may influence chemokine-GPCR signaling, thereby regulating chemokine function (9, 54–56).

THE IMPORTANCE OF CHEMOKINE-GLYCOSAMINOGLYCAN INTERACTIONS

Leukocyte Extravasation, Gradient Formation, and Transcytosis of Chemokines

A hallmark of immune cell trafficking at sites of inflammation and in normal immune surveillance is the migration of leukocytes from the circulation across the endothelium. Therefore, leukocytes need to adhere to the luminal surface of the endothelium. As an inflammatory response develops, cytokines and other inflammatory mediators stimulate the local expression of cell adhesion molecules. First, leukocytes attach to the endothelium by a low-affinity interaction between selectins on the endothelium and their carbohydrate counter-ligands mediating leukocyte tethering and rolling (52, 57–60). In this way, chemokines are able to bind to their leukocyte-specific chemokine receptor(s) resulting in the activation of integrins on the leukocyte. The interaction between the leukocyte integrins and their ligands, such as immunoglobulin-like intercellular adhesion molecules, mediates firm adhesion to the endothelium, enabling the leukocyte to force its way between endothelial cells (52). During this transendothelial migration, the leukocyte squeezes in between two neighboring endothelial cells without disrupting the integrity of the endothelial barrier (61). For neutrophils, this is accomplished by homotypic binding of platelet endothelial cell adhesion molecule-1 (PECAM-1) on the neutrophil with PECAM-1 within the endothelial junction (62). Moreover, it has been shown that PECAM-1 is able to bind heparin and HS by a site that is distinct from that required for haemophilic binding (63). In addition, leukocytes were shown to migrate through endothelial cells (64–66). This process of transcellular migration involves many of the same molecules and mechanisms that regulate paracellular migration.

To ensure the directional guidance of leukocytes across the endothelium and through the ECM into the tissue, a chemoattractant gradient is necessary. However, soluble chemokine gradients cannot persist on the luminal endothelial surface, since they are disturbed by the blood flow (67–69). In addition, soluble chemoattractant gradients would activate leukocytes in the circulation prior to their selectin-mediated adhesive interaction with the endothelium, resulting in the loss of leukocytes' ability to initiate adhesion and emigration (70). Therefore, it has been proposed that chemokines that are bound or immobilized on the luminal endothelial surface more effectively promote leukocyte adhesion to the endothelium and subsequent migration. A first proof of this haptotaxis was the *in situ* binding of CXCL8 to endothelial cells of venules and veins in human skin and the ability of immobilized CXCL8 to induce *in vitro* neutrophil migration (71, 72). In addition, chemokines undergo transcytosis through the endothelium and are presented at the luminal surface to adherent leukocytes. Both CXCL8 and CCL5 were bound at the abluminal surface of the endothelium, internalized into caveolae and transported transcellularly to the luminal surface (57). It has even been shown that a COOH-terminally truncated CXCL8 analog with impaired heparin binding and impaired immobilization on endothelial HS was unable to be transcytosed and lost its capacity to induce neutrophil migration *in vitro* and *in vivo* (57). Because many of the cell types that produce chemokines are extravascular, chemokine transcytosis and presentation by the endothelium provides a mechanism where through chemokines can stimulate leukocyte emigration (73). A similar mechanism has been shown for CCL19 in the high endothelial venules of lymphoid tissues where it mediates T cell recruitment and suggests a role for this mechanism in normal immune surveillance (74). Noteworthy, endothelial cells also produce chemokines themselves, which are stored in Weibel-Palade bodies and do not need to be transcytosed (73, 75).

In addition, ACKR1 or the duffy antigen receptor for chemokines (DARC), expressed on red blood cells and endothelial cells of postcapillary venules, was shown to bind chemokines, such as CXCL1, CXCL8, CCL2, and CCL5, in inflamed and normal human tissues (76, 77). Mice with targeted disruption of the ACKR1 gene show no developmental abnormalities, but show increased inflammatory infiltrates in lung, liver and/or peritoneum when challenged with lipopolysaccharide (LPS) and/or thioglycolate (78, 79). These data suggest that the intensity of inflammatory reactions is modulated by ACKR1 and that ACKR1 acts as a sink for chemokines. Endothelial ACKR1 may also play a role in

chemokine transcytosis in endothelial cells, since it is localized to endothelial caveolae and binds and internalizes chemokines (80, 81). Moreover, it has been suggested that ACKR1 acts as a chemokine-presenting molecule on the endothelium (82). Girbl et al. revealed a self-guided migration response of transmigrating neutrophils. More specifically, neutrophil-derived CXCL2 was presented on ACKR1 at endothelial junctions, thereby enabling unidirectional, paracellular transendothelial migration of neutrophils *in vivo* (31). However, chemokines bound to ACKR1 on red blood cells do not activate neutrophils anymore (82). Therefore, GAGs may be more important in chemokine presentation.

Although very difficult to prove *in vivo*, chemoattractant gradient formation has been reported in tissues and venules. Recently, chemokines were shown to localize within postcapillary venules in a GAG-dependent way. For example, localized extravascular release of CXCL2 induced directed migration of neutrophils along a haptotactic gradient on the endothelium toward the tissue as visualized by intravital microscopy (50). This sequestration of chemokines occurred only in venules and was HS-dependent. Transgenic mice overexpressing heparanase showed altered and random crawling of neutrophils in response to CXCL2, which was translated into a decreased number of emigrated neutrophils. In addition, fluorescently labeled CXCL8 formed an extracellular gradient in zebrafish tissue that decays within a distance of 50–100 μm from the producing cells and that was immobilized on HSPGs on the local venous vasculature (51). Inhibition of this interaction compromised both directional guidance and restriction of neutrophil motility. This suggests that leukocytes, once in the tissue, can migrate to the site of inflammation through the gradient of local GAG-bound chemokines. Analogously, endogenous HS-dependent gradients of CCL21 were detected within mouse skin, guiding dendritic cells toward lymphatic vessels (83). These data support the hypothesis that chemokine production at sites of inflammation results in the generation of GAG-mediated chemokine gradients and chemokine presentation by GAGs on the endothelial cell surface, thereby preventing their diffusion and degradation and retaining a high local concentration of the chemokines (52). Finally, blood vessels pattern HS gradients between the apical and basolateral axis (84). Resting and inflamed postcapillary skin venules, as well as high endothelial venules of lymph nodes, show higher HS densities in the basal lamina. Furthermore, the luminal glycocalyx of skin vessels and microvascular dermal cells contained much lower HS densities than their basolateral ECM. Noteworthy, progressive skin inflammation by intradermal injections of complete Freund's adjuvant resulted in massive ECM deposition and in further enrichment of the HS content nearby inflamed vessels. Recently, silencing of exostosin-1, a key enzyme in the biosynthesis of HS, was shown to reduce the directional guidance of neutrophils across inflamed endothelial barriers (85). This again suggesting an important role for basolateral HS. Strikingly, however, effector T cell transendothelial migration is not altered upon silencing of exostosin-1, suggesting that chemotactic signals from intra-endothelial chemokine stores are sufficient to induce the migration of effector T cells.

Binding to Glycosaminoglycans Is Indispensable for Chemokine Activity *in vivo*

The binding of chemokines to GAGs and oligomerization have been proven to be indispensable for chemokine activity *in vivo* (45, 48, 86, 87). Proudfoot et al. demonstrated that mutations in the GAG-binding sites of CCL2, CCL4 and CCL5 result in abrogated GAG binding and a compromised recruitment of cells *in vivo* when injected intraperitoneally, although receptor binding and *in vitro* chemotactic activity in Boyden chemotaxis chambers were seldom affected. Even at a dose 10,000-fold higher than the active dose of the wild-type chemokines, the mutants with reduced affinity for GAGs showed no activity *in vivo*. Noteworthy, the losses in potency *in vitro* can be attributed to the small losses of receptor affinity and to the impaired interaction with GAGs on the recruited cells, because GAGs can enhance the localization of chemokines to these cells *in vitro* (88). This also indicates that in general chemokines do not need to be immobilized on GAGs to induce chemotaxis *in vitro*. However, recently cis presentation of CXCL4 on GAGs, expressed on leukocytes, was reported to affect *in vitro* cell migration (89).

In addition, inactivation of bifunctional HS N-deacetylase sulphotransferase (NDST-1) in endothelial cells, which is required for sulphation of HS chains, results in impaired neutrophil infiltration in various inflammation models, although these mutant mice develop normally (53). The neutrophil adhesion and migration were reduced because of impaired chemokine transcytosis across the endothelium and reduced chemokine presentation on the endothelial surface. In addition, neutrophil infiltration was decreased to a certain extent due to altered rolling velocity and weaker binding of L-selectin to endothelial cells. In summary, endothelial HS has an important function during inflammation: acting as a ligand for L-selectin during neutrophil rolling, playing a role in chemokine transcytosis and being responsible for the binding and presentation of chemokines at the luminal surface of the endothelium.

Selectivity and Specificity in Chemokine-Glycosaminoglycan Interactions

Most chemokines are highly basic proteins and therefore it was stated that chemokine-GAG binding largely depends on non-specific electrostatic interactions. However, a certain degree of specificity mediated by van der Waals and hydrogen bonds has been ascribed to this interaction. This was exemplified by binding of the acidic chemokines CCL3 and CCL4 to GAGs (8, 45). In addition, the electrostatic interactions do not necessarily reflect the binding capacity of chemokines to heparin. Although CXCL11 and CXCL12 bound with higher affinity to a non-specific cation exchange resin than CCL5, CCL5 bound stronger to the heparin Sepharose column (9). Before, Kuschert et al. described that GAGs interact with chemokines in a selective manner, providing evidence for GAG sequence specificity. At first, chemokines were shown to exhibit a wide variation in the affinity for heparin and endothelial cells, with, for example,

higher affinity binding of CCL5 compared to CCL3 (90, 91). Second, chemokines were shown to possess selectivity in the strength of interaction with GAGs, suggesting that chemokines can discriminate between them. For CCL5, the order is heparin, DS, HS, CS, whereas for CXCL8 and CCL2 the order is heparin, HS, CS and DS. Further, CXCL8 and CXCL1 were shown to bind preferentially to a subset of heparin molecules, whereas CXCL4 and CXCL7 did not show this preference (92). It is important to realize that almost all studies rely on the use of natural GAGs, which are heterogeneous in length and carboxylation and sulphation patterns. Detailed knowledge on interaction of proteins with specific GAG structures depends on the availability of well-described, homogeneous GAG structures. However, chemical synthesis of such specific GAG structures is far more complex than the synthesis of oligonucleotides or peptides.

Several groups have determined the GAG-binding sites in chemokines by using mutagenesis studies, nuclear magnetic resonance (NMR) spectroscopy and mass spectrometry. These studies revealed that typically basic amino acids (Arg, Lys, and His) are involved in GAG binding and that the main GAG-binding motifs on chemokines frequently take the form BBXB or BBBXXBX, in which B and X represent a basic and any amino acid, respectively (93). First, it was stated that the GAG-binding domains are located at a site distant from the specific receptor-binding domain, often within the COOH-terminus of the chemokines. However, the GAG-binding domains were located sometimes in the 40 s loop or in the 20 s loop of chemokines. On the other hand, the GAG-binding motif of CXCL10 is a more widely distributed non-BBXB pattern. Thus, for some chemokines the GAG-binding site is not restricted to the COOH-terminus and has an overlap with receptor-binding sites. Therefore, the question whether chemokines simultaneously bind to GAGs on the endothelium and to their receptor on leukocytes remains unanswered and may be chemokine-dependent. Since chemokines show distinctly different GAG-binding epitopes, these data provide a strong indication for specificity of chemokine-GAG binding.

In addition to the GAG-binding motifs of chemokines, specific chemokine-binding epitopes on GAGs have been identified. Although, for example, N-sulphated groups on HS were not necessary, 2-O-sulphated groups on the iduronic acid units were required for the formation of a GAG-dependent CXCL4 tetramer (94). In addition, a binding site for CXCL8 and CCL3 was identified on HS (95, 96).

Oligomerization of Chemokines by Glycosaminoglycan Binding

Many chemokines form dimers or higher-order oligomers, thereby adding more complexity to the structural biology of the chemokine system (97). In addition, CXCL12 dimerization was reported to depend on the presence of heparin (98). CXC chemokines dimerize through the interaction of residues in their β1-strands, thereby forming a six-stranded β-sheet structure topped by two α-helices. Importantly, this dimer structure leaves the NH_2-terminus, N-loop and β3-strand exposed on the surface of the dimer. In this way, CXC chemokine dimers still bind and activate chemokine receptors. In contrast, many CC chemokines dimerize into elongated structures by the formation of an antiparallel β-sheet between the NH_2-terminal regions. Therefore, it was stated that CC chemokine dimers are inactive. In addition to dimers, several chemokines form higher-order oligomers. For example, CXCL4 and CCL3 form tetramers and polymers, respectively (97).

As discussed before, chemokine-GAG binding is important for the localization and the presentation of chemokines on cell surfaces as haptotactic gradients. Moreover, many chemokines oligomerize on GAGs and are stabilized by GAG binding. This chemokine oligomerization and stabilization is essential for chemokine activity *in vivo* (45, 86, 87, 91, 99). For example, monomeric P8A-CCL2 was incapable of recruiting leukocytes in two *in vivo* models of inflammation. Surprisingly, *in vitro*, the monomeric variants are fully active. Also in other studies, monomeric forms of CXCL8, CCL5, CCL4 and the non-oligomerizing chemokine CCL7 have been shown to bind their receptor and to induce chemotaxis *in vitro* (100–103). Therefore, it can be stated that the monomeric form is sufficient for receptor binding and induction of the directed migration of cells. However, some steps in the process of *in vivo* migration may involve oligomers. Sometimes the monomeric and dimeric forms of the chemokine show different receptor binding and GAG interactions. Both interactions are essential for *in vivo* activity, as exemplified by CXCL8 (104). Moreover, the steepness of the chemokine gradient determined by reversible oligomerization is an important factor in the chemotactic response (104, 105).

It was even stated that oligomerization of chemokines increases their affinity for GAGs by providing a more extensive binding surface. In the presence of GAGs, CCL2 formed a tetramer, whereas normally only a dimer is formed (106). In contrast, the CXCL4 tetramer is stable in the absence of GAGs. Dyer et al. showed that oligomerization-deficient mutants of CCL5 and CXCL4 have reduced affinity for heparin, HS and CS compared with their wild-type counterparts (99). In addition, oligomerization may be required for chemokines to simultaneously bind the receptor and the GAG. Certainly, when the chemokine has overlapping GAG- and receptor-binding sites. Alternatively, Graham et al. suggested a "chemokine cloud" model in which chemokines are presented as molecules sequestered in "solution" in a hydrated glycocalyx (107).

In summary, chemokine oligomerization may be important for the local concentration of the chemokine, thereby preventing their diffusion and degradation. Indeed, GAGs protected chemokines from degradation. CCL11 binding to heparin protected the chemokine from proteolysis by plasmin, cathepsin G and elastase (55). In addition, heparin and HS specifically prevented the processing of CXCL12 by CD26/dipeptidyl peptidase IV (DPP IV) (54, 56). Since cleavage of chemokines by proteases can affect their activity, this protection can serve as an additional degree of regulation prolonging the duration of the chemokine signal (108).

THE BINDING OF CHEMOKINES TO GLYCOSAMINOGLYCANS

The Binding of ELR$^+$ CXC Chemokines to Glycosaminoglycans

Consequences of CXCL1, CXCL2, and CXCL6 Binding to Glycosaminoglycans

Already in the 1980s, CXCL2 was described as a GAG-binding protein secreted by monocytes and macrophages and inducing the migration of polymorphonuclear leukocytes (109, 110). However, only years later Wang et al. described the *in vivo* importance of CXCL2 binding to GAGs (53). In mice with endothelial HS deficiency (Ndst $^{-/-}$ mice) the migration of neutrophils in response to CXCL1 and CXCL2 was significantly decreased. Moreover, in case of CXCL1, the immobilization on the endothelium was decreased in Ndst$^{-/-}$ mice and binding to CXCR2 was dependent on HSPGs (111). In addition, KSPGs formed a chemokine gradient to mediate infiltration of neutrophils to the cornea through interaction with CXCL1, indicating the importance of these PG/CXCL1 complexes in the inflammatory response in eye inflammation (112, 113). A study using CXCL2 mutants with impaired GAG binding also demonstrated that GAG regulation of chemokine activity is tissue-dependent (114). An overview of the processes that are affected by chemokine-GAG interactions is displayed in **Table 1**.

Rajasekaran et al. identified important GAG-binding residues in CXCL2, e.g., Asp19, Lys21, Lys61, Lys65, and Lys69 by NMR spectroscopy (114). Heparin binding enhanced the stability of the CXCL1 and CXCL2 homodimers (115). This enhanced stability upon interaction with GAGs is suggested to increase the lifetime of chemokines, thereby regulating the *in vivo* neutrophil recruitment. The GAG interactions with CXCL2 did not interfere with receptor binding and promoted formation of the GAG/CXCL2/CXCR2 complex. In contrast, two GAG-binding epitopes were identified in CXCL1 as an α-domain, consisting of residues in the N-loop and in the COOH-terminal helix, and a β-domain, consisting of residues in the NH_2-terminus, 40s loop and the third β-strand indicating an extensive overlap of the GAG-binding and receptor-binding domains (116). CXCL1 mutants with impaired GAG-binding affinity clearly showed reduced neutrophil recruitment to the peritoneum (117). Recently, K_D-values below 100 nM for CXCL1, CXCL2, and CXCL6 on HS were determined by surface plasmon resonance (SPR) analysis (119). Finally, it was shown that CXCL10 and a COOH-terminal GAG-binding peptide of CXCL9 were able to compete with CXCL1 for GAG binding (111, 174).

A study performed by Tanino et al. showed clear differences in GAG binding between CXCL1 and CXCL2 (118). Due to more rapid association and dissociation of murine CXCL1 from immobilized heparin, CXCL1 was more effective in the recruitment of neutrophils compared to CXCL2. This suggests that chemokines, such as CXCL2, form gradients relatively slowly compared to chemokines that interact with rapid kinetics to GAGs. Thus, different types of chemokine gradients may be formed during an inflammatory response suggesting a new model, whereby GAGs control the spatiotemporal formation of chemokine gradients and neutrophil migration in tissue (118).

Consequences of CXCL5 and CXCL7 Binding to Glycosaminoglycans

More than 20 years ago CXCL5 and CXCL7 were purified from epithelial cells and platelets, respectively, using heparin Sepharose chromatography (175–177). Only recently, the basic residues important for GAG binding were identified by NMR spectroscopy (127, 128). Those studies demonstrated that several residues involved in GAG binding are also involved in receptor binding, indicating that the GAG-bound monomer cannot activate its receptor. For CXCL5, the dimer is the high-affinity binding ligand with lysine residues from the N-loop, 40 s turn, β3-strand and COOH-terminal helix being important for GAG binding. In addition, it is known that CXCL7 forms heterodimers with other chemokines, e.g., CXCL1. This CXCL1/CXCL7 heterodimer interacts differently with GAGs compared to the CXCL7 monomer and the GAG-bound heterodimer cannot interact with the receptor (178). These data suggest that GAG interactions play a prominent role in determining heterodimer function *in vivo*.

Consequences of CXCL8 Binding to Glycosaminoglycans

CXCL8 is a pro-inflammatory member of the CXC chemokine family attracting polymorphonuclear neutrophils. This chemokine is released at sites of inflammation by cytokine-activated endothelial cells. CXCL8 triggers neutrophils via its specific GPCRs, CXCR1, and CXCR2. In addition, CXCL8 binds to GAGs on the endothelium (129). In 1993, Webb et al. described that progressive COOH-terminal truncation of CXCL8 decreased the affinity for heparin Sepharose (135). In addition, Nordsieck et al. showed that COOH-terminal truncation of this chemokine resulted in an affinity loss of CXCL8 for GAGs due to an alteration of its GAG-binding site (179). Moreover, addition of HS to CXCL8 in a Boyden chemotaxis assay increased the neutrophil chemotactic activity *in vitro*. In contrast, co-incubation of CXCL8 with heparin or dextran sulfate decreased the chemotaxis of neutrophils (133, 134). Also *in vivo* the effects of GAG binding to CXCL8 were not that clear. First, the COOH-terminus was confirmed to be important for GAG binding, transcytosis and the *in vivo* activity of CXCL8 (57). However, several CXCL8 mutants with impaired GAG binding showed higher chemoattractant activity for neutrophils when instilled into the lungs of mice (118).

CXCL8 also bound GAGs on endothelial cells and HS beads with affinities in the micromolar range (90). However, this GAG binding was inhibited by the addition of soluble GAGs. Surprisingly, different GAGs competed differentially with binding of the chemokine to immobilized GAGs, suggesting selectivity. Moreover, the presence of soluble GAGs reduced the receptor binding and the resulting calcium flux. Interestingly, GAGs could alter neutrophil responses, inhibiting the release of elastase from stimulated neutrophils and enhancing the

TABLE 1 | Overview of the processes that are affected by chemokine-GAG interactions.

Chemokine	GAG	Affected process	References
CXCL1	Heparin, HS	Stability of CXCL1 homodimer, formation of chemokine gradient for cellular trafficking, neutrophil migration in the lung	(115–118)
	HS	Binding to CXCR2 and neutrophil migration *in vivo*	(53, 111, 119)
	KS	Gradient formation in inflammatory response in the eye	(112, 113)
CXCL2	Heparin	GAG/CXCL2/CXCR2 complex formation	(114)
		Stability of CXCL2 homodimer	(115)
		Neutrophil migration in the lung	(118)
	HS	Neutrophil migration *in vivo* in response to CXCL2	(53, 119)
CXCL4	Heparin, HS, CS	High affinity binding	(92, 94, 120–124)
	Cellular GAGs	Prevention of degradation	(125, 126)
CXCL5	Heparin	Heterodimer formation *in vivo*	(127)
CXCL6	HS	High affinity binding	(119)
CXCL7	Heparin	Heterodimer formation *in vivo*	(128)
CXCL8	Heparin, DS, CS, HA	High affinity binding	(129–132)
	HS	CXCL8-induced formation of reactive oxygen species and *in vitro* chemotaxis of neutrophils	(133, 134)
		Inhibition of elastase release	(135)
		High affinity binding	(129)
		Neutrophil activity *in vivo,* inhibition of elastase release from neutrophils	(135)
	Endothelial GAGs	*In vivo* neutrophil migration, transcytosis	(57)
		Oligomerization	(91)
CXCL9	Heparin, CS, HS	Protection from CD26/DPPIV activity	(54)
	HS	Recruitment of plasmacytoid cells	(136)
	Endothelial GAGs	Recruitment and transendothelial migration of T cells	(137)
CXCL10	Heparin, HS	High affinity binding	(138–140)
		Oligomerization	(141)
		Recruitment of plasmacytoid cells	(136)
		Anti-proliferative effect on endothelial cells	(138)
		Anti-fibrotic effect in lungs	(142, 143)
		Antiviral effect against Dengue virus	(144)
	Endothelial GAGs	Recruitment and transendothelial migration of T cells	(137)
CXCL11	Heparin	Cell migration *in vivo*	(142, 145)
		High affinity binding	(99, 119)
	HS	High affinity binding	(99, 119)
		Recruitment of plasmacytoid cells	(136)
	Endothelial GAGs	Recruitment and transendothelial migration of T cells	(137)
CXCL12	Heparin, HS	High affinity binding	(146–151)
		Oligomerization	(99)
		Protection from CD26/DPPIV activity	(56)
		T cell activation in rheumatoid arthritis synovium	(150, 151)
		Intraperitoneal leukocyte accumulation and angiogenesis	(148)
		Anti-HIV activity	(152)
	Heparin, HA, CS, DS	High affinity binding	(146, 149, 153, 154)
CCL2	Heparin, HS	High affinity binding	(99, 103, 155, 156)
		Oligomerization	(106, 157)
		Heterodimerization	(158)
		In vivo cell recruitment	(106)
	Heparin, HS, HA, CS, cellular GAGs	High affinity binding	(90, 91, 159)
CCL3	Heparin, HS, DS, CS	High affinity binding and oligomerization	(88, 90, 91, 96, 160, 161)
CCL4	Heparin, HS, DS, CS	High affinity binding and oligomerization	(88, 90, 162–164) (91, 165)
CCL5	Heparin, HS	High affinity binding	(88)
		Oligomerization	(166, 167)

(Continued)

TABLE 1 | Continued

Chemokine	GAG	Affected process	References
		In vivo biological function	(168–170)
		Firm adhesion of leukocytes to endothelial cells, transendothelial migration of macrophages *in vitro*	(168, 171)
		CCL5-dependent apoptosis in T cells	(172)
CCL7	Heparin, HS	High affinity binding	(103, 155, 156, 173)
		Recruitment of leukocytes *in vivo*	(49, 106, 157)
		Heterodimerization	(158)
CCL8	Heparin	Oligomerization	(106, 157)
CCL13	Heparin	High affinity binding	(173)
		Heterodimerization	(158)

GAG, glycosaminoglycan; HS, Heparan sulfate; KS, keratan sulfate; CS, chondroitin sulfate; DS, dermatan sulfate; HA, hyaluronic acid; DPPIV, dipeptidyl peptidase IV; HIV, human immunodeficiency virus.

CXCL8-induced formation of reactive oxygen species (ROS) in neutrophils (133, 135).

More recently, another study with GAG hexasaccharides confirmed the micromolar affinities (130). Although high-affinity binding for both chondroitin-6-sulfate and heparin was determined, the binding constants for chondroitin-4-sulfate, DS and HA were considerably lower. These data indicate that the 6-O-sulfate groups in chondroitin-6-sulfate and heparin/HS are important for the interaction with CXCL8. The binding of CXCL8 to GAGs is driven by strong ionic interactions between the sulfate groups of the carbohydrates and the basic residues of the protein. In particular, the basic residues His23 and Lys25 in the proximal loop and Arg65, Lys69, Lys72, and Arg73 located in the COOH-terminal α-helix of CXCL8(1–77) were binding anchors for the anionic GAGs (**Figure 2A**) (180, 181). More recently, the importance of Lys25, Lys69, Lys72, and Glu75 for GAG binding was confirmed and evidenced (131, 132). Interestingly, using affinity co-electrophoresis, it was suggested that conserved glucuronic acid residues in the putative GAG-binding domain of CXCL8 confer GAG selectivity in chemokines. CXCL8 preferentially bound a subfraction of heparin, which was not preferentially bound by CXCL4 (92). Therefore, it was suggested that GAGs are able to determine the specificity of leukocyte recruitment *in vivo*. In addition, it was proven that the length of GAGs plays an important role for CXCL8 binding (90).

Hoogewerf et al. also revealed the importance of GAGs for the oligomerization of chemokines (91). However, the length of GAGs involved in the experimental set-up gave rise to different results. GAG oligosaccharides with chain lengths of up to 16 monosaccharide units showed higher affinity to monomeric CXCL8. In contrast, GAG 22- to 24-mers interacted well with dimeric CXCL8, which can be explained by conformational differences. Longer GAGs contain a more flexible and less sulphated linker domain which connects two terminal, fully sulphated NS-domains thereby forming a horseshoe-like conformation (95, 182). Joseph et al. investigated the structural basis underlying binding of CXCL8 monomers and dimers to GAGs. The CXCL8 dimer was shown to be the high-affinity GAG ligand. In addition, evidence was provided that the binding interface is structurally plastic, thereby mediating a multiplicity of CXCL8-GAG binding interactions. The amino acid residues involved in binding to the GAG comprise a set of core residues that function as the major recognition/binding site and a set of residues in the periphery of the core residues that define the binding geometries of the interaction (183).

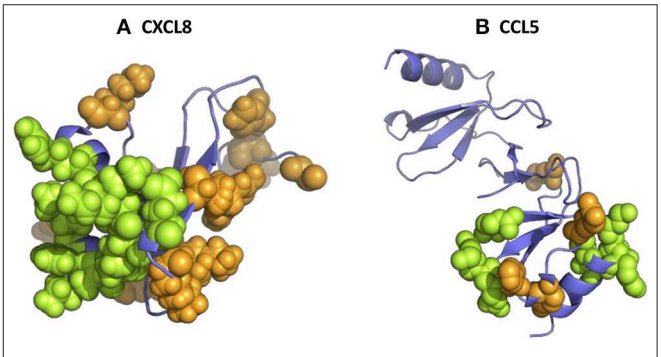

FIGURE 2 | The 3D structure of human CXCL8 and CCL5 and their glycosaminoglycan (GAG)-binding amino acids. 3D models of human CXCL8 **(A)** and CCL5 **(B)** were drawn from PDB accession codes 4XDX and 5COY, respectively, to visualize the location of the amino acids which were shown to be important for GAG binding (green). In addition, other basic amino acids are visualized in orange.

The Binding of ELR⁻ CXC Chemokines to Glycosaminoglycans

Consequences of CXCL4 and CXCL4L1 Binding to Glycosaminoglycans

One of the first properties assigned to CXCL4 was its strong affinity for GAGs. In 1976, Levine et al. introduced a purification method to isolate human CXCL4 from activated platelets, namely heparin Sepharose affinity chromatography (120, 184). In addition, CXCL4 showed high affinity for other GAGs, including HS and CS (121). CXCL4 was secreted as a tetramer in a complex with two molecules of CSPGs. In contrast, only one HS bound to the CXCL4 tetramer (94). Using SPR analysis, K_D-values of CXCL4 for GAGs in the nanomolar range were determined (92, 122–124, 185). Interestingly, CXCL4L1, which only differs from CXCL4 in three COOH-terminal amino acids, had significantly

reduced GAG-binding properties (125, 186, 187). Moreover, CXCL4L1 lost its ability to bind to CS. Therefore, it can be stated that CXCL4L1 is less tightly associated to the cell surface than CXCL4 and diffuses much more efficiently after secretion. In contrast, CXCL4 was released by activated platelets in the circulation and subsequently bound to the cell surface leading to rapid clearance from the blood and prevention of its degradation (125, 126). Treatment with heparin resulted in the release of CXCL4 into the circulation (188).

First, a cluster of four lysine residues in the COOH-terminal part of CXCL4 was believed to be critical for GAG binding (94, 120). An analog of CXCL4, with mutations in the four lysines at the COOH-terminus, showed complete loss of heparin binding but retained the ability to suppress the growth of tumors in mice (125, 189). However, other amino acids such as Arg22, His23, Arg24, Tyr25, Lys46, and Arg49 were also involved in the binding to GAGs (123). More recently, Leu67 was shown to be critical for the GAG affinity and Pro58 for binding to CS. In addition, an oligomerization-deficient mutant of CXCL4 had reduced affinity for GAGs compared to wild-type CXCL4 (99).

Recently, a multifunctional protein, TNF-stimulated gene (TSG)-6, was shown to interact with CXCL4 thereby blocking its interactions with GAGs and modulating the inflammatory response (190). In addition, TSG-6 bound GAGs directly, thereby limiting the available GAGs for chemokine interactions.

Consequences of CXCL9, CXCL10, and CXCL11 Binding to Glycosaminoglycans

The three CXCR3 ligands, CXCL9, CXCL10, and CXCL11, attract activated T lymphocytes and NK cells and interact with GAGs to conduct their *in vivo* function. Luster et al. first described the binding of CXCL10 or interferon-gamma-inducible protein-10 to cell surface HSPGs on a variety of cells including endothelial, epithelial and haematopoietic cells (138). Originally, it was stated that the chemokine-GAG binding and receptor-binding domain are distinct. However, for CXCL10, experimental evidence exists that the heparin- and CXCR3-binding sites are partially overlapping (139). Mutations of residues 20–24 and 46–47 caused both reduced heparin binding and reduced CXCR3 binding and signaling. For CXCL11, it was described that the COOH-terminus plays an important role in GAG binding since cleavage of CXCL11(5–73) to CXCL11(5–58) by matrix metalloproteinases (MMP) results in loss of heparin binding (145). Indeed, mutations of Lys17 and of basic residues in the COOH-terminal loop, namely ^{57}KSKQAR^{62}, impaired heparin binding without altering the affinity for CXCR3, indicating distinct heparin- and CXCR3-binding sites (142). However, the mutant was unable to induce cell migration *in vivo*. Interestingly, CXCL11(5–73) was a CXCR3 antagonist with enhanced affinity for heparin (145). In addition, citrullination, the deamination of Arg at position 5 into citrulline, decreased the heparin-binding properties of both CXCL10 and CXCL11 (191). Recently, SPR analysis revealed that murine CXCL10 has a higher affinity for HS than murine CXCL11 with affinities in the nanomolar range (119). As an important note, another study reported different affinities of CXCL11 for heparin and HS (below 10 nM) and revealed an important role for O-sulphation since the affinity of CXCL11 for 2-O-desulphated heparin was reduced (99). Since CXCL9 competed with CXCL8 for binding to heparin, the former chemokine was shown to bind GAGs. More recently, it was shown that GAGs protect CXCR3 ligands against processing by CD26/DPP IV and interfere with receptor signaling (54).

The recruitment of plasmacytoid dendritic cells is mediated by CXCR3, which encounters its ligands (CXCL9, CXCL10, and CXCL11) immobilized by HS (136). Furthermore, the arterial recruitment and the transendothelial migration of T cells was inhibited by soluble heparin which competes with CXCL9, CXCL10, and CXCL11 for binding to endothelial GAGs (137). This phenomenon may contribute to the therapeutic effect of heparin in inflammatory arterial diseases and supports the use of non-anticoagulant heparin derivatives as novel anti-inflammatory therapy. In addition, there is experimental evidence that GAGs not only directly regulate CXCR3 ligand function by chemokine binding. HA fragments, derived from the ECM, were demonstrated to synergize with IFN-γ, leading to enhanced CXCL9 expression in macrophages via NFκB (192). In addition, HA fragments induced the production of CXCL8 and CXCL10 in primary airway epithelial cells in a mitogen-activated protein (MAP) kinase or NFκB-dependent pathway, respectively (193). Noteworthy, this induction was specific for low-molecular-weight HA fragments. In contrast, heparin inhibited the stimulatory effect of IFN-γ on the production of CXCL9 and CXCL10 by human breast cancer cells by inhibiting cellular IFN-γ binding and modulating the IFN-γ-induced signal transducer and activator of transcription 1 (STAT1) phosphorylation (194). CXCL10 is also active on other cell types, such as endothelial cells and fibroblasts. Campanella et al. demonstrated that CXCL10 had anti-proliferative effects on endothelial cells independent of CXCR3 (195). Furthermore, it was suggested that this anti-proliferative effect and the angiostatic properties on endothelial cells are mediated by its specific HS binding site (138). However, there is experimental evidence that the angiostatic effect of CXCL10 in human melanoma was not dependent on GAGs, but was mediated by CXCR3 (196). It was even stated that Arg22 is essential for both CXCR3 binding and angiostasis. In addition, the anti-fibrotic effects of CXCL10 in lungs of mice, in the infarcted myocardium and in cardiac fibroblasts were independent of CXCR3 and required GAG binding (143, 197). Interestingly, the heparin-binding domains of CXCL10 and CXCL11, but not CXCL9, were also involved in binding to the ECM proteins fibrinogen and fibronectin (198). Moreover, fibronectin and CXCL11 synergized in keratinocyte migration and in wound healing *in vivo*, suggesting that interactions between chemokines and the ECM are not restricted to GAG binding.

Also, for CXCL10, oligomerization induced by GAG binding was required for its presentation on endothelial cells and *in vivo* activity (45, 86, 141). Furthermore, oligomerization of chemokines enhanced their affinity for GAGs and affected their ability to be presented by HS (141). In addition, chemokines rigidified and cross-linked HS, thereby changing the mobility of HS. Therefore, it was suggested that chemokine-GAG interactions may promote receptor-independent events such as the rearrangement of the endothelial ECM and signaling through

PGs. CXCL11 also displays conformational heterogeneity, explaining the multiple affinity states of CXCL11 for CXCR3 and heparin (142). In addition, interaction of the anti-inflammatory protein TSG-6 and CXCL11 through their GAG-binding epitopes was demonstrated (190).

Further, CXCL10 exerted part of its antiviral properties against dengue virus (DENV) through competition with viral binding to cell surface HS (144). Indeed, DENV rapidly induces the expression of CXCL10 in the liver. Along this line, a COOH-terminal GAG-binding CXCL9 fragment inhibited infection of cells with DENV serotype 2, herpes simplex virus-1 and respiratory syncytial virus. The CXCL9-derived peptide inhibited binding of the DENV envelope protein domain II to heparin (199). In this way, these chemokines play another important role in the host defense against viral infection.

Consequences of the Interaction of CXCL12 Proteins With Glycosaminoglycans

CXCL12, also known as stromal cell-derived factor-1 (SDF-1), is constitutively expressed within tissues during organogenesis and adult life orchestrating a lot of functions and it is involved in many pathological mechanisms (200). These physiopathological effects are mediated by CXCR4, to which the chemokine binds and triggers cell signaling. In addition, CXCL12 bound to several cell types in a GAG-dependent manner (146–151). For example, CXCL12 bound to PGs on BM endothelial cells, thereby presenting it to haematopoietic progenitor cells (147). In addition, CXCL12 and CXCL12γ were displayed on HSPGs by endothelial cells in rheumatoid arthritis (RA) synovium (150, 151). Furthermore, CXCL12/GAG interaction was mediated by inflammatory cytokines. In all of the above cases, treatment of the tissue with GAG-degrading enzymes or with sodium chlorate reduced or abrogated the binding of the chemokine. The binding of CXCL12 was diminished on GAG-deficient cells as well.

Amara et al. demonstrated that CXCL12α binds to heparin with high affinity (K_D 38.4 nM) through the first β-strand of the chemokine (146). Indeed, substitution of three basic amino acids in this β-strand, namely Lys24, His25, and Lys27, with Ser impaired the interaction with sensorchip-immobilized heparin. In addition to this typical heparin-binding consensus sequence BBXB, Arg41, and Lys43 played a role in binding of a polysaccharide fragment consisting of 13 monosaccharide units (153). Panitz et al. confirmed the distinct GAG interaction sites of CXCL12 by NMR spectroscopy and molecular modeling (154). Noteworthy, the GAG-binding domains and the receptor-binding sites of CXCL12 were spatially distant (201). Murphy et al. generated an x-ray structure of human CXCL12 in complex with unsaturated heparin disaccharides. Moreover, the specific molecular interactions between the chemokine and heparin were defined (202). The 3D structure of this human CXCL12: heparin disaccharide complex (PDB accession code 2NWG) is shown in **Figure 3**. Two interaction sites for heparin disaccharide molecules are displayed on a CXCL12 dimer configuration. One heparin disaccharide binds to the dimer interface and forms hydrogen bonds with His25 of subunit 2, Lys27 of subunit 1 and Arg41 of both CXCL12 subunits **(Figures 3A–C)**. The second disaccharide binds to the NH_2-terminal loop and the α-helix and interacts with Arg20, Ala21, and Lys64 of subunit 1 and Asn30 of subunit 2 of the CXCL12 dimer **(Figures 3D–F)**. His25 and Lys27 belong to a BBXB GAG-binding motif (Lys24 – Lys27) (202). On the contrary, the other aforementioned amino acid residues are not part of GAG-binding motifs, thereby emphasizing the importance of the 3D structural arrangement of positively charged amino acids for the ability to bind GAGs.

In contrast to CXCL12α, the splicing variant CXCL12γ has an extremely long and basic COOH-terminal extension, which contains as much as 18 basic residues, of which 9 being clustered into three putative BBXB HS-binding domains. As expected, CXCL12γ showed much higher affinity for GAGs compared to CXCL12α and CXCL12β (149). Moreover, the unstructured cationic domain of CXCL12γ extended the range of GAGs to which it can bind. The higher affinity of CXCL12γ for GAGs compared to CXCL12α was also shown by enhanced binding to cell surface-expressed HS. In addition, COOH-terminal fragments of CXCL12γ inhibited infection of cells with DENV serotype 2, herpes simplex virus-1 and respiratory syncytial virus (199). In addition, mutant chemokines were developed to evaluate the contribution of the COOH-terminal domain and the core region of CXCL12 in GAG binding. Mutation of the BBXB motif in the core region of both CXCL12β and CXCL12γ resulted in impaired GAG binding. However, mutations of the COOH-terminal domain only increased the off-rate, suggesting that this COOH-terminal domain is necessary for the stability of the chemokine-GAG complex. Although CXCL12γ showed reduced affinity for CXCR4, the sustained binding of this isoform to HS enabled it to promote *in vivo* intraperitoneal leukocyte accumulation and angiogenesis in matrigel with much higher efficiency than CXCL12α (148). This suggests that the γ isoform might exist predominantly in a GAG-bound form within tissues to either stabilize or protect the chemokine from proteolytic cleavage events that directly affect its activity and/or to immobilize CXCL12γ to allow continued and localized stimulation of cells. Indeed, binding of CXCL12α to heparin or HS prevented the proteolytic processing of CXCL12α by CD26/DPP IV (56). More recently, it was described that CXCL12γ interacts with high affinity with sulphotyrosines in the NH_2-terminal region of CXCR4 resulting in a non-productive binding and reduced signaling and chemotactic activity. However, HS prevented the interaction between CXCL12γ and CXCR4 sulphotyrosines, thereby functionally presenting the chemokine to its receptor such that its activity was similar to that of CXCL12α (203).

As mentioned before, GAG binding is necessary for chemokine function and chemokine oligomerization contributes to the affinity of chemokine-GAG interactions. Recently, a disulphide-locked dimer of CXCL12 showed an increase in affinity for GAGs compared to wild-type CXCL12, which exists as an equilibrium mixture of monomers and dimers (99).

Further, mutant CXCL12α with impaired GAG-binding capacity was not able to prevent the fusion of human immunodeficiency virus (HIV) X4 isolates in leukocytes in the same degree as wild-type CXCL12α (152). Again, the enzymatic removal of cell surface HS diminished the HIV-inhibitory

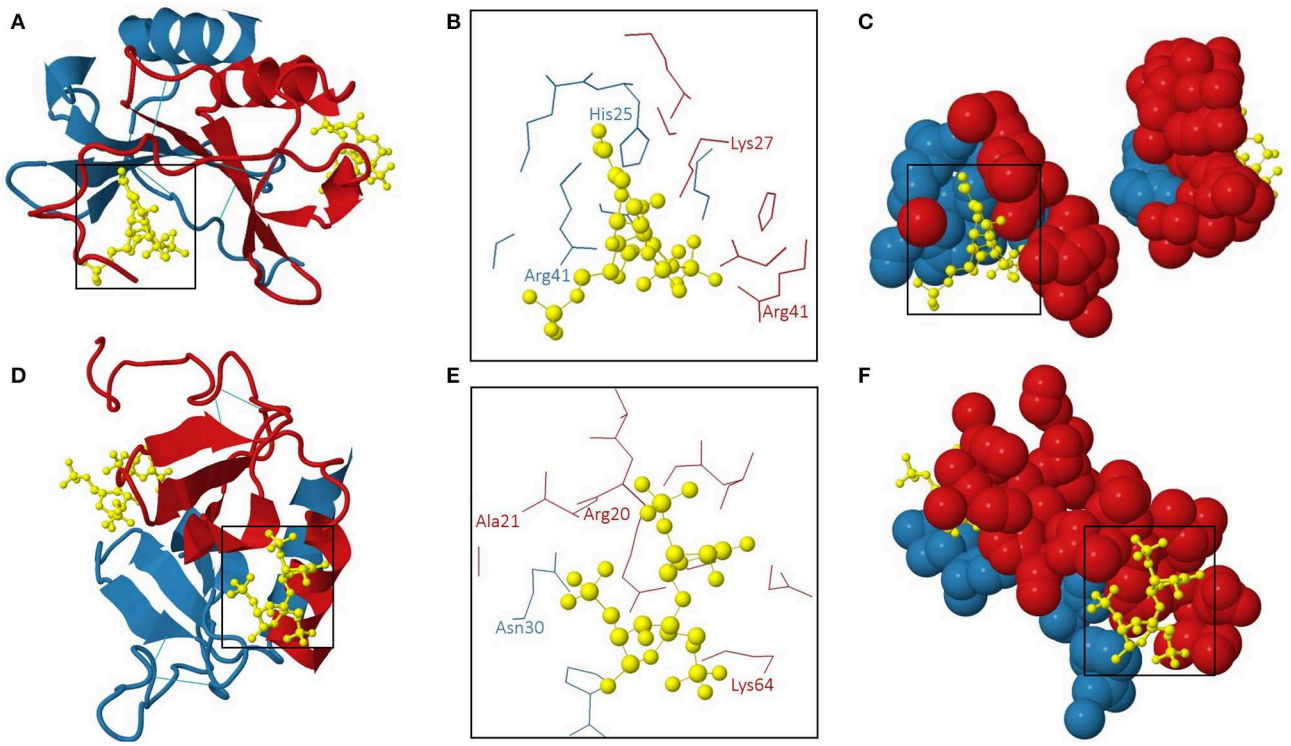

FIGURE 3 | The 3D structure of human CXCL12 dimer: heparin disaccharide complex (202). The 3D model (PDB accession code 2NWG) of the interaction of a human CXCL12 dimer with two heparin disaccharide molecules is shown from two different perspectives in **(A–C)** and **(D–F)**, respectively. **(A,D)**: overview; **(B,E)**: amino acids interacting with heparin disaccharide in the two binding pockets are indicated; **(C,F)**: 3D representation of the individual heparin disaccharide molecules in their binding pockets. The subunits of the CXCL12 dimer are displayed in red (subunit 1) and blue (subunit 2). The heparin disaccharide molecules and disulphide bridges are shown in yellow and light blue, respectively.

capacity of the chemokine. Also the anti-inflammatory protein TSG-6 interacted with CXCL12α through their GAG-binding epitopes, resulting in a decreased presentation on the endothelial surface (190).

Consequences of CXCL14 Binding to Glycosaminoglycans

Penk et al. explored the interaction between CXCL14 and various GAGs by using NMR spectroscopy, molecular modeling, heparin affinity chromatography and mutagenesis. They detected distinct GAG-binding modes dependent on the type of GAG that was used. Accordingly, the binding pose for heparin was suggested to be different from the binding poses of HA, CS-A/C, -D and DS. Moreover, it was proposed that different GAG sulphation patterns might confer specificity to the interaction (204).

The Binding of CC Chemokines to Glycosaminoglycans

Consequences of CCL2, CCL7, CCL8, and CCL13 Binding to Glycosaminoglycans

Hoogewerf et al. and Kuschert et al. described GAG-dependent binding of chemokines, including CCL2, to endothelial and CHO cells (90, 91). Amino acids Lys58 and His66 in the COOH-terminal α-helix of CCL2 were essential for GAG binding (159). However, these were less important than the amino acids Arg18, Lys19, Arg24, and Arg49 (45, 106). The [^{18}AA^{19}]-CCL2 mutant and the monomeric P8A-CCL2 mutant showed reduced GAG affinity and *in vivo* cell recruitment, although they retained chemotactic activity *in vitro*. Thus, the quaternary structure of chemokines and their interaction with GAGs may contribute to the recruitment of leukocytes beyond migration patterns defined by interactions with chemokine receptors. In addition, CCL7 and CCL13 bound to heparin with comparable affinity (173). A non-GAG-binding CCL7 mutant showed reduced recruitment of leukocytes *in vivo* indicating the importance of a BXBXXB GAG-binding motif (49). Noteworthy, the binding of monocyte attractants CCL2, CCL7, and CCL8 to GAGs was dependent on the position of sulphation, and acetylation (155, 156). More recently, SPR analysis showed high GAG affinity for CCL2 and CCL7 with K_D-values below 120 nM for heparin or HS (103). In accordance to previously obtained data, the P8A mutant of CCL2 showed reduced GAG-binding affinity to heparin, HS and 2-O-desulphated heparin (99). Mutagenesis studies revealed multiple GAG-binding sites in CCL7, enabling it to function as a non-oligomerizing chemokine (103). Noteworthy, the chemokine receptor CCR2 competed with GAGs for CCL7 binding (205). On the opposite, there exists experimental evidence reporting no interaction between GAGs and CCL2 (119, 206). For example,

under physiological salt conditions, no binding of CCL2 to mast cells and the ECM in RA synovium was detected. Noteworthy, the use of GAGs with varying length or pattern of sulphation in the binding assays can result in different binding constants.

CCL2 and CCL8 oligomerized in solution and more profoundly in the presence of GAGs (106, 157). For example, CCL2 dimers and tetramers were formed in the presence of octasaccharides. However, without GAGs, both monomers and dimers of CCL2 and CCL8 were detected. In contrast, CCL13 oligomerized in the presence or absence of GAGs. In addition, CCR2 ligands formed heterodimers, a process which is partially regulated by GAG binding (158). For example, CCL2 formed heterodimers with CCL8, CCL11 and CCL13 and CCL8 heterodimerizes with CCL13. In the presence of GAGs, also CCL8/CCL11 heterodimers were detected. Interestingly, multimerization of CCL2 was not required for transendothelial migration. However, treatment with heparin resulted in reduced GAG binding and the inhibition of migration across the endothelium (207). As described before, PTM of chemokines is an important mechanism to regulate chemokine function. Although these modifications mostly lead to changes in receptor activity, also GAG-binding affinity can be altered. Recently, nitrated CCL2 with reduced *in vitro* and *in vivo* activity was described (208). This could be partially attributed to reduced GAG binding of the nitrated chemokine.

Consequences of CCL3, CCL4, and CCL5 Binding to Glycosaminoglycans

As mentioned before, a common feature of GAGs is their overall negative charge suggesting an electrostatic interaction with basic proteins, such as chemokines. However, the chemokine-GAG interaction is not merely based on overall electrostatic interactions as exemplified by the fact that CCL3 and CCL4, both acidic chemokines, bind GAGs (90, 91). These chemokines, including CCL5, bound to GAGs on cells and/or HS beads (88). Several highly conserved basic amino acids were identified by *in vitro* mutagenesis to be involved in GAG binding, including a common heparin-binding motif of the form BBXB in the 40 s loop of CCL3, CCL4, and CCL5 (160–163, 168). The amino acids Arg18, Arg46, and Arg48 of CCL3, amino acids Arg18, Lys45, Arg46, and Lys48 of CCL4 and amino acids Arg44, Lys45, and Arg47 of CCL5 were involved in the GAG interaction (**Figure 2B**). Interestingly, the alteration of acidic residues in CCL3 led to an enhanced heparin-binding affinity (209). For CCL3, also a binding site on HS was characterized as a domain consisting of two highly sulphated regions (NS), 12–14 monosaccharide units long, separated by an N-acetylated region (NA) (96). The NS domains likely interact with the basic amino acids Arg17, Arg45, and Arg47 and may wrap around the CCL3 dimer in a horseshoe shape. Again, the CCL3 dimer showed higher affinity for HS than the monomeric or tetrameric form. NMR spectroscopy identified other residues of CCL4 involved in GAG binding, namely Arg18, Asn23, Val25, Thr44, Lys45, Lys46, and Ser47 (164). In case of CCL5, another GAG-binding domain, namely residues ^{55}KKWVR^{59} in the 50 s loop, was described as the low binding affinity site, whereas the basic amino acids ^{44}RKNR^{47} in the 40 s loop of CCL5 served as the main GAG-binding domain (169). Indeed, more recently, it was shown that the basic cluster in the 50 s loop is required for the *in vivo* biological function of CCL5 (170). The ^{55}AAWVA^{59}-CCL5 mutant lost the capacity to mediate firm adhesion of leukocytes to endothelial cells, transendothelial migration of macrophages *in vitro* and recruitment of cells to the peritoneum *in vivo*. Previously, Burns et al. suggested an important role for the amino acids 55–66 in GAG binding, since a monoclonal antibody recognizing this epitope blocked the GAG-dependent antiviral activity of CCL5 (210, 211).

Surprisingly, the non-heparin binding mutants (R46A) of CCL3 and CCL4 still bound to their receptor with similar potency, inducing similar Ca^{2+}-signals or T cell chemotactic responses. For CCL4, two residues, namely Lys48 and Arg45, had overlapping functions playing a critical role in both heparin and CCR5 binding (163). In addition, mutant CHO cells transfected with the GPCRs CCR1 or CCR5 with defective GAG expression still bound CCL3, CCL4, and CCL5, but required exposure to higher chemokine concentrations to induce similar Ca^{2+}-responses (88). Several studies with mutant CCL5 molecules showed that the interaction between the chemokine and GAGs is not essential for receptor binding, signal transduction and leukocyte migration (168, 171). However, this interaction was required for transendothelial migration, where the development of a chemokine gradient was important. The ^{44}AANA^{47}-CCL5 mutant displayed reduced GAG-binding affinity, whereas the ^{55}AAWVA^{59}-mutant retained full binding capacity (168). Mutations in the 40 s loop also abolished binding to tissue sections, and interestingly, so did mutation of the 50 s region (212). Although the ^{44}AANA^{47}-CCL5 mutant showed reduced CCR1 binding, the high-affinity binding to CCR5 and the ability to induce chemotaxis of freshly isolated monocytes in a Boyden chamber assay were retained (168). Single point mutations in the putative GAG-binding domains resulted in reduced GAG-binding affinity, but similar chemotactic responses *in vitro* (171). However, as discussed before, in more physiologic conditions the decreased binding to extracellular structures led to reduced biological activity.

As discussed before, GAG binding, but also oligomerization may be essential for the *in vivo* activity of specific chemokines. Indeed, CCL4 and CCL5 mutants with impaired GAG binding and monomeric variants were unable to recruit cells when injected into the peritoneal cavity, although they are fully active *in vitro* (45). In addition, the ^{44}AANA^{47}-CCL5 mutant was unable to form high-order oligomers, to bind to heparin and to recruit cells *in vivo* (166). This mutant also failed to induce apoptosis in T cells (172). In addition, dimeric CCL4 displayed higher affinity for heparin and disaccharide subunits (163, 164). Moreover, the dimerization affinities of CCL4 and CCL5 increased in the presence of a disaccharide (165). However, the BBXB motifs of CCL3, CCL4, and CCL5 are partially buried when they are oligomerized. For the interaction between GAGs and the CCL3 oligomer, residues from two partially buried BBXB motifs together with other residues are involved. For the CCL5 oligomer another fully exposed motif was important for GAG binding (213). Rek et al. described that CCL5 undergoes a conformational change when it binds to HS (167). This change in conformation

was suggested to be a prerequisite for oligomerization and optimal GPCR activation *in vivo*. As described before, TSG-6 was able to bind to chemokines through their GAG-binding domains (190). Pre-incubation of endothelial cells with TSG-6 inhibited the presentation of CCL5 on the endothelial surface.

In contrast to all the above, two different studies could not detect binding of CCL3 and CCL4 to GAGs by SPR analysis (99, 119). Others reported that CCL3 and CCL4 did not bind in a GAG-dependent manner to mast cells and to the ECM in the synovium of RA patients (206). In all these studies, CCL5 binding to GAGs was detected and a mutant CCL5, with decreased avidity for heparin, was not able to bind to mast cells or ECM anymore. These discrepancies in the results of these studies could be explained by the rather acidic nature of both CCL3 and CCL4 compared to other chemokines.

Consequences of CCL11 Binding to Glycosaminoglycans

Eotaxin- or CCL11-induced calcium signaling, respiratory burst and migration of eosinophils and binding of CCL11 to CCR3 was inhibited by heparin (173). However, heparin did not affect chemotactic responses to C5a. In addition, heparin inhibited CCL11, CCL24, CCL7, CCL13, and CCL5-induced eosinophil stimulation in different degrees, correlating with their relative affinities for heparin. Although HS and DS inhibited the action of CCL11, no effect was observed with CS. On the contrary, Ellyard et al. showed only binding to heparin and not to HS. Moreover, heparin protected CCL11 from proteolysis, thereby potentiating chemotactic activity *in vivo* (55). Recently, a tetrameric form of CCL11 was shown to bind the therapeutic GAG Arixtra (214).

Consequences of CCL19 and CCL21 Binding to Glycosaminoglycans

CCL21 was shown to bind to versican, a large CSPG, via its GAGs (215). Although HS supported CCL21-induced Ca^{2+}-mobilization, versican and CS B inhibited cellular responses. Moreover, the COOH-terminus of CCL21 was involved in GAG binding and the inhibitory effect of CS B on the CCL21-induced Ca^{2+}-influx (216). The COOH-terminal tail of CCL21 reduced its *in vitro* chemotactic potency in a 3D dendritic cell chemotaxis assay but enhanced its efficiency to activate ERK1/2 signaling and β-arrestin recruitment (217). In addition, full-length CCL21 induced integrin-dependent dendritic cell spreading, polarization and haptotactic movement, whereas CCL21 missing the positively charged COOH-terminus induced non-adhesive and integrin-independent directional migration (218). Interestingly, linking the COOH-terminal tail of CCL21 to the related CCR7 ligand CCL19 enhanced its affinity for heparin (219).

In accordance to CCL5 and CCL17, CCL21 also bound to mast cells and the ECM in RA synovium and this chemokine binding was inhibited by high salt concentrations and GAGs (206). Binding of CCL21 to immobilized heparin was greatly diminished upon human endosulphatase-treatment (140). Both CCL21 and CCL19 bound to a hexasaccharide as observed by SPR analysis (220). GAG binding also plays an essential role in chemokine cooperativity (221). In the absence of cooperative chemokines, CCL19 and CCL21 bound to CCR7 or GAGs on the endothelial cell surface. However, in the presence of cooperative chemokines, CCL19 and CCL21 are competed from GAGs, increasing the concentration of chemokine which can interact with their receptor. Finally, TSG-6 binding to CCL19 and CCL21 was described (190). This interaction resulted in inhibition of chemokine binding to heparin and presentation on the endothelium and the inhibition of CCL19- and CCL21-mediated transendothelial migration.

The Binding of C Chemokines XCL1 and XCL2 to Glycosaminoglycans

The two lymphocyte attractants XCL1 and XCL2 bound GAGs (222, 223). Both convert between a canonical chemokine folded monomer and a unique dimer. Interestingly, the monomer forms were responsible for receptor binding and activation, whereas the dimer forms were involved in GAG binding. Recently, a major GAG-binding site of XCL1 was determined as mutations of the amino acids Arg23 and Arg43 greatly diminished GAG binding (224). Despite their structural similarity, XCL2 displayed a higher affinity for heparin than XCL1. In addition, the XCL1 dimer was responsible for inhibiting HIV-1 activity.

In summary, it can be stated that the interaction between chemokines and GAGs on the cell surface is not essential for GPCR binding and signaling. However, GAG binding enhances the activity of low chemokine concentrations by sequestration of chemokines on the cell surface, inducing polymerization of chemokines and increasing their local concentration. Therefore, cell surface GAGs enhance the effect of chemokines on high-affinity receptors within the local microenvironment.

THERAPEUTIC APPROACHES INHIBITING CHEMOKINE-GAG INTERACTIONS

During the last two decades, research aiming at interference with chemokine activity mainly focused on the identification of inhibitors of the interaction between chemokines and their cognate GPCRs. This approach resulted in limited success with a number of compounds in clinical trials, but only two small molecule chemokine receptor antagonists on the market (for treatment of HIV and treatment of leukemia) (225–227). Since it is clear that also binding to GAGs is important for chemokine functioning *in vivo*, a few groups are investigating the inhibition of chemokine-GAG interactions (199, 228–233).

Viral Chemokine-Binding Proteins

The chemokine network exerts an indispensable role in the antiviral immune response. Accordingly, some viruses have developed strategies to modulate chemokine activity, thereby affecting leukocyte migration and aiming at evasion or manipulation of the host immune response. These viral mechanisms are highly sophisticated as they possibly have been selected during evolution over millions of years. Large DNA viruses, poxviruses and herpesviruses in particular, use a substantial part of their genome to neutralize the antiviral activity of the immune system of the host. One of their strategies

involves the expression of proteins that have the ability to modulate chemokine activity: viral chemokine homologs, viral chemokine receptor homologs and viral chemokine-binding proteins (vCKBPs). The latter group includes secreted proteins that display no sequence similarity with mammalian proteins. These vCKBPs can interfere with chemokine function via binding to either the GAG-binding epitope of chemokines or the chemokine receptor-binding epitope of chemokines, resulting in disruption of the chemokine gradient or abrogated interaction of the chemokine with its chemokine receptor, respectively (234–237). In contrast to the observed inhibitory activity of vCKBPs on chemokine function, a vCKBP that does not inhibit, but potentiates chemokine activity has been detected in both herpes simplex virus type 1 (HSV-1) and HSV-2 (238). The fact that viruses produce proteins that disrupt the chemokine gradient emphasizes the importance of the chemokine-GAG interaction (234). In this paragraph, we will focus on vCKBPs that inhibit chemokine activity by interfering with the chemokine-GAG interaction.

Poxviruses

A41

Vaccinia virus (VACV), used as vaccine for the eradication of smallpox caused by the variola virus, produces and secretes a 30 kDa glycoprotein called A41. SPR experiments could identify the CC chemokines CCL21, CCL25, CCL26, and CCL28 as binding partners for A41 (K_D values between 10^{-7} and 10^{-9} M). GAGs could disrupt the interaction of A41 with chemokines, indicating that A41 can inhibit binding of a subset of CC chemokines to GAGs via interaction with a site that overlaps with their GAG-binding site. A41 did not affect binding of these chemokines to their chemokine receptors (239).

E163

Ectromelia virus (ECTV) is closely related to the variola virus and is the causative agent of mousepox. Accordingly, ECTV infections in mice have been used as a model to study smallpox (240). ECTV encodes a 31 kDa glycoprotein called E163, which is an ortholog of the A41 protein encoded by VACV. Moreover, E163 has been identified as a vCKBP due to its ability to bind a subset of CC and CXC chemokines with high affinity. By using SPR, Ruiz-Argüello et al. demonstrated high-affinity binding (nanomolar range) of this vCKBP to three CXC chemokines (CXCL12α, CXCL12β, CXCL14) and to six CC chemokines (CCL21, CCL24, CCL25, CCL26, CCL27, CCL28). Neither the interaction of chemokines with specific GPCRs, nor leukocyte chemotaxis *in vitro* could be inhibited by E163. More specifically, heparin dose-dependently competed with chemokines for interaction with E163, suggesting that E163 binds to the GAG-binding site of chemokines and not to their receptor-binding domain. This hypothesis was confirmed as chemokines with mutated GAG-binding sites showed abrogated interaction with E163 (241). In addition, this vCKBP includes three GAG-binding motifs and correspondingly bound to a variety of sulphated GAGs. This interaction enables anchorage of E163 to the cell surface, thereby retaining it in the proximity of the infected tissue. Moreover, binding to GAGs might protect this vCKBP from degradation by proteases (241, 242). Binding of E163 to the GAG-binding domain of chemokines already suggested its potential to inhibit the chemokine-GAG interaction. Heidarieh et al. further investigated this hypothesis and by using GAG-binding mutant forms of E163, they showed that E163 interferes with the interaction between chemokines and GAGs on the cell surface. In addition, E163 appears to have the ability to interact simultaneously with chemokines and GAGs (242).

M-T7

Myxoma virus is a poxvirus that exclusively infects rabbits and causes myxomatosis. This virus secretes the myxoma virus T7 protein (M-T7) that is a soluble IFN-γ receptor homolog. Correspondingly, M-T7 bound to rabbit IFN-γ and was a potent inhibitor of the biological activity of this cytokine (243–246). Lalani et al. reported that in addition to the latter function, M-T7 interacted with multiple chemokines of the C, CC, and CXC subclasses (mXCL1, hCCL5, hCCL2, hCCL7, hCXCL8, hCXCL4, hCXCL10, hCXCL7, hCXCL1), which could be observed in a gel shift mobility assay. In contrast to the NH_2-terminal region of CXCL8, the COOH-terminal region of this chemokine appeared to be required for binding to M-T7 since COOH-terminally truncated forms had lost the ability to interact with M-T7. Moreover, heparin competed with M-T7 for binding to CCL5. Accordingly, it was proposed that M-T7 interacts with the GAG-binding domain of multiple chemokines (245).

ORFV CKBP

Orf virus (ORFV) is a parapoxvirus that infects sheep, goats, and humans. Among a range of host-modulating proteins, this virus encodes a vCKBP, namely ORFV CKBP. SPR experiments demonstrated high-affinity binding of the ORFV CKBP to the CC chemokines CCL2, CCL3, CCL4, CCL7, CCL11 and to the C chemokine XCL1 (247). In addition, ORFV CKBP bound with high affinity to CXC chemokines (CXCL2 and CXCL4) (248). Upon interaction between ORFV CKBP and a chemokine, the vCKBP masks key amino acid residues of the chemokine receptor-binding domains and the GAG-binding domains in the chemokine. Accordingly, ORFV CKBP had the ability to block chemokine binding and signaling through its cognate chemokine receptor and interfered with the chemokine-GAG interaction (247, 248).

Herpesviruses

gG

Bryant et al. identified a family of novel vCKBPs, namely glycoprotein G (gG), encoded by alphaherpesviruses including equine herpesvirus 1 (EHV-1), bovine herpesvirus 1 and 5 (BHV-1 and BHV-5) among others. Secreted forms of gG from some alphaherpesviruses are characterized by a broad binding specificity for chemokines. Moreover, gG can inhibit chemokine activity by interfering with the interaction of chemokines with their cognate chemokine receptors and with GAGs. This was exemplified by the gG vCKBP from EHV-1 that showed the

ability to disrupt pre-established chemokine-GAG (CXCL1-heparin) interactions. In addition, gG from EHV-1 and BHV-1 blocked the binding of chemokines to GAGs on the cell surface (249).

M3

Murine gammaherpesvirus-68 infects murid rodents and its *M3* gene encodes a vCKBP, namely M3 or vCKBP-3 (250, 251). This vCKBP bound to a broad range of chemokines of all four subclasses (C, CC, CXC, and CX3C chemokines). Initially, the ability of this vCKBP to inhibit binding of chemokines to their GPCRs was demonstrated (250, 252). However, further investigations by Webb et al. revealed that M3 inhibited binding to heparin of a variety of chemokines (CXCL1, CXCL8, CXCL10, CCL2, and CCL5). In addition, M3 blocked the interaction of CCL3 and CXCL8 with cell surface GAGs. Moreover, heparin-bound CCL5 and CXCL8 could be displaced from GAGs by M3 (251). Furthermore, the N-loop of chemokines was demonstrated to be required for binding to M3 (250, 252). So, it is thought that M3 binds to chemokines via their N-loop, thereby resembling binding to the chemokine receptor and apparently disrupting binding to heparin (251).

R17

R17 is a vCKBP encoded by rodent herpesvirus Peru (RHVP) that is a gammaherpesvirus related to murine gammaherpesvirus-68. This vCKBP bound a range of human and mouse C- and CC chemokines (hCCL2, hCCL3, hCCL5 and mCCL2, mCCL3, mCCL4, mCCL5, mCCL8, mCCL11, mCCL12, mCCL19, mCCL20, mCCL24, and mXCL1) with high affinity in SPR experiments. Moreover, the interaction of R17 with chemokines abrogated chemokine-mediated cell migration and calcium release, suggesting an inhibitory function on chemokine signaling for R17. In addition, binding of R17 to cell surface GAGs has been observed. R17 comprises two BBXB GAG-binding motifs, which are both crucial for GAG binding, as demonstrated by variants of R17 with mutated GAG-binding motifs. Further experiments showed that the interaction of R17 with GAGs relies on determinants that are distinct from those involved in binding to chemokines (253). Additionally, Lubman et al. used an SPR-based competition experiment to demonstrate the ability of R17 to interfere with the chemokine-GAG interaction for chemokines like CCL2 (254).

Tick Saliva Protein Evasin-3 and Synthetic Variants

Ticks are bloodsucking parasites that, like many pathogens, have developed certain mechanisms to evade the immune response of their host. Tick saliva contains a wide range of immunomodulatory proteins including a class of CKBPs, termed Evasins. These proteins bound and neutralized chemokines, thereby preventing recruitment of cells of the innate immune system and allowing ticks to remain undetected by their host (255). Until now, the class of Evasins comprises three family members: Evasin-1, Evasin-3 and Evasin-4. Since Evasin-1 and Evasin-4 are structurally related, they constitute the subclass C8 fold, whereas Evasin-3 belongs to the subclass C6 fold containing 8 and 6 cysteines, respectively. The C8 fold Evasins bound to CC chemokines: CCL3, CCL4, CCL18 (Evasin-1) and CCL5, CCL11 (Evasin-4). In contrast, the C6 fold Evasin-3 had high affinity for the CXC chemokines CXCL1 and CXCL8 (and their murine related proteins: CXCL1 and CXCL2). Potent anti-inflammatory activity of Evasins has been demonstrated in several *in vivo* animal models of disease (255, 256).

Recently, Denisov et al. explored the three-dimensional structures of Evasin-3 and the CXCL8 – Evasin-3 complex. Evasin-3 bound to the CXCL8 monomer and disrupted the interaction of CXCL8 with GAGs and with its receptor CXCR2. When Met-Evasin-3 (a variant of Evasin-3 with a methionine residue at the NH_2-terminus) was added to the CXCL8-GAG complex in *in vitro* experiments, GAG binding was abrogated. Evasin-3 disrupted the continuous stretch of positively charged amino acids of the GAG-binding domain of CXCL8, thereby preventing binding of the chemokine to GAGs. Consequently, Evasin-3 competed with GAG binding and replaced the GAGs from the CXCL8-GAG complex. Furthermore, two novel CXCL8-binding truncated Evasin-3 variants: linear tEv3 17-56 and cyclic tcEv3 16-56 dPG were synthesized. These variants demonstrated high proteolytic stability in human plasma and inhibited CXCL8-induced neutrophil migration *in vitro* to a similar extent as native Evasin-3. Both synthetic Evasin-3 variants showed high affinity for CXCL8, although lower than the affinity of native Evasin-3 for CXCL8. The long NH_2- and COOH-termini of native Evasin-3 apparently affect the internal dynamics of its structure, resulting in lower K_D values (256).

Potent *in vivo* anti-inflammatory activity of Evasin-3 has been shown in several animal models. Evasin-3 inhibited CXCL1-induced neutrophil recruitment to the peritoneal as well as the knee cavity. In addition, Evasin-3 treatment in a murine model of antigen-induced arthritis led to an overall reduction of leukocyte recruitment to the joint and periarticular tissues. Especially neutrophil influx in the knee joint was decreased (by 70%). Moreover, treatment diminished inflammatory hypernociception and the local production of TNF-α. Evasin-3 inhibited the adhesion of leukocytes to the synovial endothelium as observed in intravital microscopy experiments. In addition, Evasin-3 reduced lethality in a murine model of intestinal ischemia-reperfusion injury (255). Evasin-3 treatment was evaluated in a murine model of myocardial ischemia-reperfusion injury as well. A single administration of Evasin-3 during myocardial ischemia resulted in reduced infarct size. This beneficial effect could be allocated to the inhibition of neutrophil influx and the decrease in ROS production (257). Another study demonstrated the positive effect of Evasin-3 on atherosclerotic vulnerability for ischemic stroke. In a mouse model of carotid atherosclerosis, treatment with Evasin-3 resulted in decreased intraplaque neutrophilic inflammation and matrix metalloproteinase-9 content. However, in a murine model of ischemic stroke, no poststroke clinical outcomes were ameliorated by treatment with Evasin-3, suggesting that this treatment is not useful to prevent ischemic brain injury (258). In addition, Evasin-3 reduced neutrophilic inflammation in both lung and pancreas in a murine model of acute pancreatitis. Macrophage recruitment to the pancreas was reduced as well. Evasin-3 treatment reduced

ROS release in the lung. Furthermore, treatment with Evasin-3 was associated with reduced lung and pancreas apoptosis and pancreas necrosis (259).

Human Chemokine-Binding Protein TNF-Stimulated Gene-6

TSG-6 is an inflammation-associated protein with tissue-protective and anti-inflammatory characteristics. Its therapeutic effects have been studied in a wide range of disease models. TSG-6 interacted with various ligands including GAGs and its ability to bind to chemokines has been revealed recently. TSG-6 is the first soluble CKBP discovered in mammals (260, 261). This CKBP bound chemokines of the CC and CXC subfamilies (CCL2, CCL5, CCL7, CCL19, CCL21, CCL27, CXCL4, CXCL8, CXCL11, and CXCL12) and associated with their GAG-binding site, interfering with their interaction with GAGs (190, 262).

Chemokine-Derived GAG-Binding Peptides

GAG-binding peptides can be used as another strategy to target the chemokine-GAG interaction. The design of several GAG-binding peptides derived from different chemokines has been reported. We synthesized a CXCL9-derived GAG-binding peptide, namely CXCL9(74–103). In contrast to most other chemokines, the COOH-terminal region of CXCL9 is exceptionally long, highly positively charged and conserved among species. CXCL9 is a CXCR3 ligand and recruits activated T lymphocytes and NK cells. Moreover, this chemokine has angiostatic properties (16, 231, 263). Remarkably, when natural CXCL9 was purified, the highly charged COOH-terminus (a peptide of up to 30 amino acids) was almost always cleaved from the intact chemokine (231). In a next step, the potential role of this natural COOH-terminal peptide was evaluated. COOH-terminal CXCL9-derived peptides with different length were synthesized. These CXCL9-derived peptides do neither activate, nor recruit leukocytes through CXCR3 (231).

CXCL9(74–103) bound with high affinity to soluble and cellular GAGs. The longest 30 amino acid peptide, CXCL9(74–103), was the most potent competitor and competed with CXCL8, muCXCL1, muCXCL6, CXCL11, CCL2, and CCL3 for binding to GAGs (174, 231, 264). This indicated that CXCL9(74–103) may compete with a wide variety of chemokines that belong to different subclasses. Furthermore, the importance of amino acids 74–78 was emphasized as CXCL9(74–103) was the most potent GAG-binding peptide. Although these amino acids were required, they were not sufficient for GAG binding. CXCL9(74–103) included two typical GAG-binding motifs (BBXB: ^{75}KKQK^{78} and BBBXXB: ^{85}KKKVLK^{90}) (231). A shorter peptide, CXCL9(74–93) showed similar affinity for HS and LMWH in comparison with CXCL9(74–103). However, the affinity of the shorter peptide for binding to CS was lower compared with CXCL9(74–103), indicating that shortening of CXCL9(74–103) resulted in a narrowing of the GAG-binding spectrum (174).

Since CXCL9(74–103) competed with intact chemokines for binding to GAGs *in vitro* and showed abrogated binding to and signaling through CXCR3, it was hypothesized that CXCL9(74–103) would compete with active chemokines for GAG binding *in vivo*, thereby inhibiting leukocyte migration. In addition, as CXCL9(74–103) is derived from a chemokine, it might show specificity for certain GAG sequences expressed on the endothelium in an inflammatory situation (231). The potential anti-inflammatory activity of this peptide was first assessed in two murine acute inflammation models characterized by neutrophil infiltration. The CXCL9(74–103) peptide competed with the most potent human neutrophil-attracting chemokine, i.e., CXCL8 for GAG binding and blocked neutrophil migration in both a gout model and an inflammation model that involved intra-articular injection with CXCL8 (231). Furthermore, treatment with CXCL9(74–103) in a murine model of CXCL8-induced neutrophil recruitment to the peritoneal cavity reduced the potency of CXCL8 to induce neutrophil infiltration. In an intravital microscopy experiment, binding of CXCL9(74–103) to the endothelium was visualized in the murine cremaster muscle model. Administration of CXCL8 resulted in neutrophil recruitment. However, treatment with CXCL9(74–103) led to decreased adherence of neutrophils to the endothelial cells (174). In a murine model of antigen-induced arthritis the peptide reduced the recruitment of leukocytes, especially neutrophils, to the synovial cavity and prevented articular and cartilage damage. Moreover, CXCL9(74–103) reduced neutrophil infiltration and neutrophil-dependent inflammation in the ears of the mice in a murine contact hypersensitivity model (265).

In contrast to other strategies that interfere with the chemokine-GAG interaction, the CXCL9-derived peptide, CXCL9(74–103), was not synthesized with the intention to specifically target the action of CXCL9, but rather focuses on the inhibition of the activity of a broader range of chemokines. Recently, two other groups reported the development of chemokine-derived GAG-binding peptides as well. McNaughton et al. synthesized CCL5-, CXCL8-, and CXCL12γ-derived peptides based on the knowledge of their GAG-binding regions (232). The peptides display sequence identity with the chemokines they are derived from. This approach aims at preserving the intrinsic specificity of the chemokine for the GAG by not interfering with hydrogen binding and Van der Waals interactions. The lead peptide pCXCL8-1, consisting of ten amino acids, was modeled based on the COOH-terminal α-helix of CXCL8, a region that mediates an important role in GAG binding. This peptide showed increased affinity for HS and DS in comparison with intact CXCL8 and displayed selectivity for HS over DS. Moreover, pCXCL8-1 competed with CXCL8 for binding to HS. In contrast to pCXCL8-1, a CXCL12γ-derived peptide failed to inhibit CXCL8-induced neutrophil migration, despite its high affinity for HS. This indicates that specificity plays a role in the interaction between the peptide and HS. Accordingly, the binding sites for the CXCL8- and the CXCL12γ-derived peptides on HS may differ. The peptide pCXCL8-1 was modified (NH_2-terminal acetylation and COOH-terminal amidation) in order to protect it from proteolytic cleavage by exopeptidases upon administration *in vivo*. The resulting peptide pCXCL8-1_{aa} was tested in an *in vivo* murine model of antigen-induced arthritis. The number of neutrophils in the synovium was reduced. Furthermore, the inflammation, cellular exudate and hyperplasia were decreased

upon treatment with pCXCL8-1_{aa}. The peptide improved the arthritic score that is a measure of severity of disease in this mouse model (232). Martinez-Burgo et al. synthesized three different peptides derived from CXCL8: a COOH-terminal peptide (54–72) (wild-type peptide), a peptide (54–72) where the glutamic acid residue at position 70 was replaced with a lysine residue (E70K peptide) and a scrambled peptide consisting of the same amino acids as peptide 1 in a random order. Although only detectable at much higher concentrations compared to intact CXCL8, the three peptides, and the E70K peptide in particular, showed binding to heparin. The observed low-affinity binding of the peptides appeared to be dependent on charge. Furthermore, the peptides did not affect chemokine-GPCR binding. Only the E70K peptide showed the ability to inhibit CXCL8-mediated transendothelial migration of neutrophils (233).

Dominant-Negative Chemokine Mutants

ProtAffin Biotechnologie AG developed a protein-based technology platform, also known as the CellJammer technology platform, in order to interfere with protein-GAG interactions via protein engineering. This approach enabled the generation of GAG-binding decoy proteins, namely dominant-negative mutant proteins. On the one hand, these proteins are characterized by increased GAG-binding affinity (= dominant mutations). On the other hand, dominant-negative mutant proteins display impaired receptor binding/activation (= negative mutations) (266–268). In order to improve GAG-binding affinity, non-crucial amino acids in the GAG-binding domain of the wild-type protein were substituted with basic amino acids. This resulted in an increase of the electrostatic component of the protein-GAG interaction. Furthermore, to disrupt the bioactivity of the wild-type protein, amino acids responsible for natural chemokine-receptor interactions are either substituted with alanine residues or deleted (266). The strategy relies on the intrinsic selectivity of the GAG-binding protein for its specific GAG epitope. Consequently, dominant-negative mutant proteins that bind with higher affinity to the GAG have the ability to displace their wild-type counterpart protein from the specific GAG target sequence. With this mode of action, dominant-negative mutant proteins antagonized protein-GAG interactions (266, 267).

A series of CXCL8 mutants was engineered by site-directed mutagenesis. Subsequently, by using a combinatorial approach consisting of different techniques, the affinities of the different mutants for HS were assessed. The pro-inflammatory human CXCL8 was designed toward an anti-inflammatory dominant-negative CXCL8 mutant. On the one hand, four non-crucial amino acids of human CXCL8 were replaced with basic lysine residues in order to knock-in high GAG-binding affinity. On the other hand, the six NH_2-terminal amino acids of human CXCL8, including the ELR motif, were deleted in order to knock-out the binding to its two GPCRs, namely CXCR1 and CXCR2. This resulted in the mutant PA401 or CXCL8[Δ6F17KF21KE70KN71K] that was selected from the series of dominant-negative CXCL8 mutants as it showed the best interaction profile with HS (266, 269, 270). Moreover, complete knocked-out CXCR1 and CXCR2 activity was observed in this mutant (269, 271). The wild-type chemokine that is displaced by the dominant-negative chemokine mutant, may still activate leukocytes. However, since the endothelial contact with GAGs is disrupted, transmigration of the chemokine should not take place (271). In addition, other chemokines than CXCL8 can be displaced from GAGs by PA401 as well. PA401 had the ability to displace CCL2 from GAGs with a similar IC50 value in comparison with CXCL8. Furthermore, CXCL10, CXCL12, CCL11 and other chemokines were displaced by PA401 as well, although they were characterized by higher IC50 values (267, 271–273). PA401 had the ability to inhibit CXCL8-induced neutrophil migration (reduction by 75%) in a transendothelial migration assay (273).

The anti-inflammatory activity of PA401 was evaluated in several disease models. Treatment with PA401 reduced renal ischemia-reperfusion injury in a rat model. More specifically, proximal tubular damage was reduced and a decreased number of infiltrating granulocytes was observed. Furthermore, PA401 reduced acute allograft damage in a rat kidney transplantation model. PA401 treatment lowered glomerular infiltration of monocytes and $CD8^+$ T cells. In addition, tubular interstitial inflammation and tubulitis, which is an indication of acute allograft rejection, were diminished as well. Moreover, the highest dose of PA401 improved glomerular and vascular rejection (271). In a murine model of acute inflammation, PA401 dose-dependently inhibited neutrophil recruitment to the knee cavity after intra-articular injection with murine CXCL1. Thus, PA401 showed anti-inflammatory activity in an inflammation model that was induced by a murine functional homolog of CXCL8. Furthermore, PA401 treatment was evaluated in a murine model of antigen-induced arthritis and resulted in inhibition of leukocyte adhesion, diminished neutrophil recruitment and inflammation-related hypernociception (269). Moreover, PA401 had the ability to disrupt the CXCL8-GAG interaction in bronchoalveolar fluid samples from patients with cystic fibrosis. As a consequence, the release of CXCL8 from the GAGs rendered the chemokine susceptible to proteolytic degradation, resulting in reduced migration of neutrophils (274). PA401 was also tested as a novel therapeutic approach in two murine models characterized by neutrophilic lung inflammation. In a murine model of LPS-induced lung inflammation, the administration of PA401 reduced the total number of cells and the number of neutrophils in bronchoalveolar lavage (BAL). Furthermore, PA401 had the ability to decrease lung congestion and inflammatory cells in the lung tissue (230) and normalized plasma inflammatory markers (275). In a murine model of tobacco smoke-induced lung inflammation, PA401 treatment showed broad anti-inflammatory activities, including reduced inflammatory cells and soluble inflammatory markers. A reduction in the number of neutrophils, macrophages, lymphocytes and epithelial cells in BAL was observed (230). Furthermore, PA401 treatment was tested in a murine model of urinary tract infection and resulted in decreased recruitment of neutrophils to the urine. Normalization of the tissue architecture could be observed in mice treated with PA401 when inspecting histopathology sections of renal micro-abscesses (273). In a murine model

of bleomycin-induced pulmonary fibrosis, a dose-dependent decrease in total cell counts and neutrophils was observed in BAL samples upon PA401 treatment. Moreover, decreased levels of CXCL1 were detected in lung tissue (273). In an experimental autoimmune uveitis model in rats, treatment with PA401 influenced severity and incidence of disease. The mean maximal clinical disease scores were decreased after both pre-symptomatic and symptomatic treatment with PA401. Furthermore, slightly less retinal destruction was observed after PA401 treatment (273).

A phase I first-in-human clinical trial (NCT01627002) was performed to examine the safety, tolerability, immunogenicity and pharmacokinetics of PA401 in healthy volunteers. Moreover, the effect of PA401 on lung inflammation following an LPS challenge was investigated in this study as well.

The CellJammer approach was applied to develop a second dominant-negative chemokine mutant, namely a CCL2/MCP-1-based decoy protein named PA508. Met-CCL2[Y13AS21KQ23R] was selected out of four novel CCL2 mutants as it showed both the highest affinity for HS and knocked-out CCR2 activity. The serine and glutamine residues at position 21 and 23 respectively, are characterized by solvent-exposed areas above 30% and are located close to the GAG-binding site of the chemokine. Consequently, these amino acid residues were substituted with basic amino acids in order to increase the GAG-binding affinity. Moreover, these mutations were beneficial for the disruption of receptor activation, considering the partial overlap between the GAG-binding and receptor activation sites in CCL2. Since the tyrosine residue at position 13 is a key residue for receptor signaling, it was replaced by an alanine residue, thereby abrogating CCR2 activation and signaling. The NH_2-terminal methionine residue, originating from recombinant protein synthesis in *E. coli*, was not removed as it turned out to increase the binding affinity to heparin and decreased binding affinity for CCR2 (276). PA508 has a remarkable specificity for CCL2, as it did not influence transendothelial migration of monocytic cells induced by chemokines such as CCL5 and CXCL1. Moreover, this specificity was confirmed *in vivo* as PA508 showed no antagonistic activity in $CCR2^{-/-}$ mice, indicating that PA508 specifically targeted the CCL2-CCR2 axis (277).

The anti-inflammatory activity of PA508 has been demonstrated in several *in vivo* models. The administration of PA508 resulted in a mild ameliorating effect in rat experimental autoimmune uveitis. PA508-treated rats were protected from the development of severe inflammation of the inner eye (276). Furthermore, treatment with PA508 reduced the influx of leukocytes in a murine air pouch model of TNF-α-induced leukocyte recruitment. In a mouse model of wire-induced neointimal hyperplasia, PA508 reduced neointimal plaque area in wire-injured arteries. In addition, this reduction was associated with diminished macrophage infiltration. The smooth muscle cell content in the neointima was increased upon treatment. Thus, treatment with PA508 reduced neointima formation and resulted in a more stable, less inflammatory plaque phenotype (277). Administration of PA508 attenuated myocardial ischemia-reperfusion injury in mice. Treatment preserved heart function and reduced myocardial infarction size. The latter resulted from PA508-mediated inhibition of myocardial macrophage-related inflammation and reduction of myofibroblast and collagen content (277). In a murine model of zymosan-induced peritonitis, administration of PA508 reduced infiltration of a pro-inflammatory subset of monocytes (Gr1 and F4/80 double positive), whereas the number of peritoneal macrophages was not affected (278). PA508 treatment showed also promising results in murine experimental autoimmune encephalomyelitis. PA508-treated mice showed a delayed disease onset and an overall better clinical score. Furthermore, mice that received PA508 demonstrated decreased maximal disease severity, preserved body weight and increased survival. Treatment with PA508 resulted in a reduction of inflammatory cell infiltrates in the spinal cord and the cerebellum, as observed during histological analysis and demyelination was reduced (278).

Chemokines and their respective chemokine mutants are characterized by a short serum half-life. In order to increase the bioavailability and thus prolong the serum half-life of PA508 for chronic indications, a novel mutant CCL2-human serum albumin (HSA) fusion protein was designed. Considering the steric influence of HSA, a diminished GAG-binding affinity of this new mutant CCL2-HSA chimera was expected. Therefore, a series of novel mutants with additional basic amino acids was developed. Eventually, the fusion of the selected CCL2 mutant with HSA resulted in HSA(C34A)-$(Gly)_4$Ser-Met-CCL2[Y13AN17KS21KQ23KS34K] that demonstrated high and selective GAG-binding affinity and improved stability (279).

The CellJammer technology was used also to generate CCL5-based decoy proteins. Initially, ten CCL5 mutants were developed. All mutants retained their NH_2-terminal methionine residue that resulted from bacterial expression, rendering them into functional receptor antagonists. Two mutants, A22K and H23K, were selected since they demonstrated highest stability and improved GAG binding. Their GAG-binding affinity was increased by engineering an extended three-dimensional GAG-binding epitope in addition to the linear ^{44}RKNR^{47} GAG-binding domain. Both mutants displayed completely abrogated chemotaxis on monocytes, due to their extra NH_2-terminal methionine. Treatment with the H23K mutant in rat autoimmune uveitis led to earlier recovery from ocular inflammation, whereas treatment with the A22K mutant did not demonstrate any anti-inflammatory effect. Brandner et al. hypothesized that the minor therapeutic effect of both mutants could be due to a deficiency in GAG-induced oligomerization caused by these mutations. The H23K mutant exhibited higher GAG-binding affinity and partially retained the ability to form GAG-induced oligomers, which could explain its observed therapeutic effect in comparison with the A22K mutant of CCL5 (280).

In addition, a CXCL12α-based decoy protein was developed. Deletion of the first eight amino acids of the chemokine already resulted in completely impaired chemotaxis. Furthermore, the amino acid residues at positions 29 and 39 were mutated as these positions are important for the first receptor binding step and for GAG binding. This resulted in the dominant-negative CXCL12α mutant CXCL12α[Δ8L29KV39K], which demonstrated impaired CXCR4 signaling in combination with increased and specific GAG affinity. The effect of this mutant was assessed in an *in vivo* murine breast cancer seeding model. Treatment

with the CXCL12α mutant inhibited migration of cancer cells, resulting in a decreased number of liver metastases (281).

The Spiegelmer NOX-A12

NOX-A12 is an aptamer inhibitor of CXCL12 that can be classified more specifically as a Spiegelmer. Mirror-image aptamers or Spiegelmers are synthetic oligonucleotides that are composed of non-natural L-nucleotides. Since naturally occurring enzymes are stereoselective for nucleic acids in the D-configuration, Spiegelmers are protected from nucleolytic cleavage, implying a native biological stability (282, 283). Spiegelmers can be selected *in vitro* to bind a wide variety of molecular targets with high affinity and specificity (283, 284). Binding to a specific molecular target relies on the three-dimensional structure of a Spiegelmer, which is determined by its nucleotide sequence (283, 285). This interaction via three-dimensional structures is similar to antibody–antigen binding. Moreover, aptamers are functionally comparable to antibodies regarding binding affinity and specificity for their targets. They display advantages relative to antibodies, including smaller size, higher stability, fast *in vitro* chemical production, wide spectrum of potential targets and non-immunogenicity (285, 286).

The Spiegelmer NOX-A12 or olaptesed pegol is a 45-nucleotide long L-RNA aptamer that interferes with chemokine-GAG interactions (228, 283, 286). NOX-A12 was developed to bind and antagonize CXCL12 in the tumor microenvironment and for cell mobilization (228, 287). CXCL12 plays a critical role in physiological and pathological processes such as embryogenesis, haematopoiesis, angiogenesis and inflammation (200, 288). This chemokine functions by interaction with its two receptors CXC chemokine receptor 4 (CXCR4) and atypical chemokine receptor 3 (ACKR3) (200). NOX-A12 bound its molecular target with subnanomolar affinity (287). Because of its small size, NOX-A12 was rapidly excreted through renal filtration (285). However, in order to extend its plasma half-life, NOX-A12 was conjugated to a branched polyethylene glycol (PEG) moiety of 40 kDa (PEGylated) (289).

CXCL12 also plays a critical role in the pathogenesis of chronic lymphocytic leukemia (CLL). This chemokine is important for migration and retention of CLL cells in tissues such as the BM. Bone marrow stromal cells (BMSCs) constitutively secrete CXCL12 and consequently attract CLL cells into the supportive microenvironment via activation of the CXCR4 receptor that is expressed on these leukemic cells. CXCL12 is presented to CXCR4 by binding to GAGs on the cell surface or ECM. In the tissue microenvironment, the CLL cells are protected from cytotoxic drugs and they receive survival signals via several factors, including CXCL12. Interfering with the cross-talk between CLL and stromal cells in order to eliminate CLL cells from the protective microenvironment and sensitize CLL cells to conventional therapy can be done by targeting CXCL12/CXCR4 signaling (228, 229).

Hoellenriegel et al. investigated the effect of NOX-A12 on the migration of CLL cells and drug sensitivity. Moreover, they more thoroughly investigated the mechanism of action of NOX-A12 and revealed its ability to compete with GAGs for CXCL12 binding. SPR measurements were performed with immobilized heparin and CXCL12 was injected together with NOX-A12. The latter competed with the immobilized heparin for binding to CXCL12, resulting in detachment of heparin-bound CXCL12. Consequently, the binding site of NOX-A12 on CXCL12 was presumably close to or overlaps with the heparin-binding site of CXCL12. Hence, the mode of action of NOX-A12 involved competition with heparin for binding to CXCL12 and explained the detachment of CXCL12 from extracellular GAGs (228).

Another Spiegelmer that binds to and neutralizes a chemokine, i.e. Emapticap pegol or NOX-E36, bound to CCL2, also known as monocyte chemoattractant protein (MCP)-1 (283, 290). However, to the best of our knowledge, it has not been explored or proven whether the mechanism of action of the latter Spiegelmer is similar to the one of NOX-A12. Accordingly, NOX-E36 will not be further discussed in this review.

NOX-A12 has been used in a variety of different disease models, ranging from chronic kidney disease to several types of cancer. An overview of studies that report treatment with NOX-A12 in different (animal) models and clinical trials can be found in **Table 2**. Currently, NOX-A12 is being tested alone and in combination with the immune checkpoint inhibitor Pembrolizumab in an ongoing phase I/II clinical trial of metastatic pancreatic and colorectal cancer (NCT03168139). In addition, the recruitment of patients with newly diagnosed glioblastoma/glioma has started in order to initiate a phase I/II clinical trial to evaluate combination treatment of NOX-A12 and radiotherapy[1].

CONCLUSION

Evidence is accumulating that the chemokine-GAG interaction may be an interesting target for the inhibition of inflammation. During an exaggerated inflammatory response, the aim would be to reduce inflammation, but not to completely inhibit the inflammatory response. The use of compounds that interfere with the chemokine-GAG interaction could be feasible in this case. On the contrary, complete inhibition of inflammation is probably not feasible, and also not desired. Focusing on the chemokine-GAG interaction is often associated with lower specificity and lower efficiency in comparison with targeting chemokine-receptor interactions. However, these characteristics might actually be beneficial if a reduction of excess inflammation is the objective.

Various therapeutic approaches, including CKBPs (viral, tick, and human), chemokine-derived GAG-binding peptides, dominant-negative chemokine mutants and the Spiegelmer NOX-A12, were discussed in this review and they all showed promising results in inhibiting chemokine-GAG interactions, independent of their specific mechanisms of action. As some of these therapeutic approaches are currently in an initial stage of research, whereas other approaches are already in clinical trials, it is delicate to compare their effect and predict their future applications. In order to generate

[1]https://www.noxxon.com/index.php?option=com_content&view=article&id=21&Itemid=478.

TABLE 2 | Overview of the use of NOX-A12 as a treatment strategy in different preclinical models and clinical trials.

Species	Disease model	Treatment	Result	References
Mouse	Proliferative lupus nephritis	NOX-A12 + NOX-E36	- ↓ Proteinuria - ↓ renal excretory failure - ↓ immune complex glomerulonephritis - ↓ potentially reversible and irreversible structural kidney injury - ↓ expansion of lymphocytes and plasma cells in spleen	(291)
Mouse	Chronic kidney disease	NOX-A12	- ↑ podocyte counts - ↓ proteinuria - ↓ glomerular lesions - ↓ renal dysfunction	(292)
Mouse	Type 2 diabetes, diabetic nephropathy	NOX-A12	- ↓ glomerulosclerosis - ↑ number of podocytes - Prevention of proteinuria - Improvement of tubular damage and peritubular vasculature density	(287)
Mouse	Type 2 diabetes, diabetic nephropathy	NOX-A12 + NOX-E36	- ↓ glomerulosclerosis - ↑ number of podocytes - Prevention of proteinuria - ↓ number of glomerular leukocytes - Protective effect on GFR decline	(293)
Mouse	Islet transplantation	NOX-A12 + mNOX-E36	- Improved islet survival and function - ↓ recruitment of inflammatory monocytes in the graft site	(294)
Mouse	Type 1 diabetes	NOX-A12	- ↓ inflammation-mediated islet destruction	(294)
Mouse and cynomolgus monkey	HSC mobilization	NOX-A12	Mobilization of leukocytes and HSCs into peripheral blood	(289)
Human (phase I: first-in-human)	HSC mobilization	NOX-A12	- Benign safety profile - dose-dependent mobilization of leukocytes and HSCs into peripheral blood	(289)
Human CLL cells, human lymphoid cell lines, murine stromal cell lines	CLL	NOX-A12	- Inhibition of CXCL12-induced chemotaxis of CLL cells - ↑ CLL migration underneath a confluent layer of BMSCs - release of CXCL12 from cell-surface-bound GAGs - competition with heparin for binding to CXCL12 - Sensitization of CLL cells toward cytotoxic agents in BMSC cocultures	(228, 229)
Human (phase IIa)	Relapsed/refractory CLL	NOX-A12 + bendamustine + rituximab	- Effective mobilization of CLL cells (for at least 72 h) - Combination therapy generally well tolerated - High ORR of 86% (with 11% CR) - Median PFS of 15.4 months in ITT population - 3-year overall survival rate of >80% in ITT population	(295)
Mouse	CML	NOX-A12 + nilotinib	↓ leukemia burden	(296)
Mouse	(MM)	NOX-A12	- Microenvironment less receptive for MM cells - ↓ MM cell homing and growth - Inhibition of MM tumor progression - ↑ survival - ↓ MM cell bone metastases - chemosensitization of MM cells to bortezomib	(297)
Human (phase IIa: first-in-patient)	Relapsed/refractory MM	NOX-A12 + bortezomib-dexamethasone	- Effective mobilization of myeloma cells (for at least 72 h) - ↑ clinical activity of bortezomib-dexamethasone	(298)
MM cell lines	MM	NOX-A12 + carfilzomib	No increased cytotoxic effect compared with carfilzomib alone	(299)
Rat	Glioblastoma multiforme	NOX-A12	- Inhibition or delay of tumor recurrences following irradiation - prolongation of median life span	(300)
Mouse, rat	Glioblastoma multiforme	NOX-A12 + anti-VEGF (bevacizumab or B-20)	- ↑ survival - ↓ tumor associated macrophages - Potentiation antitumor efficacy of anti-VEGF	(301)
Tumor-stroma spheroids, mouse	Colorectal cancer	NOX-A12 + anti-PD-1 therapy	- ↑ infiltration of $CD8^+$ T cells, $CD4^+$ T cells and NK cells into spheroids - ↑ T cell activation in spheroids - ↓ tumor growth - ↑ efficacy of anti-PD-1 therapy	(302)

(Continued)

TABLE 2 | Continued

Species	Disease model	Treatment	Result	References
Rat	Idiopathic pulmonary arterial hypertension	NOX-A12	- ↓ perivascular $CD68^+$ macrophages, $CD3^+$ T cells, mast cells - ↓ pulmonary vascular remodeling - Improvement of haemodynamics and right heart hypertrophy	(303)
Mouse	Chronic allograft vasculopathy	NOX-A12	- ↓ neointima formation - ↓ expression of pro-fibrotic inflammatory cytokines - ↓ infiltrating $CD3^+$ cells	(304)
Mouse	Retinal degradation	NOX-A12 + intravitreal injection of CXCL12	- ↑ homing of bone marrow-derived stem cells into the damaged retina - ↑ visual function	(305)

GFR, glomerular filtration rate; HSC, haematopoietic stem and progenitor cell; CLL, chronic lymphocytic leukemia; ORR, overall response rate; CR, complete remission; PFS, progression-free survival; ITT, intent-to-treat; CML, chronic myeloid leukemia; MM, multiple myeloma; VEGF, vascular endothelial growth factor.

novel therapeutics that reduce inflammation by inhibiting the chemokine-GAG interaction, further research is required to elucidate the effect on inflammation in different *in vivo* models of disease and to explore thoroughly the range of therapeutic applications.

AUTHOR CONTRIBUTIONS

HC and VV wrote the initial version of the manuscript as part of their Ph.D. thesis under supervision of PP. The manuscript was finally revised by all authors.

FUNDING

This research was supported by the Fund for Scientific Research of Flanders (FWO-Vlaanderen Projects G0F7519N and G.0D25.17N) and C1 funding (C16/17/010) of KU Leuven. HC obtained a Ph.D.-SB research fellowship of the FWO-Vlaanderen.

ACKNOWLEDGMENTS

The authors would like to thank Alexandra De Zutter for correcting the author's proof.

REFERENCES

1. Mantovani A, Bonecchi R, Locati M. Tuning inflammation and immunity by chemokine sequestration: decoys and more. *Nat Rev Immunol*. (2006) 6:907–18. doi: 10.1038/nri1964
2. Moser B, Willimann K. Chemokines: role in inflammation and immune surveillance. *Ann Rheum Dis*. (2004) 63(Suppl. 2):ii84–9. doi: 10.1136/ard.2004.028316
3. Mortier A, Van Damme J, Proost P. Overview of the mechanisms regulating chemokine activity and availability. *Immunol Lett*. (2012) 145:2–9. doi: 10.1016/j.imlet.2012.04.015
4. Luster AD. Chemokines - chemotactic cytokines that mediate inflammation. *N Engl J Med*. (1998) 338:436–45. doi: 10.1056/NEJM199802123380706
5. Rollins BJ. Chemokines. *Blood*. (1997) 90:909–28. doi: 10.1182/blood.V90.3.909.909_909_928
6. Bachelerie F, Ben-Baruch A, Burkhardt AM, Combadiere C, Farber JM, Graham GJ, et al. International union of basic and clinical pharmacology. Update on the extended family of chemokine receptors and introducing a new nomenclature for atypical chemokine receptors. *Pharmacol Rev*. (2014) 66:1–79. doi: 10.1124/pr.113.04er14a
7. Rot A, von Andrian UH. Chemokines in innate and adaptive host defense: basic chemokinese grammar for immune cells. *Annu Rev Immunol*. (2004) 22:891–928. doi: 10.1146/annurev.immunol.22.012703.104543
8. Johnson Z, Proudfoot AE, Handel TM. Interaction of chemokines and glycosaminoglycans: a new twist in the regulation of chemokine function with opportunities for therapeutic intervention. *Cytokine Growth Factor Rev*. (2005) 16:625–36. doi: 10.1016/j.cytogfr.2005.04.006
9. Handel TM, Johnson Z, Crown SE, Lau EK, Sweeney M, Proudfoot AE. Regulation of protein function by glycosaminoglycans—as exemplified by chemokines. *Annu Rev Biochem*. (2005) 74:385–410. doi: 10.1146/annurev.biochem.72.121801.161747
10. Kufareva I, Salanga CL, Handel TM. Chemokine and chemokine receptor structure and interactions : implications for therapeutic strategies. *Immunol Cell Biol*. (2015) 93:372–83. doi: 10.1038/icb.2015.15
11. Moser B, Wolf M, Walz A, Loetscher P. Chemokines: multiple levels of leukocyte migration control. *Trends Immunol*. (2004) 25:75–84. doi: 10.1016/j.it.2003.12.005
12. Zlotnik A, Yoshie O. The chemokine superfamily revisited. *Immunity*. (2012) 36:705–12. doi: 10.1016/j.immuni.2012.05.008
13. Chen K, Bao Z, Tang P, Gong W, Yoshimura T, Wang JM. Chemokines in homeostasis and diseases. *Cell Mol Immunol*. (2018) 15:324–34. doi: 10.1038/cmi.2017.134
14. Gouwy M, Struyf S, Proost P, Van Damme J. Synergy in cytokine and chemokine networks amplifies the inflammatory response. *Cytokine Growth Factor Rev*. (2005) 16:561–80. doi: 10.1016/j.cytogfr.2005.03.005
15. Mahalingam S, Karupiah G. Chemokines and chemokine receptors in infectious disease. *Immunol Cell Biol*. (1999) 77:469–75. doi: 10.1046/j.1440-1711.1999.00858.x
16. Van Raemdonck K, Van den Steen PE, Liekens S, Van Damme J, Struyf S. CXCR3 ligands in disease and therapy. *Cytokine Growth Factor Rev*. (2015) 26:311–27. doi: 10.1016/j.cytogfr.2014.11.009
17. Allen SJ, Crown SE, Handel TM. Chemokine: receptor structure, interactions, and antagonism. *Annu Rev Immunol*. (2007) 25:787–820. doi: 10.1146/annurev.immunol.24.021605.090529
18. Horuk R. Chemokine receptors. *Cytokine Growth Factor Rev*. (2001) 12:313–35. doi: 10.1016/S1359-6101(01)00014-4
19. Murdoch C, Finn A. Chemokine receptors and their role in inflammation and infectious diseases. *Blood*. (2000) 95:3032–43. doi: 10.1182/blood.V95.10.3032.010k17_3032_3043
20. Patel J, Channon KM, McNeill E. The downstream regulation of chemokine receptor signalling: implications for atherosclerosis. *Mediators Inflamm*. (2013) 2013:459520. doi: 10.1155/2013/459520

21. Steen A, Larsen O, Thiele S, Rosenkilde MM. Biased and G protein-independent signaling of chemokine receptors. *Front Immunol*. (2014) 5:277. doi: 10.3389/fimmu.2014.00277
22. Rajarathnam K, Schnoor M, Richardson RM, Rajagopal S. How do chemokines navigate neutrophils to the target site: dissecting the structural mechanisms and signaling pathways. *Cell Signal*. (2019) 54:69–80. doi: 10.1016/j.cellsig.2018.11.004
23. Karin N, Wildbaum G, Thelen M. Biased signaling pathways via CXCR3 control the development and function of $CD4^+$ T cell subsets. *J Leukoc Biol*. (2016) 99:857–62. doi: 10.1189/jlb.2MR0915-441R
24. Nibbs RJB, Graham GJ. Immune regulation by atypical chemokine receptors. *Nat Rev Immunol*. (2013) 13:815–29. doi: 10.1038/nri3544
25. Mantovani A. The chemokine system: redundancy for robust outputs. *Immunol Today*. (1999) 20:254–7. doi: 10.1016/S0167-5699(99)01469-3
26. Russo R, Garcia C, Teixeira M. Anti-inflammatory drug development: broad or specific chemokine receptor antagonists? *Curr Opin Drug Discov Devel*. (2010) 13:414–27.
27. Schall TJ, Proudfoot AEI. Overcoming hurdles in developing successful drugs targeting chemokine receptors. *Nat Rev Immunol*. (2011) 11:355–63. doi: 10.1038/nri2972
28. Stone MJ, Hayward JA, Huang C, Huma ZE, Sanchez J. Mechanisms of regulation of the chemokine-receptor network. *Int J Mol Sci*. (2017) 18:342. doi: 10.3390/ijms18020342
29. Ulvmar MH, Hub E, Rot A. Atypical chemokine receptors. *Exp Cell Res*. (2011) 317:556–68. doi: 10.1016/j.yexcr.2011.01.012
30. Mortier A, Van Damme J, Proost P. Regulation of chemokine activity by posttranslational modification. *Pharmacol Ther*. (2008) 120:197–217. doi: 10.1016/j.pharmthera.2008.08.006
31. Girbl T, Lenn T, Perez L, Rolas L, Barkaway A, Thiriot A, et al. Distinct compartmentalization of the chemokines CXCL1 and CXCL2 and the atypical receptor ACKR1 determine discrete stages of neutrophil diapedesis. *Immunity*. (2018) 49:1062–76.e6. doi: 10.1016/j.immuni.2018.09.018
32. Coombs C, Georgantzoglou A, Walker HA, Patt J, Merten N, Poplimont H, et al. Chemokine receptor trafficking coordinates neutrophil clustering and dispersal at wounds in *Zebrafish*. *Nat Commun*. (2019) 10:5166. doi: 10.1038/s41467-019-13107-3
33. Dyer DP, Medina-Ruiz L, Bartolini R, Schuette F, Hughes CE, Pallas K, et al. Chemokine receptor redundancy and specificity are context dependent. *Immunity*. (2019) 50:378–389.e5. doi: 10.1016/j.immuni.2019.01.009
34. Scholten D, Canals M, Maussang D, Roumen L, Smit M, Wijtmans M, et al. Pharmacological modulation of chemokine receptor function. *Br J Pharmacol*. (2012) 165:1617–43. doi: 10.1111/j.1476-5381.2011.01551.x
35. Rajagopalan L, Rajarathnam K. Structural basis of chemokine receptor function—a model for binding affinity and ligand selectivity. *Biosci Rep*. (2006) 26:325–39. doi: 10.1007/s10540-006-9025-9
36. Thiele S, Rosenkilde M. Interaction of chemokines with their receptors–from initial chemokine binding to receptor activating steps. *Curr Med Chem*. (2014) 21:3594–614. doi: 10.2174/0929867321666140716093155
37. Jørgensen AS, Rosenkilde MM, Hjortø GM. Biased signaling of G protein-coupled receptors – from a chemokine receptor CCR7 perspective. *Gen Comp Endocrinol*. (2018) 258:4–14. doi: 10.1016/j.ygcen.2017.07.004
38. Kleist AB, Getschman AE, Ziarek JJ, Nevins AM, Gauthier PA, Chevigné A, et al. New paradigms in chemokine receptor signal transduction: moving beyond the two-site model. *Biochem Pharmacol*. (2016) 114:53–68. doi: 10.1016/j.bcp.2016.04.007
39. Proudfoot AEI. The biological relevance of chemokine–proteoglycan interactions. *Biochem Soc Trans*. (2006) 34:422–6. doi: 10.1042/BST0340422
40. Xu D, Esko JD. Demystifying heparan sulfate–protein interactions. *Annu Rev Biochem*. (2014) 83:129–57. doi: 10.1146/annurev-biochem-060713-035314
41. Lindahl U, Couchman J, Kimata K, Esko JD. *Essentials of Glycobiology*. 3rd ed. Cold Spring Harbor, NY: Cold Spring Harbor Laboratory Press (2019).
42. Gandhi NS, Mancera RL. The structure of glycosaminoglycans and their interactions with proteins. *Chem Biol Drug Des*. (2008) 72:455–82. doi: 10.1111/j.1747-0285.2008.00741.x
43. Carlsson P, Presto J, Spillmann D, Lindahl U, Kjellén L. Heparin/heparan sulfate biosynthesis: processive formation of N-sulfated domains. *J Biol Chem*. (2008) 283:20008–14. doi: 10.1074/jbc.M801652200
44. Ihrcke NS, Wrenshall LE, Lindman BJ, Platt JL. Role of heparan sulfate in immune system-blood vessel interactions. *Immunol Today*. (1993) 14:500–5. doi: 10.1016/0167-5699(93)90265-M
45. Proudfoot AEI, Handel TM, Johnson Z, Lau EK, LiWang P, Clark-Lewis I, et al. Glycosaminoglycan binding and oligomerization are essential for the *in vivo* activity of certain chemokines. *Proc Natl Acad Sci USA*. (2003) 100:1885–90. doi: 10.1073/pnas.0334864100
46. O'Boyle G, Mellor P, Kirby JA, Ali S. Anti-inflammatory therapy by intravenous delivery of non-heparan sulfate-binding CXCL12. *FASEB J*. (2009) 23:3906–16. doi: 10.1096/fj.09-134643
47. Peterson FC, Elgin ES, Nelson TJ, Zhang F, Hoeger TJ, Linhardt RJ, et al. Identification and characterization of a glycosaminoglycan recognition element of the C chemokine lymphotactin. *J Biol Chem*. (2004) 279:12598–604. doi: 10.1074/jbc.M311633200
48. Gangavarapu P, Rajagopalan L, Kolli D, Guerrero-Plata A, Garofalo RP, Rajarathnam K. The monomer-dimer equilibrium and glycosaminoglycan interactions of chemokine CXCL8 regulate tissue-specific neutrophil recruitment. *J Leukoc Biol*. (2012) 91:259–65. doi: 10.1189/jlb.0511239
49. Ali S, Robertson H, Wain JH, Isaacs JD, Malik G, Kirby JA. A non-glycosaminoglycan-binding variant of CC chemokine ligand 7 (monocyte chemoattractant protein-3) antagonizes chemokine-mediated inflammation. *J Immunol*. (2005) 175:1257–66. doi: 10.4049/jimmunol.175.2.1257
50. Massena S, Christoffersson G, Hjertström E, Zcharia E, Vlodavsky I, Ausmees N, et al. A chemotactic gradient sequestered on endothelial heparan sulfate induces directional intraluminal crawling of neutrophils. *Blood*. (2010) 116:1924–31. doi: 10.1182/blood-2010-01-266072
51. Sarris M, Masson JB, Maurin D, Van der Aa LM, Boudinot P, Lortat-Jacob H, et al. Inflammatory chemokines direct and restrict leukocyte migration within live tissues as glycan-bound gradients. *Curr Biol*. (2012) 22:2375–82. doi: 10.1016/j.cub.2012.11.018
52. Middleton J, Patterson AM, Gardner L, Schmutz C, Ashton BA. Leukocyte extravasation: chemokine transport and presentation by the endothelium. *Blood*. (2002) 100:3853–60. doi: 10.1182/blood.V100.12.3853
53. Wang L, Fuster M, Sriramarao P, Esko JD. Endothelial heparan sulfate deficiency impairs L-selectin- and chemokine-mediated neutrophil trafficking during inflammatory responses. *Nat Immunol*. (2005) 6:902–10. doi: 10.1038/ni1233
54. Metzemaekers M, Mortier A, Janssens R, Boff D, Vanbrabant L, Lamoen N, et al. Glycosaminoglycans regulate CXCR3 ligands at distinct levels: protection against processing by dipeptidyl peptidase IV/CD26 and interference with receptor signaling. *Int J Mol Sci*. (2017) 18:1513. doi: 10.3390/ijms18071513
55. Ellyard JI, Simson L, Bezos A, Johnston K, Freeman C, Parish CR. Eotaxin selectively binds heparin: an interaction that protects eotaxin from proteolysis and potentiates chemotactic activity *in vivo*. *J Biol Chem*. (2007) 282:15238–47. doi: 10.1074/jbc.M608046200
56. Sadir R, Imberty A, Baleux F, Lortat-Jacob H. Heparan sulfate/heparin oligosaccharides protect stromal cell-derived factor-1 (SDF-1)/CXCL12 against proteolysis induced by CD26/dipeptidyl peptidase IV. *J Biol Chem*. (2004) 279:43854–60. doi: 10.1074/jbc.M405392200
57. Middleton J, Neil S, Wintle J, Clark-Lewis I, Moore H, Lam C, et al. Transcytosis and surface presentation of IL-8 by venular endothelial cells. *Cell*. (1997) 91:385–95. doi: 10.1016/S0092-8674(00)80422-5
58. McEver RP. Selectins: initiators of leucocyte adhesion and signalling at the vascular wall. *Cardiovasc Res*. (2015) 107:331–9. doi: 10.1093/cvr/cvv154
59. Ivetic A, Hoskins Green HL, Hart SJ. L-selectin: a major regulator of leukocyte adhesion, migration and signaling. *Front Immunol*. (2019) 10:1068. doi: 10.3389/fimmu.2019.01068
60. Ivetic A. A head-to-tail view of L-selectin and its impact on neutrophil behaviour. *Cell Tissue Res*. (2018) 371:437–53. doi: 10.1007/s00441-017-2774-x
61. Alon R, Van Buul JD. Leukocyte breaching of endothelial barriers: the actin link. *Trends Immunol*. (2017) 38:606–15. doi: 10.1016/j.it.2017.05.002
62. Christofidou-Solomidou M, Nakada M, Williams J, Muller W, DeLisser H. Neutrophil platelet endothelial cell adhesion molecule-1 participates in neutrophil recruitment at inflammatory sites and is down-regulated after leukocyte extravasation. *J Immunol*. (1997) 158:4872–8.

63. Coombe DR, Stevenson SM, Kinnear BF, Gandhi NS, Mancera RL, Osmond RIW, et al. Platelet endothelial cell adhesion molecule 1 (PECAM-1) and its interactions with glycosaminoglycans: 2. Biochemical analyses. *Biochemistry*. (2008) 47:4863–75. doi: 10.1021/bi7024595
64. Carman CV, Springer TA. A transmigratory cup in leukocyte diapedesis both through individual vascular endothelial cells and between them. *J Cell Biol*. (2004) 167:377–88. doi: 10.1083/jcb.200404129
65. Muller WA. Mechanisms of leukocyte transendothelial migration. *Annu Rev Pathol Mech Dis*. (2011) 6:323–44. doi: 10.1146/annurev-pathol-011110-130224
66. Sage PT, Carman CV. Settings and mechanisms for trans-cellular diapedesis. *Front Biosci (Landmark Ed)*. (2009) 14:5066–83. doi: 10.2741/3587
67. Colditz I. Margination and emigration of leucocytes. *Surv Synth Pathol Res*. (1985) 4:44–68. doi: 10.1159/000156964
68. Rot A. Endothelial cell binding of NAP-1/IL-8: role in neutrophil emigration. *Immunol Today*. (1992) 13:291–4. doi: 10.1016/0167-5699(92)90039-A
69. Tanaka Y, Adams D, Shaw S. Proteoglycans on endothelial cells present adhesion-inducing cytokines to leukocytes. *Immunol Today*. (1993) 14:111–5. doi: 10.1016/0167-5699(93)90209-4
70. Ley K, Baker JB, Cybulsky MI, Gimbrone MA, Luscinskas FW. Intravenous interleukin-8 inhibits granulocyte emigration from rabbit mesenteric venules without altering L-selectin expression or leukocyte rolling. *J Immunol*. (1993) 151:6347–57.
71. Rot A. Neutrophil attractant/activation protein-1 (interleukin-8) induces *in vitro* neutrophil migration by haptotactic mechanism. *Eur J Immunol*. (1993) 23:303–6. doi: 10.1002/eji.1830230150
72. Rot A. Binding of neutrophil attractant/activation protein-1 (interleukin 8) to resident dermal cells. *Cytokine*. (1992) 4:347–52. doi: 10.1016/1043-4666(92)90077-5
73. Ebnet K, Kaldjian EP, Anderson AO, Shaw S. Orchestrated information transfer underlying leukocyte endothelial interactions. *Annu Rev Immunol*. (1996) 14:155–77. doi: 10.1146/annurev.immunol.14.1.155
74. Baekkevold ES, Yamanaka T, Palframan RT, Carlsen HS, Reinholt FP, von Andrian UH, et al. The CCR7 ligand ELC (CCL19) is transcytosed in high endothelial venules and mediates T cell recruitment. *J Exp Med*. (2001) 193:1105–12. doi: 10.1084/jem.193.9.1105
75. Wolff B, Burns A, Middleton J, Rot A. Endothelial cell "memory" of inflammatory stimulation: human venular endothelial cell store interleukin 8 in weibel-palade bodies. *J Exp Med*. (1998) 188:1757–62. doi: 10.1084/jem.188.9.1757
76. Hub E, Rot A. Binding of RANTES, MCP-1, MCP-3, and MIP-1α to cells in human skin. *Am J Pathol*. (1998) 152:749–57.
77. Patterson AM, Siddall H, Chamberlain G, Gardner L, Middleton J. Expression of the duffy antigen/receptor for chemokines (DARC) by the inflamed synovial endothelium. *J Pathol*. (2002) 197:108–16. doi: 10.1002/path.1100
78. Dawson T, Lentsch A, Wang Z, Cowhig J, Rot A, Maeda N, et al. Exaggerated response to endotoxin in mice lacking the duffy antigen/receptor for chemokines (DARC). *Blood*. (2000) 96:1681–4. doi: 10.1182/blood.V96.5.1681.h8001681a_1681_1684
79. Luo H, Chaudhuri A, Zbrezezna V, He Y, Pogo AO. Deletion of murine duffy gene (Dfy) reveals that the duffy receptor is functionally redundant. *Mol Cell Biol*. (2000) 20:3097–101. doi: 10.1128/MCB.20.9.3097-3101.2000
80. Peiper S, Wang Z, Neote K, Martin A, Showell H, Conklyn M, et al. The Duffy Antigen/Receptor for Chemokines (DARC) is expressed in endothelial cells of duffy negative individuals who lack the erythrocyte receptor. *J Exp Med*. (1995) 181:1311–7. doi: 10.1084/jem.181.4.1311
81. Chaudhuri A, Nielsen S, Elkjaer M, Zbrzezna V, Fang F, Pogo A. Detection of duffy antigen in the plasma membranes and caveolae of vascular endothelial and epithelial cells of nonerythroid organs. *Blood*. (1997) 89:701–12. doi: 10.1182/blood.V89.2.701
82. Darbonne WC, Rice GC, Mohler MA, Apple T, Hébert CA, Valente AJ, et al. Red blood cells are a sink for interleukin 8, a leukocyte chemotaxin. *J Clin Invest*. (1991) 88:1362–69. doi: 10.1172/JCI115442
83. Weber M, Hauschild R, Schwarz J, Moussion C, de Vries I, Legler DF, et al. Interstitial dendritic cell guidance by haptotactic chemokine gradients. *Science*. (2013) 339:328–32. doi: 10.1126/science.1228456
84. Stoler-Barak L, Moussion C, Shezen E, Hatzav M, Sixt M, Alon R. Blood vessels pattern heparan sulfate gradients between their apical and basolateral aspects. *PLoS ONE*. (2014) 9:e85699. doi: 10.1371/journal.pone.0085699
85. Stoler-Barak L, Barzilai S, Zauberman A, Alon R. Transendothelial migration of effector T cells across inflamed endothelial barriers does not require heparan sulfate proteoglycans. *Int Immunol*. (2014) 26:315–24. doi: 10.1093/intimm/dxt076
86. Campanella GSV, Grimm J, Manice LA, Colvin RA, Medoff BD, Wojtkiewicz GR, et al. Oligomerization of CXCL10 is necessary for endothelial cell presentation and *in vivo* activity. *J Immunol*. (2006) 177:6991–8. doi: 10.4049/jimmunol.177.10.6991
87. Handel TM, Johnson Z, Rodrigues DH, dos Santos AC, Cirillo R, Muzio V, et al. An engineered monomer of CCL2 has anti-inflammatory properties emphasizing the importance of oligomerization for chemokine activity *in vivo*. *J Leukoc Biol*. (2008) 84:1101–8. doi: 10.1189/jlb.0108061
88. Ali S, Palmer ACV, Banerjee B, Fritchley SJ, Kirby JA. Examination of the function of RANTES, MIP-1alpha, and MIP-1beta following interaction with heparin-like glycosaminoglycans. *J Biol Chem*. (2000) 275:11721–7. doi: 10.1074/jbc.275.16.11721
89. Fox JM, Kausar F, Day A, Osborne M, Hussain K, Mueller A, et al. CXCL4/platelet factor 4 is an agonist of CCR1 and drives human monocyte migration. *Sci Rep*. (2018) 8:9466. doi: 10.1038/s41598-018-27710-9
90. Kuschert GSV, Coulin F, Power CA, Proudfoot AEI, Hubbard RE, Hoogewerf AJ, et al. Glycosaminoglycans interact selectively with chemokines and modulate receptor binding and cellular responses. *Biochemistry*. (1999) 38:12959–68. doi: 10.1021/bi990711d
91. Hoogewerf AJ, Kuschert GSV, Proudfoot AEI, Borlat F, Clark-Lewis I, Power CA, et al. Glycosaminoglycans mediate cell surface oligomerization of chemokines. *Biochemistry*. (1997) 36:13570–8. doi: 10.1021/bi971125s
92. Witt DP, Lander AD. Differential binding of chemokines to glycosaminoglycan subpopulations. *Curr Biol*. (1994) 4:394–400. doi: 10.1016/S0960-9822(00)00088-9
93. Hileman RE, Fromm JR, Weiler JM, Linhardt RJ. Glycosaminoglycan-protein interactions: definition of consensus sites in glycosaminoglycan binding proteins. *BioEssays*. (1998) 20:156–67.
94. Stringer SE, Gallagher JT. Specific binding of the chemokine platelet factor 4 to heparan sulfate. *J Biol Chem*. (1997) 272:20508–14. doi: 10.1074/jbc.272.33.20508
95. Spillmann D, Witt D, Lindahl U. Defining the interleukin-8-binding domain of heparan sulfate. *J Biol Chem*. (1998) 273:15487–93. doi: 10.1074/jbc.273.25.15487
96. Stringer S, Forster M, Mulloy B, Bishop C, Graham G, Gallagher J. Characterization of the binding site on heparan sulfate for macrophage inflammatory protein 1alpha. *Blood*. (2002) 100:1543–50. doi: 10.1182/blood.V100.5.1543.h81702001543_1543_1550
97. Proudfoot AEI, Johnson Z, Bonvin P, Handel TM. Glycosaminoglycan interactions with chemokines add complexity to a complex system. *Pharmaceuticals*. (2017) 10:70. doi: 10.3390/ph10030070
98. Veldkamp CT, Peterson FC, Pelzek AJ, Volkman BF. The monomer-dimer equilibrium of stromal cell-derived factor-1 (CXCL12) is altered by pH, phosphate, sulfate, and heparin. *Protein Sci*. (2005) 14:1071–81. doi: 10.1110/ps.041219505
99. Dyer DP, Salanga CL, Volkman BF, Kawamura T, Handel TM. The dependence of chemokine-glycosaminoglycan interactions on chemokine oligomerization. *Glycobiology*. (2016) 26:312–26. doi: 10.1093/glycob/cwv100
100. Rajarathnam K, Sykes B, Kay C, Dewald B, Geiser T, Baggiolini M, et al. Neutrophil activation by monomeric interleukin-8. *Science*. (1994) 264:90–2. doi: 10.1126/science.8140420
101. Paavola CD, Hemmerich S, Grunberger D, Polsky I, Bloom A, Freedman R, et al. Monomeric monocyte chemoattractant protein-1 (MCP-1) binds and activates the MCP-1 receptor CCR2B. *J Biol Chem*. (1998) 273:33157–65. doi: 10.1074/jbc.273.50.33157
102. Laurence JS, Blanpain C, Burgner JW, Parmentier M, LiWang PJ. CC chemokine MIP-1 beta can function as a monomer and depends on Phe13 for receptor binding. *Biochemistry*. (2000) 39:3401–9. doi: 10.1021/bi9923196

103. Salanga CL, Dyer DP, Kiselar JG, Gupta S, Chance MR, Handel TM. Multiple glycosaminoglycan-binding epitopes of monocyte chemoattractant protein-3/CCL7 enable it to function as a non-oligomerizing chemokine. *J Biol Chem*. (2014) 289:14896–912. doi: 10.1074/jbc.M114.547737
104. Das ST, Rajagopalan L, Guerrero-Plata A, Sai J, Richmond A, Garofalo RP, et al. Monomeric and dimeric CXCL8 are both essential for *in vivo* neutrophil recruitment. *PLoS ONE*. (2010) 5:e11754. doi: 10.1371/journal.pone.0011754
105. Ren M, Guo Q, Guo L, Lenz M, Qian F, Koenen RR, et al. Polymerization of MIP-1 chemokine (CCL3 and CCL4) and clearance of MIP-1 by insulin-degrading enzyme. *EMBO J*. (2010) 29:3952–66. doi: 10.1038/emboj.2010.256
106. Lau EK, Paavola CD, Johnson Z, Gaudry JP, Geretti E, Borlat F, et al. Identification of the glycosaminoglycan binding site of the CC chemokine, MCP-1: implications for structure and function *in vivo*. *J Biol Chem*. (2004) 279:22294–305. doi: 10.1074/jbc.M311224200
107. Graham GJ, Handel TM, Proudfoot AEI. Leukocyte adhesion: reconceptualizing chemokine presentation by glycosaminoglycans. *Trends Immunol*. (2019) 40:472–81. doi: 10.1016/j.it.2019.03.009
108. Van Coillie E, Van Damme J, Opdenakker G. The MCP/eotaxin subfamily of CC chemokines. *Cytokine Growth Factor Rev*. (1999) 10:61–86. doi: 10.1016/S1359-6101(99)00005-2
109. Wolpe S, Davatelis G, Sherry B, Beutler B, Hesse D, Nguyen H, et al. Macrophages secrete a novel heparin-binding protein with inflammatory and neutrophil chemokinetic properties. *J Exp Med*. (1988) 167:570–81. doi: 10.1084/jem.167.2.570
110. Wolpe SD, Sherry B, Juers D, Davatelis G, Yurt RW, Cerami A. Identification and characterization of macrophage inflammatory protein 2. *Proc Natl Acad Sci USA*. (1989) 86:612–6. doi: 10.1073/pnas.86.2.612
111. Wang D, Sai J, Richmond A. Cell surface heparan sulfate participates in CXCL1-induced signaling. *Biochemistry*. (2003) 42:1071–7. doi: 10.1021/bi026425a
112. Carlson EC, Lin M, Liu CY, Kao WWY, Perez VL, Pearlman E. Keratocan and lumican regulate neutrophil infiltration and corneal clarity in lipopolysaccharide-induced keratitis by direct interaction with CXCL1. *J Biol Chem*. (2007) 282:35502–9. doi: 10.1074/jbc.M705823200
113. Carlson EC, Sun Y, Auletta J, Kao WW-Y, Liu C-Y, Perez VL, et al. Regulation of corneal inflammation by neutrophil-dependent cleavage of keratan sulfate proteoglycans as a model for breakdown of the chemokine gradient. *J Leukoc Biol*. (2010) 88:517–22. doi: 10.1189/jlb.0310134
114. Rajasekaran D, Keeler C, Syed MA, Jones MC, Harrison JK, Wu D, et al. A model of GAG/MIP-2/CXCR2 interfaces and its functional effects. *Biochemistry*. (2012) 51:5642–54. doi: 10.1021/bi3001566
115. Poluri KM, Joseph PRB, Sawant KV, Rajarathnam K. Molecular basis of glycosaminoglycan heparin binding to the chemokine CXCL1 dimer. *J Biol Chem*. (2013) 288:25143–53. doi: 10.1074/jbc.M113.492579
116. Sepuru KM, Rajarathnam K. CXCL1/MGSA is a novel glycosaminoglycan (GAG)-binding chemokine: structural evidence for two distinct non-overlapping binding domains. *J Biol Chem*. (2016) 291:4247–55. doi: 10.1074/jbc.M115.697888
117. Sawant KV, Poluri KM, Dutta AK, Sepuru KM, Troshkina A, Garofalo RP, et al. Chemokine CXCL1 mediated neutrophil recruitment: role of glycosaminoglycan interactions. *Sci Rep*. (2016) 6:33123. doi: 10.1038/srep33123
118. Tanino Y, Coombe DR, Gill SE, Kett WC, Kajikawa O, Proudfoot AEI, et al. Kinetics of chemokine–glycosaminoglycan interactions control neutrophil migration into the airspaces of the lungs. *J Immunol*. (2010) 184:2677–85. doi: 10.4049/jimmunol.0903274
119. Li S, Pettersson US, Hoorelbeke B, Kolaczkowska E, Schelfhout K, Martens E, et al. Interference with glycosaminoglycan-chemokine interactions with a probe to alter leukocyte recruitment and inflammation *in vivo*. *PLoS ONE*. (2014) 9:e104107. doi: 10.1371/journal.pone.0104107
120. Handin RI, Cohen HJ. Purification and binding properties of human platelet factor four. *J Biol Chem*. (1976) 251:4273–82.
121. Petersen F, Brandt E, Lindahl U, Spillmann D. Characterization of a neutrophil cell surface glycosaminoglycan that mediates binding of platelet factor 4. *J Biol Chem*. (1999) 274:12376–82. doi: 10.1074/jbc.274.18.12376
122. Dudek AZ, Pennell CA, Decker TD, Young TA, Key NS, Slungaard A. Platelet factor 4 binds to glycanated forms of thrombomodulin and to protein C. A potential mechanism for enhancing generation of activated protein C. *J Biol Chem*. (1997) 272:31785–92. doi: 10.1074/jbc.272.50.31785
123. Mayo KH, Ilyina E, Roongta V, Dundas M, Joseph J, Lai CK, et al. Heparin binding to platelet factor-4. An NMR and site-directed mutagenesis study: arginine residues are crucial for binding. *Biochem J*. (1995) 312:357–65. doi: 10.1042/bj3120357
124. Cochran S, Li CP, Ferro V. A surface plasmon resonance-based solution affinity assay for heparan sulfate-binding proteins. *Glycoconj J*. (2009) 26:577–87. doi: 10.1007/s10719-008-9210-0
125. Dubrac A, Quemener C, Lacazette E, Lopez F, Zanibellato C, Wu W-G, et al. Functional divergence between 2 chemokines is conferred by single amino acid change. *Blood*. (2010) 116:4703–11. doi: 10.1182/blood-2010-03-274852
126. Rucinski B, Niewiarowski S, Strzyzewski M, Holt JC, Mayo KH. Human platelet factor 4 and its C-terminal peptides: heparin binding and clearance from the circulation. *Thromb Haemost*. (1990) 63:493–8. doi: 10.1055/s-0038-1645072
127. Sepuru KM, Nagarajan B, Desai UR, Rajarathnam K. Molecular basis of chemokine CXCL5-glycosaminoglycan interactions. *J Biol Chem*. (2016) 291:20539–50. doi: 10.1074/jbc.M116.745265
128. Brown AJ, Sepuru KM, Rajarathnam K. Structural basis of native CXCL7 monomer binding to CXCR2 receptor N-domain and glycosaminoglycan heparin. *Int J Mol Sci*. (2017) 18:508. doi: 10.3390/ijms18030508
129. Pichert A, Schlorke D, Franz S, Arnhold J. Functional aspects of the interaction between interleukin-8 and sulfated glycosaminoglycans. *Biomatterials*. (2012) 2:142–8. doi: 10.4161/biom.21316
130. Pichert A, Samsonov SA, Theisgen S, Thomas L, Baumann L, Schiller J, et al. Characterization of the interaction of interleukin-8 with hyaluronan, chondroitin sulfate, dermatan sulfate and their sulfated derivatives by spectroscopy and molecular modeling. *Glycobiology*. (2012) 22:134–45. doi: 10.1093/glycob/cwr120
131. Nordsieck K, Pichert A, Samsonov SA, Thomas L, Berger C, Pisabarro MT, et al. Residue 75 of interleukin-8 is crucial for its interactions with glycosaminoglycans. *ChemBioChem*. (2012) 13:2558–66. doi: 10.1002/cbic.201200467
132. Mobius K, Nordsieck K, Pichert A, Samsonov SA, Thomas L, Schiller J, et al. Investigation of lysine side chain interactions of interleukin-8 with heparin and other glycosaminoglycans studied by a methylation-NMR approach. *Glycobiology*. (2013) 23:1260–9. doi: 10.1093/glycob/cwt062
133. Schlorke D, Thomas L, Samsonov SA, Huster D, Arnhold J, Pichert A. The influence of glycosaminoglycans on IL-8-mediated functions of neutrophils. *Carbohydr Res*. (2012) 356:196–203. doi: 10.1016/j.carres.2012.02.025
134. Ramdin L, Perks B, Sheron N, Shute J. Regulation of interleukin-8 binding and function by heparin and alpha2-macroglobulin. *Clin Exp Allergy*. (1998) 28:616–24. doi: 10.1046/j.1365-2222.1998.00283.x
135. Webb LM, Ehrengruber MU, Clark-Lewis I, Baggiolini M, Rot A. Binding to heparan sulfate or heparin enhances neutrophil responses to interleukin 8. *Proc Natl Acad Sci USA*. (1993) 90:7158–62. doi: 10.1073/pnas.90.15.7158
136. Kohrgruber N, Gröger M, Meraner P, Kriehuber E, Petzelbauer P, Brandt S, et al. Plasmacytoid dendritic cell recruitment by immobilized CXCR3 ligands. *J Immunol*. (2004) 173:6592–602. doi: 10.4049/jimmunol.173.11.6592
137. Ranjbaran H, Wang Y, Manes TD, Yakimov AO, Akhtar S, Kluger MS, et al. Heparin displaces interferon-gamma-inducible chemokines (IP-10, I-TAC, and Mig) sequestered in the vasculature and inhibits the transendothelial migration and arterial recruitment of T cells. *Circulation*. (2006) 114:1293–300. doi: 10.1161/CIRCULATIONAHA.106.631457
138. Luster AD, Greenberg SM, Leder P. The IP-10 chemokine binds to a specific cell surface heparan sulfate site shared with platelet factor 4 and inhibits endothelial cell proliferation. *J Exp Med*. (1995) 182:219–31. doi: 10.1084/jem.182.1.219
139. Campanella GSV, Lee EMJ, Sun J, Luster AD. CXCR3 and heparin binding sites of the chemokine IP-10 (CXCL10). *J Biol Chem*. (2003) 278:17066–74. doi: 10.1074/jbc.M212077200
140. Uchimura K, Morimoto-Tomita M, Bistrup A, Li J, Lyon M, Gallagher J, et al. HSulf-2, an extracellular endoglucosamine-6-sulfatase, selectively mobilizes heparin-bound growth factors and chemokines: effects on VEGF, FGF-1, and SDF-1. *BMC Biochem*. (2006) 7:2. doi: 10.1186/1471-2091-7-2

141. Dyer DP, Migliorini E, Salanga CL, Thakar D, Handel TM, Richter RP. Differential structural remodelling of heparan sulfate by chemokines: the role of chemokine oligomerization. *Open Biol*. (2017) 7:160286. doi: 10.1098/rsob.160286
142. Severin IC, Gaudry J-P, Johnson Z, Kungl A, Jansma A, Gesslbauer B, et al. Characterization of the chemokine CXCL11-heparin interaction suggests two different affinities for glycosaminoglycans. *J Biol Chem*. (2010) 285:17713–24. doi: 10.1074/jbc.M109.082552
143. Saxena A, Bujak M, Frunza O, Dobaczewski M, Gonzalez-Quesada C, Lu B, et al. CXCR3-independent actions of the CXC chemokine CXCL10 in the infarcted myocardium and in isolated cardiac fibroblasts are mediated through proteoglycans. *Cardiovasc Res*. (2014) 103:217–27. doi: 10.1093/cvr/cvu138
144. Chen J-P, Lu H-L, Lai S-L, Campanella GS, Sung J-M, Lu M-Y, et al. Dengue virus induces expression of CXC chemokine ligand 10/IFN-gamma-inducible protein 10, which competitively inhibits viral binding to cell surface heparan sulfate. *J Immunol*. (2006) 177:3185–92. doi: 10.4049/jimmunol.177.5.3185
145. Cox JH, Dean RA, Roberts CR, Overall CM. Matrix metalloproteinase processing of CXCL11/I-TAC results in loss of chemoattractant activity and altered glycosaminoglycan binding. *J Biol Chem*. (2008) 283:19389–99. doi: 10.1074/jbc.M800266200
146. Amara A, Lorthioir O, Valenzuela A, Magerus A, Thelen M, Montes M, et al. Stromal cell-derived factor-1α associates with heparan sulfates through the first β-strand of the chemokine. *J Biol Chem*. (1999) 274:23916–25. doi: 10.1074/jbc.274.34.23916
147. Netelenbos T, Van den Born J, Kessler FL, Zweegman S, Merle PA, van Oostveen JW, et al. Proteoglycans on bone marrow endothelial cells bind and present SDF-1 towards hematopoietic progenitor cells. *Leukemia*. (2003) 17:175–84. doi: 10.1038/sj.leu.2402738
148. Rueda P, Balabanian K, Lagane B, Staropoli I, Chow K, Levoye A, et al. The CXCL12γ chemokine displays unprecedented structural and functional properties that make it a paradigm of chemoattractant proteins. *PLoS ONE*. (2008) 3:e2543. doi: 10.1371/journal.pone.0002543
149. Laguri C, Sadir R, Rueda P, Baleux F, Gans P, Arenzana-Seisdedos F, et al. The novel CXCL12γ isoform encodes an unstructured cationic domain which regulates bioactivity and interaction with both glycosaminoglycans and CXCR4. *PLoS ONE*. (2007) 2:e1110. doi: 10.1371/journal.pone.0001110
150. Santiago B, Baleux F, Palao G, Gutiérrez-Cañas I, Ramírez JC, Arenzana-Seisdedos F, et al. CXCL12 is displayed by rheumatoid endothelial cells through its basic amino-terminal motif on heparan sulfate proteoglycans. *Arthritis Res Ther*. (2006) 8:R43. doi: 10.1186/ar1900
151. Santiago B, Izquierdo E, Rueda P, Del Rey MJ, Criado G, Usategui A, et al. CXCL12γ isoform is expressed on endothelial and dendritic cells in rheumatoid arthritis synovium and regulates T cell activation. *Arthritis Rheum*. (2012) 64:409–17. doi: 10.1002/art.33345
152. Valenzuela-Fernández A, Palanche T, Amara A, Magerus A, Altmeyer R, Delaunay T, et al. Optimal inhibition of X4 HIV isolates by the CXC chemokine stromal cell-derived factor 1 alpha requires interaction with cell surface heparan sulfate proteoglycans. *J Biol Chem*. (2001) 276:26550–8. doi: 10.1074/jbc.M100411200
153. Sadir R, Baleux F, Grosdidier A, Imberty A, Lortat-Jacob H. Characterization of the stromal cell-derived factor-1α-heparin complex. *J Biol Chem*. (2001) 276:8288–96. doi: 10.1074/jbc.M008110200
154. Panitz N, Theisgen S, Samsonov SA, Gehrcke J-P, Baumann L, Bellmann-Sickert K, et al. The structural investigation of glycosaminoglycan binding to CXCL12 displays distinct interaction sites. *Glycobiology*. (2016) 26:1209–21. doi: 10.1093/glycob/cww059
155. Sweeney MD, Yu Y, Leary JA. Effects of sulfate position on heparin octasaccharide binding to CCL2 examined by tandem mass spectrometry. *J Am Soc Mass Spectrom*. (2006) 17:1114–9. doi: 10.1016/j.jasms.2006.04.025
156. Schenauer MR, Yu Y, Sweeney MD, Leary JA. CCR2 chemokines bind selectively to acetylated heparan sulfate octasaccharides. *J Biol Chem*. (2007) 282:25182–8. doi: 10.1074/jbc.M703387200
157. Yu Y, Sweeney MD, Saad OM, Crown SE, Hsu AR, Handel TM, et al. Chemokine-glycosaminoglycan binding: specificity for CCR2 ligand binding to highly sulfated oligosaccharides using FTICR mass spectrometry. *J Biol Chem*. (2005) 280:32200–8. doi: 10.1074/jbc.M505738200
158. Crown SE, Yu Y, Sweeney MD, Leary JA, Handel TM. Heterodimerization of CCR2 chemokines and regulation by glycosaminoglycan binding. *J Biol Chem*. (2006) 281:25438–46. doi: 10.1074/jbc.M601518200
159. Chakravarty L, Rogers L, Quach T, Breckenridge S, Kolattukudy PE. Lysine 58 and histidine 66 at the C-terminal α-helix of monocyte chemoattractant protein-1 are essential for glycosaminoglycan binding. *J Biol Chem*. (1998) 273:29641–7. doi: 10.1074/jbc.273.45.29641
160. Koopmann W, Krangel MS. Identification of a glycosaminoglycan-binding site in chemokine macrophage inflammatory protein-1alpha . *J Biol Chem*. (1997) 272:10103–9. doi: 10.1074/jbc.272.15.10103
161. Graham GJ, Wilkinson PC, Nibbs RJ, Lowe S, Kolset SO, Parker A, et al. Uncoupling of stem cell inhibition from monocyte chemoattraction in MIP-1alpha by mutagenesis of the proteoglycan binding site. *EMBO J*. (1996) 15:6506–15. doi: 10.1002/j.1460-2075.1996.tb01041.x
162. Koopmann W, Ediriwickrema C, Krangel MS. Structure and function of the glycosaminoglycan binding site of chemokine macrophage-inflammatory protein-1 beta. *J Immunol*. (1999) 163:2120–7.
163. Laurence JS, Blanpain C, De Leener A, Parmentier M, LiWang PJ. Importance of basic residues and quaternary structure in the function of MIP-1β: CCR5 binding and cell surface sugar interactions. *Biochemistry*. (2001) 40:4990–9. doi: 10.1021/bi002593w
164. McCornack MA, Cassidy CK, LiWang PJ. The binding surface and affinity of monomeric and dimeric chemokine macrophage inflammatory protein 1β for various glycosaminoglycan disaccharides. *J Biol Chem*. (2003) 278:1946–56. doi: 10.1074/jbc.M207440200
165. McCornack MA, Boren DM, LiWang PJ. Glycosaminoglycan disaccharide alters the dimer dissociation constant of the chemokine MIP-1 beta. *Biochemistry*. (2004) 43:10090–101. doi: 10.1021/bi049751u
166. Johnson Z, Kosco-Vilbois MH, Herren S, Cirillo R, Muzio V, Zaratin P, et al. Interference with heparin binding and oligomerization creates a novel anti-inflammatory strategy targeting the chemokine system. *J Immunol*. (2004) 173:5776–85. doi: 10.4049/jimmunol.173.9.5776
167. Rek A, Brandner B, Geretti E, Kungl AJ. A biophysical insight into the RANTES–glycosaminoglycan interaction. *Biochim Biophys Acta*. (2009) 1794:577–82. doi: 10.1016/j.bbapap.2009.01.001
168. Proudfoot AEI, Fritchley S, Borlat F, Shaw JP, Vilbois F, Zwahlen C, et al. The BBXB motif of RANTES is the principal site for heparin binding and controls receptor selectivity. *J Biol Chem*. (2001) 276:10620–6. doi: 10.1074/jbc.M010867200
169. Vivès RR, Crublet E, Andrieu J-P, Gagnon J, Rousselle P, Lortat-Jacob H. A novel strategy for defining critical amino acid residues involved in protein/glycosaminoglycan interactions. *J Biol Chem*. (2004) 279:54327–33. doi: 10.1074/jbc.M409760200
170. Segerer S, Johnson Z, Rek A, Baltus T, von Hundelshausen P, Kungl AJ, et al. The basic residue cluster (55)KKWVR(59) in CCL5 is required for *in vivo* biologic function. *Mol Immunol*. (2009) 46:2533–8. doi: 10.1016/j.molimm.2009.05.015
171. Ali S, Fritchley SJ, Chaffey BT, Kirby JA. Contribution of the putative heparan sulfate-binding motif BBXB of RANTES to transendothelial migration. *Glycobiology*. (2002) 12:535–43. doi: 10.1093/glycob/cwf069
172. Murooka TT, Wong MM, Rahbar R, Majchrzak-Kita B, Proudfoot AEI, Fish EN. CCL5-CCR5-mediated apoptosis in T cells: requirement for glycosaminoglycan binding and CCL5 aggregation. *J Biol Chem*. (2006) 281:25184–94. doi: 10.1074/jbc.M603912200
173. Culley FJ, Fadlon EJ, Kirchem A, Williams TJ, Jose PJ, Pease JE. Proteoglycans are potent modulators of the biological responses of eosinophils to chemokines. *Eur J Immunol*. (2003) 33:1302–10. doi: 10.1002/eji.200323509
174. Vanheule V, Boff D, Mortier A, Janssens R, Petri B, Kolaczkowska E, et al. CXCL9-derived peptides differentially inhibit neutrophil migration *in vivo* through interference with glycosaminoglycan interactions. *Front Immunol*. (2017) 8:530. doi: 10.3389/fimmu.2017.00530
175. Proost P, Wuyts A, Conings R, Lenaerts J, Put W, Van Damme J. Purification and identification of natural chemokines. *Methods*. (1996) 10:82–92. doi: 10.1006/meth.1996.0082
176. Walz A, Dewald B, von Tscharner V, Baggiolini M. Effects of the neutrophil-activating peptide NAP-2, platelet basic protein, connective tissue-activating

peptide III and platelet factor 4 on human neutrophils. *J Exp Med*. (1989) 170:1745–50. doi: 10.1084/jem.170.5.1745
177. Walz A, Burgener R, Car B, Baggiolini M, Kunkel S, Strieter R. Structure and neutrophil-activating properties of a novel inflammatory peptide (ENA-78) with homology to interleukin 8. *J Exp Med*. (1991) 174:1355–62. doi: 10.1084/jem.174.6.1355
178. Brown AJ, Joseph PRB, Sawant KV, Rajarathnam K. Chemokine CXCL7 heterodimers: structural insights, CXCR2 receptor function, and glycosaminoglycan interactions. *Int J Mol Sci*. (2017) 18:748. doi: 10.3390/ijms18040748
179. Nordsieck K, Baumann L, Hintze V, Pisabarro MT, Schnabelrauch M, Beck-Sickinger AG, et al. The effect of interleukin-8 truncations on its interactions with glycosaminoglycans. *Biopolymers*. (2018) 109:e23103. doi: 10.1002/bip.23103
180. Kuschert GSV, Hoogewerf AJ, Proudfoot AEI, Chung C, Cooke RM, Hubbard RE, et al. Identification of a glycosaminoglycan binding surface on human interleukin-8. *Biochemistry*. (1998) 37:11193–201. doi: 10.1021/bi972867o
181. Krieger E, Geretti E, Brandner B, Goger B, Wells TN, Kungl AJ. A structural and dynamic model for the interaction of interleukin-8 and glycosaminoglycans: support from isothermal fluorescence titrations. *Proteins*. (2004) 54:768–75. doi: 10.1002/prot.10590
182. Goger B, Halden Y, Rek A, Mösl R, Pye D, Gallagher J, et al. Different affinities of glycosaminoglycan oligosaccharides for monomeric and dimeric interleukin-8: a model for chemokine regulation at inflammatory sites. *Biochemistry*. (2002) 41:1640–6. doi: 10.1021/bi011944j
183. Joseph PRB, Mosier PD, Desai UR, Rajarathnam K. Solution NMR characterization of chemokine CXCL8/IL-8 monomer and dimer binding to glycosaminoglycans: structural plasticity mediates differential binding interactions. *Biochem J*. (2015) 472:121–33. doi: 10.1042/BJ20150059
184. Levine SP, Wohl H. Human platelet factor 4: purification and characterization by affinity chromatography. Purification of human platelet factor 4. *J Biol Chem*. (1976) 251:324–8.
185. Kolset S, Mann D, Uhlin-Hansen L, Winberg J, Ruoslahti E. Serglycin-binding proteins in activated macrophages and platelets. *J Leukoc Biol*. (1996) 59:545–54. doi: 10.1002/jlb.59.4.545
186. Struyf S, Burdick MD, Proost P, Van Damme J, Strieter RM. Platelets release CXCL4L1, a nonallelic variant of the chemokine platelet factor-4/CXCL4 and potent inhibitor of angiogenesis. *Circ Res*. (2004) 95:855–7. doi: 10.1161/01.RES.0000146674.38319.07
187. Struyf S, Salogni L, Burdick MD, Vandercappellen J, Gouwy M, Noppen S, et al. Angiostatic and chemotactic activities of the CXC chemokine CXCL4L1 (platelet factor-4 variant) are mediated by CXCR3. *Blood*. (2011) 117:480–8. doi: 10.1182/blood-2009-11-253591
188. Rao AK, Niewiarowski S, James P, Holt JC, Harris M, Elfenbein B, et al. Effect of heparin on the *in vivo* release and clearance of human platelet factor 4. *Blood*. (1983) 61:1208–14. doi: 10.1182/blood.V61.6.1208.1208
189. Maione TE, Gray GS, Hunt AJ, Sharpe RJ. Inhibition of tumor growth in mice by an analogue of platelet factor 4 that lacks affinity for heparin and retains potent angiostatic activity. *Cancer Res*. (1991) 51:2077–83.
190. Dyer DP, Salanga CL, Johns SC, Valdambrini E, Fuster MM, Milner CM, et al. The anti-inflammatory protein TSG-6 regulates chemokine function by inhibiting chemokine/glycosaminoglycan interactions. *J Biol Chem*. (2016) 291:12627–40. doi: 10.1074/jbc.M116.720953
191. Loos T, Mortier A, Gouwy M, Ronsse I, Put W, Lenaerts J-P, et al. Citrullination of CXCL10 and CXCL11 by peptidylarginine deiminase: a naturally occurring posttranslational modification of chemokines and new dimension of immunoregulation. *Blood*. (2008) 112:2648–56. doi: 10.1182/blood-2008-04-149039
192. Horton MR, Boodoo S, Powell JD. NF-κB activation mediates the cross-talk between extracellular matrix and interferon-γ (IFN-γ) leading to enhanced monokine induced by IFN-γ (MIG) expression in macrophages. *J Biol Chem*. (2002) 277:43757–62. doi: 10.1074/jbc.M206007200
193. Boodoo S, Spannhake EW, Powell JD, Horton MR. Differential regulation of hyaluronan-induced IL-8 and IP-10 in airway epithelial cells. *Am J Physiol Cell Mol Physiol*. (2006) 291:L479–86. doi: 10.1152/ajplung.00518.2005
194. Fluhr H, Seitz T, Zygmunt M. Heparins modulate the IFN-γ-induced production of chemokines in human breast cancer cells. *Breast Cancer Res Treat*. (2013) 137:109–18. doi: 10.1007/s10549-012-2334-8
195. Campanella GSV, Colvin RA, Luster AD. CXCL10 can inhibit endothelial cell proliferation independently of CXCR3. *PLoS ONE*. (2010) 5:e12700. doi: 10.1371/journal.pone.0012700
196. Yang J, Richmond A. The angiostatic activity of interferon-inducible protein-10/CXCL10 in human melanoma depends on binding to CXCR3 but not to glycosaminoglycan. *Mol Ther*. (2004) 9:846–55. doi: 10.1016/j.ymthe.2004.01.010
197. Jiang D, Liang J, Campanella GS, Guo R, Yu S, Xie T, et al. Inhibition of pulmonary fibrosis in mice by CXCL10 requires glycosaminoglycan binding and syndecan-4. *J Clin Invest*. (2010) 120:2049–57. doi: 10.1172/JCI38644
198. Tortelli F, Pisano M, Briquez PS, Martino MM, Hubbell JA. Fibronectin binding modulates CXCL11 activity and facilitates wound healing. *PLoS ONE*. (2013) 8:e79610. doi: 10.1371/journal.pone.0079610
199. Vanheule V, Vervaeke P, Mortier A, Noppen S, Gouwy M, Snoeck R, et al. Basic chemokine-derived glycosaminoglycan binding peptides exert antiviral properties against dengue virus serotype 2, herpes simplex virus-1 and respiratory syncytial virus. *Biochem Pharmacol*. (2016) 100:73–85. doi: 10.1016/j.bcp.2015.11.001
200. Janssens R, Struyf S, Proost P. The unique structural and functional features of CXCL12. *Cell Mol Immunol*. (2018) 15:299–311. doi: 10.1038/cmi.2017.107
201. Laguri C, Arenzana-Seisdedos F, Lortat-Jacob H. Relationships between glycosaminoglycan and receptor binding sites in chemokines—the CXCL12 example. *Carbohydr Res*. (2008) 343:2018–23. doi: 10.1016/j.carres.2008.01.047
202. Murphy JW, Cho Y, Sachpatzidis A, Fan C, Hodsdon ME, Lolis E. Structural and functional basis of CXCL12 (stromal cell-derived factor-1 alpha) binding to heparin. *J Biol Chem*. (2007) 282:10018–27. doi: 10.1074/jbc.M608796200
203. Connell BJ, Sadir R, Baleux F, Laguri C, Kleman J-P, Luo L, et al. Heparan sulfate differentially controls CXCL12- and CXCL12-mediated cell migration through differential presentation to their receptor CXCR4. *Sci Signal*. (2016) 9:ra107. doi: 10.1126/scisignal.aaf1839
204. Penk A, Baumann L, Huster D, Samsonov SA. NMR and molecular modeling reveal specificity of the interactions between CXCL14 and glycosaminoglycans. *Glycobiology*. (2019) 29:715–25. doi: 10.1093/glycob/cwz047
205. Jen CH, Leary JA. A competitive binding study of chemokine, sulfated receptor, and glycosaminoglycan interactions by nano-electrospray ionization mass spectrometry. *Anal Biochem*. (2010) 407:134–40. doi: 10.1016/j.ab.2010.08.005
206. Patel DD, Koopmann W, Imai T, Whichard LP, Yoshie O, Krangel MS. Chemokines have diverse abilities to form solid phase gradients. *Clin Immunol*. (2001) 99:43–52. doi: 10.1006/clim.2000.4997
207. Ali S, Palmer ACV, Fritchley SJ, Maley Y, Kirby JA. Multimerization of monocyte chemoattractant protein-1 is not required for glycosaminoglycan-dependent transendothelial chemotaxis. *Biochem J*. (2001) 358:737–45. doi: 10.1042/bj3580737
208. Barker CE, Thompson S, O'Boyle G, Lortat-Jacob H, Sheerin NS, Ali S, et al. CCL2 nitration is a negative regulator of chemokine-mediated inflammation. *Sci Rep*. (2017) 7:44384. doi: 10.1038/srep44384
209. Ottersbach K, Graham GJ. Aggregation-independent modulation of proteoglycan binding by neutralization of C-terminal acidic residues in the chemokine macrophage inflammatory protein 1alpha. *Biochem J*. (2001) 354:447–53. doi: 10.1042/bj3540447
210. Burns JM, Gallo RC, DeVico AL, Lewis GK. A new monoclonal antibody, mAb 4A12, identifies a role for the glycosaminoglycan (GAG) binding domain of RANTES in the antiviral effect against HIV-1 and intracellular Ca2+ signaling. *J Exp Med*. (1998) 188:1917–27. doi: 10.1084/jem.188.10.1917
211. Burns JM, Lewis GK, DeVico AL. Soluble complexes of regulated upon activation, normal T cells expressed and secreted (RANTES) and glycosaminoglycans suppress HIV-1 infection but do not induce (Ca2+) signaling. *Proc Natl Acad Sci USA*. (1999) 96:14499–504. doi: 10.1073/pnas.96.25.14499

212. Segerer S, Djafarzadeh R, Gröne H-J, Weingart C, Kerjaschki D, Weber C, et al. Selective binding and presentation of CCL5 by discrete tissue microenvironments during renal inflammation. *J Am Soc Nephrol*. (2007) 18:1835–44. doi: 10.1681/ASN.2006080837
213. Liang WG, Triandafillou CG, Huang T-Y, Zulueta MML, Banerjee S, Dinner AR, et al. Structural basis for oligomerization and glycosaminoglycan binding of CCL5 and CCL3. *Proc Natl Acad Sci USA*. (2016) 113:5000–5. doi: 10.1073/pnas.1523981113
214. Dykstra A, Sweeney M, Leary J. Structural evidence for the tetrameric assembly of chemokine CCL11 and the glycosaminoglycan Arixtra^{TM}. *Biomolecules*. (2013) 3:905–22. doi: 10.3390/biom3040905
215. Hirose J, Kawashima H, Yoshie O, Tashiro K, Miyasaka M. Versican interacts with chemokines and modulates cellular responses. *J Biol Chem*. (2001) 276:5228–34. doi: 10.1074/jbc.M007542200
216. Hirose J, Kawashima H, Willis MS, Springer TA, Hasegawa H, Yoshie O, et al. Chondroitin sulfate B exerts its inhibitory effect on secondary lymphoid tissue chemokine (SLC) by binding to the C-terminus of SLC. *Biochim Biophys Acta*. (2002) 1571:219–24. doi: 10.1016/S0304-4165(02)00232-5
217. Hjortø GM, Larsen O, Steen A, Daugvilaite V, Berg C, Fares S, et al. Differential CCR7 targeting in dendritic cells by three naturally occurring CC-chemokines. *Front Immunol*. (2016) 7:568. doi: 10.3389/fimmu.2016.00568
218. Schumann K, Lämmermann T, Bruckner M, Legler DF, Polleux J, Spatz JP, et al. Immobilized chemokine fields and soluble chemokine gradients cooperatively shape migration patterns of dendritic cells. *Immunity*. (2010) 32:703–13. doi: 10.1016/j.immuni.2010.04.017
219. Barmore AJ, Castex SM, Gouletas BA, Griffith AJ, Metz SW, Muelder NG, et al. Transferring the C-terminus of the chemokine CCL21 to CCL19 confers enhanced heparin binding. *Biochem Biophys Res Commun*. (2016) 477:602–6. doi: 10.1016/j.bbrc.2016.06.098
220. de Paz JL, Moseman EA, Noti C, Polito L, von Andrian UH, Seeberger PH. Profiling heparin–chemokine interactions using synthetic tools. *ACS Chem Biol*. (2007) 2:735–44. doi: 10.1021/cb700159m
221. Verkaar F, van Offenbeek J, van der Lee MMC, van Lith LHCJ, Watts AO, Rops ALWMM, et al. Chemokine cooperativity is caused by competitive glycosaminoglycan binding. *J Immunol*. (2014) 192:3908–14. doi: 10.4049/jimmunol.1302159
222. Fox JC, Nakayama T, Tyler RC, Sander TL, Yoshie O, Volkman BF. Structural and agonist properties of XCL2, the other member of the C-chemokine subfamily. *Cytokine*. (2015) 71:302–11. doi: 10.1016/j.cyto.2014.11.010
223. Fox JC, Tyler RC, Guzzo C, Tuinstra RL, Peterson FC, Lusso P, et al. Engineering metamorphic chemokine lymphotactin/XCL1 into the GAG-binding, HIV-inhibitory dimer conformation. *ACS Chem Biol*. (2015) 10:2580–8. doi: 10.1021/acschembio.5b00542
224. Fox JC, Tyler RC, Peterson FC, Dyer DP, Zhang F, Linhardt RJ, et al. Examination of glycosaminoglycan binding sites on the XCL1 dimer. *Biochemistry*. (2016) 55:1214–25. doi: 10.1021/acs.biochem.5b01329
225. Perry CM. Maraviroc: a review of its use in the management of CCR5-tropic HIV-1 infection. *Drugs*. (2010) 70:1189–213. doi: 10.2165/11203940-000000000-00000
226. De Clercq E. The AMD3100 story: the path to the discovery of a stem cell mobilizer (Mozobil). *Biochem Pharmacol*. (2009) 77:1655–64. doi: 10.1016/j.bcp.2008.12.014
227. Andrews SP, Cox RJ. Small molecule CXCR3 antagonists. *J Med Chem*. (2016) 59:2894–917. doi: 10.1021/acs.jmedchem.5b01337
228. Hoellenriegel J, Zboralski D, Maasch C, Rosin NY, Wierda WG, Keating MJ, et al. The spiegelmer NOX-A12, a novel CXCL12 inhibitor, interferes with chronic lymphocytic leukemia cell motility and causes chemosensitization. *Blood*. (2014) 123:1032–9. doi: 10.1182/blood-2013-03-493924
229. Marasca R, Maffei R. NOX-A12: mobilizing CLL away from home. *Blood*. (2014) 123:952–3. doi: 10.1182/blood-2013-12-542480
230. Adage T, Konya V, Weber C, Strutzmann E, Fuchs T, Zankl C, et al. Targeting glycosaminoglycans in the lung by an engineered CXCL8 as a novel therapeutic approach to lung inflammation. *Eur J Pharmacol*. (2015) 748:83–92. doi: 10.1016/j.ejphar.2014.12.019
231. Vanheule V, Janssens R, Boff D, Kitic N, Berghmans N, Ronsse I, et al. The positively charged COOH-terminal glycosaminoglycan-binding CXCL9(74-103) peptide inhibits CXCL8-induced neutrophil extravasation and monosodium urate crystal-induced gout in mice. *J Biol Chem*. (2015) 290:21292–304. doi: 10.1074/jbc.M115.649855
232. McNaughton EF, Eustace AD, King S, Sessions RB, Kay A, Farris M, et al. Novel anti-inflammatory peptides based on chemokine–glycosaminoglycan interactions reduce leukocyte migration and disease severity in a model of rheumatoid arthritis. *J Immunol*. (2018) 200:3201–17. doi: 10.4049/jimmunol.1701187
233. Martínez-Burgo B, Cobb SL, Pohl E, Kashanin D, Paul T, Kirby JA, et al. A C-terminal CXCL8 peptide based on chemokine–glycosaminoglycan interactions reduces neutrophil adhesion and migration during inflammation. *Immunology*. (2019) 157:173–84. doi: 10.1111/imm.13063
234. Lindow M, Lüttichau HR, Schwartz TW. Viral leads for chemokine-modulatory drugs. *Trends Pharmacol Sci*. (2003) 24:126–30. doi: 10.1016/S0165-6147(03)00033-6
235. González-Motos V, Kropp KA, Viejo-Borbolla A. Chemokine binding proteins: an immunomodulatory strategy going viral. *Cytokine Growth Factor Rev*. (2016) 30:71–80. doi: 10.1016/j.cytogfr.2016.02.007
236. Heidarieh H, Hernáez B, Alcamí A. Immune modulation by virus-encoded secreted chemokine binding proteins. *Virus Res*. (2015) 209:67–75. doi: 10.1016/j.virusres.2015.02.028
237. Seet BT, McFadden G. Viral chemokine-binding proteins. *J Leukoc Biol*. (2002) 72:24–34. doi: 10.1189/jlb.72.1.24
238. Viejo-Borbolla A, Martinez-Martín N, Nel HJ, Rueda P, Martín R, Blanco S, et al. Enhancement of chemokine function as an immunomodulatory strategy employed by human herpesviruses. *PLoS Pathog*. (2012) 8:e1002497. doi: 10.1371/journal.ppat.1002497
239. Bahar MW, Kenyon JC, Putz MM, Abrescia NGA, Pease JE, Wise EL, et al. Structure and function of A41, a vaccinia virus chemokine binding protein. *PLoS Pathog*. (2008) 4:0055–68. doi: 10.1371/journal.ppat.0040005
240. Esteban DJ, Buller RML. Ectromelia virus: the causative agent of mousepox. *J Gen Virol*. (2005) 86:2645–59. doi: 10.1099/vir.0.81090-0
241. Ruiz-Argüello MB, Smith VP, Campanella GSV, Baleux F, Arenzana-Seisdedos F, Luster AD, et al. An ectromelia virus protein that interacts with chemokines through their glycosaminoglycan binding domain. *J Virol*. (2008) 82:917–26. doi: 10.1128/JVI.02111-07
242. Heidarieh H, Alcamí A. Mechanism of action of the viral chemokine-binding protein E163 from ectromelia virus. *J Biol Chem*. (2018) 293:17418–29. doi: 10.1074/jbc.RA118.004432
243. Upton C, Mossman K, McFadden G. Encoding of a homolog of the IFN-gamma receptor by myxoma virus. *Science*. (1992) 258:1369–72. doi: 10.1126/science.1455233
244. Mossman K, Upton C, McFadden G. The myxoma virus-soluble interferon-receptor homolog, M-T7, inhibits interferon- in a species-specific manner. *J Biol Chem*. (1995) 270:3031–8. doi: 10.1074/jbc.270.7.3031
245. Lalani AS, Graham K, Mossman K, Rajarathnam K, Clark-Lewis I, Kelvin D, et al. The purified myxoma virus gamma interferon receptor homolog M-T7 interacts with the heparin-binding domains of chemokines. *J Virol*. (1997) 71:4356–63. doi: 10.1128/JVI.71.6.4356-4363.1997
246. Lalani AS, McFadden G. Secreted poxvirus chemokine binding proteins. *J Leukoc Biol*. (1997) 62:570–6. doi: 10.1002/jlb.62.5.570
247. Seet BT, McCaughan CA, Handel TM, Mercer A, Brunetti C, McFadden G, et al. Analysis of an orf virus chemokine-binding protein: shifting ligand specificities among a family of poxvirus viroceptors. *Proc Natl Acad Sci USA*. (2003) 100:15137–42. doi: 10.1073/pnas.2336648100
248. Couñago RM, Knapp KM, Nakatani Y, Fleming SB, Corbett M, Wise LM, et al. Structures of orf virus chemokine binding protein in complex with host chemokines reveal clues to broad binding specificity. *Structure*. (2015) 23:1199–213. doi: 10.1016/j.str.2015.04.023
249. Bryant NA, Davis-Poynter N, Vanderplasschen A, Alcami A. Glycoprotein G isoforms from some alphaherpesviruses function as broad-spectrum chemokine binding proteins. *EMBO J*. (2003) 22:833–46. doi: 10.1093/emboj/cdg092
250. Parry CM, Simas JP, Smith VP, Stewart CA, Minson AC, Efstathiou S, et al. A broad spectrum secreted chemokine binding protein encoded by a herpesvirus. *J Exp Med*. (2000) 191:573–8. doi: 10.1084/jem.191.3.573
251. Webb LMC, Smith VP, Alcami A. The gammaherpesvirus chemokine binding protein can inhibit the interaction of chemokines with

glycosaminoglycans. *FASEB J*. (2004) 18:571–3. doi: 10.1096/fj.03-0485fje
252. van Berkel V, Barrett J, Tiffany HL, Fremont DH, Murphy PM, McFadden G, et al. Identification of a gammaherpesvirus selective chemokine binding protein that inhibits chemokine action. *J Virol*. (2000) 74:6741–7. doi: 10.1128/JVI.74.15.6741-6747.2000
253. Lubman OY, Cella M, Wang X, Monte K, Lenschow DJ, Huang YH, et al. Rodent herpesvirus peru encodes a secreted chemokine decoy receptor. *J Virol*. (2014) 88:538–46. doi: 10.1128/JVI.02729-13
254. Lubman OY, Fremont DH. Parallel evolution of chemokine binding by structurally related herpesvirus decoy receptors. *Structure*. (2016) 24:57–69. doi: 10.1016/j.str.2015.10.018
255. Déruaz M, Frauenschuh A, Alessandri AL, Dias JM, Coelho FM, Russo RC, et al. Ticks produce highly selective chemokine binding proteins with antiinflammatory activity. *J Exp Med*. (2008) 205:2019–31. doi: 10.1084/jem.20072689
256. Denisov SS, Ippel JH, Heinzmann ACA, Koenen RR, Ortega-Gomez A, Soehnlein O, et al. Tick saliva protein Evasin-3 modulates chemotaxis by disrupting CXCL8 interactions with glycosaminoglycans and CXCR2. *J Biol Chem*. (2019) 294:12370–9. doi: 10.1074/jbc.RA119.008902
257. Montecucco F, Lenglet S, Braunersreuther V, Pelli G, Pellieux C, Montessuit C, et al. Single administration of the CXC chemokine-binding protein evasin-3 during ischemia prevents myocardial reperfusion injury in mice. *Arterioscler Thromb Vasc Biol*. (2010) 30:1371–7. doi: 10.1161/ATVBAHA.110.206011
258. Copin JC, Da Silva RF, Fraga-Silva RA, Capettini L, Quintao S, Lenglet S, et al. Treatment with Evasin-3 reduces atherosclerotic vulnerability for ischemic stroke, but not brain injury in mice. *J Cereb Blood Flow Metab*. (2013) 33:490–8. doi: 10.1038/jcbfm.2012.198
259. Montecucco F, Mach F, Lenglet S, Vonlaufen A, Gomes Quinderé AL, Pelli G, et al. Treatment with Evasin-3 abrogates neutrophil-mediated inflammation in mouse acute pancreatitis. *Eur J Clin Invest*. (2014) 44:940–50. doi: 10.1111/eci.12327
260. Day AJ, Milner CM. TSG-6: a multifunctional protein with anti-inflammatory and tissue-protective properties. *Matrix Biol*. (2019) 78–79:60–83. doi: 10.1016/j.matbio.2018.01.011
261. Lee TH, Wisniewski HG, Vilcek J. A novel secretory tumor necrosis factor-inducible protein (TSG-6) is a member of the family of hyaluronate binding proteins, closely related to the adhesion receptor CD44. *J Cell Biol*. (1992) 116:545–57. doi: 10.1083/jcb.116.2.545
262. Dyer DP, Thomson JM, Hermant A, Jowitt TA, Handel TM, Proudfoot AEI, et al. TSG-6 inhibits neutrophil migration via direct interaction with the chemokine CXCL8. *J Immunol*. (2014) 192:2177–85. doi: 10.4049/jimmunol.1300194
263. Farber JM. HuMig: a new human member of the chemokine family of cytokines. *Biochem Biophys Res Commun*. (1993) 192:223–30. doi: 10.1006/bbrc.1993.1403
264. Boff D, Crijns H, Janssens R, Vanheule V, Menezes GB, Macari S, et al. The chemokine fragment CXCL9(74–103) diminishes neutrophil recruitment and joint inflammation in antigen-induced arthritis. *J Leukoc Biol*. (2018) 104:413–22. doi: 10.1002/JLB.3MA1217-502R
265. Vanheule V, Crijns H, Poosti F, Ruytinx P, Berghmans N, Gerlza T, et al. Anti-inflammatory effects of the GAG-binding CXCL9(74-103) peptide in dinitrofluorobenzene-induced contact hypersensitivity in mice. *Clin Exp Allergy*. (2018) 48:1333–44. doi: 10.1111/cea.13227
266. Adage T, Piccinini AM, Falsone A, Trinker M, Robinson J, Gesslbauer B, et al. Structure-based design of decoy chemokines as a way to explore the pharmacological potential of glycosaminoglycans. *Br J Pharmacol*. (2012) 167:1195–205. doi: 10.1111/j.1476-5381.2012.02089.x
267. Trinker MU, Kungl AJ. Targeting chemokine-glycan interactions: the celljammer® technology platform. *Drug Discov Today Technol*. (2012) 9:253–9. doi: 10.1016/j.ddtec.2012.07.005
268. Potzinger H, Geretti E, Brandner B, Wabitsch V, Piccinini AM, Rek A, et al. Developing chemokine mutants with improved proteoglycan affinity and knocked-out GPCR activity as anti-inflammatory recombinant drugs. *Biochem Soc Trans*. (2006) 34:435–7. doi: 10.1042/BST0340435
269. Falsone A, Wabitsch V, Geretti E, Potzinger H, Gerlza T, Robinson J, et al. Designing CXCL8-based decoy proteins with strong anti-inflammatory activity *in vivo*. *Biosci Rep*. (2013) 33:743–54. doi: 10.1042/BSR20130069
270. Gerlza T, Hecher B, Jeremic D, Fuchs T, Gschwandtner M, Falsone A, et al. A combinatorial approach to biophysically characterise chemokine-glycan binding affinities for drug development. *Molecules*. (2014) 19:10618–34. doi: 10.3390/molecules190710618
271. Bedke J, Nelson PJ, Kiss E, Muenchmeier N, Rek A, Behnes CL, et al. A novel CXCL8 protein-based antagonist in acute experimental renal allograft damage. *Mol Immunol*. (2010) 47:1047–57. doi: 10.1016/j.molimm.2009.11.012
272. Rek A, Krenn E, Kungl AJ. Therapeutically targeting protein-glycan interactions. *Br J Pharmacol*. (2009) 157:686–94. doi: 10.1111/j.1476-5381.2009.00226.x
273. Gschwandtner M, Strutzmann E, Teixeira MM, Anders HJ, Diedrichs-Möhring M, Gerlza T, et al. Glycosaminoglycans are important mediators of neutrophilic inflammation *in vivo*. *Cytokine*. (2017) 91:65–73. doi: 10.1016/j.cyto.2016.12.008
274. McElvaney OJ, O'Reilly N, White M, Lacey N, Pohl K, Gerlza T, et al. The effect of the decoy molecule PA401 on CXCL8 levels in bronchoalveolar lavage fluid of patients with cystic fibrosis. *Mol Immunol*. (2015) 63:550–8. doi: 10.1016/j.molimm.2014.10.013
275. Adage T, del Bene F, Fiorentini F, Doornbos RP, Zankl C, Bartley MR, et al. PA401, a novel CXCL8-based biologic therapeutic with increased glycosaminoglycan binding, reduces bronchoalveolar lavage neutrophils and systemic inflammatory markers in a murine model of LPS-induced lung inflammation. *Cytokine*. (2015) 76:433–41. doi: 10.1016/j.cyto.2015.08.006
276. Piccinini AM, Knebl K, Rek A, Wildner G, Diedrichs-Möhring M, Kungl AJ. Rationally evolving MCP-1/CCL2 into a decoy protein with potent anti-inflammatory activity *in vivo*. *J Biol Chem*. (2010) 285:8782–92. doi: 10.1074/jbc.M109.043299
277. Liehn EA, Piccinini AM, Koenen RR, Soehnlein O, Adage T, Fatu R, et al. A new monocyte chemotactic protein-1/chemokine cc motif ligand-2 competitor limiting neointima formation and myocardial ischemia/reperfusion injury in mice. *J Am Coll Cardiol*. (2010) 56:1847–57. doi: 10.1016/j.jacc.2010.04.066
278. Gschwandtner M, Piccinini AM, Gerlza T, Adage T, Kungl AJ. Interfering with the CCL2-glycosaminoglycan axis as a potential approach to modulate neuroinflammation. *Neurosci Lett*. (2016) 626:164–73. doi: 10.1016/j.neulet.2016.05.037
279. Gerlza T, Winkler S, Atlic A, Zankl C, Konya V, Kitic N, et al. Designing a mutant CCL2-HSA chimera with high glycosaminoglycan-binding affinity and selectivity. *Protein Eng Des Sel*. (2015) 28:231–40. doi: 10.1093/protein/gzv025
280. Brandner B, Rek A, Diedrichs-Möhring M, Wildner G, Kungl AJ. Engineering the glycosaminoglycan-binding affinity, kinetics and oligomerization behavior of RANTES: a tool for generating chemokine-based glycosaminoglycan antagonists. *Protein Eng Des Sel*. (2009) 22:367–73. doi: 10.1093/protein/gzp013
281. Gschwandtner M, Trinker MU, Hecher B, Adage T, Ali S, Kungl AJ. Glycosaminoglycan silencing by engineered CXCL12 variants. *FEBS Lett*. (2015) 589:2819–24. doi: 10.1016/j.febslet.2015.07.052
282. Klußmann S, Nolte A, Bald R, Erdmann VA, Fürste JP. Mirror-image RNA that binds D-adenosine. *Nat Biotechnol*. (1996) 14:1112–5. doi: 10.1038/nbt0996-1112
283. Vater A, Klussmann S. Turning mirror-image oligonucleotides into drugs: the evolution of spiegelmer(®) therapeutics. *Drug Discov Today*. (2015) 20:147–55. doi: 10.1016/j.drudis.2014.09.004
284. Eulberg D, Klussmann S. Spiegelmers: biostable aptamers. *ChemBioChem*. (2003) 4:979–83. doi: 10.1002/cbic.200300663
285. Zhou J, Rossi J. Aptamers as targeted therapeutics: current potential and challenges. *Nat Rev Drug Discov*. (2017) 16:181–202. doi: 10.1038/nrd.2016.199
286. Keefe AD, Pai S, Ellington A. Aptamers as therapeutics. *Nat Rev Drug Discov*. (2010) 9:537–50. doi: 10.1038/nrd3141
287. Sayyed SG, Hägele H, Kulkarni OP, Endlich K, Segerer S, Eulberg D, et al. Podocytes produce homeostatic chemokine stromal cell-derived factor-1/CXCL12, which contributes to glomerulosclerosis, podocyte loss and

albuminuria in a mouse model of type 2 diabetes. *Diabetologia*. (2009) 52:2445–54. doi: 10.1007/s00125-009-1493-6
288. Bleul CC, Fuhlbrigge RC, Casasnovas JM, Aiuti A, Springer TA. A highly efficacious lymphocyte chemoattractant, stromal cell-derived factor 1 (SDF-1). *J Exp Med*. (1996) 184:1101–9. doi: 10.1084/jem.184.3.1101
289. Vater A, Sahlmann J, Kröger N, Zöllner S, Lioznov M, Maasch C, et al. Hematopoietic stem and progenitor cell mobilization in mice and humans by a first-in-class mirror-image oligonucleotide inhibitor of CXCL12. *Clin Pharmacol Ther*. (2013) 94:150–7. doi: 10.1038/clpt.2013.58
290. Kulkarni O, Pawar RD, Purschke W, Eulberg D, Selve N, Buchner K, et al. Spiegelmer inhibition of CCL2/MCP-1 ameliorates lupus nephritis in MRL-(Fas)lpr mice. *J Am Soc Nephrol*. (2007) 18:2350–8. doi: 10.1681/ASN.2006121348
291. Devarapu SK, Kumar VR S, Rupanagudi KV, Kulkarni OP, Eulberg D, Klussmann S, et al. Reprint of "Dual blockade of the pro-inflammatory chemokine CCL2 and the homeostatic chemokine CXCL12 is as effective as high dose cyclophosphamide in murine proliferative lupus nephritis." *Clin Immunol*. (2017) 185:119–27. doi: 10.1016/j.clim.2017.10.011
292. Romoli S, Angelotti ML, Antonelli G, Kumar VR S, Mulay SR, Desai J, et al. CXCL12 blockade preferentially regenerates lost podocytes in cortical nephrons by targeting an intrinsic podocyte-progenitor feedback mechanism. *Kidney Int*. (2018) 94:1111–26. doi: 10.1016/j.kint.2018.08.013
293. Darisipudi MN, Kulkarni OP, Sayyed SG, Ryu M, Migliorini A, Sagrinati C, et al. Dual blockade of the homeostatic chemokine CXCL12 and the proinflammatory chemokine CCL2 has additive protective effects on diabetic kidney disease. *Am J Pathol*. (2011) 179:116–24. doi: 10.1016/j.ajpath.2011.03.004
294. Citro A, Pellegrini S, Dugnani E, Eulberg D, Klussmann S, Piemonti L. CCL2/MCP-1 and CXCL12/ SDF-1 blockade by L-aptamers improve pancreatic islet engraftment and survival in mouse. *Am J Transplant*. (2019) 19:3131–8. doi: 10.1111/ajt.15518
295. Steurer M, Montillo M, Scarfò L, Mauro FR, Andel J, Wildner S, et al. Olaptesed pegol (NOX-A12) with bendamustine and rituximab: a phase IIa study in patients with relapsed/refractory chronic lymphocytic leukemia. *Haematologica*. (2019) 104:2053–60. doi: 10.3324/haematol.2018.205930
296. Weisberg EL, Sattler M, Azab AK, Eulberg D, Kruschinski A, Manley PW, et al. Inhibition of SDF-1-induced migration of oncogene-driven myeloid leukemia by the L-RNA aptamer (spiegelmer), NOX-A12, and potentiation of tyrosine kinase inhibition. *Oncotarget*. (2017) 8:109973–84. doi: 10.18632/oncotarget.22409
297. Roccaro AM, Sacco A, Purschke WG, Moschetta M, Buchner K, Maasch C, et al. SDF-1 inhibition targets the bone marrow niche for cancer therapy. *Cell Rep*. (2014) 9:118–28. doi: 10.1016/j.celrep.2014.08.042
298. Ludwig H, Weisel K, Petrucci MT, Leleu X, Cafro AM, Garderet L, et al. Olaptesed pegol, an anti-CXCL12/SDF-1 spiegelmer, alone and with bortezomib-dexamethasone in relapsed/refractory multiple myeloma: a phase IIa study. *Leukemia*. (2017) 31:997–1000. doi: 10.1038/leu.2017.5
299. Waldschmidt JM, Simon A, Wider D, Müller SJ, Follo M, Ihorst G, et al. CXCL12 and CXCR7 are relevant targets to reverse cell adhesion-mediated drug resistance in multiple myeloma. *Br J Haematol*. (2017) 179:36–49. doi: 10.1111/bjh.14807
300. Liu SC, Alomran R, Chernikova SB, Lartey F, Stafford J, Jang T, et al. Blockade of SDF-1 after irradiation inhibits tumor recurrences of autochthonous brain tumors in rats. *Neuro Oncol*. (2014) 16:21–8. doi: 10.1093/neuonc/not149
301. Deng L, Stafford JH, Liu SC, Chernikova SB, Merchant M, Recht L, et al. SDF-1 blockade enhances anti-VEGF therapy of glioblastoma and can be monitored by MRI. *Neoplasia*. (2017) 19:1–7. doi: 10.1016/j.neo.2016.11.010
302. Zboralski D, Hoehlig K, Eulberg D, Frömming A, Vater A. Increasing tumor-infiltrating T cells through inhibition of CXCL12 with NOX-A12 synergizes with PD-1 blockade. *Cancer Immunol Res*. (2017) 5:950–6. doi: 10.1158/2326-6066.CIR-16-0303
303. Savai R, Pullamsetti SS, Kolbe J, Bieniek E, Voswinckel R, Fink L, et al. Immune and inflammatory cell involvement in the pathology of idiopathic pulmonary arterial hypertension. *Am J Respir Crit Care Med*. (2012) 186:897–908. doi: 10.1164/rccm.201202-0335OC
304. Thomas MN, Kalnins A, Andrassy M, Wagner A, Klussmann S, Rentsch M, et al. SDF-1/CXCR4/CXCR7 is pivotal for vascular smooth muscle cell proliferation and chronic allograft vasculopathy. *Transpl Int*. (2015) 28:1426–35. doi: 10.1111/tri.12651
305. Enzmann V, Lecaudé S, Kruschinski A, Vater A. CXCL12/SDF-1-dependent retinal migration of endogenous bone marrow-derived stem cells improves visual function after pharmacologically induced retinal degeneration. *Stem Cell Rev Rep*. (2017) 13:278–86. doi: 10.1007/s12015-016-9706-0

Conflict of Interest: The authors declare that the research was conducted in the absence of any commercial or financial relationships that could be construed as a potential conflict of interest.

frontiers in Immunology

PERSPECTIVE
published: 03 April 2020
doi: 10.3389/fimmu.2020.00570

HS and Inflammation: A Potential Playground for the Sulfs?

*Rana El Masri, Yoann Crétinon, Evelyne Gout and Romain R. Vivès**

Université Grenoble Alpes, CNRS, CEA, Institut de Biologie Structurale (IBS), Grenoble, France

Heparan sulfate (HS) is a complex polysaccharide abundantly found in extracellular matrices and cell surfaces. HS participates in major cellular processes, through its ability to bind and modulate a wide array of signaling proteins. HS/ligand interactions involve saccharide domains of specific sulfation pattern. Assembly of such domains is orchestrated by a complex biosynthesis machinery and their structure is further regulated at the cell surface by post-synthetic modifying enzymes. Amongst them, extracellular sulfatases of the Sulf family catalyze the selective removal of 6-*O*-sulfate groups, which participate in the binding of many proteins. As such, increasing interest arose on the regulation of HS biological properties by the Sulfs. However, studies of the Sulfs have so far been essentially restricted to the fields of development and tumor progression. The aim of this review is to survey recent data of the literature on the still poorly documented role of the Sulfs during inflammation, and to widen the perspectives for the study of this intriguing regulatory mechanism toward new physiopathological processes.

Keywords: heparan sulfate (HS), inflammation, glycosaminoglycan/protein interactions, sulfatase, chemokine, leukocyte migration

OPEN ACCESS

Edited by:
Rogier M. Reijmers, Leiden University Medical Center, Netherlands

Reviewed by:
Kenji Uchimura, UMR8576 Unité de Glycobiologie Structurale et Fonctionnelle, France
Mark Michael Fuster, University of California, San Diego, United States
Steven David Rosen, University of California, San Francisco, United States

****Correspondence:***
Romain R. Vivès
romain.vives@ibs.fr

Specialty section:
This article was submitted to Inflammation, a section of the journal Frontiers in Immunology

Received: *04 December 2019*
Accepted: *12 March 2020*
Published: *03 April 2020*

Citation:
El Masri R, Crétinon Y, Gout E and Vivès RR (2020) HS and Inflammation: A Potential Playground for the Sulfs? Front. Immunol. 11:570. doi: 10.3389/fimmu.2020.00570

INTRODUCTION

Heparan sulfate proteoglycans (HSPGs) are major components of the cell surface, extracellular matrix (ECM) and basement membrane in most animal cells. They are composed of a protein core, onto which are covalently attached complex, anionic Heparan Sulfate (HS) chains of the glycosaminoglycan (GAG) polysaccharide family. Through the ability of their HS chains to bind, modulate and control bioavailability of a multitude of protein ligands, HSPGs are involved in a plethora of biological processes, including cell adhesion, migration, proliferation and differentiation, embryo development, inflammation, control of angiogenesis, blood coagulation, tumor growth, and metastasis (1–3). Structurally, a HS chain is characterized by the linear repetition of a disaccharide unit, composed of alternating N-acetyl glucosamine (GlcNAc) and glucuronic acid (GlcA). During biosynthesis, the polymer undergoes a series of modifications, which include the *N*-deacetylation/*N*-sulfation of glucosamine to form N-sulfo glucosamine (GlcNS), the C5 epimerization of GlcA into iduronic acid (IdoA), and *O*-sulfations at positions C2 of IdoA and C6 (more rarely C3) of glucosamine residues. Tight regulation of these modification steps leads to the generation of specialized saccharide regions termed S-domains, exhibiting both remarkable structural diversity and high sulfation content. These S-domains are involved in the recognition and binding of most HS ligands (4–6). HS is structurally closely related to heparin, although the latter displays a much higher sulfation content. Therefore, heparin has been widely used as a surrogate of HS S-domains for protein interaction studies.

HS IN INFLAMMATION

Inflammation is a complex, multi-step process leading to the rapid recruitment of leukocytes from the blood to the inflammation site. Briefly, emission of an inflammatory signal triggers the secretion of cytokines and chemokines that diffuse throughout the tissue and activate leukocytes and vascular endothelial cells. Cell activation leads to the adhesion and rolling of leukocytes on the endothelium toward the inflammatory site. Leukocytes will then cross the endothelium to the basement membrane, and migrate toward the inflamed tissue to initiate immune responses. Through its large protein binding properties, HS participates in various steps of inflammation [for review, see (7, 8)].

Inflammation is first initiated by the production, upon endogenous or exogenous signals, of inflammatory cytokines. Amongst these, chemokines are a family of small proteins involved in many biological processes such as development, inflammation and immunosurveillance (9). Chemokines induce the activation of the endothelium and the migration of leukocytes from blood toward inflammatory sites. To elicit their functions, they bind to their primary G-coupled receptors that trigger downstream signaling. In addition, all chemokines bind to cell surface and ECM HS. The structural basis of these interactions has been intensively studied and is now well documented (10–12).

Functionally, HS does not seem to be essential for chemokine signaling *in vitro*. However, *in vivo* studies showed that chemokines unable to bind to HS failed to recruit leukocytes (13), and that HS modulated chemokine activity through different mechanisms [for review, see (12, 14)]. HS first regulates chemokine diffusion and sequestration. In some instance, the capture of the chemokine/cytokine by HS prevents its release and thus its activity (15). However, by regulating chemokine diffusion, HS participates in the formation and stabilization of chemotactic gradients providing directional cues for migrating leukocytes. In support to this, *in vivo* inhibition of CXCL12/HS interaction using sulfated polysaccharide tilted the chemokine distribution from bone marrow toward the plasma, thereby causing the release of hematopoietic progenitor cells in the blood circulation (16). HS also mediates chemokine transcytosis across the endothelial cell wall (17, 18), and protects chemokines/cytokines from enzymatic degradation and inactivation (19–21). Finally, HS may further modulate chemokine activity by inducing chemokine oligomerization [for review, see (11)], which has been shown to be functionally relevant *in vivo* (13). In that context, an original HS-dependent cooperative mechanism driving CCL5 dimerization has been characterized (22).

Activation by pro-inflammatory chemokines and cytokines induces the expression of endothelial C-type lectins E- and P-selectins. These bind a variety of glycosylated ligands present on the leukocyte cell surface to initiate adhesion and rolling of leukocytes on the endothelium. Recruitment is further promoted through additional interactions, involving L-selectin constitutively expressed on leukocytes with leukocyte and endothelial ligands (23, 24). HS may participate to this process, as studies reported binding to L-selectin (24, 25), P-selectin (26), and E-selectin (27, 28). However, it should be noted that the physiological relevance of these interactions remains to be clarified. Studies showed that the removal of cell surface HS with heparinases reduced L-selectin dependent binding of monocytes, and leukocyte rolling on endothelial cells (29, 30). During acute inflammation, HS was shown to support L-selectin dependent rolling of neutrophils on lung microvasculature (31). On the contrary, lymphocyte rolling on high endothelial venules (HEV) exclusively relied on interactions of L-selectin with ligands bearing sialyl Lewis X (sLe^x) glycosylation motifs, suggesting no involvement of HS in L-selectin-dependent lymphocyte homing (32). One could speculate that these discrepancies could be due to the presence of distinct HS structures and/or sLe^x ligands on these different cell types.

Leukocyte rolling is then arrested through increased integrin-mediated cell-cell adhesion. In a recent study, it has been proposed that endothelial cell surface HS could participate indirectly to this process, by capturing and presenting CCL21, which would in turn activate integrin LFA-1 on rolling lymphocytes (32). Following arrest, leukocytes get access to inflamed tissues through extravasation across the endothelial cell wall. They then reach the basement membrane that comprises numerous interacting molecules and a variety of HSPGs, including perlecan, agrin and XVIII collagen, which may further modulate the extravasation process. These HSPGs can bind many chemokines, cytokines and growth factors that are critical for leukocyte migration, and contribute to the formation of chemokine gradients. On the contrary, they can act as a physical barrier hindering leukocyte migration.

Finally, studies have also suggested a role of HS in the phagocytosis process (33, 34). A proposed mechanism is that newly-exposed HS binding sites at the surface of apoptotic cells could facilitate their recognition, uptake and clearance by macrophages (35). However, *in vivo* data are still needed to clarify this process.

Most of these inflammatory steps are generally accompanied by changes in the expression of their cell-surface HPSGs and HS structure. Many studies have reported an upregulation of cell-surface HSPG Syndecan-1 upon endothelial cell activation by pro-inflammatory cytokines [reviewed in (25)]. Differentiation of monocytes into macrophages leads to high expression of Syndecan-1, -2 and -4, whereas macrophage activation by Interleukin (IL)-1 results in the overexpression of Syndecan-2 only (36). Furthermore, the activation of T cells induces the expression of Syndecans and Glypicans, while the differentiation of B cells into plasma cells specifically triggers Syndecan-1 expression (37, 38). Depending on the inflammatory *stimuli*, HS length, structure and sulfation profiles may also be affected. For instance, the size and 6-*O*-sulfation patterns of HS are altered in primary human endothelial cells upon treatment with tumor necrosis factor (TNFα) or IL-1 (39). Pro-inflammatory effectors have been shown to modulate the expression of NDSTs (40–42). In particular induction of NDST1 led to the production of highly sulfated HS that increased the sequestration of CCL5, thereby promoting leukocyte extravasation (42). Vascular lesions in mice have also been associated with a significant increase

of NDST1 expression (43). In line with this, inactivation of NDSTs in endothelial cells led to impaired rolling and infiltration of neutrophils and macrophages into inflammatory sites (31, 44). In contrast, restricted inactivation of NDSTs to leukocytes had no effect on leukocyte infiltration (31). Changes in HS *O*-sulfotransferases (OSTs) expression have also been reported, during macrophage M1/M2 polarization (45), or the development of renal fibrosis (46). Interestingly, the stimulation of human monocytes by LPS or TNFα upregulates only one out of the seven 3OST isoform: 3OST3b, thus highlighting the fine tuning of sulfotransferase expression pattern during inflammation (47). Finally, the silencing of 2OST in mouse endothelial cells during acute inflammation resulted in enhanced HS 6-*O*- and *N*-sulfation, leading to increased neutrophil infiltration (48).

POST-EDITING MECHANISMS REGULATING HS DISTRIBUTION, STRUCTURE AND FUNCTION

Although HS expression and structure is primarily controlled during polysaccharide biosynthesis, increasing evidence have also highlighted the importance of the additional regulatory step provided by post-editing enzymes, including Heparanase, sheddases, and sulfatases of the Sulfs family.

In inflammatory processes, post-synthesis regulation of HS plays a significant role. Heparanase is an endo-β-D-glucuronidase targeting [GlcA-GlcNS] linkages within HS. Heparanase cleaves long HS chains from ECM and cell-surface HSPGs into shorter fragments of 10–20 sugar units. This results in the release of sequestered HS bound ligands, such as growth factors, chemokines and morphogens, which can then induce angiogenesis, cell proliferation and motility (49). Consequently, Heparanase has been associated with various pathologies, including cancer, inflammation, thrombosis, atherosclerosis, fibrosis, diabetes, and kidney disease (50). During inflammation, Heparanase plays multiple roles. It favors neutrophil adhesion onto the endothelium, by degrading endothelial cell-surface HS and unmasking membrane adhesion molecules (51). It also facilitates leukocyte extravasation, by degrading basement membrane HSPGs (52). More recently, Heparanase has been shown to enhance T-cell activity (53). Furthermore, intracellular heparanase upregulated the transcription of genes involved in T-cell differentiation (54). Finally and noteworthy, Heparanase expression is also markedly increased during neuroinflammation (55).

Shedding of HSPGs takes place upon activation of metalloproteinases, plasmins and elatases by inflammatory cytokines (56–59). These proteases target the core protein of HSPGs like Syndecans, thus releasing soluble HS-peptide conjugates. Shedding regulates the amount of HSPGs found at the cell surface or in the ECM and facilitate the release of sequestered chemokines, which contributes to the resolution of neutrophilic inflammation (58, 60). In combination with Heparanase, shedding also facilitate leukocyte migration by altering the architecture of the ECM and basement membranes (52).

In addition, soluble released HS fragments/conjugates (produced by sheddases or Heparanase) induce the secretion by macrophages and splenocytes of pro-inflammatory cytokines through activation of the NF-κB signaling pathway (61–63). Soluble HS fragments also activate neutrophils and promote an immune response via toll like receptor-4 (64, 65). They can also trigger the maturation of dendritic cells, leading to their migration toward lymphoid organs to elicit primary immune responses (66). In line with this, it was shown that an exogenous administration of HS or elastase resulted in a systemic inflammatory response syndrome (SIRS)-like reaction (67).

THE SULFS: POST-SYNTHETIC REGULATORS OF HS STRUCTURE AND FUNCTION

Sulfs are extracellular endosulfatases that catalyze the 6-*O*-desulfation of HS. Sulf-1 was first discovered in Quail (68), then orthologs were later identified in mouse, rat, chick, *C. elegans*, zebrafish, and human, as well as a second related enzyme, Sulf-2 (69). In human, HSulf-1 and HSulf-2 (encoded by two distinct genes) feature a common structural organization (69). Maturation of the sulfs involves furin-type processing of pro-enzyme proteins, yielding two sub-units linked by one or more disulfide bonds (see **Figure 1** inset). The N-terminal regions features the enzyme catalytic (CAT) domain, which shows strong homology with most eukaryotic sulfatases. The CAT domain comprises the enzyme active site, including the two conserved sulfatase signature amino acid sequences as well as the cysteine modified, catalytic FGly residue. The second functional domain of the Sulfs is the highly charged basic domain (HD), which spans over both N-terminal and C-terminal sub-units. The HD domain is a unique feature of the Sulfs, as it shares no homology with any other known protein. It is responsible for high affinity binding to HS substrate and is therefore required for the enzyme endo-6-*O*-sulfatase activity (70–73). In addition, the HD domain has been shown to mediate the capture of Sulfs on cell-surface HS thereby modulating enzyme diffusion (71). Finally, Sulf C-terminal region shows homology to Glucosamine-6-sulfatase (G6S) and *Arabidopsis thaliana* GlcNAc transferase, suggesting a role of this domain in the recognition of glucosamine motifs (69).

Sulfs catalyze the 6-*O*-desulfation of HS with a strong preference for [Glc/IdoA(2S)-GlcNS(6S)] trisulfated disaccharides that are essentially found within S-domains. Although abundant in heparin, this disaccharide motif is relatively scarce in HS. Sulf-induced modification of HS structure is therefore structurally subtle, but with great functional consequences, as 6-*O*-sulfation pattern of HS S-domains is critical for the binding of many signaling proteins (74). Sulfs are therefore implicated in a number of physiological and pathological processes, including development, tissue repair, neurodegenerative disease and cancer [for reviews, see (75–77)].

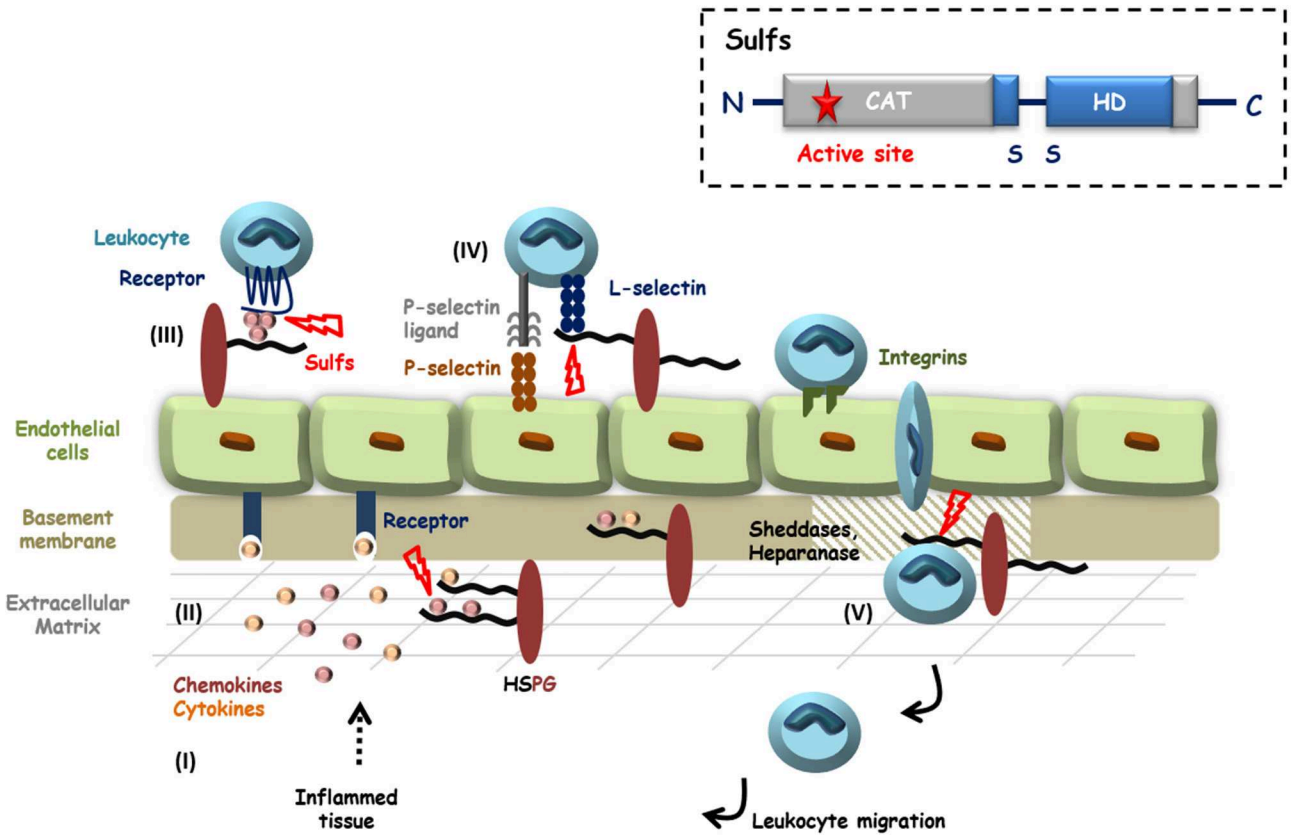

FIGURE 1 | HS in inflammation and potential roles of the Sulfs. Inflammatory *stimuli* induce the secretion of cytokines and chemokines (I) that activate endothelial cells and blood circulating leukocytes. HS controls the diffusion of these pro-inflammatory proteins, their oligomerization and the establishment of chemotactic gradients (II and III). Activated Leukocytes then adhere and roll over endothelial cells, through interactions of E- and P-selectins with their counter ligands. L-selectin tightens cell-contacts by binding to sLe^X decorated glycoproteins and HSPGs (IV). After passage through the endothelial layer, efficient migration of leukocytes toward inflammatory sites requires the degradation of basement membrane HSPGs by proteases and Heparanase (V). HS is thus largely involved during inflammation and HS 6-*O*-sulfation is critical for most of these interactions. Although still poorly investigated, Sulfs could therefore play different roles during inflammation. In the figure, steps during which Sulfs could be implicated are highlighted with red bolts. Inset: schematic representation of Sulf structural organization.

DISCUSSION: POTENTIAL ROLES OF THE SULFS DURING INFLAMMATION

Over the recent years, Sulfs have emerged as critical regulators of HS functions, with well documented roles during development and cancer. However and despite growing evidence, Sulfs have remained largely unstudied in the context of inflammation (see **Figure 1**).

It is first well established that HS 6-*O*-sulfation is a major structural determinant for the interaction with many chemokines, including CXCL12 (78–80), CXCL8 (81, 82), CXCL4 (83, 84) and CCL5 (85). For the latter, the resolution of the CCL5 crystal structure in complex with heparin provided further evidence of the contribution of 6-*O*-S group in the interaction (85). Furthermore, HS mimetic glycopolymers featuring [IdoA(2S), GlcNS(6S)] disaccharides efficiently inhibited CCL5/heparin interaction (86). In this context, it is therefore most likely that Sulfs would significantly affect HS binding properties toward many of these chemokines, with consequences on chemokine oligomerization, storage, bioavailability and diffusion. Interestingly, a recent study investigating chemokine inhibition using synthetic sulfated $[IdoA(2S), GlcNS(\pm 6S)]_6$ dodecasaccharides showed that the presence of a 6-*O*-sulfate group on the non-reducing end residue switched saccharide binding properties from CXCL8 toward CXCL12 (87). In light of this, it was also recently reported that HSulfs catalyzed the 6-*O*-desulfation of HS following a processive and orientated mechanism, starting from S-domain non-reducing end (88). Together, these data thus suggest that Sulfs could tune HS binding selectivity for chemokines. Despite these findings and most surprisingly, the effect of Sulfs on HS/chemokine interaction has so far only been investigated in one study, which showed the inhibition of CXCL12-α binding to heparin by the Sulfs in an *in vitro* immunoassay (79).

Studies have reported that the 6-*O*-sulfation of endothelial HS was critical for leukocyte rolling (89), and that 6-*O*-sulfation of heparin was necessary to block L-selectin mediated leukocyte adhesion (80, 90). Sulfs could thus be involved in the

control of leukocyte adhesion and migration on the activated endothelium. Vascular glycocalyx and especially endothelial HS undergo significant degradation during inflammation (91). A role of the Sulfs in these mechanisms could thus be postulated, as suggested by a first study on post-septic mice. Sepsis is associated with a hyper-inflammatory process, followed by a delayed period of immunosuppression called compensatory anti-inflammatory response syndrome (CARS), which can lead to secondary infections. This study showed that HS of lung endothelial glycocalyx displayed higher 6-*O*-sulfation content after septic injury, which was due to a downregulation of Sulf-1. Interestingly, the post-septic loss of Sulf-1 was necessary for CARS to occur, as the administration of exogenous recombinant Sulf-1 intravenously reversed the immunosuppression phenotype (92). In the same context, Sulfs could also participate in the degradation of the basement membrane, along with Heparanase and proteases to facilitate leukocyte migration toward inflammatory sites. Although there is no evidence of such an involvement yet, a study preceding the discovery of the Sulfs showed that activation of endothelial cells with pro-inflammatory cytokines led to the detection of a sulfatase activity, which was required for the degradation of the basement membrane (52).

Changes in the expression of the Sulfs upon inflammatory conditions have been reported. An *in vivo* study on renal allograft biopsies showed that Sulf-1 expression was repressed in inflammatory conditions (93). In contrast, HSulf-1 was up-regulated in human fibroblasts upon TNF-α treatment (94). Likewise, TGF-β1 induced the expression of Sulf-2 in renal epithelial cells (95), and of both Sulf-1 and Sulf-2 in lung fibroblasts (96). In line with this, Sulf-2 was overexpressed in idiopathic pulmonary fibrosis (97) and would act as a regulator, in a negative feedback loop, of TGF-β1 signaling in type 2 alveolar epithelial cells (96, 97). Furthermore, it was shown that Sulf-2 expression in type II alveolar epithelial cells played a protective role in epithelial lung injury, inflammation and mortality (98). Surprisingly, Sulf-2 overexpression in human hepatocellular carcinoma cells promoted TGF-β1 signaling (99). Altogether, these data clearly underline the complex interplay between Sulf activities and TGF-β1 signaling.

One still intriguing and yet poorly understood issue about the Sulfs is that the two human forms, HSulf-1 and HSulf-2, feature very similar enzyme activities *in vitro*, but show clear functional discrepancies *in vivo*. As such, a study on Sulf KO mice indicated that both forms exhibit redundant or overlapping functions during development (100, 101), while accumulating data describe opposite activities in cancer (75, 76). Furthermore, it has been reported that alternative splicing of *Sulf1/Sulf2* genes generated functionally active variants. In Quail, a QSulf-1 variant (QSulf-1B) encoding for a shorter protein form exhibited opposite activities to full length QSulf-1, QSulf-1B inhibiting Wnt signaling and promoting angiogenesis (102). Mammalian variants of Sulf1 and Sulf2 were later identified in tumors (103, 104). The occurrence and biological significance of Sulf variants are still poorly understood. However, some of these variants have been shown to regulate growth factor signaling pathways and to display anti-oncogenic and anti-angiogenic properties (105). Noteworthy, the expression of Sulf-1 and Sulf-2 variants was also reported in the context of inflammation (105). Studying the spatial and temporal expression and activity of the two Sulf forms as well as their respective splice variants may therefore be critical to fully understand the role of these enzymes in a given biological process such as inflammation.

Finally, another interesting observation arose from our recent article reporting the expression and purification of recombinant HSulf-2 (73). In this work, we showed that the protein HD domain was very sensitive to proteolytic digestion. This observation is in agreement with secondary structure predictions based on amino-acid sequence, which suggests the presence of large unstructured regions within the HD domain. Most surprisingly, we found that these degraded forms of HSulf-2 displayed endosulfatase activity. This is in agreement with a previous study, which demonstrated that deletion of the inner region of HSulf-1 HD domain did not abrogate enzyme activity (71). However, partial degradation of the HD domain may significantly affect HS substrate selectivity and/or the HD-dependent immobilization of Sulfs on cell-surface HS (71). It could thus be hypothesized that, under inflammatory conditions, protease-driven processing of the HD could affect both Sulf biological activity and diffusion throughout tissues.

In conclusion, the structural and functional regulation of HS by the Sulfs is undeniably a significant topic of interest, which merits further investigation in the context of inflammation. Evidence of Sulf involvement in inflammatory processes and in the modulation of pro-inflammatory effectors are slowly arising, but progress in the field has been hampered by the complexity of these enzymes, which markedly distinguishes them from other eukaryotic sulfatases. Nevertheless, recent access to purified recombinant protein solved a critical technical bottleneck, which should boost progress in their study. In this context, we reported for the first time the intravenous injection of recombinant enzyme *in vivo* to analyze an inflammatory process (92), and we anticipate that this study will pave the way to further investigations in this field.

AUTHOR CONTRIBUTIONS

All authors listed have made a substantial, direct and intellectual contribution to the work, and approved it for publication.

FUNDING

The authors would like to acknowledge the support of Grenoble Instruct centre (ISBG; UMS 3518 CNRS-CEA-UJF-EMBL) with support from FRISBI (ANR-10-INSB-05-02) and GRAL (ANR-10-LABX-49-01) within the Grenoble Partnership for Structural Biology (PSB), of the GDR GAG (GDR 3739) and the Investissements d'avenir program Glyco@Alps (ANR-15-IDEX-02), and of grants from the Agence Nationale de la Recherche (ANR-12-BSV8-0023 and ANR-17-CE11-0040) and Université Grenoble-Alpes (UGA AGIR program).

ACKNOWLEDGMENTS

The authors would like to thank Professor John Gallagher for his diligent proofreading of the manuscript.

REFERENCES

1. Sarrazin S, Lamanna WC, Esko JD. Heparan sulfate proteoglycans. *Cold Spring Harb Perspect Biol.* (2011) 3:4952. doi: 10.1101/cshperspect.a004952
2. Iozzo RV, Schaefer L. Proteoglycan form and function: a comprehensive nomenclature of proteoglycans. *Matrix Biol.* (2015) 42:11–55. doi: 10.1016/j.matbio.2015.02.003
3. Kjellén L, Lindahl U. Specificity of glycosaminoglycan-protein interactions. *Curr Opin Struct Biol.* (2018) 50:101–8. doi: 10.1016/j.sbi.2017.12.011
4. Li J-P, Kusche-Gullberg M. Heparan sulfate: biosynthesis, structure, and function. *Int Rev Cell Mol Biol.* (2016) 325:215–73. doi: 10.1016/bs.ircmb.2016.02.009
5. Gallagher J. Fell-Muir lecture: heparan sulphate and the art of cell regulation: a polymer chain conducts the protein orchestra. *Int J Exp Pathol.* (2015) 96:203–31. doi: 10.1111/iep.12135
6. Lindahl U, Li JP. Interactions between heparan sulfate and proteins-design and functional implications. *Int Rev Cell Mol Biol.* (2009) 276:105–59. doi: 10.1016/S1937-6448(09)76003-4
7. Parish CR. The role of heparan sulphate in inflammation. *Nat Rev Immunol.* (2006) 6:633–43. doi: 10.1038/nri1918
8. Collins LE, Troeberg L. Heparan sulfate as a regulator of inflammation and immunity. *J Leukoc Biol.* (2019) 105:81–92. doi: 10.1002/JLB.3RU0618-246R
9. Zlotnik A, Yoshie O. The chemokine superfamily revisited. *Immunity.* (2012) 36:705–16. doi: 10.1016/j.immuni.2012.05.008
10. Lortat-Jacob H, Grosdidier A, Imberty A. Structural diversity of heparan sulfate binding domains in chemokines. *Proc Natl Acad Sci USA.* (2002) 99:1229–34. doi: 10.1073/pnas.032497699
11. Salanga CL, Handel TM. Chemokine oligomerization and interactions with receptors and glycosaminoglycans: the role of structural dynamics in function. *Exp Cell Res.* (2011) 317:590–601. doi: 10.1016/j.yexcr.2011.01.004
12. Monneau Y, Arenzana-Seisdedos F, Lortat-Jacob H. The sweet spot: how GAGs help chemokines guide migrating cells. *J Leukoc Biol.* (2016) 99:935–53. doi: 10.1189/jlb.3MR0915-440R
13. Proudfoot AE, Handel TM, Johnson Z, Lau EK, LiWang P, Clark-Lewis I, et al. Glycosaminoglycan binding and oligomerization are essential for the *in vivo* activity of certain chemokines. *Proc Natl Acad Sci U A.* (2003) 100:1885–90. doi: 10.1073/pnas.0334864100
14. Proudfoot AE. The biological relevance of chemokine-proteoglycan interactions. *Biochem Soc Trans.* (2006) 34:422–6. doi: 10.1042/BST0340422
15. Miller JD, Clabaugh SE, Smith DR, Stevens RB, Wrenshall LE. Interleukin-2 is present in human blood vessels and released in biologically active form by heparanase. *Immunol Cell Biol.* (2012) 90:159–67. doi: 10.1038/icb.2011.45
16. Sweeney EA, Lortat-Jacob H, Priestley GV, Nakamoto B, Papayannopoulou T. Sulfated polysaccharides increase plasma levels of SDF-1 in monkeys and mice: involvement in mobilization of stem/progenitor cells. *Blood.* (2002) 99:44–51. doi: 10.1182/blood.V99.1.44
17. Middleton J, Neil S, Wintle J, Clark-Lewis I, Moore H, Lam C, et al. Transcytosis and surface presentation of IL-8 by venular endothelial cells. *Cell.* (1997) 91:385–95. doi: 10.1016/S0092-8674(00)80422-5
18. Middleton J, Patterson AM, Gardner L, Schmutz C, Ashton BA. Leukocyte extravasation: chemokine transport and presentation by the endothelium. *Blood.* (2002) 100:3853–60. doi: 10.1182/blood.V100.12.3853
19. Sadir R, Imberty A, Baleux F, Lortat-Jacob H. Heparan sulfate/heparin oligosccharides protect stromal cell-derived factor-1 (SDF-1)/CXCL12 against proteolysis induced by CD26/dipeptidyl peptidase IV. *J Biol Chem.* (2004) 279:43854–60. doi: 10.1074/jbc.M405392200
20. Lortat-Jacob H, Baltzer F, Grimaud JA. Heparin decreases the blood clearance of interferon-gamma and increases its activity by limiting the processing of its carboxyl-terminal sequence. *J Biol Chem.* (1996) 271:16139–43. doi: 10.1074/jbc.271.27.16139
21. Jayanthi S, Koppolu BP, Nguyen KG, Smith SG, Felber BK, Kumar TKS, et al. Modulation of interleukin-12 activity in the presence of heparin. *Sci Rep.* (2017) 7:5360. doi: 10.1038/s41598-017-05382-1
22. Vives RR, Sadir R, Imberty A, Rencurosi A, Lortat-Jacob H. A kinetics and modeling study of RANTES(9-68) binding to heparin reveals a mechanism of cooperative oligomerization. *Biochemistry.* (2002) 41:14779–89. doi: 10.1021/bi026459i
23. Rosen SD. Ligands for l-selectin: homing, inflammation, and beyond. *Annu Rev Immunol.* (2004) 22:129–56. doi: 10.1146/annurev.immunol.21.090501.080131
24. Ivetic A, Hoskins Green HL, Hart SJ. L-selectin: a Major regulator of leukocyte adhesion, migration and signaling. *Front Immunol.* (2019) 10:1068. doi: 10.3389/fimmu.2019.01068
25. Gotte M. Syndecans in inflammation. *Faseb J.* (2003) 17:575–91. doi: 10.1096/fj.02-0739rev
26. Nelson RM, Cecconi O, Roberts WG, Aruffo A, Linhardt RJ, Bevilacqua MP. Heparin oligosaccharides bind l- and p-selectin and inhibit acute inflammation. *Blood.* (1993) 82:3253–58. doi: 10.1182/blood.V82.11.3253.3253
27. Koenig A, Norgard-Sumnicht K, Linhardt R, Varki A. Differential interactions of heparin and heparan sulfate glycosaminoglycans with the selectins. *Implications for the use of unfractionated and low molecular weight heparins as therapeutic agents*. *J Clin Invest.* (1998) 101:877–89. doi: 10.1172/JCI1509
28. Luo J, Kato M, Wang H, Bernfield M, Bischoff J. Heparan sulfate and chondroitin sulfate proteoglycans inhibit e-selectin binding to endothelial cells. *J Cell Biochem.* (2001) 80:522–31. doi: 10.1002/1097-4644(20010315)80:4<522::AID-JCB1006>3.0.CO;2-H
29. Giuffrè L, Cordey AS, Monai N, Tardy Y, Schapira M, Spertini O. Monocyte adhesion to activated aortic endothelium: role of l-selectin and heparan sulfate proteoglycans. *J Cell Biol.* (1997) 136:945–56. doi: 10.1083/jcb.136.4.945
30. Rops AL, Jacobs CW, Linssen PC, Boezeman JB, Lensen JF, Wijnhoven TJ, et al. Heparan sulfate on activated glomerular endothelial cells and exogenous heparinoids influence the rolling and adhesion of leucocytes. *Nephrol Dial Transplant Off Publ Eur Dial Transpl Assoc - Eur Ren Assoc.* (2007) 22:1070–7. doi: 10.1093/ndt/gfl801
31. Wang L, Fuster M, Sriramarao P, Esko JD. Endothelial heparan sulfate deficiency impairs l-selectin- and chemokine-mediated neutrophil trafficking during inflammatory responses. *Nat Immunol.* (2005) 6:902–10. doi: 10.1038/ni1233
32. Bao X, Moseman EA, Saito H, Petryniak B, Petryanik B, Thiriot A, et al. Endothelial heparan sulfate controls chemokine presentation in recruitment of lymphocytes and dendritic cells to lymph nodes. *Immunity.* (2010) 33:817–29. doi: 10.1016/j.immuni.2010.10.018
33. Fukasawa M, Sekine F, Miura M, Nishijima M, Hanada K. Involvement of heparan sulfate proteoglycans in the binding step for phagocytosis of latex beads by chinese hamster ovary cells. *Exp Cell Res.* (1997) 230:154–62. doi: 10.1006/excr.1996.3403
34. Dehio C, Freissler E, Lanz C, Gómez-Duarte OG, David G, Meyer TF. Ligation of cell surface heparan sulfate proteoglycans by antibody-coated beads stimulates phagocytic uptake into epithelial cells: a model for cellular invasion by neisseria gonorrhoeae. *Exp Cell Res.* (1998) 242:528–39. doi: 10.1006/excr.1998.4116
35. Gebska MA, Titley I, Paterson HF, Morilla RM, Davies DC, Gruszka-Westwood AM, et al. High-affinity binding sites for heparin generated on leukocytes during apoptosis arise from nuclear structures segregated during cell death. *Blood.* (2002) 99:2221–7. doi: 10.1182/blood.V99.6.2221
36. Clasper S, Vekemans S, Fiore M, Plebanski M, Wordsworth P, David G, et al. Inducible expression of the cell surface heparan sulfate proteoglycan syndecan-2 (fibroglycan) on human activated macrophages can regulate fibroblast growth factor action. *J Biol Chem.* (1999) 274:24113–23. doi: 10.1074/jbc.274.34.24113
37. Jones KS, Petrow-Sadowski C, Bertolette DC, Huang Y, Ruscetti FW. Heparan sulfate proteoglycans mediate attachment and entry of human t-cell leukemia virus type 1 virions into CD4+ t cells. *J Virol.* (2005) 79:12692–702. doi: 10.1128/JVI.79.20.12692-12702.2005
38. Sanderson RD, Børset M. Syndecan-1 in b lymphoid malignancies. *Ann Hematol.* (2002) 81:125–35. doi: 10.1007/s00277-002-0437-8
39. Reine TM, Kusche-Gullberg M, Feta A, Jenssen T, Kolset SO. Heparan sulfate expression is affected by inflammatory stimuli in primary human endothelial cells. *Glycoconj J.* (2012) 29:67–76. doi: 10.1007/s10719-011-9365-y
40. Berninsone P, Hirschberg CB. Heparan sulfate/heparin n-deacetylase/N-sulfotransferase. The N-sulfotransferase activity domain is at the

carboxyl half of the holoenzyme. *J Biol Chem.* (1998) 273:25556–9. doi: 10.1074/jbc.273.40.25556
41. Krenn EC, Wille I, Gesslbauer B, Poteser M, van Kuppevelt TH, Kungl AJ. Glycanogenomics: a CPCR-approach to investigate biological glycan function. *Biochem Biophys Res Commun.* (2008) 375:297–302. doi: 10.1016/j.bbrc.2008.07.144
42. Carter NM, Ali S, Kirby JA. Endothelial inflammation: the role of differential expression of n-deacetylase/N-sulphotransferase enzymes in alteration of the immunological properties of heparan sulphate. *J Cell Sci.* (2003) 116:3591–600. doi: 10.1242/jcs.00662
43. Adhikari N, Rusch M, Mariash A, Li Q, Selleck SB, Hall JL. Alterations in heparan sulfate in the vessel in response to vascular injury in the mouse. *J Cardiovasc Transl Res.* (2008) 1:236–40. doi: 10.1007/s12265-008-9047-8
44. Rops ALWMM, Loeven MA, van Gemst JJ, Eversen I, Van Wijk XM, Dijkman HB, et al. Modulation of heparan sulfate in the glomerular endothelial glycocalyx decreases leukocyte influx during experimental glomerulonephritis. *Kidney Int.* (2014) 86:932–42. doi: 10.1038/ki.2014.115
45. Martinez P, Denys A, Delos M, Sikora AS, Carpentier M, Julien S, et al. Macrophage polarization alters the expression and sulfation pattern of glycosaminoglycans. *Glycobiology.* (2015) 25:502–13. doi: 10.1093/glycob/cwu137
46. Ferreras L, Moles A, Situmorang GR, El Masri R, Wilson IL, Cooke K, et al. Heparan sulfate in chronic kidney diseases: exploring the role of 3-O-sulfation. *Biochim Biophys Acta Gen Subj.* (2019) 1863:839–48. doi: 10.1016/j.bbagen.2019.02.009
47. Sikora A-S, Delos M, Martinez P, Carpentier M, Allain F, Denys A. Regulation of the expression of heparan sulfate 3-O-Sulfotransferase 3B (HS3ST3B) by inflammatory stimuli in human monocytes. *J Cell Biochem.* (2016) 117:1529–42. doi: 10.1002/jcb.25444
48. Axelsson J, Xu D, Kang BN, Nussbacher JK, Handel TM, Ley K, et al. Inactivation of heparan sulfate 2-O-sulfotransferase accentuates neutrophil infiltration during acute inflammation in mice. *Blood.* (2012) 120:1742–51. doi: 10.1182/blood-2012-03-417139
49. Parish CR, Freeman C, Hulett MD. Heparanase: a key enzyme involved in cell invasion. *Biochim Biophys Acta.* (2001) 1471:M99–108. doi: 10.1016/S0304-419X(01)00017-8
50. Vlodavsky I, Gross-Cohen M, Weissmann M, Ilan N, Sanderson RD. Opposing functions of heparanase-1 and heparanase-2 in cancer progression. *Trends Biochem Sci.* (2018) 43:18–31. doi: 10.1016/j.tibs.2017.10.007
51. Schmidt EP, Yang Y, Janssen WJ, Gandjeva A, Perez MJ, Barthel L, et al. The pulmonary endothelial glycocalyx regulates neutrophil adhesion and lung injury during experimental sepsis. *Nat Med.* (2012) 18:1217–23. doi: 10.1038/nm.2843
52. Bartlett MR, Underwood PA, Parish CR. Comparative analysis of the ability of leucocytes, endothelial cells and platelets to degrade the subendothelial basement membrane: evidence for cytokine dependence and detection of a novel sulfatase. *Immunol Cell Biol.* (1995) 73:113–24. doi: 10.1038/icb.1995.19
53. Digre A, Singh K, Åbrink M, Reijmers RM, Sandler S, Vlodavsky I, Li J-P. Overexpression of heparanase enhances t lymphocyte activities and intensifies the inflammatory response in a model of murine rheumatoid arthritis. *Sci Rep.* (2017) 7:46229. doi: 10.1038/srep46229
54. Parish CR, Freeman C, Ziolkowski AF, He YQ, Sutcliffe EL, Zafar A, et al. Unexpected new roles for heparanase in type 1 diabetes and immune gene regulation. *Matrix Biol J Int Soc Matrix Biol.* (2013) 32:228–33. doi: 10.1016/j.matbio.2013.02.007
55. O'Callaghan P, Zhang X, Li J-P. Heparan sulfate proteoglycans as relays of neuroinflammation. *J Histochem Cytochem Off J Histochem Soc.* (2018) 66:305–19. doi: 10.1369/0022155417742147
56. Buczek-Thomas JA, Nugent MA. Elastase-mediated release of heparan sulfate proteoglycans from pulmonary fibroblast cultures. A mechanism for basic fibroblast growth factor (bFGF) release and attenuation of bfgf binding following elastase-induced injury. *J Biol Chem.* (1999) 274:25167–72. doi: 10.1074/jbc.274.35.25167
57. Marshall LJ, Ramdin LSP, Brooks T, DPhil PC, Shute JK. Plasminogen activator inhibitor-1 supports IL-8-mediated neutrophil transendothelial migration by inhibition of the constitutive shedding of endothelial IL-8/heparan sulfate/syndecan-1 complexes. *J Immunol Baltim.* (2003) 171:2057–65. doi: 10.4049/jimmunol.171.4.2057
58. Nissinen L, Kähäri V-M. Matrix metalloproteinases in inflammation. *Biochim Biophys Acta.* (2014) 1840:2571–80. doi: 10.1016/j.bbagen.2014.03.007
59. Ihrcke NS, Platt JL. Shedding of heparan sulfate proteoglycan by stimulated endothelial cells: evidence for proteolysis of cell-surface molecules. *J Cell Physiol.* (1996) 168:625–37.
60. Hayashida K, Parks WC, Park PW. Syndecan-1 shedding facilitates the resolution of neutrophilic inflammation by removing sequestered CXC chemokines. *Blood.* (2009) 114:3033–43. doi: 10.1182/blood-2009-02-204966
61. Wrenshall LE, Cerra FB, Singh RK, Platt JL. Heparan sulfate initiates signals in murine macrophages leading to divergent biologic outcomes. *J Immunol Baltim.* (1995) 154:871–80.
62. Wrenshall LE, Platt JL. Regulation of t cell homeostasis by heparan sulfate-bound IL-2. *J Immunol Baltim.* (1999) 163:3793–800.
63. Goodall KJ, Poon IKH, Phipps S, Hulett MD. Soluble heparan sulfate fragments generated by heparanase trigger the release of pro-inflammatory cytokines through TLR-4. *PLoS ONE.* (2014) 9:e109596. doi: 10.1371/journal.pone.0109596
64. Platt JL, Wrenshall LE, Johnson GB, Cascalho M. Heparan sulfate proteoglycan metabolism and the fate of grafted tissues. *Adv Exp Med Biol.* (2015) 865:123–40. doi: 10.1007/978-3-319-18603-0_8
65. Akbarshahi H, Axelsson JBF, Said K, Malmström A, Fischer H, Andersson R. TLR4 dependent heparan sulphate-induced pancreatic inflammatory response is IRF3-mediated. *J Transl Med.* (2011) 9:219. doi: 10.1186/1479-5876-9-219
66. Kodaira Y, Nair SK, Wrenshall LE, Gilboa E, Platt JL. Phenotypic and functional maturation of dendritic cells mediated by heparan sulfate. *J Immunol Baltim.* (2000) 165:1599–604. doi: 10.4049/jimmunol.165.3.1599
67. Johnson GB, Brunn GJ, Platt JL. Cutting edge: an endogenous pathway to systemic inflammatory response syndrome (SIRS)-like reactions through toll-like receptor 4. *J Immunol Baltim.* (2004) 172:20–4. doi: 10.4049/jimmunol.172.1.20
68. Dhoot GK, Gustafsson MK, Ai X, Sun W, Standiford DM, Emerson CP Jr. Regulation of Wnt signaling and embryo patterning by an extracellular sulfatase. *Science.* (2001) 293:1663–6. doi: 10.1126/science.293.5535.1663
69. Morimoto-Tomita M, Uchimura K, Werb Z, Hemmerich S, Rosen SD. Cloning and characterization of two extracellular heparin-degrading endosulfatases in mice and humans. *J Biol Chem.* (2002) 277:49175–85. doi: 10.1074/jbc.M205131200
70. Ai X, Do AT, Kusche-Gullberg M, Lindahl U, Lu K, Emerson CP Jr. Substrate specificity and domain functions of extracellular heparan sulfate 6-O-endosulfatases, QSulf1 and QSulf2. *J Biol Chem.* (2006) 281:4969–76. doi: 10.1074/jbc.M511902200
71. Frese MA, Milz F, Dick M, Lamanna WC, Dierks T. Characterization of the human sulfatase sulf1 and its high affinity heparin/heparan sulfate interaction domain. *J Biol Chem.* (2009) 284:28033–44. doi: 10.1074/jbc.M109.035808
72. Tang R, Rosen SD. Functional consequences of the subdomain organization of the sulfs. *J Biol Chem.* (2009) 284:21505–14. doi: 10.1074/jbc.M109.028472
73. Seffouh A, El Masri R, Makshakova O, Gout E, Hassoun ZEO, Andrieu J-P, et al. Expression and purification of recombinant extracellular sulfatase HSulf-2 allows deciphering of enzyme sub-domain coordinated role for the binding and 6-O-desulfation of heparan sulfate. *Cell Mol Life Sci CMLS.* (2019) 76:1807–19. doi: 10.1007/s00018-019-03027-2
74. El Masri R, Seffouh A, Lortat-Jacob H, Vivès RR. The "in and out" of glucosamine 6-O-sulfation: the 6th sense of heparan sulfate. *Glycoconj J.* (2017) 34:285–98. doi: 10.1007/s10719-016-9736-5
75. Rosen SD, Lemjabbar-Alaoui H. Sulf-2: an extracellular modulator of cell signaling and a cancer target candidate. *Expert Opin Ther Targets.* (2010) 14:935–49. doi: 10.1517/14728222.2010.504718
76. Vives RR, Seffouh A, Lortat-Jacob H. Post-Synthetic regulation of HS structure: the yin and yang of the sulfs in cancer. *Front Oncol.* (2014) 3:331. doi: 10.3389/fonc.2013.00331

77. Nishitsuji K. Heparan sulfate s-domains and extracellular sulfatases (Sulfs): their possible roles in protein aggregation diseases. *Glycoconj J.* (2018) 35:387–96. doi: 10.1007/s10719-018-9833-8
78. Sadir R, Baleux F, Grosdidier A, Imberty A, Lortat-Jacob H. Characterization of the stromal cell-derived factor-1alpha-heparin complex. *J Biol Chem.* (2001) 276:8288–96. doi: 10.1074/jbc.M008110200
79. Uchimura K, Morimoto-Tomita M, Bistrup A, Li J, Lyon M, Gallagher J, et al. HSulf-2, an extracellular endoglucosamine-6-sulfatase, selectively mobilizes heparin-bound growth factors and chemokines: effects on VEGF, FGF-1, and SDF-1. *BMC Biochem.* (2006) 7:2. doi: 10.1186/1471-2091-7-2
80. Zhang S, Condac E, Qiu H, Jiang J, Gutierrez-Sanchez G, Bergmann C, et al. Heparin-induced leukocytosis requires 6-O-sulfation and is caused by blockade of selectin- and CXCL12 protein-mediated leukocyte trafficking in mice. *J Biol Chem.* (2012) 287:5542–53. doi: 10.1074/jbc.M111.314716
81. Spillmann D, Witt D, Lindahl U. Defining the interleukin-8-binding domain of heparan sulfate. *J Biol Chem.* (1998) 273:15487–93. doi: 10.1074/jbc.273.25.15487
82. Pichert A, Schlorke D, Franz S, Arnhold J. Functional aspects of the interaction between interleukin-8 and sulfated glycosaminoglycans. *Biomatter.* (2012) 2:142–8. doi: 10.4161/biom.21316
83. Stringer SE, Gallagher JT. Specific binding of the chemokine platelet factor 4 to heparan sulfate. *J Biol Chem.* (1997) 272:20508–14. doi: 10.1074/jbc.272.33.20508
84. Pempe EH, Burch TC, Law CJ, Liu J. Substrate specificity of 6-O-endosulfatase (Sulf-2) and its implications in synthesizing anticoagulant heparan sulfate. *Glycobiology.* (2012) 22:1353–62. doi: 10.1093/glycob/cws092
85. Shaw JP, Johnson Z, Borlat F, Zwahlen C, Kungl A, Roulin K, et al. The X-Ray structure of RANTES; heparin-derived disaccharides allows the rational design of chemokine inhibitors. *Struct Camb.* (2004) 12:2081–93. doi: 10.1016/j.str.2004.08.014
86. Sheng GJ, Oh YI, Chang S-K, Hsieh-Wilson LC. Tunable heparan sulfate mimetics for modulating chemokine activity. *J Am Chem Soc.* (2013) 135:10898–901. doi: 10.1021/ja4027727
87. Jayson GC, Hansen SU, Miller GJ, Cole CL, Rushton G, Avizienyte E, et al. Synthetic heparan sulfate dodecasaccharides reveal single sulfation site interconverts CXCL8 and CXCL12 chemokine biology. *Chem Commun Camb Engl.* (2015) 51:13846–9. doi: 10.1039/C5CC05222J
88. Seffouh A, Milz F, Przybylski C, Laguri C, Oosterhof A, Bourcier S, et al. HSulf sulfatases catalyze processive and oriented 6-O-desulfation of heparan sulfate that differentially regulates fibroblast growth factor activity. *Faseb J.* (2013) 27:2431–9. doi: 10.1096/fj.12-226373
89. Rops AL, van den Hoven MJ, Baselmans MM, Lensen JF, Wijnhoven TJ, van den Heuvel LP, et al. Heparan sulfate domains on cultured activated glomerular endothelial cells mediate leukocyte trafficking. *Kidney Int.* (2008) 73:52–62. doi: 10.1038/sj.ki.5002573
90. Wang L, Brown JR, Varki A, Esko JD. Heparin's anti-inflammatory effects require glucosamine 6-O-sulfation and are mediated by blockade of l- and p-selectins. *J Clin Invest.* (2002) 110:127–36. doi: 10.1172/JCI0214996
91. Uchimido R, Schmidt EP, Shapiro NI. The glycocalyx: a novel diagnostic and therapeutic target in sepsis. *Crit Care.* (2019) 23:6. doi: 10.1186/s13054-018-2292-6
92. Oshima K, Han X, Ouyang Y, El Masri R, Yang Y, Haeger SM, et al. Loss of endothelial sulfatase-1 after experimental sepsis attenuates subsequent pulmonary inflammatory responses. *Am J Physiol Lung Cell Mol Physiol.* (2019) 317:L667–L77. doi: 10.1152/ajplung.00175.2019
93. Celie JW, Rutjes NW, Keuning ED, Soininen R, Heljasvaara R, Pihlajaniemi T, et al. Subendothelial heparan sulfate proteoglycans become major l-selectin and monocyte chemoattractant protein-1 ligands upon renal ischemia/reperfusion. *Am J Pathol.* (2007) 170:1865–78. doi: 10.2353/ajpath.2007.070061
94. Sikora A-S, Hellec C, Carpentier M, Martinez P, Delos M, Denys A, et al. Tumour-necrosis factor-α induces heparan sulfate 6-O-endosulfatase 1 (Sulf-1) expression in fibroblasts. *Int J Biochem Cell Biol.* (2016) 80:57–65. doi: 10.1016/j.biocel.2016.09.021
95. Alhasan AA, Spielhofer J, Kusche-Gullberg M, Kirby JA, Ali S. Role of 6-O-sulfated heparan sulfate in chronic renal fibrosis. *J Biol Chem.* (2014) 289:20295–306. doi: 10.1074/jbc.M114.554691
96. Yue X, Li X, Nguyen HT, Chin DR, Sullivan DE, Lasky JA. Transforming growth factor-beta1 induces heparan sulfate 6-O-endosulfatase 1 expression *in vitro* and *in vivo*. *J Biol Chem.* (2008) 283:20397–407. doi: 10.1074/jbc.M802850200
97. Yue X, Lu J, Auduong L, Sides MD, Lasky JA. Overexpression of sulf2 in idiopathic pulmonary fibrosis. *Glycobiology.* (2013) 23:709–19. doi: 10.1093/glycob/cwt010
98. Yue X. Epithelial deletion of sulf2 exacerbates bleomycin-Induced lung injury, inflammation, and mortality. *Am J Respir Cell Mol Biol.* (2017) 57:560–9. doi: 10.1165/rcmb.2016-0367OC
99. Chen G, Nakamura I, Dhanasekaran R, Iguchi E, Tolosa EJ, Romecin PA, et al. Transcriptional induction of periostin by a sulfatase 2-TGFβ1-SMAD signaling axis mediates tumor angiogenesis in hepatocellular carcinoma. *Cancer Res.* (2017) 77:632–45. doi: 10.1158/0008-5472.CAN-15-2556
100. Holst CR, Bou-Reslan H, Gore BB, Wong K, Grant D, Chalasani S, et al. Secreted sulfatases sulf1 and sulf2 have overlapping yet essential roles in mouse neonatal survival. *PLoS ONE.* (2007) 2:e575. doi: 10.1371/journal.pone.0000575
101. Lum DH, Tan J, Rosen SD, Werb Z. Gene trap disruption of the mouse heparan sulfate 6-O-endosulfatase gene, sulf2. *Mol Cell Biol.* (2007) 27:678–88. doi: 10.1128/MCB.01279-06
102. Sahota AP, Dhoot GK. A novel SULF1 splice variant inhibits wnt signalling but enhances angiogenesis by opposing SULF1 activity. *Exp Cell Res.* (2009) 315:2752–64. doi: 10.1016/j.yexcr.2009.06.029
103. Gill RB, Day A, Barstow A, Liu H, Zaman G, Dhoot GK. Sulf2 gene is alternatively spliced in mammalian developing and tumor tissues with functional implications. *Biochem Biophys Res Commun.* (2011) 414:468–73. doi: 10.1016/j.bbrc.2011.09.088
104. Gill RBS, Day A, Barstow A, Zaman G, Chenu C, Dhoot GK. Mammalian sulf1 RNA alternative splicing and its significance to tumor growth regulation. *Tumour Biol J Int Soc Oncodev Biol Med.* (2012) 33:1669–1680. doi: 10.1007/s13277-012-0423-2
105. Gill RM, Michael A, Westley L, Kocher HM, Murphy JI, Dhoot GK. SULF1/SULF2 splice variants differentially regulate pancreatic tumor growth progression. *Exp Cell Res.* (2014) 324:157–71. doi: 10.1016/j.yexcr.2014.04.001

Conflict of Interest: The authors declare that the research was conducted in the absence of any commercial or financial relationships that could be construed as a potential conflict of interest.

frontiers in Immunology

REVIEW
published: 24 April 2020
doi: 10.3389/fimmu.2020.00660

Structural Insights Into How Proteoglycans Determine Chemokine-CXCR1/CXCR2 Interactions: Progress and Challenges

Krishna Rajarathnam[1,2,3]* *and Umesh R. Desai*[4]

[1] Department of Biochemistry and Molecular Biology, The University of Texas Medical Branch at Galveston, Galveston, TX, United States, [2] Sealy Center for Structural Biology and Molecular Biophysics, The University of Texas Medical Branch at Galveston, Galveston, TX, United States, [3] Department of Microbiology and Immunology, The University of Texas Medical Branch at Galveston, Galveston, TX, United States, [4] Department of Medicinal Chemistry, Institute for Structural Biology, Drug Discovery and Development, Virginia Commonwealth University, Richmond, VA, United States

OPEN ACCESS

Edited by:
Linda Troeberg,
University of East Anglia,
United Kingdom

Reviewed by:
Brian F. Volkman,
Medical College of Wisconsin,
United States
Daniel F. Legler,
Biotechnology Institute Thurgau,
Switzerland

***Correspondence:**
Krishna Rajarathnam
krrajara@utmb.edu

Specialty section:
This article was submitted to Cytokines and Soluble Mediators in Immunity, a section of the journal Frontiers in Immunology

Received: 17 January 2020
Accepted: 23 March 2020
Published: 24 April 2020

Citation:
Rajarathnam K and Desai UR (2020) Structural Insights Into How Proteoglycans Determine Chemokine-CXCR1/CXCR2 Interactions: Progress and Challenges. Front. Immunol. 11:660. doi: 10.3389/fimmu.2020.00660

Proteoglycans (PGs), present in diverse environments, such as the cell membrane surface, extracellular milieu, and intracellular granules, are fundamental to life. Sulfated glycosaminoglycans (GAGs) are covalently attached to the core protein of proteoglycans. PGs are complex structures, and are diverse in terms of amino acid sequence, size, shape, and in the nature and number of attached GAG chains, and this diversity is further compounded by the phenomenal diversity in GAG structures. Chemokines play vital roles in human pathophysiology, from combating infection and cancer to leukocyte trafficking, immune surveillance, and neurobiology. Chemokines mediate their function by activating receptors that belong to the GPCR class, and receptor interactions are regulated by how, when, and where chemokines bind GAGs. GAGs fine-tune chemokine function by regulating monomer/dimer levels and chemotactic/haptotactic gradients, which are also coupled to how they are presented to their receptors. Despite their small size and similar structures, chemokines show a range of GAG-binding geometries, affinities, and specificities, indicating that chemokines have evolved to exploit the repertoire of chemical and structural features of GAGs. In this review, we summarize the current status of research on how GAG interactions regulate ELR-chemokine activation of CXCR1 and CXCR2 receptors, and discuss knowledge gaps that must be overcome to establish causal relationships governing the impact of GAG interactions on chemokine function in human health and disease.

Keywords: glycosaminoglycan, proteoglycan, chemokine, nuclear magnetic resonance, structure, heparan sulfate, chondroitin sulfate, heparin

Abbreviations: CS, chondroitin sulfate; CXCL, CXC ligand; CXCR2, CXC chemokine receptor 2; DS, dermatan sulfate; ECM, extracellular matrix; GAG, glycosaminoglycan; HA, hyaluronic acid; HS, heparan sulfate; ITC, isothermal titration calorimetry; KS, keratan sulfate; MD, molecular dynamics; NMR, nuclear magnetic resonance; PCM, pericellular matrix; PG, proteoglycan; Sdn, syndecan; SPR, surface plasmon resonance.

INTRODUCTION

Proteoglycans (PGs), a diverse class of forty three members, are expressed by most cell types and tissues and play vital roles in human physiology and disease (1–5). PGs are classified into four classes: cell-surface, pericellular, extracellular, and intracellular (1). Sulfated glycosaminoglycans (GAGs) are a family of linear polysaccharides covalently attached to core proteins, and are the glycan part of PGs (6). Mammals express five sulfated GAGs that differ in their backbone structure and sulfation pattern: heparin, HS, CS, DS, and KS. Cell surface PGs consist of two classes – transmembrane (TM) and glycosylphosphatidylinositol (GPI) PGs, and both carry HS and/or CS chains (7, 8). Pericellular and extracellular PGs are secreted and exist as macromolecular complexes with other PGs and proteins (1, 9, 10). Pericellular PGs predominantly carry HS, and extracellular PGs predominantly carry CS (1). Intracellular PG consists of only one member, serglycin, which serves as a storage for granule proteins. Whereas serglycin in mast cells carries predominantly heparin, serglycin in platelets carries CS and DS (1, 11, 12).

A PG can have one single GAG chain or hundreds of GAG chains, and one or two types of GAGs; additionally, the prevalence of the individual GAGs can vary, with HS and CS being the most preferred. GAGs are intrinsically heterogeneous due to differential sulfation and epimerization. Therefore, the complexity of PG structures arise not only from their amino acid sequence, size, shape, and the type and number of attached GAG chains, but also from the diversity in GAG structures. PG physiology is equally diverse and includes both structural and functional roles that are highly context-dependent. Whereas their structural role as a component of the ECM and PCM in providing cellular and tissue integrity and stability is relatively well understood, their functional roles – as a platform for binding hundreds of proteins of various classes, from chemokines and growth factors to proteases – are less well understood.

Humans express around 47 chemokines that share the following fundamental properties. They are around 70 to 100 amino acids in length, have the same tertiary structure consisting of three β-strands and an α-helix stabilized by disulfide bonds, exist reversibly as monomers and dimers and occasionally as higher order oligomers, bind GAGs, activate receptors of the GPCR (G protein-coupled receptor) class, and mediate trafficking of various immune and non-immune cells to distal and remote locations (13–15). Fundamental to any given chemokine or cell type, chemokine function must be highly regulated so that the right number of cells reach their target site at the right time to elicit the right response. For instance, seven human chemokines – CXCL1, CXCL2, CXCL3, CXCL5, CXCL6, CXCL7, and CXCL8, all characterized by the conserved N-terminal "ELR" motif – are agonists for CXCR1 and CXCR2 receptors. Whereas all ELR-chemokine monomers are potent CXCR2 agonists, ELR-chemokine dimers are differentially active for CXCR2, and CXCL8 monomer alone functions as a potent CXCR1 agonist. CXCR1 and CXCR2 are expressed in diverse cell types, including neutrophils that combat infection, oligodendrocytes in spinal cord patterning, and neuronal cells that regulate pain, in addition to regulating trafficking and proliferation of cancer cells (16–19). In this review, we focus on the structural basis and molecular mechanisms by which GAGs regulate ELR-chemokine activation of CXCR1 and CXCR2 receptors that are expressed on neutrophils and other cell types. Insights from this subset of chemokines and cell type reflect the current status and challenges for the GAG interactions of the entire chemokine family at large.

To appreciate the diversity in PG structures, we discuss syndecans as an example. Syndecans are cell surface PGs, and vertebrates express four syndecans: syndecan-1, -2, -3, and -4 (3, 20, 21). Whereas syndecan-4 (Sdc-4) is widely expressed in most tissues, Sdc-1 is expressed on epithelial and endothelial cells, and Sdc-2 and Sdc-3 are expressed selectively in cells of mesenchymal and neuronal origin, respectively. Studies using *Sdc-1* and *Sdc-4* KO mice and cell-based assays show that Sdc-1 and Sdc-4 regulate chemokine-mediated neutrophil recruitment (22–29). Chemokine binding to syndecans has been implicated in the activation of signaling pathways, changes in actin cytoskeleton, downregulation of gap junction proteins, and an increase in permeability (30–32). Reorganization of endothelial PGs also facilitates neutrophil adhesion, an early critical step that precedes crossing the endothelium (33). However, Sdc-1 and Sdc-4 are of varying molecular weights, show low amino acid sequence homology in their ectodomains, and whereas Sdc-1 carries 3 HS and 2 CS chains, Sdc-4 carries only 3 HS chains. HS chains are located close to the N-terminus at the distal end of the ectodomains; therefore, HS-bound GAGs are more accessible for interacting with infiltrating leukocytes. CS chains are closer to the membrane surface, and thus CS-bound chemokine could play a prominent role in mediating signaling events in the endothelium. From biophysical studies that have shown chemokine binding can induce crosslinking and clustering of GAGs, it has been proposed chemokine binding to GAGs can result in clustering and reorganization of the glycocalyx triggering endothelial signaling (34).

The basic building block of HS consists of repeating disaccharide units of D-glucuronic acid (GlcA) and N-acetyl-D-glucosamine (GlcNAc). HS has a modular structure, with sulfated sequences separated by non-sulfated regions, and is also more diverse due to differential N-sulfation and O-sulfation. In addition to N-sulfation, glucosamine can have 6-O sulfation, and GlcA can have 2-O sulfation and epimerize at C5 to L-iduronic acid (IdoA). The basic building block of CS consists of D-GlcA and N-acetyl-D-galactosamine (GalNAc), and on average, the disaccharide unit has one sulfate with O-sulfation either at C4 or C6 of GalNAc. Knowledge of the manner in which differences in CS and HS structures and fine structure of a given GAG impact chemokine binding and function is necessary.

In response to infection or injury, ELR-chemokines released by resident cells at the site of insult navigate across the epithelium, ECM, and endothelium to the vasculature, and provide directional cues by establishing haptotactic and chemotactic gradients that direct neutrophils to the insult site (35–39). GAG interactions impact most aspects of chemokine function, including chemokine blood levels, lifetime by preventing proteolysis and being washed away with blood flow, makeup of chemokine gradients, and chemokine presentation to the receptor on neutrophils (37–45). During an inflammatory

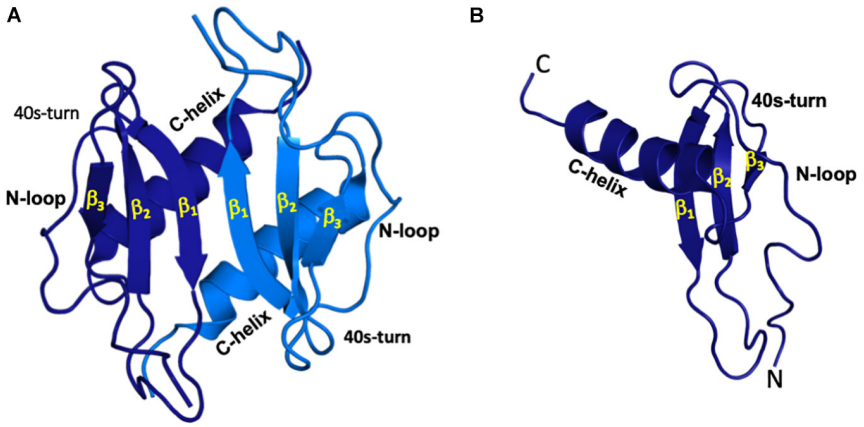

FIGURE 1 | All ELR-chemokines share the same structural fold. Structures of CXCL5 dimer **(A)** and monomer **(B)** as a representative of ELR chemokines are shown. The individual monomers in the dimer are shown in dark and light blue for clarity and different GAG-binding regions (N-terminal loop, 40s turn, and C-terminal α-helix) are labeled.

response, neutrophils are observed in as early as an hour and can last over a day or more; chemokine levels during this period can vary by orders of magnitude as a function of time and space (46–48). The chemokine concentration is higher close to the membrane surface due to GAG interactions, and fall steeply toward the center of the vessel; it is also higher at sites where neutrophils extravasate into the tissue due to small dimensions of the capillaries and high numbers of endothelial venules.

ELR-chemokines reversibly exist as monomers and dimers (**Figure 1**), and it is well established that the dimeric form binds GAG with higher affinity (49–55). At any given time and location, all four forms – monomer and dimer in solution and in GAG-bound forms – must exist in dynamic equilibrium. However, their relative amounts will depend on chemokine and GAG concentrations and four equilibrium constants – between monomer and dimer, monomer and GAG, dimer and GAG, and monomer-bound GAG and dimer-bound GAG. Engineered trapped monomers and dimers in animal models show distinctly different neutrophil recruitment profiles, indicating that the monomer-dimer equilibrium regulates recruitment (56–59). These observations indicate that chemokine dimerization and GAG interactions control chemotactic and haptotactic gradients that are coupled to the flux, duration, and kinetics of circulating neutrophil egress to the tissue. In disease situations, dysregulation in chemokine expression and/or disruption in monomer/dimer ratio could lead to either low or uncontrolled neutrophil trafficking resulting in unresolved inflammation and significant collateral tissue damage and disease.

Neutrophil trafficking is orchestrated by the interaction of ELR-chemokines with the endothelial, ECM, PCM, and glycocalyx PGs (**Figure 2**). Chemokines released at the site of insult first encounter ECM PGs, then cross the rather thin PCM located on the abluminal side of the endothelium, and then the endothelium before interacting with the endothelial cell surface PGs (60). Chemokines then enter the glycocalyx, which is a specific form of PCM as it functions as an interface between the endothelial cell surface and the blood flow (61). The dimensions of the glycocalyx are much larger (∼1000 nm) in comparison with the dimensions of a chemokine (∼3 nm), syndecan ectodomain (<100 nm), or a typical GAG (∼80 nm) (62). The glycocalyx, besides several PGs and proteins, also contains the non-sulfated GAG HA, and syndecan ectodomain and free HS generated upon cleavage by bacterial and endogenous proteases during an inflammatory response (4, 63–66). HA, which can be a few microns long, plays an important role in keeping the components of the glycocalyx together. From the perspective of chemokine interactions, endothelial PGs and the glycocalyx must be considered as a continuum rather than as two distinct compartments, and GAG interactions at this location are crucial as they set the stage for the subsequent steps of neutrophil trafficking to the target site. Chemokines then finally diffuse into the vasculature, where they encounter neutrophils before being washed away with the blood flow.

Understanding how PG interactions impact chemokine function requires knowledge of the molecular mechanisms and the structural basis, such as binding-interface residues, geometry, affinity, and stoichiometry of both monomer and dimer binding to different GAG types, as well as how PG structures and distribution of GAGs in a given PG impact chemokine binding interactions. There is no evidence that chemokines bind to the protein component of the PGs, and so we confine our discussion to binding to GAGs. A schematic of different GAG-chemokine complexes that could exist during neutrophil recruitment at different locations is shown in **Figure 3**. At low concentrations, essentially a single chemokine monomer or dimer will bind each GAG chain (models A and B). GAGs are long linear polysaccharides; therefore, when chemokines are in excess, multiple chemokines – either as monomers or dimers – can bind a single GAG, like beads on a string (models C and D). Model C will be sparsely populated as chemokines form dimers at higher concentrations, and dimers bind GAG with higher affinity. Because most proteoglycans carry two or more GAG chains, binding could also occur due to proximity effects, as shown in

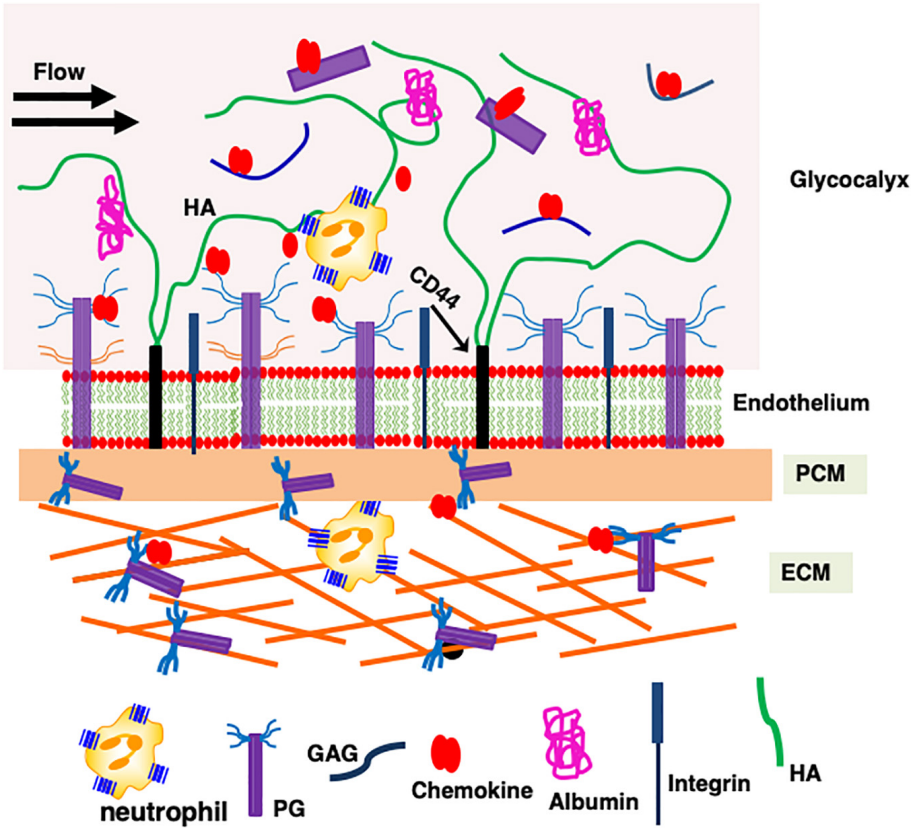

FIGURE 2 | A schematic showing how proteoglycan interactions regulate chemokine-mediated neutrophil trafficking. Endothelial glycocalyx consists of a number of secreted PGs and various proteins such as albumin that functions as a barrier between blood flow and the endothelium. Critical components of the endothelium and glycocalyx are labeled. This figure is not drawn to scale, and its purpose is to illustrate different anatomical regions that are involved in chemokine-mediated neutrophil recruitment to the insult site.

models E to H. HS has also been proposed to adopt horseshoe geometry (model I) due to its modular structure (67).

MOLECULAR BASIS OF HEPARIN INTERACTIONS

The molecular basis of the binding of human CXCL1, CXCL5, CXCL7, and CXCL8 and of mouse KC/mCXCL1 and MIP2/mCXCL2 to heparin oligosaccharides has been characterized using solution NMR spectroscopy (53–55, 68–72). GAGs are acidic, and ELR-chemokines are basic, indicating that electrostatic and H-bonding interactions play a major role in driving the binding process. NMR chemical shifts of the backbone amides are sensitive to their environment; therefore binding-induced chemical shift changes were used to identify the GAG-binding interface residues, which were then used in generating models of the chemokine-GAG complex using HADDOCK docking software. These studies used oligosaccharides from a disaccharide to a 26 mer, and the results indicated that an octasaccharide or longer is necessary for capturing the binding interface. Shorter oligosaccharides were ineffective in identifying all of the binding residues due to weaker binding, because binding affinity decreases with decreasing size. These studies also indicated that (i) dimerization and GAG binding are coupled and that the dimer binds GAG with higher affinity; (ii) the binding-interface is extensive and plastic; (iii) electrostatic and H-bonding interactions mediate affinity and specificity; (iv) lysines (Lys) dominate over arginines (Arg) at the binding interface; and (v) GAG-binding geometries differ among chemokines.

GAG-BINDING SIGNATURE AND BINDING INTERACTIONS

As ELR chemokines share a similar structural fold, any differences in GAG interactions must be due to differences in the amino acid sequence. NMR, mutagenesis, and *in vivo* neutrophil trafficking studies have shown that GAG binding is driven by conserved and chemokine-specific lysine, arginine, and histidine residues located in the N-loop, 40s turn, and C-terminal helix (**Figure 4**). A GAG-binding residue is labeled as conserved if present in five or more of the seven human sequences. Conserved GAG-binding residues, labeled B1 to B7, are in red. Binding residues that are not conserved and unique to a given chemokine are in blue. Whereas CXCL1, CXCL7, and

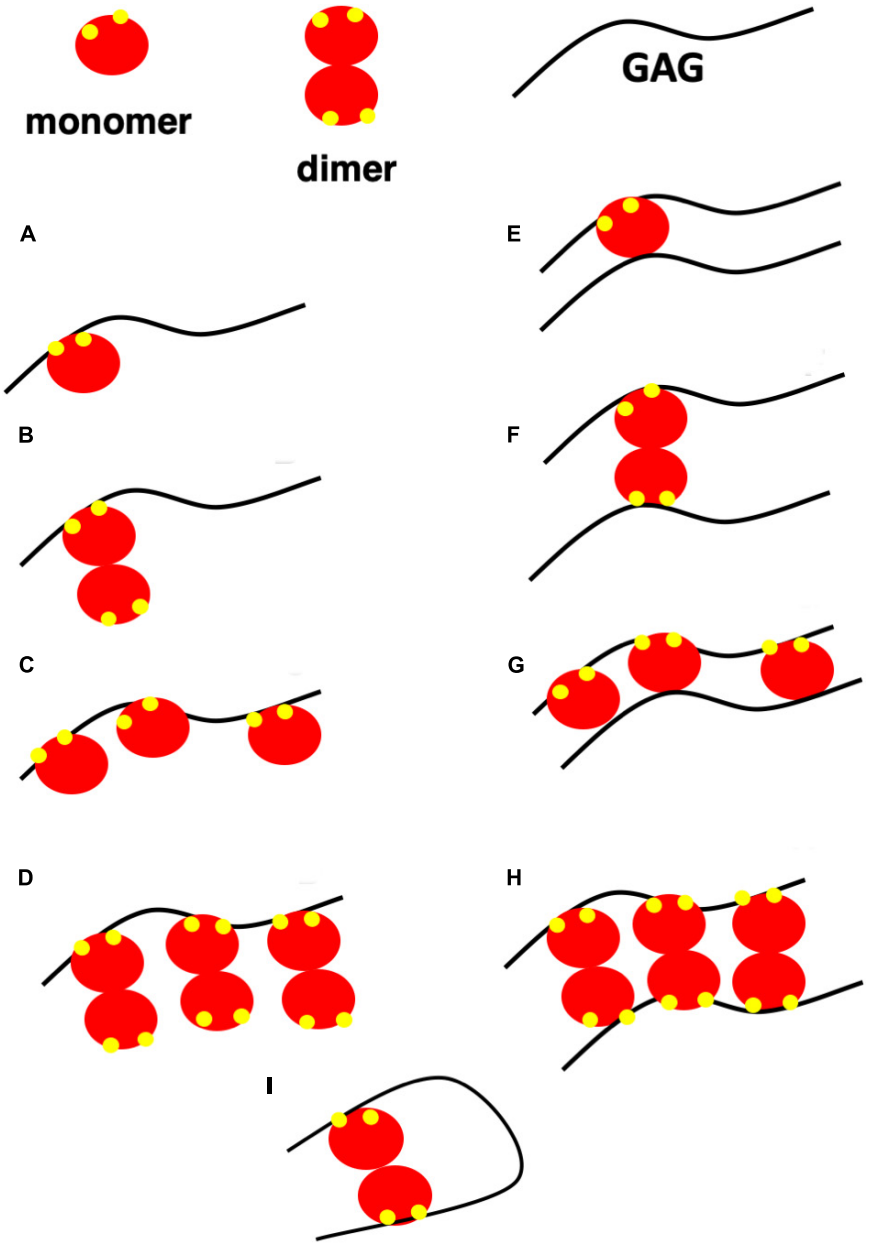

FIGURE 3 | A schematic showing possible GAG-bound ELR chemokine structures. In this schematic, a GAG corresponds to heparin or HS, monomer and dimer corresponds to CXCL5 monomer and dimer, and GAG-binding residues are shown in yellow. **(A,B)** A single chemokine monomer or dimer binding a single GAG occurs at low chemokine concentrations. With increasing concentration, dimer-bound GAG is favored due to higher binding affinity. **(C,D)** Chemokines bind GAGs like beads on a string at high chemokine concentrations. Of the two, model **(D)** is favored due to higher binding affinity of the dimer. **(E–H)** Chemokines bind two GAGs within a PG or between PGs. Of the different models, models E and G are unlikely as a monomer has only one GAG binding site. **(I)** Horseshoe model of HS binding to a chemokine dimer. HS structure consists of sulfated regions (NS) interspersed with non-sulfated regions (NA). HS is of the form NS-NA-NS in the horseshoe model.

CXCL8 have unique GAG-binding residues, CXCL5 has none. The large numbers of unique GAG-binding residues in CXCL1 and CXCL8 are noteworthy. In CXCL1 alone, an N-terminal arginine is involved in binding, and this arginine is absolutely conserved and is critical for receptor activation in all ELR-chemokines (66). Therefore this residue, from a GAG-binding perspective, is labeled as a specific and not a conserved residue. GAG interactions for CXCL2, CXCL3, and CXCL6 are not known. Sequences of CXCL2 and CXCL3 are highly similar to CXCL1 but are missing a basic residue at positions B4 and B5, respectively, and CXCL6 is also distinct as it is missing B3. Residues B2, B3, B6, and B7 are involved in binding in both mouse chemokines (KC/mCXCL1 and MIP2/mCXCL2). However, MIP2 is missing B1 and B4, but has two unique

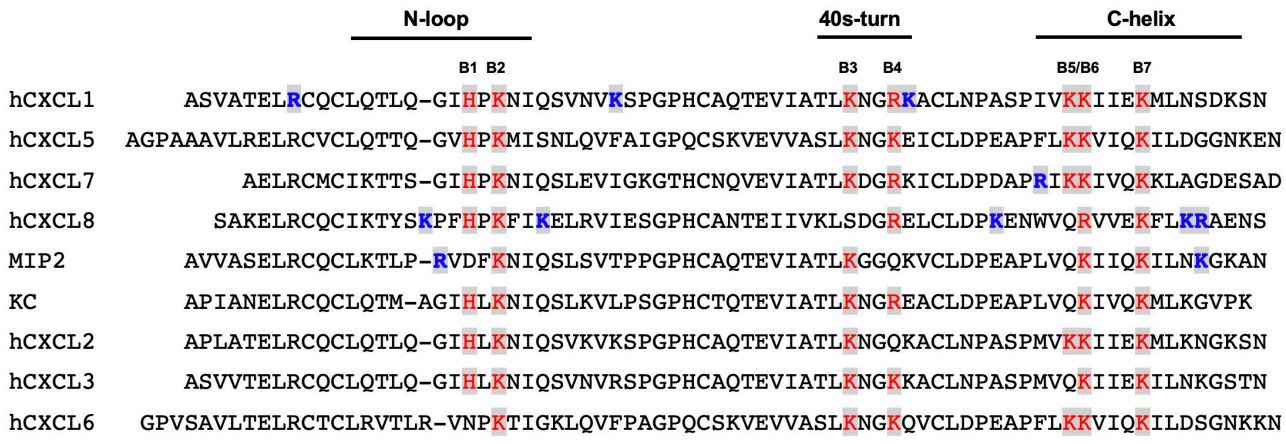

FIGURE 4 | GAG-binding residues in human and mouse ELR-chemokines. A GAG-binding residue is labeled as conserved if present in five or more of the seven human sequences. Conserved GAG-binding residues are labeled B1 to B7 and are in red. Binding residues unique to a given chemokine are in blue.

GAG-binding residues whereas KC has none. These observations collectively suggest that each member of ELR-chemokines has a unique GAG-binding signature by differential combination of conserved and chemokine-specific residues.

GEOMETRY OF BINDING

Mapping heparin-binding residues on chemokine structures suggests multiple binding geometries. Therefore, to gain more definitive insights into the binding geometry, we generated structures of heparin-bound chemokine complexes using HADDOCK modeling software, which uses residues implicated in binding from NMR chemical shift changes as ambiguous restraints, shape complementarity, and energetics to drive the docking process (73). Three different HADDOCK runs were performed to ensure that the input constraints did not bias specific structural models, and that all possible binding geometries within a monomer and across the dimer interface were considered – binding of one heparin with constraints given to both monomers of the dimer, binding of two heparins with constraints given to both monomers of the dimer, and binding of one heparin with constraints given to only one monomer of the dimer. Models generated from these studies for CXCL1, CXCL5, KC, and MIP2 are shown in **Figure 5**. For CXCL1, modeling indicates two heparin chains span the dimer interface that are located on opposite faces of the protein (defined as the α-domain and β-domain). For CXCL5, modeling suggests two models, of which only one model (model-I; in which CXCL5 binds within the monomer) is consistent with all of the NMR data. In the second model, CXCL5 binds across the dimer interface and does not involve 40s turn residues (model-II). Isothermal titration calorimetry studies indicate two heparins bind per CXCL5 dimer that are consistent only with Model-I (71). Modeling studies for KC/mCXCL1 and MIP2/mCXCL2 also suggest two binding geometries, one within the monomer and one across the dimer interface. NMR data are consistent only with model-I, and ITC data also indicate a stoichiometry of two heparins per dimer (54). Modeling studies for CXCL8 suggest three binding geometries within a monomer and one across the dimer interface (74). Additional studies are required to determine whether binding occurs across the dimer or within the monomer. Modeling studies for CXCL7 also suggest two binding geometries, one within the monomer and one across the dimer interface (53). Additional studies are required to unambiguously define whether binding occurs via one or both interactions.

STOICHIOMETRY AND THERMODYNAMICS

Knowledge of the stoichiometry is essential not only to validate GAG-binding geometry but also to understand whether a GAG-bound chemokine can bind its receptor. Unlike protein-protein and protein-DNA complexes, defining the stoichiometry for GAG-chemokine complexes is not straightforward. The stoichiometry can vary because GAGs are linear polysaccharides consisting of repeating disaccharide units resulting in multiple binding sites (**Figure 2**). Further, the stoichiometry and the number of species will vary with GAG size, chemokine:GAG ratio, and experimental conditions such as pH and ionic strength. Commonly used techniques such as SPR and fluorescence spectroscopy report a binding constant and cannot provide insights into the stoichiometry. ITC, in addition to providing a binding constant and thermodynamic signatures (enthalpy and entropy), also provides stoichiometry (75). ITC has additional advantages: it is quite sensitive, does not require modification of the protein or GAG, and can measure binding constants from the micromolar (μM) to nanomolar (nM) range. Interestingly, despite similar binding affinities, thermodynamic signatures for KC and MIP2 are quite different. Molecular dynamic (MD) simulations also indicate striking differences in binding

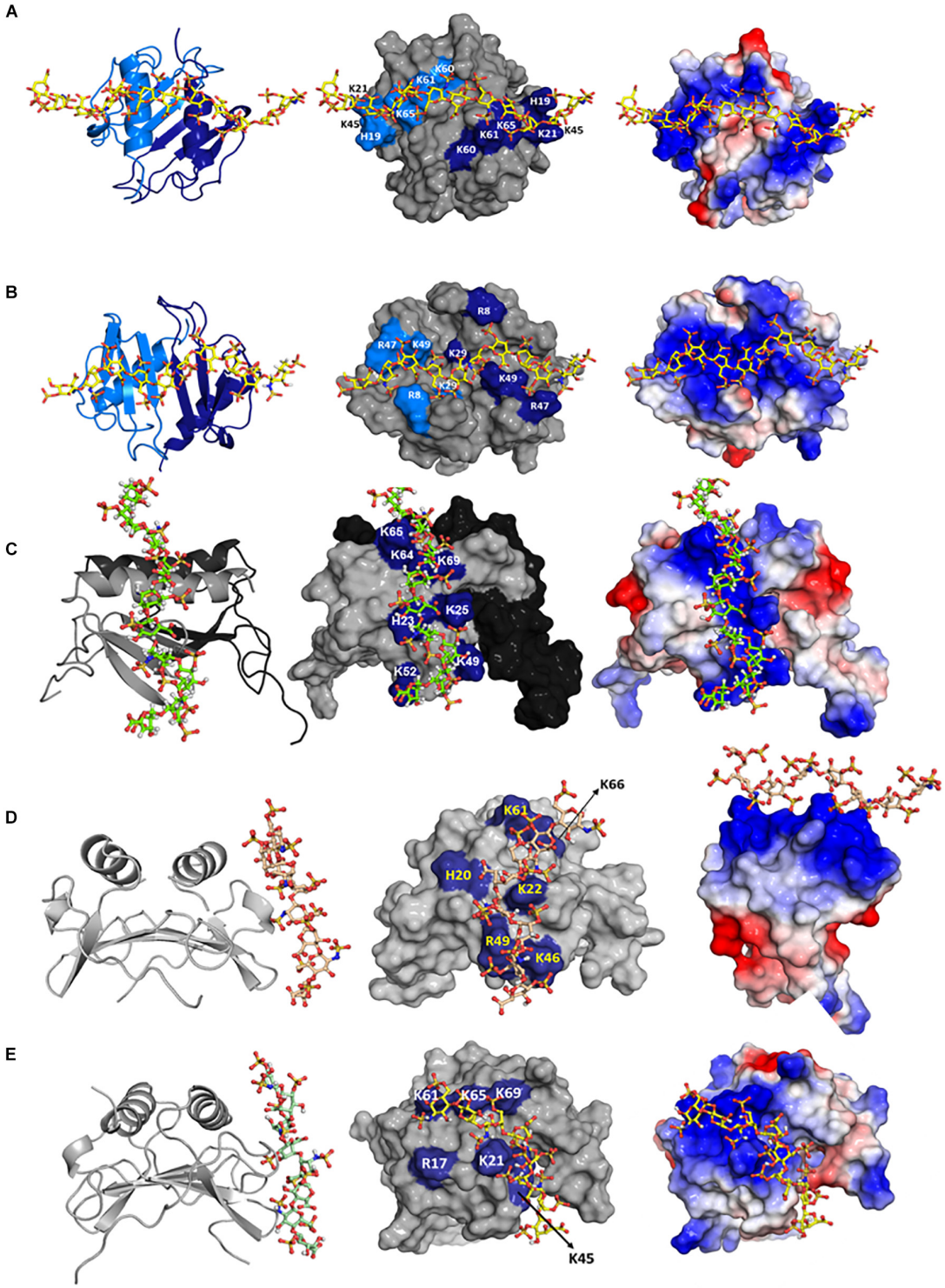

FIGURE 5 | Structural models of heparin bound to **(A)** CXCL1 α-domain, **(B)** CXCL1 β-domain, **(C)** CXCL5, **(D)** KC/mCXCL1, and **(E)** MIP2/mCXCL2. Left column: chemokine dimer structures are shown in ribbon presentation and heparin as sticks. Middle column: Heparin binding residues are highlighted on a space-filling model. Right column: Heparin binding residues are shown as the electrostatic surface. In panels **(A,B)**, two monomers of the dimer are shown in light and dark blue (left column) and heparin-binding residues from both monomers are highlighted in light and dark blue (middle column). In panel **(C)**, two monomers of the dimer are shown in gray and black (left and middle columns), and GAG-binding residues are labeled only in the gray monomer. In panels **(D,E)**, both monomers are shown in gray, and only one monomer of the dimer is labeled.

interactions at a residue-specific level, and suggest that binding interactions are not additive but coupled, and that the binding of any given residue is governed by the binding interactions of all residues.

MOLECULAR BASIS OF HS INTERACTIONS

In the context of *in vivo* function, chemokines interact with HS and not heparin. Both HS and heparin share a repeating disaccharide unit composed of glucosamine and hexuronic acid. Heparin is preferred for structural and biophysical studies as it is more uniformly sulfated and because of the availability of size-defined oligosaccharides. Heparin is assumed to be a good surrogate for describing HS interactions; this could be an oversimplification considering that their solution structures are different, and the fine structure of HS due to differential sulfation cannot be captured by heparin (76–78). We recently characterized the binding of heparin and HS polymers to CXCL1 and CXCL5 using NMR spectroscopy (79). Binding-induced chemical shift changes for HS were similar to heparin, indicating that the same basic residues mediate binding both GAGs and that their binding geometry is the same (**Figures 5**, **6**). Because HS fine structure arises due to differential N- and O-sulfation, HS variants that are either missing N-sulfate, 2-O sulfate, or 6-O sulfate were modeled for binding both chemokines. The binding geometries of all variants were similar to that of heparin, suggesting that the binding interface is plastic, and that differences in sulfation do not impact the binding geometry (79). In principle, a single HS polymer could bind both binding sites as a horseshoe (**Figure 3**), but NMR studies cannot distinguish between two HS chains binding two binding sites or a single HS binding both sites. This is the first NMR study for any protein that has characterized residue-specific binding interactions to heparin and HS polymers, and it validates the premise that heparin is a good surrogate at least for describing structural features such as the binding interface. Whether this is universally applicable to all HS binding proteins remains to be determined.

MOLECULAR BASIS OF CS AND DS INTERACTIONS

Very little is known regarding the structural basis of the binding interactions of CS, DS, or KS, or how the distribution of basic residues in a given protein mediate binding different GAGs. To address this knowledge gap, we characterized the binding of CS and DS oligosaccharides to CXCL1 and CXCL5 using NMR spectroscopy (79). DS can be considered a variant of CS, with the difference arising from C5 epimerization of GlcA to IdoA. For both chemokines, the dimer compared to the monomer bound CS and DS with higher affinity similar to what was observed for HS, the binding affinities were lower than for HS, and binding interactions were quite different from HS. For both chemokines, chemical shift changes were observed for N-loop and 40s turn basic residues, but not for the helical residues, which is quite striking, as helical residues in ELR-chemokines have long been implicated as important in GAG binding. For CXCL1, CS and DS bind a set of basic resides that lie within the monomer (defined as the γ-domain) in contrast to two HS chains spanning the dimer interface that are located on opposite faces of the protein (**Figure 6**). For CXCL5, in addition to perturbation of the N-loop and 40s turn basic residues, several N-loop and 30s loop non-basic residues were also perturbed, and modeling studies indicated a binding geometry across the dimer interface (**Figure 6**). CS exists in two forms with a sulfate at either 4-O or 6-O position, and modeling studies indicate that their binding interactions are similar (79). In contrast to CXCL1 and CXCL5, an NMR study has reported that the binding interactions of CS, DS, and heparin to CXCL8 are similar (80). Collectively, these data demonstrate how differences in the participation of a few basic residues and GAG backbone structure and sulfation pattern can result in diverse binding interactions.

MOLECULAR BASIS OF PROTEOGLYCAN GAG INTERACTIONS

Studies described so far have characterized chemokine binding to free GAGs; the question therefore arises to what extent these studies capture binding to *in vivo* PG GAGs. PG GAG chains are assembled on serine residues in core proteins by a series of glycosyltransferases and modification enzymes in the Golgi; therefore all GAG chains have the same orientation within a PG, and further, their mobility is restricted compared to free GAGs due to its covalent linkage to the core protein. Biophysical, cellular, and *ex vivo* studies have shown that a single GAG can bind multiple chemokines, binding promotes chemokine accumulation and GAG crosslinking, and that *in vivo* binding occurs at distinct anatomical sites (34, 41, 81–83). A chemokine dimer can bind a single GAG chain, bind two GAG chains within a PG, and/or two GAG chains from different PGs (**Figure 7**). For a chemokine dimer to bind two GAG chains within a PG, the dimensions of the chemokine dimer must be compatible to the distance between the GAGs. However, GAG binding sites in the chemokine dimer are antiparallel due to two-fold symmetry, and so GAG binding at the second site will not occur unless GAG interactions are non-specific. Molecular modeling studies indicate that GAGs show a preferred directionality (polarity). Binding to two GAGs within a PG can occur if the binding surface in two monomers of the dimer are different and are therefore not restricted by symmetry considerations. A chemokine dimer can bind two GAGs from two different PGs as it is not restricted by symmetry considerations. Further, structures of the GAG chains in the same PG are not necessarily equivalent or have to be perfectly aligned as GAGs are dynamic and flexible. Fluorescence recovery after photobleaching (FRAP) experiments have shown CXCL12 dimer binding can induce crosslinking of HS chain (84). In this setup, HS chains are immobilized and so they have the same orientation. NMR studies show heparin binds across the CXCL12 dimer interface suggesting a stoichiometry of one GAG per dimer (85). Therefore, how CXCL12 is able to crosslink HS chains is not clear, suggesting

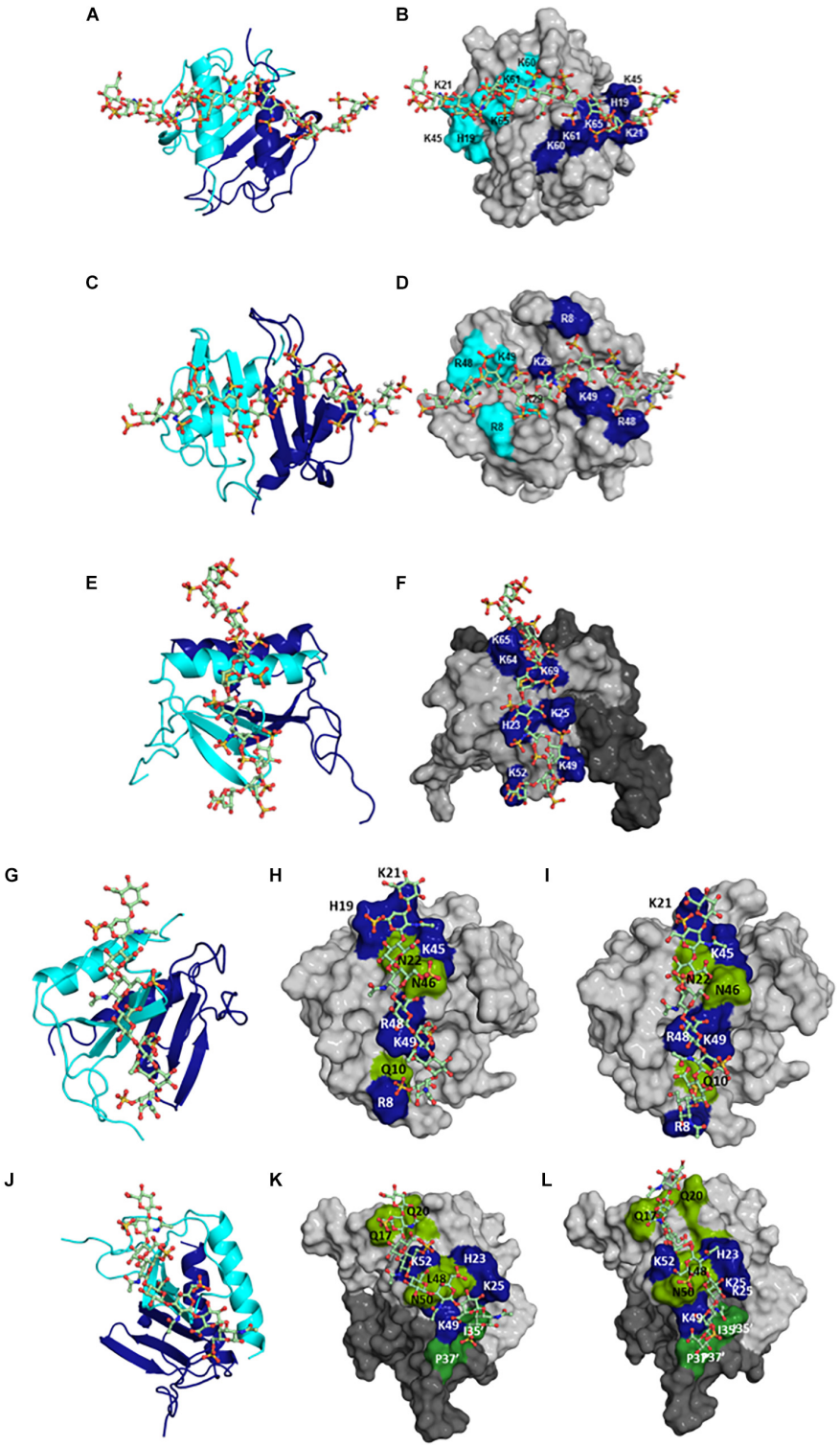

FIGURE 6 | Structural models of HS bound to **(A,B)** CXCL1 α-domain, **(C,D)** CXCL1 β-domain, and **(E,F)** to CXCL5; of CS bound to **(G,H)** CXCL1 γ-domain and to **(J,K)** CXCL5; of DS bound to **(I)** CXCL1 γ-domain and to **(L)** CXCL5. In panels **(A,C,E,G,J)**, CXCL1 and CXCL5 dimer structures are shown in ribbon presentation and GAG as sticks. Two monomers of the dimer are shown in blue and cyan. In panels **(B,D,F,H,I,K,L)**, GAG binding residues are highlighted on a space-filling model. In panels **(F,K,L)**, two monomers of the dimer are colored in light and dark gray. In panels **(H–K)**, polar residues are in green. In panels **(K,L)**, residues from the second monomer are distinguished by the ′ symbol. HS binds across the dimer interface in CXCL1 and within the monomer in CXCL5; CS and DS bind within a monomer in CXCL1 and bind both monomers of the dimer in CXCL5.

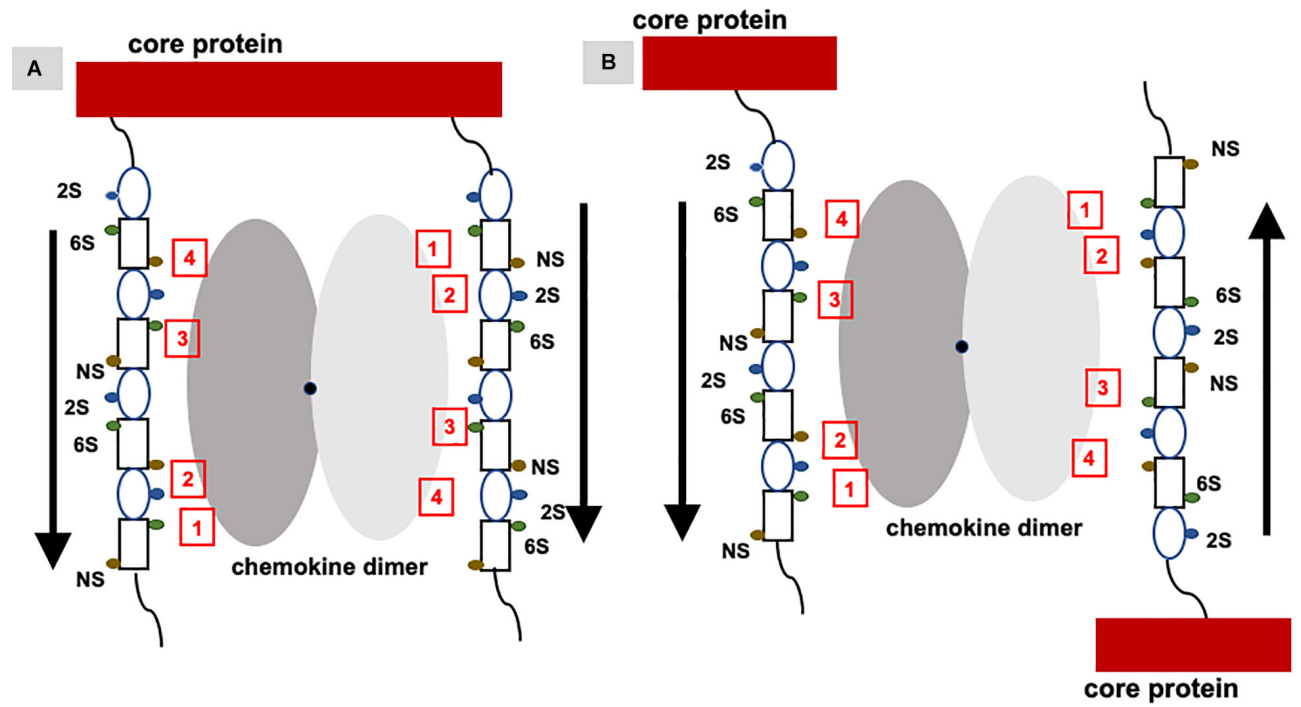

FIGURE 7 | Binding of a chemokine dimer to PG GAGs. Monomers of the chemokine dimer are shown in different shades of gray. For illustrative purposes, GAG-binding residues in each monomer of the chemokine dimer are labeled 1 to 4, which run in opposite directions because of two-fold symmetry about the dimer interface (shown by a black dot). Schematic of an heparin octasaccharide with iduronate and glucosamine shown as an oval and rectangle, and N-sulfate (NS), 2-sulfate (2S), and 6-sulfate (6S) shown as spheres in different colors. Helical structure of heparin clusters the 3 sulfate groups on opposite faces of the helical axis (44). **(A)** Binding of a chemokine dimer to two GAG chains within a PG. Direction of the GAG orientation are shown by arrows. The schematic shows GAG interactions of the two monomers cannot be the same, and that binding to both GAG chains is only possible if the binding interactions of the two monomers are different. **(B)** Binding of a chemokine to two GAG chains from two PGs. Direction of the GAG orientation are shown by arrows. In this case, two monomers of the dimer can encounter GAG chains running in opposite directions and so similar interactions to both monomers are possible. Such binding could occur in PCM and ECM due to some degree of motional freedom of the PGs.

the structural basis of binding cell surface GAGs could be more complex. Experiments specifically designed to address chemokine binding to PG GAGs both in the context of cell surface and ECM environments are essential to address this critical missing knowledge.

CAN A GAG-BOUND CHEMOKINE FORM A TERNARY COMPLEX WITH ITS RECEPTOR?

Functional studies show receptor activation involves interactions between the chemokine N-loop/β_3-strand and receptor N-domain residues (defined as Site-I) and between the ligand N-terminal and receptor extracellular/transmembrane residues (Site-II) (16, 86, 87). For all ELR-chemokines, some of the N-loop residues involved in GAG binding are also involved in receptor binding (49, 68–72, 74, 79, **Figure 8**), indicating that GAG interactions disrupt receptor binding. NMR experiments have shown that a GAG-bound monomer cannot form a ternary complex due to occlusion of receptor-binding residues, indicating only the free monomer can activate the receptor (74, 88). Similarly, residues that mediate receptor interactions are occluded in a chemokine dimer sandwiched between GAGs, and a ternary complex cannot be formed. For a chemokine dimer bound to a single GAG, the second receptor binding site is available for receptor interactions, which is the case when the chemokine dimer is bound at the edge of HS chains in syndecan (**Figures 9**, **10**). This model will only apply if GAG binding occurs within a monomer; therefore, HS-bound CXCL1, or a chemokine in which HS binds both monomers of the dimer like a horseshoe cannot bind the receptor. Both Sdc-1 and Sdc-4 carry HS chains, and Sdc-1 also carries CS chains that are located close to the membrane; therefore, CS-bound chemokines are likely to be less important for CXCR2 activation. ECM and PCM PGs and free HS and cleaved PG ectodomains in the glycocalyx are not restricted by constraints of the membrane, and a chemokine dimer bound to a single GAG chain can therefore bind the receptor (**Figure 10**). However, direct experimental evidence in support of GAG-bound dimer binding the receptor is lacking. CC chemokines, in addition to dimers, also form oligomers and polymers. However, their dimer interactions involve N-loop residues, and so dimers and oligomers cannot activate the receptor. CC oligomers also bind GAG with higher affinity, and so it is very unlikely that receptor binding residues are accessible in the GAG-bound form. Recently, it has been

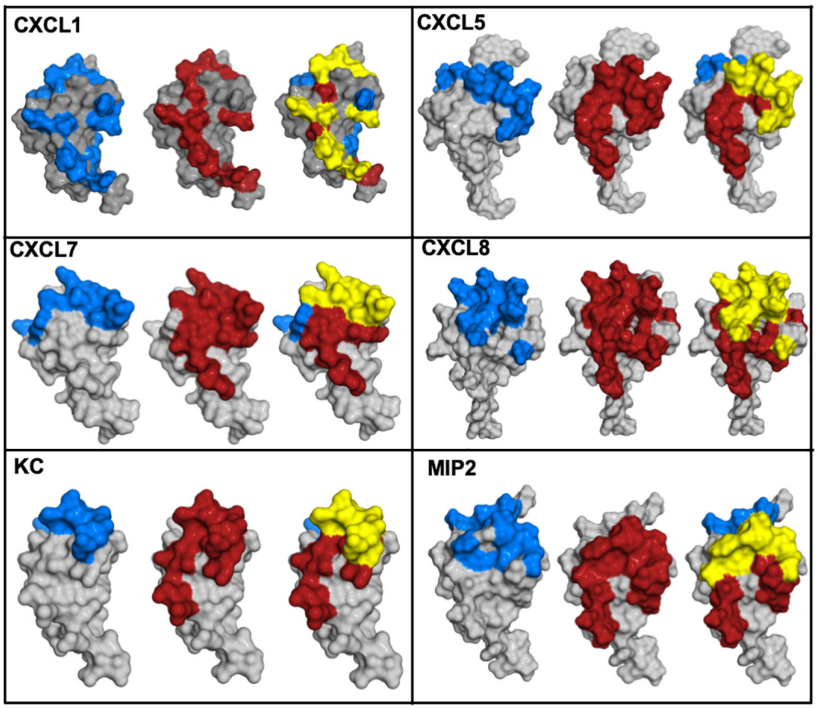

FIGURE 8 | Chemokine structures showing GAG and receptor binding regions. Receptor-binding domains are in red, GAG-binding domains are in blue, and residues that are common to both are in yellow.

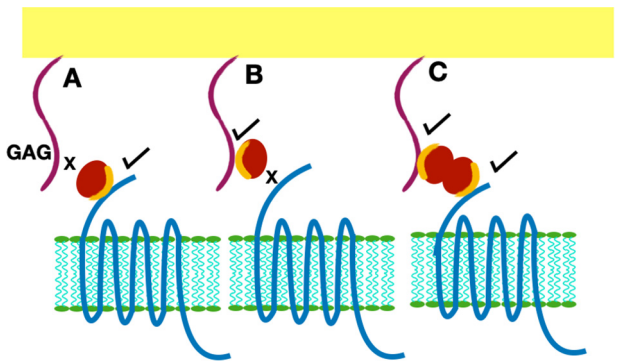

FIGURE 9 | Presentation of GAG-bound chemokine for receptor interactions. Chemokine is shown as a red sphere, and shared residues for GAG and receptor binding are shown in orange. **(A)** Chemokine monomer bound to the receptor cannot bind the GAG. **(B)** Chemokine monomer bound to a GAG chain cannot bind the receptor. **(C)** A chemokine dimer bound to a single GAG chain. In this case, one monomer can bind the GAG and the second monomer of the dimer is available for receptor interactions.

proposed that GAG-bound chemokine regulates a "cloud" of solution phase chemokines within the glycocalyx (labeled as "chemokine cloud" model), and that it is this soluble form for any chemokine that interacts with leukocyte-bound receptors (89). Our model is in agreement with the "chemokine cloud" model for the ELR chemokine monomer but not necessarily for the dimer. Structural features of ELR chemokine dimer allows GAG-bound dimer to interact with the receptor (**Figures 9**, **10**). The availability of well-characterized trapped dimeric and monomeric chemokines, such as those used in the NMR studies, would be most useful in designing experiments that address how chemokine dimers bind PG GAGs and whether PG GAG-bound chemokine can access the receptor (53, 54, 74).

SPECIFICITY OF GAG-BINDING RESIDUES

A characteristic feature of ELR-chemokines is the preference of GAG-binding residues for Lys over Arg (**Figure 4**). In general, arginines are enriched relative to lysines in protein-protein and protein-DNA Interfaces (90, 91). The pKa of the surface Lys amino and Arg guanidinium groups are >10, indicating that they are always protonated and charged at physiological pH. Whereas the Lys NH_3^+ group is symmetric and has a simple structure, the guanidinium group of Arg is planar and asymmetric with a more complex structure. The guanidinium group, compared to the NH_3^+ group, can form stronger electrostatic interactions with the sulfate anion (92). To understand the preference for lysines, three of the lysines in CXCL8 known to be involved in GAG interactions were mutated to arginine. The Lys to Arg mutants bound heparin with higher affinity as expected, but interestingly, exhibited highly impaired neutrophil recruitment activity in a mouse model (93). Mutating these lysines to alanine results in reduced GAG affinity and also reduced neutrophil

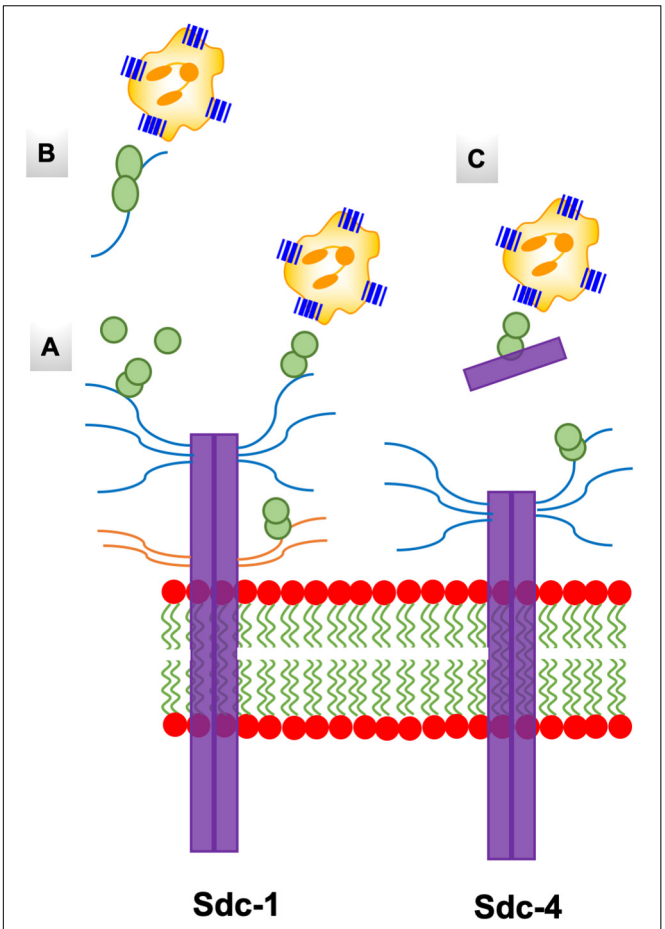

FIGURE 10 | A schematic of the endothelial syndecans and glycocalyx. Syndecans span the membrane and exist as dimers. Sdc-1 is larger (33 kDa) compared to Sdc-4 (22 kDa), and the extracellular domains carry HS and CS chains that are shown in blue and orange, respectively. Chemokine dimer bound to HS chain on syndecans **(A)**, and to free HS and syndecan ectodomain in the glycocalyx **(B,C)** are accessible to the CXCR2 receptor on neutrophils.

recruitment (59). These data make a compelling case that the specificity imparted by a lysine cannot be replaced by an arginine, and that enhanced GAG binding as a result of arginine substitution is actually detrimental, and most likely impacts one or more GAG-related functions, which in turn impairs neutrophil recruitment function.

$$\text{Lys NH} - C_\alpha H - C_\beta H_2 - C_\gamma H_2 - C_\delta H_2 - C_\varepsilon H_2 - N_\zeta H_3^+$$

$$\text{Arg NH} - C_\alpha H - C_\beta H_2 - C_\gamma H_2 - C_\delta H_2 - N_\varepsilon H - C_\zeta = (N_\eta H_2)_2^+$$

FUTURE DIRECTIONS AND CHALLENGES

We contend that the current knowledge on GAG interactions is just the "tip of the iceberg," and there is still much to be learnt if we were to compare to what is known for protein-protein and protein-DNA interactions. In particular, knowledge of how individual residues and their crosstalk with other binding residues mediate GAG interactions, the role of dynamics, and the relationship between structure, dynamics, thermodynamics, and function is lacking. NMR, ITC, and MD studies of KC and MIP2 binding to heparin highlight the importance of such knowledge for deeper and more quantitative insights (54). GAGs and Lys and Arg side chains are conformationally dynamic (94–96), and very little is known regarding how dynamic characteristics of the protein and GAG drive binding interactions. NMR studies tailored to probe lysine NH_3^+, arginine guanidinium, and histidine imidazole groups can provide crucial insights that are not accessible based on backbone chemical shifts (69, 93, 97). Chemical shifts of the lysine NH_3^+ group are not observed in the free protein due to rapid exchange with the solvent, but are observed in the bound form due to its interaction with GAG acidic groups; these shifts are more sensitive than backbone chemical shifts in defining whether a particular lysine is involved in binding or not (69). Side chain chemical shifts are essential for characterizing side chain dynamics, and such studies have proven to be quite useful for describing the properties of the individual lysines in protein-DNA complexes (96). The histidine imidazole side chain can exist in three forms due to two titratable nitrogens. NMR chemical shifts of the conserved histidine (B2) in CXCL1 and CXCL8 indicate that the structural state and their GAG interactions are different (97), emphasizing differences in chemokine-specific and residue-specific interactions that could not have been inferred from any other experiment. There is evidence that GAG binding is also driven by H-bonding interactions mediated by polar residues such as asparagine (Asn) and glutamine (Gln) (98, 99). NMR and MD studies of several ELR chemokines suggest Asn and Gln are involved in GAG interactions (54, 100). Considering these residues form weak H-bonds compared to lysines and arginines, the impact of mutating these residues on affinity, geometry, and neutrophil trafficking should give definitive insights into whether they play a role in defining specificity or affinity or both.

Much less is known regarding how GAG backbone structure and distribution of sulfates and carboxylates dictate binding. NMR-based structural models provide such knowledge but need to be independently validated. Whereas measuring binding-induced chemical shifts of protein GAG-binding residues is straightforward, the reciprocal experiment where binding-induced changes in GAG chemical shifts or assigning it to a specific sulfate and carboxylate is not trivial. Knowledge of the structures of GAG-bound chemokine complexes allows describing which sulfate and carboxylate interacts with which protein residue. However, structure determination of GAG-protein complexes, either by crystallography or NMR spectroscopy, faces many challenges, including lack of crystals suitable for crystallography and isotopically labeled homogeneous GAGs for NMR methods. This is evident if we consider that of the more than 100,000 structures deposited in the protein data bank (PDB), only around 100 correspond to those of protein-GAG complexes. The majority of these structures correspond to select proteins such as proteases and

growth factors bound to small heparin oligosaccharides. As far as chemokines go, a crystal structure of chemokine CCL2 bound to a heparin octasaccharide, and an NMR structure of CCL5 bound to CS have been reported (101, 102). Homogeneous heparin and HS oligosaccharides have been produced by chemoenzymatic methods by a few select labs (103–105), but are not routinely available for researchers. Glycan Therapeutics (106), founded by academic researchers with the aid of a STTR grant from the NIH, recently announced it will make homogeneous GAGs including ^{13}C-labeled oligosaccharides commercially available. These will be a major boon not only for structural studies using NMR and X-ray methods but also for studies focused on understanding how GAG structural features impact binding interactions and function.

Considering that there are tens of thousands of possible structures of, say, an HS octasaccharide, synthesis of all HS variants or their characterization is not realistic. However, in principle, their interactions can be characterized *in silico*. In recent years, much effort has gone into this arena, including developing energy functions, MD and docking programs, and user-friendly software that can be accessed by the GAG community at large (107–112). Promising variants from this exercise could then be tested by experimental methods. Advances in structural and computational methods will also have a major impact for GAG-based therapeutics. Heparin is used extensively as an anticoagulant, and several heparin-based drugs have shown protection in human diseases (113–115). Heparin (unfractionated, low molecular weight and other derivatives) has been investigated in clinical trials for various forms of inflammation (116–119), although it is not clear which sequences, if any, would offer the best response. A recent discovery that a HS hexasaccharide selectively targets cancer stem cells is exciting (120). Though HS is known to engage diverse mitogenic factors, this observation suggests that one or more HS oligosaccharides could display selectivity for a specific chemokine and thereby exhibit a distinct anti-inflammatory phenotype. However, heparin-based drugs have their own limitations, including intrinsic heterogeneity, potential CS contamination that could be detrimental, and an unknown mode of action *in vivo,* as it binds a number of proteins (121). Hydrogels based on heparin and heparin derivatives were also shown to outperform the standard-of-care product Promogran, by their ability to scavenge chemokines, and effectively reducing neutrophil activity and alleviating disease symptoms in humans (122). Therefore, advances in understanding GAG interactions will also be useful for designing GAG-based drugs that could have high clinical relevance for treating a number of human pathologies.

CONCLUSION

There is now compelling evidence that GAG interactions and binding geometries can be quite diverse for closely related chemokines, indicating that GAG interactions are highly specific and that this information is coded in the chemokine sequence. Chemokines were first reported around 30 years ago, and the fact that they are ligands for GPCRs and bind GAGs was reported a few years later. Studies characterizing chemokines and/or related to chemokines continue to be an area of active research, which is evident if we consider a PubMed search for the word "chemokine" results in >100,000 hits, with >5000 hits for 2019 alone. Though all ELR-chemokines activate CXCR2, animal models and clinical data provide convincing evidence that they are not redundant and are selectively and differentially expressed in different tissues for eliciting diverse physiological roles. We propose that differences in GAG interactions play important roles in defining the unique *in vivo* phenotype of each chemokine. Continued advances in structural, biophysical and computational methods for characterizing protein-GAG and protein-PG complexes, and the availability of homogeneous GAGs should lead to significant expansion of the knowledge base on the many ways through which these fascinating biopolymers orchestrate function in human pathophysiology.

AUTHOR CONTRIBUTIONS

KR conceived and wrote the manuscript with input and suggestions from UD. Both authors approved the final version of the manuscript.

FUNDING

This work was supported by a grant from the National Institutes of Health P01 HL107152 to KR and UD and 1R21AI135606 to KR and U01CA241951 to UD.

ACKNOWLEDGMENTS

We thank Dr. Krishna Mohan Sepuru for some of the figures.

REFERENCES

1. Iozzo RV, Schaefer L. Proteoglycan form and function: a comprehensive nomenclature of proteoglycans. *Matrix Biol.* (2015) 42:11–55. doi: 10.1016/j.matbio.2015.02.003
2. Karamanos NK, Piperigkou Z, Theocharis AD, Watanabe H, Franchi M, Baud S, et al. Proteoglycan chemical diversity drives multifunctional cell regulation and therapeutics. *Chem Rev.* (2018) 118:9152–232. doi: 10.1021/acs.chemrev.8b00354
3. Couchman JR. Transmembrane signaling proteoglycans. *Annu Rev Cell Dev Biol.* (2010) 26:89–114. doi: 10.1146/annurev-cellbio-100109-104126
4. Weinbaum S, Tarbell JM, Damiano ER. The structure and function of the endothelial glycocalyx layer. *Annu Rev Biomed Eng.* (2007) 9:121–67. doi: 10.1146/annurev.bioeng.9.060906.151959
5. Schaefer L, Schaefer RM. Proteoglycans: from structural compounds to signaling molecules. *Cell Tissue Res.* (2010) 339:237–46. doi: 10.1007/s00441-009-0821-y
6. Pomin VH, Mulloy B. Glycosaminoglycans and proteoglycans. *Pharmaceuticals.* (2018) 11:27. doi: 10.3390/ph11010027
7. Choi Y, Chung H, Jung H, Couchman JR, Oh ES. Syndecans as cell surface receptors: unique structure equates with functional diversity. *Matrix Biol.* (2011) 30:93–9. doi: 10.1016/j.matbio.2010.10.006

8. Filmus J, Capurro M, Rast J. Glypicans. *Genome Biol.* (2008) 9:224. doi: 10.1186/gb-2008-9-5-224
9. Mouw JK, Ou G, Weaver VM. Extracellular matrix assembly: a multiscale deconstruction. *Nat Rev Mol Cell Biol.* (2014) 15:771–85. doi: 10.1038/nrm3902
10. Wilusz RE, Sanchez-Adams J, Guilak F. The structure and function of the pericellular matrix of articular cartilage. *Matrix Biol.* (2014) 39:25–32. doi: 10.1016/j.matbio.2014.08.009
11. Mulloy B, Lever R, Page CP. Mast cell glycosaminoglycans. *Glycoconj J.* (2017) 34:351–61. doi: 10.1007/s10719-016-9749-0
12. Lord MS, Cheng B, Farrugia BL, McCarthy S, Whitelock JM. Platelet factor 4 binds to vascular proteoglycans and controls both growth factor activities and platelet activation. *J Biol Chem.* (2017) 292:4054–63. doi: 10.1074/jbc.M116.760660
13. Stone MJ, Hayward JA, Huang CE, Huma Z, Sanchez J. Mechanisms of regulation of the chemokine-receptor network. *Int J Mol Sci.* (2017) 18:2. doi: 10.3390/ijms18020342
14. Salanga CL, Handel TM. Chemokine oligomerization and interactions with receptors and glycosaminoglycans: the role of structural dynamics in function. *Exp Cell Res.* (2011) 317:590–601. doi: 10.1016/j.yexcr.2011.01.004
15. Miller MC, Mayo KH. Chemokines from a structural perspective. *Int J Mol Sci.* (2017) 18:10. doi: 10.3390/ijms18102088
16. Rajarathnam K, Schnoor M, Richardson RM, Rajagopal S. How do chemokines navigate neutrophils to the target site: dissecting the signaling pathways. *Cell Signal.* (2019) 54:69–80. doi: 10.1016/j.cellsig.2018.11.004
17. Tsai HH, Frost E, To V, Robinson S, Ffrench-Constant C, Geertman R, et al. The chemokine receptor CXCR2 controls positioning of oligodendrocyte precursors in developing spinal cord by arresting their migration. *Cell.* (2002) 110:373–83. doi: 10.1016/s0092-8674(02)00838-3
18. Zhang ZJ, Cao DL, Zhang X, Ji RR, Gao YJ. Chemokine contribution to neuropathic pain: respective induction of CXCL1 and CXCR2 in spinal cord astrocytes and neurons. *Pain.* (2013) 154:2185–97. doi: 10.1016/j.pain.2013.07.002
19. Cheng Y, Ma XL, Wei YQ, Wei XW. Potential roles and targeted therapy of the CXCLs/CXCR2 axis in cancer and inflammatory diseases. *Biochim Biophys Acta Rev Cancer.* (2019) 1871:289–312. doi: 10.1016/j.bbcan.2019.01.005
20. Xian X, Gopal S, Couchman JR. Syndecans as receptors and organizers of the extracellular matrix. *Cell Tissue Res.* (2010) 339:31–46. doi: 10.1007/s00441-009-0829-3
21. Yoneda A, Couchman JR. Regulation of cytoskeletal organization by syndecan transmembrane proteoglycans. *Matrix Biol.* (2003) 22:25–33. doi: 10.1016/s0945-053x(03)00010-6
22. Ishiguro K, Kadomatsu K, Kojima T, Muramatsu H, Iwase M, Yoshikai Y, et al. Syndecan-4 deficiency leads to high mortality of lipopolysaccharide-injected mice. *J Biol Chem.* (2001) 276:47483–8. doi: 10.1074/jbc.M106268200
23. Partovian C, Ju R, Zhuang ZW, Martin KA, Simons M. Syndecan-4 regulates subcellular localization of mTOR complex2 and Akt activation in a PKCalpha-dependent manner in endothelial cells. *Mol Cell.* (2008) 32:140–9. doi: 10.1016/j.molcel.2008.09.010
24. Stepp MA, Gibson HE, Gala PH, Iglesia DD, Pajoohesh-Ganji A, Pal-Ghosh S, et al. Defects in keratinocyte activation during wound healing in the syndecan-1 deficient mouse. *J Cell Sci.* (2002) 115:4517–31. doi: 10.1242/jcs.00128
25. Tanino Y, Chang MY, Wang X, Gill SE, Skerrett S, McGuire JK, et al. Syndecan-4 regulates early neutrophil migration and pulmonary inflammation in response to lipopolysaccharide. *Am J Respir Cell Mol Biol.* (2012) 47:196–202. doi: 10.1165/rcmb.2011-0294OC
26. Marshall LJ, Ramdin LS, Brooks TD, Phil PC, Shute JK. Plasminogen activator inhibitor-1 supports IL-8-mediated neutrophil transendothelial migration by inhibition of the constitutive shedding of endothelial IL-8/heparan sulfate/syndecan-1 complexes. *J Immunol.* (2003) 171:2057–65. doi: 10.4049/jimmunol.171.4.2057
27. Bass MD, Roach KA, Morgan MR, Mostafavi-Pour Z, Schoen T, Muramatsu T, et al. Syndecan-4-dependent Rac1 regulation determines directional migration in response to the extracellular matrix. *J Cell Biol.* (2007) 177:527–38. doi: 10.1083/jcb.200610076
28. Lim ST, Longley RL, Couchman JR, Woods A. Direct binding of syndecan-4 cytoplasmic domain to the catalytic domain of protein kinase C alpha (PKC alpha) increases focal adhesion localization of PKC alpha. *J Biol Chem.* (2003) 278:13795–802. doi: 10.1074/jbc.M208300200
29. Teng YH, Aquino RS, Park PW. Molecular functions of syndecan-1 in disease. *Matrix Biol.* (2012) 31:3–16. doi: 10.1016/j.matbio.2011.10.001
30. Yang Y, Schmidt EP. The endothelial glycocalyx: an important regulator of the pulmonary vascular barrier. *Tissue Barriers.* (2013) 1:e23494. doi: 10.4161/tisb.23494
31. Derler R, Gesslbauer B, Weber C, Strutzmann E, Miller I, Kungl A. Glycosaminoglycan-mediated downstream signaling of CXCL8 binding to endothelial cells. *Int J Mol Sci.* (2017) 18:12. doi: 10.3390/ijms18122605
32. Dull RO, Dinavahi R, Schwartz L, Humphries DE, Berry D, Sasisekharan R, et al. Lung endothelial heparan sulfates mediate cationic peptide-induced barrier dysfunction: a new role for the glycocalyx. *Am J Physiol Lung Cell Mol Physiol.* (2003) 285:L986–95. doi: 10.1152/ajplung.00022.2003
33. Schmidt EP, Lee WL, Zemans RL, Yamashita C, Downey GP. On, around, and through: neutrophil-endothelial interactions in innate immunity. *Physiology.* (2011) 26:334–47. doi: 10.1152/physiol.00011.2011
34. Dyer DP, Migliorini E, Salanga CL, Thakar D, Handel TM, Richter RP. Differential structural remodelling of heparan sulfate by chemokines: the role of chemokine oligomerization. *Open Biol.* (2017) 7:160286. doi: 10.1098/rsob.160286
35. Kobayashi Y. The role of chemokines in neutrophil biology. *Front Biosci.* (2008) 13:2400–7. doi: 10.2741/2853
36. Mayadas TN, Cullere X, Lowell CA. The multifaceted functions of neutrophils. *Annu Rev Pathol.* (2014) 9:181–218. doi: 10.1146/annurev-pathol-020712-164023
37. Massena S, Christoffersson G, Hjertstrom E, Zcharia E, Vlodavsky I, Ausmees N, et al. A chemotactic gradient sequestered on endothelial heparan sulfate induces directional intraluminal crawling of neutrophils. *Blood* (2010) 116:1924–31. doi: 10.1182/blood-2010-01-266072
38. Rot A. Neutrophil attractant/activation protein-1 (interleukin-8) induces in vitro neutrophil migration by haptotactic mechanism. *Eur J Immunol.* (1993) 23:303–6. doi: 10.1002/eji.1830230150
39. Middleton J, Neil S, Wintle J, Clark-Lewis I, Moore H, Lam C, et al. Transcytosis and surface presentation of IL-8 by venular endothelial cells. *Cell.* (1997) 91:385–95. doi: 10.1016/s0092-8674(00)80422-5
40. Sarris M, Masson JB, Maurin D, Van der Aa LM, Boudinot P, Lortat-Jacob H, et al. Inflammatory chemokines direct and restrict leukocyte migration within live tissues as glycan-bound gradients. *Curr Biol.* (2012) 22:2375–82. doi: 10.1016/j.cub.2012.11.018
41. Frevert CW, Kinsella MG, Vathanaprida C, Goodman RB, Baskin DG, Proudfoot A, et al. Binding of interleukin-8 to heparan sulfate and chondroitin sulfate in lung tissue. *Am J Respir Cell Mol Biol.* (2003) 28:464–72. doi: 10.1165/rcmb.2002-0084OC
42. Monneau Y, Arenzana-Seisdedos F, Lortat-Jacob H. The sweet spot: How GAGS help chemokines guide migrating cells. *Leukoc Biol.* (2016) 99:935–53. doi: 10.1189/jlb.3MR0915-440R
43. Celie JW, Beelen RH, van den Born J. Heparan sulfate proteoglycans in extravasation: assisting leukocyte guidance. *Front Biosci.* (2009) 14:4932–49. doi: 10.2741/3578
44. Gallagher J. Heparan sulphate and the art of cell regulation: a polymer chain conducts the protein orchestra. *Int J Exp Pathol.* (2015) 96:203–31. doi: 10.1111/iep.12135
45. Stoler-Barak L, Moussion C, Shezen E, Hatzav M, Sixt M, Alon R. Blood vessels pattern heparan sulfate gradients between their apical and basolateral aspects. *PLoS One.* (2014) 9:e85699. doi: 10.1371/journal.pone.0085699
46. De Filippo K, Dudeck A, Hasenberg M, Nye E, van Rooijen N, Hartmann K, et al. Mast cell and macrophage chemokines CXCL1/CXCL2 control the early stage of neutrophil recruitment during tissue inflammation. *Blood.* (2013) 121:4930–7. doi: 10.1182/blood-2013-02-486217
47. Wengner AM, Pitchford SC, Furze RC, Rankin SM. The coordinated action of G-CSF and ELR + CXC chemokines in neutrophil mobilization during acute inflammation. *Blood.* (2008) 111:42–9. doi: 10.1182/blood-2007-07-099648
48. Craciun FL, Schuller ER, Remick DG. Early enhanced local neutrophil recruitment in peritonitis-induced sepsis improves bacterial clearance and survival. *J. Immunol.* (2010) 185:6930–8. doi: 10.4049/jimmunol.1002300

49. Rajarathnam K, Kay CM, Dewald B, Wolf M, Baggiolini M, Clark-Lewis I, et al. Neutrophil activating peptide-2 and melanoma growth stimulatory activity are functional as monomers for neutrophil activation. *J Biol Chem.* (1997) 272:1725–9. doi: 10.1074/jbc.272.3.1725
50. Joseph PR, Sawant KV, Rajarathnam K. Heparin-bound chemokine CXCL8 monomer and dimer are impaired for CXCR1 and CXCR2 activation: implications for gradients and neutrophil trafficking. *Open Biology*. (2017) 7:170168. doi: 10.1098/rsob.170168
51. Sepuru KM, Poluri KM, Rajarathnam K. Solution structure of CXCL5–a novel chemokine and adipokine implicated in inflammation and obesity. *PLoS One.* (2014) 9:e93228. doi: 10.1371/journal.pone.0093228
52. Shao W, Jerva LF, West J, Lolis E, Schweitzer BI. Solution structure of murine macrophage inflammatory protein-2. *Biochemistry*. (1998) 37:8303–13. doi: 10.1021/bi980112r
53. Brown AJ, Sepuru KM, Sawant KV, Rajarathnam K. Platelet-derived Chemokine CXCL7 dimer preferentially exists in the Glycosaminoglycan-bound form: implications for neutrophil-platelet crosstalk. *Front Immunol*. (2017) 8:1248. doi: 10.3389/fimmu.2017.01248
54. Sepuru KM, Nagarajan B, Desai UR, Rajarathnam K. Structural basis, stoichiometry, and thermodynamics of chemokines KC/mCXCL1 and MIP2/mCXCL2 binding to glycosaminoglycan heparin. *J Biol Chem.* (2018) 293:17817–28. doi: 10.1074/jbc.RA118.004866
55. Rajasekaran D, Keeler C, Syed MA, Jones MC, Harrison JK, Wu D, et al. A model of GAG/MIP-2/CXCR2 interfaces and its functional effects. *Biochemistry.* (2012) 51:5642–54. doi: 10.1021/bi3001566
56. Sawant KV, Poluri KM, Dutta A, Sepuru KM, Troshkina A, Garofalo RP, et al. Chemokine CXCL1 mediated neutrophil recruitment: role of glycosaminoglycan interactions. *Sci Rep*. (2016) 6:33123. doi: 10.1038/srep33123
57. Das ST, Rajagopalan L, Guerrero-Plata A, Sai J, Richmond A, Garofalo RP, et al. Monomeric and Dimeric CXCL8 are both essential for in vivo neutrophil recruitment. *PLoS One*. (2010) 5:e11754. doi: 10.1371/journal.pone.0011754
58. Sawant K, Xu R, Cox R, Hawkins H, Kolli D, Garofalo RP, et al. Chemokine CXCL1-mediated neutrophil recruitment in the lung – Role CXCR2 activation. *J Innate Immun.* (2015) 54:5113–9. doi: 10.1159/000430914
59. Gangavarapu P, Rajagopalan L, Kohli D, Guerrero-Plata A, Garofalo RP, Rajarathnam K. The monomer-dimer equilibrium and glycosaminoglycan interactions of chemokine CXCL8 regulate tissue-specific neutrophil recruitment. *J Leukoc Biol.* (2012) 91:259–65. doi: 10.1189/jlb.0511239
60. Rot A. Chemokine patterning by glycosaminoglycans and interceptors. *Front Biosci.* (2010) 15:645–60. doi: 10.2741/3638
61. Nijenhuis N, Mizuno D, Spaan JA, Schmidt CF. High-resolution microrheology in the pericellular matrix of prostate cancer cells. *J R Soc Interface.* (2012) 9:1733–44. doi: 10.1098/rsif.2011.0825
62. Marki A, Esko JD, Pries AR, Ley K. Role of the endothelial surface layer in neutrophil recruitment. *J Leukoc Biol.* (2015) 98:503–15. doi: 10.1189/jlb.3MR0115-011R
63. Gill SE, Nadler ST, Li Q, Frevert CW, Park PW, Chen P, et al. Shedding of syndecan-1/CXCL1 complexes by matrix metalloproteinase 7 functions as an epithelial checkpoint of neutrophil activation. *Am J Respir Cell Mol Biol.* (2016) 55:243–51. doi: 10.1165/rcmb.2015-0193OC
64. Hayashida K, Parks WC, Park PW. Syndecan-1 shedding facilitates the resolution of neutrophilic inflammation by removing sequestered CXC chemokines. *Blood.* (2009) 114:3033–43. doi: 10.1182/blood-2009-02-204966
65. Lipowsky HH. The endothelial glycocalyx as a barrier to leukocyte adhesion and its mediation by extracellular proteases. *Ann Biomed Eng.* (2012) 40:840–8. doi: 10.1007/s10439-011-0427-x
66. Reitman S, Slaaf DW, Vink H, van Zandvoort MA, Egbrink MG. The endothelial glycocalyx: composition, functions, and visualization. *Pflugers Arch.* (2007) 454:345–59. doi: 10.1007/s00424-007-0212-8
67. Spillmann D, Witt D, Lindahl U. Defining the interleukin-8-binding domain of heparan sulfate. *J. Biol. Chem.* (1998) 273:15487–93. doi: 10.1074/jbc.273.25.15487
68. Poluri KM, Joseph PR, Sawant KV, Rajarathnam K. Molecular basis of glycosaminoglycan binding to chemokine CXCL1 dimer. *J Biol Chem.* (2013) 288:25143–53. doi: 10.1074/jbc.M113.492579
69. Sepuru KM, Iwahara J, Rajarathnam K. Direct detection of lysine side chain NH_3^+ in protein-heparin complexes using NMR spectroscopy. *Analyst.* (2018) 143:635–8. doi: 10.1039/c7an01406f
70. Sepuru KM, Rajarathnam K. CXCL1/MGSA Is a Novel Glycosaminoglycan (GAG)-binding chemokine: structural evidence for two distinct non-overlapping binding domains. *J Biol Chem.* (2016) 291:4247–55. doi: 10.1074/jbc.M115.697888
71. Sepuru KM, Nagarajan B, Desai UR, Rajarathnam K. Molecular basis of chemokine CXCL5-glycosaminoglycan interactions. *J Biol Chem.* (2016) 291:20539–50. doi: 10.1074/jbc.M116.745265
72. Rajarathnam K, Sepuru KM, Joseph PB, Sawant K, Brown AJ. Glycosaminoglycan interactions finetune chemokine-mediated neutrophil trafficking: Structural insights and molecular mechanisms. *J Histochem Cytochem.* (2018) 66:229–39. doi: 10.1369/0022155417739864
73. de Vries SJ, van Dijk AD, Krzeminski M, van Dijk M, Thureau A, Hsu V, et al. HADDOCK versus HADDOCK: new features and performance of HADDOCK2.0 on the CAPRI targets. *Proteins.* (2007) 69:726–33. doi: 10.1002/prot.21723
74. Joseph PR, Mosier PD, Desai UR, Rajarathnam K. Solution NMR characterization of chemokine CXCL8/IL-8 monomer and dimer binding to glycosaminoglycans: Structural plasticity mediates differential binding interactions. *Biochem J.* (2015) 472:121–33. doi: 10.1042/BJ20150059
75. Dutta AK, Rösgen J, Rajarathnam K. Using isothermal titration calorimetry to determine thermodynamic parameters of protein-glycosaminoglycan interactions. *Methods Mol Biology*. (2015) 1229:315–22. doi: 10.1007/978-1-4939-1714-3_25
76. Khan S, Fung KW, Rodriguez E, Patel R, Gor J, Mulloy B, et al. The solution structure of heparan sulfate differs from that of heparin: implications for function. *J Biol Chem.* (2013) 288:27737–51. doi: 10.1074/jbc.A111.226027
77. Meneghetti MC, Hughes AJ, Rudd TR, Nader HB, Powell AK, Yates EA, et al. Heparan sulfate and heparin interactions with proteins. *J R Soc Interface.* (2015) 12:0589. doi: 10.1098/rsif.2015.0589
78. Yates EA, Gallagher JT, Guerrini M. Heparan sulfate and heparin: challenges and controversies: some outstanding questions in heparan sulfate and heparin research. *Molecules.* (2019) 24:7. doi: 10.3390/molecules24071399
79. Sepuru KM, Rajarathnam K. Structural basis of chemokine interactions with heparan sulfate, chondroitin sulfate, and dermatan sulfate. *J Biol Chem.* (2019) 294:15650–61. doi: 10.1074/jbc.RA119.009879
80. Pichert A, Samsonov SA, Theisgen S, Thomas L, Baumann L, Schiller J, et al. Characterization of the interaction of interleukin-8 with hyaluronan, chondroitin sulfate, dermatan sulfate and their sulfated derivatives by spectroscopy and molecular modeling. *Glycobiology.* (2012) 22:134–45. doi: 10.1093/glycob/cwr120
81. Kuschert GS, Coulin F, Power CA, Proudfoot AE, Hubbard RE, Hoogewerf AJ, et al. Glycosaminoglycans interact selectively with chemokines and modulate receptor binding and cellular responses. *Biochemistry*. (1999) 38:12959–68. doi: 10.1021/bi990711d
82. Kuschert GS, Hoogewerf AJ, Proudfoot AE, Chung CW, Cooke RM, Hubbard RE, et al. Identification of a glycosaminoglycan binding surface on human interleukin-8. *Biochemistry*. (1998) 37:11193–201. doi: 10.1021/bi972867o
83. Hoogewerf AJ, Kuschert GS, Proudfoot AE, Borlat F, Clark-Lewis I, Power CA, et al. Glycosaminoglycans mediate cell surface oligomerization of chemokines. *Biochemistry.* (1997) 36:13570–8. doi: 10.1021/bi971125s
84. Migliorini E, Thakar D, Kühnle J, Sadir R, Dyer DP, Li Y, et al. Cytokines and growth factors cross-link heparan sulfate. *Open Biol.* (2015) 5:150046. doi: 10.1098/rsob.150046
85. Ziarek JJ, Veldkamp CT, Zhang F, Murray NJ, Kartz GA, Liang X, et al. Heparin oligosaccharides inhibit chemokine (CXC motif) ligand 12 (CXCL12) cardioprotection by binding orthogonal to the dimerization interface, promoting oligomerization, and competing with the chemokine (CXC motif) receptor 4 (CXCR4) N terminus. *J Biol Chem.* (2013) 288:737–46. doi: 10.1074/jbc.M112.394064
86. Rajagopalan L, Rajarathnam K. Structural basis of chemokine receptor function – A model for binding affinity and ligand selectivity. *Biosci Rep.* (2006) 26:325–39. doi: 10.1007/s10540-006-9025-9
87. Crump MP, Gong JH, Loetscher P, Rajarathnam K, Amara A, Arenzana-Seisdedos F, et al. Solution structure and basis for functional activity of stromal cell-derived factor-1; dissociation of CXCR4 activation from binding

and inhibition of HIV-1. *EMBO J.* (1997) 16:6996–7007. doi: 10.1093/emboj/16.23.6996
88. Brown AJ, Sepuru KM, Rajarathnam K. Structural Basis of Native CXCL7 monomer binding to CXCR2 receptor N-domain and glycosaminoglycan heparin. *Int J Mol Sci.* (2017) 18:508. doi: 10.3390/ijms18030508
89. Graham GJ, Handel TM, Proudfoot AEI. Leukocyte Adhesion: Reconceptualizing Chemokine Presentation by Glycosaminoglycans. *Trends Immunol.* (2019) 40:472–81. doi: 10.1016/j.it.2019.03.009
90. Tsai CJ, Lin SL, Wolfson HJ, Nussinov R. Studies of protein-protein interfaces: a statistical analysis of the hydrophobic effect. *Protein Sci.* (1997) 6:53–64. doi: 10.1002/pro.5560060106
91. Nadassy K, Wodak SJ, Janin J. Structural features of protein-nucleic acid recognition sites. *Biochemistry.* (1999) 38:1999–2017. doi: 10.1021/bi982362d
92. Fromm JR, Hileman RE, Caldwell EE, Weiler JM, Linhardt RJ. Differences in the interaction of heparin with arginine and lysine and the importance of these basic amino acids in the binding of heparin to acidic fibroblast growth factor. *Arch Biochem Biophys.* (1995) 323:279–87. doi: 10.1006/abbi.1995.9963
93. Joseph PR, Sawant K, Iwahara J, Desai UR, Garofalo R, Rajarathnam K. Lysines and Arginines play non-redundant roles in mediating chemokine-glycosaminoglycan interactions. *Sci Rep.* (2018) 8:12289. doi: 10.1038/s41598-018-30697-y
94. Mulloy B, Forster MJ. Conformation and dynamics of heparin and heparan sulfate. *Glycobiology.* (2000) 10:1147–56. doi: 10.1093/glycob/10.11.1147
95. Zandarashvili L, Esadze A, Iwahara J. NMR studies on the dynamics of hydrogen bonds and ion pairs involving lysine side chains of proteins. *Adv Protein Chem Struct Biol.* (2013) 93:37–80. doi: 10.1016/B978-0-12-416596-0.00002-6
96. Esadze A, Chen C, Zandarashvili L, Roy S, Pettitt BM, Iwahara J. Changes in conformational dynamics of basic side chains upon protein-DNA association. *Nucleic Acids Res.* (2016) 44:6961–70. doi: 10.1093/nar/gkw531
97. Sepuru KM, Rajarathnam K. Distinct differences in structural states of conserved histidines in two related proteins: NMR studies of chemokines CXCL1 and CXCL8 in the free form and macromolecular complexes. *Biochemistry.* (2018) 57:5969–77. doi: 10.1021/acs.biochem.8b00756
98. Capila I, Linhardt RJ. Heparin-protein interactions. *Angew Chem Int Ed.* (2002) 41:391–412. doi: 10.4172/2168-9652.1000241
99. Sarkar A, Desai UR. Simple method for discovering druggable, specific glycosaminoglycan-protein systems. elucidation of key principles from heparin/heparan sulfate-binding proteins. *PLoS One.* (2015) 10:e0141127. doi: 10.1371/journal.pone.0141127
100. Brown AJ, Joseph PB, Sawant K, Rajarathnam K. Chemokine CXCL7 Heterodimers: structural insights, CXCR2 receptor function, and glycosaminoglycan interactions. *Int J Mol Sci.* (2017) 18:748. doi: 10.3390/ijms18040748
101. Liang WG, Triandafillou CG, Huang TY, Zulueta MM, Banerjee S, Dinner AR, et al. Structural basis for oligomerization and glycosaminoglycan binding of CCL5 and CCL3. *Proc Natl Acad Sci USA.* (2016) 113:5000–5. doi: 10.1073/pnas.1523981113
102. Deshauer C, Morgan AM, Ryan EO, Handel TM, Prestegard JH, Wang X. Interactions of the chemokine CCL5/RANTES with medium-sized chondroitin sulfate ligands. *Structure.* (2015) 23:1066–77. doi: 10.1016/j.str.2015.03.024
103. Xu D, Arnold K, Liu J. Using structurally defined oligosaccharides to understand the interactions between proteins and heparan sulfate. *Curr Opin Struct Biol.* (2018) 50:155–61. doi: 10.1016/j.sbi.2018.04.003
104. Zhang X, Lin L, Huang H, Linhardt RJ. Chemoenzymatic synthesis of glycosaminoglycans. *Acc Chem Res.* (2010) 53:335–46. doi: 10.1021/acs.accounts.9b00420
105. Zulueta MM, Lin SY, Hu YP, Hung SC. Synthetic heparin and heparan sulfate oligosaccharides and their protein interactions. *Curr Opin Chem Biol.* (2013) 17:1023–9. doi: 10.1016/j.cbpa.2013.10.008
106. Glycan Therapeutics Available online at: https://www.glycantherapeutics.com/ (accessed April 16, 2020).
107. Nagarajan B, Sankaranarayanan NV, Desai UR. Perspective on computational simulations of glycosaminoglycans. *Wiley Interdiscip Rev Comput Mol Sci.* (2019) 9:2. doi: 10.1002/wcms.1388
108. Sankaranarayanan NV, Nagarajan B, Desai UR. So you think computational approaches to understanding glycosaminoglycan-protein interactions are too dry and too rigid? Think again! *Curr Opin Struct Biol.* (2018) 50:91–100. doi: 10.1016/j.sbi.2017.12.004
109. Samsonov SA, Gehrcke JP, Pisabarro MT. Flexibility and explicit solvent in molecular-dynamics-based docking of protein-glycosaminoglycan systems. *J Chem Inf Model.* (2014) 54:582–92. doi: 10.1021/ci400 6047
110. Singh A, Tessier MB, Pederson K, Wang X, Venot AP, Boons GJ, et al. Extension and validation of the GLYCAM force field parameters for modeling glycosaminoglycans. *Can J Chem.* (2016) 94:927–35. doi: 10.1139/cjc-2015-0606
111. Kozakov D, Hall DR, Xia B, Porter KA, Padhorny D, Yueh C, et al. The ClusPro web server for protein-protein docking. *Nat Protoc.* (2017) 12:255–78. doi: 10.1038/nprot.2016.169
112. Gandhi NS, Mancera RL. Free energy calculations of glycosaminoglycan–protein interactions. *Glycobiology.* (2009) 19:1103–15. doi: 10.1093/glycob/cwp101
113. Mulloy B, Hogwood J, Gray E, Lever R, Page CP. Pharmacology of heparin and related drugs. *Pharmacol Rev.* (2016) 68:76–141. doi: 10.1124/pr.115.011247
114. Alquwaizani M, Buckley L, Adams C, Fanikos J. Anticoagulants: a review of the pharmacology, dosing, and complications. *Curr Emerg Hosp Med Rep.* (2013) 1:83–97. doi: 10.1007/s40138-013-0014-6
115. Morla S. Glycosaminoglycans and Glycosaminoglycan Mimetics in Cancer and Inflammation. *Int J Mol Sci.* (2019) 20:8. doi: 10.3390/ijms20081963
116. Clinical Trials Available online at: https://clinicaltrials.gov/ct2/show/NCT02026765 (accessed April 16, 2020).
117. Clinical Trials Available online at: https://clinicaltrials.gov/ct2/show/NCT02135770 (accessed April 16, 2020).
118. Clinical Trials Available online at: https://clinicaltrials.gov/ct2/show/NCT00986076 (accessed April 16, 2020).
119. Clinical Trials Available online at: https://clinicaltrials.gov/ct2/show/NCT03539718 (accessed April 16, 2020).
120. Patel NJ, Sharon C, Baranwal S, Boothello RS, Desai UR, Patel BB. Heparan sulfate hexasaccharide selectively inhibits cancer stem cells self-renewal by activating p38 MAP kinase. *Oncotarget.* (2016) 7:84608–22. doi: 10.18632/oncotarget.12358
121. Guerrini M, Beccati D, Shriver Z, Naggi A, Viswanathan K, Bisio A, et al. Oversulfated chondroitin sulfate is a contaminant in heparin associated with adverse clinical events. *Nat Biotechnol.* (2008) 26:669–75. doi: 10.1038/nbt1407
122. Lohmann N, Schirmer L, Atallah P, Wandel E, Ferrer RA, Werner C, et al. Glycosaminoglycan-based hydrogels capture inflammatory chemokines and rescue defective wound healing in mice. *Sci Transl Med.* (2017) 9:386. doi: 10.1126/scitranslmed.aai9044

Conflict of Interest: The authors declare that the research was conducted in the absence of any commercial or financial relationships that could be construed as a potential conflict of interest.

frontiers in Immunology

ORIGINAL RESEARCH
published: 28 April 2020
doi: 10.3389/fimmu.2020.00732

MASP-2 Is a Heparin-Binding Protease; Identification of Blocking Oligosaccharides

Ditmer T. Talsma[1], Felix Poppelaars[1], Wendy Dam[1], Anita H. Meter-Arkema[1], Romain R. Vivès[2], Peter Gál[3], Geert-Jan Boons[4,5], Pradeep Chopra[5], Annamaria Naggi[6], Marc A. Seelen[1], Stephan P. Berger[1], Mohamed R. Daha[1], Coen A. Stegeman[1], Jacob van den Born[1] and the COMBAT Consortium*

[1] Department of Nephrology, University Medical Center Groningen, Groningen, Netherlands, [2] Univ. Grenoble Alpes, CNRS, CEA, IBS, Grenoble, France, [3] Institute of Enzymology, Research Centre for Natural Sciences, Budapest, Hungary, [4] Department of Chemical Biology and Drug Discovery, Utrecht Institute for Pharmaceutical Sciences, and Bijvoet Center for Biomolecular Research, Utrecht University, Utrecht, Netherlands, [5] Complex Carbohydrate Research Center, University of Georgia, Athens, GA, United States, [6] Ronzoni Institute, Milan, Italy

OPEN ACCESS

Edited by:
Megan S. Lord, University of New South Wales, Australia

Reviewed by:
Jeremy Turnbull, University of Liverpool, United Kingdom
Douglas Philip Dyer, University of Manchester, United Kingdom

***Correspondence:**
Jacob van den Born
j.van.den.born@umcg.nl

Specialty section:
This article was submitted to Molecular Innate Immunity, a section of the journal Frontiers in Immunology

Received: *09 October 2019*
Accepted: *31 March 2020*
Published: *28 April 2020*

Citation:
Talsma DT, Poppelaars F, Dam W, Meter-Arkema AH, Vivès RR, Gál P, Boons G-J, Chopra P, Naggi A, Seelen MA, Berger SP, Daha MR, Stegeman CA, van den Born J and the COMBAT Consortium (2020) MASP-2 Is a Heparin-Binding Protease; Identification of Blocking Oligosaccharides. Front. Immunol. 11:732. doi: 10.3389/fimmu.2020.00732

It is well-known that heparin and other glycosaminoglycans (GAGs) inhibit complement activation. It is however not known whether fractionation and/or modification of GAGs might deliver pathway-specific inhibition of the complement system. Therefore, we evaluated a library of GAGs and their derivatives for their functional pathway specific complement inhibition, including the MASP-specific C4 deposition assay. Interaction of human MASP-2 with heparan sulfate/heparin was evaluated by surface plasmon resonance, ELISA and in renal tissue. *In vitro* pathway-specific complement assays showed that highly sulfated GAGs inhibited all three pathways of complement. Small heparin- and heparan sulfate-derived oligosaccharides were selective inhibitors of the lectin pathway (LP). These small oligosaccharides showed identical inhibition of the ficolin-3 mediated LP activation, failed to inhibit the binding of MBL to mannan, but inhibited C4 cleavage by MASPs. Hexa- and pentasulfated tetrasaccharides represent the smallest MASP inhibitors both in the functional LP assay as well in the MASP-mediated C4 assay. Surface plasmon resonance showed MASP-2 binding with heparin and heparan sulfate, revealing high Kon and Koff rates resulted in a Kd of $\sim 2\,\mu M$ and confirmed inhibition by heparin-derived tetrasaccharide. In renal tissue, MASP-2 partially colocalized with agrin and heparan sulfate, but not with activated C3, suggesting docking, storage, and potential inactivation of MASP-2 by heparan sulfate in basement membranes. Our data show that highly sulfated GAGs mediated inhibition of all three complement pathways, whereas short heparin- and heparan sulfate-derived oligosaccharides selectively blocked the lectin pathway via MASP-2 inhibition. Binding of MASP-2 to immobilized heparan sulfate/heparin and partial co-localization of agrin/heparan sulfate with MASP, but not C3b, might suggest that *in vivo* heparan sulfate proteoglycans act as a docking platform for MASP-2 and possibly prevent the lectin pathway from activation.

Keywords: lectin pathway, MASP-2, tetrasaccharide, heparin, complement, glycosaminoglycans

INTRODUCTION

As a part of the innate immune system, complement consists of soluble, and cell bound proteins. The complement system is activated *via* three different pathways; the classical pathway (CP), lectin pathway (LP), and alternative pathway (AP). The CP is initiated by the binding of C1q to IgG or IgM and the LP by pattern recognition molecules binding to carbohydrates of pathogens or self-antigen. This leads to a conformational change and subsequent activation of the associated serine proteases C1r/C1s and MASP-1/MASP-2, respectively. These serine proteases cleave C2 and C4, forming the C4bC2a complex, a C3 convertase which deposits C3b initiating the amplification loop. The AP can be initiated either by auto activation of C3 eventually forming the C3 convertase C3bBb, or by *in situ* binding of AP stimulator properdin to the cell surface. Formation of the C5 convertase in the end leads to the generation of the C5b-9 membrane attack complex, resulting in cell lysis (1).

In the field of nephrology, complement has gained increased attention in recent years as studies have identified complement as a key player in multiple renal diseases. The classical pathway (CP) has been shown to play a major role in the auto-immune disease lupus erythematosus (2). In addition, lectin pathway (LP) components, either in plasma, or deposited within the kidney, have been correlated to disease progression following human kidney transplantation and hemodialysis, IgA nephropathy and diabetic nephropathy (3–6). Furthermore, it has been shown that mannan binding lectin (MBL) and collectin-11 recognize epitopes in I/R damaged kidneys and increase I/R induced damage (7, 8). Finally, the alternative pathway (AP) has been identified as a factor in the physiopathology of dense deposit disease, C3 glomerulopathy, atypical hemolytic uremic syndrome, and progression of proteinuric renal diseases (9–13). Therefore, complement-targeted therapies can potentially be of great use in a variety of renal diseases and conditions.

The *in vivo* inhibitory potential of heparin on the complement system has been known for ∼25 years (14). Since then, numerous interactions have been described between glycosaminoglycans (GAGs) such as heparin, and complement components. In the lectin route of complement, anti-thrombin bound to heparin is a strong inhibitor of C4 cleavage by MASPs (15). Besides the lectin pathway, heparin can also block the classical pathway by directly inhibiting the C1q subunit of C1 or by potentiating the effect of C1-inhibitor (16–18). Studies by our group showed that the binding of both properdin, an alternative pathway initiator and stabilizer, and factor H, an alternative pathway inhibitor, to heparan sulfates (HS) on proximal tubular epithelial cells can be prevented by heparin and some other GAGs (12, 13). Combined, these studies indicate that GAGs have the potential to inhibit different components of the three pathways of the complement system.

Proteoglycans are glycoconjugates consisting of a core protein to which GAGs are covalently attached. Proteoglycans, such as the members of the syndecan and the glypican families, can be found on the cell membrane, others like versican, perlecan, and agrin are found in the extracellular matrix. Membrane proteoglycans function as highly abundant, relatively low affinity co-receptors for growth factors, chemokines, and adhesion molecules and modulate proliferation, migration, and adhesion events (19). Matrix-associated proteoglycans mostly function as storage depot for mediators, which can be released for paracrine functions upon tissue remodeling by proteases, sulfatases, and/or heparanase (20–22). GAGs consist of repetitive disaccharide units, which can be modified enzymatically in their length and sulfation pattern to alter their binding capacity and function. The effects on binding capacity and pharmacokinetics of GAG length modifications have been known for some time and have led to the introduction of low molecular weight heparins. Modifications of heparan sulfate (HS) sulfation are well-known from *in vivo* modifications of proteoglycan side chains upon stimuli like inflammation and fibrosis (23, 24). HS/Heparin can carry sulfate groups on the N position and/or on the 3-O, 6-O, and 2-O position of glucosamine and iduronic acid residues, respectively. Degree of sulfation is positively correlated to the electro-negativity of HS/Heparin and therefore to their binding capacity, making it an important factor in various cellular functions. It has for example been shown that the binding of heparin to anti-thrombin III depends on a specific pentasaccharide structure, in which 3-O sulfation is essential (25). Moreover, our group has shown that properdin and factor H require different GAG sulfation patterns for HS binding (13). These examples illustrate the important role of chain length and sulfation pattern of GAGs for specific interactions related to biological properties.

In this study, we aimed at identifying pathway-specific complement inhibiting GAGs from a library of natural and enzymatically and chemically modified and/or depolymerized GAGs. We show that small heparin- and HS-derived oligosaccharides are specific inhibitors of the LP of complement and that these sugars inhibit the LP *via* inhibition of the MASP-2 enzyme. By surface plasmon resonance we confirm MASP-2 to be a HS/heparin binding protein. Moreover, we provide some evidence that HS proteoglycans *in situ* might bind and eventually regulate MASP-2 *in vivo*.

MATERIALS AND METHODS

Polysaccharides

Heparin from ovine intestinal mucosa, heparin from bovine lung, heparin (∼2.5 sulfate groups/disacch) and HS from porcine intestinal mucosa (∼1.0 sulfate groups/disacch), Chondroitin sulfate-A, -B, -and C, dextran T40, dextran sulfate, fucoidan, were purchased from Sigma (Sigma, Zwijndrecht, The Netherlands). Nadroparin (Fraxiparine®) was purchased from Sanofi Winthrop (Maassluis, The Netherlands), Dalteparin (Fragmin®) was purchased from Pharmacia & Upjohn, and enoxaparin (Clexane®) was purchased from Rhone-Poulenc Rorer (Paris, France). HS isolated from bovine kidney (∼0.8 sulfate groups/disacch) or from Engelbreth-Holm-Swarm sarcoma (∼0.6 sulfate groups/disacch) were obtained from Seikagaku Corp (Tokyo, Japan). *Escherichia coli* capsular polysaccharide K5, with the same $(GlcUA\rightarrow GlcNAc)_n$ structure as the non-sulfated HS/heparin biosynthetic precursor polysaccharide (0.0 sulfate groups/disacch) (26); *O*-sulfated K5 and low molecular weight *O*-sulfated K5; were kindly provided

by Dr. G. van Dedem (Diosynth, Oss, The Netherlands), as well as the heparin-derived octasaccharides (Org32100), hexasaccharides (Org 32101), and tetrasaccharides (Org 32102). HS from bovine intestine was kindly provided by Marco Maccarana (Department of Experimental Medical Science, Biomedical Center, University of Lund, Sweden) (27). HS from human aorta was isolated essentially as described by Iverius (∼0.6 sulfate groups/disacch) (28). *N* + *O*-sulfated K5 was produced by *N*-deacetylation (hydrazinolysis), subsequent *N*-sulfation with sulfur trioxide-trimethylamine (29) of O-sulfated K5, followed by *N*-acetylation. Heparin and HS-derived oligosaccharides were prepared as previously described (30, 31) by partial heparinase I (Grampian enzymes, Orkney, UK) depolymerization of porcine mucosal heparin and exhaustive digestion of porcine mucosal HS with heparinase III (Grampian enzymes). Disaccharide analysis of SAGAG heparin tetrasaccharides was achieved by reverse-phase ion-pair high-performance liquid chromatography (RPIP-HPLC) as described before (32). Treatment of heparin by the 6-O-endosulfatase HSulf-2 was performed as described previously (33), for details on the disaccharide composition, see (34). Enoxaparin tetrasaccharides (Ron G11237) were kindly provided by dr. Annamaria Naggi (Ronzoni Institute, Milan, Italy) isolated and characterized by NMR spectroscopy as described before (35), N-desulfated, re-acetylated heparin and periodate-oxidized and reduced heparin were also provided by dr. Annamaria Naggi and were prepared and characterized as described before (36). Synthetic HS tetrasaccharides were kindly provided by prof. dr. G.J.P.H. Boons (Pharmacy, State University of Utrecht, The Netherlands) and were produced as described before (37).

Wieslab Pathway-Specific Complement Assay

The Wieslab complement assay (WieLISA) kits were obtained from Euro Diagnostica, Malmö, Sweden. The WieLISA assay is a straightforward ELISA-based format for the evaluation of the three pathways of complement activation. The assays are based on specific coatings for each pathway in combination with specific buffer systems and measure the deposition of the terminal C5b-9 MAC complex. The measurement of the lectin pathway is either done by using mannan coated plates, allowing binding of the MBL-MASP complex from serum (in the standard WieLISA assay), or by using acetylated BSA coated plated, allowing binding of ficolin-3-MASP complexes from serum (in the ficolin-3 LP assay). The assays have been described by Seelen et al. (38). Positive control serum delivered with the kits was used as serum source for all measurements. GAGs were diluted in route specific buffer delivered with the kit. Final GAG concentration was 100 μg/ml in the CP and LP assay and due to a higher incubated serum concentration 200 μg/ml in the AP assay. Serum was added to the diluted GAGs right before the plates were incubated at 37°C for 60 min. Except for the serum (+/– GAGs) incubation, the kit protocol was followed. Data were expressed as % inhibition compared to the positive control. Dose dependent assays with variable amounts of GAGs were performed as described above. Data was presented as representative experiments.

MBL Binding Assay

To evaluate whether GAGs could inhibit the mannan—MBL interaction, Maxisorp immunoassay plates were incubated overnight with 100 μg/ml mannan (Sigma, Zwijndrecht, The Netherlands) diluted in 0,1 M $NaCO_3$, pH 9,6. After washing three times, plates were blocked with 1% BSA in PBS for 1 h. Thereafter, pooled serum diluted 1:50 in GVB++ buffer, described by Roos et al. (39), were pre-incubated with a concentration range of GAGs, for 15 min at room temperature. GVB++ buffer is Veronal-buffered saline (1,8 mM Na-5,5-diethylbarbital, 0,2 mM 5,5-diethylbarbituric acid, 145 mM NaCl) containing 0,5 mM MgCl2, 2 mM CaCl2, 0,05% Tween-20 and 0,1% gelatin, pH 7.5. The pre-incubated mixture was then incubated for 60 min on the mannan coated plates at 37°C. In the dose dependent binding of MBL to mannan, no GAGs were added. Bound MBL was detected with a DIG-labeled mouse anti-human MBL antibody 1:1,000 (mAb 3e7 from Hycult Biotech, Uden, the Netherlands) and a Sheep anti-DIG HRP labeled conjugate 1:8,000 (Roche Diagnostics, Mannheim, Germany). The assay was developed using tetramethylbenzidine (TMB) (Sigma, Zwijndrecht, The Netherlands) and the reaction was stopped with 1 M H2SO4. Absorbance was measured at 450 nm in a microplate reader. Data was expressed as % inhibition compared to non-inhibited control. Data was presented as representative experiment.

C4 Inhibition Assays

To evaluate whether GAGs inhibit the C4 cleavage (by C4d deposition) by MASPs, we performed a C4 cleaving assay, as first described by Petersen and colleagues (40). Maxisorp immunoassay plates were incubated overnight with 100 μg/ml mannan (Sigma, Zwijndrecht, The Netherlands) diluted in 0,1 M $NaCO_3$, pH 9,6. Thereafter, plates were blocked for 1 h using 10 mM Tris-HCl, 140 mM NaCl, 0,1% BSA, pH 7,4. Next, pooled serum diluted 1:100 in 20 mM Tris-HCl, 10 mM $CaCl_2$, 1 M NaCl, 0,05% Triton X-100, 0,1% BSA, pH 7,4 was incubated overnight at 4°C, allowing the MBL/MASP complex to bind to mannan, but prevents MASP activation and subsequent complement activation. Incubation of serum in 1 M NaCl was done to prevent classical pathway activation through anti-mannan IgG3 antibodies, prevalent in the majority of the healthy population. High ionic buffers prevent the binding of C1q to immune complexes and disrupt the C1 complex, whereas the carbohydrate-binding activity of MBL and the integrity of the MBL complex are maintained under hypertonic conditions. After washing, MBL/MASP coated plates were pre-incubated with 50 μl GAG at twice the final concentration in 10 mM Tris-HCl, 140 mM NaCl, 5 mM $CaCl_2$, 0,05% Tween, 0,1% BSA, pH 7,4 for 30 min at 37°C. Non-inhibited control wells were incubated with buffer only. Without washing, 50 μl of 5 μg/ml purified C4 (Hycult Biotech, Uden, the Netherlands) diluted in 10 mM Tris-HCl, 140 mM NaCl, 5 mM $CaCl_2$, 0,05% Tween, 0,1% BSA, pH 7,4 was added to the pre-incubated GAGs and incubated for 1 h at 37°C. After washing, C4d deposition was detected using a DIG

labeled mouse anti-human C4 antibody, diluted 1:4,000, followed by incubation with a Sheep anti-DIG HRP labeled antibody (Roche Diagnostics, Mannheim, Germany, dilution 1:8,000). The assay was developed using TMB (Sigma, Zwijndrecht, The Netherlands) and the reaction was stopped with 1 M H_2SO_4. Absorbance was measured at 450 nm in a microplate reader. Data was expressed as % inhibition compared to non-inhibited control. Experiments were independently reproduced in triplicate.

Heparin-MBL/MASP Interaction ELISA

In three independent experiments, we tested the binding of serum MASP-2 and recombinant MASP2 to heparin. To this end, we coated Maxisorp immunoassay plates overnight with 5 μg/ml heparin-albumin or 5 μg/ml albumin diluted in PBS. Heparin-albumin was from Sigma-Aldrich (Saint Louis, MO, USA). According to the data sheet, this artificial proteoglycan contained 4.8 moles heparin per mole albumin, protein content is about 55%. After washing, plates were blocked using 1% BSA in PBS for 1 h. Thereafter, recombinant MASP2 or pooled human serum diluted in GVB++ buffer was incubated for 2 h at 4°C. Binding of MASP-2 was detected by incubating rat anti-human MASP-2 (Hycult Biotech, Uden, the Netherlands) diluted at 1:200 in PBS, 1% BSA and 0,05% Tween. Rabbit anti-Rat HRP labeled (DAKO, Glostrup, Denmark) diluted 1:500 in PBS, 1% BSA and 0,05% Tween was incubated for 1 h. The assay was developed using TMB (Sigma, Zwijndrecht, The Netherlands), the reaction was stopped with 1 M H_2SO_4. Absorbance was measured at 450 nm in a microplate reader.

Surface Plasmon Resonance Analysis

To define the binding affinity of MASP-2 to heparin derivatives surface plasmon resonance (SPR) experiments were performed using recombinant human MASP-2 protein containing the catalytic fragment (CCP1-CCP2-SP), which was prepared as described earlier (41). All experiments were performed on a BIAcore T200 (GE healthcare), using as previously described standard procedures and GAG biotinylation techniques (40). Briefly, reducing-end biotinylated 6 and 15 kDa heparin, and HS (porcine mucosa) were captured on three streptavidin-activated flowcells of a S-CM4 sensorchip (41.2 and 44.1 RU for 6 and 15 kDa heparin respectively, and 61.9 RU for HS, a fourth one being used as negative control surface. Using HBS-P+ running buffer (10 mM HEPES, 150 mM NaCl, 0.05% surfactant P20, pH 7.4) at a flow rate of 20 μl/min, series of 0–3,000 nM of MASP-2 were injected over the heparin, HS and negative control surfaces, followed by a 3 min washing step with HBS-P+ buffer to allow dissociation of the complexes formed. At the end of each cycle, surfaces were regenerated with a 2.5 min injection of 2M NaCl. Sensorgram shown correspond to on-line subtraction of the negative control to the heparin surface signal. Kds were determined using the BIAcore T200 evaluation (version 3.1) software, by steady state analysis (1:1 binding model). For this, resonance values (Req) were taken within the equilibrium phase (just before the end of injection) and plotted against MASP-2 concentration. Calculated $\chi 2$ values provided quality control of experimental data fitting. Competition assays were performed similarly, by injecting 200 nM of MASP-2 pre-incubated with GAGs (30 μg/ml) over the heparin and negative control surfaces. Tested GAGs included a heparin tetrasaccharide (ΔHexA2S-GlCNS6S-IdoA2S-GlcNS6S) and chondroitin sulfate A, B and C, the 15 kDa heparin being used as a positive control (also 30 μg/ml, a 10-fold excess compared to the concentration used to load the sensor chip). Noteworthy, this experiments was conducted using fixed tetrasaccharide and heparin mass concentrations to reflect the fact that a 15 kDa heparin chain comprises multiple highly sulfated tetrasaccharide (composition of 15 kDa Heparin is provided in Seffouh et al. (42). All experiments were independently replicated three times.

Immunohistochemistry

Four μm frozen kidney sections of five human donor kidneys not suitable for transplantation for anatomical reasons were used for immunofluorescent stainings. Sections were double stained for MASP-2 in combination with the basement membrane HS proteoglycan agrin, or in combination with HS (clone 10E4 recognizing mixed N-sulfated/N-acetylated sequences) or triple stained with HS and activated complement factor C3 (recognizing a neoepitope on C3b, iC3b, and C3c after cleavage of C3 by C3-convertase). Details of the immunofluorescence procedures and the antibodies used are given in **Table 1**. Photomicrographs were taken at 630x magnification with confocal microscope (Leica SP8, Leica microsystems BV, Rijswijk, the Netherlands) at the Imaging and Microscopy Center of the University Medical Center Groningen.

RESULTS

Small Heparan Sulfate- and Heparin-Derived Oligosaccharides Specifically Inhibit the Lectin Pathway, While Longer Highly Sulfated GAGs Block All Three Routes of Complement

A library of naturally, chemically, or enzymatically modified and synthetic GAGs, as well as size-defined HS/heparin depolymerization products were tested for their complement inhibiting potential in the WieLISA, which allows separate evaluation of the three pathways of the complement system. From the results (**Table 2**), it can be seen that unfractionated heparins inhibited all three complement pathways. Heparin from different sources e.g., porcine intestinal mucosa and bovine lung showed strong inhibitory potential for all pathways.

Selective desulfation of heparin, either 6-O desulfation by SULF2 (80% reduction of the 6-O content in NS2S6S disaccharides), or by chemical N-desulfation followed by reacetylation, resulted in some loss of complement inhibitory potential, mostly in the classical and alternative route.

Periodate-oxidized and reduced heparin is a non-anticoagulant heparin derivate in which the structure of the antithrombin binding site was modified, and the results in **Table 2** show that despite losing the ability to interact with antithrombin III, it remained able to inhibit all complement pathways. LMW-heparins like fragmin, fraxiparin and

TABLE 1 | Details on immunofluorescence stainings on human cryosections.

Procedure	MASP-2	Agrin	Heparan sulfate	Activated C3
Fixation	Icecold 100% aceton for 10 min	Icecold 100% aceton for 10 min	Icecold 100% aceton for 10 min	Icecold 100% aceton for 10 min
Peroxidase inactivation	0.03% H_2O_2 in PBS for 30 min in the dark	–	–	–
Blocking a-specific background	1% BSA in PBS for 15 min	1% BSA in PBS for 15 min	1% BSA in PBS for 15 min	1% BSA in PBS for 15 min
Blocking endogenous biotin	–	–	Avidin/Biotin blocking kit (SP-2001; Vector Laboratories; Burlingame CA, USA)	–
Primary antibody	Rat mAb anti-human MASP-2, clone 8B5, 1:100 (Hycult, Uden, The Netherlands)	Mouse mAb JM-72 anti-human agrin, 1:750 (43)	Biotinylated mouse mAb anti-heparan sulfate, clone 10E4, 1:50 (Amsbio, Abingdon, UK)	Mouse IgG2a mouse mAb anti-neoepitope on C3b, iC3b and C3c, clone bH6, 1:200 (Hycult)
Secondary antibody	Rabbit anti-rat IgG-HRP, 1:200 + 5% normal human serum for (Dako, Glostrup, Denmark)	Donkey anti-Mouse IgG-Alexa 488, 1:250 (Life Technologies, Carlsbad CA, USA)	–	Donkey anti-mouse IgG-Alexa647, 1:250 (Life Technologies, Carlsbad CA, USA)
Tertiary antibody	Goat anti-rabbit IgG-HRP, 1:200 + 5% normal human serum (Dako)	–	–	–
Amplification HRP signal	TSA Tyramide-TRITC, 1:50 for 10 min (PerkinElmer, Waltham MA, USA)	–	–	–
Detection biotinylated antibody	–	–	Streptavidin-FITC, 1:300 (Invitrogen, Waltham MA, USA)	–
Nuclear staining	Dapi for 10 min	Dapi for 10 min	Dapi for 10 min	Dapi for 10 min
Embedment	Citifluor (Haffield PA, USA)	Citifluor (Haffield PA, USA)	Citifluor (Haffield PA, USA)	Citifluor (Haffield PA, USA)

Stainings are performed as MASP2/agrin double staining, as MASP2/HS double staining, and as MASP2/HS/actC3 triple staining.
All antibody incubations were done for 30 min at room temperature in PBS + 1% BSA. Sections were washed with PBS in between the incubation steps. Double- and triple stainings were designed in such a way that all cross-reactions among the stainings were avoided.

enoxaparin are widely used in the clinic as anticoagulants and showed strong potential to inhibit the three complement pathways. N-desulfation followed by reacetylation of LMW heparin reduced the ability to inhibit all complement pathways, mostly the classical pathway. Size fractionation products of limited heparinase I treated heparin showed that smaller heparin fragments retain their ability to inhibit the LP, but were no longer able to inhibit the CP and AP, indicating that GAG chain length is a major determinant for CP and AP inhibition. The smallest heparin fragment tested, i.e., tetrasaccharides (4-mer), were found to be completely selective for inhibition of the LP.

Escherichia coli -derived K5 polysaccharides share their polysaccharide backbone with heparin except that K5 polysaccharides carry exclusively GlcA uronic acid epimers, while heparin features >80% IdoA C5 uronic epimers. Native K5 does not contain any sulfate groups and did not inhibit the complement system. O-sulfated and N + O-sulfated K5 both showed equally strong inhibitory capacity for all three complement pathways, indicating that neither GlcA to IdoA conversion nor N-sulfation (next to O-sulfation) is crucial for complement inhibition, when the density of O-sulfates is high enough (∼1,5 O-sulfates/disacch in O-sulfated K5). O-sulfated K5 hexasaccharide did not inhibit the complement unlike heparin hexasaccharides (see above). Whether this is due to different positioning of the O-sulfate groups is unknown, but suggestive, which in regular heparin is mostly IdoA2S-GlcNs6S, and in chemically O-sulfated K5 mostly at C2 and C3 of GlcA along with N-sulfation of Glc units.

We also tested GAGs and polysaccharides with a different backbone structure than heparin. These results indicate that the chemical nature of the monosaccharides and their bonds between the monosaccharide units is of lesser importance compared to the degree of sulfation when looking at complement inhibitory potential. Highly sulfated polysaccharides like fucoidan and dextran sulfate and to a lesser extent sulodexide [mixture of heparin (80%) and dermatan sulfate (20%)] showed inhibition of all complement pathways. Chondroitin sulfate B (dermatan sulfate) with an intermediate amount of sulfates and high content of iduronic acid showed some inhibition of the LP, but not of the CP and AP, while chondroitin sulfates -A and -C and the non-sulfated dextran T40 didn't inhibit the three complement routes.

HS have a slightly different disaccharide composition compared to heparin and are less and more variably sulfated (25, 44). HS from different sources (e.g., bovine kidney and porcine

TABLE 2 | Complement inhibition by heparin(oids), (derivatives of) K5 polysaccharide, (derivatives of) heparan sulfates, and some other glycosaminoglycans.

Glycosaminoglycans	Classical pathway	Lectin pathway	Alternative pathway	Repeats
HEPARINS AND HEPARIN DERIVATIVES				
Porcine intestinal mucosa	73 (12)	97 (1)	94 (5)	2
Ovine intestinal mucosa	83	97	96	1
Bovine lung	66	90	74	1
SULF-2 treated heparin	54	96	48	1
N-desulfated, re-acetylated heparin	6	52	42	1
Periodate-oxidized and reduced heparin	60	91	97	1
LMW-heparin (Fragmin) Mw: 6000	73	98	98	1
LMW-heparin (Fraxiparin) Mw: 4500	48	95	92	1
LMW-heparin (Enoxaparin) Mw: 4500	65	97	95	1
LMW N-desulfated, reacetylated heparin	8	46	44	1
Heparin-derived 18-mer	13	71	20	1
Heparin-derived 16-mer	27	90	25	1
Heparin-derived 14-mer	26	92	35	1
Heparin-derived 12-mer	26	94	38	1
Heparin-derived 10-mer	14	87	21	1
Heparin-derived 8-mer	20	93	26	1
Heparin-derived 6-mer	12	93	0	1
Heparin-derived 4-mer	0	74	0	1
***E. coli* K5-DERIVED POLYSACCHARIDES**				
Native K5	0	1	3	1
O-sulfated K5	100 (0)	88 (4)	92 (3)	3
N-+ O-sulfated K5	100	93	97	1
O-sulfated K5 hexasaccharides	0	2	0	1
GLYCOSAMINOGLYCANS				
Chondroitin sulfate A	3 (4)	6 (7)	8 (9)2	3
Chondroitin sulfate C	0 (0)	0 (0)	0 (0)	2
Chondroitin sulfate B (Dermatan sulfate)	5 (7)	39 (5)	10 (10)	3
Sulodexide	52	93	73	1
POLYSACCHARIDES				
Dextran T40	4	8	17	1
Dextran sulfate	100	99	100	1
Fucoidan	98	78	79	1
HEPARAN SULFATE AND HEPARAN SULFATE DERIVATIVES				
HS human aorta	5	23	7	1
HS EHS mouse sarcoma	17	31	22	1
HS bovine intestine	21	76	39	1
HS bovine kidney	2 (1)	73 (0)	18 (18)	2
HS porcine mucosa	9	95	26	1
Heparan sulfate derived 18-mer	5	91	25	1
Heparan sulfate derived 16-mer	11	92	32	1
Heparan sulfate derived 14-mer	4	92	18	1
Heparan sulfate derived 12-mer	0	93	3	1
Heparan sulfate derived 10-mer	0	87	0	1
Heparan sulfate derived 8-mer	0	74	0	1
Heparan sulfate derived 4-mer	0	0	0	1

A library of GAG-derived polysaccharides was tested in the WieLISA for their complement inhibiting potential. Values are expressed as percentage inhibition compared to control values without inhibitor as mean ± SD or from a single experiment. GAGs were added in a concentration of 100 ug/ml in the CP and LP assay and due to a higher serum concentration at 200 ug/ml in the AP assay.

mucosa) showed in general substantial LP inhibition without inhibiting the CP and AP. Smaller HS fragments were found to be more specific inhibitors of the LP. 12-mer, 10-mer and 8-mer HS fragments showed complete specificity for the LP and did not show any inhibition of the CP and AP (**Figures 1A,C,D**). The HS-derived 4-mer did not show any inhibitory capacity for any pathway (HS-derived 6-mer was not available) in contrast to heparin-derived tetrasaccharide, probably because of a lower degree of sulfation (**Table 2**).

To test the effect of GAG length on the inhibitory potential of the complement system, 5 heparin fragments ranging from unfractionated heparin to heparin-derived tetrasaccharides were tested in the WieLISA in a dose dependent fashion. As expected, unfractionated heparin showed the strongest inhibition in all pathways (**Figures 1A–C**). Interestingly, the LP was inhibited most potently by unfractionated heparin with an IC50 value of 2 μg/ml in 100-times diluted serum, in contrast to the CP (IC50: 39 μg/ml) and the AP (IC50: 76 μg/ml) (**Figure 1D**). Heparin octasaccharides and smaller heparin fragments become, up to the concentrations tested, specific LP inhibitors; IC50: octasaccharides: 3 μg/ml, hexasaccharides: 4 μg/ml and tetrasaccharides: 21 μg/ml (**Figure 1D**). These results indicate that a certain heparin chain length is required for inhibition of the CP and AP, while heparin fragments down to 4 saccharides in length can inhibit the LP.

To illustrate the effect of heparin/HS sulfation on the inhibitory capacity of complement, we selected 6 heparin/HS/K5 preparations with different sulfation degrees from **Table 1** and displayed them in **Figure 1E**. Heparin with >2,5 sulfate groups per disaccharide showed, as observed before, strong inhibitory potential for all complement pathways. A reduced number of sulfate groups to 1,0 or 0,8 per disaccharide, attenuated predominantly the ability to inhibit the CP and AP. Further lowering the sulfate content resulted in a reduced inhibition of all complement pathways (**Figure 1E**).

Altogether, all three complement pathways can be blocked by highly sulfated polysaccharides such as heparin, fucoidan, dextran sulfate and O-sulfated K5 and to a lesser extent by some HS preparations and dermatan sulfate. Specific complement inhibition of the LP is achieved by some HS preparations and small heparin- and HS-derived oligosaccharides.

Heparin Oligosaccharides Inhibit the Proteolytic Activity of MASPs and Thereby Reduce C4d Deposition

The previous results showed that HS/heparin-derived oligosaccharides can specifically inhibit the LP of complement. The LP differs from the CP only in the pattern recognition molecule: MBL (in the WieLISA) vs. C1q, and the serine proteases, MASP-1 and−2 vs. C1r and C1s. To pinpoint whether the small heparin oligosaccharides interfere with MBL or MASPs, the inhibitory effect of heparin (fragments) on the MBL-mannan interaction was tested. Serum was co-incubated with or without the heparin (fragments) on a mannan coated plate and MBL binding to mannan was used as a read out. MBL binding to mannan in the absence of inhibitors showed a dose

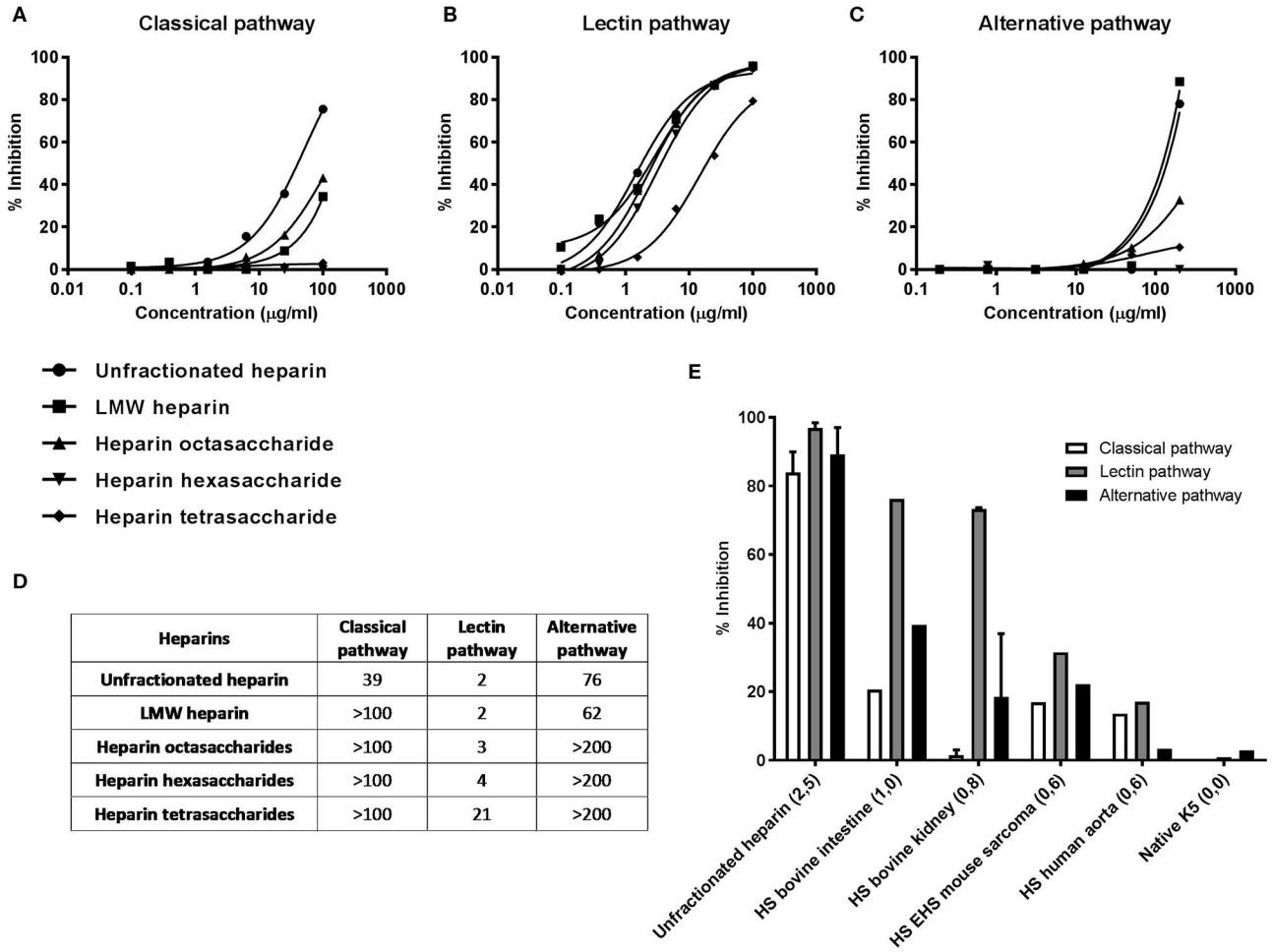

D

Heparins	Classical pathway	Lectin pathway	Alternative pathway
Unfractionated heparin	39	2	76
LMW heparin	>100	2	62
Heparin octasaccharides	>100	3	>200
Heparin hexasaccharides	>100	4	>200
Heparin tetrasaccharides	>100	21	>200

FIGURE 1 | Effect of GAG length and sulfation on complement inhibition. Complement inhibitory potential of selected heparin derivatives was evaluated in a dose dependent fashion. The concentration-response curves show that all heparin derivatives tested are strong LP inhibitors **(B)**, while the CP and AP are only inhibited by heparin and LMW heparin in concentrations of ≥50 μg/ml **(A,C)**. Heparin hexa-and tetrasaccharides are fully specific LP inhibitors **(A–C)**. **(D)** IC50 values (μg/ml) of the dose dependent inhibition assays **(A–C)** of the heparin fragments tested. **(E)** Illustration of the role of sulfation on complement inhibition. The average amount of sulfate groups per disaccharide is between brackets. Heparin shows inhibitory potential for all pathways. Reducing the number of sulfate groups per disaccharide results predominantly in a reduced potential to inhibit the CP and AP while the inhibitory potential for the LP is initially preserved. GAGs were tested at 100 (CP and LP) or 200 μg/ml (AP). Data shown are the result of a single experiment, after careful optimization of all conditions before. Heparin and HS from bovine kidney **(E)** as mean +/– SEM of two independent experiments.

dependent binding, a serum concentration of 1:50 was used for the inhibition experiments (OD: 0.96) (**Figure 2A**). The results revealed that none of the selected heparin preparations, which all inhibit the LP in the WieLISA, could inhibit the MBL binding to mannan in any of the concentrations tested (**Figure 2B**). To strengthen the conclusion that heparin did not interfere with the MBL-mannan interaction, heparin (fragments) were tested in a ficolin-3 mediated LP activity assay. This assay measures LP activity with ficolin-3 as pattern recognition molecule for immobilized acetylated BSA instead of MBL with immobilized mannan. In ficolin-3 mediated LP activation cleaving of C4 and C2 is, like in the MBL mediated route, dependent on MASP activity (45). The heparin (fragments) showed a dose dependent inhibitory pattern in the ficolin-3 mediated LP assay identical to the MBL mediated WieLISA (**Figure 2C** vs. **Figure 1B**). Unfractionated heparin showed the strongest inhibitory effect with an IC50 of 3 μg/ml. Decreasing the GAG length resulted in reduced inhibitory potential for LMW heparin, octasaccharides, hexasaccharides, and tetrasaccharides heparin (IC50: 7, 11, 16, and 342 μg/ml, respectively). Since the LP and CP differ only in their pattern recognition molecules and their serine proteases and we showed that the heparin (oligoaccharides) are unable to inhibit the binding of pattern recognition molecules to pathogen associated molecular patterns, we suggest, based on these data, that the LP is inhibited by heparin (oligosaccharides) via the serine proteases, the MASP enzymes.

To prove this assumpsion, we next used an assay to measure the C4 cleavage potential (by measuring C4d deposition)

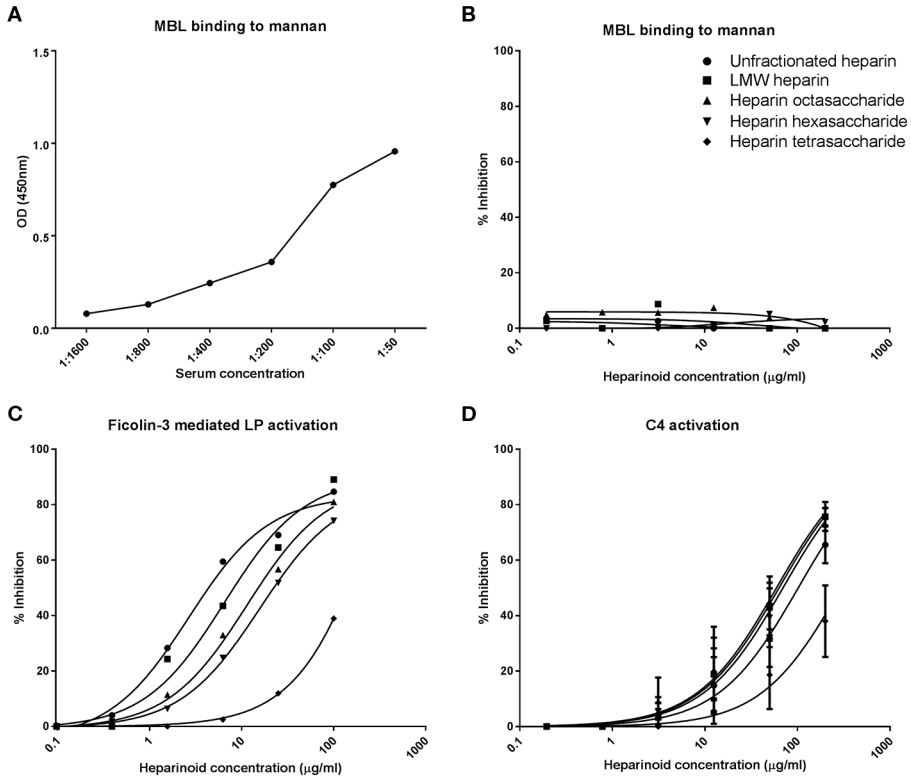

FIGURE 2 | Heparin-derived oligosaccharides inhibit the lectin pathway of complement *via* inhibition of C4d deposition. To determine which LP component is inhibited by heparin derivatives MBL and MASP inhibition were tested. Representative experiments show that MBL binds dose dependent to mannan **(A)**. Heparin derivatives did not inhibit the binding of MBL to mannan **(B)**. The selected heparin fragments did however show inhibition of the LP when the LP was initiated by ficolin-3 binding **(C)**. Heparin fragments did also show an inhibitory effect in a C4d deposition assay, as a measure for MASP-2 activity **(D)**. Data is expressed as a representative measurement **(A–C)** or as mean ± SEM of three independent experiments **(D)**.

of the MASPs. Since C4 is completely cleaved by MASP-2 and not by MASP-1, this is predominantly a MASP-2 assay (46). Interestingly, unfractionated heparin showed a relatively mild inhibitory potential (IC50: 102 μg/ml) compared to the LMW-heparin enoxaparin, heparin oligosaccharide and heparin hexasaccharide (IC50: 63, 59, and 70 μg/ml, respectively). The weakest inhibitory effect was shown by the heparin tetrasaccharide with an IC50 of 296 μg/ml (**Figure 2D**). This assay revealed that heparin oligosaccharides inhibit the LP at the level of the MASP enzymes, most likely MASP-2, in a dose dependent manner.

Recombinant Human MASP-2 Shows Similar Binding Affinity for Short and Long HS GAGs

To further strengthen the hypothesis that heparin/HS fragments predominantly inhibit MASP-2 we performed SPR experiments to evaluate the binding kinetics between catalytically active recombinant human MASP-2 fragment (CCP1-CCP2-SP) and different heparin/HS preparations. **Figure 3A** shows the sensorgram of recMASP-2 binding to an immobilized 15 kDa heparin fragment. Immobilized HS (porcine mucosa) and 6 kDa LMW-heparin showed similar sensorgrams (**Supplementary Figure 1**). Interestingly the on and off rates were very fast indicating a transient interaction, which could indicate moderate affinity. In **Figure 3B** we show the fit of the experimental data for the binding of MASP-2 to 15 kDa heparin upon representative steady-state analysis. Calculations of the affinity indeed show Kd values between 1.5 and 2.0 μM for the heparins and HS tested (**Figure 3C**). The observation that MASP-2 showed similar affinity for the 6 kDa heparin and the 15 kDa heparin and HS (usually between 12 and 20 kDa) indicates that MASP-2 recognizes a rather short and comparable motif on heparin/HS. Using the 15 kDa heparin as a scaffold for MASP-2, competition assays were performed using unfractionated heparin, heparin-derived tetrasaccharide (identical composition as Org 32102, namely ΔHexA2S-GlCNS6S-IdoA2S-GlCNS6S) and chondroitin A, B, and C as competitors. Results show that the heparin-derived tetrasaccharide reduced the binding of MASP-2 to 15 kDa heparin by ±40%. Although further experiments (including direct MASP-2/tetrasaccharide binding analysis) would be needed to ascertain that a tetrasaccharide is the actual minimal size required for MASP-2 binding, these data again suggest that MASP-2 is recognized by a short heparin/HS motif (**Figure 3D**).

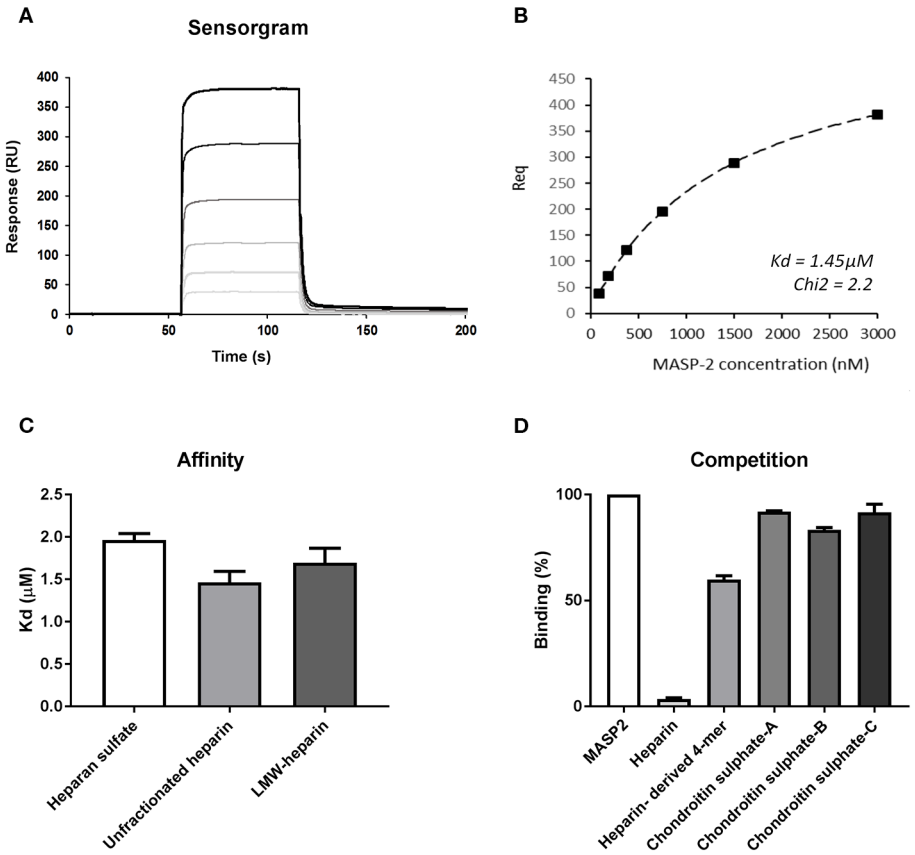

FIGURE 3 | The recombinant catalytic CCP1-CCP2-SP domain of MASP-2 shows equal affinity for heparan sulfate, small, and larger heparin preparations. **(A)** Surface plasmon resonance sensorgram of binding of a (from clear to dark lines) 0–3,000 nM concentration range of recombinant MASP-2 to 15 kDa heparin, showing rapid on and off rates, indicating a transient interaction. Binding of MASP-2 to HS and 6 kDa heparin produced similar graphs (**Supplementary Figure 1**). **(B)** Representative steady-state analysis and fit of the experimental data for the binding of MASP-2 to 15 kDa heparin. **(C)** Affinity calculations reveal micro molar affinity for MASP-2 binding to HS, 6 kDa, and 15 kDa heparin. **(D)** Competition experiments using a tetrasaccharide (4-mer) heparin fragment results in a 40% reduction of the binding of MASP-2 to immobilized 15 kDa heparin, while chondroitin sulfates fail to inhibit the MASP-2/heparin interaction. Experiments were expressed as mean ± SEM from three independent experiments.

Sulfation Pattern Determines the MASP-2-Mediated Lectin Pathway Inhibitory Potential of Tetrasaccharides

To determine the importance of sulfate group positioning within tetrasaccharides for the inhibition of the LP, various heparin-derived tetrasaccharides obtained after limited heparinase I digestion as well as a set of synthetic tetrasaccharides were tested in the WieLISA and the C4 activation assay (37). As a reference the heparin tetrasaccharide Org 32102 (>90% ΔUA2S-GlcNS6S-IdoA2S-GlcNS6S as evaluated by NMR) and unfractionated heparin used in the experiments above were added. The tetrasaccharides were tested in both the WieLISA and MASP-2-mediated C4 deposition assay. None of the tetrasaccharides affected the CP and the AP (data not shown). As shown before, results in the LP WieLISA and the MASP-mediated C4 deposition assay showed comparable results (**Table 3** and **Figure 4**). Strongest inhibition in both assays was obtained by the fully hexasulfated ΔUA2S-GlcNS6S-IdoA2S-GlcNS6S (Org 32102) tetrasaccharide. The hexasulfated preparations with the ΔUA2S at the non-reducing end (by heparinase I elimination reaction), like Org32102 and SAGAG peak 3, showed better inhibitory capacity compared to the synthetic variant, tetrasaccharide T40. Pentasulfated tetrasaccharides also showed inhibitory capacity in both assays, although to a lesser extent compared to the hexasulfated tetrasaccharide. Thus, SAGAG Peak 1 and 2 (having 5 sulfate groups) vs. SAGAG peak 3 (six sulfate groups), and synthetic tetrasaccharide T38 (having 5 sulfate groups) vs. T40 (having 6 sulfate groups). The data indicate that one of the 2-O or 6-O sulfates within the tetrasaccharide can be missed, leaving a pentasulfated HS/heparin tetrasaccharide being the minimal MASP-2 binding sequence in HS and heparin. Further reduction in sulfation to four or less sulfate groups/tetrasaccharide led to loss of all inhibitory potential in both the LP Wielisa and the MASP-2 C4 deposition assay (**Table 3**). Not tested in these experiments are the influence of 3-O sulfation and the eventual effect of GlcNAc or $GlcNH_3^+$ modifications.

TABLE 3 | Inhibitory capacity of heparin-derived and synthetic tetrasaccharides in the Lectin Pathway WieLISA and MASP-mediated C4 deposition assay.

Tetrasaccharide	Structure	Inhibition (%) in WieLISA	Repeats	Inhibition (%) in C4 assay	Repeats
BY HEPARINASE I TREATMENT OF (LMW-) HEPARIN					
Org 32102	ΔUA**2S**-Glc**NS6S**-IdoA**2S**-Glc**NS2S** (90%)[a]	76 (2)	3	61 (6)	3
Ron G11237	ΔUA**2S**-Glc**NS6S**-IdoA**2S**-Glc**NS2S** (37%)	81	1	ND	1
	ΔUA**2S**-Glc**NS6S**-IdoA**2S**-An**S**1,6an (18%)				
	ΔUA**2S**-Glc**NS6S**-IdoA**2S**-Man**NS6S** (18%)				
	ΔUA**2S**-Glc**NS6S**-GlcA-Glc**NS3S6S** (8%)				
	ΔUA**2S**-Glc**NS6S**-GlcA-Glc**NS6S** (12%)[b]				
SAGAG Peak 1	ΔUA**2S**-Glc**NS6S** + ΔUA**2S**-Glc**NS**[c]	46	1	55	1
SAGAG Peak 2	ΔUA**2S**-Glc**NS6S** + ΔUA-Glc**NS6S**[c]	28	1	47	1
SAGAG Peak 3	ΔUA**2S**-Glc**NS6S** + ΔUA**2S**-Glc**NS6S**[c]	68	1	66	1
SYNTHETIC TETRASACCHARIDES					
T7	IdoA-GlcNAc**6S**-IdoA-GlcNAc**6S**-$(CH_2)_5NH_2$	0	1	0 (0)	3
T11	IdoA-GlcNAc**6S**-IdoA**2S**-GlcNAc**6S**-$(CH_2)_5NH_2$	0	1	0 (0)	3
T13	IdoA-Glc**NS6S**-IdoA-Glc**NS6S**-$(CH_2)_5NH_2$	0	1	0 (0)	3
T38	IdoA-Glc**NS6S**-IdoA**2S**-Glc**NS6S**-$(CH_2)_5NH_2$	24	1	10 (10)	3
T39	IdoA**2S**-GlcNAc**6S**-IdoA**2S**-GlcNAc**6S**-$(CH_2)_5NH_2$	0	1	0 (0)	3
T40	IdoA**2S**-Glc**NS6S**-IdoA**2S**-Glc**NS6S**-$(CH_2)_5NH_2$	30	1	16 (3)	3

Values are expressed as percentage inhibition compared to control values without inhibitor expressed as mean ± SD or from a single experiment. GAGs were added in a concentration of 100 ug/ml in the LP and C4 assay.

[a]Composition and purity by NMR spectroscopy.

[b]Composition by NMR spectroscopy.

[c]Composition after digestion of the tetrasaccharide with a cocktail of heparinase I, II, and III followed by RPIP-HPLC disaccharide identification.

MBL-MASP Complex Binds to Immobilized Heparin and Tissue Heparan Sulfate

We have shown in this study that specific domains in heparins and HS can inhibit the LP of complement by inhibiting the enzymatic activity of the MASP2 enzyme. To test whether the MASP-2 in serum indeed binds to solid phase heparin/HS, we incubated serum in heparin-albumin coated wells and measured whether MASP-2 was bound to the immobilized heparin. Results showed binding of serum-derived MASP-2 to immobilized heparin in a dose dependent fashion (**Figure 5A**), indicating that serum MASP-2 could bind to HS/heparin on cells and tissues. RecMASP-2 showed binding to heparin albumin as well (**Figure 5B**).

We thus hypothesized that HS in extracellular matrices and cell membranes could function as docking platforms for MASP-2 *in vivo*. To test this hypothesis we double stained human donor kidneys for MASP-2 and basement membrane HS proteoglycan agrin, which is localized in renal glomerular, tubular and vascular basement membranes. We also performed a double staining for MASP-2 and HS (mAb 10E4). Both double stainings revealed MASP-2 to be present in a subset of tubular basement membranes, partly colocalizing with agrin and HS (**Figures 5C–H**, **6A–C**). The fact that not all basement membranes showed MASP-2 positivity might be because MASP-2 is just very locally produced and stored in the underneath basement membrane, and/or that just a small subset of renal basement membranes displayed HS with a MASP-2 binding motif.

However, from these data it is not clear whether MASP-2 is enzymatically active or not when co-localized to basement membrane HSPGs. Therefore, we performed a triple staining for HS using mAb 10E4, MASP-2 and C3b, the cleaved product of C3, also called active C3. Although the 10E4 and MASP-2 epitopes of HS are different from each other, in **Figures 6D–G** it can be appreciated that MASP-2 and HS showed partial co localization in some basement membranes of vascular structures and in Bowman's capsule. Cleaved C3 within the glomerulus did not colocalize with MASP-2 and/or HS. It can also be seen that cleaved C3 occasionally showed co localization with MASP-2, but not when MASP-2 is co localized with 10E4/HS. Within the limitations of this approach, we speculate that MASP-2 bound to tissue HS is not able to activate the LP and thus no C3b can be formed i.e., MASP-2 might be enzymatically inhibited by the binding to HSPGs.

DISCUSSION

The interaction of GAGs (especially heparin-related GAGs) with complement has been known for some decades, but it has never been tested on a larger scale whether GAGs and derivatives thereof could be specific inhibitors of either of the complement pathways. In this study we tested a library of GAG-related polysaccharides for their complement inhibitory capacity and showed that the LP of complement can be specifically blocked by some HS and heparin- and HS-derived oligosaccharides. Decreasing the disaccharide length of the HS and heparin oligosaccharides resulted in more specificity for the LP and loss of CP and AP inhibitory activity. Since the LP shares the C3 convertase C4b2a with the CP, LP-specific GAGs must inhibit either the MASP enzymes or the pattern recognition molecules

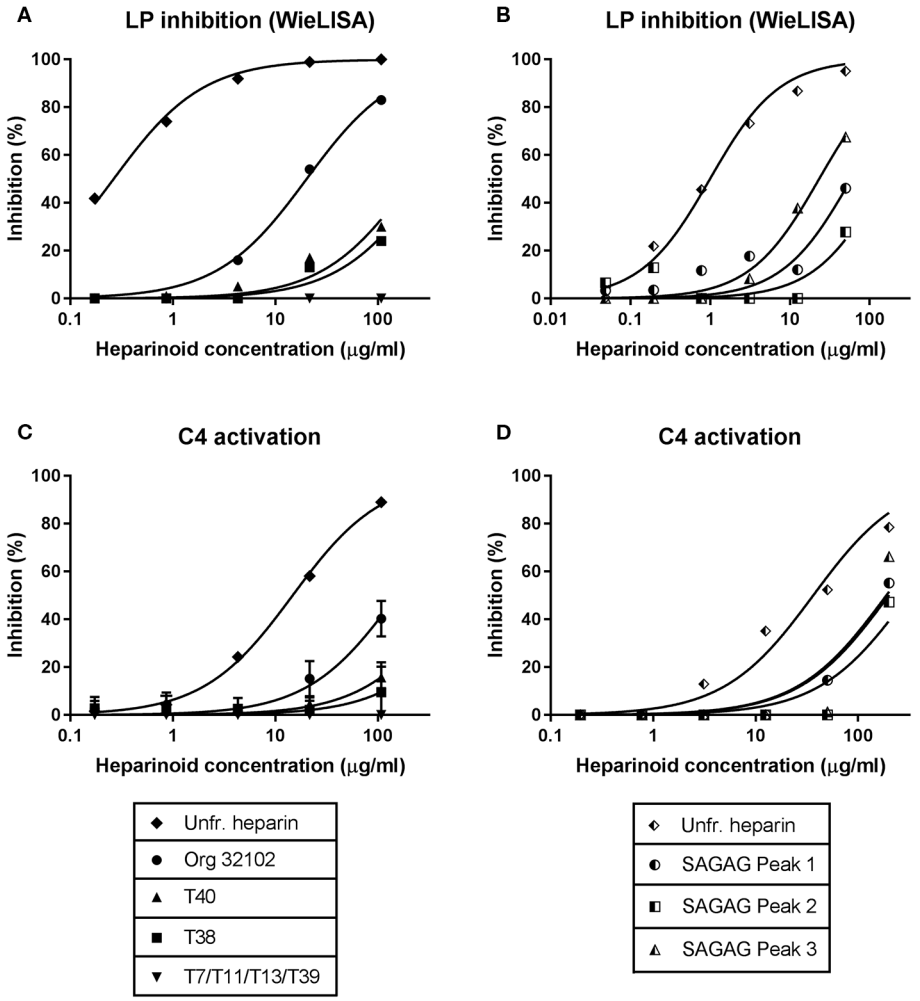

FIGURE 4 | Inhibition of the lectin pathway by tetrasaccharides requires at least pentasulfation. Using synthetic tetrasaccharides **(A,C)** and purified tetrasaccharides **(B,D)**, we determined that LP inhibition requires at least a pentasulfated tetrasaccharide. All penta- and hexa-sulfated oligosaccharides showed inhibition in both the LP WieLISA and the C4 activation test. Removing both IdoA2S sulfate groups or both N-sulfate groups resulted in vanishing of the inhibitory potential. Displacement of an iduronic acid by an unsaturated uronic or hexuronic acid results in an improvement of inhibitory potential in both assays. For data on the sulfation degree of the tetrasaccharides see **Table 3**. As a reference the non-synthetic heparin tetrasaccharide 32102 and unfractionated heparin, used in the former experiments, was added to experiment **(A,C)**. Data is expressed as representative measurement **(A,B,D)** or as the mean ± SEM of three independent experiments **(C)**.

of the LP. Our results show that heparin fragments inhibited the cleaving of C4, but did not affect the binding of MBL to mannan, suggesting a blocking effect of GAGs on either MASP-1 or MASP-2 activity. This conclusion is further strengthened by the finding that the tested GAGs are also able to inhibit the LP initiated by ficolin-3 as a pattern recognition molecule. We could also show binding of serum-derived MASP-2 as well as recMASP-2 to immobilized heparin and demonstrated the binding affinity of recombinant MASP-2 to heparins and HS. Moreover, partial co-localization was seen of MASP-2 and agrin/10E4 HS epitope in some basement membrane of tubuli and vessels in human kidney, while activated C3 did not co-localize. These data might suggest that HS *in situ* might function as a docking platform for MASP-2 rendering the enzyme inactive, thereby eventually protecting the tissue from LP complement activation.

GAG length, disaccharide backbone composition, and sulfation pattern form the main determinants for protein binding properties of GAGs in general and this study shows that this holds true for complement components as well. Although the heparin/HS (oligosaccharides) were tested in a fixed μg/ml concentration, increasing the difficulty to directly compare small and large fractions, it can be appreciated that in larger GAGs, the complement inhibitory capacity is predominantly determined by sulfation degree and less by disaccharide composition and linkages. GAGs carrying a different backbone compared to heparin like O-sulfated *E. coli* K5 polysaccharide, and GAG-like polysaccharides fucoidan and dextran sulfate show equally strong inhibition of all complement pathways, stressing the role of GAG sulfation in complement inhibition. It can be appreciated from **Table 2** that in most cases the inhibitory

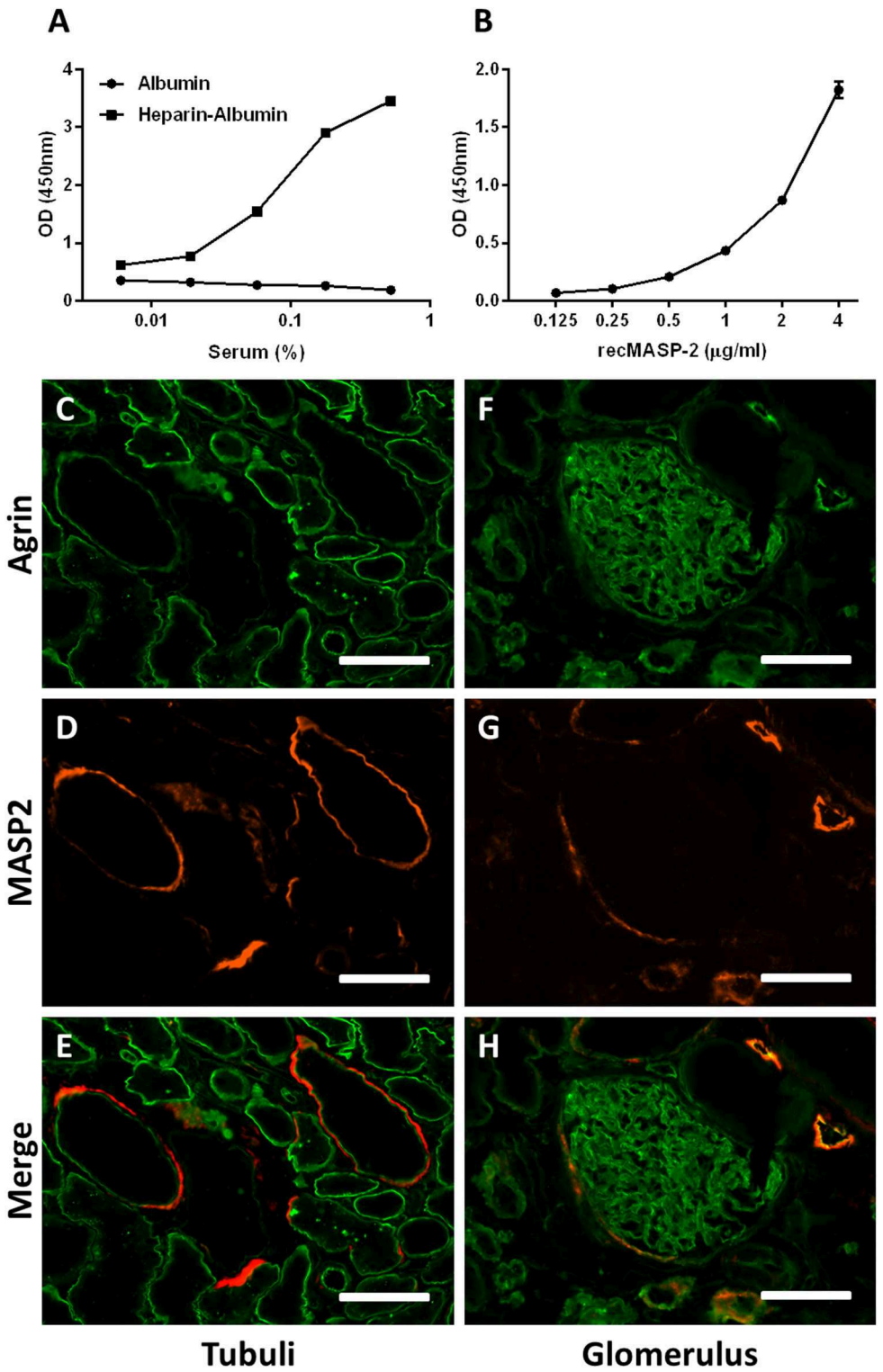

FIGURE 5 | HSPG's might serve as a docking platform for the MBL/MASP complex. **(A)** Incubation of serum on a heparin-albumin coated plate results in binding of MASP-2 to the heparin. **(B)** recMASP-2 binds to heparin-albumin coated on a plate. **(C–H)** Confocal immunofluorescence double staining of human donor kidneys for MASP-2 (red) and agrin (green) showed partial co localization in the basement membranes of some tubuli, within Bowman's capsule and some blood/lymph vessel basement membranes. Data is expressed as representative measurement **(A)** or as mean ± SEM of two independent experiments **(B)**. Scale bars indicate 50 µm.

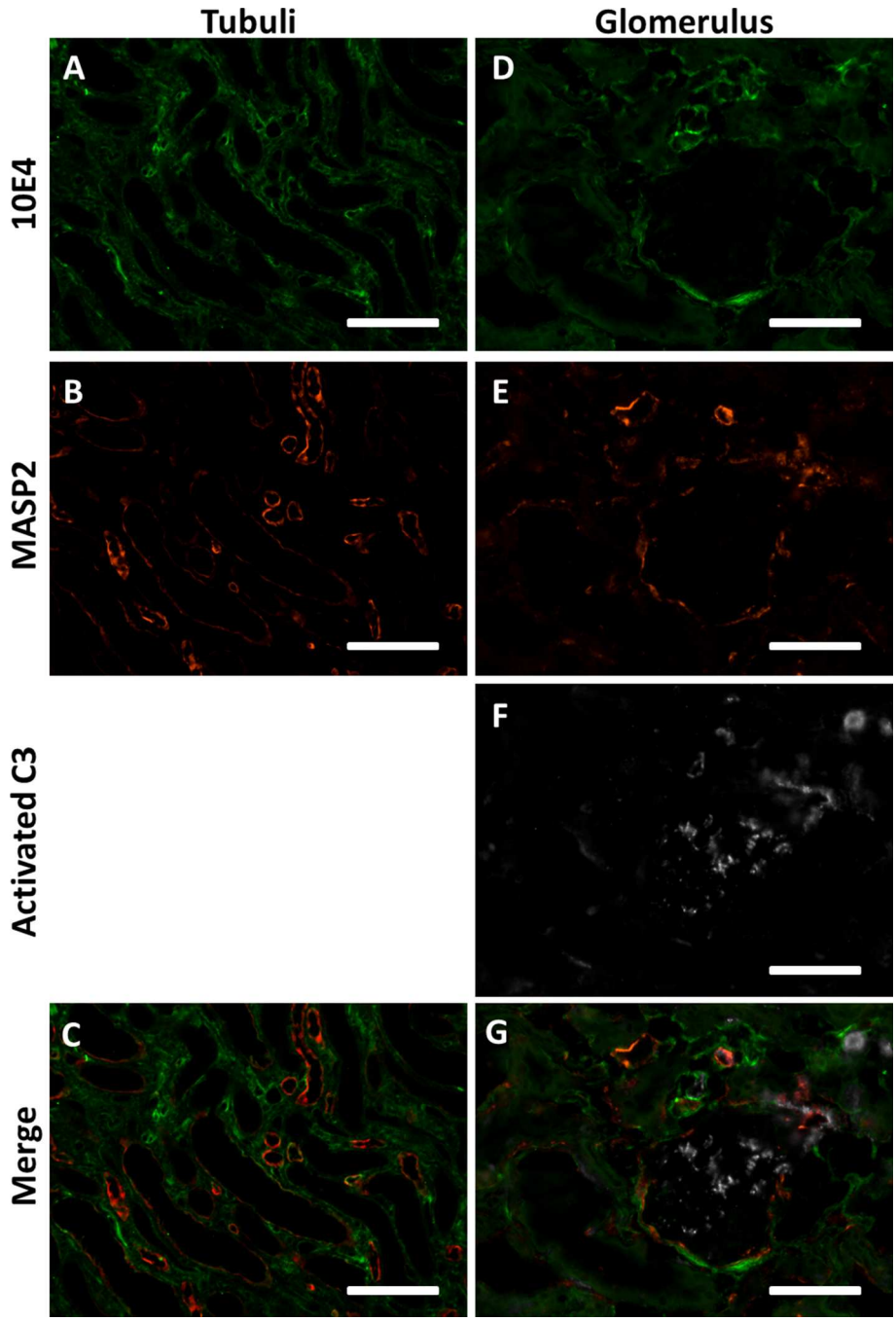

FIGURE 6 | MASP2 is bound to HSPGs in an enzymatically inactive state. **(A–C)** Confocal immunofluorescence double staining of HS marker 10E4 (green) showed partial co localization with MASP-2 (red) in some tubular and vascular basement membranes of human donor kidneys. **(D–G)** Confocal immunofluorescence triple staining for HS mAb 10E4 (green), MASP-2 (red) and cleaved C3 (white). MASP-2 colocalized partially with HS in some vascular basement membranes and Bowmans capsule, but not with activated C3. Activated C3 is predominantly localized in the glomerulus (single positive) and not seen where MASP-2 co localizes with 10E4, indicating that MASP2 is bound the HSPGs in an inactive state. Scale bars indicate 50 μm.

capacity of GAGs is comparable for the CP and AP. This might suggest that the CP and AP share an inhibitory GAG binding protein and that the GAG binding site in the LP is unique within the complement system. The known interactions between GAGs and the complement system have been summarized by us before (47) and we have more extensively investigated the interaction between GAGs and properdin (12). Interestingly, the GAGs showing the highest affinity for properdin in the study conducted

earlier also show the strongest CP and AP inhibition (12). This might indicate a role for the GAG/properdin interaction in our current results. Properdin is a stimulator of the AP, by stabilizing the C3 convertase, but can have the same effect in the CP since cleaving of C3 by the C3 convertase C4bC2a can be followed by AP activation. Whether the inhibition by GAGs of the CP and AP is indeed properdin mediated or not should be studied further, since interactions between GAGs on one hand and AP activator properdin, AP inhibitor factor H (13) and CP inhibitors like C1-inhibitor on the other hand have been described Caughman et al. (48).

This study showed that smaller heparin and HS depolymerization products lose their ability to inhibit the CP and AP and become specific inhibitors for the LP. HS oligosaccharides start to be LP specific from dp12 and heparin from dp6. Our surface plasmon resonance experiments indicated that MASP-2 recognizes a small GAG epitope. Of note, heparin is significantly more sulfated than HS (∼2.5 and ∼0.85 sulfates per disaccharide, respectively). Furthermore, HS oligosaccharides were generated using heparinase III, which specificity for (GlcNAc ± 6S–GlcA) disaccharides will produce fragments with low/non-sulfated saccharide extremities. We therefore assume that larger (dp6–dp12) HS oligosaccharides may contain just one MASP2 binding site connected to low sulfated, biologically inactive HS stretches. Whereas, larger (dp6–dp12) heparin oligo's, due to high sulfation, also start to recognize C1inh, ATIII and other members of the complement serine proteases and therefore start to inhibit the CP and AP besides the LP. The smallest component capable of inhibiting the LP is a tetrasaccharide, which needs to have at least pentasulfation to show inhibitory function. This is interesting because other GAG/protein interactions e.g., heparin and ATIII have shown to require larger high sulfation stretches. Therefore, the interaction of a tetrasaccharide with MASP enzymes holds clinical potential. Interestingly, replacing the iduronic acid at the non-reducing end of the tetrasaccharide by unsaturated ΔHexA could increase the inhibitory potential, suggesting the importance of the backbone structure. Alternatively, the reducing terminal—$(CH_2)_5NH_2$ derivatization of the synthetic tetrasaccharides might interfere the interaction with MASP-2 to some extent.

We showed in this study that the inhibitory effect of GAGs on the lectin route of complement is not pattern recognition molecule related, but rather MASP related. As elegantly shown by Héja and colleagues, MASP-2 is solely responsible for the activation of C4 and both MASP-1 and 2 are responsible for the activation of C2 (46). This study shows that GAGs inhibit the C4 activation and that GAGs show interaction with the catalytic domain of MASP-2. Therefore, we can conclude that GAGs interact with MASP-2 and inhibit the enzymatic activity. Literature has demonstrated that MASP-2, but not MASP-1, has a highly positively charged exosite located in the serine protease domain, which differs from de described exosite in C1s (49, 50). Under physiological conditions, this positively charged exosite is believed to be the binding site of C4. C4 carries a negatively charged cluster consisting of three tyrosine-sulfate residues, interaction of these tyrosine-sulfate residues with the positively charged exosite on MASP-2 and C1s is crucial for cleaving, and therefore activity, of C4 (51, 52). Since heparin, and HS to a lesser extent, is negatively charged due to their sulfate groups, we propose that specific LP inhibition by HS and heparin oligosaccharides occurs *via* binding to this positively charged exosite. In **Figure 7**, we aligned the amino acid sequence of the serine protease domains of MASP-2, MASP-1, and C1s. In green we indicated the positively charged arginine and lysine residues in MASP-2 involved in the recognition of the tyrosine-sulfate residues in C4 (K450, K503, R578, and R583). In red we showed them in C1s (K575, R576, R581, and K583). As can be seen, such an exosite is lacking in MASP-1. Moreover, MASP-1 is not cleaving C4, just C2. Moreover, because we found the inhibition of the C4 deposition assay we studied MASP-2 and not MASP-1. Therefore, these data strongly suggest that the heparin oligo's block the interaction of MASP-2/C4 interaction at the interface of the MASP-2 exosite with the tyrosin-sulfate residues of C4, and thereby prevents cleavage of C4.

It has been described that protease inhibitors like C1inh, ATIII, and tissue factor pathway inhibitor can form complexes with the MASP proteases (15, 54) and could therefore influence our results by heparin mediated activation of these serine protease inhibitors followed by inactivation of the MASP enzymes by proteolytic cleavage. We deem it however unlikely since ATIII needs minimally a 3-O sulfated pentasaccharide which is not present in the synthetic tetrasaccharides tested (25). C1inh and TFPI are also not very likely involved, since according to literature both protease inhibitors show an increased protease activity at low heparin concentrations and blocking of the protease activity at high heparin concentrations (15, 55). We never observed such kinetics using the WIELISA or C4 deposition assays. Besides, the 1M NaCl conditions in the C4 deposition assay the MASPs will not react with the serpins.

This study shows that the serum-derived MASP-2 can bind to heparin and HS GAGs and inhibit the LP of complement. These findings suggest that HS proteoglycans *in vivo* can act as a docking station for MASP-2 and preclude LP activity. In support to this, we found some co-localization of MASP-2 and HS proteoglycan agrin and HS in Bowman's capsule and the basement membranes of some tubuli and vessels. We were not able to show cleaved C3 to co-localize with HS and MASP-2. To test HS-dependent MASP-2 binding renal sections were pretreated with heparitinase. Effective enzymatic cleavage of HS was shown by induced staining using anti-ΔHS stub mAb 3G10, which after heparitinase became brilliant positive in all extracellular matrices of the kidney. Nevertheless, the intensity of the MASP-2 staining did not diminish after heparitinase (data not shown). This could mean that MASP-2 is not physically bound with HS. However, we cannot exclude that its binding to HS precludes the heparitinase enzyme to cleave HS. Another explanation could be that the MASP-2 in renal tissue is part of a larger complement complex, including MASP-1, MBL, and eventually other complement factors (C2 and C4 eg). These other complement factors also might interact with renal determinants, other than HS. This means that digestion of HS will not reduce MASP-2 presence. All in all, such an enzymatic approach is not conclusive. Although our immunofluorescence data is far from robust proof, this might suggest that MASP-2 is stored inactively

```
Masp2-SP  433 - VCGLSARTTG--GRIYGGQKAKPGDFPWQVLILGG---TTAAGALLYDNWVLTAAHAVYE
C1s-SP    424 - VCGVPREPFEEKQRIIGGSDADIKNFPWQVFFDN----PWAGGALINEYWVLTAAHVVEG
Masp-1-SP 435 - VCGLPKFSRKLMARIFNGRPAQKGTTPWIAMLSHLNGQPFCGGSLLGSSWIVTAAHCLHQ
                ***:.  .     ** .*  *.    ** .::      . ..*:*: . *::**** :

Masp2-SP        QKHDASALDIRMGTLKRLSPHYTQAWSEAVFIHEGYTHDAG-------------FDNDIA
C1s-SP          NREPTMYVGSTSVQTSRLAKSKMLTP-EHVFIHPGWKLLEVPEGRTN-------FDNDIA
Masp-1-SP       SLDPEDPTLRDSDLLSPSDFKIILGKHWRLRSDENEQHLGVKHTTLHPQYDPNTFENDVA
                . .           .             :  . .                    *:**:*

Masp2-SP        LIKLNNKVVINSNITPICLPRKEAESFMRTDDIGTASGWGLTQRGFLARNLMYVDIPIVD
C1s-SP          LVRLKDPVKMGPTVSPICLPGTSSDYNLMDGDLGLISGWGRTEKRDRAVRLKAARLPVAP
Masp-1-SP       LVELLESPVLNAFVMPICLP----EGPQQEGAMVIVSGWGKQFLQRFPETLMEIEIPIVD
                *:.* :   :.. : *****    :     . :   ****       .  *    :*:.

Masp2-SP        HQKCTAAYEKPPYPRGS---VTANMLCAGLESGGKDSCRGDSGGALVFLDS-ETERWFVG
C1s-SP          LRKCKEVKVEKPTADAEAYVFTPNMICAGGEKG-MDSCKGDSGGAFAVQDPNDKTKFYAA
Masp-1-SP       HSTCQKAYAPLKK------KVTRDMICAGEKEGGKDACAGDSGGPMVTLNR-ERGQWYLV
                  .*  .             .* :*:*** :.*  *:* *****.:.  :  :  :::

Masp2-SP        GIVSWGSMNCGEAGQYGVYTKVINYIPWIENIISDF------ - 686
C1s-SP          GLVSWG----PQCGTYGLYTRVKNYVDWIMKTMQENSTPRED - 688
Masp-1-SP       GTVSWG-DDCGKKDRYGVYSYIHHNKDWIQRVTGVRN----- - 699
                * ****     : . **:*: : :   ** .
```

FIGURE 7 | Amino acid sequence alignment of the serine protease domains of MASP-2, C1s and MASP-1. Sequence alignment was done by Clustal W (https://www.genome.jp/tools-bin/clustalw) as described by Thompson et al. (53). Amino acid sequences were obtained in Uniprot (https://www.uniprot.org/). Indicated in green are the positively charged arginine and lysine residues in MASP-2 involved in the recognition of the tyrosine-sulfate residues in C4 (K450, K503, R578, and R583). In red these residues are shown in C1s (K575, R576, R581, and K583). As can be seen, the positively charged exocites of MASP-2 and C1s clearly differs from each other, while such a positively charged exosite is lacking in MASP-1.

in the basement membrane and we speculate that it might be released upon the right stimuli e.g., by the action of heparanase or oxidative stress.

We show in this study that HS and small heparin fragments are specific LP inhibitors, although the interaction is in the micromolar affinity range resulting in rather high IC50 values. To date there is no specific LP inhibitor clinically available, although a phase II clinical trial in renal patients using humanized anti-MASP-2 mAb (OMS721 by OMEROS, Saettle WA, USA) was recently closed with promising results in patients suffering from IgA nephropathy and lupus nephritis. Furthermore, an interesting study was recently published introducing a modified TFPI 1 domain as a potential MASP-2 inhibitor (56). Current treatment option for LP mediated conditions would be C5 inhibitor eculizumab. However, eculizumab is very expensive and inhibits all three complement pathways. The use of polysaccharide-based therapeutics has the advantages: production can be cheap and easy, and polysaccharides are not susceptible to proteolytic enzymes, making them less vulnerable to degradation. Moreover, decades of experience has been obtained with heparin based therapeutics in the field of anti-coagulation. Therefore, we believe that polysaccharide based specific LP inhibitors have good potential for further development. The comparison of four different β-elimination heparin-derived tetrasaccharide fragments and synthetic tetrasaccharides revealed the best LP/MASP inhibition by the fully hexasulfated ΔHexA, 2S-GlcNS, 6S-ΔHexA,2S-GlcNS, 6S structure. This structure could be a promising starting molecule to develop related small glycan-based LP/MASP inhibitors with higher affinity.

DATA AVAILABILITY STATEMENT

All datasets generated for this study are included in the article/**Supplementary Material**.

AUTHOR CONTRIBUTIONS

DT, MD, CS, MS, SB, and JB contributed to the conception and design of the study. DT, FP, WD, AM-A, and RV conducted the experiments. AN, PC, G-JB, and PG delivered crucial reagents. DT wrote the first draft of the manuscript. All authors contributed to manuscript revision, read, and approved the submitted version.

FUNDING

The research was funded by the graduate school of Medical Sciences of the University Medical Center of Groningen in

the form of a Ph.D. stipend to DT and by the Dutch Kidney Foundation (grants IP 12.90 and Consortium grant COMBAT #130CA27. This work used the SPR platform of the Grenoble Instruct centre (ISBG; UMS 3518 CNRS-CEA-UJF-EMBL) with support from FRISBI (ANR-10-INSB-05-02) and GRAL (ANR-10-LABX-49-01) within the Grenoble Partnership for Structural Biology (PSB). This work was also supported by the CNRS and the GDR GAG (GDR 3739), the Investissements d'avenir program Glyco@Alps (ANR-15-IDEX-02), and by a Agence Nationale de la Recherche grant (ANR-17-CE11-0040). The study was supported by the Hungarian National Research, Development and Innovation Office OTKA grant K119374.

ACKNOWLEDGMENTS

We thank Justyna Dobruchowska for performing the structural analysis of the Org 32102 tetrasaccharide and Evelyne Gout for technical help with the SPR experiments. We are grateful to Júlia Balczer for the technical assistance. This study was performed on behalf of the COMBAT Consortium. This is an interuniversity collaboration in the Netherlands that is formed to study basic mechanisms, assay development, and therapeutic translation of complement-mediated renal diseases. Principal investigators are (in alphabetical order): SB (Department of Internal Medicine-Nephrology, University Medical Center Groningen, Groningen, Netherlands), JB (Department of Internal Medicine-Nephrology, University Medical Center Groningen, Groningen, Netherlands), P. Gros (Department of Chemistry, Utrecht University, Utrecht, Netherlands), L.P. van den Heuvel (Department of Pediatric Nephrology, Radboud University Medical Center, Nijmegen, Netherlands), N. van de Kar (Department of Pediatric Nephrology, Radboud University Medical Center, Nijmegen, Netherlands), C. van Kooten (Department of Internal Medicine-Nephrology, Leiden University Medical Center, Leiden, Netherlands), MS (Department of Internal Medicine-Nephrology, University Medical Center Groningen, Groningen, Netherlands), A. de Vries (Department of Internal Medicine-Nephrology, Leiden University Medical Center, Leiden, Netherlands).

SUPPLEMENTARY MATERIAL

The Supplementary Material for this article can be found online at: https://www.frontiersin.org/articles/10.3389/fimmu.2020.00732/full#supplementary-material

REFERENCES

1. Thurman JM, Nester CM. All things complement. *Clin J Am Soc Nephrol*. (2016) 11:1856–66. doi: 10.2215/CJN.01710216
2. Leffler J, Bengtsson AA, Blom AM. The complement system in systemic lupus erythematosus: an update. *Ann Rheum Dis*. (2014) 73:1601–6. doi: 10.1136/annrheumdis-2014-205287
3. Hovind P, Hansen TK, Tarnow L, Thiel S, Steffensen R, Flyvbjerg A, et al. Mannose-binding lectin as a predictor of microalbuminuria in type 1 diabetes: an inception cohort study. *Diabetes*. (2005) 54:1523–7. doi: 10.2337/diabetes.54.5.1523
4. Berger SP, Roos A, Mallat MJ, Fujita T, de Fijter JW, Daha MR. Association between mannose-binding lectin levels and graft survival in kidney transplantation. *Am J Transplant*. (2005) 5:1361–6. doi: 10.1111/j.1600-6143.2005.00841.x
5. Roos A, Rastaldi MP, Calvaresi N, Oortwijn BD, Schlagwein N, van Gijlswijk-Janssen DJ, et al. Glomerular activation of the lectin pathway of complement in IgA nephropathy is associated with more severe renal disease. *J Am Soc Nephrol*. (2006) 17:1724–34. doi: 10.1681/ASN.2005090923
6. Poppelaars F, Faria B, Gaya da Costa M, Franssen CFM, van Son WJ, Berger SP, et al. The complement system in dialysis: a forgotten story? *Front Immunol*. (2018) 9:71. doi: 10.3389/fimmu.2018.00071
7. Moller-Kristensen M, Wang W, Ruseva M, Thiel S, Nielsen S, Takahashi K, et al. Mannan-binding lectin recognizes structures on ischaemic reperfused mouse kidneys and is implicated in tissue injury. *Scand J Immunol*. (2005) 61:426–434. doi: 10.1111/j.1365-3083.2005.01591.x
8. Farrar CA, Tran D, Li K, Wu W, Peng Q, Schwaeble W, et al. Collectin-11 detects stress-induced L-fucose pattern to trigger renal epithelial injury. *J Clin Invest*. (2016) 126:1911–25. doi: 10.1172/JCI83000
9. Gaarkeuken H, Siezenga MA, Zuidwijk K, van Kooten C, Rabelink TJ, Daha MR, et al. Complement activation by tubular cells is mediated by properdin binding. *Am J Physiol Renal Physiol*. (2008) 295:F1397–403. doi: 10.1152/ajprenal.90313.2008
10. Hawfield A, Iskandar SS, Smith RJ. Alternative pathway dysfunction in kidney disease: a case report and review of dense deposit disease and C3 glomerulopathy. *Am J Kidney Dis*. (2013) 61:828–31. doi: 10.1053/j.ajkd.2012.11.045
11. Sethi S, Fervenza FC. Pathology of renal diseases associated with dysfunction of the alternative pathway of complement: C3 glomerulopathy and atypical hemolytic uremic syndrome (aHUS). *Semin Thromb Hemost*. (2014) 40:416–21. doi: 10.1055/s-0034-1375701
12. Zaferani A, Vives RR, van der Pol P, Hakvoort JJ, Navis GJ, van Goor H, et al. Identification of tubular heparan sulfate as a docking platform for the alternative complement component properdin in proteinuric renal disease. *J Biol Chem*. (2011) 286:5359–67. doi: 10.1074/jbc.M110.167825
13. Zaferani A, Vives RR, van der Pol P, Navis GJ, Daha MR, van Kooten C, et al. Factor h and properdin recognize different epitopes on renal tubular epithelial heparan sulfate. *J Biol Chem*. (2012) 287:31471–81. doi: 10.1074/jbc.M112.380386
14. Weiler JM, Edens RE, Linhardt RJ, Kapelanski DP. Heparin and modified heparin inhibit complement activation *in vivo*. *J Immunol*. (1992) 148:3210–15.
15. Parej K, Dobo J, Zavodszky P, Gal P. The control of the complement lectin pathway activation revisited: both C1-inhibitor and antithrombin are likely physiological inhibitors, while alpha2-macroglobulin is not. *Mol Immunol*. (2013) 54:415–22. doi: 10.1016/j.molimm.2013.01.009
16. Rent R, Myhrman R, Fiedel BA, Gewurz H. Potentiation of C1-esterase inhibitor activity by heparin. *Clin Exp Immunol*. (1976) 23:264–71.
17. Loos M, Bitter-Suermann D. Mode of interaction of different polyanions with the first (C1,C1) the second (C2) and the fourth (C4) component of complement. IV. Activation of C1 in serum by polyanions. *Immunology*. (1976) 31:931–4. doi: 10.1016/0161-5890(76)90026-2
18. Poppelaars F, Damman J, de Vrij EL, Burgerhof JG, Saye J, Daha MR, et al. New insight into the effects of heparinoids on complement inhibition by C1-inhibitor. *Clin Exp Immunol*. (2016) 184:378–88. doi: 10.1111/cei.12777
19. Talsma DT, Daha MR, van den Born J. The bittersweet taste of tubulo-interstitial glycans. *Nephrol Dial Transplant*. (2017) 32:611–19. doi: 10.1093/ndt/gfw371
20. Sarrazin S, Lamanna WC, Esko JD. Heparan sulfate proteoglycans. *Cold Spring Harb Perspect Biol*. (2011) 3:a004952. doi: 10.1101/cshperspect.a004952
21. Vlodavsky I, Beckhove P, Lerner I, Pisano C, Meirovitz A, Ilan N, et al. Significance of heparanase in cancer and inflammation. *Cancer Microenviron*. (2012) 5:115–32. doi: 10.1007/s12307-011-0082-7

22. El Masri R, Seffouh A, Lortat-Jacob H, Vives RR. The "in and out" of glucosamine 6-O-sulfation: the 6th sense of heparan sulfate. *Glycoconj J*. (2017) 34:285–98. doi: 10.1007/s10719-016-9736-5
23. Celie JW, Reijmers RM, Slot EM, Beelen RH, Spaargaren M, Ter Wee PM, et al. Tubulointerstitial heparan sulfate proteoglycan changes in human renal diseases correlate with leukocyte influx and proteinuria. *Am J Physiol Renal Physiol*. (2008) 294:F253–63. doi: 10.1152/ajprenal.00429.2007
24. Katta K, Boersema M, Adepu S, Rienstra H, Celie JW, Mencke R, et al. Renal heparan sulfate proteoglycans modulate fibroblast growth factor 2 signaling in experimental chronic transplant dysfunction. *Am J Pathol*. (2013) 183:1571–84. doi: 10.1016/j.ajpath.2013.07.030
25. Casu B, Lindahl U. Structure and biological interactions of heparin and heparan sulfate. *Adv Carbohydr Chem Biochem*. (2001) 57:159–206. doi: 10.1016/S0065-2318(01)57017-1
26. Vann WF, Schmidt MA, Jann B, Jann K. The structure of the capsular polysaccharide (K5 antigen) of urinary-tract-infective Escherichia coli 010:K5:H4. A polymer similar to desulfo-heparin. *Eur J Biochem*. (1981) 116:359–64. doi: 10.1111/j.1432-1033.1981.tb05343.x
27. Maccarana M, Sakura Y, Tawada A, Yoshida K, Lindahl U. Domain structure of heparan sulfates from bovine organs. *J Biol Chem*. (1996) 271:17804–10. doi: 10.1074/jbc.271.30.17804
28. Iverius PH. Coupling of glycosaminoglycans to agarose beads (sepharose 4B). *Biochem J*. (1971) 124:677–83. doi: 10.1042/bj1240677
29. Rej RN, Ludwig-Baxter KG, Perlin AS. Sulfation of some chemically-modified heparins. Formation of a 3-sulfate analog of heparin. *Carbohydr Res*. (1991) 210:299–310. doi: 10.1016/0008-6215(91)80130-F
30. Vives RR, Sadir R, Imberty A, Rencurosi A, Lortat-Jacob H. A kinetics and modeling study of RANTES(9-68) binding to heparin reveals a mechanism of cooperative oligomerization. *Biochemistry*. (2002) 41:14779–89. doi: 10.1021/bi026459i
31. Pye DA, Vives RR, Turnbull JE, Hyde P, Gallagher JT. Heparan sulfate oligosaccharides require 6-O-sulfation for promotion of basic fibroblast growth factor mitogenic activity. *J Biol Chem*. (1998) 273:22936–42. doi: 10.1074/jbc.273.36.22936
32. Henriet E, Jager S, Tran C, Bastien P, Michelet JF, Minondo AM, et al. A jasmonic acid derivative improves skin healing and induces changes in proteoglycan expression and glycosaminoglycan structure. *Biochim Biophys Acta Gen Subj*. (2017) 1861:2250–60. doi: 10.1016/j.bbagen.2017.06.006
33. Seffouh A, Milz F, Przybylski C, Laguri C, Oosterhof A, Bourcier S, et al. HSulf sulfatases catalyze processive and oriented 6-O-desulfation of heparan sulfate that differentially regulates fibroblast growth factor activity. *FASEB J*. (2013) 27:2431–9. doi: 10.1096/fj.12-226373
34. Chabrol E, Nurisso A, Daina A, Vassal-Stermann E, Thepaut M, Girard E, et al. Glycosaminoglycans are interactants of langerin: comparison with gp120 highlights an unexpected calcium-independent binding mode. *PLoS ONE*. (2012) 7:e50722. doi: 10.1371/journal.pone.0050722
35. Alekseeva A, Elli S, Cosentino C, Torri G, Naggi A. Susceptibility of enoxaparin reducing end amino sugars to periodate oxidation. *Carbohydr Res*. (2014) 400:33–43. doi: 10.1016/j.carres.2014.08.016
36. Casu B, Guerrini M, Guglieri S, Naggi A, Perez M, Torri G, et al. Undersulfated and glycol-split heparins endowed with antiangiogenic activity. *J Med Chem*. (2004) 47:838–48. doi: 10.1021/jm030893g
37. Zong C, Venot A, Li X, Lu W, Xiao W, Wilkes JL, et al. Heparan sulfate microarray reveals that heparan sulfate-protein binding exhibits different ligand requirements. *J Am Chem Soc*. (2017) 139:9534–43. doi: 10.1021/jacs.7b01399
38. Seelen MA, Roos A, Wieslander J, Mollnes TE, Sjoholm AG, Wurzner R, et al. Functional analysis of the classical, alternative, and MBL pathways of the complement system: standardization and validation of a simple ELISA. *J Immunol Methods*. (2005) 296:187–98. doi: 10.1016/j.jim.2004.11.016
39. Roos A, Bouwman LH, Munoz J, Zuiverloon T, Faber-Krol MC, Fallaux-van den Houten FC, et al. Functional characterization of the lectin pathway of complement in human serum. *Mol Immunol*. (2003) 39:655–68. doi: 10.1016/S0161-5890(02)00254-7
40. Petersen SV, Thiel S, Jensen L, Steffensen R, Jensenius JC. An assay for the mannan-binding lectin pathway of complement activation. *J Immunol Methods*. (2001) 257:107–16. doi: 10.1016/S0022-1759(01)00453-7
41. Ambrus G, Gal P, Kojima M, Szilagyi K, Balczer J, Antal J, et al. Natural substrates and inhibitors of mannan-binding lectin-associated serine protease-1 and−2: a study on recombinant catalytic fragments. *J Immunol*. (2003) 170:1374–82. doi: 10.4049/jimmunol.170.3.1374
42. Seffouh A, El Masri R, Makshakova O, Gout E, Hassoun ZEO, Andrieu JP, et al. Expression and purification of recombinant extracellular sulfatase HSulf-2 allows deciphering of enzyme sub-domain coordinated role for the binding and 6-O-desulfation of heparan sulfate. *Cell Mol Life Sci*. (2019) 76:1807–19. doi: 10.1007/s00018-019-03027-2
43. van den Born J, van den Heuvel LP, Bakker MA, Veerkamp JH, Assmann KJ, Weening JJ, et al. Distribution of GBM heparan sulfate proteoglycan core protein and side chains in human glomerular diseases. *Kidney Int*. (1993) 43:454–63. doi: 10.1038/ki.1993.67
44. Sasisekharan R, Venkataraman G. Heparin and heparan sulfate: biosynthesis, structure and function. *Curr Opin Chem Biol*. (2000) 4:626–31. doi: 10.1016/S1367-5931(00)00145-9
45. Hein E, Honore C, Skjoedt MO, Munthe-Fog L, Hummelshoj T, Garred P. Functional analysis of ficolin-3 mediated complement activation. *PLoS ONE*. (2010) 5:e15443. doi: 10.1371/journal.pone.0015443
46. Heja D, Kocsis A, Dobo J, Szilagyi K, Szasz R, Zavodszky P, et al. Revised mechanism of complement lectin-pathway activation revealing the role of serine protease MASP-1 as the exclusive activator of MASP-2. *Proc Natl Acad Sci USA*. (2012) 109:10498–503. doi: 10.1073/pnas.1202588109
47. Zaferani A, Talsma D, Richter MK, Daha MR, Navis GJ, Seelen MA, et al. Heparin/heparan sulphate interactions with complement–a possible target for reduction of renal function loss? *Nephrol Dial Transplant*. (2014) 29:515–22. doi: 10.1093/ndt/gft243
48. Caughman GB, Boackle RJ, Vesely J. A postulated mechanism for heparin's potentiation of C1 inhibitor function. *Mol Immunol*. (1982) 19:287–95. doi: 10.1016/0161-5890(82)90342-X
49. Dobo J, Harmat V, Beinrohr L, Sebestyen E, Zavodszky P, Gal P. MASP-1, a promiscuous complement protease: structure of its catalytic region reveals the basis of its broad specificity. *J Immunol*. (2009) 183:1207–14. doi: 10.4049/jimmunol.0901141
50. Kjaer TR, Thiel S, Andersen GR. Toward a structure-based comprehension of the lectin pathway of complement. *Mol Immunol*. (2013) 56:413–22. doi: 10.1016/j.molimm.2013.05.007
51. Duncan RC, Mohlin F, Taleski D, Coetzer TH, Huntington JA, Payne RJ, et al. Identification of a catalytic exosite for complement component C4 on the serine protease domain of C1s. *J Immunol*. (2012) 189:2365–73. doi: 10.4049/jimmunol.1201085
52. Kidmose RT, Laursen NS, Dobo J, Kjaer TR, Sirotkina S, Yatime L, et al. Structural basis for activation of the complement system by component C4 cleavage. *Proc Natl Acad Sci USA*. (2012) 109:15425–30. doi: 10.1073/pnas.1208031109
53. Thompson JD, Higgins DG, Gibson TJ. CLUSTAL W: improving the sensitivity of progressive multiple sequence alignment through sequence weighting, position-specific gap penalties and weight matrix choice. *Nucleic Acids Res*. (1994) 22:4673–80. doi: 10.1093/nar/22.22.4673
54. Keizer MP, Pouw RB, Kamp AM, Patiwael S, Marsman G, Hart MH, et al. TFPI inhibits lectin pathway of complement activation by direct interaction with MASP-2. *Eur J Immunol*. (2015) 45:544–50. doi: 10.1002/eji.201445070
55. Peraramelli S, Thomassen S, Heinzmann A, Hackeng TM, Hartmann R, Scheiflinger F, et al. Role of exosite binding modulators in the inhibition of Fxa by TFPI. *Thromb Haemost*. (2016) 115:580–90. doi: 10.1160/th15-04-0354
56. Szakacs D, Kocsis A, Szasz R, Gal P, Pal G. Novel MASP-2 inhibitors developed via directed evolution of human TFPI1 are potent lectin pathway inhibitors. *J Biol Chem*. (2019) 294:8227–37. doi: 10.1074/jbc.RA119.008315

Conflict of Interest: The authors declare that the research was conducted in the absence of any commercial or financial relationships that could be construed as a potential conflict of interest.

frontiers in Immunology

ORIGINAL RESEARCH
published: 29 April 2020
doi: 10.3389/fimmu.2020.00731

Proteoglycan-Dependent Endo-Lysosomal Fusion Affects Intracellular Survival of *Salmonella* Typhimurium in Epithelial Cells

*Alibek Galeev[1], Abdulhadi Suwandi[1], Hans Bakker[2], Ade Oktiviyari[1], Françoise H. Routier[2], Lena Krone[3], Michael Hensel[3] and Guntram A. Grassl[1]**

[1] *Institute of Medical Microbiology and Hospital Epidemiology, Hannover Medical School and German Center for Infection Research (DZIF), Hanover, Germany,* [2] *Institute of Clinical Biochemistry, Hannover Medical School, Hanover, Germany,* [3] *Division of Microbiology, University of Osnabrück, Osnabrück, Germany*

OPEN ACCESS

Edited by:
Megan S. Lord, University of New South Wales, Australia

Reviewed by:
Peter Monk, University of Sheffield, United Kingdom
Inger Øynebråten, Oslo University Hospital, Norway

****Correspondence:***
Guntram A. Grassl
grassl.guntram@mh-hannover.de

Specialty section:
This article was submitted to Molecular Innate Immunity, a section of the journal Frontiers in Immunology

Received: *13 December 2019*
Accepted: *31 March 2020*
Published: *29 April 2020*

Citation:
Galeev A, Suwandi A, Bakker H, Oktiviyari A, Routier FH, Krone L, Hensel M and Grassl GA (2020) Proteoglycan-Dependent Endo-Lysosomal Fusion Affects Intracellular Survival of Salmonella Typhimurium in Epithelial Cells. Front. Immunol. 11:731. doi: 10.3389/fimmu.2020.00731

Proteoglycans (PGs) are glycoconjugates which are predominately expressed on cell surfaces and consist of glycosaminoglycans (GAGs) linked to a core protein. An initial step of GAGs assembly is governed by the β-D-xylosyltransferase enzymes encoded in mammals by the *XylT1/XylT2* genes. PGs are essential for the interaction of a cell with other cells as well as with the extracellular matrix. A number of studies highlighted a role of PGs in bacterial adhesion, invasion, and immune response. In this work, we investigated a role of PGs in *Salmonella enterica* serovar Typhimurium (*S*. Typhimurium) infection of epithelial cells. Gentamicin protection and chloroquine resistance assays were applied to assess invasion and replication of *S*. Typhimurium in wild-type and xylosyltransferase-deficient (Δ*XylT2*) Chinese hamster ovary (CHO) cells lacking PGs. We found that *S*. Typhimurium adheres to and invades CHO WT and CHO Δ*XylT2* cells at comparable levels. However, 24 h after infection, proteoglycan-deficient CHO Δ*XylT2* cells are significantly less colonized by *S*. Typhimurium compared to CHO WT cells. This proteoglycan-dependent phenotype could be rescued by addition of PGs to the cell culture medium, as well as by complementation of the *XylT2* gene. Chloroquine resistance assay and immunostaining revealed that in the absence of PGs, significantly less bacteria are associated with *Salmonella*-containing vacuoles (SCVs) due to a re-distribution of endocytosed gentamicin. Inhibition of endo-lysosomal fusion by a specific inhibitor of phosphatidylinositol phosphate kinase PIKfyve significantly increased *S*. Typhimurium burden in CHO Δ*XylT2* cells demonstrating an important role of PGs for PIKfyve dependent vesicle fusion which is modulated by *Salmonella* to establish infection. Overall, our results demonstrate that PGs influence survival of intracellular *Salmonella* in epithelial cells via modulation of PIKfyve-dependent endo-lysosomal fusion.

Keywords: *Salmonella*, proteoglycans, glycosaminoglycans, xylosyltransferase, PIKfyve, gentamicin

INTRODUCTION

Proteoglycans (PGs) are heavily glycosylated proteins facilitating cell-matrix and cell-cell interactions and are also playing an important role in bacterial adhesion, invasion, and immune response (1). All PGs consist of a core protein substituted with glycosaminoglycans (GAGs) – long linear polysaccharides comprised of repeating disaccharide units. Based on the structure of the disaccharide unit, GAGs are divided into four distinct families: heparan sulfate (HS)/heparin, chondroitin/dermatan sulfate, keratan sulfate, and hyaluronan (2). The biosynthesis of the first two GAGs is initiated by the assembly of the tetrasaccharide linker D-GlcA-β1-3-Gal-β1-3-Gal-β1-4-Xyl-β-Ser. The initial, rate-limiting step is the transfer of Xyl from UDP-D-α-xylose to serine moieties of the core protein and is catalyzed by the isoenzymes β-D-xylosyltransferase-I and -II (EC 2.4.2.26) (3) encoded in humans by the *XYLT1* and *XYLT2* genes, respectively.

In the past years, a number of studies highlighted an importance of PGs in bacterial pathogenesis. Proteoglycan-mediated adhesion and invasion has been previously reported for various gram-positive and gram-negative bacteria, including *Listeria monocytogenes* (4), *Neisseria gonorrhoeae* (5), *Borrelia burgdorferi* (6), and *Salmonella enterica* serovar Typhimurium (*S.* Typhimurium) (7). *S.* Typhimurium is a successful food-borne pathogen able to colonize the human gastrointestinal tract and to cause severe diarrhea. *S.* Typhimurium manipulates actin and membrane trafficking pathways of epithelial cells initiating entry via actin-mediated macropinocytosis (8). A hallmark of *Salmonella* infection is an extensive alteration of the endo-lysosomal system and phosphoinositide metabolism of the host (9). After invasion, *S.* Typhimurium translocates effectors through a type 3 secretion system (T3SS) encoded by genes in *Salmonella* pathogenicity island 2 (SPI2) into the host cytoplasm in order to establish a replicative niche called the *Salmonella*-containing vacuole (SCV). At later stages of infection, mature SCVs acquire late endosomal markers, such as LAMP1, and fuse with the late endosomes and other organelles (ER, Golgi apparatus) forming an extensive network of tubules called *Salmonella*-induced filaments (SIFs) (10, 11). Previous studies identified that SIF formation by *S.* Typhimurium is dependent on various host factors, including the lysosomal glycoproteins LAMPs (12), vacuolar vATPase (13), the late endosomal small GTPase Rab7 (14), and secretory carrier membrane proteins (SCAMPs) (15). Moreover, there is a growing body of evidence suggesting that *Salmonella* interferes with the exocytic transport machinery and with secretory pathways (16, 17).

Phosphatidylinositol (PI) belongs to the class of the phosphatidylglycerides – glycerol-based phospholipids which are a major component of biological cell membranes. Phosphorylated forms of PI (called phosphoinositides) play important roles in cell signaling, cell growth and death, and membrane trafficking (18). For example, the monophosphorylated phosphatidylinositol-3-phosphate (PtdIns3P) orchestrates recruitment and membrane association of early endosomal proteins EEA1 and Rab5 (19). Furthermore, it was demonstrated that phosphatidylinositol-3,5-bisphosphate (PtdIns(3,5)P_2) regulates endosomal fission and fusion, as well as multivesicular body (MVB) formation and detachment (20). PIKfyve is a lipid kinase that converts PtdIns3P into PtdIns(3,5)P_2 in the endocytic microdomains of mammalian cells (21). While it is known that *Salmonella* can modulate phosphoinositide pathways in host cells (22, 23), limited knowledge exists on possible interactions of phosphoinositides with PGs.

To investigate the contribution of surface and intracellular PGs to *Salmonella* infection we utilized a proteoglycan-deficient Chinese hamster ovary (CHO) cell line (3). We demonstrate that absence of PGs in epithelial CHO cells results in an altered PIKfyve-dependent endo-lysosomal trafficking affecting intracellular *Salmonella* survival.

MATERIALS AND METHODS

Cell Lines

Chinese hamster ovary (CHO) CHO-K1 WT and CHO-K1 pgsA745 (aka Δ*XylT2*, referred to as Δ*XylT*) (3) cells were routinely cultured in DMEM/F-12 GlutaMAX growth medium (Life Technologies) supplemented with 10% (v/v) fetal bovine serum (Biochrom).

CHO Δ*XylT* Cell Line Complementation

CHO Δ*XylT* mutant was complemented with a plasmid expressing human *XYLT2* as described (24). Complementation of a G418-selected clone was confirmed by flow cytometry using the heparan sulfate-specific phage display antibody AO4B08 (25). The overlaid histograms with the peak heights were normalized to mode (% of Max). The data were analyzed using FlowJo v.10 software (TreeStar).

Bacteria and Growth Conditions

Salmonella enterica serovar Typhimurium (*S.* Typhimurium) 14028s (26), *S.* Typhimurium SL1344 WT (27), *S.* Typhimurium SL1344 eGFP (pFPV25.1) (28), *S.* Typhimurium SL1344 Δ*ssaR* (29), and *S.* Typhimurium SL1344 Δ*sifA* (30) were grown overnight at 37°C with shaking in lysogeny broth (LB) supplemented with 100 μg/mL streptomycin, 100 μg/mL ampicillin, or 50 μg/mL kanamycin, when appropriate. The reporter strain *S.* Typhimurium SL1344 p4889 (31) was grown in presence of carbenicillin 50 μg/mL. *Listeria monocytogenes* EGD strain (32) was grown at 37°C in Brain Hearth Infusion (BHI) broth. For infection, overnight cultures of bacteria were sub-cultured and grown for 3 h at 37°C to mid-log phase.

Generation of Acid Shock Reporter Plasmid

The acid shock-responsive promoter of *asr* was used to control expression of sfGFP. A dual fluorescence reporter was generated based on p4889, and P_{uhpT} in p4889 was replaced by P_{asr} by Gibson assembly (GA) cloning. Primers Vf-p4889 and Vr-p4889 were used to PCR amplify the vector backbone of p4889, and 1f p4889-Pasr and 1r Pasr-sfGFP were used to amplify the P_{asr} region from genomic DNA of *S.* Typhimurium. GA resulted

in plasmid p5386 that was confirmed by DNA sequencing, and functional analyses of response of sfGFP expression upon acid shock exposure in synthetic media buffered to various pH.

Gentamicin Protection Assay

CHO WT, CHO Δ*XylT*, or complemented CHO Δ*XylT* cells (CHO cX) were seeded in 24-well plates (10^5 cells/well) and incubated overnight in 5% CO_2 at 37°C. The next day, cells were infected with either *Listeria monocytogenes* EGD, or with different *Salmonella* strains at MOI 10, 50, or 100 (as indicated). For quantification of adherent bacteria, 30 min (or 60 min for *Listeria*) post infection (p.i.), cells were washed 3 times with PBS and lysed in PBS containing 1% (v/v) Triton X-100 and 0.1% (v/v) sodium dodecyl sulfate (SDS). The cell lysates were then serially diluted in PBS and plated on LB agar or on BHI agar for colony-forming unit (CFU) count. For later time points, upon washing, culture medium was replaced with a medium supplemented with 100 μg/mL gentamicin (Sigma) to kill extracellular bacteria. The number of invaded bacteria was determined by plating the cells lysates 1.5 h p.i. (2.5 h p.i. for *Listeria*). Medium was replaced by medium containing the indicated concentrations of gentamicin and bacterial intracellular survival or replication was assessed 4 and 24 h p.i.

Gene Expression Analysis

Total RNA was extracted from CHO cells using the High Pure RNA Isolation Kit (Roche) following the manufacturer's guidelines. Reverse transcription of 1 μg RNA of each sample was done with the High Capacity cDNA Reverse Transcription Kit (Applied Biosystems). Gene expression was assessed by qPCR using the Power SYBR® Green PCR Master Mix (Applied Biosystems) using gene specific primers (**Supplementary Table S1**). Relative gene expression was calculated by the ΔΔCt method (33) and normalized to *Gapdh* and *Rps9* housekeeping genes.

Gentamicin ELISA

To determine levels of intracellular gentamicin, CHO WT and CHO Δ*XylT* cells were washed four times with PBS and lysed. The concentration of gentamicin in cell lysates was measured using the GEN ELISA Kit (Cusabio) according to the manufacturer's protocol.

Gentamicin Cy3 Conjugation and Cell Labeling Experiments

Gentamicin sulfate salt (Sigma-Aldrich) was mixed with the Sulfo-Cyanine3 NHS ester (Lumiprobe) in 50:1 molar ratio and incubated for 1 h at room temperature. The conjugate (Gen-Cy3) was isolated by reversed-phase chromatography (column C18), aliquoted, dried, and stored in the dark at -20°C. Prior to usage, the conjugate was resuspended in sterile water, absorbance at 548 nm was measured, and a concentration was calculated using the molar attenuation coefficient of the Sulfo-Cyanine3 NHS ester. In the cell labeling experiments, gentamicin sulfate used in a protection assay was replaced with Cy3-conjugated gentamicin (GEN-Cy3) at the indicated concentrations. CHO WT and CHO Δ*XylT* cells incubated with GEN-Cy3 were fixed at different time points post infection.

CHO WT and CHO Δ*XylT* cells were seeded on coverslips and then infected with *S.* Typhimurium eGFP at an MOI of 50. Upon bacterial invasion, CHO cells were incubated for 2, 7, or 24 h in presence of 50 nM Lysotracker Red DND-99 (Sigma-Aldrich). Then, CHO cells were extensively washed with PBS, fixed with 4% paraformaldehyde (PFA) and stained with 4′,6-diamidino-2-phenylindole (DAPI) (Invitrogen) (1:1000) to visualize nuclei. Images were recorded on a Zeiss Apotome.2 microscope using AxioVision 4.9.1 software (Zeiss).

Immunocytochemistry

CHO WT and CHO Δ*XylT* cells were seeded on coverslips in 24 well plates, fixed with 4% PFA, washed 3 times with PBS, and permeabilized with Triton-X100 (0.1%). Unspecific binding was blocked using 2% normal goat serum (NGS), cells were then incubated with the AO4B08 antibody (25) (1:100) recognizing both heparin and HS. Infected cells were additionally stained with rabbit anti-*Salmonella* antibody (1:100). Upon washing, bound AO4B08 antibodies were detected by incubation with mouse anti-VSV tag IgG antibody P5D5 (1:400), followed by Alexa 488-conjugated goat anti-mouse IgG (1:1000) and Alexa 568-conjugated goat anti-rabbit IgG (1:1000) (Thermo Fisher Scientific). Phalloidin-iFluor 647 (1:1000) (Abcam) and DAPI (Invitrogen) were applied to visualize F-actin and nuclei, respectively. For a list of antibodies used see **Supplementary Table S2**.

Chloroquine Resistance Assay

To determine the number of cytosolic *S.* Typhimurium within the CHO cells, chloroquine (CHQ) resistance assay was performed as described (34). Briefly, CHO WT and CHO Δ*XylT* cells were infected as described above. 24 h p.i., the cells were incubated for 1 h in the presence of CHQ (400 μM) and gentamicin (cytosolic bacteria) or with gentamicin only (total intracellular bacteria). CHO cells were then lysed, and serial dilutions plated on LB agar plates.

Infection With *S.* Typhimurium Reporter Strains

CHO WT and CHO Δ*XylT* cells seeded on coverslips were infected with *S.* Typhimurium p4889 reporter strain at MOI 100. Upon bacterial invasion, CHO medium was supplemented with 100 μg/mL gentamicin. 24 h p.i., the infected cells and uninfected controls were fixed with 4% PFA, and then incubated with DAPI (1:1000). Images were recorded with a Zeiss Apotome.2 microscope using AxioVision 4.9.1 software (Zeiss). Bacteria in cytoplasm and in *Salmonella*-containing vacuole were enumerated in 20 random fields of view (FOV) using the Fiji software (35).

To test exposure of intracellular bacteria to acidic endosomal environments, CHO WT and CHO Δ*XylT* were infected with *S.* Typhimurium harboring p5386 at MOI of 10. Cells were incubated with or without gentamicin as indicated. CHO cells were detached 2 h after infection, chloramphenicol was added

in a final concentration of 200 μg/mL to stop further bacterial protein biosynthesis, and incubation was continued at 4°C in order to allow full maturation of all synthesized sfGFP molecules. To control the effect of host cell endosomal acidification on intracellular *S.* Typhimurium, acidification was abrogated by vATPase inhibitor bafilomycin added after infection in a final concentration of 100 nM. For quantification, at least 50,000 CHO cells were analyzed by flow cytometry on an Attune NxT (Thermo Fisher) instrument. Cells were gated for DsRed-positive, i.e., *S.* Typhimurium-infected population, and sfGFP fluorescence of this population was determined as proxy for the level of acidification.

Transfection

10^6 CHO WT and CHO Δ*XylT* cells were resuspended in 100 μl Nucleofector Solution and mixed with 5 μg of p4605 plasmid encoding human ARL8B (ADP Ribosylation Factor Like GTPase 8B) (36) and transfected using the Nucleofector Program U-027 (Lonza). Immediately after transfection, cells were resuspended in CHO medium, seeded onto cover slips in 24 well plates, and incubated for at least 18 h prior to infection.

Antibody Uptake Assay

CHO WT and CHO Δ*XylT* cells seeded on coverslips were infected with *S.* Typhimurium WT or with *S.* Typhimurium WT eGFP at an MOI of 50. 1.5 h p.i., medium was replaced with medium containing 10 μg/mL gentamicin and rabbit anti-*Salmonella* antibody (Difco). 24 h p.i., cells were fixed with 4% PFA, and bacteria were stained with the Alexa 546-conjugated donkey anti-rabbit IgG. In case of WT bacteria, samples were additionally stained with mouse anti-*Salmonella* antibody (Meridian Life Science) and Alexa 488-conjugated donkey anti-mouse IgG secondary antibody (Thermo Fisher Scientific). Bacteria were enumerated in 20 random FOVs.

Endo-Lysosomal Fusion Assay

CHO WT and CHO Δ*XylT* cells were seeded on coverslips for pulse-chase experiments. In brief, CHO cells were first incubated with dextran-Alexa568 (10,000 MW, 0.4 mg/mL) (Invitrogen) for 4 h, washed and incubated in dextran-free CHO medium for 18 h. Cells were then pulsed with dextran-Alexa488 (10,000 MW, 0.4 mg/mL) for 10 min, washed and incubated in CHO medium for 30 min. CHO WT and CHO Δ*XylT* cells were fixed with 4% PFA, and stained with phalloidin-iFluor 647 Reagent (1:1000) (Abcam) and DAPI. Images of 20 random FOVs were acquired on Zeiss Apotome.2 microscope with 63 × oil immersion objective using AxioVision 4.9.1 software (Zeiss). Spatial resolution of images was 9.7674 pixels per micron, pixel size: 0.1024 × 0.1024 micron^2. Endo-lysosomal fusion was scored by quantifying co-localization between the two labeled dextrans using ImageJ version 1.52e and JACoP plugin for pixel intensity spatial correlation analysis (37). Pearson's correlation coefficient and Manders split coefficients (M1 and M2, thresholds set manually for both channels) were calculated.

Cytotoxicity Assay

CHO cells were infected with *S.* Typhimurium WT strain as described previously. 24 h p.i., supernatants were collected and an activity of the lactate dehydrogenase (LDH) was measured using the Pierce LDH Cytotoxicity Assay Kit (Thermo Fisher Scientific) following the manufacturer's instructions.

Statistical Analysis

Data were analyzed using Prism V7.0d software (GraphPad). Statistical analysis was done using one-way analysis of variance (ANOVA) followed by Tukey's multiple comparison test, or Dunnett's multiple comparison test, the Kruskal-Wallis test followed by Dunn's multiple comparison test, unpaired two-tailed t-test, or Wilcoxon-Mann-Whitney test as indicated. The results were considered statistically significant when *p*-values were smaller than 0.033. Graphs display the mean values ± SD and represent three independent biological repetitions unless stated otherwise.

RESULTS

Proteoglycans Are Crucial for *Salmonella* Survival Within CHO Cells

Proteoglycans were shown to contribute to *Salmonella* invasion via interaction with the bacterial adhesin PagN (7). However, PagN is only expressed under intracellular (SPI2)-inducing conditions and when PagN is not expressed, invasion of host cells is PG-independent. Furthermore, it is not known if PGs are important for intracellular survival or replication. To test this, CHO WT and proteoglycan-deficient CHO Δ*XylT* cells were infected with *S.* Typhimurium WT strains. Bacterial adhesion (30 min p.i), invasion (1.5 h p.i), and early replication (4 h p.i) were comparable between CHO WT and CHO Δ*XylT* cells. However, 24 h p.i., we detected a significant reduction of intracellular bacteria in CHO Δ*XylT* compared to CHO WT cells incubated in presence of 100 μg/mL gentamicin (**Figure 1A**). Gentamicin-mediated killing of *S.* Typhimurium 14028S and SL1344 strains CHO Δ*XylT* cells was dose-dependent (**Figure 1B**). In contrast, when ampicillin was applied instead of gentamicin, a dose-dependent reduction of bacterial intracellular numbers was detected in the both CHO WT and CHO Δ*XylT* cells infected with *S.* Typhimurium 14028S at 24 p.i. (**Supplementary Figure S1**). To determine whether the effect on intracellular survival is *Salmonella*-specific, we infected CHO WT and CHO Δ*XylT* cells with another intracellular pathogen, *Listeria monocytogenes*. In contrast to *Salmonella*, reduction of intracellular *Listeria* was dependent on the gentamicin dose but not dependent on the presence of proteoglycans (**Figure 1C**).

Next, we asked whether proteoglycan can affect the uptake of gentamicin into CHO cells as increased uptake of gentamicin by CHO Δ*XylT* cells could contribute to increased killing of intracellular *Salmonella*. CHO cells were infected with *S.* Typhimurium WT as described above and intracellular gentamicin concentrations were measured by ELISA. No differences in intracellular gentamicin levels were detected

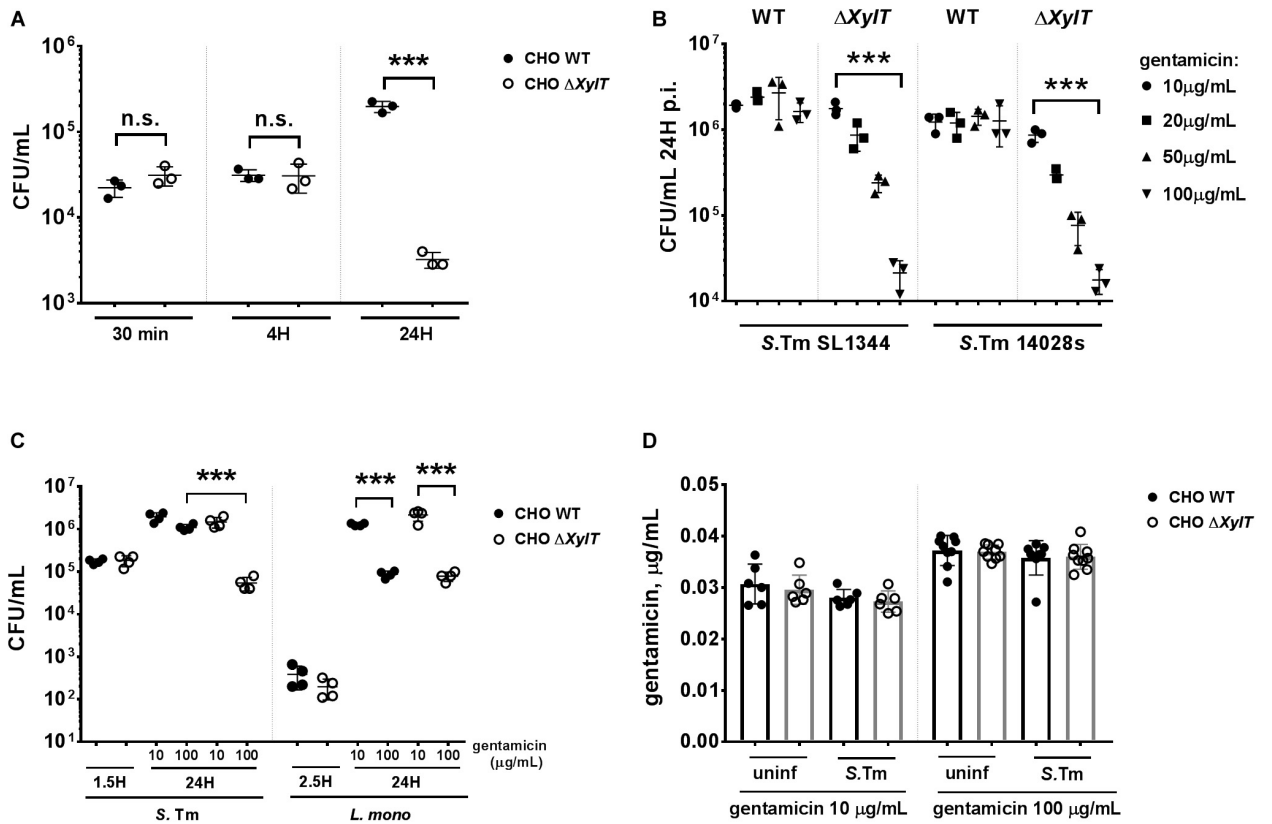

FIGURE 1 | Proteoglycans influence survival of intracellular *S.* Typhimurium. **(A)** CHO WT and CHO Δ*XylT* cells were infected with *S*. Typhimurium WT at MOI 10 for 30 min, washed three times with PBS and then lysed to assess adherence. Remaining wells were incubated for 1 h with 100 μg/mL gentamicin to kill extracellular bacteria, and then either lysed immediately to evaluate invasion or at various time points post infection (p.i.) following incubation with media supplemented with 100 μg/mL gentamicin, as indicated. Lysates were collected, serially diluted and plated on agar plates. CHO Δ*XylT* (open circles), CHO WT cells (closed circles). **(B)** CHO WT and CHO Δ*XylT* cells were infected with *S*. Typhimurium SL1344 or with *S*. Typhimurium 14028s at MOI 50. Inhibition of bacterial growth (of both strains) in CHO Δ*XylT* cells was dependent on the gentamicin concentration used. **(C)** CHO WT and CHO Δ*XylT* cells were infected with either *S*. Typhimurium WT for 30 min., or with *L. monocytogenes* for 1 h (MOI 50) followed by treatment with 100 μg/mL gentamicin for 60 min. At 1.5 h (*Salmonella*) or 2.5 h (*Listeria*) medium was replaced with medium containing the indicated concentration of gentamicin. **(D)** Total cell lysates of the CHO WT and CHO Δ*XylT* cells at 24 h p.i. (non-infected, or infected with *S*. Typhimurium WT) incubated with 10 mg/mL or 100 μg/mL gentamicin were collected and levels of the intracellular gentamicin were measured by ELISA. Data points, means and SD of representative results of three independent experiments are depicted. One-way ANOVA with Tukey's multiple comparison test, n.s. (not significant), ***$p < 0.001$.

between CHO WT and CHO Δ*XylT* cells, or between uninfected and infected cells (**Figure 1D**). Previous studies emphasized a role of the transient receptor potential channels (Trpv), Trpv1 (38) and Trpv4 (39), and the multidrug resistance protein 2 (Mrp2 or Abcc2) (40) in the cellular uptake and transport of gentamicin, respectively. Expression of *Trpv1*, *Trpv4*, and *Mrp2* genes was comparable in non-infected and infected CHO WT and CHO Δ*XylT* cells (**Supplementary Figures S2A–C**). Collectively, these findings indicate that a lack of proteoglycans in CHO cells does not affect active or passive gentamicin uptake.

To verify that the observed phenotype is indeed due to the proteoglycan deficiency, we complemented the CHO Δ*XylT* cells with the human *XYLT2* gene. When compared to the proteoglycan-deficient CHO Δ*XylT* cells, complemented CHO c*XylT* cells harbored similar levels of *Salmonella* after invasion (at 1.5 h p.i.), but significantly more bacteria at 24 h p.i. (**Figure 2A**). However, while compared to CHO WT cells, complemented CHO c*XylT* cells still had lower *S.* Typhimurium loads 24 h p.i., which correlated with lower amounts of proteoglycans present on CHO c*XylT* cells, as assessed by flow cytometry (**Supplementary Figure S3**A), indicating only partial complementation of PGs. Next, we tested if addition of proteoglycans to the medium could also complement *Salmonella* survival in CHO Δ*XylT* cells. Addition of heparin (a structural analog of heparan sulfate) to the medium increased bacterial survival in CHO Δ*XylT* cells in a dose-dependent manner, but did not affect *Salmonella* survival in CHO WT cells (**Figure 2B**). In contrast, addition of equimolar amounts of chondroitin sulfate A (**Figure 2C**) or 2-fucosyllactose (**Figure 2D**) did not affect intracellular bacterial numbers in either CHO cell line. Notably, heparin did not support or inhibit growth of *S.* Typhimurium in LB medium and did not affect killing of *Salmonella* in LB broth supplemented with 100 μg/mL gentamicin (**Supplementary Figure S3**B). To summarize, these results indicate that host proteoglycans are important for the

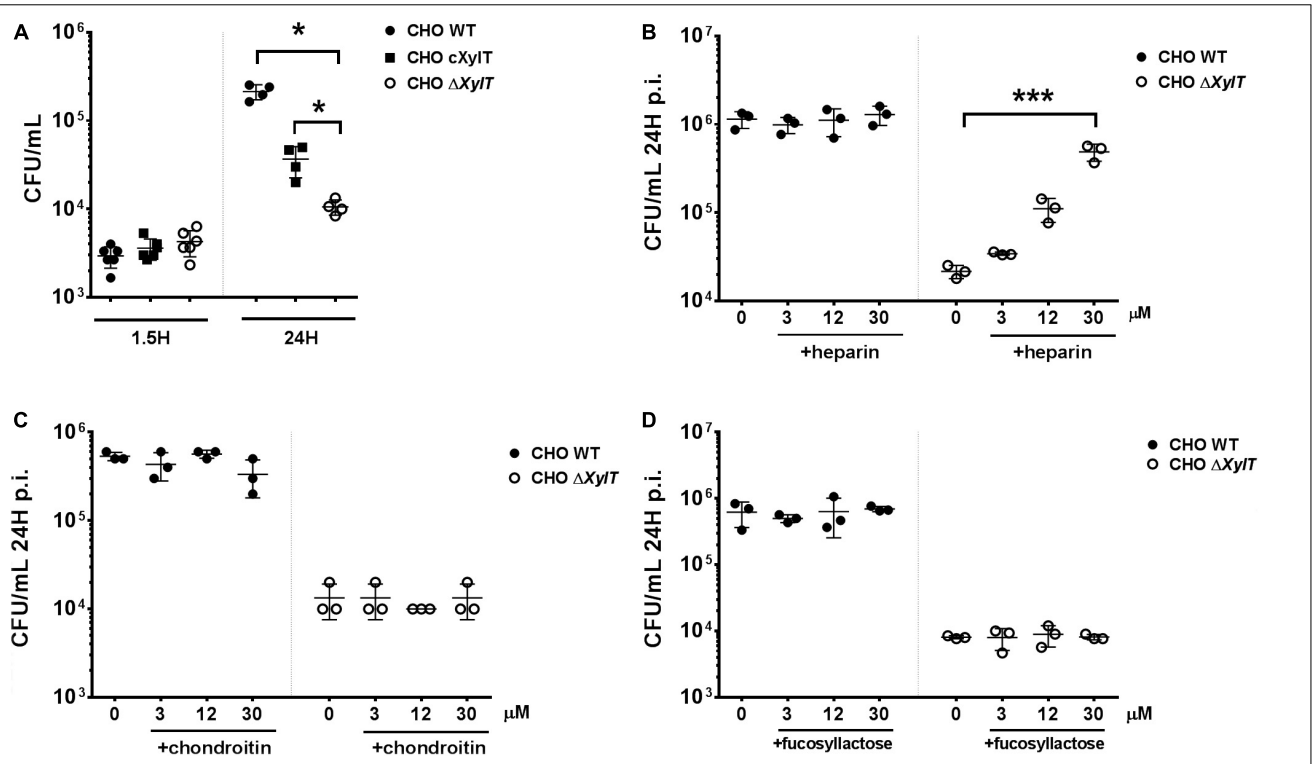

FIGURE 2 | Proteoglycan-dependent phenotype can be rescued by an addition of the external GAGs as well as by *XylT2* gene complementation. CHO WT and CHO Δ*XylT* cells were infected with *S.* Typhimurium WT and incubated for 24 h with 100 μg/mL gentamicin or lysed immediately to evaluate invasion. **(A)** Infection of complemented of CHO Δ*XylT* cells (indicated as cXylT, in black squares) resulted in significantly higher numbers of intracellular *Salmonella* in comparison to CHO Δ*XylT* cells. Mann–Whitney *U* test, $*p < 0.033$. CHO WT and CHO Δ*XylT* cells were infected with *S.* Typhimurium WT at MOI 50. Gentamicin (100 μg/mL) was added 30 min p.i. Heparin sodium salt **(B)**, chondroitin sulfate **(C)** or 2′-fucosyllactose **(D)** was added at indicated concentrations 1.5 h p.i. Data points, means and SD of representative results of three independent experiments are depicted. One-way ANOVA with Dunnett's multiple comparison test, not significant differences are not indicated, $***p < 0.001$.

survival of *Salmonella* in epithelial cells when gentamicin is added to the tissue culture medium.

CHO Cells Lacking Proteoglycans Display a Lower Abundance of SCV-Associated *Salmonella*

To investigate if a lack of proteoglycans might affect subcellular localization of intracellular bacteria, CHO WT and CHO Δ*XylT* cells were infected with a *S.* Typhimurium reporter strain expressing DsRed protein constitutively and sfGFP only when bacteria are located in the cytosol (31). Microscopy revealed that CHO Δ*XylT* cells incubated with 100 μg/mL gentamicin had significantly lower numbers of total bacteria, but significantly higher numbers of GFP-expressing, cytosolic *Salmonella* compared to CHO WT at 24 h p.i., as shown by an elevated ratio of cytosolic/total bacteria in infected cells (**Figures 3A,B**). Addition of chloroquine selectively kills *Salmonella* within SCVs (34). Therefore, we used a combination of chloroquine resistance assay and gentamicin protection assay to determine cytosolic and intra-SCV bacteria corroborating our results obtained with the reporter strains (**Figure 3C**). To further investigate the subcellular localization of *Salmonella*, *S.* Typhimurium Δ*sifA* strain was utilized. This mutant is not able to maintain SCV integrity upon infection, which results in an extensive cytosolic replication of bacteria (30). Intracellular replication was analyzed by gentamicin protection assay, and expressed as a ratio of replicated (CFU at 24 h p.i)/invaded (CFU at 1.5 h p.i) bacteria. Intracellular proliferation of *S.* Typhimurium Δ*sifA* in CHO WT cells in the presence of 100 μg/mL gentamicin was about two times higher when compared to *S.* Typhimurium WT. In contrast, in CHO Δ*XylT* cells, *S.* Typhimurium Δ*sifA* intracellular replication was about 50 times higher compared to *S.* Typhimurium WT strain (**Figure 3D**). The differences in late replication were even more pronounced in CHO and CHO Δ*XylT* cells incubated with 200 μg/mL gentamicin (**Figure 3D**). Overall, these data indicate that the reduction of bacterial burden in CHO Δ*XylT* cells was due to a diminished number of bacteria in SCV, while cytosolic bacteria were largely unaffected by increasing concentrations of gentamicin.

Recently, it has been shown that *Salmonella*-induced filaments (SIFs) can increase the exposure of bacteria to internalized antibiotics in the SCV (41). To evaluate a contribution of the SIF network to the observed phenotype, CHO WT and CHO Δ*XylT* cells were infected with either *S.* Typhimurium WT or *S.* Typhimurium Δ*ssaR* (a SPI-2 mutant lacking SIFs) (29). In

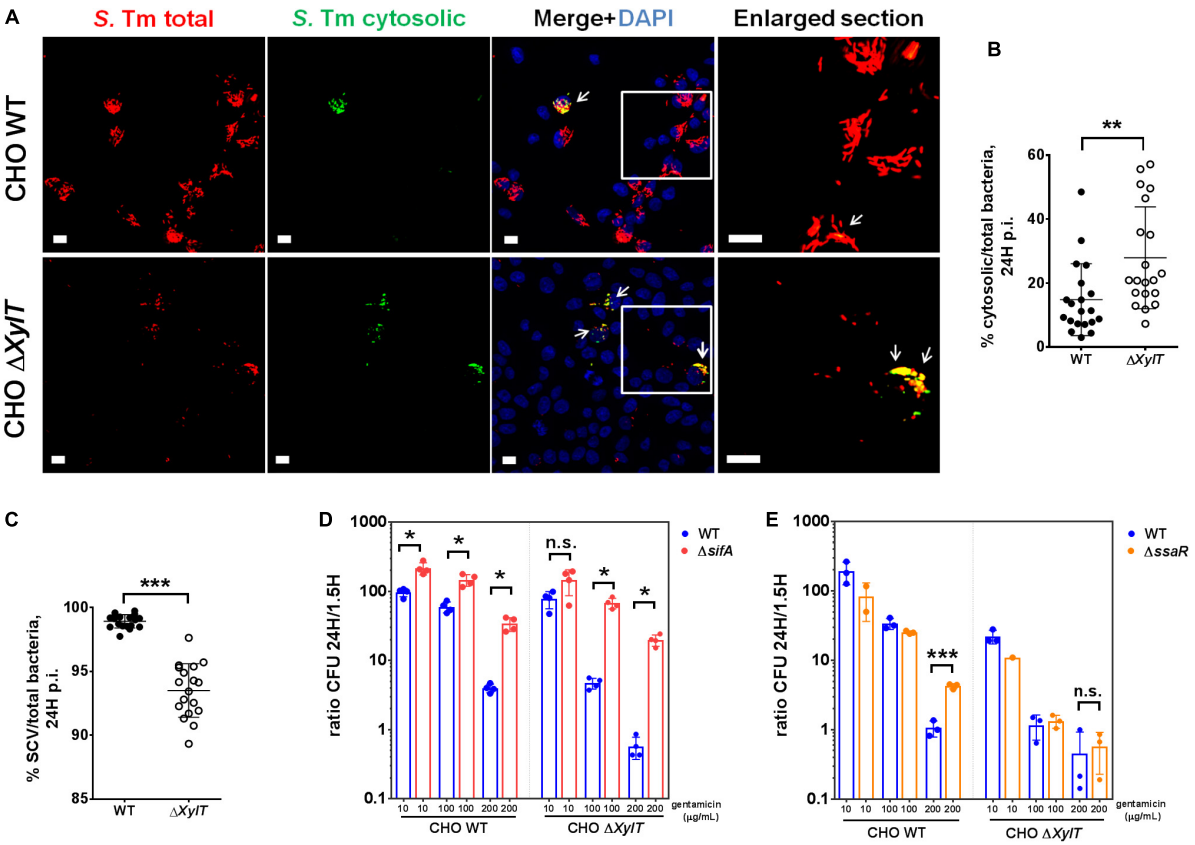

FIGURE 3 | *Salmonella* in SCV, but not cytosolic bacteria, are affected by gentamicin in proteoglycan-deficient cells. **(A,B)** CHO WT and CHO Δ*XylT* cells were infected at MOI 100 with *S.* Typhimurium [p4889] and then incubated in presence of 100 μg/mL gentamicin. 24 h p.i., cell monolayers were washed, fixed with 4% PFA and stained with DAPI. Microscopy revealed a significantly higher number of GFP-expressing, cytosolic *Salmonella* (indicated by arrows) in CHO Δ*XylT* cells compared to CHO WT. Scale bars, 10 μm. Mann–Whitney *U* test, $^{**}p < 0.002$. **(C)** CHO WT and CHO Δ*XylT* cells were infected with *S.* Typhimurium WT at MOI 50, and gentamicin (100 μg/mL) was added 30 min after infection. 24 h p.i., cells were treated with 400 μM chloroquine for 1 h, then washed with PBS and lysed. Mann–Whitney *U* test, $^{***}p < 0.001$. **(D–E)** CHO WT and CHO Δ*XylT* cells were infected with either *S.* Typhimurium WT, *S.* Typhimurium Δ*sifA*, or *S.* Typhimurium Δ*ssaR* at MOI 50. Gentamicin (100 μg/mL) was added 30 min after infection. 1.5 h p.i. medium was replaced with medium containing gentamicin at 10, 100, or 200 μg/mL as indicated. Intracellular CFU counts were determined 1.5 and 24 h p.i. and depicted is the intracellular replication (CFU ratio of 24 to 1.5 h). **(D)** Cytosolic bacteria (Δ*sifA*) showed higher intracellular replication than WT *Salmonella* in both CHO cell types. Data points, means and SD of representative results of two independent experiments are depicted. Mann–Whitney *U* test, n.s. (not significant), $^{*}p < 0.033$. **(E)** Intracellular replication of *S.* Typhimurium Δ*ssaR* mutant compared to WT *S.* Typhimurium was increased in CHO WT but not in CHO Δ*XylT* cells. Data points, means and SD of representative results of three independent experiments are depicted. Unpaired *t*-test, n.s. (not significant), $^{***}p < 0.001$.

agreement with the findings by Liss et al. (41), incubation of the infected CHO WT cells with 200 μg/mL gentamicin for 24 h resulted in a significantly higher intracellular proliferation of *S.* Typhimurium Δ*ssaR* compared to the WT strain. In contrast, numbers of both intracellular *Salmonella* WT and Δ*ssaR* were strongly decreased in CHO Δ*XylT* cells (**Figure 3E**) indicating that the gentamicin-mediated inhibition of bacterial growth in CHO Δ*XylT* cells is independent of SIFs.

Proteoglycans Are Important for PIKfyve-Dependent Endo-Lysosomal Fusion

Our observation that CHO WT and CHO Δ*XylT* cells had similar levels of intracellular gentamicin was based on ELISA measurements of whole cell lysates. Next, we tested whether intracellular localization of gentamicin is altered in the absence of proteoglycans. Indeed, in infected CHO Δ*XylT* cells Cy3-labeled gentamicin was found close to *Salmonella*, or bacterial debris, while in CHO WT cells gentamicin-Cy3 was distributed more randomly (**Figure 4A**). Of note, uninfected CHO WT and Δ*XylT* cells were similar in terms of a distribution of labeled gentamicin (**Supplementary Figure S4**). Such re-distribution of an antibiotic may enhance *Salmonella* killing within modified compartments of CHO Δ*XylT* cells. Association of bacteria with vacuolar markers such as LAMP-1 or ARL8B was similar in CHO WT and CHO Δ*XylT* cells (**Figure 4B**).

We hypothesized that a lack of PGs may also alter intracellular routing of cargo other than antibiotics. To test this, we employed an antibody uptake assay. Cells were infected with GFP-expressing *S.* Typhimurium, and an anti-*Salmonella* antibody was added to cell culture medium 1.5 h p.i. (after invasion of

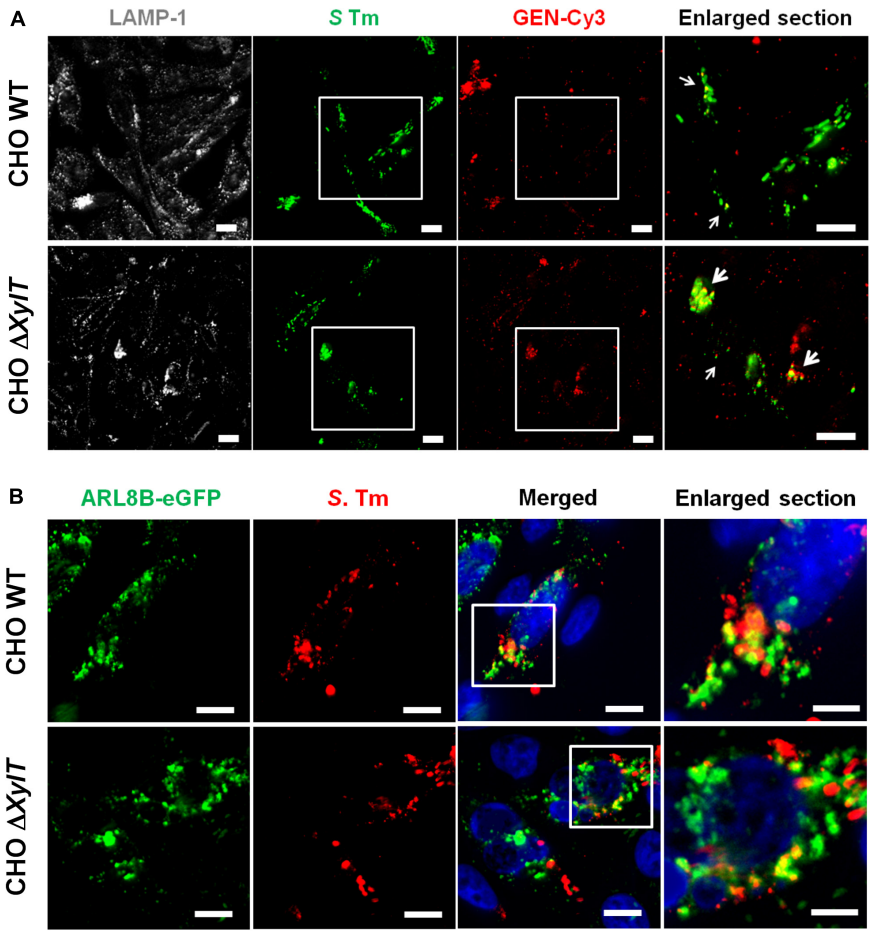

FIGURE 4 | Intracellular gentamicin is associated with *Salmonella* in CHO Δ*XylT* cells. **(A)** CHO cells were infected with *S*. Typhimurium WT, incubated with Cy3-labeled gentamicin 30 min p.i., and 7 h p.i. fixed with 4% PFA, stained with anti-*Salmonella* antibody, Phalloidin-iFluor647 and DAPI. Microscopy revealed an enhanced co-localization of Cy3-labeled gentamicin and *Salmonella* in CHO Δ*XylT* cells (bottom row) resulting in a degradation of bacteria (enlarged section, indicated by arrows). Scale bars, 10 μm. A representative image of three biological repetitions is shown. **(B)** CHO WT and CHO Δ*XylT* cells were transfected with a plasmid encoding the human ARL8B gene fused to eGFP. Cells were infected with *S*. Typhimurium WT at MOI of 50. Eight hours p.i. cells were fixed and stained for *S*. Typhimurium (in red). Representative images of two biological repetitions, scale bars, 10 μm or 5 μm (in enlarged sections).

bacteria). 24 h p.i., we observed that significantly higher numbers of intracellular *S*. Typhimurium were stained with the anti-*Salmonella* antibody in infected CHO Δ*XylT* cells compared to CHO WT cells (**Figures 5A,B**). Addition of heparin to the cell culture medium 1.5 h p.i. reduced the number of double-positive bacteria in the infected CHO Δ*XylT* cells, while the total number of *S*. Typhimurium increased. These data indicates an important role of PGs in proper vesicle trafficking (**Figure 5C**).

Vacuole acidification is sensed and manipulated by *Salmonella*. To test whether endo-lysosomal trafficking and acidic vacuole formation is affected by proteoglycans we stained acidic organelles by incubation with Lysotracker. Strikingly, CHO Δ*XylT* cells (both non-infected and infected) were less stained than CHO WT cells when incubated with Lysotracker (**Figure 6A**). Interestingly, complemented CHO c*XylT* cells displayed an intermediate degree of Lysotracker staining (**Supplementary Figure S5**). To test if a lack of PG affects SCV acidification, we used a *Salmonella* strain harboring dual fluorescence reporter p5386 to monitor exposure of intracellular *Salmonella* to acidic pH (**Supplementary Figures S6AB**). The reporter features constitutive expression of DsRed, allowing the localization of intracellular *Salmonella*, and sfGFP under control of the acid shock response-activated promoter P_{asr} (42, 43). *In vitro* analyses demonstrated the P_{asr} is activated if *Salmonella* is exposed to media of pH 5.0 or lower. Exposure to media with higher pH did not lead to synthesis of sfGFP under control of P_{asr} (**Supplementary Figure S6C**). Inhibition of acidification of the SCV by addition of vATPase inhibitor bafilomycin fully ablated expression of P_{asr}:sfGFP (**Supplementary Figure S6D**). Expression of P_{asr}:sfGFP at 2 h p.i. was not affected by presence of absence of gentamicin in the cell culture medium (**Figure 6B**). However, at 8 h p.i, we observed lower expression of P_{asr}:sfGFP in CHO Δ*XylT* cells compared to CHO WT cells (**Figure 6C**). Taken together, the acidification of endosomal compartments is impaired in PG-deficient cells as indicated by the lower signal intensity

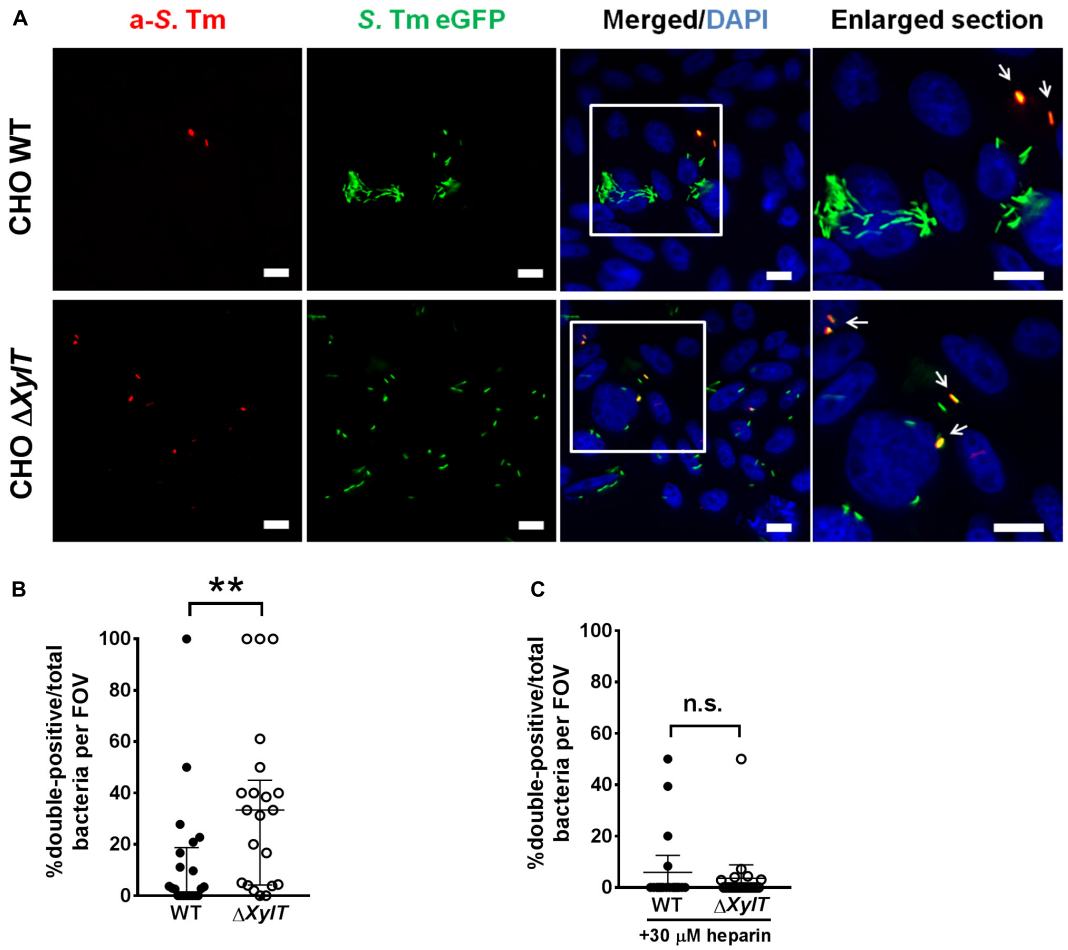

FIGURE 5 | Endocytosed cargo in infected proteoglycan-deficient CHO Δ*XylT* cells co-localizes with *Salmonella*. CHO cells were infected with *S.* Typhimurium eGFP. Gentamicin (100 μg/mL) was added 30 min after infection and 1.5 h p.i. anti-*Salmonella* antibody was added to the medium. 24 h p.i. cells were fixed with 4% PFA, and stained with DAPI. **(A)** Double-positive bacteria are indicated with arrows in enlarged section. Scale bars, 10 μm. **(B)** Number of double-positive bacteria was counted in 20 FOVs. Mann–Whitney *U* test, $^{**}p < 0.002$. **(C)** 1.5 h p.i. heparin (30 μM) was added to growth medium containing anti-*Salmonella* antibody. 20 random FOVs were counted, mean values with 95% CI are shown. Mann–Whitney *U* test, n.s., not significant.

of Lysotracker labeling and lower expression of P_{asr}:sfGFP in Δ*XylT* cells.

To identify, at which stage trafficking of endocytosed cargo is affected by the lack of PGs, we utilized inhibitors of clathrin-mediated endocytosis (dynasore), phosphoinositide 3-kinase PI3K (wortmannin), as well as an inhibitor of FYVE finger-containing phosphoinositide kinase (PIKfyve) activity (YM201636). Application of dynasore 1.5 h p.i. (added after invasion of bacteria resulted in a significantly higher recovery of *S.* Typhimurium from CHO Δ*XylT* cells compared to the non-treated controls. In contrast, dynasore treatment had no significant effect on intracellular bacterial numbers in CHO WT cells (**Figure 7A**). In addition, treatment of either CHO WT or CHO Δ*XylT* cells with wortmannin had no significant effect on intracellular *S.* Typhimurium numbers (**Supplementary Figure S7**). When PIKfyve activity in CHO WT cells was inhibited with YM201636, *S.* Typhimurium numbers were reduced in a dose-dependent manner in agreement with the results by Kerr et al. (44). However, YM201636 treatment of CHO Δ*XylT* cells resulted in significantly more intracellular bacteria compared to non-treated cells (**Figure 7B**). Heparin treatment abrogated the dose-dependent effect of YM201636 on *Salmonella* survival (**Figure 7C**) implying a direct effect of PGs on PIKfyve activity. Soluble heparin was detected within endosomal compartments and SCVs in the heparin-treated CHO Δ*XylT* cells as revealed by immunostaining (**Supplementary Figure S10**). Application of YM201636 also resulted in diminished numbers of double-positive bacteria in both CHO cell lines in an antibody uptake assay (**Figure 7D**). Furthermore, incubation of CHO WT and CHO Δ*XylT* cells with PIKfyve-inhibitor dramatically enhanced the size of acidic lysosomes (**Supplementary Figure S8**). These data demonstrate a critical role of proteoglycans in PIKfyve-mediated fusion events.

To assess if endo-lysosomal fusion is abrogated in CHO Δ*XylT* cells, we employed a modified pulse-chase assay using Alexa568- and Alexa488-labeled dextrans to label lysosomes/late

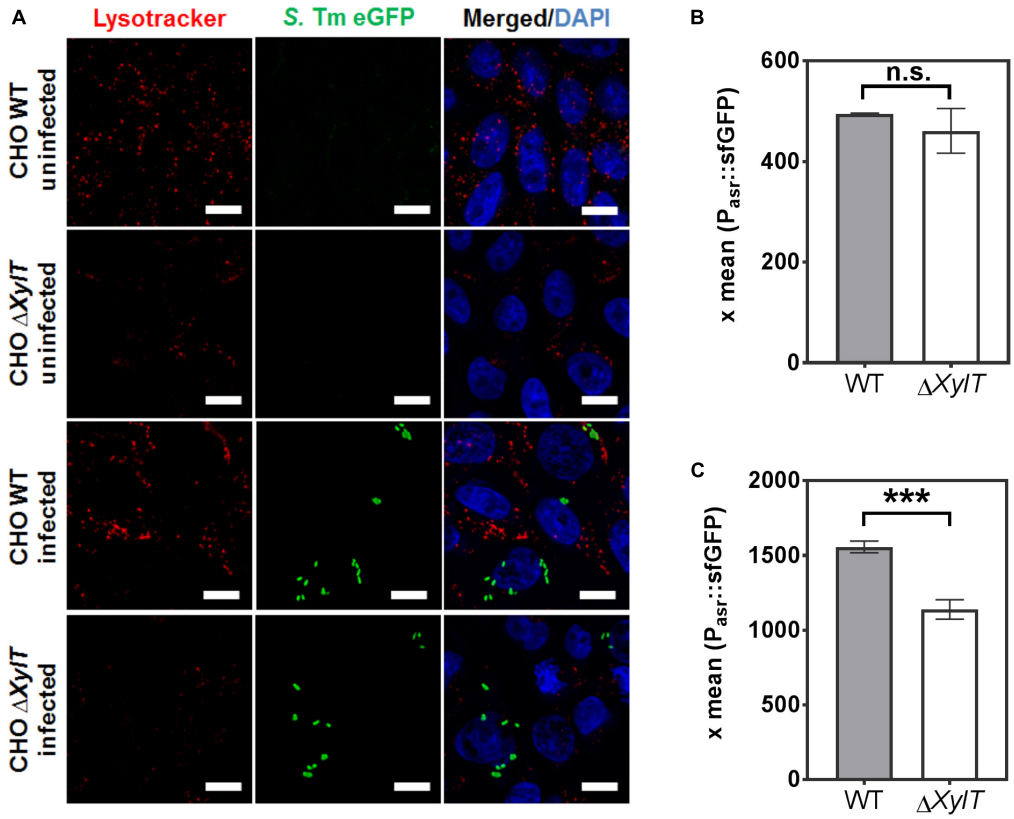

FIGURE 6 | Acidic organelles in CHO Δ*XylT* cells display reduced labeling by Lysotracker. **(A)** Uninfected CHO WT and CHO Δ*XylT* cells, or cells infected with *S.* Typhimurium EGFP at MOI of 50, were incubated for 2 h with 50 nM Lysotracker Red. Cells were fixed with 4% PFA. Representative images of three biological repetitions, scale bars, 10 μm. **(B,C)** Acidification of *Salmonella* is dependent on the presence of PGs. CHO WT or CHO Δ*XylT* cells were infected with *Salmonella* WT harboring an acid shock sensor. Infection and analyses by flow cytometry were performed as described in **Supplementary Figure S6**. After infection for 30 min, cells were treated with 100 μg/mL gentamicin for 1 h followed by 10 μg/mL gentamicin for 1 h **(B)** or 7 h **(C)**. The mean sfGFP fluorescence intensity is displayed for CHO cells harboring DsRed-positive *Salmonella*. X-means and standard deviations are shown for triplicate samples, and the data shown are representative for three biological replicates with similar outcome. Unpaired *t*-test, n.s., not significant, ***$p < 0.001$.

endosomes and early endosomes, respectively, as described by Kerr et al. (44). CHO WT and CHO Δ*XylT* cells were incubated with dextran-Alexa568 for 4 h, followed by incubation in dextran-free CHO medium. 18 h later, cells were incubated with dextran-Alexa488 for 10 min, washed and incubated in CHO medium for another 30 min before fixation with 4% PFA. To assess vesicle fusion events, Pearson's correlation coefficient and Manders split coefficients (M1 and M2, thresholds set manually for both channels) were calculated. CHO Δ*XylT* cells had significantly lower degree of co-localization between the two dextrans compared to CHO WT cells indicating a delayed or reduced endo-lysosomal fusion in proteoglycan-deficient cells (**Figure 8**).

DISCUSSION

In the present study, we report a novel role of PGs for endo-lysosomal fusion. PG deficiency abrogates endo-lysosomal fusion which affects *Salmonella* survival within epithelial cells in a context of gentamicin protection assay. Wild-type CHO cells exclusively utilize *Xylt2* for PGs biosynthesis and lack detectable *Xylt1* gene expression (45). CHO pgsA745 (Δ*XylT2*) cells lack the xylosyltransferase-II enzyme and thus, are PG-deficient (3). This cell line has been extensively used to investigate the contribution of PGs to the entry of bacterial and viral pathogens into host cells (46). Recently, it has been identified that CHO Δ*XylT* cells also carry a mutation in the *Lama2* gene. The resulting deletion of the long isoform of the laminin subunit α-2 significantly reduced invasion of group B *Streptococcus* in CHO Δ*XylT* compared to CHO WT cells (47). Indeed, while both the short and the long isoforms of laminin-2 were expressed in our CHO WT cells, CHO Δ*XylT* cells lacked the long isoform expression (**Supplementary Figure S9**). In addition, it was shown that when *Salmonella* is grown under *pagN*-inducing conditions there was a reduced uptake into CHO Δ*XylT* cells (7). However, in our study, no differences in terms of *S.* Typhimurium adhesion to and invasion into the CHO WT and CHO ΔXylT cell lines were detected.

Upon invasion, *Salmonella* hijack endo-lysosomal trafficking and acquire host factors including LAMP1 and ARL8B in

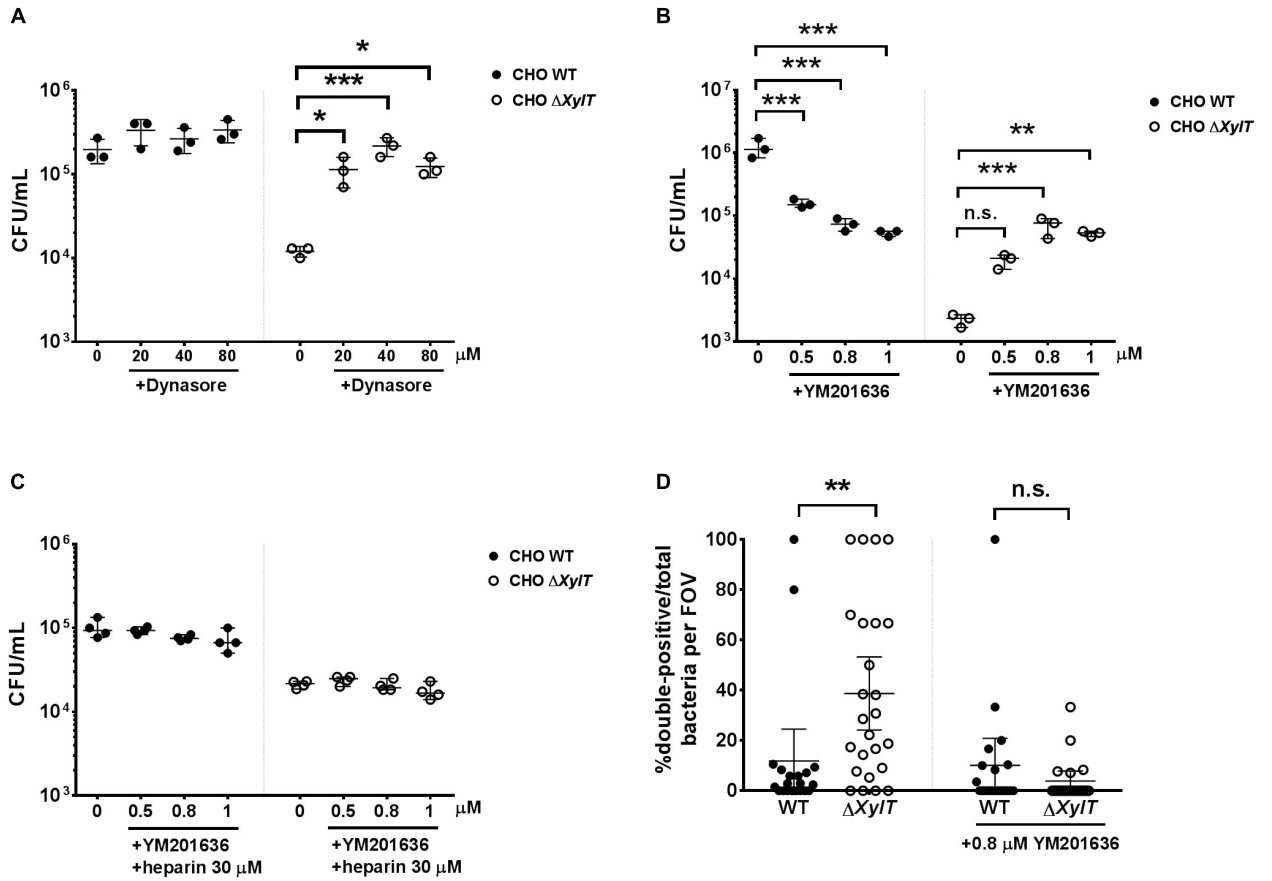

FIGURE 7 | Inhibition of endo-lysosomal fusion increases *Salmonella* burdens in CHO Δ*XylT* cells. CHO WT and CHO Δ*XylT* cells were infected with *S*. Typhimurium WT at MOI = 50 and incubated for 24 h in presence of 100 μg/mL gentamicin and increasing concentrations of **(A)** dynasore or **(B)** YM201636. One-way ANOVA with Dunnett's multiple comparison test, n.s. (not significant), $^{*}p < 0.033$, $^{**}p < 0.002$, $^{***}p < 0.001$. **(C)** CHO WT and CHO Δ*XylT* cells were first infected with *S*. Typhimurium WT at MOI of 50. After 30 min, cells were incubated with 100 μg/mL gentamicin, heparin (30 μM), and different concentrations of YM201636 for 24 h. One-way ANOVA with Dunnett's multiple comparison test, not significant differences are not indicated**. (D)** CHO cells were infected with *S*. Typhimurium eGFP. Gentamicin (100 μg/mL) was added 30 min after infection and 1.5 h p.i. anti-*Salmonella* antibody and 0.8 μM YM201636 were added to the medium. 24 h p.i., cells were fixed with 4% PFA. 20 random FOV were counted. Graph shows mean values with 95% CI. Mann–Whitney *U* test, $^{**}p < 0.002$, n.s., not significant.

order to establish a *Salmonella*-containing vacuole (SCV) and later on, *Salmonella*–induced filaments (SIFs). Microscopy and chloroquine resistance assays revealed that in the absence of PGs, significantly less bacteria were associated with SCVs when compared to WT CHO cells, while similar numbers of cytosolic bacteria were found in CHO WT and CHO Δ*XylT* cells. It should be noted that no differences in the levels of a total intracellular gentamicin between CHO WT and CHO Δ*XylT* cells were detected. Thus, we reasoned that an intracellular localization of gentamicin might be altered in the infected CHO Δ*XylT* cells, which leads to an increased exposure of specific bacterial populations to the antibiotic. Although cell membranes are generally regarded to be impermeable to gentamicin, aminoglycosides can be transported into epithelial cells via endocytosis-dependent and -independent pathways (48). It was previously reported that endocytosis of gentamicin resulted in its accumulation within lysosomes and in increased lysosomal ROS production in kidney epithelial cells (49). CHO Δ*XylT* cells are not defective in terms of endocytosis/phagocytosis (47), which is supported by our data regarding uptake of gentamicin (Cy3-labeled and by ELISA). However, during infection, we observed an increased co-localization of gentamicin and SCV-associated bacteria in proteoglycan-deficient CHO cells. Indeed, the *S.* Typhimurium Δ*sifA* mutant, which cannot establish a functional SCV and therefore localizes to the cytoplasm (50), was significantly less affected by increasing gentamicin concentrations than WT *Salmonella,* in both CHO cell lines. To conclude, the intracellular re-distribution of gentamicin in proteoglycan-deficient CHO cells was associated with a drastic reduction of *Salmonella* counts.

In addition, we detected increased accumulation of an anti-*Salmonella* antibody in SCV/SIF compartments in CHO Δ*XylT* compared to CHO WT cells. This process could be blocked by addition of heparin to cell culture medium or by inhibiting of PIKfyve activity in CHO Δ*XylT* cells. CHO WT cells treated with a specific PIKfyve inhibitor

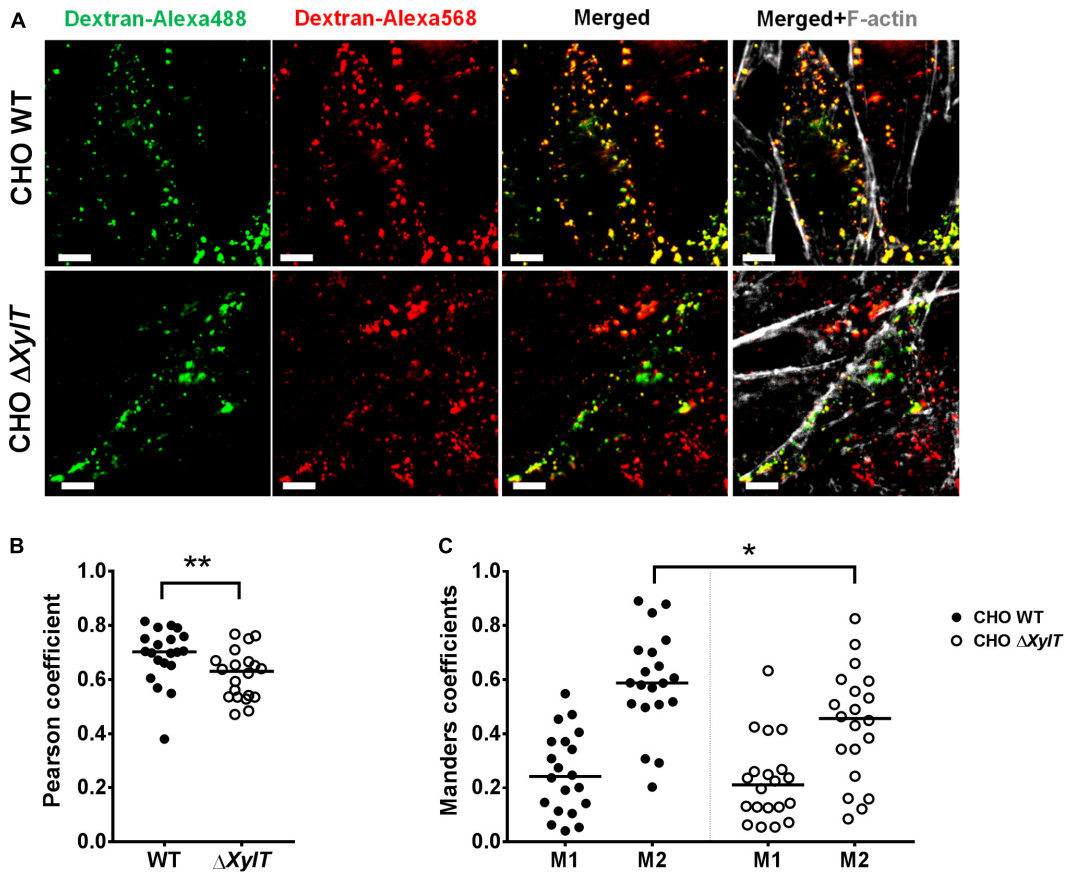

FIGURE 8 | CHO Δ*XylT* cells display reduced degree of endo-lysosomal fusion. CHO WT and CHO Δ*XylT* cells were seeded on cover slips and pulsed for 4 h with dextran-Alexa568, followed by incubation with CHO medium. 18 h later dextran-Alexa488 was added for 10 min, cells were washed and 30 min later, cells were fixed with 4% PFA. **(A)** Co-localization of Alexa-labeled vesicles can be seen in the merged section. Scale bars, 5 μm. **(B)** Pearson correlation coefficient was calculated for 20 FOVs per cell line. **(C)** CHO Δ*XylT* cells have same fraction of late endosomes overlapping with early endosomes (M1), but smaller fraction of early endosomes co-localizing with late endosomes (M2). Mander's overlap coefficient calculated for each of 20 FOVs, Mann–Whitney *U* test, $^{*}p < 0.033$, $^{**}p < 0.002$. Data are representative of two biological repetitions, median values are indicated on graphs.

(YM201636) were characterized by significantly reduced bacterial loads compared to untreated controls which is in line with observations by Kerr et al. (44). In contrast, inhibition of PIKfyve in CHO Δ*XylT* cells increased *S.* Typhimurium counts. PIKfyve is a kinase that converts PtdIns3P into PtdIns(3,5)P_2. It has been suggested that PIKfyve orchestrates the fusion of *Salmonella* macropinosomes with organelles of the late endosomal/lysosomal system (44), and more recent data link PIKfyve activity with the recycling of tight junction proteins (51) and with a re-distribution of endocytosed cargo from/to lysosomes occurring at late stages of endocytic vacuole maturation (52). As we observed a different distribution of Cy3-labeled gentamicin and endocytosed antibody within the CHO WT and CHO Δ*XylT* cells, we speculated that proteoglycans are required for PIKfyve-dependent endo-lysosomal fusion and subsequent trafficking/recycling pathways. Interestingly, CHO Δ*XylT* cells displayed reduced labeling with Lysotracker, which was increased upon treatment with YM201636. The pH inside the SCV can affect bacterial survival in multiple ways: for example, phagosomal pH in macrophages is important for susceptibility of *S.* Typhimurium to gentamicin (53). In addition, there is evidence that autophagosome-lysosome fusion in CHO cells is affected by the pH in acidic compartments (54). While, in our experiments, early acidification of the SCV in CHO WT and CHO Δ*XylT* cells was similar as determined by acid shock response reporter strains, at the later time points acidification of SCV in CHO Δ*XylT* cells was impaired.

Our results raise the question of specific interactions between phosphoinositides and PGs in the context of infection. For example, it was shown that binding of the transmembrane heparan sulfate PG syndecan-4 to phosphatidylinositol 4,5-bisphosphate (PtdIns(4,5)P_2) is required for formation of focal adhesions (55). Because phosphoinositides are essential for actin assembly, it is not surprising that *Salmonella* can deplete PtdIns(4,5)P_2 by the effector SigD which results in membrane fission during bacterial invasion (56). However, the role of PGs in SCV/SIF biogenesis and endo-lysosomal trafficking is less clear. Several studies showed that syndecans, along with the endosomal sorting complex required for transport (ESCRT) proteins, are involved in the formation of multivesicular endosomes or bodies

(MVBs) (57, 58). MVBs can fuse with lysosomes or be exported as exosomes. It is known that *Salmonella* disturbs normal endosome to lysosome trafficking, affecting the ESCRT system (23) and exocytosis (16, 17). PtdIns(3,5)P_2 (hence, PIKfyve) regulates endosomal fission and fusion, and MVB formation (20).

Taken together, our data show that altered routes of endocytosed cargo in PG-deficient epithelial cells interfere with vesicle acidification and *Salmonella*-modulated PIKfyve-dependent fusion to establish a replicative niche and thereby elucidate a novel role of PGs in intracellular vesicle trafficking and SCV formation.

DATA AVAILABILITY STATEMENT

All datasets generated for this study are included in the article/**Supplementary Material**.

AUTHOR CONTRIBUTIONS

AG, AS, HB, FR, MH, and GG: conceptualization. AG, AO, AS, HB, and LK: investigation. AG, AO, AS, LK, FR, HB, MH, and GG: data analysis. AG, AS, and GG: manuscript writing. AG, AO, AS, HB, FR, LK, MH, and GG: manuscript editing and approval.

FUNDING

GG was supported by the Deutsche Forschungsgemeinschaft (DFG) priority program SPP1656/2, the German Federal Ministry of Education and Research (BMBF) Infect-ERA consortium grant 031L0093B and DFG collaborative research center SFB 900 TP08 (Project number 158989968). AG was supported by the Hannover Biomedical Research School (HBRS) and by the Center for Infection Biology (ZIB). MH was supported by the DFG SFB 944 P4 and Infect-ERA consortium grant 031L0093A.

ACKNOWLEDGMENTS

We would like to thank Nicoletta Schwermann for excellent help in performing inhibitor experiments, and Janina Noster for experimental support in flow cytometry of the P_{asr} reporter.

SUPPLEMENTARY MATERIAL

The Supplementary Material for this article can be found online at: https://www.frontiersin.org/articles/10.3389/fimmu.2020.00731/full#supplementary-material

FIGURE S1 | Intracellular *Salmonella* are sensitive to treatment with ampicillin. **(A)** CHO cells were infected with *S*. Typhimurium 14028s WT at MOI 10, and ampicillin was used instead of gentamicin in a protection assay. 24 h p.i., cells had similar low CFU counts. Dotted line indicates limit of detection, ND – not detected. **(B)** Infected CHO WT and CHO Δ*XylT* cells had comparable levels of released lactate dehydrogenase as measured by LDH assay kit. Dotted line indicates limit of detection. Kruskal–Wallis test with Dunn's multiple comparison test, n.s. (not significant).

FIGURE S2 | CHO WT and Δ*XylT* cells had comparable expression levels of gentamicin transporters genes. Gene expression was measured in CHO WT and CHO Δ*XylT* cells, non-infected and infected with *S*. Typhimurium WT. Control CHO cells were incubated without gentamicin. Gene expression was normalized to *Gapdh* and *Rps9*, and control CHO WT data used as a calibrator. Comparable levels of *Abcc2* **(A)**, *Trpv1* **(B)**, and *Trpv4* **(C)**, expression were observed in both CHO WT and Δ*XylT* cells, regardless infected or not. One-way ANOVA with Tukey's multiple comparison test and Mann-Whitney test, not significant differences are not indicated.

FIGURE S3 | Presence of PGs in CHO cells. **(A)** CHO WT, CHO Δ*XylT*, and complemented CHO Δ*XylT* cells (indicated as CHO cXylT) were stained with heparan sulfate-specific antibody and analyzed by flow cytometry. **(B)** *S*. Typhimurium WT was grown for 6 h in LB broth in presence/absence of 30 μM heparin, and OD600 was recorded every 10 min. Mean values of three technical replicates of a representative experiment out of two are shown.

FIGURE S4 | Gentamicin uptake in CHO WT and CHO Δ*XylT* cells. CHO cells were incubated for 7 h with gentamicin-Cy3 conjugate and then fixed with 4% PFA. Microscopy revealed a similar distribution of the labeled antibiotic within the CHO WT and CHO Δ*XylT* cells.

FIGURE S5 | Labeling by Lysotracker correlates with PGs expression in CHO cells. CHO WT, CHO Δ*XylT*, and complemented CHO c*XylT* cells were infected with *S*. Typhimurium EGFP at MOI 50 and incubated for 24 h with 50 nM Lysotracker Red added upon invasion of bacteria. CHO c*XylT* cells had an intermediate staining (compare to **Supplementary Figure S3A**). Representative images of two biological repetitions. Scale bars, 10 μm.

FIGURE S6 | A dual fluorescence reporter for acid shock exposure of *Salmonella*. **(A)** Plasmid map of p5386, encoding DsRed constitutively under control of promoter P_{EM7}, and sfGFP under control the acid shock-inducible promoter P_{asr}. **(B)** Flow cytometry and gating of *Salmonella* without fluorescent protein expression, or constitutive expression of DsRed or sfGFP. **(C)** Acid shock of cultured bacteria induces sfGFP expression. *Salmonella* WT harboring p5386 (*S*.Tm WT) was grown in PCN, pH 7.5 to mid-log phase. Bacteria were pelleted, washed twice in sterile saline, and resuspended in PCN buffered to the indicated pH. Culture was continued for 1 h, bacteria were harvested by centrifugation and resuspended in PCB containing 200 μg/mL chloramphenicol to stop further protein biosynthesis. The bacteria were incubated for at least 2 h at 4°C to allow full maturation of sfGFP, and subjected to flow cytometry. **(D)** For *in vivo* analyses, *S*.Tm WT harboring p5386 was subcultured for 3 h and used to infect ca. 2×10^5 CHO WT or CHO Δ*XylT* cells at MOI of 10. If indicated (+ Baf), bafilomycin was added to a final concentration of 100 nM. Cells were infected for 30 min, washed three times to remove non-internalized bacteria and incubated 2 h with or without gentamicin addition as indicated in Fig 6B. A representative example of an assay with a constant concentration of 10 μg/mL gentamicin is shown. After washing, cells were detached using biotase, chloramphenicol was added to final concentration of 200 μg/mL and incubated for at least 4 h at 4°C for allow full maturation of sfGFP. Flow cytometry was performed by gating of CHO cells and the level of DsRed and sfGFP fluorescence was determined for at least 50,000 infected host cells.

FIGURE S7 | Inhibition of PI3K does not affect intracellular *Salmonella*. CHO WT and CHO Δ*XylT* cells were infected with *S*. Typhimurium WT at MOI of 50 and incubated for 24 h with 100 μg/mL gentamicin and increasing concentrations of specific inhibitors. Addition of wortmannin had no effect on *Salmonella* survival in either CHO cell line. One-way ANOVA with Dunnett's multiple comparison test, only significant differences are indicated.

FIGURE S8 | PIKfyve kinase inhibition increased labeling by Lysotracker in both CHO WT and CHO Δ*XylT* cells. CHO cells infected with *S*. Typhimurium EGFP were incubated for 24 h with 50 nM Lysotracker Red added upon invasion, in presence/absence of 0.8 μM YM201636. Microscopy revealed enlarged lysosomes/endosomes in YM201636-treated CHO cells. Representative images, scale bars, 10 μm.

FIGURE S9 | CHO Δ*XylT* cells lack *Lama2* expression. cDNA of the uninfected CHO cells was used to screen for an expression of *Lama2* isoforms. ND – not detected.

FIGURE S10 | Addition of heparin to the medium results in intracellular accumulation of heparin in the endo-lysosomal system. CHO Δ*XylT* cells, uninfected and infected with *S*. Typhimurium WT at MOI of 50 were incubated for 24 h with 100 μg/mL gentamicin and with 30 μM heparin. Heparin (green) was detected inside CHO Δ*XylT* cells, in the same compartment as bacteria (red). In CHO WT cells, in the absence of added heparin, HS staining shows localization of HS at the cell surface but also in endo-lysosomal compartments. Representative images of two biological repetitions, scale bars, 10 μm or 5 μm (in enlarged sections).

TABLE S1 | Primers used in this study.

TABLE S2 | Antibodies used in this study.

REFERENCES

1. Iozzo RV, Schaefer L. Proteoglycan form and function: a comprehensive nomenclature of proteoglycans. *Matrix Biol.* (2015) 42:11–55. doi: 10.1016/j.matbio.2015.02.003
2. Taylor KR, Gallo RL. Glycosaminoglycans and their proteoglycans: host-associated molecular patterns for initiation and modulation of inflammation. *FASEB J.* (2006) 20:9–22. doi: 10.1096/fj.05-4682rev
3. Esko JD, Stewart TE, Taylor WH. Animal cell mutants defective in glycosaminoglycan biosynthesis. *Proc Natl Acad Sci USA.* (1985) 82:3197–201. doi: 10.1073/pnas.82.10.3197
4. Henry-Stanley MJ, Hess DJ, Erickson EA, Garni RM, Wells CL. Role of heparan sulfate in interactions of Listeria monocytogenes with enterocytes. *Med Microbiol Immunol (Berl).* (2003) 192:107–15. doi: 10.1007/s00430-002-0165-7
5. van Putten JP, Paul SM. Binding of syndecan-like cell surface proteoglycan receptors is required for *Neisseria gonorrhoeae* entry into human mucosal cells. *EMBO J.* (1995) 14:2144–54. doi: 10.1002/j.1460-2075.1995.tb07208.x
6. Leong JM, Wang H, Magoun L, Field JA, Morrissey PE, Robbins D, et al. Different classes of proteoglycans contribute to the attachment of Borrelia burgdorferi to cultured endothelial and brain cells. *Infect Immun.* (1998) 66:994–9.
7. Lambert MA, Smith SGJ. The PagN protein mediates invasion via interaction with proteoglycan. *FEMS Microbiol Lett.* (2009) 297:209–16. doi: 10.1111/j.1574-6968.2009.01666.x
8. Francis CL, Starnbach MN, Falkow S. Morphological and cytoskeletal changes in epithelial cells occur immediately upon interaction with *Salmonella* typhimurium grown under low-oxygen conditions. *Mol Microbiol.* (1992) 6:3077–87. doi: 10.1111/j.1365-2958.1992.tb01765.x
9. Alonso A, García-del Portillo F. Hijacking of eukaryotic functions by intracellular bacterial pathogens. *Int Microbiol.* (2004) 7:181–91. doi: http://hdl.handle.net/10261/2135
10. Knuff K, Finlay BB. What the SIF Is Happening—The Role of Intracellular *Salmonella*-Induced Filaments. *Front Cell Infect Microbiol.* (2017) 7:335. doi: 10.3389/fcimb.2017.00335
11. Rajashekar R, Liebl D, Seitz A, Hensel M. Dynamic remodeling of the endosomal system during formation of *Salmonella* -induced filaments by intracellular *Salmonella enterica*. *Traffic.* (2008) 9:2100–16. doi: 10.1111/j.1600-0854.2008.00821.x
12. Garcia-del Portillo F, Zwick MB, Leung KY, Finlay BB. *Salmonella* induces the formation of filamentous structures containing lysosomal membrane glycoproteins in epithelial cells. *Proc Natl Acad Sci USA.* (1993) 90:10544–8. doi: 10.1073/pnas.90.22.10544
13. Steele-Mortimer O, Meresse S, Gorvel J-P, Toh B-H, Finlay BB. Biogenesis of *Salmonella* typhimurium-containing vacuoles in epithelial cells involves interactions with the early endocytic pathway. *Cell Microbiol.* (1999) 1:33–49. doi: 10.1046/j.1462-5822.1999.00003.x
14. Meresse S. The rab7 GTPase controls the maturation of *Salmonella* typhimurium-containing vacuoles in HeLa cells. *EMBO J.* (1999) 18:4394–403. doi: 10.1093/emboj/18.16.4394
15. Mota LJ, Ramsden AE, Liu M, Castle JD, Holden DW. SCAMP3 is a component of the *Salmonella* -induced tubular network and reveals an interaction between bacterial effectors and post-Golgi trafficking. *Cell Microbiol.* (2009) 11:1236–53. doi: 10.1111/j.1462-5822.2009.01329.x
16. Kuhle V, Abrahams GL, Hensel M. Intracellular *Salmonella enterica* redirect exocytic transport processes in a *Salmonella* pathogenicity Island 2-dependent manner: *Salmonella* redirect exocytosis. *Traffic.* (2006) 7:716–30. doi: 10.1111/j.1600-0854.2006.00422.x
17. Perrett CA, Zhou D. *Salmonella* type III effector SopB modulates host cell exocytosis. *Emerg Microbes Infect.* (2013) 2:1–6. doi: 10.1038/emi.2013.31
18. Toker A. Phosphoinositides and signal transduction. *Cell Mol Life Sci CMLS.* (2002) 59:761–79. doi: 10.1007/s00018-002-8465-z
19. Gillooly DJ, Morrow IC, Lindsay M, Gould R, Bryant NJ, Gaullier J-M, et al. Localization of phosphatidylinositol 3—phosphate in yeast and mammalian cells. *EMBO J.* (2000) 19:4577–88. doi: 10.1093/emboj/19.17.4577
20. Shaw JD, Hama H, Sohrabi F, DeWald DB, Wendland B. PtdIns(3,5)P2 is required for delivery of endocytic cargo into the multivesicular body. *Traffic.* (2003) 4:479–90. doi: 10.1034/j.1600-0854.2003.t01-1-00106.x
21. Sbrissa D, Ikonomov OC, Shisheva A. PIKfyve, a mammalian ortholog of yeast fab1p lipid kinase, synthesizes 5-phosphoinositides effect of insulin. *J Biol Chem.* (1999) 274:21589–97. doi: 10.1074/jbc.274.31.21589
22. Drecktrah D, Knodler LA, Steele-Mortimer O. Modulation and utilization of host cell phosphoinositides by *Salmonella* spp. *Infect Immun.* (2004) 72:4331–5. doi: 10.1128/IAI.72.8.4331-4335.2004
23. Dukes JD, Lee H, Hagen R, Reaves BJ, Layton AN, Galyov EE, et al. The secreted *Salmonella* dublin phosphoinositide phosphatase, SopB, localizes to PtdIns(3)P-containing endosomes and perturbs normal endosome to lysosome trafficking. *Biochem J.* (2006) 395:239–47. doi: 10.1042/BJ20051451
24. Bakker H, Oka T, Ashikov A, Yadav A, Berger M, Rana NA, et al. Functional UDP-xylose transport across the endoplasmic reticulum/golgi membrane in a chinese hamster ovary cell mutant defective in UDP-xylose synthase. *J Biol Chem.* (2009) 284:2576–83. doi: 10.1074/jbc.M804394200
25. Dam GB, Hafmans T, Veerkamp JH, van Kuppevelt TH. Differential expression of heparan sulfate domains in rat spleen. *J Histochem Cytochem.* (2003) 51:727–39. doi: 10.1177/002215540305100604
26. Matsuura M, Kawasaki K, Kawahara K, Mitsuyama M. Evasion of human innate immunity without antagonizing TLR4 by mutant *Salmonella enterica* serovar Typhimurium having penta-acylated lipid A. *Innate Immun.* (2012) 18:764–73. doi: 10.1177/1753425912440599
27. Hoiseth SK, Stocker BAD. Aromatic-dependent *Salmonella* typhimurium are non-virulent and effective as live vaccines. *Nature.* (1981) 291:238–9. doi: 10.1038/291238a0
28. Cormack BP, Valdivia RH, Falkow SF. ACS-. optimized mutants of the green fluorescent protein (GFP). *Gene.* (1996) 173:33–8. doi: 10.1016/0378-1119(95)00685-0
29. Brumell JH, Goosney DL, Finlay BB. SifA, a Type III Secreted Effector of *Salmonella* typhimurium, directs *Salmonella*-induced filament (Sif) formation along microtubules. *Traffic.* (2002) 3:407–15. doi: 10.1034/j.1600-0854.2002.30604.x
30. Beuzon CR. *Salmonella* maintains the integrity of its intracellular vacuole through the action of SifA. *EMBO J.* (2000) 19:3235–49. doi: 10.1093/emboj/19.13.3235
31. Noster J, Chao T-C, Sander N, Schulte M, Reuter T, Hansmeier N, et al. Proteomics of intracellular *Salmonella enterica* reveals roles of *Salmonella* pathogenicity island 2 in metabolism and antioxidant defense. *PLoS Pathog.* (2019) 15:e1007741. doi: 10.1371/journal.ppat.1007741
32. Bécavin C, Bouchier C, Lechat P, Archambaud C, Creno S, Gouin E, et al. Comparison of widely used listeria monocytogenes strains EGD, 10403S, and EGD-e highlights genomic differences underlying variations in pathogenicity. *mBio.* (2014) 5:e969-14. doi: 10.1128/mBio.00969-14
33. Livak KJ, Schmittgen TD. Analysis of relative gene expression data using real-time quantitative PCR and the 2−ΔΔCT method. *Methods.* (2001) 25:402–8. doi: 10.1006/meth.2001.1262
34. Knodler LA, Nair V, Steele-Mortimer O. Quantitative assessment of cytosolic *Salmonella* in epithelial cells. *PLoS One.* (2014) 9:e84681. doi: 10.1371/journal.pone.0084681
35. Schindelin J, Arganda-Carreras I, Frise E, Kaynig V, Longair M, Pietzsch T, et al. Fiji: an open-source platform for biological-image analysis. *Nat Methods.* (2012) 9:676–82. doi: 10.1038/nmeth.2019

36. Reuter T, Vorwerk S, Liss V, Chao T-C, Hensel M, Hansmeier N. Proteomic analysis of *Salmonella*-modified membranes reveals adaptations to macrophage hosts. *Mol Cell Proteomics MCP.* (2020) [epub ahead of print]. doi: 10.1074/mcp.RA119.001841
37. Bolte S, Cordelières FP. A guided tour into subcellular colocalization analysis in light microscopy. *J Microsc.* (2006) 224:213–32. doi: 10.1111/j.1365-2818.2006.01706.x
38. Myrdal SE, Steyger PS. TRPV1 regulators mediate gentamicin penetration of cultured kidney cells. *Hear Res.* (2005) 204:170–82. doi: 10.1016/j.heares.2005.02.005
39. Karasawa T, Wang Q, Fu Y, Cohen DM, Steyger PS. TRPV4 enhances the cellular uptake of aminoglycoside antibiotics. *J Cell Sci.* (2008) 121:2871–9. doi: 10.1242/jcs.023705
40. Notenboom S. Increased apical insertion of the multidrug resistance protein 2 (MRP2/ABCC2) in renal proximal tubules following gentamicin exposure. *J Pharmacol Exp Ther.* (2006) 318:1194–202. doi: 10.1124/jpet.106.104547
41. Liss V, Swart AL, Kehl A, Hermanns N, Zhang Y, Chikkaballi D, et al. *Salmonella enterica* remodels the host cell endosomal system for efficient intravacuolar nutrition. *Cell Host Microbe.* (2017) 21:390–402. doi: 10.1016/j.chom.2017.02.005
42. Allam US, Krishna MG, Sen M, Thomas R, Lahiri A, Gnanadhas DP, et al. Acidic pH induced STM1485 gene is essential for intracellular replication of *Salmonella*. *Virulence.* (2012) 3:122–35. doi: 10.4161/viru.19029
43. Seputiene V, Motiejûnas D, Suziedelis K, Tomenius H, Normark S, Melefors O, et al. Molecular characterization of the acid-inducible asr gene of *Escherichia coli* and its role in acid stress response. *J Bacteriol.* (2003) 185:2475–84. doi: 10.1128/jb.185.8.2475-2484.2003
44. Kerr MC, Wang JTH, Castro NA, Hamilton NA, Town L, Brown DL, et al. Inhibition of the PtdIns(5) kinase PIKfyve disrupts intracellular replication of *Salmonella*. *EMBO J.* (2010) 29:1331–47. doi: 10.1038/emboj.2010.28
45. Cuellar K, Chuong H, Hubbell SM, Hinsdale ME. Biosynthesis of chondroitin and heparan sulfate in chinese hamster ovary cells depends on xylosyltransferase II. *J Biol Chem.* (2007) 282:5195–200. doi: 10.1074/jbc.M611048200
46. Rostand KS, Esko JD. Microbial adherence to and invasion through proteoglycans. *Infect Immun.* (1997) 65:1–8.
47. van Wijk XM, Döhrmann S, Hallström BM, Li S, Voldborg BG, Meng BX, et al. Whole-genome sequencing of invasion-resistant cells identifies laminin α2 as a host factor for bacterial invasion. *mBio.* (2017) 8:e2128-16. doi: 10.1128/mBio.02128-16
48. Nagai J, Takano M. Entry of aminoglycosides into renal tubular epithelial cells via endocytosis-dependent and endocytosis-independent pathways. *Biochem Pharmacol.* (2014) 90:331–7. doi: 10.1016/j.bcp.2014.05.018
49. Denamur S, Tyteca D, Marchand-Brynaert J, Van Bambeke F, Tulkens PM, Courtoy PJ, et al. Role of oxidative stress in lysosomal membrane permeabilization and apoptosis induced by gentamicin, an aminoglycoside antibiotic. *Free Radic Biol Med.* (2011) 51:1656–65. doi: 10.1016/j.freeradbiomed.2011.07.015
50. Brumell JH, Tang P, Zaharik ML, Finlay BB. Disruption of the *Salmonella*-containing vacuole leads to increased replication of *Salmonella enterica* serovar typhimurium in the cytosol of epithelial cells. *Infect Immun.* (2002) 70:3264–70. doi: 10.1128/IAI.70.6.3264-3270.2002
51. Dukes JD, Whitley P, Chalmers AD. The PIKfyve inhibitor YM201636 blocks the continuous recycling of the tight junction proteins claudin-1 and claudin-2 in MDCK cells. *PLoS One.* (2012) 7:e28659. doi: 10.1371/journal.pone.0028659
52. Krishna S, Palm W, Lee Y, Yang W, Bandyopadhyay U, Xu H, et al. PIKfyve regulates vacuole maturation and nutrient recovery following engulfment. *Dev Cell.* (2016) 38:536–47. doi: 10.1016/j.devcel.2016.08.001
53. Menashe O, Kaganskaya E, Baasov T, Yaron S. Aminoglycosides affect intracellular *Salmonella enterica* serovars typhimurium and virchow. *Antimicrob Agents Chemother.* (2008) 52:920–6. doi: 10.1128/AAC.00382-07
54. Kawai A, Uchiyama H, Takano S, Nakamura N, Ohkuma S. Autophagosome-lysosome fusion depends on the pH in acidic compartments in CHO cells. *Autophagy.* (2007) 3:154–7. doi: 10.4161/auto.3634
55. Oh E-S, Woods A, Lim S-T, Theibert AW, Couchman JR. Syndecan-4 proteoglycan cytoplasmic domain and phosphatidylinositol 4,5-bisphosphate coordinately regulate protein kinase C activity. *J Biol Chem.* (1998) 273:10624–9. doi: 10.1074/jbc.273.17.10624
56. Terebiznik MR, Vieira OV, Marcus SL, Slade A, Yip CM, Trimble WS, et al. Elimination of host cell PtdIns(4,5)P2 by bacterial SigD promotes membrane fission during invasion by *Salmonella*. *Nat Cell Biol.* (2002) 4:766–73. doi: 10.1038/ncb854
57. Friand V, David G, Zimmermann P. Syntenin and syndecan in the biogenesis of exosomes: syndecan-syntenin pathway in exosome biogenesis. *Biol Cell.* (2015) 107:331–41. doi: 10.1111/boc.201500010
58. Hessvik NP, Llorente A. Current knowledge on exosome biogenesis and release. *Cell Mol Life Sci.* (2018) 75:193–208. doi: 10.1007/s00018-017-2595-9

Conflict of Interest: The authors declare that the research was conducted in the absence of any commercial or financial relationships that could be construed as a potential conflict of interest.

frontiers in Immunology

REVIEW
published: 29 April 2020
doi: 10.3389/fimmu.2020.00569

The Role of Hyaluronan Treatment in Intestinal Innate Host Defense

*Yeojung Kim and Carol A. de la Motte**

Department of Inflammation and Immunity, Lerner Research Institute, Cleveland Clinic Foundation, Cleveland, OH, United States

Hyaluronan (HA) is best known as an abundantly present extracellular matrix component found throughout the body of all vertebrates, including humans. Recent evidence, however, has demonstrated benefits of providing HA exogenously as a therapeutic modality for several medical conditions. Here we discuss the effects of providing HA treatment to increase innate host defense of the intestine, elucidate the size specific effects of HA, and discuss the role of various HA receptors as potential mediators of the HA effects in the intestine. This review especially focuses on HA interaction with the epithelium because it is the primary cellular barrier of the intestine and these cells play a critical balancing role between allowing water and nutrient absorption while excluding microbes and harmful dietary metabolites that are constantly in that organ's environment.

Keywords: hyaluronan, innate host defense, intestinal epithelium, tight junctions, antimicrobial responses

OPEN ACCESS

Edited by:
Aaron C. Petrey,
The University of Utah, United States

Reviewed by:
Guntram A. Grassl,
Hannover Medical School, Germany
Suryasarathi Dasgupta,
Takeda, United States

***Correspondence:**
Carol A. de la Motte
delamoc@ccf.org

Specialty section:
This article was submitted to Molecular Innate Immunity, a section of the journal Frontiers in Immunology

Received: *10 December 2019*
Accepted: *12 March 2020*
Published: *29 April 2020*

Citation:
Kim Y and de la Motte CA (2020) The Role of Hyaluronan Treatment in Intestinal Innate Host Defense. Front. Immunol. 11:569. doi: 10.3389/fimmu.2020.00569

HYALURONAN

Hyaluronan (HA), also known as hyaluronic acid or sodium hyaluronate, is a polymer made up of repeating disaccharides of N-acetylglucosamine and glucuronic acid (1).

HA is found in many places in our body including most connective tissues, the skin, the vitreous of the eyes, synovial fluid, in the joints, and the umbilical cord (1). HA is synthesized on cell surfaces as a high molecular weight polymer reaching up to 10,000 kDa and is an important component of the extracellular matrix (2, 3). Since HA lacks a protein core, the process of cellular HA synthesis is a unique process as it occurs at the cell membrane, not in Golgi networks where most glycosaminoglycans are usually made (1). Vertebrates have three evolutionarily conserved and highly homologous (55–70% protein identity) HA synthases enzymes (HAS1-3) (4). During the process of HA synthesis, UDP-D-glucuronic acid (GlcA), and UDP-N-acetyl-D-glucosamine (GlcNAC) monomers are added in an alternating assembly to form HA polymers (3). Interestingly, reports suggest that each of these three HAS enzymes may prefer to synthesize different ranges of HA sizes. In general, HAS1 produces a wide range of HA, HAS2 generates large HA (200–2,000 kDa), and HAS3 synthesizes relatively short HA (100–1,000 kDa) (4).

Upon tissue injury or damage, high molecular weight HA is degraded through multiple pathways into small fragments that can act as danger signals (2, 5). The degradation of HA is accomplished by specific proteins including hyaluronidases (HYAL1 and 2) (6), Cell Migration-inducing and Hyaluronan-binding Protein (CEMIP, also known as KIAA1199) (7), transmembrane protein 2 (TMEM2) (8), as well as non-specifically by reactive oxygen species (ROS) (6). Depolymerization can be roughly categorized into three distinct mechanisms. The first one occurs at the local cellular level. HA binds to specific cell surface receptors such as CD44,

TABLE 1 | Summary of HA used in pre-clinical models.

HA sizes	Route of delivery	Effects
HA 35 kDa	Oral	Protection from ethanol-induced liver injury *in vitro* and *in vivo* (9, 10)
Undefined	Topical	Treatment for interstitial cystitis/painful bladder syndrome (11)
HA 750 kDa	IP	Proliferation of colonic epithelium *in vivo* (12)
HA 750 kDa	IP	Protection from DSS-induced colitis *in vitro* and *in vivo* (13)
HA 750 kDa	IP	Protection from irradiation *in vivo* (14)
HA 35 kDa	Oral	Induction of an antimicrobial peptide *in vitro* and *in vivo* (15)
HA 35 kDa	Oral	Decreases bacterial infection *in vitro* and *in vivo* (16–18)
HA 35 kDa	Oral	Increases the expression of a tight junction protein *in vitro* and *in vivo* (16, 17, 19)
HA 35 kDa	Oral	Reduce intestinal permeability in DSS-induced colitis mouse model (16)
HA 35 kDa	Oral	Protection from NEC model *in vivo* (20)

HA molecular mass and route of administration appear to be important for specific efficacy.

before being internalized, and degraded within lysosome of cells by hyaluronidases (21). The second pathway occurs at the tissue level. HA present in extracellular matrices it may be degraded to fragments in the extracellular cellular space where the fragments may signal neighboring cells as Damage Associated Molecular Pattern molecules (DAMPs) via multiple receptors, including CD44, TLR4 and TLR2, RHAMM, and Layilin. Free HA fragments may also be generated in the vasculature by platelets using HYAL2 (22). Ultimately HA reaching the vasculature and lymphatics, travels to the liver, kidney, and possibly the spleen for clearance (2). Clearance of HA is mediated by the HA receptor for endocytosis (HARE), and lymphatic vessel endothelial HA receptor (LYVE)-1 (1). The third pathway of HA depolymerization is non-specific, and mediated by free radicals generated under oxidative conditions. This process is promoted by combined action of oxygen and transition metal cations (22). Once HA fragments are generated by catabolism, for example upon tissue injury, they are thought to initiate an innate immune response and induce inflammation (2, 5).

CURRENT CLINICAL USES OF HA

HA is currently being used in medical/ patient applications both in HA-containing medical device and as well as treatments. In particular, HA has efficacy as a viscoelastic tool during the ophthalmological surgeries (23), and for viscosupplementation in intra-articular spaces in patients with osteoarthritis (24, 25). Interestingly, for osteoarthritis patients, in addition to the intra-articular injections, the effects from orally delivered HA have also been investigated. Randomized, double-blinded, placebo-controlled clinical trials have proven the effectiveness of orally administrated HA for osteoarthritis in US, EU, and Asia (26, 27). Furthermore, based on HA's ability to promote cellular wound healing, HA based wound-dressings have proven beneficial to patients with burns, trauma, and ulcers (28). Endogenous HA, as well as its degradation products are generated during the process of wound healing and they are capable of inducing fibroblast proliferation and angiogenesis to promote the repair (29).

Although studies of efficacy of exogenous HA treatment effects are currently limited to specific fields, i.e., orthopedics, ophthalmology, and dermatology, results of clinical trials using HA provide evidence that exogenous HA is a safe molecule that may be used in humans (25, 27, 30).

INNATE HOST DEFENSE IN THE GASTROINTESTINAL TRACT

The two major physiological functions of the gastrointestinal (GI) tract are digestion of food and absorption of nutrients, electrolytes, and water. The GI tract also provides a major habitat for the body's beneficial commensal bacterial population, or microbiota. The organ's physiologic challenge is to host the beneficial microbial populations while at the same time protecting the host from pathogenic organisms (31). The mucosal barrier of the digestive tract is a key element in mediating this important balance.

The GI tract is an organ system in direct contact with the non-sterile external environment, and one, which continues to protect against the environmental challenges experienced throughout the continuous lumen in the body. To cope with the substantial microbial challenge, the GI tract possesses multiple layers of host defense mechanisms. The first protective layer is a physical barrier of mucus that is produced by, and lies directly on, the luminal side of the epithelium. Mucins form a physical impediment to contact of microbes and are continuously sloughed off to decrease bacterial contact. The mucus lining also retains antimicrobial peptides (AMPs), an additional mode of protection. AMPs are a family of natural antibiotic molecules produced by cells within an organism that can kill bacteria, fungi, viruses, and parasites (32). Defensin proteins are a class of antimicrobial peptides which act against both gram- positive and -negative bacteria. Alpha-defensins are produced by Paneth cells and neutrophils and beta-defensins are expressed by most epithelial cells. The expression of alpha-defensins is constitutive and does not require bacterial signals to be expressed but bacterial stimuli may induce higher levels (33). Several studies have suggested that a defective inner mucus layer may result in closer contact between epithelium and bacteria as well as their products, which could drive pro-inflammatory responses and lead to the development of diseases like ulcerative colitis and self-limiting colitis (34–36).

The second layer is a tightly bound, single layer of cells, called the epithelium. Intestinal epithelial cells arise from the bottom of crypts from stem cells and as they divide and differentiate into specific type of epithelial cells, they migrate toward surface epithelium area (37). Once epithelial cells are differentiated and matured, these cells are gradually turned over through shedding into the lumen and by apoptotic cell death. Importantly, this

process occurs naturally without disruption of the epithelial barrier integrity (38). The epithelium controls the flow of water and nutrients from the external to the internal environment of the body. The epithelial barrier is selectively permeable and absorbs nutrients and water, while at the same time, keeping the tight integrity between epithelial cells preventing bacterial invasion. The integrity of the epithelial barrier is regulated by apical junctional complex (AJC). In the intestinal epithelium the AJC is composed of tight junctions and adherens junctions (39). Even though both types of junction complexes are involved in cell-cell adhesions, the functions of each complex are different. Adherens junctions consist of the transmembrane protein E-cadherin, alpha-, gamma-, and delta-catenin and they initiate cell-cell contacts, and maintain the contacts (40). On the other hand, the tight junction is the most apical junctional complex and it is critical in the regulation of permeability in the intestinal epithelium. Tight junctions are composed of transmembrane proteins [i.e., claudins, occludin, and junctional adhesion molecule (JAM)], as well as cytoplasmic scaffolding proteins [i.e., zonula occludens (ZO-1, ZO-2, and ZO-3)] (39, 40). Most tight junction proteins mediate the formation of a tight epithelial barrier. However, there are also reports of tight junction proteins, including Claudin-2, inducing a leaky gut barrier to modulate absorption of ions and water as part of the normal physiology (38). The importance of the functional tight epithelial barrier has been emphasized through the association with diseases. Dysregulation of tight junction proteins have been reported in diseases such as inflammatory bowel disease (IBD) and celiac disease (41, 42). Upregulation of claudin-2 and downregulation of occludin and ZO-1 have been observed in IBD patients (39, 43). Current data suggests that HA can strengthen barrier integrity and therapeutic approaches that enhance epithelial barrier integrity may prove beneficial for patients with gastrointestinal disease.

Beneath the epithelium resides a loose connective tissue, known as the *lamina propria*, largely made up of extracellular matrix, sub-epithelial fibroblasts, smooth muscle cells, and resident immune cells. The *lamina propria* contains a population of leukocytes that provides immune surveillance and protection against invading organisms. Maintaining a healthy, functional mucosa is critical for the prevention of bacterial infections in our gut and many diseases are directly linked to an imbalance in one or more functions of the mucosal barrier (39).

EXOGENOUS HYALURONAN TREATMENT AND INTESTINAL INNATE HOST DEFENSE

In addition to the clinical device uses of exogenous HA treatments for osteoarthritis, wound healing, and in ophthalmological surgery, there are also a number of pre-clinical studies (**Table 1**) examining the effects of orally administered HA on other organs and diseases (15–17, 44). Overall, oral treatment with exogenous HA has been proven to be beneficial. For example, a recent study has demonstrated that treatment with HA 35 kDa reduces the proinflammatory signaling in Kupffer cells and protects mice from ethanol-induced liver injury by regulating the expression of micro RNA (9, 10). Furthermore, the potential use of intravesical instillations of HA in interstitial cystitis/painful bladder syndrome has also been suggested (11, 29).

Multiple studies have shown a variety of effects of HA treatment on intestinal epithelium. Riehl et al. has shown that long-term (5 weeks) intraperitoneal administration of HA 750 kDa induces the proliferation of colonic epithelium in healthy mice (12). Additional studies have revealed that the HA receptors, CD44 and TLR-4, mediate the proliferative phenotype of colonic epithelium post HA treatment *in vivo,* although *in vitro* the same report has shown that HA 750 kDa treatment does not alter proliferation of intestinal epithelial organoids (45). On the other hand, Zheng et al. have demonstrated that the same treatment protects mice from dextran sulfate sodium (DSS)-induced colitis when the HA treatment was started at the same time as DSS treatment (13). In that study, exogenous HA treatment induces the expression of tumor necrosis factor α (TNFα), macrophage inflammatory protein-2 (MIP-2), and cyclooxygenase-2 (COX-2) in a MyD88-dependent manner in mouse peritoneal macrophages *in vitro* and in the distal colon *in vivo* (13). Even though Zheng et al. have shown that COX-2 is induced in macrophages as a result of HA 750 kDa treatment, another study has shown that HA 200 kDa treatment has no effect of COX-2 expression in HIEC cell line (human normal small intestine cell line) (13, 46). Additional studies by Riehl et al. have also shown that intraperitoneal HA 750 kDa treatment 8 h before irradiation is radioprotective and increases crypt survival and diminishes radiation-induced apoptosis in proximal jejunum of mice in a TLR-4 dependent manner (14). Taken together, all these studies suggest that while intra-peritoneal delivery of HA in mice modulates intestinal epithelium indirectly, it directly affects macrophages in the *lamina propria*. Plausibly, changes observed in epithelium may be dependent on the HA-affected immune cells present in *lamina propria*.

In addition to exploring the role of intraperitoneally administered HA, the effects of oral delivery have also been investigated. Hill et al. have shown that oral administration of specifically HA 35 kDa, but not significantly larger or smaller sizes, induces the expression of beta defensin-2, an antimicrobial peptide, in intestinal epithelium *in vitro* and *in vivo* through TLR-4 (15). Furthermore, Hill et al. has reported that HA isolated from human milk also increases the expression of beta defensin-2 *in vitro* and *in vivo via* CD44 and TLR-4 as well as inhibits *Salmonella enterica* infection *in vitro* (18).

Oral HA35 has shown protective effects in *in vivo* bacterial infection models as well. HA 35 kDa treatment has been reported to decrease severity of murine *Citrobacter rodentium* infection, a model organism which is similar to enteropathogenic *E. coli* in humans (16). Both recoverable *C. rodentium* CFU (colony forming units) and epithelial bacterial translocation were reduced in these studies. In this same report, HA 35 kDa treatment increased the expression of a tight junction protein zonula occludens-1 (ZO-1), a critical component in forming tight junction complexes between intestinal epithelial cells that prevents bacterial infection (16). In agreement, HA 35 kDa mediated ZO-1 induction has been shown to act directly on

mouse epithelium *in vitro* (19). Accordingly, oral gavage with HA 35 kDa also diminishes the observed increase in intestinal permeability post DSS treatment of mice (16). Recently, Kessler et al. have shown that oral treatment with HA 35 kDa inhibits *Salmonella* infection *in vivo* and decreases the expression of Claudin-2, a leaky tight junction protein (17).

In two additional models of colitis which are also bacterially driven, the dextran sulfate sodium (DSS) (13) and the murine necrotizing enterocolitis (NEC) model (20), oral HA35 was shown to be protective. HA 35 kDa treatment diminishes the observed increase in intestinal permeability post DSS treatment of mice (16). Interestingly, oral gavage with large sizes of HA such as 2,000 kDa does not induce expression of either beta defensin-2 or ZO-1 in mouse intestinal epithelium. Clearly, intraperitoneal injection of large HA 750 kDa and oral treatment of small HA 35 kDa have obvious beneficial effects on intestinal epithelium while oral treatment of large HA 2,000 kDa has no effect. Moreover, the result of a study using HA isolated from human milk (milk-HA), which contains 95% of HA ∼500 kDa and 5% of HA ∼35 kDa, indicates that orally administered 500 kDa size of HA or combination of both 500 kDa and 35 kDa HA may be effective for protecting intestinal epithelium (18, 47). Hill et al. has shown that milk HA is a more potent inducer of defensin-2 than HA 35 kDa, since a lower concentration of milk HA (up to 700-fold less) is sufficient to obtain the effects comparable to HA 35 kDa *in vitro* and *in vivo* (18). Although requiring further studies, it is provocative to speculate that HA 2,000 kDa may be simply too large to physically cross the mucus layer present on the intestinal barrier.

In a model of NEC, mouse pups receiving HA35 had increased survival and lower intestinal injury compared to untreated NEC. HA 35 also reduced intestinal permeability, bacterial translocation, and proinflammatory cytokine release in NEC pups as well as upregulating epithelial tight junction proteins claudin-2,-3,-4, occludin, and ZO-1, suggesting that HA 35 protects against NEC at least partly by enhancing epithelial barrier defenses (20).

HA SIZING EFFECTS ON INTESTINAL EPITHELIUM

A still unanswered question that remains is "why are HA effects frequently size specific?" In theory, each HA receptor recognizes a 6–10 sugar residues of HA and this should be the case independent of the HA length (48). However, multiple studies have described the effects of HA to be size specific (3, 9, 15, 49).

Based on the studies demonstrating that HA effects may be obtained only from a small-, but not a large size HA, one of the possible explanations may be the inability of certain size of HA to reach the cell surface and to bind the HA receptors expressed there. Moreover, before HA reaches the cell surface, environmental components including extracellular matrix and mucus might affect the capacity of HA to bind to cell surface receptors. For example, while HA is given orally, to be able to bind to HA receptors on the intestinal epithelial surface, HA must pass through the mucus layer. The mucus is comprised of many highly glycosylated proteins and it is possible that a large HA such as HA 2,000 kDa may be unable to reach the epithelial cells. Kessler et al. show that oral HA 35 kDa indeed makes its way to the colon and comes in contact with epithelium (17).

Interestingly, although the large HA is able to reach the surface of the cells *in vitro*, it is not internalized by cells unlike a small size HA 35 kDa (**Figure 1**) (19). These data indicate that the internalization of HA is size dependent and may not occur with large sizes of HA. Absence of CD44 receptors in mouse intestinal epithelial cells may be another possible explanation (19). This, however, requires further investigation, as in mouse lung epithelial cells, which express CD44, similar size specific effects as those found by Kim et al. were shown by Forteza et al. (49) Multiple studies have investigated binding of HA to CD44 receptors and have shown that larger HA binds to CD44 with higher affinity than the smaller size HA (50, 51). Future studies are needed to address the question of whether CD44 or additional receptors may be involved in the internalization of HA in a size dependent manner and whether the internalization of HA is required for induction of any downstream signaling pathways.

HA RECEPTORS IN INTESTINAL EPITHELIUM

High molecular weight HA and fragments of HA can bind to several HA binding receptors including the CD44 receptor, the receptor for HA-mediated motility (RHAMM), HA receptor for endocytosis (HARE), lymphatic vessel endothelial HA receptor (LYVE1), layilin, and toll-like receptors (TLRs-2 and 4) (2) Some investigators have proposed that the signal transduction activated by HA is dependent on the cell-type dependent available HA receptors, cooperatively and/or clustering of HA receptors (3). As mentioned, CD44 is the most highly investigated HA receptor and biochemical studies have shown that larger sizes of HA bind to CD44 with higher affinity (50). Interestingly, the clustering of CD44 upon binding to high molecular weight HA binding can be inhibited by small HA oligosaccharides (51).

Several studies have indicated that toll-like receptors (TLRs) are capable of signaling in response to HA and many of the HA effects have been suggested to be through TLR-2 and TLR-4 (5, 52, 53). Interestingly, for monocytes to respond to HA, TLR-4, and CD44 must form a complex together with MD2 (lymphocyte antigen 96) (54). However, to date, HA has not been demonstrated to directly bind to TLRs.

Among all HA receptors identified, the least studied HA receptor is layilin. Layilin is a transmembrane membrane protein, first identified as a HA receptor in 2001 by *Hynes* group (55). Layilin contains C-type lectin domain, which is similar to the link domain, also known as a HA binding domain (56, 57). Layilin plays important roles in cell migration and membrane ruffling as demonstrated by layilin knockdown inhibiting cell migration *in vitro, and inhibiting* cancer cell metastases *in vivo* (58). Furthermore, layilin is essential for induction of epithelial-mesenchymal transformation (EMT) induced by TNF (tumor necrosis factor)-α in kidneys (59). In addition to HA, cytoskeletal proteins, including talin, merlin, and radixin also bind to layilin,

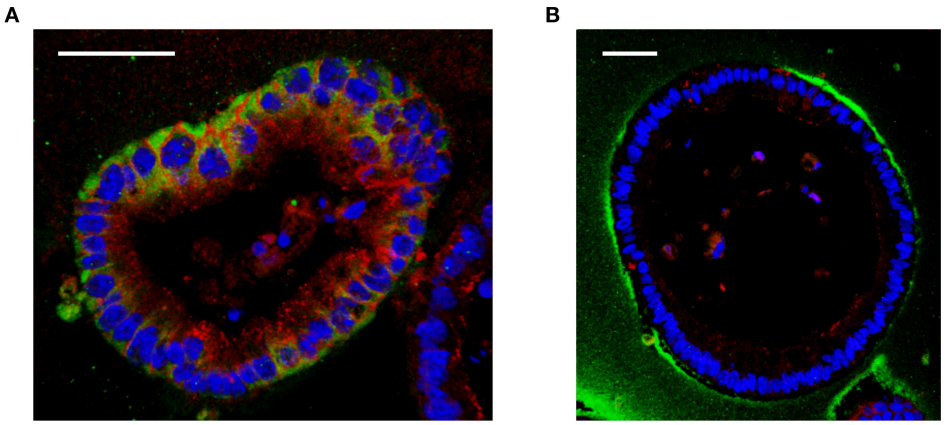

FIGURE 1 | Effect of different sizes of HA on cultured mouse intestinal organoids. **(A)** Immunofluorescent staining of HA 35 kDa (350 micrograms/ml, 30 h) treated mouse intestinal organoids show internalized HA (*green*) and increased ZO-1 expression (*red*) compared to **(B)** HA2000 kDa (350 micrograms/ml, 30 h) treated mouse intestinal organoids, which show no uptake of HA (*green*). DAPI = blue. Scale bar = 50 mm. Immunohistochemical staining for HA was performed using biotinylated HA binding protein. Z-stack images were obtained using confocal microscopy and 3D images were generated using Velocity.

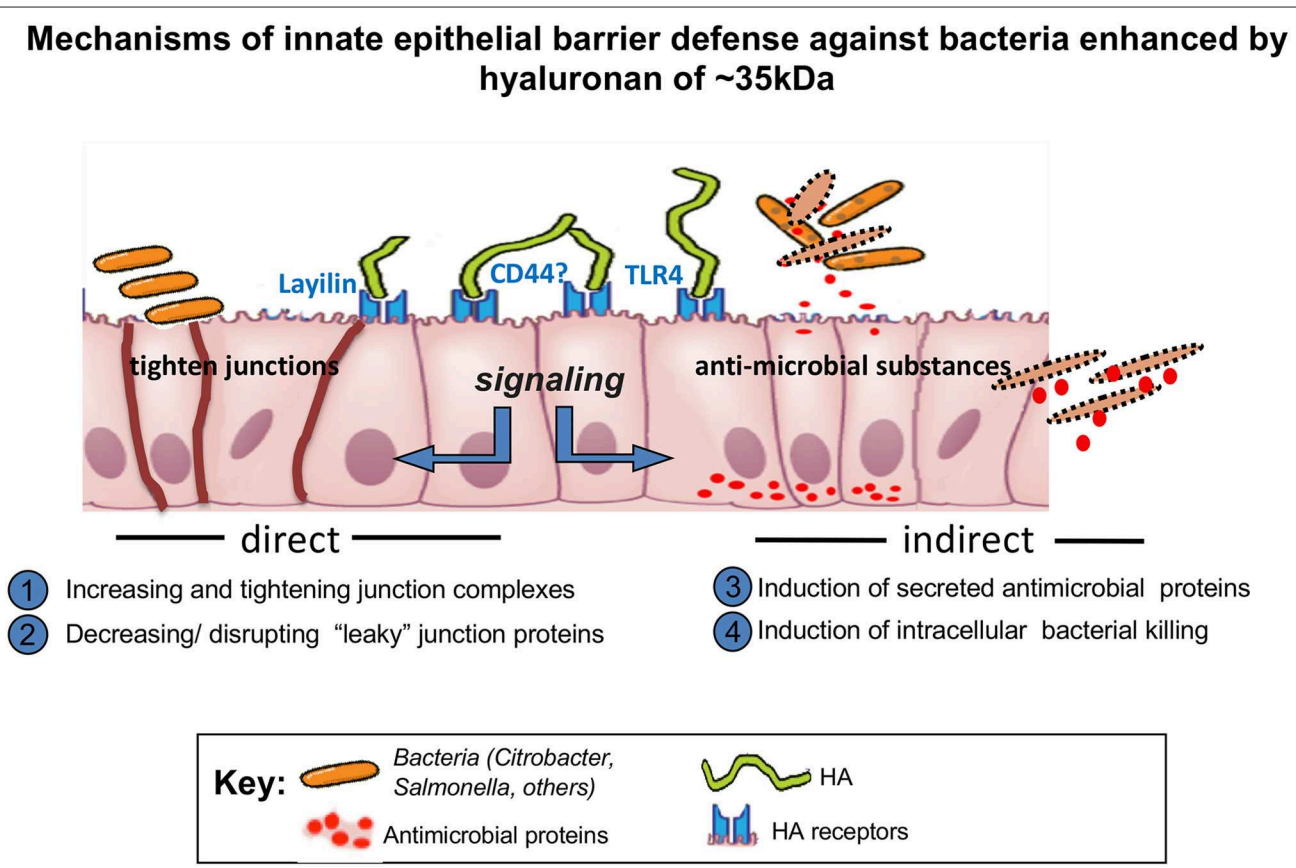

FIGURE 2 | Schematic depicting the activity of HA 35 kDa.

however, the function of this binding has not been investigated (55, 60). Only a few studies have been conducted investigating the effects of HA through layilin. Forteza et al. has demonstrated that in lung epithelial cells expressing layilin, HA 35 kDa or smaller HA, treatment decreases E-cadherin expression while larger HA does not (49). In the report from Kim et al. HA 35 kDa but not HA 2,000 kDa was shown to increases the expression of ZO-1 through layilin while HA 35 kDa treatment does not change

the expression of E-cadherin in colonic epithelial organoids (19). The differing results of E-cadherin expression post HA treatment between lung epithelial cells and intestinal epithelial organoids may be due to the fact that layilin is expressed in colonic epithelial organoids in the absence of CD44, while both receptors are expressed in lung epithelial cells (19, 49). Additional studies investigating the significance of the layilin in receptor mediated HA effects on various cells are warranted, and may provide further insight into its cellular signaling and functions.

Although multiple types of HA binding receptors have been identified the specific HA receptors expressed in human or murine intestinal epithelium and the location of HA receptors present have not been clarified. The majority of studies investigating HA effects have been conducted using HA receptor knockout mouse models, which do not directly prove that any of the observed effects of HA requires binding of HA to any of its receptors (15, 19, 45) Studies have shown that in normal human colon CD44 is expressed in the crypts, while mature intestinal epithelial cells do not express CD44 (61). Interestingly, in the mouse, CD44 shows the same expression pattern as human from proximal to transverse colon but distally, CD44 expression is lost even in the crypts (19). Most studies that have been done using human colon tissues have not specified the region within the colon from where samples taken, so we do not as yet know whether there is a regional difference in CD44 expression in human colon, similar to what we observe in mouse colonic epithelium. While TLR-4 is expressed on the cell surface in immune cells, it is also expressed intracellularly in a mouse small intestinal epithelial cell line (62). In human and mouse colonic epithelium, TLR-4 is intracellularly expressed in fetal colon during gestation, however the expression is significantly reduced postpartum (63). Low expression of TLR-4 in colonic epithelium in human colon has been reported in another study comparing colon tissues of normal and IBD patients (64). On the other hand, the regional differences in expression of TLR-4 have not yet been addressed either in human or mouse colonic epithelium. Certainly interesting, and potentially important, is understanding where HA receptors are expressed in the intestinal epithelium. So far, only CD44 has been investigated in a limited number of studies. Limited data indicates that CD44 is expressed in basolateral side of intestinal epithelium in human and mouse tissue which suggests that the effect of ingested HA would not be directly mediated by CD44 (45, 65). Still, we cannot exclude the possibility that the location of CD44 can be changed to an apical location in the presence of HA. **Figure 1** suggests that HA receptors bind to exogenous HA might be located apically. Unfortunately, the location of layilin could not been shown due to the technical limitation of detection antibodies. Further studies using the microinjection of HA in spheroid-cultured intestinal organoids could help to address these questions.

CONCLUSION

HA is a natural product and is present in human milk at the highest levels immediately post-partum, which supports the notion of its participation in process of maturing the neonatal digestive system. A number of pre-clinical studies highlight functions of exogenous HA promoting intestinal epithelial defense mechanisms and inhibiting bacterial infections in the intestine. Effects of exogenous HA treatment on the intestine have been investigated in multiple studies looking at oral and intraperitoneal delivery *in vivo*. In the case of orally delivered HA, HA 35 kDa appears to be the most potent size of HA for protection of intestinal epithelium (Schematic-**Figure 2**), different from large size of HA. In the case of intraperitoneally delivered HA, size dependent studies have not been reported, with only HA 750 kDa being used for the intraperitoneal injection *in vivo* (12). In this context, the detailed mechanisms of how certain specific range of HA sizes may be effective in colonic epithelium especially in the *in vivo* setting have not been identified. The complex environment in the intestine including the presence of mucus layer and microflora may be one of the main reasons of why it is difficult to recapitulate the *in vivo* setting using the *in vitro* models. Further studies dissecting mechanisms of how HA treatment promotes defense in the intestine will be helpful to advance any possible future clinical trials utilizing HA treatment to improve intestinal health.

Through the numerous clinical trials of HA intra-articular injections and oral delivery for osteoarthritis patients, as well as clinical usages of HA in ophthalmology, the safety of using HA as a therapeutic modality appears to be most promising. A recent pilot study has also shown that HA 35 kDa is safe for human oral consumption (66). This is not surprising, since many successful and minimally toxic compounds have been of natural origin; the use of probiotics for treatment of colitis is a good example of beneficial use of natural products (67). Recent studies have revealed an underappreciated feature of HA, as a promoter of the epithelial defense mechanisms against pathogens in the intestine (16, 17). We envision HA has the potential to be a novel supplement and prophylactic treatment for pre-mature infants who cannot be breastfed, as well as patients who may have a dysregulated intestinal barrier and who are at increased risk for enteric bacterial translocation.

AUTHOR CONTRIBUTIONS

The review was outlined and jointly written by YK and CM.

FUNDING

This research was supported by the National Institutes of Health HD061918, R21AA024387, AA026764, and the Programs of Excellence in Glycosciences Grant HL107147, as well as the Cleveland Clinic Innovators Research Fund (all to CM). This work utilized the Leica SP5 confocal/multi-photon microscope that was purchased with partial funding from National Institutes of Health SIG grant [1S10RR026820-01].

REFERENCES

1. Necas J, Bartosikova L, Brauner P, Kolar J. Hyaluronic acid (hyaluronan): a review. *Vet Med*. (2008) 53:397–411. doi: 10.17221/1930-VETMED
2. Stern R, Asari AA, Sugahara KN. Hyaluronan fragments: an information-rich system. *Eur J Cell Biol.* (2006) 85:699–715. doi: 10.1016/j.ejcb.2006.05.009
3. Cyphert JM, Trempus CS, Garantziotis S. Size matters: molecular weight specificity of hyaluronan effects in cell biology. *Int J Cell Biol.* (2015) 2015:563818–8. doi: 10.1155/2015/563818
4. Itano N, Sawai T, Yoshida M, Lenas P, Yamada Y, Imagawa M, et al. Three isoforms of mammalian hyaluronan synthases have distinct enzymatic properties. *J Biol Chem.* (1999) 274:25085–92. doi: 10.1074/jbc.274.35.25085
5. Scheibner KA, Lutz MA, Boodoo S, Fenton MJ, Powell JD, Horton MR. Hyaluronan fragments act as an endogenous danger signal by engaging TLR2. *J Immunol.* (2006) 177:1272–81. doi: 10.4049/jimmunol.177.2.1272
6. Stern R, Kogan G, Jedrzejas MJ, Soltés L. The many ways to cleave hyaluronan. *Biotechnol Adv*. (2007) 25:537–57. doi: 10.1016/j.biotechadv.2007.07.001
7. Yoshida H, Nagaoka A, Kusaka-Kikushima A, Tobiishi M, Kawabata K, Sayo T, et al. KIAA1199, a deafness gene of unknown function, is a new hyaluronan binding protein involved in hyaluronan depolymerization. *Proc Natl Acad Sci USA*. (2013) 110:5612–7. doi: 10.1073/pnas.1215432110
8. Yamaguchi Y, Yamamoto H, Tobisawa Y, Irie F. TMEM2: a missing link in hyaluronan catabolism identified? *Matrix Biol.* (2019) 78–9:139–46. doi: 10.1016/j.matbio.2018.03.020
9. Saikia P, Bellos D, McMullen MR, Pollard KA, de la Motte CA, Nagy LE. miR181b-3p and its target importin α5 regulate TLR4 signaling in kupffer cells and liver injury in mice in response to ethanol. *Hepatology*. (2017) 66:602–15. doi: 10.1002/hep.29144
10. Saikia P, Roychowdhury S, Bellos D, Pollard KA, McMullen MR, McCullough RL, et al. Hyaluronic acid 35 normalizes TLR4 signaling in kupffer cells from ethanol-fed rats via regulation of microRNA291b and its target Tollip. *Sci Rep*. (2017) 7:15671. doi: 10.1038/s41598-017-15760-4
11. Riedl CR, Engelhardt PF, Daha KL, Morakis N, Pflüger H. Hyaluronan treatment of interstitial cystitis/painful bladder syndrome. *Int Urogynecol J*. (2008) 19:717–21. doi: 10.1007/s00192-007-0515-5
12. Riehl TE, Ee X, Stenson WF. Hyaluronic acid regulates normal intestinal and colonic growth in mice. *Am J Physiol Gastrointest Liver Physiol.* (2012) 303:G377–88. doi: 10.1152/ajpgi.00034.2012
13. Zheng L, Riehl TE, Stenson WF. Regulation of colonic epithelial repair in mice by Toll-like receptors and hyaluronic acid. *Gastroenterology.* (2009) 137:2041–51. doi: 10.1053/j.gastro.2009.08.055
14. Riehl TE, Foster L, Stenson WF. Hyaluronic acid is radioprotective in the intestine through a TLR4 and COX-2-mediated mechanism. *Am J Physiol Gastrointest Liver Physiol.* (2012) 302:G309–16. doi: 10.1152/ajpgi.00248.2011
15. Hill DR, Kessler SP, Rho HK, Cowman MK, de la Motte CA. Specific-sized hyaluronan fragments promote expression of human -defensin 2 in intestinal epithelium. *J Biol Chem.* (2012) 287:30610–24. doi: 10.1074/jbc.M112.356238
16. Kim Y, Kessler SP, Obery DR, Homer CR, McDonald C, de la Motte CA. Hyaluronan 35kDa treatment protects mice from citrobacter rodentium infection and induces epithelial tight junction protein ZO-1 *in vivo*. *Matrix Biol*. (2016) 62:28–39. doi: 10.1016/j.matbio.2016.11.001
17. Kessler SP, Obery DR, Nickerson KP, Petrey AC, McDonald C, de la Motte CA. Multifunctional role of 35 kilodalton hyaluronan in promoting defense of the intestinal epithelium. *J Histochem Cytochem.* (2018) 66:273–87. doi: 10.1369/0022155417746775
18. Hill DR, Rho HK, Kessler SP, Amin R, Homer CR, McDonald C, et al. Human milk hyaluronan enhances innate defense of the intestinal epithelium. *J Biol Chem.* (2013) 288:29090–104. doi: 10.1074/jbc.M113.468629
19. Kim Y, West GA, Ray G, Kessler SP, Petrey AC, Fiocchi C, et al. Layilin is critical for mediating hyaluronan 35kDa-induced intestinal epithelial tight junction protein ZO-1 *in vitro* and *in vivo*. *Matrix Biol*. (2017) 66:93–109. doi: 10.1016/j.matbio.2017.09.003
20. Gunasekaran A, Eckert J, Burge K, Zheng W, Yu Z, Kessler S, et al. Hyaluronan 35 kDa enhances epithelial barrier function and protects against the development of murine necrotizing enterocolitis. *Pediatr Res.* (2019). doi: 10.1038/s41390-019-0563-9. [Epub ahead of print].
21. Albeiroti S, Soroosh A, de la Motte CA. Hyaluronan's role in fibrosis: a pathogenic factor or a passive player? *Biomed Res Int.* (2015) 2015:790203. doi: 10.1155/2015/790203
22. de la Motte C, Nigro J, Vasanji A, Rho H, Kessler S, Bandyopadhyay S, et al. Platelet-derived hyaluronidase 2 cleaves hyaluronan into fragments that trigger monocyte-mediated production of proinflammatory cytokines. *Am J Pathol.* (2009) 174:2254–64. doi: 10.2353/ajpath.2009.080831
23. Goa KL, Benfield P. Hyaluronic acid. a review of its pharmacology and use as a surgical aid in ophthalmology, and its therapeutic potential in joint disease and wound healing. *Drugs.* (1994) 47:536–66. doi: 10.2165/00003495-199447030-00009
24. Trigkilidas D, Anand A. The effectiveness of hyaluronic acid intra-articular injections in managing osteoarthritic knee pain. *Ann R Coll Surg Engl.* (2013) 95:545–51. doi: 10.1308/rcsann.2013.95.8.545
25. Ayhan E, Kesmezacar H, Akgun I. Intraarticular injections (corticosteroid, hyaluronic acid, platelet rich plasma) for the knee osteoarthritis. *World J Orthop*. (2014) 5:351–61. doi: 10.5312/wjo.v5.i3.351
26. Oe M, Tashiro T, Yoshida H, Nishiyama H, Masuda Y, Maruyama K, et al. Oral hyaluronan relieves knee pain: a review. *Nutr J.* (2016) 15:11. doi: 10.1186/s12937-016-0128-2
27. Tashiro T, Seino S, Sato T, Matsuoka R, Masuda Y, Fukui N. Oral administration of polymer hyaluronic acid alleviates symptoms of knee osteoarthritis: a double-blind, placebo-controlled study over a 12-month period. *Sci World J.* (2012) 2012:167928–8. doi: 10.1100/2012/167928
28. Longinotti C. The use of hyaluronic acid based dressings to treat burns: a review *Burns Trauma.* (2014). 2:162–68. doi: 10.4103/2321-3868.142398
29. Prosdocimi M, Bevilacqua C. Exogenous hyaluronic acid and wound healing: an updated vision. *Panminerva Med*. (2012) 54:129–35.
30. Becker LC, Bergfeld WF, Belsito DV, Klaassen CD, Marks JG Jr, Shanket RC, et al. Final report of the safety assessment of hyaluronic acid, potassium hyaluronate, and sodium hyaluronate. *Int J Toxicol.* (2009) 28:5–67. doi: 10.1177/1091581809337738
31. Mazmanian SK, Round JL, Kasper DL. A microbial symbiosis factor prevents intestinal inflammatory disease. *Nature.* (2008) 453:620–5. doi: 10.1038/nature07008
32. Gallo RL, Hooper LV. Epithelial antimicrobial defence of the skin and intestine. *Nat Rev Immunol.* (2012) 12:503–16. doi: 10.1038/nri3228
33. Hooper LV, Macpherson AJ. Immune adaptations that maintain homeostasis with the intestinal microbiota. *Nat Rev Immunol.* (2010) 10:159–69. doi: 10.1038/nri2710
34. Johansson MEV, Sjövall H, Hansson GC. The gastrointestinal mucus system in health and disease. *Nat Rev Gastroenterol Hepatol.* (2013) 10:352–61. doi: 10.1038/nrgastro.2013.35
35. Swidsinski A, Loening-Baucke V, Theissig F, Engelhardt H, Bengmark S, Koch S, et al. Comparative study of the intestinal mucus barrier in normal and inflamed colon. *Gut.* (2007) 56:343–50. doi: 10.1136/gut.2006.098160
36. Wehkamp J, Koslowski M, Wang G, Stange EF. Barrier dysfunction due to distinct defensin deficiencies in small intestinal and colonic Crohn's disease. *Mucosal Immunol.* (2008) 1:S67–74. doi: 10.1038/mi.2008.48
37. Peterson LW, Artis D. Intestinal epithelial cells: regulators of barrier function and immune homeostasis. *Nat Rev Immunol.* (2014) 14:141–53. doi: 10.1038/nri3608
38. Delgado ME, Grabinger T, Brunner T. Cell death at the intestinal epithelial front line *FEBS J.* (2016) 283:2701–19. doi: 10.1111/febs.13575
39. Turner JR. Intestinal mucosal barrier function in health and disease. *Nat Rev Immunol.* (2009) 9:799–809. doi: 10.1038/nri2653
40. Hartsock A, Nelson WJ. Adherens and tight junctions: structure, function and connections to the actin cytoskeleton. *Biochim Biophys Acta.* (2008) 1778:660–9. doi: 10.1016/j.bbamem.2007.07.012
41. Groschwitz KR, Hogan SP. Intestinal barrier function: molecular regulation and disease pathogenesis. *J Allergy Clin Immunol.* (2009) 124:3–20. doi: 10.1016/j.jaci.2009.05.038
42. Antoni L, Nuding S, Wehkamp J, Stange EF. Intestinal barrier in inflammatory bowel disease. *WJG.* (2014) 20:1165–79. doi: 10.3748/wjg.v20.i5.1165
43. Gassler N, Rohr C, Schneider A, Kartenbeck J, Bach A, Obermüller N, et al. Inflammatory bowel disease is associated with changes of enterocytic junctions. *Am J Physiol Gastrointest Liver Physiol.* (2001) 281:G216–28. doi: 10.1152/ajpgi.2001.281.1.G216

44. Asari A, Kanemitsu T, Kurihara H. Oral administration of high molecular weight hyaluronan (900 kDa) controls immune system via toll-like receptor 4 in the intestinal epithelium. *J Biol Chem.* (2010) 285:24751–8. doi: 10.1074/jbc.M110.104950
45. Riehl TE, Santhanam S, Foster L, Ciorba M, Stenson WF. CD44 and TLR4 mediate hyaluronic acid regulation of Lgr5+ stem cell proliferation, crypt fission, and intestinal growth in postnatal and adult mice. *Am J Physiol Gastrointest Liver Physiol.* (2015) 309:G874–87. doi: 10.1152/ajpgi.00123.2015
46. Misra S, Obeid LM, Hannun YA, Minamisawa S, Berger FG, Markwald RR, et al. Hyaluronan constitutively regulates activation of COX-2-mediated cell survival activity in intestinal epithelial and colon carcinoma cells. *J Biol Chem.* (2008) 283:14335–44. doi: 10.1074/jbc.M703811200
47. Yuan H, Amin R, Ye X, de la Motte CA, Cowman MK. Determination of hyaluronan molecular mass distribution in human breast milk. *Anal Biochem.* (2015) 474:78–88. doi: 10.1016/j.ab.2014.12.020
48. Lesley J, Hascall VC, Tammi M, Hyman R. Hyaluronan binding by cell surface CD44. *J Biol Chem.* (2000) 275:26967–75. doi: 10.1074/jbc.M002527200
49. Forteza RM, Casalino-Matsuda SM, Falcon NS, Valencia Gattas M, Monzon ME. Hyaluronan and layilin mediate loss of airway epithelial barrier function induced by cigarette smoke by decreasing E-cadherin. *J Biol Chem.* (2012) 287:42288–98. doi: 10.1074/jbc.M112.387795
50. Wolny PM, Banerji S, Gounou C, Brisson AR, Day AJ, Jackson DG, et al. Analysis of CD44-hyaluronan interactions in an artificial membrane system insights into the distinct binding properties of high and low molecular weight hyaluronan. *J Biol Chem.* (2010) 285:30170–80. doi: 10.1074/jbc.M110.137562
51. Yang C, Cao M, Liu H, He Y, Xu J, Du Y, et al. The high and low molecular weight forms of hyaluronan have distinct effects on CD44 clustering. *J Biol Chem.* (2012) 287:43094–107. doi: 10.1074/jbc.M112.349209
52. Jiang D, Liang J, Fan J, Yu S, Chen S, Luo Y, et al. Regulation of lung injury and repair by toll-like receptors and hyaluronan. *Nat Med.* (2005) 11:1173–9. doi: 10.1038/nm1315
53. Jiang D, Liang J, Noble PW. Hyaluronan in tissue injury and repair. *Annu Rev Cell Dev Biol.* (2007) 23:435–61. doi: 10.1146/annurev.cellbio.23.090506.123337
54. Taylor KR, Yamasaki K, Radek KA, Nardo AD, Goodarzi H, Golenbock D, et al. Recognition of hyaluronan released in sterile injury involves a unique receptor complex dependent on toll-like receptor 4, CD44, and MD-2. *J Biol Chem.* (2007) 282:18265–75. doi: 10.1074/jbc.M606352200
55. Bono P, Rubin K, Higgins JM, Hynes RO. Layilin, a novel integral membrane protein, is a hyaluronan receptor. *Mol Biol Cell.* (2001) 12:891–900. doi: 10.1091/mbc.12.4.891
56. Kohda D, Morton CJ, Parkar AA, Hatanaka H, Inagaki FM, Campbell ID, et al. Solution structure of the link module: a hyaluronan-binding domain involved in extracellular matrix stability and cell migration. *Cell.* (1996) 86:767–75. doi: 10.1016/S0092-8674(00)80151-8
57. Borowsky ML, Hynes RO. Layilin, a novel talin-binding transmembrane protein homologous with C-type lectins, is localized in membrane ruffles. *J Cell Biol.* (1998) 143:429–42. doi: 10.1083/jcb.143.2.429
58. Chen Z, Zhuo W, Wang Y, Ao X, An J. Down-regulation of layilin, a novel hyaluronan receptor, via RNA interference, inhibits invasion and lymphatic metastasis of human lung A549 cells. *Biotechnol Appl Biochem.* (2008) 50:89–96. doi: 10.1042/BA20070138
59. Adachi T, Arito M, Suematsu N, Kamijo-Ikemori A, Omoteyama K, Sato T, et al. Roles of layilin in TNF-α-induced epithelial-mesenchymal transformation of renal tubular epithelial cells. *Biochem Biophys Res Commun.* (2015) 467:63–9. doi: 10.1016/j.bbrc.2015.09.121
60. Bono P, Cordero E, Johnson K, Borowsky M, Ramesh V, Jacks T, et al. Layilin, a cell surface hyaluronan receptor, interacts with merlin and radixin. *Exp Cell Res.* (2005) 308:177–87. doi: 10.1016/j.yexcr.2005.04.017
61. Huang EH, Hynes MJ, Zhang T, Ginestier C, Dontu G, Appelman H, et al. Aldehyde dehydrogenase 1 is a marker for normal and malignant human colonic stem cells (SC) and tracks SC overpopulation during colon tumorigenesis. *Cancer Res.* (2009) 69:3382–9. doi: 10.1158/0008-5472.CAN-08-4418
62. Hornef MW, Normark BH, Vandewalle A, Normark S. Intracellular recognition of lipopolysaccharide by toll-like receptor 4 in intestinal epithelial cells. *J Exp Med.* (2003) 198:1225–35. doi: 10.1084/jem.20022194
63. Meng D, Zhu W, Shi HN, Lu L, Wijendran V, Xu W, et al. Toll-like receptor-4 in human and mouse colonic epithelium is developmentally regulated: a possible role in necrotizing enterocolitis. *Pediatr Res.* (2015) 77:416–24. doi: 10.1038/pr.2014.207
64. Cario E, Podolsky DK. Differential alteration in intestinal epithelial cell expression of toll-like receptor 3 (TLR3) and TLR4 in inflammatory bowel disease. *Infect Immun.* (2000) 68:7010–7. doi: 10.1128/IAI.68.12.7010-7017.2000
65. Gracz AD, Fuller MK, Wang F, Li L, Stelzner M, Dunn JCY, et al. Brief report: CD24 and CD44 mark human intestinal epithelial cell populations with characteristics of active and facultative stem cells. *Stem Cells.* (2013) 31:2024–30. doi: 10.1002/stem.1391
66. Bellar A, Kessler SP, Obery DR, Sangwan N, Welch N, Nagy LE, et al. Safety of hyaluronan 35 in healthy human subjects: a pilot study. *Nutrients.* (2019). 22:E1135. doi: 10.3390/nu11051135
67. Ganji-Arjenaki M, Rafieian-Kopaei M. Probiotics are a good choice in remission of inflammatory bowel diseases: a meta-analysis and systematic review. *J Cell Physiol.* (2018) 233:2091–103. doi: 10.1002/jcp.25911

Conflict of Interest: The authors declare that the research was conducted in the absence of any commercial or financial relationships that could be construed as a potential conflict of interest.

frontiers in Immunology

REVIEW
published: 19 May 2020
doi: 10.3389/fimmu.2020.00769

Proteoglycans in Obesity-Associated Metabolic Dysfunction and Meta-Inflammation

Ariane R. Pessentheiner[1], G. Michelle Ducasa[1] and Philip L. S. M. Gordts[1,2]**

[1] Department of Medicine, Division of Endocrinology and Metabolism, University of California, San Diego, La Jolla, CA, United States, [2] Glycobiology Research and Training Center, University of California, San Diego, La Jolla, CA, United States

Proteoglycans are a specific subset of glycoproteins found at the cell surface and in the extracellular matrix, where they interact with a plethora of proteins involved in metabolic homeostasis and meta-inflammation. Over the last decade, new insights have emerged on the mechanism and biological significance of these interactions in the context of diet-induced disorders such as obesity and type-2 diabetes. Complications of energy metabolism drive most diet-induced metabolic disorders, which results in low-grade chronic inflammation, thereby affecting proper function of many vital organs involved in energy homeostasis, such as the brain, liver, kidney, heart and adipose tissue. Here, we discuss how heparan, chondroitin and keratan sulfate proteoglycans modulate obesity-induced metabolic dysfunction and low-grade inflammation that impact the initiation and progression of obesity-associated morbidities.

Keywords: diabetes, extracellular matrix, metabolic inflammation, obesity, proteoglycans

OPEN ACCESS

Edited by:
Rogier M. Reijmers, Leiden University Medical Center, Netherlands

Reviewed by:
Luciana D'Apice, Italian National Research Council, Italy
Paul Proost, KU Leuven, Belgium

****Correspondence:***
Ariane R. Pessentheiner
apessentheiner@health.ucsd.edu
Philip L. S. M. Gordts
pgordts@health.ucsd.edu

Specialty section:
This article was submitted to Cytokines and Soluble Mediators in Immunity, a section of the journal Frontiers in Immunology

Received: *12 February 2020*
Accepted: *06 April 2020*
Published: *19 May 2020*

Citation:
Pessentheiner AR, Ducasa GM and Gordts PLSM (2020) Proteoglycans in Obesity-Associated Metabolic Dysfunction and Meta-Inflammation. Front. Immunol. 11:769. doi: 10.3389/fimmu.2020.00769

INTRODUCTION

Obesity and its co-morbidities are responsible for a global health problem carrying a significant economic burden. The most common obesity-mediated complications include type-2 diabetes (T2D), cardiovascular disease and chronic kidney disease, yet the contributing mechanisms to these diseases remain to be fully established (1, 2). Obesity and in particular central adiposity – the excess deposition of visceral fat – is associated with increased serum levels of pro-inflammatory cytokines such as interleukin 6 (IL-6), C-reactive protein (CRP), and tumor necrosis factor (TNF) (3–5). This type of low-grade tissue inflammation, also called meta-inflammation, of multiple organs such as liver, adipose tissue, pancreas, kidney, heart, and brain is an important contributing risk factor for the development of insulin resistance.

Abbreviations: αMSH, A-melanocyte stimulating hormone; AgRP, agouti-related protein; ApoB, apolipoprotein B; ApoE, apolipoprotein E; AT, adipose tissue; BAT, brown adipose tissue; Bgn, biglycan; BMI, body-mass index; CD, cluster of differentiation; CRP, C-reactive protein; CSPG, chondroitin sulfate proteoglycans; DAMPs, danger-associated molecular patterns; DCN, decorin; DIO, diet induced obesity; DKD, diabetic kidney disease; DSPG, dermatan sulfate proteoglycans; ECM, extracellular matrix; ESM1, endothelial cell-specific molecule 1; FGFs, fibroblast growth factors; GAG, glycosaminoglycan; Gal, galactose; GlcA, glucoronic acid; GlcNAc, *N*-acetyl glucosamine; GlcNS, *N*-sulfated glucosamine; GPC, glypicans; GPI, glycosylphosphatidylinositol; GWAS, genome-wide association study; HFD, high fat diet; HIF1, hypoxia inducible factor 1; HPSE, heparanase; HS, heparan sulfate; HS6ST, HS 6-*O*-sulfotransferase; HSPG, heparan sulfate proteoglycans; HSPG2, perlecan; ICAM-1, intercellular adhesion molecule; IdoA, iduronic acid; IL-1β, interleukin 1 beta; IL-6, interleukin 6; KS, keratan sulfate; KSPG, keratan sulfate proteoglycans; LDL, low-density lipoproteins; LDLR, low-density lipoprotein receptor; LPS, lipopolysaccharide; Lum, lumican; MC-4R, melanocortin-4-receptor; MCH, melanin concentrating hormone; NAFLD, non-alcoholic fatty liver disease; NASH, non-alcoholic steatohepatitis; NDST, N-deacetylase/N-sulfotransferase; NLRP3, NLR family pyrin domain containing 3; OGN, osteoglycin; PGs, proteoglycans; SDC, Syndecan; SGBS, Simpson-Golabi-Behmel syndrome; SLRP, small leucine-rich proteoglycans; SNPs, single nucleotide polymorphisms; SULF2, sulfatase 2; T1/2D, type-1/2 diabetes; T4, thyroxine; TGF-β, transforming growth factor beta; Th1, T-helper type 1; TLR, toll-like receptor; TNF, tumor necrosis factor; TRL, triglyceride-rich lipoproteins; VLDL, very low-density lipoproteins; XYLT, xylosyltransferases.

The ensuing chronic tissue inflammation is also associated with fibrosis and necrosis, leading to progressive tissue damage. While obesity-associated inflammation is well recognized, the exact etiology is still poorly understood. The complex nature of obesity-induced inflammation presents a challenge to understand the underlying molecular mechanisms that contribute to development of obesity and its associated inflammation. The extracellular matrix (ECM) surrounding cells is a central hub in mediating metabolic and inflammatory signal transduction, regulating fibrotic processes and ensuring the functional integrity of cells. In this review we will describe the central role of heparan, chondroitin and keratan sulfate proteoglycans found in the ECM in processes critical for initiation, progression and the chronic nature of meta-inflammation in the context of obesity and T2D.

DIET-INDUCED META-INFLAMMATION AFFECTS SPECIFIC TISSUES CRITICAL FOR ENERGY HOMEOSTASIS

Adipose Tissue Inflammation

Adipose tissue (AT) has an enormous plasticity to adapt to nutritional changes. However, under conditions of constant overnutrition, AT expands beyond its limits and is associated with the development of inflammation, impaired angiogenesis and ectopic fat deposition in organs such as liver and skeletal muscle. This detrimental cycle leads to tissue dysfunction and development of insulin resistance. Adipose depots are a conglomerate of various cell types, such as mature adipocytes embedded in the stroma with preadipocytes, fibroblasts, immune cells and endothelial cells. Immune cells, primarily macrophages, residing in AT maintain the integrity and hormonal sensitivity of adipocytes in a normal lean state. Macrophages are characterized by their "polar" state, displaying more of a pro-inflammatory or anti-inflammatory and, resolving phenotype. Resident macrophages of lean subjects present an M2-polarized or resolving state which is generally associated with anti-inflammatory properties. However, during progressive weight gain and development of obesity macrophages change into pro-inflammatory M1-like macrophages, which produce pro-inflammatory cytokines attracting more M1-macrophages to infiltrate the AT. The thereby activated inflammatory program has an overall T-helper type 1 (Th1) nature, which is usually associated with infection. Unlike acute inflammation, the meta-inflammation in an obese state is not resolved, which leads to a chronic inflammatory response that triggers insulin resistance of adipocytes resulting in lipid spill-over to peripheral organs (5, 6).

Liver Is a Central Hub for Energy Homeostasis

One of the major organs affected by diet-induced meta-inflammation and AT insulin resistance is the liver. It plays a central role in maintaining whole body energy homeostasis and is considered an energy storage and redistribution node. Consisting predominantly of hepatocytes it is also populated by fenestrated sinusoidal endothelium and Kupffer-cells, which are specific resident hepatic macrophages important for normal liver function especially in the lean state. However, in the context of energy excess, such as obesity, Kupffer-cells get activated analogous to resident AT macrophages thereby recruiting more immune cells and promoting hepatic insulin resistance. Consequently, this negatively affects insulin-mediated inhibition of hepatic glucose production (gluconeogenesis) thereby driving elevated glucose levels in afflicted patients (7, 8). Hepatic insulin resistance also prevents insulin-mediated inhibition of production of very-low density lipoproteins (VLDL) in hepatocytes and impairs hepatic lipoprotein clearance of low-density lipoproteins (LDL) and triglyceride-rich lipoprotein (TRL) remnants. This results in the onset of metabolic dyslipidemia, which in conjunction with chronic inflammation drives the progression of cardiovascular disease. Importantly, insulin resistance favors the development of excessive fat accumulation in the liver, also called steatohepatitis creating a vicious cycle of escalating inflammation, insulin resistance and fibrosis which leads to non-alcoholic fatty liver disease (NAFLD). Furthermore, AT-derived circulating cytokines and adipokines promote NAFLD (9–11). Without intervention NAFLD progresses to liver cirrhosis and ultimately to hepatocellular carcinoma. However, even after weight loss intervention, a permanent inflammatory fingerprint lingers in AT and liver (12).

Kidney Dysfunction Induced by Meta-Inflammation

While the consequences of obesity and insulin resistance in liver and AT are often discussed, less attention is paid to the kidneys which are important for detoxifying processes and contribute to organ dysfunction in disease states. Increased obesity prevalence has been associated with a rise in chronic kidney disease progression and not surprisingly obese individuals are at elevated risk for developing end-stage kidney disease (13). Similarly, experimental mouse models of obesity, such as high fat diet (HFD) fed models, develop increased kidney injury (14). HFD-mediated kidney injury results in leakage of albumin in the urine (albuminuria), renal fibrosis, insulin resistance, and elevated inflammation in mice (15). Obesity and diabetes mediated end-stage kidney disease is characterized by an accumulation of lipids within the kidney met with increased inflammation (2). IL-6, TNF, IL-1β and MCP-1 levels are elevated in kidneys from a diet-induced obesity rat model, associated with increased kidney fibrosis and sclerotic lesions (16). Similarly, TNF is elevated in sera obtained from patients with diabetic kidney disease (DKD), as well as in an obese-diabetic mouse model that presents with kidney disease (17). Furthermore, oxidative stress is upregulated in kidneys from preclinical obesity-induced DKD models (18) together with increased inflammation in perirenal visceral AT, all of which was reversed after treatment with an angiotensin II inhibitor (ANG 1-7) (19). Collectively, these data suggest that obesity and AT inflammation contribute to kidney complications observed in obese experimental and clinical models.

THE EXTRACELLULAR MATRIX SURROUNDING ADIPOCYTES PLAYS A CENTRAL ROLE IN METABOLIC INFLAMMATION

In recent years the importance of the adipocyte microenvironment has gained more prominence as ECM composition, remodeling and interacting factors significantly contribute to the detrimental consequences of obesity. The ECM is a key regulator for maintaining optimal cell and tissue homeostasis by disseminating and integrating cues from and to surrounding cells as well as distant organs. ECM remodeling is critical for differentiation of adipocytes, the integrity of expanding adipocytes as well as recruitment of immune cells (20). AT has the capacity to expand either through hyperplasia, a result of increased preadipocyte proliferation and differentiation into adipocytes, or through hypertrophy by expanding the lipid storage capacity of existing adipocytes. In the process of adipocyte differentiation, the ECM undergoes structural changes from a fibrillar to a laminar structure. The fibrillar structure of preadipocytes, mainly containing collagen I, plasmin, and fibronectin, is replaced by a laminar structure built by collagen VI, laminin, and a high amounts of collagen IV (21). During excessive AT expansion, imbalances in ECM synthesis and degradation lead to fibrosis, one of the hallmarks of AT dysfunction associated with meta-inflammation and progression of advanced insulin resistance (22). Moreover, hypertrophy induces hypoxia and mechanical stress (6, 23, 24). Hypoxia contributes to meta-inflammation through activation of hypoxia inducible factor 1 (HIF1) resulting in increased transcription of a pro-inflammatory gene program in adipocytes and patrolling immune cells (23, 24). Concomitantly, angiogenesis is induced during AT expansion to support the growing tissue with essential nutrients, hormones, growth factors, and oxygen. However, in an obese state, the angiogenic capacity of endothelial cells declines, resulting in augmented tissue hypoxia and cell apoptosis. This process requires infiltration of immune cells including macrophages to clear dying adipocytes thereby forming so-called crown-like structures. Although flexible to some degree, the ECM provides a rigid mesh that puts mechanical pressure on adipocytes. This occurs during hypertrophy and induces an inflammatory signature during excessive expansion (20). Modulating that mechanical stress by targeting collagen VI levels improves lipid and energy metabolism in adipocytes and attenuates fibrosis and metabolic inflammation (25). These observations emphasize the therapeutic potential of ECM modulation.

PROTEOGLYCANS ARE UBIQUITOUS EXTRACELLULAR ENVIRONMENT COMPONENTS REGULATING NUMEROUS METABOLIC PROCESSES

Proteoglycans (PGs) are an integral part of the cellular glycocalyx in the ECM and exhibit important roles in cell and tissue homeostasis by regulating various processes such as proliferation, differentiation, angiogenesis, and inflammation. They consist of a core protein with one or more covalently attached glycosaminoglycan (GAG) chains (**Figure 1**). The building block of those GAG chains are repeating disaccharide units consisting of an amino sugar and a uronic acid which depending on the alternating glycan units determine the class of proteoglycans. Keratan sulfate (KS) does not contain a uronic acid but is built of repeating units of galactose (Gal) and *N*-Acetyl-glucosamine (GlcNAc) attached to *N*- (KS-I) or *O*-glycan (KS-II) chains (**Figure 1**). Chondroitin sulfate (CS) consists of repeating units of *N*-acetyl-D-galactosamine (GalNAc) and glucuronic acid (GlcA) residues (**Figure 1**). Dermatan sulfate differs from CS only by the additional presence of iduronic acids (IdoA) as a result of GlcA epimerization. In contrast, heparan sulfate (HS) features repeating units of GlcNAc or *N*-sulfated glucosamine (GlcNS) and a combination of either GlcA or IdoA (**Figure 1**). Hence, there are three main proteoglycan subclasses – chondroitin/dermatan sulfate proteoglycans (CS/DSPG), heparan sulfate proteoglycans (HSPG), and keratan sulfate proteoglycans (KSPG) (**Figure 1**). One important feature of GAG chains attached to proteoglycans is their high degree of sulfation resulting in generation of a strongly negatively charged polysaccharide. This gives proteoglycans an enormous capacity to act as a charge-barrier in the ECM, hindering some factors to bind and allowing others to interact (26). Many ligands of PGs have been identified over the years, including growth factors such as fibroblast growth factors (FGFs), cytokines and chemokines, cell surface receptors, cell adhesion molecules, and other ECM components such as collagen and fibronectin. Some proteoglycan interactions require GAG chains, others are depending on the core protein (27–29). Not surprisingly, proteoglycans are crucial regulators of many metabolic homeostatic processes as well as of acute and chronic inflammation (30–34). Several proteoglycans, including lumican, perlecan, decorin, aggrecan, versican, betaglycan, biglycan, and proteoglycan 4, have been described to be either secreted by adipocytes or are at least abundantly present in their ECM (20, 35). Proteoglycan composition is influenced by the diabetic condition (36), however, the amount of PGs produced during differentiation of preadipocytes to adipocytes is controversial with some studies noting decreased PG production during differentiation (37), and others reporting the opposite trend (38). The interaction of ECM components, such as collagens and proteoglycans, with cell surface receptors is crucial during the differentiation and expansion of adipocytes. Therefore, a detailed understanding of the role proteoglycans and their interaction partners play can provide novel solutions to tackle obesity-related meta-inflammation. The link between diet-induced metabolic inflammation and the development of insulin resistance has been well-established over the past years, but specific mechanisms of how the microenvironment surrounding cells influences the progression of inflammation are still under investigation. In this review, we will focus on the roles of proteoglycans and their structural modifications in metabolic homeostasis as well as their influence on AT hypertrophy and hyperplasia and their impact on meta-inflammation in critical

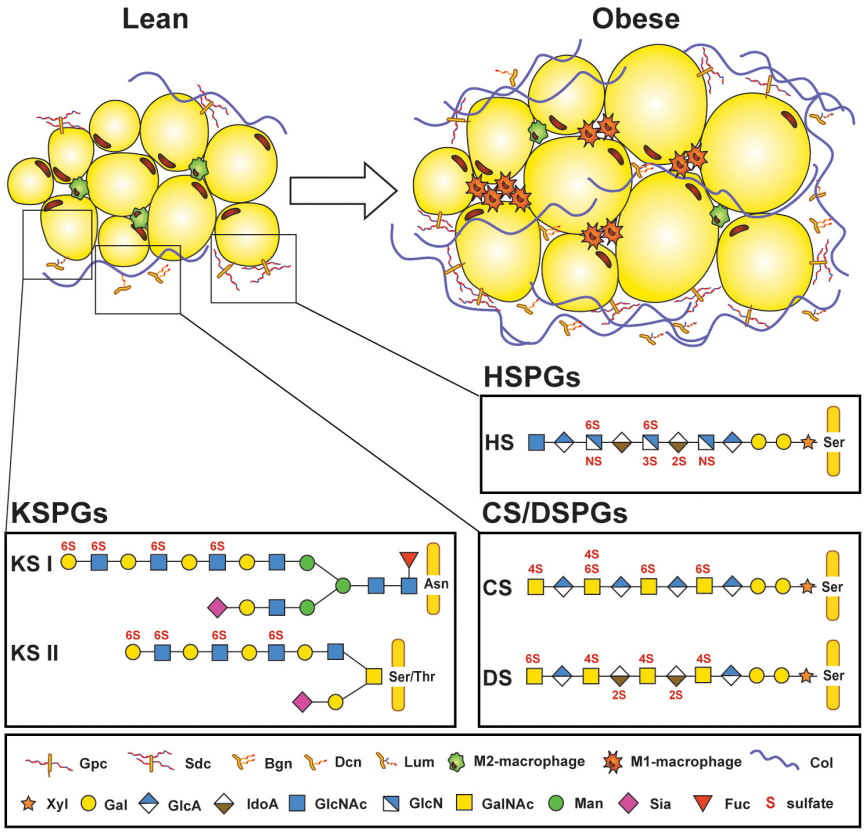

FIGURE 1 | Proteoglycans are part of the microenvironment surrounding adipocytes. Lean adipose tissue expresses low amounts of proteoglycans found in the extracellular matrix surrounding adipocytes and stromal vascular cells, but their expression increases in obese adipose tissue, along with increased infiltration of M1-macrophages and deposition of collagen. Several core proteins are linked to adipose tissue homeostasis, such as glypican (Gpc) and syndecans (Sdc); biglycan (Bgn), decorin (Dcn), and lumican (Lum). Three different types of glycosaminoglycan (GAG) chains that are covalently attached to protein cores can be found in adipose tissue. Keratan sulfate (KS) chains are either attached to asparagine (Asn) or serine/threonine (Ser/Thr) at the protein core and consist of repeating *N*-acetylglucosamine (GlcNAc) and galactose (Gal) subunits. KS chains can also be sialylated (Sia) or fucosylated (Fuc). Heparan sulfate (HS) and chondroitin/dermatan sulfates (CS/DS) are attached through a tetrasaccharide linker region starting with a xylose (Xyl), two Gal, and a glucuronic acid (GlcA) at a Ser on the protein core. HS consists of *N*-acetyl-glucosamine (GlcNAc) and a combination of either GlcA or iduronic acid (IdoA). CS features *N*-acetyl galactosamine (GalNAc) and GlcA residues which can be replaced by IdoA in DS. GAG chains are sulfated on various positions (*N*-,2-*O*, 3-*O*, 4-*O*, or 6-*O*-sulfations depicted in red). Col: Collagen. [Proteoglycan structures adapted from Ref. (26)].

organs for obesity-associated metabolic complications such as AT, liver and kidney.

HEPARAN SULFATE PROTEOGLYCANS, A DEFINED GROUP OF GLYCOPROTEINS, ACT AS REOSTATS IN METABOLIC DISEASE

HSPGs are a group of 17 family members of proteoglycans found in the basement membrane of cells. Despite their relatively small number of core proteins, they are structurally very diverse. Their primary GAG are HS chains reaching up to 40–300 sugar residues in length which can be modified by sulfotransferases on three different carbon positions (C2 on IdoA or C3 and C6 on GlcNAc) or an amine group (GlcNS) (**Figure 1**). Sulfation occurs in clusters of variable length generating heavily sulfated domains interspersed by unsulfated domains. A functional consequence of this molecular sulfation diversity is the formation of defined structural motifs which allow HS to bind and modulate the action of numerous specific extracellular ligands, such as cytokines and growth factors (39). HSPGs have many functions in inflammation, including: (i) building morphogen, growth factor, chemokine and cytokine gradients (**Figure 2A**); (ii) protecting chemo- and cytokines from proteolysis (**Figure 2A**); (iii) acting as co-receptors, for example with FGF receptors (FGFRs), to stabilize receptor/ligand complexes (**Figure 2A**); (iv) mediating signal transduction independently or by engaging inflammatory receptors such as toll-like receptors (**Figure 2B**); (v) regulating immune cell adhesion, migration, and activation (**Figure 2C**); and (vi) binding and regulating ECM components (**Figure 2D**) (40, 41). In addition, HSPGs play a central role in liver lipid homeostasis and thus influence hyperlipidemia and atherosclerosis development (42). Furthermore, HSPGs, such as perlecan and agrin play an essential role in the charge-mediated

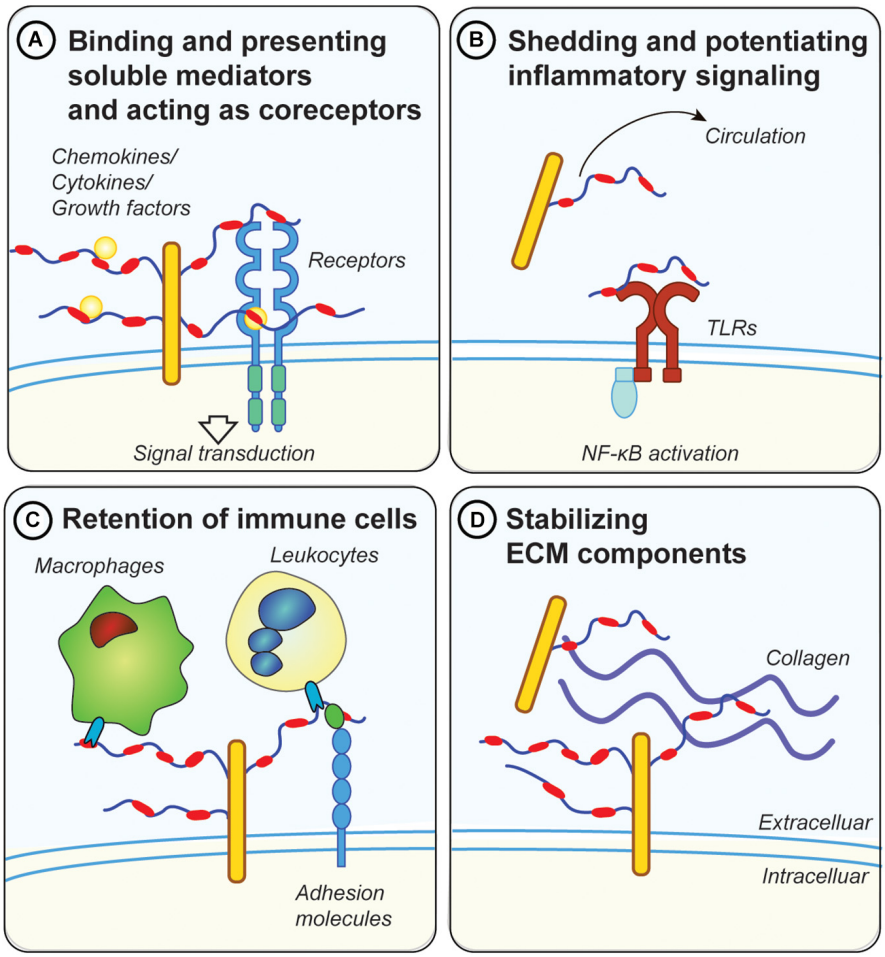

FIGURE 2 | Possible mechanisms for proteoglycans in metabolic inflammation. **(A)** GAG chains, in particular HS, bind and present soluble inflammatory mediators, such as cytokines and chemokines at the cell surface. They also protect those factors from proteolytic degradation. Moreover, they act as co-receptors for ligand/receptor complexes, such as fibroblast growth factor 1 (FGF1) with FGF receptors. **(B)** Diabetes and metabolic inflammation lead to increased shedding of proteoglycans from the ECM, either by cleaving the protein core or the attached GAG chains. Shed proteoglycans and GAG chains have been shown to engage with toll-like receptors (TLRs), thereby potentiating the inflammatory response via NF-κB downstream signaling. Proteoglycans and GAGs released in the circulation can therefore have systemic effects and could be used as biomarkers for metabolic disease (e.g., GPC4). **(C)** Membrane bound proteoglycans (e.g., syndecans or glypicans) are in involved in retention of immune cells by directly engaging with lectins on the surface of immune cells. Proteoglycans also regulate the accessibility of adhesion molecules such as ICAM-1 on the cell surface which are important for the attachment of leucocytes. **(D)** Proteoglycans mediate the interaction between other ECM components such as collagens and fibrinogen. Dysregulations in ECM deposition lead to the development of fibrosis, a common pathology associated with metabolic disease.

barrier of the glomerulus, important for the proper filtration of the kidney, and are associated with inflammation during kidney disease (43).

Proteoglycan Biosynthetic and Modifying Enzymes in Meta-Inflammation

Due to the functional importance of GAG chains, enzymes that are involved in the assembly and functionalization of HS are consequential for HSPG-related processes making them important to consider in the context of obesity and meta-inflammation. The biosynthesis and modification of GAGs require several glycosyltransferases, sulfotransferases, and epimerases, all of which are well investigated. However, the regulatory circuits that impact their expression and activity in a spatial and temporal manner remain less clear.

Xylosyltransferases (XYLT) 1 and 2 initiate HS, CS and DS biosynthesis via catalyzing a covalent linkage of xylose to serine residues at the GAG-attachment site of the core protein (**Figure 1**). Given their critical role for GAG biosynthesis it is not surprising that their genetic inactivation results in gross phenotypic changes. Indeed, loss of XYLT1 in humans (and mice) is associated with short-stature due to bone development issues making it difficult to assess the impact in the context of meta-inflammation (44). Loss of XYLT2 in mice leads to decreased AT mass and local inflammation, concomitant with decreased glucose tolerance similar to a lipodystrophy phenotype (45). Also, *Xylt2*-deficient mice are afflicted by multi-organ dysfunction,

making it difficult to assess to what extent the observed AT dysfunction plays an exclusive role in the observed metabolic effects (45). Nevertheless, it is important to consider the impact of *Xylt2* inactivation in diet-induced obesity.

HS undergoes extensive modifications beginning with *N*-deacetylation followed immediately by *N*-sulfation, a reaction catalyzed by *N*-deacetylase/*N*-sulfotransferases (NDST1-4). The structural complexity is further enhanced by epimerization and the sulfation of several positions by 2-*O*, 3-*O*, and 6-*O*-sulfotransferases. The sulfation reactions are non-template driven and require initial *N*-sulfation. Altered sulfation patterns influence the binding and signaling capacity of HS/ligand interactions (39) and compositional variation in sulfation within the population might influence their susceptibility for obesity and cardiovascular disease. An example of intrinsic variation of HS-sulfation are venous and aortic endothelial cells which differ in their degree of sulfation (46). This discrepancy might be the reason why there is increased leukocyte recruitment into small veins compared to capillaries and arteries (46). Global knock-out of *Ndst1* is perinatal lethal, but conditional knock-out mice allow investigating the impact of altered HS sulfation under various obesity- and inflammation-related conditions. In endothelial cells, inactivation of *Ndst1* inhibits granulocyte adhesion and diminishes binding of L-selectin *in vitro* (47) and results in reduced leukocyte recruitment in DKD *in vivo* (48). Embryonic stem cells from *Ndst1/2* double knock-out mice fail to differentiate into adipocytes *in vitro* (49) and decreased sulfation of macrophage HS through targeted deletion of *Ndst1* leads to increased atherosclerosis and obesity development driven by increased AT inflammation via type I interferon signaling (50, 51). However, to date no studies investigating the role of adipose NDSTs have been reported.

WNT and FGF binding to HS and hence their respective signaling modalities are regulated by HS, in particular via 6-*O*-sulfation (52, 53). Three different HS 6-*O*-sulfotransferases (HS6STs) having slightly different substrate specificities have been identified (54) and expression of *Hs6st1* is increased in macrophages from mice suffering from CVD and obesity (55–57). The importance of 6-*O*-sulfation in maintaining energy homeostasis has been evaluated in male *Hs6st2* knock-out mice. The systemic null mice present with increased weight gain and impaired glucose metabolism, even on a low-fat diet. Mechanistically, this was explained by reduced brown adipose tissue (BAT) mediated non-shivering thermogenesis as a result of reduced circulating thyroid hormone thyroxine (T4) levels that activate BAT (58). It is still unclear if this alteration in T4 levels is due to impaired uptake of the HS-binding thyroid hormone precursor thyroglobulin or due to the impact of HS on thyroid functionality to produce and secrete T4.

Heparanase (HPSE) is an extracellular HS degrading endo-β-D glucuronidase that is expressed in a variety of tissues. HPSE is involved in shedding of HSPGs from the ECM, which generates HS fragments ranging between 10 to 20 disaccharide units that remain biologically active. This leads to a re-organization of the ECM and therefore impacts cell motility and invasion (59). In an inflammatory context, this facilitates the recruitment of immune cells (60). HPSE activity also leads to upregulation of cytokine expression in macrophages (61, 62) and its expression in turn is induced by a variety of inflammatory cytokines, fatty acids (63) and high glucose (64). Diabetic patients often present with elevated HPSE in their circulation and urine (65) and *HPSE* upregulation is associated with DKD (66), as well as diabetes-associated cardiovascular diseases (67). Soluble HS fragments generated by HPSE have been shown to promote toll-like receptor (TLR) 4 signaling in dendritic cells (68) and human peripheral blood monocytes (69). Not surprisingly, infusion of mice with HS fragments resulted in marked pancreatic inflammation, while infusion in TLR4 knockout mice did not produce this inflammatory response (70). However, soluble HS fractions can also have protective functions and prevent bone marrow transplant rejection (71). It remains to be elucidated if HS fragments are released more prominently in metabolic dysfunctional patients and if their functions under obese conditions are beneficial or detrimental for infiltrating immune cells and the surrounding metabolic active cells.

Overall, investigation of HS-modifying enzymes comprises certain difficulties for the development of intervention strategies mostly due to their pleiotropic impact on all proteoglycans in every tissue, which makes it difficult to dissect and target the function of individual proteoglycans. Specific PGs have been implicated in metabolic homeostasis and inflammation and as such will be further discussed in the following sections.

Syndecans – Major Hubs for Inflammation, Lipid Metabolism and Satiety Control

In mammalian cells, the Syndecan (SDC) family consist of four type I transmembrane HSPG (SDC1-4) (**Table 1**). They are expressed in a developmental and cell-type specific manner and involved in diverse biological processes ranging from morphogenesis to energy metabolism. The major functional groups of syndecans are the 1-3 attached HS chains on the N-terminus. They also carry 1-3 shorter CS chains closer to the plasma membrane. The number of attached GAG chains, their size, composition and sulfation pattern largely influence SDC's binding capacity of its natural ligands. In this fashion syndecans bind and retain multiple heparan sulfate binding proteins (HSBPs). This will either attenuate or propagate HSBP functions, including properties of chemokines/cytokines and their interactions with leukocytes and endothelial cells (**Figure 2**) (31, 34). Several *in vitro* and *in vivo* studies have highlighted the diverse roles of SDCs in inflammation (31, 34, 72), but reports investigating the impact of SDCs on obesity-related metabolic inflammation are sparse (73–77). Using whole-genome linkage studies a SNP in chromosomal region 20q12-13, which contains the *SDC4* gene, has been linked with increased predisposition for T2D and obesity (78, 79). De Luca and coworkers showed in a small cohort that children homozygous for the minor *SDC4* SNP (rs1981429) allele presented with decreased lean mass and increased intra-abdominal fat mass (80). Fruit flies express one functionally conserved SDC isoform and its loss in female Drosophila reduced their body weight and body lipid content, while males did not show body weight changes. This was

TABLE 1 | Overview of proteoglycans associated with phenotypes in the context of metabolic dysregulation and meta-inflammation.

Proteoglycan	Core mass (kDa)[a]	Chain type (number)[b]	Subcellular localization	Phenotypic observations	
				Humans	Relevant preclinical models
Heparan sulfate proteoglycans					
Syndecan 1–4 (SDC1–4)	31–45	HS (2–3) in SDC2 and 4; HS/CS (3–4 HS/1-2 CS) in SDC1 and 3	Membrane-bound	Plasma SDC1 correlates with T1D and DKD (77) and hypertriglyceridemia in T2D patients (84); SNP in SDC4 linked with predisposition to T2D and obesity (78, 79, 80)	Increased atherosclerosis in *Apoe*$^{-/-}$*Sdc1*$^{-/-}$ mice (73); All SDCs: regulation of feeding behavior (89-92)
Glypican 1–6 (GPC 1–6)	57–69	HS (1–3)	Membrane-bound	Simpson-Golabi-Behmel syndrome (overgrowth) (GPC3-4) (98); GPC4 (serum, AT) increases with BMI, insulin resistance, NAFLD (100–106); GPC5 risk allele in DKD (107)	GPC5 correlates with DKD (108);
Perlecan (HSPG2)	∼470	HS (1–3)	Secreted/ECM	No data reported.	Obesity resistance in cartilage-rescued *Hspg2*$^{-/-}$ mice (109); Role in lipoprotein retention in atherosclerosis (113, 117, 118)
Chondroitin/Dermatan sulfate proteoglycans					
Endocan (ESM1)	20	DS (1)	Secreted	Serum and AT levels increase in obesity (126, 134, 135); T2D (128, 129); atherosclerosis (130); DKD (131, 135); NAFLD (132); and psoriasis (133)	Correlation with DKD (136)
Decorin (DCN)	38–42	DS/CS (1)	Secreted/ECM	Increased expression in AT in obesity and T2D (143, 149, 151); Upregulated in DKD (156)	*Dcn*$^{-/-}$ mice: increased obesity, AT inflammation, and glucose intolerance (151, 153); aggravated DKD (157)
Biglycan (BGN)	38–42	DS/CS (2)	Secreted/ECM	Upregulation in atherosclerotic plaques (166, 167); Increased in kidney injuries met with elevated inflammation, including DKD (171)	*Bgn*$^{-/-}$ mice*:* reduced AT inflammation upon obesity (160); overexpression in mice promotes atherosclerosis (166, 167); *Bgn* accumulates in glomeruli of DKD mice (170)
Keratan sulfate proteoglycans					
Lumican (LUM)	∼37	KS (1)	Secreted	Liver expression correlates with severity of NASH and NAFLD (174–176)	*Lum*$^{-/-}$ mice (females): increased obesity (177)
Osteoglycin (OGN)	25–72	KS and *O*-linked glycans	Secreted	OGN serum levels increase in response to weight loss in severely obese patients (184); Associated with atherosclerotic plaques (183)	Increased in atherosclerotic plaques in rabbits (182); Reduced levels of *Ogn* in obesity (185); *Ogn*$^{-/-}$ mice: glucose intolerance and insulin resistance in diet-induced obesity (185)

AT, adipose tissue; HS, heparan sulfate; DS, dermatan sulfate; CS, chondroitin sulfate; ECM, extracellular matrix; T2D, type 2 diabetes; NASH, non-alcoholic steatohepatitis; NAFLD, non-alcoholic fatty liver disease; DKD, diabetic kidney disease. [a]*Variation in core mass is due to species differences.* [b]*Number of chains is based on the number of putative attachment sites for chain initiation as well as data from the literature; the actual number of chains varies by method, tissue, and species.*

associated with reduced metabolic activity, measured by O_2 and CO_2 production, in mutant flies suggesting that SDCs play a key role in the regulation of body metabolism (80).

Insulin promotes shedding of SDC1 ectodomains (81, 82) and increased inflammatory mediators and proinflammatory monocytes in patients with type-1 diabetes and nephropathy have been correlated with increased plasma SDC1 levels (77). Insulin also increases expression of SDC1 in a human hepatoma cell line but is downregulated by increasing fatty acids levels (83). In the liver, SDC1 is particularly important for TRL uptake from the circulation. Hence, reduced SDC1 expression or increased shedding contributes to the associated hypertriglyceridemia in T2D patients (84). In fact, T2D patients present with increased expression of an ECM enzyme, called sulfatase-2 (SULF2), that removes 6-*O* sulfate groups from HS chains on SDC1 and other HSPGs (85–87). Increased SULF2 expression was also observed in *db*/*db* mice, a diabetic and obese mouse model lacking leptin receptor expression. The increased liver SULF2 levels in *db*/*db* mice associated with reduced HS sulfation on hepatocytes accompanied by reduced SDC1-mediated TRL clearance. Moreover, therapeutic lowering of SULF2 using antisense oligonucleotides reduced hypertriglyceridemia in *db*/*db* mice (88) and introduced a new therapeutic window for T2D-associated hyperlipidemia.

SDC1 is also presented at the cell surface of macrophages where it influences migration and inflammatory resolution response (73). Expression of SDC1 differs between macrophage subclasses depending on their inflammatory profile. Resolving or M2 polarized macrophages express high levels of SDC1, in contrast pro-inflammatory M1-polarized macrophages completely lack SDC1 expression. In particular, macrophages derived from *Sdc1* knock-out mice have reduced motility

of M2-resolving macrophages, which is associated with increased atherosclerosis development in *Apoe*$^{-/-}$*Sdc1*$^{-/-}$ mice fed a Western-type diet (73). This might be explained by SDC1 sequestering inflammatory and chemotactic mediators away from signaling receptors on macrophages to promote anti-inflammatory properties. Although these data have been observed in the context of atherosclerosis, it is likely that macrophage-expressed SDC1 impacts other metabolic complications such as obesity-induced diabetes.

All SDCs have been implicated in the regulation of feeding behavior by guiding neuronal development and plasticity (89–92). Energy intake is centrally regulated in the hypothalamus via orexigenic/pro-feeding (agouti-related protein, AgRP) and anorexigenic/anti-feeding, pro-opiomelanocortic neurons. Both types of neurons make contact with melanocortin-4 receptor (MC-4R) expressing neurons. Secretion of satiety hormones including α-melanocyte stimulating hormone (αMSH) and anti-satiety peptides such as AgRP and melanin concentrating hormone (MCH) lead to inhibition or stimulation of food intake, respectively (93). SDC3 is expressed in the hypothalamus and its cell surface levels are regulated by nutrient conditions. Fasting induces hypothalamic expression of SDC3 and its ectodomain is shed in response to feeding. *Sdc3*$^{-/-}$ mice are resistant to diet-induced obesity (94) due to reduced food intake. Lack of SDC3 at the cell surface increases orexigenic signaling via AgRP by preventing engagement of the anti-satiety hormone MCH with MC-4R and potentiation of αMSH (90). During feeding, SDC3 is cleaved by metalloproteases inducing satiety via MCH/MC-4R signaling. Furthermore, the shedding process appears to be regulated under fasting conditions as well since a putative inhibitor of the shedding process, tissue inhibitor of metalloprotease−3, is increased by food deprivation. Transgenic overexpression of SDC1 in the hypothalamus promotes obesity due to increased food intake as overabundant SDC1 at the cell membrane interacts with AgRP to potentiate its orexigenic activity (91). Loss of SDC1 also induces hyperphagia, especially after fasting periods. However, this is a result of reduced intradermal adipogenic differentiation. Lack of insulating intradermal fat promotes cold-stress resulting in hyperphagia. However, this increased food intake does not promote weight gain since it meets the increased energy demand of BAT to maintain body temperature via enhanced non-shivering thermogenesis (95). Food intake was also decreased in *Sdc4*$^{-/-}$ mice independent of the diet. Although unclear at this point which role SDC4 plays in feeding behavior, it further emphasizes the overall relevance of Syndecans in satiety control (89).

Glypicans – Biomarkers for Metabolic Syndrome and Insulin Resistance

Glypicans (GPC) are a six-member family of cell surface glycosylphosphatidylinositol (GPI)-anchored HSPGs (96) (**Table 1**). GPC can be shed from the cell surface by phospholipase-mediated cleavage of the GPI-anchor (97) which gives them the potential not only to influence cell surface processes, but also processes in the extracellular environment and to act systemically (**Figure 2**). In humans, mutations in GPC3 and GPC4 are associated with the development of the Simpson-Golabi-Behmel syndrome (SGBS), an X-linked inherited overgrowth syndrome characterized by a broad spectrum of clinical manifestations, such as congenital, facial and cardiac abnormalities, organomegaly, and reduced viability primarily in male patients (98). Interestingly, pre-adipocytes from a male SGBS patient have been used as a model system for human adipogenic differentiation ever since their isolation in 2001 (99).

In an unbiased screen GPC4 was identified as an adipokine in a set of developmentally regulated genes that are differentially expressed in subcutaneous and visceral AT of mice and men (100). In healthy humans, subcutaneous AT has the highest GPC4 expression while in obese patients GPC4 expression decreases in subcutaneous AT and increased in visceral AT (100, 101). The most clinically relevant observation is a positive association between GPC4 expression in human white AT and both body-mass index (BMI) and central AT distribution. Since its discovery as a novel adipokine, several studies further confirmed this strong correlation using serum GPC4 levels and also identified that increased GPC4 serum levels positively associated with the prevalence of NAFLD and insulin resistance in at risk patients (101–106). When considering GPC4 as a biomarker for insulin resistance and NAFLD it is important to consider sex-specific differences as healthy men present with higher plasma GPC4 levels compared to women. However, circulating GPC4 levels in obese and insulin resistant female patients are dramatically elevated, reaching comparable levels as their male counterparts (101, 105). Collectively, GPC4 seems to be a potent biomarker for metabolic disease, however its exact functions in obesity development and metabolic inflammation remains to be fully established. Functionally, research supports the concept of GPC4 as an insulin sensitizer as GPC4 directly binds the insulin receptor, an interaction that is disrupted by insulin. Hence, it is plausible that the insulin receptor interaction with GPC4 stabilizes insulin receptor to prolong its presentation and insulin reception. Recombinant GPC4 administration increases insulin signaling in cultured adipocytes independent of its GPI anchor, but the importance of the HS chains for the GPC4-mediated insulin sensitization is unclear and remains to be determined (101).

GPC5, another GPI-anchored HSPG, associated in a genome-wide association study (GWAS) with acquired DKD [odds ratio 1.45 (95% CI, 1.18–1.79)] (107). The risk allele in the GWAS correlated with elevated GPC5 expression in podocytes. Similarly, GPC5 expression gradually increased in glomerular mesangial cells in murine T2D models and associated with progression and severity of DKD (108). In contrast, podocyte specific GPC5 knockdown in a preclinical FGF2 induced DKD model conferred resistance to podocyte and glomerular injury. These studies validate the importance of GPC5 in progression of DKD. It remains unclear how GPC5 influences the pathology, but it might involve sequestration of FGF2 and local modulation of FGF receptor activity (107, 108). Therefore, future studies are warranted to elucidate the involvement of GPC5 in DKD pathophysiology.

Perlecan – Driver of Atherogenesis and Adipocyte Hypertrophy

The largest secreted proteoglycan (∼500 kDa) is Perlecan (HSPG2) carrying up to three HS attachments. It is an integral component of the ECM where it interacts with the basement membrane (109–113) (**Table 1**). HSPG2 is implicated in various pathological processes, such as tumor development, osteoarthritis, muscle hypertrophy, atherosclerosis and diet-induced obesity (113). Its physiological importance and complex biology is illustrated by the fact that a null-allele of *Hspg2* in mice is embryonic lethal, but can be perinatally rescued via transgenic expression of *HSPG2* in cartilage (111). Regulation of perlecan expression is intricate and modulated by many external factors including growth factors, chemokines, cytokines and cellular danger signals. Its expression and secretion is suppressed by interferon γ but activated by nuclear factor kappa-light-chain-enhancer of activated B cells (NF-κB) signaling (114, 115), as well as in macrophages by HIF1α and HIF1β upon hypoxia, a pertinent condition in atherosclerotic lesions and hypertrophic AT (116). HSPG2 is abundant in the arterial wall, specifically the intima. In this sub-endothelial layer of the artery HSPG2 binds and traps LDL via interaction of LDL-associated apolipoprotein B (apoB) and E (apoE) in an HS chain dependent manner. Knock-in mice expressing perlecan lacking the HS binding sites present with reduced subendothelial lipoprotein retention and atherosclerosis development (113, 117, 118). Hence, hypoxia-induced perlecan expression in macrophages could accelerate lipoprotein trapping in the subendothelial layers of arteries as well as promote hypertrophy (over hyperplasia) in expanding AT. It is thus not surprising that perinatally rescued *Hspg2*-deficient ($Hspg2^{-/-}$tg) mice are resistant to diet-induced obesity due to reduced AT hypertrophy (109). The additional improvements in hepatic steatosis and insulin sensitivity might also be attributed to elevated muscle energy metabolism. However, the impact of *Hspg2*-loss on metabolic/adipose inflammation and insights as to how perlecan can affect adipocyte hypertrophy remain to be determined.

CHONDROITIN, DERMATAN AND KERATAN SULFATE PROTEOGLYCANS HAVE PLEOTROPIC ROLES IN META-INFLAMMATION INITIATION AND PROGRESSION

Unlike HSPGs, CSPG and DSPGs are a group of mostly secreted proteins forming an integral part of the ECM (**Figure 1**). They are involved in many essential physiological functions such as morphogenesis, inflammation and neuronal plasticity and play central roles in pathological processes such as cancer, osteoarthritis and thrombosis making them potential therapeutic targets (119, 120). Several secreted matrix CS/DS and KS proteoglycans contain leucine-rich repeats (LRRs) in their protein core (around 42 kDa), categorizing them as small leucine-rich proteoglycans (SLRPs). Five classes based on their structural relationship and associated GAG chain are described: Class I consists of CS/DS containing biglycan (Bgn), decorin (Dcn) and asporin, class II is formed by KS-associated PGs such as fibromodulin and lumican (Lum), class III consists of osteoglycin and opticin and non-canonical classes IV and V lack GAG attachments (121). SLRPs have been implicated in maintaining matrix assembly, thereby fine-tune the tissue-specific micro-environment and are involved in multiple metabolic processes, including inflammation (27).

The first step in CS/DS biosynthesis is building the shared GAG tetrasaccharide linker on a serine residue of the core protein (**Figure 1**). Subsequent polymerization, sulfation, epimerization and degradation of the disaccharide subunits requires a distinct set of enzymes not shared with HSPGs (122). Little is known about how alterations in CS/DS composition affect metabolic dysfunctions and meta-inflammation except for a report on a spontaneous mutated mouse line, small with kinky tail. This mouse model lacks functional chondroitin sulfate synthase 1 and presents with increased age-related, low-grade inflammation (123). Overall, this lack of knowledge is due to the fact that the number, diversity and redundancy of CSPG-specific biosynthetic enzymes make it difficult to probe this issue. Historically this has shifted the focus to evaluating core proteoglycans in meta-inflammation, which we will discuss in the following sections.

Endocan – Potential Biomarker for T2D Severity and Co-morbidities

Transcription of the endothelial cell-specific molecule 1 (*ESM1*) gene produces Endocan, a DSPG that is secreted in the ECM carrying a single DS chain covalently linked to serine 137 (**Table 1**) (124). Primarily expressed by lung and kidney endothelial cells, endocan is upregulated by pro-inflammatory cytokines such as TNF and interleukin 1-β (IL1-β) (124). Once in the circulation ESM1 can interfere with leucocyte extravasation by blocking the interaction of leukocyte function-associated antigen-1 and intercellular adhesion molecule (ICAM-1), suggesting that endocan is part of a negative feedback loop to attenuate the inflammatory recruitment response (125). ESM1 is secreted by adipocytes and its expression progressively increases during adipogenesis. As expected AT *ESM1* expression and circulating ESM1 levels increased in obese patients (126). In contrast, insulin and cortisol administration inhibit ESM1 expression in adipocytes *in vitro* (126, 127). Because of its potential as a marker for endothelial dysfunction and its association with AT and obesity, endocan is evaluated as a potential biomarker for several obesity associated conditions. Several studies observed elevated plasma endocan levels in T2D patients (128, 129) as well as a correlation with the onset of T2D associated morbidities including atherosclerosis (130), nephropathy (131), and NAFLD (132). In psoriasis patients, a common chronic inflammatory skin disease, elevated endocan levels correlated with enhanced mean carotid artery intima-media thickness, BMI, and TNF levels (133). However, conflicting data in T2D patients indicated that using endocan as a prognostic biomarker is a much more sophisticated endeavor, as plasma endocan concentrations were significantly reduced and correlated inversely with waist circumference and CRP levels, a

marker for systemic inflammation (126, 134, 135). In the same T2D patient population endocan serum levels associated with increased urinary albumin to creatinine ratios, suggesting a role for endocan in the progression of kidney injury in obesity-mediated diabetes (135). Evaluation of a DKD mouse model confirmed that ESM1 expression decreased in glomeruli with an ensuing reduction in endocan plasma levels and increased urinary concentration (136). Thus, evidence is mounting that endocan can be a useful biomarker for the severity of T2D and the onset of its co-morbidities. Collectively, functional studies of the role of endocan are needed to help to clarify the contribution of endocan to the development of T2D.

Opposing Roles of Biglycan and Decorin in Obesity and Meta-Inflammation

Bgn and Dcn are ECM proteins with high expression in AT that share similar structural features (**Table 1**). Multiple roles have been attributed to Bgn and Dcn, including matrix remodeling via interaction with collagens (137), regulation of growth factor signaling such as transforming growth factor β (TGF-β) (138), and contribution to the proliferation of cells such as preadipocytes (139, 140). Both SLRPs regulate innate immune responses through direct interaction with TLR2 and TLR4 (**Figure 2**) (141, 142). However, despite their similarities they tend to have opposing roles in the context of diet-induced obesity (DIO) with Dcn having protective attributes and Bgn promoting meta-inflammation.

Decorin – Friend or a Foe in Inflammatory Diseases?

One of the best studied SLRPs is DCN, an ECM CSPG that regulates both innate and adaptive immunity in opposing manner. DCN interacts with TLR2 and TLR4 on innate immune cells to promote expression of pro-inflammatory cytokines such as TNF and IL12p70. Support for its physiological importance as an enhancer of innate immunity was provided by the observation that LPS-induced sepsis is mitigated in $Dcn^{-/-}$ mice (142). In contrast, DCN, as well as BGN, are inhibitors of adaptive immunity and specifically of classical complement activation. Both PGs bind and sequester complement component 1q thereby preventing its recruitment to antigen-antibody complexes. This event prevents proper C1 complex activation and suppresses the adaptive inflammatory response and cytokine production. This, in the context of metabolic inflammation, can attenuate complement overactivation at the onset of its manifestation (143, 144). DCN also modulates engagement of cytokines with their receptors. For example, DCN interacts with TGF-β, a major activator of fibrinogenesis, to suppress its response. The reduced TGF-β reception can further mitigate inflammation, fibrosis and tissue hypoxia in the context of metabolic disorders such as obesity and non-alcoholic steatohepatitis (NASH) (145).

Many factors, including cytokines, modulate DCN expression that result in upregulation, such as TGF-β and TNF (146), as well as down-regulation by IL-1, IL-6, and IL-10 (30, 147, 148). Its expression also exhibits regional variation, particularly between subcutaneous and visceral AT depots, with higher DCN expression in the latter (149, 150). DCN is predominantly expressed by the stromal vascular pre-adipocyte fraction and to a lesser extent by mature adipocytes (151). The complex transcriptional regulation also translates in a multifaceted impact of decorin expression on adipogenesis. Silencing of *Dcn in vitro* increased the differentiation potential of visceral preadipocytes without affecting subcutaneous preadipocyte differentiation. High levels of recombinant DCN protein was able to overcome this divergences as it inhibited adipogenic differentiation in both depots (150). It is generally well-accepted that subcutaneous and visceral ATs display distinct features such as different gene expression, higher lipolytic rate and decreased insulin sensitivity in visceral AT (152). Future research needs to elucidate if DCN is a key determinant of some of these depot-specific differences.

Obese and T2D patients present with increased *DCN* expression in AT. This phenomenon is attenuated after administration of thiazolidinediones, a potent class of insulin sensitizing drugs. This suggests that insulin resistance is partially responsible for the increase in AT *DCN* expression in T2D (143, 149). However, after bariatric surgery, which induces substantial weight loss and improved glucose tolerance, *DCN* expression is further upregulated in subcutaneous AT (151). Systemic *Dcn* knock-out mice have increased HFD-induced obesity, aggravated glucose intolerance and a higher risk of developing spontaneous intestinal tumors (151, 153). The study provided indirect evidence suggesting that altered DCN-associated ECM remodeling mediated some of these effects. In addition the lack of DCN production in white AT from HFD-fed $Dcn^{-/-}$ mice associated with augmented AT inflammation measured by increased expression of complement and coagulation related genes (151). Other reports described DCN as a resistin receptor on adipose progenitor cells (140). Resistin is an adipokine promoting inflammation and insulin resistance in rodents (154) and in humans it is positively associated with AT macrophage content and increased during bouts of systemic inflammation (154). Single nucleotide polymorphisms (SNPs) in the human DCN gene locus correlate with elevated plasma resistin levels, while SNPs in the resistin gene correlate with higher susceptibility for T2D (155). It remains to be determined how and to what extend DCN impacts metabolic consequence associated with elevated resistin expression. One possibility is that DCN serves as a decoy receptor or scavenging agent which buffers the increased resistin secretion associated with excessive AT expansion.

In a patient study of DKD, both DCN and BGN were identified to be upregulated in kidney cortex and glomerular biopsies from patients with DKD. Only DCN was increased in the plasma of these DKD patients and correlated with a significant reduction in glomerular filtration rate (a clinical characteristic of DKD progression) (156). *Dcn* deficiency in a streptozotocin-induced type 1 diabetes mouse model promoted DKD, resulting in elevated albumin to creatinine ratios and increased fibrosis (157). Moreover, in a follow-up study, diabetic $Dcn^{-/-}$ mice showed aggravated kidney injury met with an accumulation in renal BGN content, accentuating potential opposing roles of DCN and BGN in kidney injury (158). The protective effect of decorin in DKD is a multifactorial process and evidence

supports that the impact is mediated via decorin binding to TGF and the insulin-like growth factor-I receptor. Binding to the former attenuates inflammation, while binding to the latter will promote anti-apoptotic effects in tubular epithelial cells, synthesis of fibrillin-1 in renal fibroblasts and inhibition of proliferation and migration. Decorin seems to have the potential to attenuate metabolic inflammation. Hence, factors that modulate its expression as well as decorin itself have great potential as future therapeutic targets for inflammation-associated morbidities in metabolic disease.

Biglycan – Danger Signal in Metabolic Disease

Both biglycan and decorin are signaling molecules and established ECM-derived danger-associated molecular patterns (DAMPs). Under normal conditions BGN is sequestered in the ECM but gets released during cellular stress and inflammation, as for instance during obesity. Once in its soluble form BGN is a ligand for TLR2 and TLR4 present on innate immune cells. The complex between BGN, TLRs and their co-receptors cluster of differentiation (CD) 14 and lymphocyte antigen 96 promotes activation of an inflammatory cascade engaging the NLR family pyrin domain containing 3 (NLRP3) inflammasome leading to IL-1β and IL-6 secretion (141, 159). Because of its role as a DAMP, *Bgn*-deficient mice were studied to evaluate the impact of BGN on meta-inflammation in the context of diet-induced obesity. The lack of BGN expression in this HFD-fed model was associated with a reduction in obesity-driven inflammation in visceral AT independent of changes in adiposity (160). *Bgn* expression in AT reportedly increases during obesity which correlates positively with the expression of inflammatory genes and inversely with adiponectin (139, 160–163). The exact mechanism regulating *Bgn* expression during obesogenic conditions remains unknown, but involves factors such as pro-inflammatory cytokines (IL-6 and IL-1β) as well as adipokines such as adiponectin (141). Adiponectin prevents hyperglycemia and promotes fatty acid oxidation. Unlike most adipokines, plasma and AT adiponectin levels are reduced in obese patients and mice (164, 165). A correlation between biglycan and adiponectin expression is evident in *Bgn*-null mice as they have elevated adiponectin levels, independent of their diet. However, *Bgn* knock-down in adipocytes *in vitro* had the opposite effect on adiponectin expression (162). Thus, the mechanisms leading to the increased adiponectin expression *in vivo* might be a metabolic adaption and needs to be further studied.

In addition to its detrimental roles in obesity, BGN also influences atherosclerosis development. BGN is the proteoglycan that is most co-localized with apoB in murine and human atherosclerotic plaques (166, 167). When overexpressed in smooth muscle cells of mice lacking low-density lipoprotein receptor (LDLR), it promotes atherosclerosis likely because it enhances the retention of apoCIII-enriched LDL and TRLs in the subendothelial matrix (168, 169).

BGN has also been demonstrated to play a role in the development and progression of kidney disease in obese and diabetic experimental models. Thompson et al. demonstrated that *Ldlr* knockout mice which were induced to be diabetic through streptozotocin injections, experienced glomerular BGN accumulation. Interestingly, this was met with elevated renal lipid accumulation and an increase in TGF-β, suggesting the involvement of BGN in lipotoxicity-mediated DKD (170). Soluble BGN is being considered a biomarker for kidney injuries, which are met with elevated inflammation, including obesity-mediated DKD (171). Collectively, studies show that elevated BGN expression and shedding was associated with obesity associated co-morbidities, rendering BGN as a potential diagnostic marker and therapeutic target.

Lumican – Pro-inflammatory Diagnostic Marker for NAFLD Progression?

Lumican (Lum) belongs to class II SLRPs that carry KS-chains (121). In contrast to HS, CS and DS which attach to the core protein at a serine residue, keratan sulfate is attached via *O*- or *N*-glyosidic bindings at asparagine and serine/threonine residues (**Table 1** and **Figure 1**). Similar to BGN and DCN, Lum is found in the ECM where it interacts with collagens and is associated with repair processes in collagen-rich connective tissues (137). In contrast to BGN and DCN, Lum does not directly interact with TLR2/4, but interferes with the adaptor protein CD14 which facilitates LPS presentation to CD14 (172). Moreover, TNF-stimulated fibroblasts produce Lum that in turn promotes fibrocyte differentiation (173). In fact, Lum expression in the liver is tightly correlated with the severity of NAFLD and NASH and is currently evaluated as a biomarker for progression of such liver complications (174–176).

A recent report described a role for Lum in obesity and inflammation (177). As for other SLRPs, visceral AT exhibits higher Lum expression compared to subcutaneous AT and increases during obesity progression. Interestingly, Wolff and coworkers observed sex-specific differences in weight gain and obesity-related inflammation in Lum full body knock-out mice during diet-induced obesity (177). Based on its positive correlation with inflammation, loss of Lum should be protective against obesity and meta-inflammation. However, female $Lum^{-/-}$ mice showed increased fat accumulation and AT inflammation which was also associated with accelerated progression of insulin resistance, whereas male mice were devoid of detrimental phenotypes (177). This study also tested the therapeutic potential of Lum by Adeno-associated Virus-mediated overexpression of Lum in male mice which mildly improved insulin sensitivity. As with other SLRPs, Lum's role in obesity-related morbidities is controversial and could be based on the disease-specific context. Mechanisms explaining sex- and tissue-depending impacts of Lum pose interesting aspects for future investigations.

Osteoglycin – Coordinator of Bone Formation With Novel Roles in Controlling Energy Homeostasis

Osteoglycin (OGN), also known as mimecan, is a class III SLRP associated with KS GAG chains. In addition to

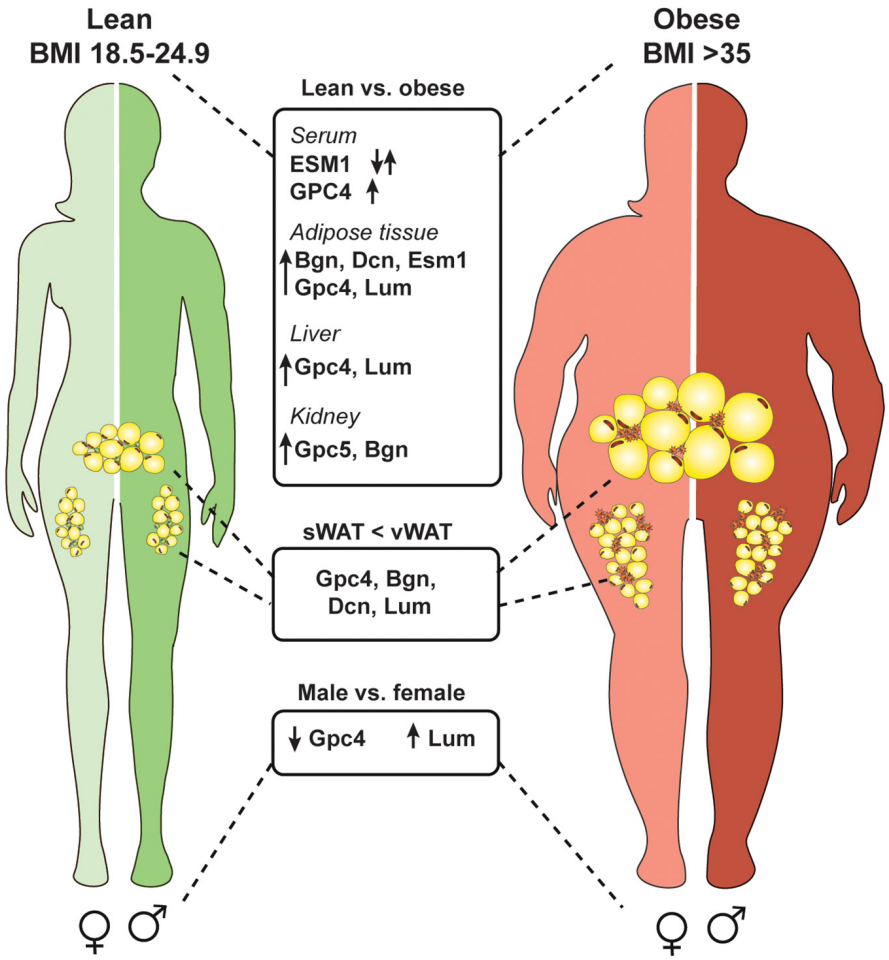

FIGURE 3 | Several proteoglycans are deregulated in the obese state and differentially expressed in an adipose depot and sex specific manner. Obesity is defined by a body mass index of over 35 (weight in kg/height in m^2). Multiple proteoglycans are upregulated in an obese state in adipose tissue, kidney, and liver. Also, serum levels of glypican-4 (GPC4) increase which could be used as a marker for insulin resistance. Serum endocan (ESM1) levels are deregulated in obese subjects and depending on the specific disease context can be up- or downregulated. Interestingly, some proteoglycans are higher expressed in visceral white adipose tissue (vWAT) compared to subcutaneous white adipose tissue (sWAT) which might account for depot specific differences (biglycan, Bgn; decorin, Dcn; lumican, Lum). Also, proteoglycans show differential expression in males and females independent of the diet.

GAG chains other *O*-linked glycosylation of OGN have been described, but the glycan-type remains unidentified (**Table 1**). OGN is expressed in several isoforms resulting from differential splicing, alternative polyadenylation, and posttranslational modifications such as glycosylation (178). In an inflammatory context, the largest 72 kDa glycosylated leukocyte-derived isoform has been described to enhance the activation of TLR4 during viral cardiac inflammation (179). *Ogn* expression is upregulated by INF-y and TNF in an NF-κB dependent manner (180, 181). These phenomena could be connected to increased OGN expression found in atherosclerotic plaques, where these pathways are activated (182, 183). OGN binds and increases collagen cross-linking and bone formation, respectively. OGN is highly expressed in osteoblasts, but also expressed, albeit to a lesser degree, in cardiomyocytes, vascular smooth muscle cells, fibroblasts and neurons (178). Recent data shows that OGN is expressed in AT and involved in regulation of glucose homeostasis (184). Lack of *Ogn* expression increases glucose intolerance and elevates insulin levels in HFD-fed $Ogn^{-/-}$ mice and ectopic administration of OGN improves glucose tolerance (185). Lee et al., showed that *Ogn* expression levels negatively correlate with diet-induced obesity and blood glucose levels and that ectopic administered OGN increases insulin secretion and glucose intolerance in mice. In severely obese humans, OGN serum levels increased in response to weight loss (185). It is assumed that this weight loss could be mediated by OGN regulating food intake. A previous study reported that injection of recombinant OGN in db/db mice induced an anorexic effect (184). However, this could not be reproduced in the later study of Lee et al., who showed the opposite effect (185). Different mouse models and technical differences might explain the discrepancies, but future studies are needed to clarify the effect of OGN on food intake.

CLINICAL SIGNIFICANCE AND POTENTIAL THERAPEUTIC APPLICATION OF PROTEOGLYCANS

Heparin, a naturally derived, heavily sulfated HS, is an essential and commonly used anti-coagulant in the clinic worldwide. Low molecular weight heparin analogs have anti-inflammatory properties without unwarranted anti-coagulant activity rendering these analogs as interesting candidates for clinical evaluation (186). Proteoglycans and associated GAG chains are utilized in the clinic for drug delivery methods and several experimental studies have evaluated the benefit of applying proteoglycans in the clinic as biomarkers and therapeutic targets for various diseases (187–189). This current review highlights several key clinical studies implicating proteoglycans as potential therapeutic targets or biomarkers for obesity-mediated inflammatory diseases. In summary, several proteoglycans are modulated in clinical and experimental models of obesity and its co-morbidities (summarized in **Table 1** and **Figure 3**). Specifically, diabetic patients have been observed to have increased heparinase in the blood and urine, demonstrating that heparin and HS chain modifications could be important in diabetes and its co-morbidities (65). In separate studies authors demonstrated that soluble fragments generated from heparinase activity resulted in activation of TLR4 signaling, further implicating their involvement in meta-inflammation. Several studies mentioned above include strong association for many PGs and disease outcome in distinct patient cohorts of obesity and diabetes, such as GPC4 and ESM1. Interestingly, obese mice treated with oral administration of salmon cartilage proteoglycans experienced improvement in hyperglycemia and insulin sensitivity associated with a reduction in the expression of key inflammatory modulators such as TNF, IL-6 and C-X-C motif chemokine ligand 2 in AT (190). Studies like this one highlight the overall benefit of implementing the therapeutic potential of proteoglycans.

CONCLUSION AND OUTLOOK

Undoubtful, proteoglycans play significant roles in mediating metabolic inflammation. Despite recent advances, our understanding of the specific roles of PGs during obesity progression and metabolic inflammation is still nascent. Many of the reports discussed in this review are primarily observational and lack mechanistic explanations. Model systems that allow studying proteoglycan interactions with inflammatory components have been generated in the past several years. However, few studies discriminate between the protein and GAG moiety of proteoglycans. This lack of properly addressing the importance of the glycoforms might explain discrepancies in study outcomes. Also, many of the proteoglycans' functions might be triggered in a context- and tissue-dependent fashion. Thus, generation and investigation of conditional proteoglycan knock-out models is warranted to clarify the roles of proteoglycans upon diet-induced obesity and meta-inflammation. Overall it is evident that proteoglycans are interesting diagnostic or therapeutic targets, and specific roles in obesity-related inflammation and receptor interactions need to be fully identified and understood prior to consider them as such in the future.

AUTHOR CONTRIBUTIONS

PG and AP: conceptualization, writing – review and editing, and funding acquisition. AP, GD, and PG: writing – original draft. AP: Visualization; PG: supervision and project administration.

FUNDING

This work was supported by a Erwin-Schrödinger FWF Grant J4031-B21 (AP), A NIH K12 UCSD biomedical scientist career development program in glycoscience 12HL141956 (GD), and a Fondation Leducq grant 16CVD01 (PG).

REFERENCES

1. Bhupathiraju SN, Hu FB. Epidemiology of obesity and diabetes and their cardiovascular complications. *Circ Res*. (2016) 118:1723–35. doi: 10.1161/CIRCRESAHA.115.306825
2. Winocour PH. Diabetes and chronic kidney disease: an increasingly common multi-morbid disease in need of a paradigm shift in care. *Diabet Med*. (2018) 35:300–5. doi: 10.1111/dme.13564
3. Festa A, D'Agostino R, Williams K, Karter AJ, Mayer-Davis EJ, Tracy RP, et al. The relation of body fat mass and distribution to markers of chronic inflammation. *Int J Obes Relat Metab Disord*. (2001) 25:1407–15. doi: 10.1038/sj.ijo.0801792
4. Saltiel AR, Olefsky JM. Inflammatory mechanisms linking obesity and metabolic disease. *J Clin Invest*. (2017) 127:1–4. doi: 10.1172/JCI92035
5. Lee YS, Wollam J, Olefsky JM. An integrated view of immunometabolism. *Cell*. (2018) 172:22–40. doi: 10.1016/j.cell.2017.12.025
6. Crewe C, An YA, Scherer PE. The ominous triad of adipose tissue dysfunction: inflammation, fibrosis, and impaired angiogenesis. *J Clin Invest*. (2017) 127:74–82. doi: 10.1172/JCI88883
7. Liu R, Nikolajczyk BS. tissue immune cells fuel obesity-associated inflammation in adipose tissue and beyond. *Front Immunol*. (2019) 10:1587. doi: 10.3389/fimmu.2019.01587
8. Morinaga H, Mayoral R, Heinrichsdorff J, Osborn O, Franck N, Hah N, et al. Characterization of distinct subpopulations of hepatic macrophages in HFD/obese mice. *Diabetes*. (2015) 64:1120–30. doi: 10.2337/db14-1238
9. Park EJ, Lee JH, Yu GY, He G, Ali SR, Holzer RG, et al. Dietary and genetic obesity promote liver inflammation and tumorigenesis by enhancing IL-6 and TNF expression. *Cell*. (2010) 140:197–208. doi: 10.1016/j.cell.2009.12.052
10. Jung UJ, Choi MS. Obesity and its metabolic complications: the role of adipokines and the relationship between obesity, inflammation, insulin resistance, dyslipidemia and nonalcoholic fatty liver disease. *Int J Mol Sci*. (2014) 15:6184–223. doi: 10.3390/ijms15046184
11. Chitturi S, Abeygunasekera S, Farrell GC, Holmes-Walker J, Hui JM, Fung C, et al. NASH and insulin resistance: insulin hypersecretion and specific association with the insulin resistance syndrome. *Hepatology*. (2002) 35:373–9. doi: 10.1053/jhep.2002.30692

12. Fischer IP, Irmler M, Meyer CW, Sachs SJ, Neff F, Hrabì de Angelis M, et al. A history of obesity leaves an inflammatory fingerprint in liver and adipose tissue. *Int J Obes (Lond)*. (2018) 42:507–17. doi: 10.1038/ijo.2017.224
13. Saran R, Robinson B, Abbott KC, Agodoa LYC, Bragg-Gresham J, Balkrishnan R, et al. US renal data system 2018 annual data report: epidemiology of kidney disease in the United States. *Am J Kidney Dis*. (2019) 73(3 Suppl. 1):A7–8. doi: 10.1053/j.ajkd.2019.01.001
14. Wicks SE, Nguyen TT, Breaux C, Kruger C, Stadler K. Diet-induced obesity and kidney disease – in search of a susceptible mouse model. *Biochimie*. (2016) 124:65–73. doi: 10.1016/j.biochi.2015.08.001
15. Wang XX, Jiang T, Shen Y, Adorini L, Pruzanski M, Gonzalez FJ, et al. The farnesoid X receptor modulates renal lipid metabolism and diet-induced renal inflammation, fibrosis, and proteinuria. *Am J Physiol Renal Physiol*. (2009) 297:F1587–96. doi: 10.1152/ajprenal.00404.2009
16. Stemmer K, Perez-Tilve D, Ananthakrishnan G, Bort A, Seeley RJ, Tschöp MH, et al. High-fat-diet-induced obesity causes an inflammatory and tumor-promoting microenvironment in the rat kidney. *Dis Model Mech*. (2012) 5:627–35. doi: 10.1242/dmm.009407
17. Pedigo CE, Ducasa GM, Leclercq F, Sloan A, Mitrofanova A, Hashmi T, et al. Local TNF causes NFATc1-dependent cholesterol-mediated podocyte injury. *J Clin Invest*. (2016) 126:3336–50. doi: 10.1172/JCI85939
18. Ducasa GM, Mitrofanova A, Mallela SK, Liu X, Molina J, Sloan A, et al. ATP-binding cassette A1 deficiency causes cardiolipin-driven mitochondrial dysfunction in podocytes. *J Clin Invest*. (2019) 129:3387–400. doi: 10.1172/JCI125316
19. Mori J, Patel VB, Ramprasath T, Alrob OA, DesAulniers J, Scholey JW, et al. Angiotensin 1-7 mediates renoprotection against diabetic nephropathy by reducing oxidative stress, inflammation, and lipotoxicity. *Am J Physiol Renal Physiol*. (2014) 306:F812–21. doi: 10.1152/ajprenal.00655.2013
20. Mariman EC, Wang P. Adipocyte extracellular matrix composition, dynamics and role in obesity. *Cell Mol Life Sci*. (2010) 67:1277–92. doi: 10.1007/s00018-010-0263-4
21. Huang G, Greenspan DS. ECM roles in the function of metabolic tissues. *Trends Endocrinol Metab*. (2012) 23:16–22. doi: 10.1016/j.tem.2011.09.006
22. Sun K, Tordjman J, Clément K, Scherer PE. Fibrosis and adipose tissue dysfunction. *Cell Metab*. (2013) 18:470–7. doi: 10.1016/j.cmet.2013.06.016
23. Gonzalez FJ, Xie C, Jiang C. The role of hypoxia-inducible factors in metabolic diseases. *Nat Rev Endocrinol*. (2018) 15:21–32. doi: 10.1038/s41574-018-0096-z
24. Lee YS, Kim JW, Osborne O, Oh DY, Sasik R, Schenk S, et al. Increased adipocyte O2 consumption triggers HIF-1α, causing inflammation and insulin resistance in obesity. *Cell*. (2014) 157:1339–52. doi: 10.1016/j.cell.2014.05.012
25. Khan T, Muise ES, Iyengar P, Wang ZV, Chandalia M, Abate N, et al. Metabolic dysregulation and adipose tissue fibrosis: role of collagen VI. *Mol Cell Biol*. (2009) 29:1575–91. doi: 10.1128/MCB.01300-08
26. Varki A, Cummings RD, Esko JD, Stanley P, Hart GW, Aebi M, et al. *Essentials of Glycobiology*. 3rd ed. New York, NY: Cold Spring Harbor Laboratory Press. (2015).
27. Neill T, Schaefer L, Iozzo RV. Decoding the matrix: instructive roles of proteoglycan receptors. *Biochemistry*. (2015) 54:4583–98. doi: 10.1021/acs.biochem.5b00653
28. Gallagher J. Fell-muir lecture: heparan sulphate and the art of cell regulation: a polymer chain conducts the protein orchestra. *Int J Exp Pathol*. (2015) 96:203–31. doi: 10.1111/iep.12135
29. Mizumoto S, Yamada S, Sugahara K. Molecular interactions between chondroitin-dermatan sulfate and growth factors/receptors/matrix proteins. *Curr Opin Struct Biol*. (2015) 34:35–42. doi: 10.1016/j.sbi.2015.06.004
30. Frey H, Schroeder N, Manon-Jensen T, Iozzo RV, Schaefer L. Biological interplay between proteoglycans and their innate immune receptors in inflammation. *FEBS J*. (2013) 280:2165–79. doi: 10.1111/febs.12145
31. Götte M. Syndecans in inflammation. *FASEB J*. (2003) 17:575–91. doi: 10.1096/fj.02-0739rev
32. Wight TN, Kang I, Merrilees MJ. Versican and the control of inflammation. *Matrix Biol*. (2014) 35:152–61. doi: 10.1016/j.matbio.2014.01.015
33. Roedig H, Nastase MV, Wygrecka M, Schaefer L. Breaking down chronic inflammatory diseases: the role of biglycan in promoting a switch between inflammation and autophagy. *FEBS J*. (2019) 286:2965–79. doi: 10.1111/febs.14791
34. Agere SA, Kim EY, Akhtar N, Ahmed S. Syndecans in chronic inflammatory and autoimmune diseases: pathological insights and therapeutic opportunities. *J Cell Physiol*. (2018) 233:6346–58. doi: 10.1002/jcp.26388
35. Lim JM, Sherling D, Teo CF, Hausman DB, Lin D, Wells L. Defining the regulated secreted proteome of rodent adipocytes upon the induction of insulin resistance. *J Proteome Res*. (2008) 7:1251–63. doi: 10.1021/pr7006945
36. Gowd V, Gurukar A, Chilkunda ND. Glycosaminoglycan remodeling during diabetes and the role of dietary factors in their modulation. *World J Diabetes*. (2016) 7:67–73. doi: 10.4239/wjd.v7.i4.67
37. Musil KJ, Malmström A, Donnér J. Alteration of proteoglycan metabolism during the differentiation of 3T3-L1 fibroblasts into adipocytes. *J Cell Biol*. (1991) 114:821–6. doi: 10.1083/jcb.114.4.821
38. Calvo JC, Rodbard D, Katki A, Chernick S, Yanagishita M. Differentiation of 3T3-L1 preadipocytes with 3-isobutyl-1-methylxanthine and dexamethasone stimulates cell-associated and soluble chondroitin 4-sulfate proteoglycans. *J Biol Chem*. (1991) 266:11237–44.
39. Sarrazin S, Lamanna WC, Esko JD. Heparan sulfate proteoglycans. *Cold Spring Harb Perspect Biol*. (2011) 3:a004952. doi: 10.1101/cshperspect.a004952
40. Collins LE, Troeberg L. Heparan sulfate as a regulator of inflammation and immunity. *J Leukoc Biol*. (2019) 105:81–92. doi: 10.1002/JLB.3RU0618-246R
41. Swart M, Troeberg L. Effect of polarization and chronic inflammation on macrophage expression of heparan sulfate proteoglycans and biosynthesis enzymes. *J Histochem Cytochem*. (2019) 67:9–27. doi: 10.1369/0022155418798770
42. Gordts PLSM, Esko JD. The heparan sulfate proteoglycan grip on hyperlipidemia and atherosclerosis. *Matrix Biol*. (2018) 7:262–82. doi: 10.1016/j.matbio.2018.05.010
43. Rops AL, van der Vlag J, Lensen JF, Wijnhoven TJ, van den Heuvel LP, van Kuppevelt TH, et al. Heparan sulfate proteoglycans in glomerular inflammation. *Kidney Int*. (2004) 65:768–85. doi: 10.1111/j.1523-1755.2004.00451.x
44. Mis EK, Liem KF, Kong Y, Schwartz NB, Domowicz M, Weatherbee SD. Forward genetics defines Xylt1 as a key, conserved regulator of early chondrocyte maturation and skeletal length. *Dev Biol*. (2014) 385:67–82. doi: 10.1016/j.ydbio.2013.10.014
45. Sivasami P, Poudel N, Munteanu MC, Hudson J, Lovern P, Liu L, et al. Adipose tissue loss and lipodystrophy in xylosyltransferase II deficient mice. *Int J Obes (Lond)*. (2019) 43:1783–94. doi: 10.1038/s41366-019-0324-1
46. Lowe-Krentz LJ, Joyce JG. Venous and aortic porcine endothelial cells cultured under standardized conditions synthesize heparan sulfate chains which differ in charge. *Anal Biochem*. (1991) 193:155–63. doi: 10.1016/0003-2697(91)90001-a
47. Rops AL, Loeven MA, van Gemst JJ, Eversen I, Van Wijk XM, Dijkman HB, et al. Modulation of heparan sulfate in the glomerular endothelial glycocalyx decreases leukocyte influx during experimental glomerulonephritis. *Kidney Int*. (2014) 86:932–42. doi: 10.1038/ki.2014.115
48. Talsma DT, Katta K, Ettema MAB, Kel B, Kusche-Gullberg M, Daha MR, et al. Endothelial heparan sulfate deficiency reduces inflammation and fibrosis in murine diabetic nephropathy. *Lab Invest*. (2018) 98:427–38. doi: 10.1038/s41374-017-0015-2
49. Forsberg M, Holmborn K, Kundu S, Dagälv A, Kjellén L, Forsberg-Nilsson K. Undersulfation of heparan sulfate restricts differentiation potential of mouse embryonic stem cells. *J Biol Chem*. (2012) 287:10853–62. doi: 10.1074/jbc.M111.337030
50. Gordts PLSM, Foley EM, Lawrence R, Sinha R, Lameda-Diaz C, Deng L, et al. Reducing macrophage proteoglycan sulfation increases atherosclerosis and obesity through enhanced type I interferon signaling. *Cell Metab*. (2014) 20:813–26. doi: 10.1016/j.cmet.2014.09.016
51. Gordts PL, Esko JD. Heparan sulfate proteoglycans fine-tune macrophage inflammation via IFN-β. *Cytokine*. (2015) 72:118–9. doi: 10.1016/j.cyto.2014.12.013
52. Sugaya N, Habuchi H, Nagai N, Ashikari-Hada S, Kimata K. 6-O-sulfation of heparan sulfate differentially regulates various fibroblast growth factor-dependent signalings in culture. *J Biol Chem*. (2008) 283:10366–76. doi: 10.1074/jbc.M705948200

53. Habuchi H, Nagai N, Sugaya N, Atsumi F, Stevens RL, Kimata K. Mice deficient in heparan sulfate 6-O-sulfotransferase-1 exhibit defective heparan sulfate biosynthesis, abnormal placentation, and late embryonic lethality. *J Biol Chem*. (2007) 282:15578–88. doi: 10.1074/jbc.M607434200
54. Habuchi H, Tanaka M, Habuchi O, Yoshida K, Suzuki H, Ban K, et al. The occurrence of three isoforms of heparan sulfate 6-O-sulfotransferase having different specificities for hexuronic acid adjacent to the targeted N-sulfoglucosamine. *J Biol Chem*. (2000) 275:2859–68. doi: 10.1074/jbc.275.4.2859
55. Berisha SZ, Hsu J, Robinet P, Smith JD. Transcriptome analysis of genes regulated by cholesterol loading in two strains of mouse macrophages associates lysosome pathway and ER stress response with atherosclerosis susceptibility. *PLoS One*. (2013) 8:e65003. doi: 10.1371/journal.pone.0065003
56. Xu X, Grijalva A, Skowronski A, van Eijk M, Serlie MJ, Ferrante AW. Obesity activates a program of lysosomal-dependent lipid metabolism in adipose tissue macrophages independently of classic activation. *Cell Metab*. (2013) 18:816–30. doi: 10.1016/j.cmet.2013.11.001
57. Prieur X, Mok CY, Velagapudi VR, Núñez V, Fuentes L, Montaner D, et al. Differential lipid partitioning between adipocytes and tissue macrophages modulates macrophage lipotoxicity and M2/M1 polarization in obese mice. *Diabetes*. (2011) 60:797–809. doi: 10.2337/db10-0705
58. Nagai N, Habuchi H, Sugaya N, Nakamura M, Imamura T, Watanabe H, et al. Involvement of heparan sulfate 6-O-sulfation in the regulation of energy metabolism and the alteration of thyroid hormone levels in male mice. *Glycobiology*. (2013) 23:980–92. doi: 10.1093/glycob/cwt037
59. Parish CR, Freeman C, Hulett MD. Heparanase: a key enzyme involved in cell invasion. *Biochim Biophys Acta*. (2001) 1471:M99–108. doi: 10.1016/s0304-419x(01)00017-8
60. Gingis-Velitski S, Zetser A, Flugelman MY, Vlodavsky I, Ilan N. Heparanase induces endothelial cell migration via protein kinase B/Akt activation. *J Biol Chem*. (2004) 279:23536–41. doi: 10.1074/jbc.M400554200
61. Parish CR. The role of heparan sulphate in inflammation. *Nat Rev Immunol*. (2006) 6:633–43. doi: 10.1038/nri1918
62. Masola V, Bellin G, Gambaro G, Onisto M. Heparanase: a multitasking protein involved in extracellular matrix (ECM) remodeling and intracellular events. *Cells*. (2018) 7:236. doi: 10.3390/cells7120236
63. Chen G, Wang D, Vikramadithyan R, Yagyu H, Saxena U, Pillarisetti S, et al. Inflammatory cytokines and fatty acids regulate endothelial cell heparanase expression. *Biochemistry*. (2004) 43:4971–7. doi: 10.1021/bi0356552
64. Han J, Hiebert LM. Alteration of endothelial proteoglycan and heparanase gene expression by high glucose, insulin and heparin. *Vascul Pharmacol*. (2013) 59:112–8. doi: 10.1016/j.vph.2013.08.001
65. Shafat I, Ilan N, Zoabi S, Vlodavsky I, Nakhoul F. Heparanase levels are elevated in the urine and plasma of type 2 diabetes patients and associate with blood glucose levels. *PLoS One*. (2011) 6:e17312. doi: 10.1371/journal.pone.0017312
66. Goldberg R, Rubinstein AM, Gil N, Hermano E, Li JP, van der Vlag J, et al. Role of heparanase-driven inflammatory cascade in pathogenesis of diabetic nephropathy. *Diabetes*. (2014) 63:4302–13. doi: 10.2337/db14-0001
67. Osterholm C, Folkersen L, Lengquist M, Pontén F, Renné T, Li J, et al. Increased expression of heparanase in symptomatic carotid atherosclerosis. *Atherosclerosis*. (2013) 226:67–73. doi: 10.1016/j.atherosclerosis.2012.09.030
68. Kodaira Y, Nair SK, Wrenshall LE, Gilboa E, Platt JL. Phenotypic and functional maturation of dendritic cells mediated by heparan sulfate. *J Immunol*. (2000) 165:1599–604. doi: 10.4049/jimmunol.165.3.1599
69. Goodall KJ, Poon IK, Phipps S, Hulett MD. Soluble heparan sulfate fragments generated by heparanase trigger the release of pro-inflammatory cytokines through TLR-4. *PLoS One*. (2014) 9:e109596. doi: 10.1371/journal.pone.0109596
70. Akbarshahi H, Axelsson JB, Said K, Malmström A, Fischer H, Andersson R. TLR4 dependent heparan sulphate-induced pancreatic inflammatory response is IRF3-mediated. *J Transl Med*. (2011) 9:219. doi: 10.1186/1479-5876-9-219
71. Brennan TV, Lin L, Huang X, Cardona DM, Li Z, Dredge K, et al. Heparan sulfate, an endogenous TLR4 agonist, promotes acute GVHD after allogeneic stem cell transplantation. *Blood*. (2012) 120:2899–908. doi: 10.1182/blood-2011-07-368720
72. Teng YH, Aquino RS, Park PW. Molecular functions of syndecan-1 in disease. *Matrix Biol*. (2012) 31:3–16. doi: 10.1016/j.matbio.2011.10.001
73. Angsana J, Chen J, Smith S, Xiao J, Wen J, Liu L, et al. Syndecan-1 modulates the motility and resolution responses of macrophages. *Arterioscler Thromb Vasc Biol*. (2015) 35:332–40. doi: 10.1161/ATVBAHA.114.304720
74. Cai P, Lu Z, Jiang T, Wang Z, Yang Y, Zheng L, et al. Syndecan-4 involves in the pathogenesis of rheumatoid arthritis by regulating the inflammatory response and apoptosis of fibroblast-like synoviocytes. *J Cell Physiol*. (2019) 235:1746–58. doi: 10.1002/jcp.29093
75. Vuong TT, Reine TM, Sudworth A, Jenssen TG, Kolset SO. Syndecan-4 is a major syndecan in primary human endothelial cells in vitro, modulated by inflammatory stimuli and involved in wound healing. *J Histochem Cytochem*. (2015) 63:280–92. doi: 10.1369/0022155415568995
76. Wang JB, Zhang YJ, Guan J, Zhou L, Sheng Y, Zhang Y, et al. Enhanced syndecan-1 expression on neutrophils in patients with type 2 diabetes mellitus. *Acta Diabetol*. (2012) 49:41–6. doi: 10.1007/s00592-011-0265-1
77. Kolseth IB, Reine TM, Parker K, Sudworth A, Witczak BJ, Jenssen TG, et al. Increased levels of inflammatory mediators and proinflammatory monocytes in patients with type I diabetes mellitus and nephropathy. *J Diabetes Complications*. (2017) 31:245–52. doi: 10.1016/j.jdiacomp.2016.06.029
78. Ji L, Malecki M, Warram JH, Yang Y, Rich SS, Krolewski AS. New susceptibility locus for NIDDM is localized to human chromosome 20q. *Diabetes*. (1997) 46:876–81. doi: 10.2337/diab.46.5.876
79. Klupa T, Malecki MT, Pezzolesi M, Ji L, Curtis S, Langefeld CD, et al. Further evidence for a susceptibility locus for type 2 diabetes on chromosome 20q13.1-q13.2. *Diabetes*. (2000) 49:2212–6. doi: 10.2337/diabetes.49.12.2212
80. De Luca M, Klimentidis YC, Casazza K, Chambers MM, Cho R, Harbison ST, et al. A conserved role for syndecan family members in the regulation of whole-body energy metabolism. *PLoS One*. (2010) 5:e11286. doi: 10.1371/journal.pone.0011286
81. Wang JB, Guan J, Shen J, Zhou L, Zhang YJ, Si YF, et al. Insulin increases shedding of syndecan-1 in the serum of patients with type 2 diabetes mellitus. *Diabetes Res Clin Pract*. (2009) 86:83–8. doi: 10.1016/j.diabres.2009.08.002
82. Reizes O, Goldberger O, Smith AC, Xu Z, Bernfield M, Bickel PE. Insulin promotes shedding of syndecan ectodomains from 3T3-L1 adipocytes: a proposed mechanism for stabilization of extracellular lipoprotein lipase. *Biochemistry*. (2006) 45:5703–11. doi: 10.1021/bi052263h
83. Olsson U, Egnell AC, Lee MR, Lundén GO, Lorentzon M, Salmivirta M, et al. Changes in matrix proteoglycans induced by insulin and fatty acids in hepatic cells may contribute to dyslipidemia of insulin resistance. *Diabetes*. (2001) 50:2126–32. doi: 10.2337/diabetes.50.9.2126
84. Stanford KI, Bishop JR, Foley EM, Gonzales JC, Niesman IR, Witztum JL, et al. Syndecan-1 is the primary heparan sulfate proteoglycan mediating hepatic clearance of triglyceride-rich lipoproteins in mice. *J Clin Invest*. (2009) 119:3236–45. doi: 10.1172/JCI38251
85. Matikainen N, Burza MA, Romeo S, Hakkarainen A, Adiels M, Folkersen L, et al. Genetic variation in SULF2 is associated with postprandial clearance of triglyceride-rich remnant particles and triglyceride levels in healthy subjects. *PLoS One*. (2013) 8:e79473. doi: 10.1371/journal.pone.0079473
86. Hassing HC, Surendran RP, Derudas B, Verrijken A, Francque SM, Mooij HL, et al. SULF2 strongly prediposes to fasting and postprandial triglycerides in patients with obesity and type 2 diabetes mellitus. *Obesity (Silver Spring)*. (2014) 22:1309–16. doi: 10.1002/oby.20682
87. Chen K, Liu ML, Schaffer L, Li M, Boden G, Wu X, et al. Type 2 diabetes in mice induces hepatic overexpression of sulfatase 2, a novel factor that suppresses uptake of remnant lipoproteins. *Hepatology*. (2010) 52:1957–67. doi: 10.1002/hep.23916
88. Hassing HC, Mooij H, Guo S, Monia BP, Chen K, Kulik W, et al. Inhibition of hepatic sulfatase-2 in vivo: a novel strategy to correct diabetic dyslipidemia. *Hepatology*. (2012) 55:1746–53. doi: 10.1002/hep.25580
89. De Luca M, Vecchie D, Athmanathan B, Gopalkrishna S, Valcin JA, Swain TM, et al. Genetic deletion of syndecan-4 alters body composition, metabolic phenotypes, and the function of metabolic tissues in female mice fed a high-fat diet. *Nutrients*. (2019) 11:2810. doi: 10.3390/nu11112810
90. Zheng Q, Zhu J, Shanabrough M, Borok E, Benoit SC, Horvath TL, et al. Enhanced anorexigenic signaling in lean obesity resistant syndecan-3 null

mice. *Neuroscience*. (2010) 171:1032–40. doi: 10.1016/j.neuroscience.2010.09.060
91. Reizes O, Lincecum J, Wang Z, Goldberger O, Huang L, Kaksonen M, et al. Transgenic expression of syndecan-1 uncovers a physiological control of feeding behavior by syndecan-3. *Cell*. (2001) 106:105–16. doi: 10.1016/s0092-8674(01)00415-9
92. Reizes O, Benoit SC, Clegg DJ. The role of syndecans in the regulation of body weight and synaptic plasticity. *Int J Biochem Cell Biol*. (2008) 40:28–45. doi: 10.1016/j.biocel.2007.06.011
93. Heisler LK, Lam DD. An appetite for life: brain regulation of hunger and satiety. *Curr Opin Pharmacol*. (2017) 37:100–6. doi: 10.1016/j.coph.2017.09.002
94. Strader AD, Reizes O, Woods SC, Benoit SC, Seeley RJ. Mice lacking the syndecan-3 gene are resistant to diet-induced obesity. *J Clin Invest*. (2004) 114:1354–60. doi: 10.1172/JCI20631
95. Kasza I, Suh Y, Wollny D, Clark RJ, Roopra A, Colman RJ, et al. Syndecan-1 is required to maintain intradermal fat and prevent cold stress. *PLoS Genet*. (2014) 10:e1004514. doi: 10.1371/journal.pgen.1004514
96. Tamori Y, Kasuga M. Glypican-4 is a new comer of adipokines working as insulin sensitizer. *J Diabetes Investig*. (2013) 4:250–1. doi: 10.1111/jdi.12071
97. Traister A, Shi W, Filmus J. Mammalian notum induces the release of glypicans and other GPI-anchored proteins from the cell surface. *Biochem J*. (2008) 410:503–11. doi: 10.1042/BJ20070511
98. Tenorio J, Arias P, Martínez-Glez V, Santos F, García-Miñaur S, Nevado J, et al. Simpson-golabi-behmel syndrome types I and II. *Orphanet J Rare Dis*. (2014) 9:138. doi: 10.1186/s13023-014-0138-0
99. Wabitsch M, Brenner RE, Melzner I, Braun M, Möller P, Heinze E, et al. Characterization of a human preadipocyte cell strain with high capacity for adipose differentiation. *Int J Obes Relat Metab Disord*. (2001) 25:8–15. doi: 10.1038/sj.ijo.0801520
100. Gesta S, Blüher M, Yamamoto Y, Norris AW, Berndt J, Kralisch S, et al. Evidence for a role of developmental genes in the origin of obesity and body fat distribution. *Proc Natl Acad Sci USA*. (2006) 103:6676–81. doi: 10.1073/pnas.0601752103
101. Ussar S, Bezy O, Blüher M, Kahn CR. Glypican-4 enhances insulin signaling via interaction with the insulin receptor and serves as a novel adipokine. *Diabetes*. (2012) 61:2289–98. doi: 10.2337/db11-1395
102. Jędrzejuk D, Lwow F, Kuliczkowska-Płaksej J, Hirnle L, Trzmiel-Bira A, Lenarcik-Kabza A, et al. Association of serum glypican-4 levels with cardiovascular risk predictors in women with polycystic ovary syndrome – a pilot study. *Gynecol Endocrinol*. (2016) 32:223–6. doi: 10.3109/09513590.2015.1110137
103. Leelalertlauw C, Korwutthikulrangsri M, Mahachoklertwattana P, Chanprasertyothin S, Khlairit P, Pongratanakul S, et al. Serum glypican 4 level in obese children and its relation to degree of obesity. *Clin Endocrinol (Oxf)*. (2017) 87:689–95. doi: 10.1111/cen.13435
104. Li K, Xu X, Hu W, Li M, Yang M, Wang Y, et al. Glypican-4 is increased in human subjects with impaired glucose tolerance and decreased in patients with newly diagnosed type 2 diabetes. *Acta Diabetol*. (2014) 51:981–90. doi: 10.1007/s00592-014-0652-5
105. Yoo HJ, Hwang SY, Cho GJ, Hong HC, Choi HY, Hwang TG, et al. Association of glypican-4 with body fat distribution, insulin resistance, and nonalcoholic fatty liver disease. *J Clin Endocrinol Metab*. (2013) 98:2897–901. doi: 10.1210/jc.2012-4297
106. Zhu HJ, Pan H, Cui Y, Wang XQ, Wang LJ, Li NS, et al. The changes of serum glypican4 in obese patients with different glucose metabolism status. *J Clin Endocrinol Metab*. (2014) 99:E2697–701. doi: 10.1210/jc.2014-2018
107. Okamoto K, Tokunaga K, Doi K, Fujita T, Suzuki H, Katoh T, et al. Common variation in GPC5 is associated with acquired nephrotic syndrome. *Nat Genet*. (2011) 43:459–63. doi: 10.1038/ng.792
108. Okamoto K, Honda K, Doi K, Ishizu T, Katagiri D, Wada T, et al. Glypican-5 increases susceptibility to nephrotic damage in diabetic kidney. *Am J Pathol*. (2015) 185:1889–98. doi: 10.1016/j.ajpath.2015.03.025
109. Yamashita Y, Nakada S, Yoshihara T, Nara T, Furuya N, Miida T, et al. Perlecan, a heparan sulfate proteoglycan, regulates systemic metabolism with dynamic changes in adipose tissue and skeletal muscle. *Sci Rep*. (2018) 8:7766. doi: 10.1038/s41598-018-25635-x
110. Ang XM, Lee MH, Blocki A, Chen C, Ong LL, Asada HH, et al. Macromolecular crowding amplifies adipogenesis of human bone marrow-derived mesenchymal stem cells by enhancing the pro-adipogenic microenvironment. *Tissue Eng Part A*. (2014) 20:966–81. doi: 10.1089/ten.TEA.2013.0337
111. Xu Z, Ichikawa N, Kosaki K, Yamada Y, Sasaki T, Sakai LY, et al. Perlecan deficiency causes muscle hypertrophy, a decrease in myostatin expression, and changes in muscle fiber composition. *Matrix Biol*. (2010) 29:461–70. doi: 10.1016/j.matbio.2010.06.001
112. Nakamura R, Nakamura F, Fukunaga S. Perlecan diversely regulates the migration and proliferation of distinct cell types in vitro. *Cells Tissues Organs*. (2015) 200:374–93. doi: 10.1159/000440950
113. Gubbiotti MA, Neill T, Iozzo RV. A current view of perlecan in physiology and pathology: a mosaic of functions. *Matrix Biol*. (2017) 5:285–98. doi: 10.1016/j.matbio.2016.09.003
114. Sharma B, Iozzo RV. Transcriptional silencing of perlecan gene expression by interferon-gamma. *J Biol Chem*. (1998) 273:4642–6. doi: 10.1074/jbc.273.8.4642
115. Warren CR, Grindel BJ, Francis L, Carson DD, Farach-Carson MC. Transcriptional activation by NFκB increases perlecan/HSPG2 expression in the desmoplastic prostate tumor microenvironment. *J Cell Biochem*. (2014) 115:1322–33. doi: 10.1002/jcb.24788
116. Asplund A, Stillemark-Billton P, Larsson E, Rydberg EK, Moses J, Hultén LM, et al. Hypoxic regulation of secreted proteoglycans in macrophages. *Glycobiology*. (2010) 20:33–40. doi: 10.1093/glycob/cwp139
117. Tran-Lundmark K, Tran PK, Paulsson-Berne G, Fridén V, Soininen R, Tryggvason K, et al. Heparan sulfate in perlecan promotes mouse atherosclerosis: roles in lipid permeability, lipid retention, and smooth muscle cell proliferation. *Circ Res*. (2008) 103:43–52. doi: 10.1161/CIRCRESAHA.108.172833
118. Xu YX, Ashline D, Liu L, Tassa C, Shaw SY, Ravid K, et al. The glycosylation-dependent interaction of perlecan core protein with LDL: implications for atherosclerosis. *J Lipid Res*. (2015) 56:266–76. doi: 10.1194/jlr.M053017
119. Benito-Arenas R, Zarate S, Revuelta GJ, Bastida A. chondroitin sulfate-degrading enzymes as tools for the development of new pharmaceuticals. *Catalysts*. (2019) 9:322. doi: 10.3390/catal9040322
120. Morla S. Glycosaminoglycans and glycosaminoglycan mimetics in cancer and inflammation. *Int J Mol Sci*. (2019) 20:1963. doi: 10.3390/ijms20081963
121. Chen S, Birk DE. The regulatory roles of small leucine-rich proteoglycans in extracellular matrix assembly. *FEBS J*. (2013) 280:2120–37. doi: 10.1111/febs.12136
122. Mikami T, Kitagawa H. Biosynthesis and function of chondroitin sulfate. *Biochim Biophys Acta*. (2013) 1830:4719–33. doi: 10.1016/j.bbagen.2013.06.006
123. Macke EL, Henningsen E, Jessen E, Zumwalde NA, Landowski M, Western DE, et al. Loss of chondroitin sulfate modification causes inflammation and neurodegeneration in skt Mice. *Genetics*. (2020) 214:121–34. doi: 10.1534/genetics.119.302834
124. Lassalle P, Molet S, Janin A, Heyden JV, Tavernier J, Fiers W, et al. ESM-1 is a novel human endothelial cell-specific molecule expressed in lung and regulated by cytokines. *J Biol Chem*. (1996) 271:20458–64. doi: 10.1074/jbc.271.34.20458
125. Béchard D, Scherpereel A, Hammad H, Gentina T, Tsicopoulos A, Aumercier M, et al. Human endothelial-cell specific molecule-1 binds directly to the integrin CD11a/CD18 (LFA-1) and blocks binding to intercellular adhesion molecule-1. *J Immunol*. (2001) 167:3099–106. doi: 10.4049/jimmunol.167.6.3099
126. Janke J, Engeli S, Gorzelniak K, Feldpausch M, Heintze U, Böhnke J, et al. Adipose tissue and circulating endothelial cell specific molecule-1 in human obesity. *Horm Metab Res*. (2006) 38:28–33. doi: 10.1055/s-2006-924973
127. Wellner M, Herse F, Janke J, Gorzelniak K, Engeli S, Bechart D, et al. Endothelial cell specific molecule-1–a newly identified protein in adipocytes. *Horm Metab Res*. (2003) 35:217–21. doi: 10.1055/s-2003-39477
128. Arman Y, Akpinar TS, Kose M, Emet S, Yuruyen G, Akarsu M, et al. Effect of glycemic regulation on endocan levels in patients with diabetes: a preliminary study. *Angiology*. (2016) 67:239–44. doi: 10.1177/0003319715585664
129. Balamir I, Ates I, Topcuoglu C, Turhan T. Association of endocan, ischemia-modified albumin, and hsCRP levels with endothelial dysfunction

in type 2 diabetes mellitus. *Angiology*. (2018) 69:609–16. doi: 10.1177/0003319717740781
130. Lv Y, Zhang Y, Shi W, Liu J, Li Y, Zhou Z, et al. The association between endocan levels and subclinical atherosclerosis in patients with type 2 diabetes mellitus. *Am J Med Sci*. (2017) 353:433–8. doi: 10.1016/j.amjms.2017.02.004
131. Ekiz-Bilir B, Bilir B, Aydın M, Soysal-Atile N. Evaluation of endocan and endoglin levels in chronic kidney disease due to diabetes mellitus. *Arch Med Sci*. (2019) 15:86–91. doi: 10.5114/aoms.2018.79488
132. Dallio M, Masarone M, Caprio GG, Di Sarno R, Tuccillo C, Sasso FC, et al. Endocan serum levels in patients with non-alcoholic fatty liver disease with or without type 2 diabetes mellitus: a pilot study. *J Gastrointestin Liver Dis*. (2017) 26:261–8. doi: 10.15403/jgld.2014.1121.263.dal
133. Elkamshoushi AM, Omar SS, El Abd AM, Hassan SZ, Sultan EA, Abd Elkawy E. Subclinical atherosclerosis in psoriatic disease: relation to endocan, TNF-α, age of onset, and body fat. *Int J Dermatol*. (2019) 58:456–64. doi: 10.1111/ijd.14290
134. Rodrigues KF, Pietrani NT, Bosco AA, Sousa LP, Ferreira CN, Sandrim VC, et al. Endocan: a new biomarker associated with inflammation in type 2 diabetes mellitus? *Diabetes Metab Res Rev*. (2015) 31:479–80. doi: 10.1002/dmrr.2639
135. Cikrikcioglu MA, Erturk Z, Kilic E, Celik K, Ekinci I, Yasin Cetin A. I, et al. Endocan and albuminuria in type 2 diabetes mellitus. *Ren Fail*. (2016) 38:1647–53. doi: 10.1080/0886022X.2016.1229966
136. Zheng X, Soroush F, Long J, Hall ET, Adishesha PK, Bhattacharya S, et al. Murine glomerular transcriptome links endothelial cell-specific molecule-1 deficiency with susceptibility to diabetic nephropathy. *PLoS One*. (2017) 12:e0185250. doi: 10.1371/journal.pone.0185250
137. Svensson L, Närlid I, Oldberg A. Fibromodulin and lumican bind to the same region on collagen type I fibrils. *FEBS Lett*. (2000) 470:178–82. doi: 10.1016/s0014-5793(00)01314-4
138. Hildebrand A, Romarís M, Rasmussen LM, Heinegård D, Twardzik DR, Border WA, et al. Interaction of the small interstitial proteoglycans biglycan, decorin and fibromodulin with transforming growth factor beta. *Biochem J*. (1994) 302(Pt 2):527–34. doi: 10.1042/bj3020527
139. Ward M, Ajuwon KM. Regulation of pre-adipocyte proliferation and apoptosis by the small leucine-rich proteoglycans, biglycan and decorin. *Cell Prolif*. (2011) 44:343–51. doi: 10.1111/j.1365-2184.2011.00763.x
140. Daquinag AC, Zhang Y, Amaya-Manzanares F, Simmons PJ, Kolonin MG. An isoform of decorin is a resistin receptor on the surface of adipose progenitor cells. *Cell Stem Cell*. (2011) 9:74–86. doi: 10.1016/j.stem.2011.05.017
141. Schaefer L, Babelova A, Kiss E, Hausser HJ, Baliova M, Krzyzankova M, et al. The matrix component biglycan is proinflammatory and signals through Toll-like receptors 4 and 2 in macrophages. *J Clin Invest*. (2005) 115:2223–33. doi: 10.1172/JCI23755
142. Merline R, Moreth K, Beckmann J, Nastase MV, Zeng-Brouwers J, Tralhão JG, et al. Signaling by the matrix proteoglycan decorin controls inflammation and cancer through PDCD4 and MicroRNA-21. *Sci Signal*. (2011) 4:ra75. doi: 10.1126/scisignal.2001868
143. Zhang J, Wright W, Bernlohr DA, Cushman SW, Chen X. Alterations of the classic pathway of complement in adipose tissue of obesity and insulin resistance. *Am J Physiol Endocrinol Metab*. (2007) 292:E1433–40. doi: 10.1152/ajpendo.00664.2006
144. Groeneveld TW, Oroszlán M, Owens RT, Faber-Krol MC, Bakker AC, Arlaud GJ, et al. Interactions of the extracellular matrix proteoglycans decorin and biglycan with C1q and collectins. *J Immunol*. (2005) 175:4715–23. doi: 10.4049/jimmunol.175.7.4715
145. Vu TT, Marquez J, Le LT, Nguyen ATT, Kim HK, Han J. The role of decorin in cardiovascular diseases: more than just a decoration. *Free Radic Res*. (2018) 52:1210–9. doi: 10.1080/10715762.2018.1516285
146. Mauviel A, Santra M, Chen YQ, Uitto J, Iozzo RV. Transcriptional regulation of decorin gene expression. Induction by quiescence and repression by tumor necrosis factor-alpha. *J Biol Chem*. (1995) 270:11692–700. doi: 10.1074/jbc.270.19.11692
147. Edwards IJ, Xu H, Wright MJ, Wagner WD. Interleukin-1 upregulates decorin production by arterial smooth muscle cells. *Arterioscler Thromb*. (1994) 14:1032–9.
148. Strazynski M, Eble JA, Kresse H, Schönherr E. Interleukin (IL)-6 and IL-10 induce decorin mRNA in endothelial cells, but interaction with fibrillar collagen is essential for its translation. *J Biol Chem*. (2004) 279:21266–70. doi: 10.1074/jbc.M309782200
149. Bolton K, Segal D, McMillan J, Jowett J, Heilbronn L, Abberton K, et al. Decorin is a secreted protein associated with obesity and type 2 diabetes. *Int J Obes (Lond)*. (2008) 32:1113–21. doi: 10.1038/ijo.2008.41
150. Meissburger B, Perdikari A, Moest H, Müller S, Geiger M, Wolfrum C. Regulation of adipogenesis by paracrine factors from adipose stromal-vascular fraction - a link to fat depot-specific differences. *Biochim Biophys Acta*. (2016) 1861(9 Pt A):1121–31. doi: 10.1016/j.bbalip.2016.06.010
151. Svärd J, Røst TH, Sommervoll CEN, Haugen C, Gudbrandsen OA, Mellgren AE, et al. Absence of the proteoglycan decorin reduces glucose tolerance in overfed male mice. *Sci Rep*. (2019) 9:4614. doi: 10.1038/s41598-018-37501-x
152. Ibrahim MM. Subcutaneous and visceral adipose tissue: structural and functional differences. *Obes Rev*. (2010) 11:11–8. doi: 10.1111/j.1467-789X.2009.00623.x
153. Bi X, Tong C, Dockendorff A, Bancroft L, Gallagher L, Guzman G, et al. Genetic deficiency of decorin causes intestinal tumor formation through disruption of intestinal cell maturation. *Carcinogenesis*. (2008) 29:1435–40. doi: 10.1093/carcin/bgn141
154. Park HK, Ahima RS. Resistin in rodents and humans. *Diabetes Metab J*. (2013) 37:404–14. doi: 10.4093/dmj.2013.37.6.404
155. Osawa H, Yamada K, Onuma H, Murakami A, Ochi M, Kawata H, et al. The G/G genotype of a resistin single-nucleotide polymorphism at -420 increases type 2 diabetes mellitus susceptibility by inducing promoter activity through specific binding of Sp1/3. *Am J Hum Genet*. (2004) 75:678–86. doi: 10.1086/424761
156. Schaefer L, Raslik I, Grone HJ, Schonherr E, Macakova K, Ugorcakova J, et al. Small proteoglycans in human diabetic nephropathy: discrepancy between glomerular expression and protein accumulation of decorin, biglycan, lumican, and fibromodulin. *FASEB J*. (2001) 15:559–61. doi: 10.1096/fj.00-0493fje
157. Williams KJ, Qiu G, Usui HK, Dunn SR, McCue P, Bottinger E, et al. Decorin deficiency enhances progressive nephropathy in diabetic mice. *Am J Pathol*. (2007) 171:1441–50. doi: 10.2353/ajpath.2007.070079
158. Merline R, Lazaroski S, Babelova A, Tsalastra-Greul W, Pfeilschifter J, Schluter KD, et al. Decorin deficiency in diabetic mice: aggravation of nephropathy due to overexpression of profibrotic factors, enhanced apoptosis and mononuclear cell infiltration. *J Physiol Pharmacol*. (2009) 60(Suppl. 4):5–13.
159. Babelova A, Moreth K, Tsalastra-Greul W, Zeng-Brouwers J, Eickelberg O, Young MF, et al. Biglycan, a danger signal that activates the NLRP3 inflammasome via toll-like and P2X receptors. *J Biol Chem*. (2009) 284:24035–48. doi: 10.1074/jbc.M109.014266
160. Adapala VJ, Ward M, Ajuwon KM. Adipose tissue biglycan as a potential anti-inflammatory target of sodium salicylate in mice fed a high fat diet. *J Inflamm (Lond)*. (2012) 9:15. doi: 10.1186/1476-9255-9-15
161. Kim J, Lee SK, Shin JM, Jeoun UW, Jang YJ, Park HS, et al. Enhanced biglycan gene expression in the adipose tissues of obese women and its association with obesity-related genes and metabolic parameters. *Sci Rep*. (2016) 6:30609. doi: 10.1038/srep30609
162. Ward MG, Ajuwon KM. Biglycan deletion alters adiponectin expression in murine adipose tissue and 3T3-L1 adipocytes. *PLoS One*. (2012) 7:e50554. doi: 10.1371/journal.pone.0050554
163. Bolton K, Segal D, Walder K. The small leucine-rich proteoglycan, biglycan, is highly expressed in adipose tissue of *Psammomys obesus* and is associated with obesity and type 2 diabetes. *Biologics*. (2012) 6:67–72. doi: 10.2147/BTT.S27925
164. Yamauchi T, Kamon J, Waki H, Terauchi Y, Kubota N, Hara K, et al. The fat-derived hormone adiponectin reverses insulin resistance associated with both lipoatrophy and obesity. *Nat Med*. (2001) 7:941–6. doi: 10.1038/90984
165. Díez JJ, Iglesias P. The role of the novel adipocyte-derived hormone adiponectin in human disease. *Eur J Endocrinol*. (2003) 148:293–300. doi: 10.1530/eje.0.1480293
166. Nakashima Y, Fujii H, Sumiyoshi S, Wight TN, Sueishi K. Early human atherosclerosis: accumulation of lipid and proteoglycans in intimal thickenings followed by macrophage infiltration. *Arterioscler Thromb Vasc Biol*. (2007) 27:1159–65. doi: 10.1161/ATVBAHA.106.134080

167. Kunjathoor VV, Chiu DS, O'Brien KD, LeBoeuf RC. Accumulation of biglycan and perlecan, but not versican, in lesions of murine models of atherosclerosis. *Arterioscler Thromb Vasc Biol*. (2002) 22:462–8. doi: 10.1161/hq0302.105378
168. Thompson JC, Tang T, Wilson PG, Yoder MH, Tannock LR. Increased atherosclerosis in mice with increased vascular biglycan content. *Atherosclerosis*. (2014) 235:71–5. doi: 10.1016/j.atherosclerosis.2014.03.037
169. Olin-Lewis K, Krauss RM, La Belle M, Blanche PJ, Barrett PH, Wight TN, et al. ApoC-III content of apoB-containing lipoproteins is associated with binding to the vascular proteoglycan biglycan. *J Lipid Res*. (2002) 43:1969–77. doi: 10.1194/jlr.m200322-jlr200
170. Thompson J, Wilson P, Brandewie K, Taneja D, Schaefer L, Mitchell B, et al. Renal accumulation of biglycan and lipid retention accelerates diabetic nephropathy. *Am J Pathol*. (2011) 179:1179–87. doi: 10.1016/j.ajpath.2011.05.016
171. Hsieh LT, Nastase MV, Zeng-Brouwers J, Iozzo RV, Schaefer L. Soluble biglycan as a biomarker of inflammatory renal diseases. *Int J Biochem Cell Biol*. (2014) 54:223–35. doi: 10.1016/j.biocel.2014.07.020
172. Wu F, Vij N, Roberts L, Lopez-Briones S, Joyce S, Chakravarti S. A novel role of the lumican core protein in bacterial lipopolysaccharide-induced innate immune response. *J Biol Chem*. (2007) 282:26409–17. doi: 10.1074/jbc.M702402200
173. Pilling D, Vakil V, Cox N, Gomer RH. TNF-α-stimulated fibroblasts secrete lumican to promote fibrocyte differentiation. *Proc Natl Acad Sci USA*. (2015) 112:11929–34. doi: 10.1073/pnas.1507387112
174. Krishnan A, Li X, Kao WY, Viker K, Butters K, Masuoka H, et al. Lumican, an extracellular matrix proteoglycan, is a novel requisite for hepatic fibrosis. *Lab Invest*. (2012) 92:1712–25. doi: 10.1038/labinvest.2012.121
175. Sharma DL, Lakhani HV, Klug RL, Snoad B, El-Hamdani R, Shapiro JI, et al. Investigating molecular connections of non-alcoholic fatty liver disease with associated pathological conditions in west virginia for biomarker analysis. *J Clin Cell Immunol*. (2017) 8:523. doi: 10.4172/2155-9899.1000523
176. Charlton M, Viker K, Krishnan A, Sanderson S, Veldt B, Kaalsbeek AJ, et al. Differential expression of lumican and fatty acid binding protein-1: new insights into the histologic spectrum of nonalcoholic fatty liver disease. *Hepatology*. (2009) 49:1375–84. doi: 10.1002/hep.22927
177. Wolff G, Taranko AE, Meln I, Weinmann J, Sijmonsma T, Lerch S, et al. Diet-dependent function of the extracellular matrix proteoglycan Lumican in obesity and glucose homeostasis. *Mol Metab*. (2019) 19:97–106. doi: 10.1016/j.molmet.2018.10.007
178. Deckx S, Heymans S, Papageorgiou AP. The diverse functions of osteoglycin: a deceitful dwarf, or a master regulator of disease? *FASEB J*. (2016) 30:2651–61. doi: 10.1096/fj.201500096R
179. Rienks M, Papageorgiou A, Wouters K, Verhesen W, Leeuwen RV, Carai P, et al. A novel 72-kDa leukocyte-derived osteoglycin enhances the activation of toll-like receptor 4 and exacerbates cardiac inflammation during viral myocarditis. *Cell Mol Life Sci*. (2017) 74:1511–25. doi: 10.1007/s00018-016-2423-7
180. Tasheva ES, Conrad GW. Interferon-gamma regulation of the human mimecan promoter. *Mol Vis*. (2003) 9:277–87.
181. Li X, Massa PE, Hanidu A, Peet GW, Aro P, Savitt A, et al. IKKalpha, IKKbeta, and NEMO/IKKgamma are each required for the NF-kappa B-mediated inflammatory response program. *J Biol Chem*. (2002) 277:45129–40. doi: 10.1074/jbc.M205165200
182. Fernández B, Kampmann A, Pipp F, Zimmermann R, Schaper W. Osteoglycin expression and localization in rabbit tissues and atherosclerotic plaques. *Mol Cell Biochem*. (2003) 246:3–11. doi: 10.1007/978-1-4615-0298-2_1
183. Malaud E, Merle D, Piquer D, Molina L, Salvetat N, Rubrecht L, et al. Local carotid atherosclerotic plaque proteins for the identification of circulating biomarkers in coronary patients. *Atherosclerosis*. (2014) 233:551–8. doi: 10.1016/j.atherosclerosis.2013.12.019
184. Cao HM, Ye XP, Ma JH, Jiang H, Li SX, Li RY, et al. Mimecan, a hormone abundantly expressed in adipose tissue, reduced food intake independently of leptin signaling. *EBioMedicine*. (2015) 2:1718–24. doi: 10.1016/j.ebiom.2015.09.044
185. Lee NJ, Ali N, Zhang L, Qi Y, Clarke I, Enriquez RF, et al. Osteoglycin, a novel coordinator of bone and glucose homeostasis. *Mol Metab*. (2018) 13:30–44. doi: 10.1016/j.molmet.2018.05.004
186. Pan Q, Zhang C, Wu X, Chen Y. Identification of a heparosan heptasaccharide as an effective anti-inflammatory agent by partial desulfation of low molecular weight heparin. *Carbohydr Polym*. (2020) 227:115312. doi: 10.1016/j.carbpol.2019.115312
187. Tanaka Y, Tateishi R, Koike K. Proteoglycans are attractive biomarkers and therapeutic targets in hepatocellular carcinoma. *Int J Mol Sci*. (2018) 19:3070. doi: 10.3390/ijms19103070
188. Lepedda AJ, De Muro P, Capobianco G, Formato M. Significance of urinary glycosaminoglycans/proteoglycans in the evaluation of type 1 and type 2 diabetes complications. *J Diabetes Complications*. (2017) 31:149–55. doi: 10.1016/j.jdiacomp.2016.10.013
189. Theocharis AD, Skandalis SS, Tzanakakis GN, Karamanos NK. Proteoglycans in health and disease: novel roles for proteoglycans in malignancy and their pharmacological targeting. *FEBS J*. (2010) 277:3904–23. doi: 10.1111/j.1742-4658.2010.07800.x
190. Hirose S, Asano K, Nakane A. Attenuation of obesity-induced inflammation in mice orally administered with salmon cartilage proteoglycan, a prophylactic agent. *Biochem Biophys Res Commun*. (2017) 484:480–5. doi: 10.1016/j.bbrc.2017.01.056

Conflict of Interest: The authors declare that the research was conducted in the absence of any commercial or financial relationships that could be construed as a potential conflict of interest.

Advantages of publishing in Frontiers

OPEN ACCESS
Articles are free to read for greatest visibility and readership

FAST PUBLICATION
Around 90 days from submission to decision

HIGH QUALITY PEER-REVIEW
Rigorous, collaborative, and constructive peer-review

TRANSPARENT PEER-REVIEW
Editors and reviewers acknowledged by name on published articles

Frontiers
Avenue du Tribunal-Fédéral 34
1005 Lausanne | Switzerland

Visit us: www.frontiersin.org
Contact us: info@frontiersin.org | +41 21 510 17 00

REPRODUCIBILITY OF RESEARCH
Support open data and methods to enhance research reproducibility

DIGITAL PUBLISHING
Articles designed for optimal readership across devices

FOLLOW US
@frontiersin

IMPACT METRICS
Advanced article metrics track visibility across digital media

EXTENSIVE PROMOTION
Marketing and promotion of impactful research

LOOP RESEARCH NETWORK
Our network increases your article's readership